

---

# Directed Evolution of Gold-based Artificial Metalloenzymes and Design of Gold-triggered Drug-Release Systems

---

## **Inauguraldissertation**

zur

Erlangung der Würde eines Doktors der Philosophie

vorgelegt der

Philosophisch-Naturwissenschaftlichen Fakultät

der Universität Basel

von

**Fadri Christoffel**

Basel, 2021

*Originaldokument gespeichert auf dem Dokumentenserver der Universität Basel  
edoc.unibas.ch*

Genehmigt von der Philosophisch-Naturwissenschaftlichen Fakultät  
auf Antrag von

Prof. Dr. Thomas R. Ward

Prof. Dr. Olivier Baudoin

Prof. Dr. Cristina Nevado

Basel, den 22. Juni 2021

---

Prof. Dr. Marcel Mayor

Dekan

# Acknowledgement

---

First of all, I would like to thank Prof. Dr. Thomas R. Ward for not only giving me the opportunity to do my PhD in this group but also for providing me with such challenging and interesting projects. I am thankful for the guidance and support that I received during the last four years and for the chance to be part of this amazing team. I would like to thank Prof. Dr. Olivier Baudoin for his commitment of being the co-examiner of my PhD thesis, the supervisor of my MSc thesis and for inspiring lectures around organic chemistry. A thanks goes to Prof. Dr. Cristina Nevado for being the external expert of my PhD defense.

A big thank you goes to Nico V. Igareta, “mein Biologe des Vertrauens”. Thank you very much for the great teamwork, the many proteins you prepared and the many weekends we powered through. It has been quite a journey with the biot-Au · Sav-SOD project and it was nice to have someone to share the challenges but also to share the passion, the success, and celebrations. A special thanks goes to Juliane Klehr and Prof. Dr. Ryan Peterson for all the assistance with the biological part of our projects. I would like to thank all the other people who have contributed to this thesis: Dr. Michaela M. Pellizzoni, Dr. Valerio Sabatino, Boris Lozhkin, Philipp Meyer, Tobias Vornholt, Dr. Isabel T. Alt, Laura Tiessler-Sala, Prof. Dr. Jean D. Maréchal, Prof. Dr. Agusti Iledos, Dr. Markus Jeschek and Prof. Dr. Sven Panke.

*Teamwork makes the DrEAM  
(Directed Evolution of Artificial Metalloenzymes)  
work.*

I would like to thank Prof. Dr. Daniel Häussinger (NMR analysis), Michael Pfeffer, Jonas Zurflüh and Sylvie Mittelheisser (HR-MS analysis), the Werkstatt-team as well as the secretary office for their precious support.

I would like to thank all actual and former members of the Ward group and the Köhler group, in particular Lab-4039 (Alexandria, Boris, Coentín, Martina, Daniel, Valerio and Yoann), the hiking team (Jonas, Fabian, Juliane and Miriam) and the gym bros (Alain, Coentín, Nico). I really enjoyed the time we spent together.

Zum Schluss möchte ich meiner Familie, Fabian Fatima und Flurin Christoffel sowie meiner geliebten Frau, Miriam Christoffel für die unglaubliche Unterstützung, die ich über all die Jahre hinweg erfahren durfte, danken. Herzlichen Dank!

# Abstract

---

Nature has evolved enzymes to solve the complex biochemical problems of life through directed evolution over millions of years. But, to solve the needs of today's society, enzymes must be able to evolve more quickly and "smartly". Artificial metalloenzymes are an elegant solution to add new functionality to enzymes while utilizing the power of genetic memory from the host protein matrix. These systems can be especially useful in establishing biorthogonal reactions in living systems and have been extensively investigated in the Ward Lab at the University of Basel.

The aim of this thesis is to expand the current repertoire of biorthogonal catalysts by synthesizing gold(I)-based artificial metalloenzymes as well as gold(I)-functionalized somatostatin analogues and optimize their catalytic potential via directed evolution or systematic screening. This includes the design of new "close-to-release" substrates for controlled uncaging of fluorophores upon reaction with gold catalysts.



# Table of Contents

---

Acknowledgement -----	i
Abstract-----	ii
1. General Introduction-----	1
1.1 The Biotin-(Strept)Avidin Technology -----	1
1.2 Gold in Catalysis -----	2
2. Aim & Summary of individual Chapters -----	3
2.1 Aim of this Thesis: -----	3
2.2 Chapter 1: Dual-Gold-based chimeric ArMs -----	3
2.3 Chapter 2: Systematic Screening of Gold-based ArMs -----	3
2.4 Chapter 3: Intramolecular Heck Reaction -----	4
2.5 Chapter 4: Gold-triggered Drug-Release Systems -----	4
3. Chapter 1: Dual-Gold-based chimeric ArMs-----	5
3.1 Outline of the Authors Contribution -----	5
3.2 Introduction -----	5
3.3 Results and Discussion-----	6
3.4 Conclusion-----	17
3.5 Appendix: Mechanistic Studies -----	18
3.6 Appendix: Cooperativity Studies-----	23
3.7 Appendix: Linker Studies -----	27
3.8 Appendix: Unreactive Substrates for Dual-Gold Catalysis -----	29
4. Chapter 2: Systematic Screening of Gold-based ArMs-----	31
4.1 Outline of the Authors Contribution -----	31
4.2 Introduction -----	31
4.3 Results and Discussion-----	32
4.4 Conclusion-----	37
4.5 Appendix: Unreactive Substrates & Proline Metabolism-----	37
5. Chapter 3: Intramolecular Heck Reaction-----	40

5.1 Outline of the Authors Contribution -----	40
5.2 Introduction -----	40
5.3 Results and Discussion -----	42
5.4 Conclusion -----	47
6. Chapter 4: Gold-triggered Drug-Release Systems -----	48
6.1 Outline of the Authors Contribution -----	48
6.2 Introduction -----	48
6.3 Results and Discussion -----	50
6.4 Conclusion -----	57
6.5 Appendix: Unreactive Substrates -----	57
6.6 Appendix: Sulfimide Gold-NHC complex -----	59
7. Final Conclusion and Outlook -----	62
8. Experimental and Supplementary Information -----	64
8.1 General Methods: -----	64
8.2 Chapter 1: Dual-Gold-based chimeric ArMs -----	66
8.3 Chapter 2: Systematic Screening of Gold-based ArMs -----	176
8.4 Chapter 3: Palladium-based ArMs -----	184
8.5 Chapter 4: Gold-triggered Drug-Release Systems -----	205
9. Bibliography: -----	227
10. Self Citations & Reprint Permissions -----	235
11. Curriculum Vitae -----	238
12. Publication List -----	240

# 1. General Introduction

---

Enzymes display unmatched catalytic activity while functioning in sophisticated cascades and in complex biological environments. Artificial metalloenzymes (ArMs) are one way of mimicking nature's most efficient catalysts in order to introduce complex organometallic reactivities *in vivo*. ArMs are composed of a synthetic, catalytically competent metallocofactor integrated into a protein matrix. The result is a hybrid catalyst capable of combining the benefits of homogeneous and enzymatic catalysis.<sup>1</sup>

## 1.1 The Biotin-(Strept)Avidin Technology

Avidin and its relation to the vitamin biotin were initially discovered while investigating egg white in the late 1920s.<sup>2</sup> Its function may be linked to bacterial inhibition by removing biotin, a crucial bacterial metabolite, from the environment.<sup>3</sup> Despite the low sequence identity (~30%),<sup>4</sup> Avidin and the structurally related Streptavidin (Sav) isolated first from *Streptomyces avidinii*, both form homotetrameric structures constituting of  $\beta$ -barrel motifs that each bind biotin nearly irreversibly ( $K_d > 10^{-14}$  M).<sup>5-7</sup> In the 1970s, Whitesides and Wilson utilized this supramolecular anchoring strategy to incorporate biotinylated diphosphinerhodium(I) into avidin.<sup>8</sup> The goal was to benefit from the second coordination sphere of the host protein to induce enantioselectivity to rhodium(I)-based asymmetric hydrogenation. This innovative approach achieved modest enantioselectivity as the biotechnological tools necessary to optimize the protein matrix were missing. These limitations also affected the development of other ArM designs e.g. based on metal substitution of carboxypeptidase A.<sup>9</sup>

Decades later and with new tools with regards to protein engineering and organometallic catalyst design in hands, the field of ArMs including the biotin-Sav technology experienced a revival.<sup>10</sup> The applications of Sav in biotechnology go far beyond ArM design and include the purification and detection of biomolecules,<sup>11,12</sup> the construction of nanomaterials,<sup>13,14</sup> its use in immunotherapy<sup>15-17</sup> as well as the transport of drugs via protein-delivery systems.<sup>18</sup> In contrast to avidin, Sav does not bear any glycosylation domains and consists of a very different primary sequence. As a result, Sav is more acidic which reduces nonspecific binding, prevents pseudo-catalysis and minimizes undesired agglomeration. Furthermore, Sav displays exceptional stability: it tolerates large variations in pH, high amounts of organic solvent and remains stable even above 70 °C.<sup>19</sup> This versatile protein was used to incorporate a diverse range of biotinylated organometallic catalyst for the preparation of ArMs with applications in: hydrogenation,<sup>20,21</sup> sulfoxidation,<sup>22</sup> dihydroxylation,<sup>23</sup> alcohol oxidation,<sup>24</sup> transfer hydrogenation,<sup>25-27</sup> Suzuki cross-coupling,<sup>28</sup> C-H activation,<sup>29</sup> and metathesis.<sup>30</sup> In combination with established Sav expression systems, it can be fairly straight-forward to develop Sav-

based directed evolution protocols in order to optimize these ArMs towards high catalytic activity but also towards new regio- and/or enantioselectivities.<sup>30–33</sup>

## 1.2 Gold in Catalysis

Gold has been used by humans for ten-thousands of years. It is associated with intrinsic worth (monetary system), divine principles (golden ratio, golden rule) and great achievements (Nobel prize, Olympic medal). Gold crafts have retained their “shining dawn” (aurum) over millennia due to the outstanding stability of this element towards oxidation.<sup>34</sup> While catalyst derived from transition metals including palladium, iridium, rhodium and ruthenium have been extensively explored since the 1970s, gold has been undeservedly neglected for decades. Already back in 1973 Geoffrey Bond stated: “We are at a loss to understand why these catalytic properties of gold have not been reported before, especially since the preparative methods we have used are in no way remarkable.”<sup>35</sup> And in 1998 David Thompson followed: “In addition, it is noticeable that most areas of gold science are at an earlier stage of evolution than that already attained for neighboring elements in the Periodic Table, and although some of the potential applications are at an early stage of development, many significant developments can be anticipated in the future.”<sup>36</sup> In the shadow of Nobel-prize winning osmium (2001), rhodium (2001), titanium (2001), ruthenium (2001 and 2005) and palladium (2010) catalysis, it took another decade for the field of gold catalysis to seriously take off.<sup>37–40</sup>

While elemental gold is inert, gold nanoparticles, gold(I) complexes or gold (III) complexes can be used for gold catalysis. The strong Lewis acidity, the potential to stabilize cationic intermediates and coordinate unsaturated bonds combined with exceptional stability towards both oxygen and acidic protons imparts unique reactivity to this set of catalysts.<sup>41</sup> In contrast to other transition metals, gold(I) and gold (III) complexes do not readily cycle between oxidation states and thus rarely follow the typical oxidative addition/reductive elimination pattern.<sup>42</sup> Instead, new modes of reactivity were discovered, including dual-gold catalysis.<sup>43</sup> The strong relativistic contractions in the 6s orbital of gold does not only result in strengthened gold-ligand bonds but also in stabilizing gold-gold interactions, a phenomenon referred to as “aurophilicity”.<sup>42</sup> In this study, we are especially interested in utilizing the alkynophilic, Lewis acid-like properties of Au(I) complexes to convert alkynes in a biorthogonal and selective manner under mild reaction conditions.

## 2. Aim & Summary of individual Chapters

---

### 2.1 Aim of this Thesis:

The aim of this thesis is to expand the current repertoire of biorthogonal catalysts by synthesizing palladium(II)- and gold(I)-based artificial metalloenzymes. The course of action was: i) the synthesis of biotinylated *N*-heterocyclic cofactors, ii) the synthesis of compatible substrates, iii) the introduction of the cofactors into Sav and chimeric analogues thereof and finally iv) the optimization of the corresponding ArM via directed evolution or systematic screening. Additionally, gold(I)-functionalized somastatin analogues were investigated for the controlled uncaging of fluorophores via a newly developed “close-to-release” reaction.

### 2.2 Chapter 1: Dual-Gold-based chimeric ArMs

An artificial hydroaminase was engineered and evolved to perform either single- or dual-gold catalysis. Guided by modeling, a chimeric streptavidin equipped with a hydrophobic lid shielding its active site was designed, which enforces the advantageous positioning of two synergistic biotinylated gold cofactors. Three rounds of directed evolution using *E. coli* cell-free extracts led to the identification of mutants favoring either the anti-Markovnikov product (an indole carboxamide with 96% regioselectivity, 51 TONs) resulting from a dual gold  $\sigma,\pi$ -activation of an ethynylphenylurea substrate or the Markovnikov product (a phenyl-dihydroquinazolinone with 99% regioselectivity, 333 TONs) resulting from the  $\pi$ -activation of the alkyne to gold.

### 2.3 Chapter 2: Systematic Screening of Gold-based ArMs

Gold-based ArMs were systematically screened to optimize their performance in the periplasm of *E. coli*. Various reactions were investigated including the uncaging of protected-indole and the hydroamination of 2-aminopent-4-ynoic acid to 2,3-dihydroproline. However, only two reactions proved viable: (i) the hydroamination of 2-ethynylaniline towards indole and (ii) the hydroarylation of pro-coumarin derivatives. The use of a systematic screening platform provided sufficient training set data for machine learning approaches. Furthermore, efficient smart libraries could be deduced from the screening data to optimize screening efforts in the future.

## 2.4 Chapter 3: Intramolecular Heck Reaction

The synthesis of 2-iodo-N-vinylaniline derivatives and their role in the intramolecular Heck cyclization was investigated. The corresponding substrates should be transformed to pro-metabolites, with the goal to implement the Heck reaction in an artificial Tryptophan synthase pathway. Different palladium complexes were prepared to catalyze the cyclization of tosyl-protected 2-iodo-N-vinylaniline to the corresponding indole in aqueous THF. Attempts to deprotect the substrate and/or the product were not successful, while the synthesis of unprotected substrates failed. As a result, the project was not further pursued, and palladium(II)-based ArM were not further investigated in this thesis.

## 2.5 Chapter 4: Gold-triggered Drug-Release Systems

A new “close-to-release” methodology was developed utilizing intramolecular gold-cyclization followed by spontaneous 1,2-elimination to release umbelliferone. Chimeric gold ArMs proved highly efficient in uncaging umbelliferone in MES buffer. The simple reaction procedure could prove useful for systematic screening efforts. In order to facilitate medical applications, gold-functionalized peptides were prepared based on cyclic somatostatin analogues. These peptides catalyzed the close-to-release reaction albeit with lower conversions. What’s more, in aqueous mixtures of acetonitrile, the gold-functionalized peptides quantitatively performed the hydroarylation of pro-coumarin derivatives to afford the corresponding fluorescent products.

## 3. Chapter 1: Dual-Gold-based chimeric ArMs

---

**Christoffel, F.**, Igareta, N., Pellizzoni, M., Tiessler-Sala, L., Lozhkin, B., Spiess, D., Lledos, A., Maréchal, J., Peterson, R., Ward, T. R., Design and Evolution of Chimeric Streptavidin for Protein-Enabled Dual Gold Catalysis. *Nat. Catal.* **4**, 643-653 (2021).  
&  
*unpublished results*

### 3.1 Outline of the Authors Contribution

TRW, RLP and FC conceived and designed the study. FC, MMP and BL contributed to the synthesis of the substrates, products and complexes. NVI, DCS, RLP and FC contributed to mutagenesis, protein expression, protein purification and protein characterization. NVI performed the crystallization, X-ray structure determinations and the native MS experiments. FC performed the catalytic, preparative, and deuterium-labeling experiments, designed the screening protocol and recorded the data. TRW, FC and NVI analyzed the data. JDM, AL, and LTS contributed to the molecular modelling experiments.

### 3.2 Introduction

Thanks to their unique affinity towards alkynes, allenes and alkenes, gold complexes have attracted significant attention for their catalytic potential.<sup>44-49</sup> In addition to the activation of unsaturated substrates via  $\pi$ -coordination, terminal alkynes undergo dual-gold activation via synergistic  $\sigma, \pi$ -coordination.<sup>43,50-55</sup> This mode of activation, which proceeds via a diaurated transition state, affords distinct products/regioisomers, significantly broadening the scope of gold-catalyzed reactions. Such synergistic action of two metals in catalysis is reminiscent of polynuclear metalloenzymes, whereby (at least) two metals act in concert to catalyze challenging reactions.<sup>56-59</sup>

In the context of *in vivo* ligation and bioconjugation, alkynes occupy a place of choice, as this functional group was shown to be bio-orthogonal, thus finding widespread use in “click” chemistry.<sup>60-63</sup> Although Cu and Ru are privileged catalysts in this context,<sup>64,65</sup> recent reports suggest that gold-complexes maintain catalytic activity in a cellular environment, albeit for a different type of reactivity.<sup>66-72</sup> To the best of our knowledge however, these biocompatible reactions rely on a  $\pi$ -activation of the alkyne, rather than the dual activation, so distinctive of gold-catalysis.

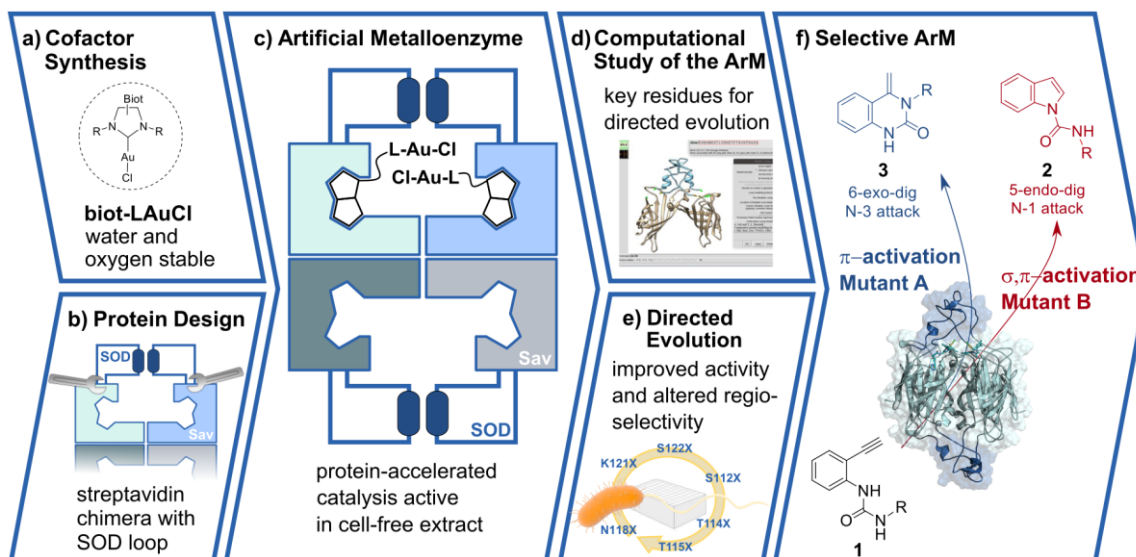


**Figure 1 Engineering and evolving an artificial hydroaminase (HAMase) based on dual-gold activation of alkynes.** Chemo-genetic optimization of the catalytic performance relies on combining: **a** a biotinylated cofactor and **b** a tailored chimeric protein to assemble **c** an ArM equipped with two adjacent gold cofactors. Genetic optimization is guided by **d** modelling to identify **e** advantageous amino acids for directed evolution to favor **f** either  $\sigma,\pi$ -activation or  $\pi$ -activation of the alkyne to afford either indole **2** or quinazolinone **3** respectively. Modified and reprinted with permission from Springer Nature.<sup>73</sup>

With the aim of complementing natural enzymes,<sup>74</sup> ArMs have experienced a renaissance in the past two decades.<sup>8,75–81</sup> For this purpose, an abiotic metal cofactor is compartmentalized within a protein scaffold which can be optimized by genetic means. Thus far, more than 40 reactions can be catalyzed by ArMs.<sup>10</sup> Current challenges in the field include i) protein-accelerated catalysis, whereby a pre-catalyst is activated upon incorporation within the host protein,<sup>29,82</sup> ii) dual catalysis<sup>83,84</sup> and iii) compatibility of the ArM with a cytosolic environment.<sup>10,85,86</sup> Privileged scaffolds for ArMs include: carbonic anhydrase,<sup>87</sup> hemoproteins,<sup>88,89</sup> prolyl oligopeptidase,<sup>90</sup> lactococcal multiresistance regulator,<sup>78</sup> four helix-bundles,<sup>58,91</sup> nitrobindin,<sup>92</sup> human serum albumin,<sup>93</sup> and (strept)avidin.<sup>8,86,94</sup> As a result of the unique topology of Sav favoring the localization of two close-lying biotinylated probes in a hydrophobic environment, we set out to engineer and evolve a biocompatible artificial hydroaminase (HAMase hereafter) based on either single<sup>95</sup> or dual-gold activation of the alkyne, **Figure 1**.

### 3.3 Results and Discussion

As reported by Asensio<sup>52,96</sup> and van der Vlugt<sup>97</sup>, the regioselectivity for the hydroamination of ethynylurea **1** is by-and-large governed by the mode of activation of the alkyne by gold: the canonical  $\pi$ -activation favors the quinazolinone **3** (Markovnikov, 6-exo-dig addition product), while the dual  $\sigma,\pi$ -gold activation affords preferentially the indole **2** (anti-Markovnikov, 5-endo-dig addition product)<sup>52,97,98</sup> Upon  $\pi$ -coordination of the alkyne to gold, the pKa of the terminal



C–H bond is lowered, thus favoring its deprotonation and coordination by a second gold to afford the  $\sigma,\pi$ -activation mode.<sup>96</sup> Accordingly, the spatial arrangement of the two gold species is critical in determining the regioselectivity of the reaction. We thus selected the gold-catalyzed cyclization of the ethynylurea **1** to engineer and evolve a dual-gold catalyzed hydroaminase (HAMase) based on the biotin-streptavidin technology.

Thanks to its dimer of dimers quaternary structure, which places the valeric acid side chains of two proximal biotins 19.8 Å apart (pdb: 3ry2<sup>99</sup>), we designed *N*-heterocyclic carbene ligands equipped with a biotin anchor introduced at various positions, **Figure 2 a**.<sup>100</sup> We hypothesized that the relative position of two gold moieties within the biotin binding vestibule may influence the mode of alkyne-activation as reflected by the indole **2** vs the quinazolinone **3** ratio. Sterically-crowded imidazolium precursors were metalated using a one-step procedure,<sup>101</sup> and less-hindered carbenes were prepared through transmetalation of the silver-carbene complex,<sup>102</sup> to afford the corresponding gold complexes: **biot-Au 1-5**, **SI Figure 1**<sup>103–105</sup> These are air- and water stable and can be stored for months as stock solutions in DMSO at 5 °C.

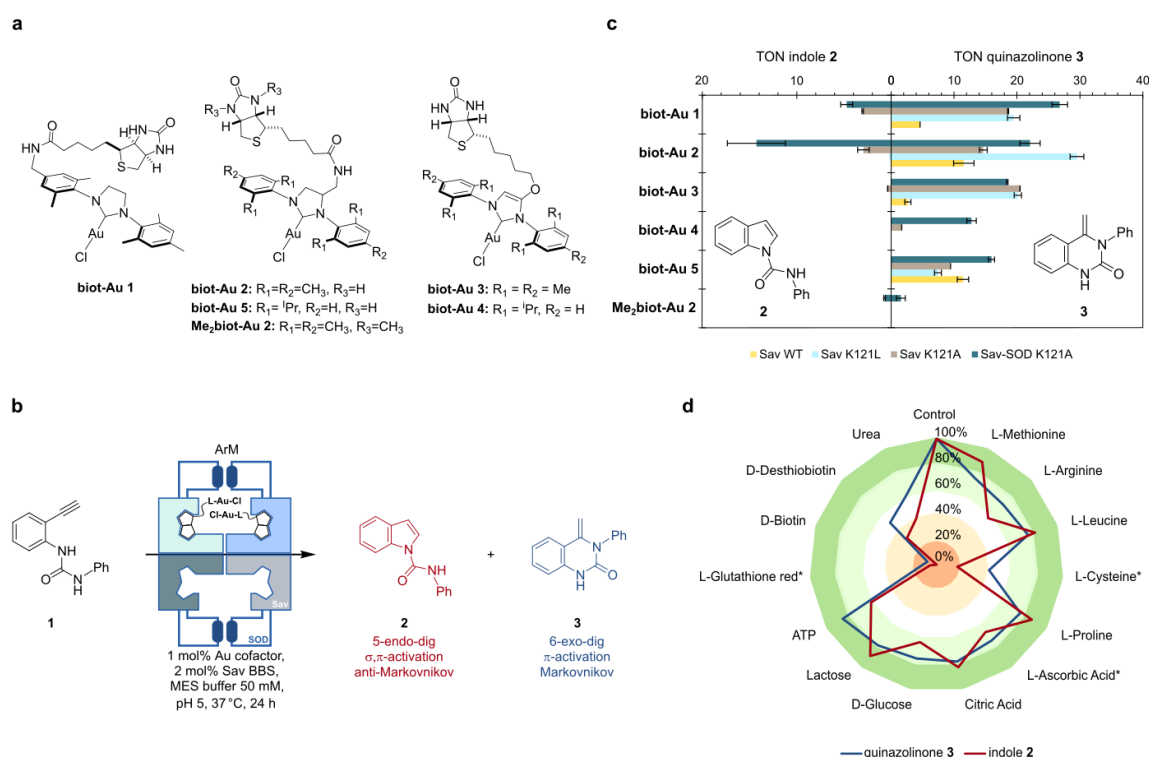


**Figure 2 Chemo-genetic optimization of HAMase activity.** **a** Biotinylated gold complexes **biot-Au 1-5** tested **b** in the presence of streptavidin isoforms **c** for the hydroamination of substrate **1** to afford indole **2** or quinazolinone **3**. Screening conditions using purified Sav samples:  $V_{\text{tot}}$  200  $\mu\text{L}$  ( $V_{\text{DMSO}}$  15  $\mu\text{L}$ ), [Sub] 5 mM, [Au] 50  $\mu\text{M}$ , [Sav] 100  $\mu\text{M}$ , [MES-buffer] 50 mM, pH 5, 37 °C for 24 h. **d** Bio-additive-based screening of **biot-Au 2** · Sav-SOD K121A allows identifying detrimental cellular components. Reaction conditions:  $V_{\text{tot}}$  200  $\mu\text{L}$  ( $V_{\text{DMSO}}$  15  $\mu\text{L}$ ), [Sub] 2.5 mM, [bio-additive] 2.5 mM, [**biot-Au 2**] 50  $\mu\text{M}$ , [Sav] 100  $\mu\text{M}$ , [MES-buffer] 50 mM, pH 5, 37 °C for 24 h. \*cross-reaction with the substrate. Modified and reprinted with permission from Springer Nature.<sup>73</sup>

Initial studies using Au(I)-complexes bearing either commercially-available NHCs or **biot-Au 1-5** in buffered aqueous solutions afforded < 1 turnover (TON, using 7.5 % DMSO, [substrate **1**] = 5 mM and [Au] = 50  $\mu$ M = 1 mol %, 24 hours at room temperature), SI Table 1. Addition of wild-type streptavidin (Sav WT hereafter, 25  $\mu$ M, corresponding to 100  $\mu$ M biotin-binding sites, BBS) to a biotinylated cofactor **biot-Au 1-5** improved the catalytic activity leading to up to 12 TONs and affording the quinazolinone **3** exclusively, **Figure 2 b-c**, **SI Figure 2** and **SI Table 1**. This “protein-acceleration” phenomenon upon addition of Sav was not observed with cofactors devoid of biotin or with **Me<sub>2</sub>biot-Au 2** which bears a dimethylated biotin anchor and thus a markedly decreased affinity towards streptavidin as highlighted by a HABA displacement assay, **SI Figure 3**.<sup>106</sup> Fine-tuning the reaction conditions revealed that MES buffer at pH = 5 affords the highest TONs, without significantly affecting the regioselectivity, **SI Figure 4-8**. Next, we selected **biot-Au 2** and screened it in the presence of a focused library of Sav isoforms bearing mutations at S112 and/or K121. While the TON could be improved, especially in the presence of small/hydrophobic residues at position K121, the critical **3:2** ratio, diagnostic of the gold-activation mode, remained heavily biased in favor of the 6-exo-dig product **3**, **SI Figure 9** and **SI Table 2**. The addition of various bio-additives in fiftyfold excess vs. catalyst was tolerated in most cases. Reduced glutathione and cysteine poisoned the catalytic system, fortunately only at higher concentrations (> 20x[**biot-Au 2**]). Strikingly, biotin inhibits the ArM already at low concentrations (> 4x[**biot-Au 2**]). These results highlight the promising bio-robustness of the ArM, suggesting it may be used in a cellular medium, **SI Table 3**. With directed evolution in mind, this is a highly desirable feature as it allows screening cell-free extracts (cfe), without the need to purify the streptavidin mutants.<sup>107,108</sup>

Inspection of the > 30 X-ray structures of ArMs based on the biotin-streptavidin technology reveal a tendency for biotinylated metal cofactors to be poorly localized within the biotin-binding vestibule.<sup>94</sup> We attribute this to its shallow topology, thus allowing a biotinylated cofactor to adopt multiple poses, resulting in reduced occupancy.<sup>109</sup> Multiscale-modeling strategies on some of these systems illustrate that the pronounced flexibility of the cofactor may compromise the regiospecificity of the reaction.<sup>110</sup> With the aim of shielding the biotin-binding vestibule, consisting of two eight-stranded  $\beta$ -barrels facing each other, we surveyed the literature for naturally-occurring dimerization domains present in  $\beta$ -sheet-rich proteins. We identified a potential candidate fitting this criterion: the superoxide dismutase C (sodC) from *M. tuberculosis* (pdb: 1pzs<sup>111</sup>), which includes a ~ 30 amino acid dimerization domain. This lid forms an interface that spans across the ~ 29 Å of the two Greek Key  $\beta$ -barrel subunits of sodC. We thus set out to engineer a chimera consisting of the dimerization domain of sodC inserted in the 3-4 loop of the Sav to yield a Sav-SOD, **Figure 3 a**. To our delight, Sav-SOD

could be expressed in the soluble fraction in high yield (typically > 100 mg/L) in shake flasks using *E. coli* BL21 DE3, **SI Figure 10-11**.

To scrutinize the effect on the perturbation resulting from the addition of the sodC dimerization domain, we performed Isothermal Titration Calorimetry measurements (ITC) with biotin. Nanomolar binding affinity for biotin is retained over a wide range of temperatures (10 to 40 °C). At 25 °C, the  $K_d$  is 4.2 nM with standard binding enthalpy  $\Delta H^\circ = -20.90$  kcal/mol and binding enthalpy  $T\Delta S^\circ = -9.49$  kcal/mol. The standard free energy  $\Delta G^\circ = -11.4$  kcal/mol at 25 °C.<sup>112</sup> These parameters suggest that the biotin-binding is primarily enthalpically-driven. Comparison of the turn-on fluorescence upon incorporation of the biotinylated solvatochromic fluorescent reporter 4-*N,N*-dimethylamino-1,8-naphthalimide (**biot-4DMN**) in Sav and Sav-SOD K121A reveals a > 2.5 and 20 fold increase in fluorescence compared to the free **biot-4DMN**, accompanied by a blue shift ( $\lambda_{em} = 532$  and 526 nm vs. 556 nm). Such increase in fluorescence accompanied by an ipsochromic shift, have been attributed to increased hydrophobicity.<sup>112,113</sup> Furthermore, thermal shift assay highlights an increased thermal stability of the apo chimeric protein compared to apo Sav WT. We thus surmise that the SOD-lid stabilizes the protein and significantly contributes to provide a hydrophobic and shielded environment for organometallic catalysis.

To gain structural and mechanistic insight on the influence of the protein scaffold, we refined an integrative computational procedure that we have developed to model various ArMs, **Figure 3 b**.<sup>114</sup> We analyzed the formation of the 6-exo-dig product **3** and 5-endo-dig product **2** catalyzed by **biot-Au 2** · Sav WT, **biot-Au 2** · Sav K121A and **biot-Au 2** · Sav-SOD K121A. For this purpose, we applied the following workflow: i) DFT calculations on the “theozyme”, the core catalytic center (urea **1** coordinated to one or two biotinylated gold catalysts) for both  $\pi$ - and dual  $\sigma, \pi$ -activation modes. DFT calculations (B3LYP-D3 functional) were performed using continuum water solvent conditions.<sup>115,116</sup> ii) With no X-ray structure of the Sav-SOD available, structural modelling (with Modeller<sup>117</sup>) was carried out on this system followed by classical Molecular Dynamics (MD) simulations (AMBER Force field<sup>118</sup>) up to convergence. Then, after inclusion of **biot-Au 2** into the protein vestibule by protein-ligand docking, MD on the three Sav scaffolds **biot-Au 2** · Sav-WT, **biot-Au 2** · Sav K121A and **biot-Au 2** · Sav-SOD K121A were performed to determine the conformational space available for substrate binding. iii) Incorporation of the transition state structures for the 6-exo-dig and 5-endo-dig pathways in water (see i)) by protein-ligand docking approaches (using GaudiMM<sup>119</sup> and Gold5.8.1<sup>120</sup>) into the most representative structures of the MD simulations for the three Sav scaffolds (we term these “pseudo-transition states”), and iv) further refinement by MD of the best results obtained for systems with reasonable predicted affinity (in iii)). The final simulations were analyzed

focusing on: a) the complementarity of transition state structures for the 6-exo-dig and 5-endo-dig within the Sav vestibule, and b) the number of gold cofactors **biot-Au 2** involved (i.e. one or two). The influence of the host protein on the transition state structures helped identify amino acid residues to randomize during directed evolution.

The DFT calculations revealed that the competition between  $\pi$ - and dual  $\sigma,\pi$ -activation modes also operates in water. The difference between the Gibbs energy barriers for both pathways is about 2 kcal mol<sup>-1</sup> (19.5 vs. 21.5 kcal mol<sup>-1</sup> for 6-exo-dig and 5-endo-dig mechanisms, respectively), suggesting that subtle changes in the first or second coordination sphere of the metal may significantly affect the ratio between both products. Calculations of the barriers in solvents of different dielectric constant suggest that the regioselectivity is not significantly affected by the polarity of the medium. We surmised that a shift in regioselectivity may be promoted by the protein environment. DFT calculations carried out on small models were used to evaluate the impact on the ground- and transition states structures of the gold complexes both in bulk water and in the confined, hydrophobic environment provided by the biotin-binding vestibule. Scrutiny of the active site led us to hypothesize that, following  $\pi$ -coordination, the alkyne's C-H may be deprotonated by close-lying amino acids or a water molecule to afford a di-aurated  $\sigma,\pi$ -acetylide species: (Au-C $\sigma$  = 2.01 Å) and (Au-C $\pi$  = 2.28, 2.33 Å) and a Au—Au distance ~3 Å.

Having identified transition state structures in water for the isolated cofactor (in the absence of the protein scaffold), three different pseudo-transition states embedded in the protein were evaluated whereby **1TS-1Au** and **2TS-2Au**—and **1TS-2Au**. The transition state **1TS-1Au** corresponds to the  $\pi$ -activated TS which occupies half of the biotin-binding vestibule, with a second, unligated **biot-Au 2** occupying the neighboring biotin binding site. The transition state **2TS-2Au** is similar to **1TS-1Au**, but includes two gold complexes, each activating an alkyne via  $\pi$ -coordination. Finally, the transition state **1TS-2Au2** contains two gold complexes interacting with a single alkyne substrate via  $\sigma,\pi$ -coordination, **Figure 4 a**.

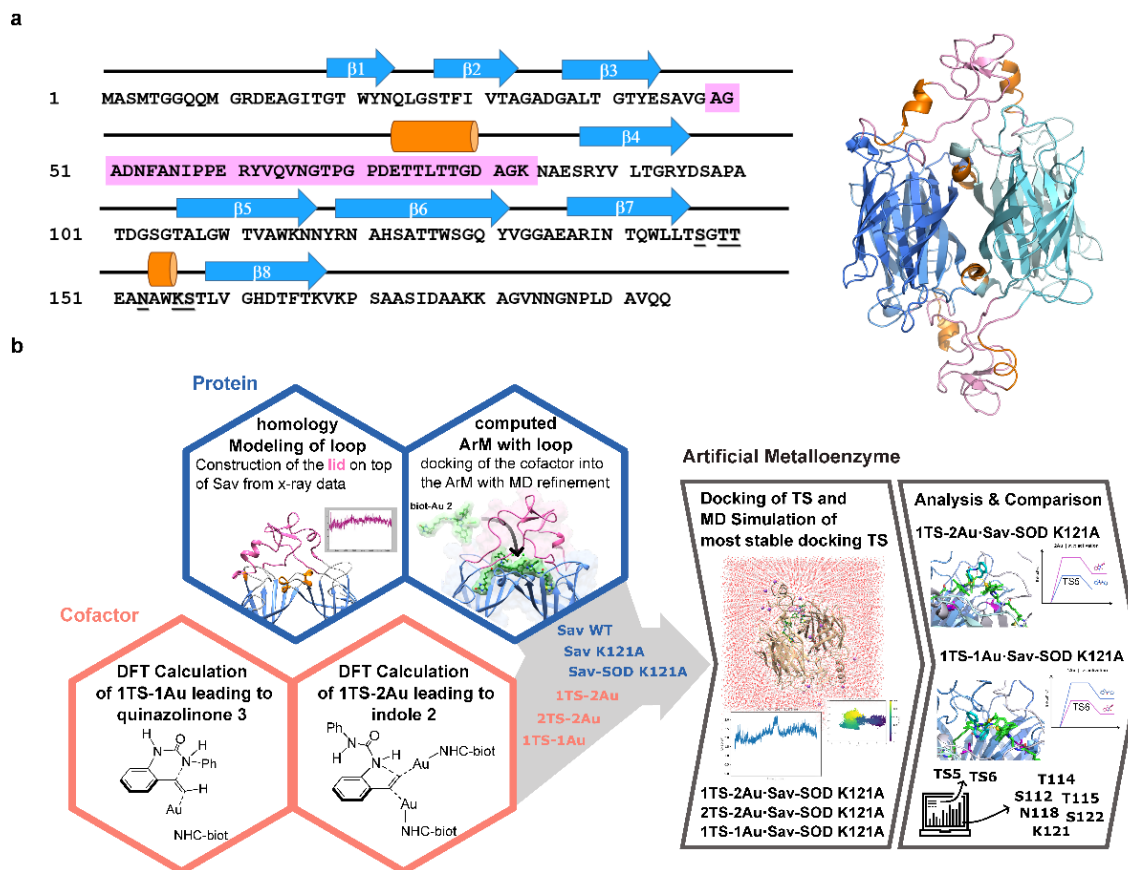


**Figure 3 Design and structural characterization of the chimeric ArM:** **a** Protein topology diagram of the sequence of one Sav-SOD monomer (left) and the computed structure of chimeric Sav-SOD resulting from a 200 ns MD simulation (right); the SOD insert is highlighted in pink; residues subjected to saturation mutagenesis are underlined; blue arrows and orange cylinders represent  $\beta$ -sheets and  $\alpha$ -helices respectively. **b** Workflow for the computational design and optimization of transition states in chimeric streptavidin. Identification of most promising amino acid residues to subject to mutagenesis. Modified and reprinted with permission from Springer Nature.<sup>73</sup>

Molecular modeling of **biot-Au 2** · Sav WT provides the best fit for the pseudo-transition state **1TS-1Au** when inserted into the catalytic vestibule of Sa. Worse complementarities were computed for **2TS-2Au** and severe clashes with the amino acids on position 121 were predicted for **1TS-2Au**. All these pseudo-transition state structures are rather solvent-exposed, with minimal impact of the second coordination sphere, resulting in similar energy barriers and similar predicted regioselectivity compared to the free cofactor. Both the free cofactor and **biot-Au 2** · Sav WT are thus predicted to favor  $\pi$ -activation to afford quinazolinone **3**. Gratifyingly, *in vitro* experiments support the model, revealing that **biot-Au 2** · Sav WT affords exclusively quinazolinone **3**, **Figure 2 c**.

In the case of **biot-Au 2** · Sav K121A, similar or worse fitting scores compared to Sav WT are computed for all pseudo-transition states, except for **1TS-2Au**. In fact, the score associated per cofactor reveals that the binding affinity of **1TS-2Au** is close to the value obtained for **1TS-1Au** (that corresponds to a single transition state geometry with no geometric constraint from

the adjacent Sav monomer), SI Table 6. These results suggest that a single-point mutation K121A improves the docking score of **1TS-2Au** compared to **1TS-1Au**. This reflects a modest shift in favor of  $\sigma,\pi$ -alkyne coordination which should allow for the formation of the anti-Markovnikov product indole **2**. These findings are supported by experiments: the regioselectivity (**3:2**) varies from 100:0 (for **biot-Au 2** · Sav WT) to 83:17 for **biot-Au 2** · Sav K121A, **Figure 2 c** and **Table 1**.

X-ray quality crystals of **biot-Au 2** · Sav-SOD (including various point mutants) were obtained through co-crystallization. Although a resolution down to 1.8 Å was achieved, the SOD-lid could not be fully resolved due to its high flexibility, PDB 7ALX. We thus set out to model the structure of **biot-Au 2** · Sav-SOD K121A, starting with homology modeling, followed by a long classical MD (200 ns), **Figure 4 b**.<sup>121</sup> The resulting models are stable with the SOD-lid presenting the highest degree of flexibility (RMSF 2.63). Next, we docked **biot-Au 2** into the system. Good complementarities were obtained by collective motion of the entire SOD-lid. This hydrophobic lid contributes to shield both cofactors from the solvent. A second MD (300 ns) placed both **biot-Au 2** cofactors sufficiently close to synergistically engage in  $\sigma,\pi$ -activation of a terminal alkyne. To our delight, **biot-Au 2** · Sav-SOD K121A indeed displayed the highest 5-endo-dig regioselectivity (i.e. 62:38 for **3:2**) and TONs of up to 40, **Figure 2 c** and **Table 1**. We thus selected **biot-Au 2** · Sav-SOD K121A for directed evolution.

Docking of the three pseudo-transition state models into Sav-SOD K121A reveal that the best complementarity is obtained for **1TS-1Au** and **1TS-2Au** (especially for TS5), **Figure 4 c-d**. Scoring values for **2TS-2Au** were extremely low as there is limited space for such a large pseudo-transition state in the Sav-SOD's vestibule. This also suggests that the possibility of another substrate approaching **1TS-2Au** to form **2TS-2Au** is unlikely in chimeric Sav-SOD. Depending on the transition state, the substrate(s) occupies different positions within the active site, **Figure 4 c vs d**.

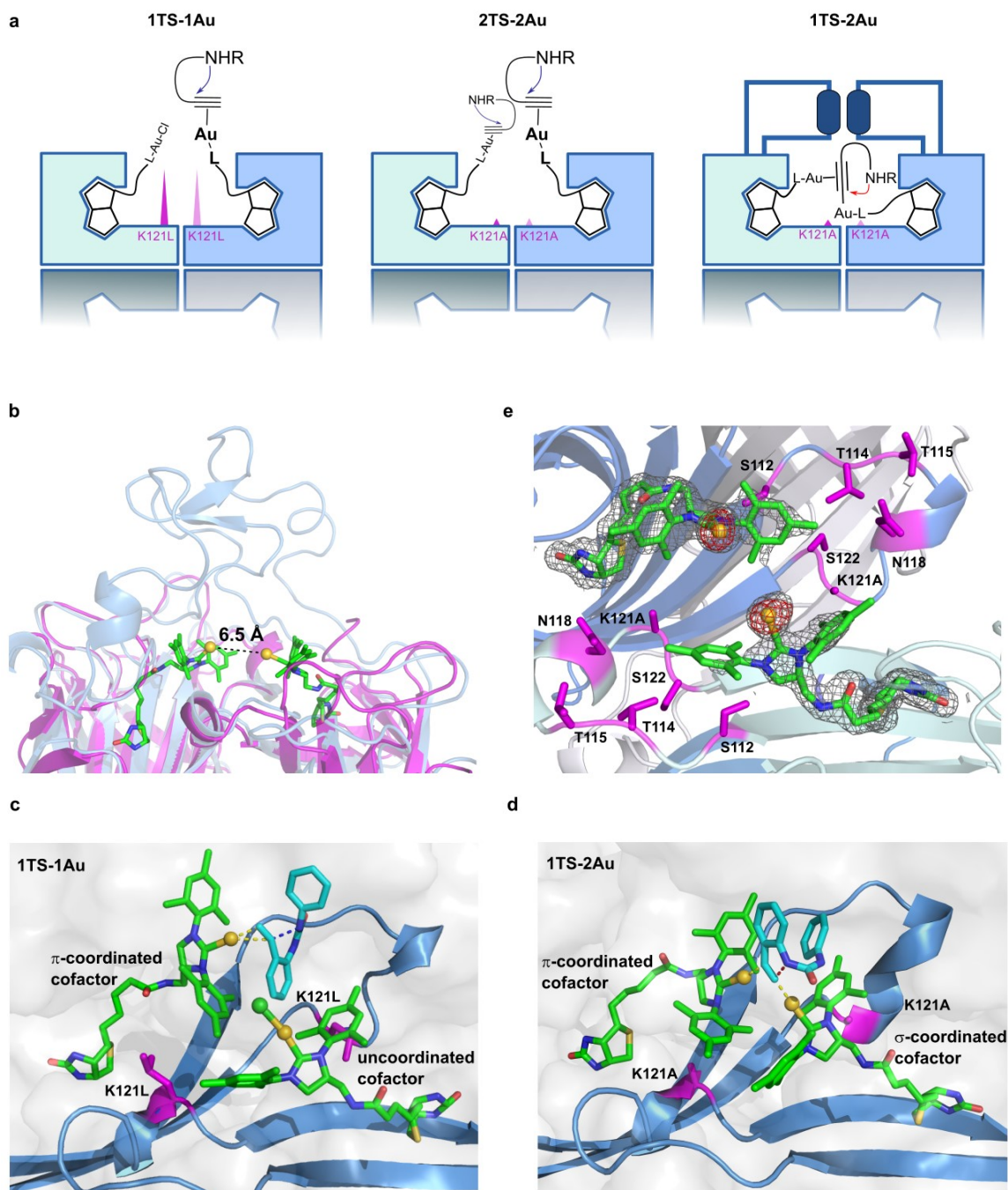


**Figure 4 Analysis of the transition state structure and close-lying amino acid residues in chimeric Sav:** **a** Schematic representation of postulated gold-catalyzed hydroamination reaction mechanisms within the biotin-binding vestibule. **b** X-ray crystal structure of **biot-Au 2** · Sav-SOD K121A (magenta) overlaid with the MD model (blue). **c,d** Computed transition state for the **biot-Au 2**-catalyzed 6-exo-dig (**1TS-1Au**) and for the 5-endo-dig cyclization (**1TS-2Au**) docked within Sav-SOD K121A. **e** Close-up view of the X-ray structure of **biot-Au 2** · Sav-SOD K121A. Anomalous electron density (displayed as red mesh at  $5\sigma$ ) assigned to Au and modeled with a 50% occupancy; no electron density for Cl was detected. Electron density map ( $2F_o - F_c$ ) for the **biot-Au 2** (displayed as grey mesh at  $1\sigma$ ). **biot-Au 2** (green stick), close-lying amino acid residues (magenta stick representation), Au as golden sphere, Cl as green sphere and the protein as cartoon representation. Reprinted with permission from Springer Nature.<sup>73</sup>

The most notable difference is a 180-degree rotation of the substrate between **1TS-1Au** (6-exo-dig) compared to **1TS-2Au** (5-endo-dig). Further residue- contribution analysis of **1TS-**



**2Au** and **1TS-1Au** (to afford 5-endo-dig and 6-exo-dig products respectively) in the active ArM were performed. Calculations were carried out using Cytoscape<sup>122</sup> as implemented in UCSF Chimera<sup>123</sup> (for a qualitative analysis of main interactions along the MDs) followed by MMGBSA (to extract indicative energetic values). Direct interactions of gold with close-lying amino acids are very weak (e.g. purely VdW contacts). Both pseudo-transition state structures reveal common interactions between the coordinated substrate **1** and the residues SOD-N8, SOD-I9, SOD-A3 and Sav-N118. For **1TS-1Au**, additional contacts were identified: from Sav-S112 to S122, especially T114. This increased number of contacts is traced back to the high level of flexibility of the **1TS-1Au** versus the **1TS-2Au**. As the SOD lid is highly flexible (and disordered in the X-ray structure), we selected close-lying residues belonging to Sav rather than the SOD-lid. Accordingly, the following amino acids were selected for the directed evolution campaign: S112, T114, T115, N118, K121 and S122, **Figure 4 e**.

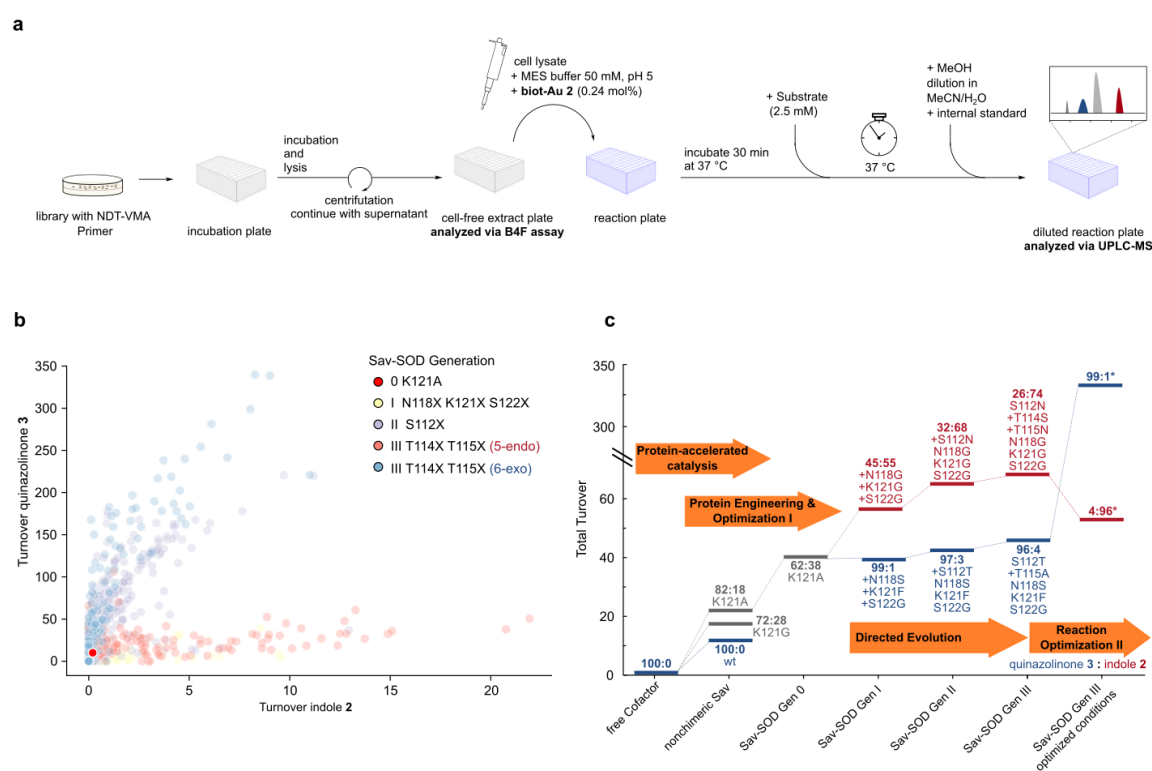


**Figure 5 Directed Evolution of an HAMase Based on Sav-SOD.** **a** Streamlined protocol for the genetic optimization of **biot-Au 2** · Sav-SOD in cfe using a 96-well plate assay. **b** Scatterplot of 2500 cfe experiments displaying the two evolutionary trajectories Sav-SOD GGG (red) and Sav-SOD SFG (blue), for amino acid positions selected for mutagenesis, see panel **c**, ultimately leading to the identification of **biot-Au 2** · Sav-SOD T-A-SFG and **biot-Au 2** · Sav-SOD N-SN-GGG. Reaction conditions for 96-well cfe screening:  $V_{\text{tot}}$  400  $\mu\text{L}$  ( $V_{\text{DMSO}}$  20  $\mu\text{L}$ ), [Sub] 2.5 mM, [Cofactor] 6.25  $\mu\text{M}$ , MES-buffer:lysis-buffer (1:1), pH ~5.5, sealed at 37 °C for 4 days. **c** Evolution trajectory of HAMase using purified Sav isoforms of the evolution of **biot-Au 2** · Sav-SOD. Reaction conditions for catalysis with purified protein samples:  $V_{\text{tot}}$  200  $\mu\text{L}$  ( $V_{\text{DMSO}}$  15  $\mu\text{L}$ ), [Sub] 5 mM, [Cofactor] 50  $\mu\text{M}$ , [Sav] 100  $\mu\text{M}$ , [MES-buffer] 50 mM, pH 5, 37 °C for 24 h except optimized reaction conditions\* for 6-exo-dig:  $V_{\text{tot}}$  400  $\mu\text{L}$  (365  $\mu\text{L}$  of MES-buffer, 50 mM, pH 5) [Sub] 2.5 mM, [**biot-Au 2**] 2.5  $\mu\text{M}$ , [Sav] 5  $\mu\text{M}$ , 39 °C for 72 h and for 5-endo-dig:  $V_{\text{tot}}$  100  $\mu\text{L}$  ( $V_{\text{MES}}$  45  $\mu\text{L}$ ), [Sub] 15 mM, [Diamide] 15 mM, [**biot-Au 2**] 100  $\mu\text{M}$ , [Sav] 200  $\mu\text{M}$ , 37 °C for 72 h. Reprinted with permission from Springer Nature.<sup>73</sup>



Having engineered an evolvable hydrophobic environment lining the biotin-binding vestibule and identified promising residues, we set out to optimize the HAMase by directed evolution. Building on the computational insight, we selected **biot-Au 2** · Sav-SOD K121A as starting scaffold for the iterative saturation mutagenesis. The free cofactor **biot-Au 2** did not display significant HAMase activity in the absence of Sav, either using MES buffer or cfe, **Table 1** and **SI Table 4**. We hypothesize that as **biot-Au 2** is insoluble in the aqueous cfe, the gold is shielded from poisoning by the cellular debris (in particular soluble thiols). Upon compartmentalization within Sav, a soluble and active ArM results, whereby the protein (partially) shields the cofactor from these detrimental metabolites, thus restoring catalytic activity, as previously observed in related studies.<sup>93,124</sup> We were delighted to observe HAMase activity upon addition of **biot-Au 2** to *E. coli* cfe (BL21 DE3) containing Sav and Sav-SOD, **SI Table 4** and **SI Figure 10**. This strategy allows bypassing the laborious protein purification step and complements our previous high-throughput screening platforms based on periplasmic and surface-display.<sup>10,31,32,125–127</sup>

**Table 1** Selected Results of evolved ArMs using purified HAMases<sup>a</sup>. Best hits for either regioisomer are highlighted in bold<sup>b,c</sup> and were tested on preparative scale<sup>d,e</sup>.

Entry	Sav-Mutants	Total TON <sup>a</sup>	Selectivity ( <b>3:2</b> )
1	no streptavidin	0.3 ± 0.1	100:0
2	Sav K121A	21.2 ± 0.9	82:18
3	Sav-SOD K121A	39.3 ± 1.9	62:38
4	Sav-SOD N118G K121G S122G	57.5 ± 4.7	45:55
5	Sav-SOD S112N N118G K121G S122G	64.6 ± 2.1	32:68
<b>6</b>	<b>Sav-SOD S112N T114S T115N N118G K121G S122G</b>	<b>51.2 ± 3.5<sup>b</sup></b> <b>39<sup>d</sup></b>	<b>4:96<sup>b</sup></b> <b>8:92<sup>d</sup></b>
7	Sav-SOD N118S K121F S122G	38.6 ± 1.0	99:1
8	Sav-SOD S112T N118S K121F S122G	42.0 ± 1.1	97:3
<b>9</b>	<b>Sav-SOD S112T T115A N118S K121F S122G</b>	<b>333 ± 57<sup>c</sup></b> <b>94<sup>e</sup></b>	<b>99:1<sup>c</sup></b> <b>&gt;99:1<sup>e</sup></b>

<sup>a</sup>The analytical experiments were carried out in quadruplicates. The combined turnover for both products in relation to **[biot-Au 2]** is displayed as well as the quinazolinone:indole ratio (**3:2**) with standard reaction conditions: V<sub>tot</sub> 200 μL (V<sub>DMSO</sub> 15 μL), [Sub] 5 mM, **[biot-Au 2]** 50 μM, [Sav] 100 μM, [MES-buffer] 50 mM, pH 5, 37 °C for 24 h.; <sup>b</sup>Optimized reaction conditions 5-endo-dig with the following changes: V<sub>tot</sub> 100 μL (V<sub>MES</sub> 45 μL, V<sub>DMSO</sub> 20 μL), [Sub] 15 mM, [Diamide] 15 mM, **[biot-Au 2]** 100 μM, [Sav] 200 μM, 37 °C for 72 h; <sup>c</sup>Optimized reaction conditions 6-exo-dig with the following changes: V<sub>tot</sub> 400 μL (365 μL of MES-buffer 50 mM, pH 5) [Sub] 2.5 mM, **[biot-Au 2]** 2.5 μM, [Sav] 5 μM, 39 °C for 72 h; <sup>d</sup>Preparative reaction (0.2 mmol): 72% yield of indole **2** and 6% yield of quinazolinone **3**; <sup>e</sup>Preparative reaction (0.1 mmol): 47% yield of quinazolinone **3** and no isolable trace of indole **2**.

First, positions N118, K121 and S122 were mutated simultaneously using a library consisting of NDT codons at these three positions, **Figure 5 a**, **SI Table 5** and **SI Figure 11**.<sup>128,129</sup> For this purpose, thirteen 96-well plates, representing 24% coverage, were grown. Each well was subjected to a biotin-4-fluorescein (B4F) binding assay to identify biotin-binding Sav-SOD-

mutants that were then evaluated in catalysis. Twelve hits including Sav-SOD N118G K121G S122G (GGG hereafter) and Sav-SOD N118S K121F S122G (SFG hereafter) were quantified by UPLC-MS and displayed either the highest TON or the highest regioselectivity. They were sequenced, expressed, purified by affinity chromatography and tested *in vitro*. Next, the twelve hits were subjected to another round of directed evolution targeting position S112 with 18-possible amino acid combinations using VMA and NDT codons. The best six hits were expressed, purified and evaluated. Mutants Sav-SOD S112N N118G K121G S122G (N-GGG) and Sav-SOD S112T N118S K121F S122G (T-SFG) were identified as most promising for 5-endo-dig product **2** and 6-exo-dig product **3** respectively. These two quadruple mutants were subjected to another round of mutagenesis, targeting simultaneously positions T114 and T115.

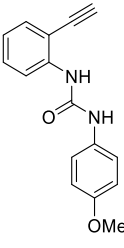
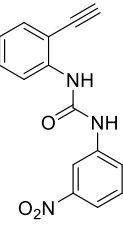
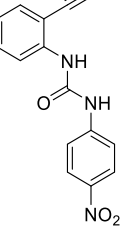
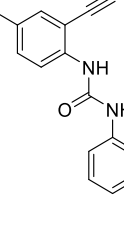
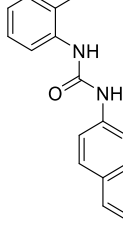
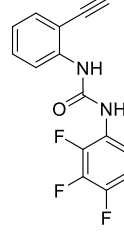
From this screening campaign, the following trends emerge: *i*) large amino acids at position K121 favor the 6-exo-dig product **3**, suggesting that the clashes observed via computational studies between K121 and the  $\sigma,\pi$ -gold intermediate are also valid for other mutants. *ii*) Reactions conditions used for cfe experiments tend to generally favor the formation of 6-exo-dig product **3**. *iii*) After two rounds of directed evolution starting from Sav-SOD K121A, clear evolutionary trajectories favoring either regioisomer emerge (scaffold GGG favors the indole **2** and SFG favors the quinazolinone **3** pathways respectively), **Figure 5 b** and **SI Figure 10**. To validate these trends, the most promising Sav chimeras were expressed in shake flasks and purified. Significant improvement of activity and selectivity over various generations were observed. Ultimately, we identified two chimeras Sav-SOD S112N T114S T115N N118G K121G S122G (N-SN-GGG) and Sav-SOD S112T T115A N118S K121F S122G (T-A-SFG) for the production of either regioisomer: **biot-Au 2** · Sav-SOD T-A-SFG and Sav-SOD N-SN-GGG afforded 333 and 51 TONs with a ratio **3:2** of 99:1 and 4:96 respectively, **Figure 5 c**, **Table 1** and **SI Table 6**. To further validate these results, the two best chimeras were scaled-up (> 500 mg) and the two HAMases were tested on preparative scale (0.1 mmol and 0.2 mmol respectively): **biot-Au 2** · Sav-SOD T-A-SFG afforded quinazolinone **3** with 47% isolated yield and no isolable amount of indole **2** (> 99:1 regioselectivity) while **biot-Au 2** · Sav-SOD N-SN-GGG afforded quinazolinone **3** and indole **2** in 6% and 72% isolated yield respectively (8:92 regioselectivity), **SI Figure 12-15**.

To confirm that the 5-endo-dig product **2** isolated using the evolved HAMase Sav-SOD N-SN-GGG and Sav-SOD T-A-SFG indeed results from a dual-gold mechanism –rather than a single-gold mechanism– we carried out preparative-scale reactions in D<sub>2</sub>O. The dual activation mechanism proceeds via a di-aurated intermediate, which then undergoes deutero-deauration to regenerate the catalyst and release the (di-deuterated) product **2-d<sub>2</sub>**, **SI Figure 16**. Gratifyingly, both <sup>1</sup>H-NMR and HR-MS studies confirm that the isolated indole **2-d<sub>2</sub>**, is indeed equally di-deuterated at its C2

and C3 position (> 98% by <sup>1</sup>H-NMR), **SI Figure 16-17**. We thus conclude that the formation of the indole **2** through either evolved HAMase indeed proceeds via a dual-gold mechanism.

Finally, six structurally-related ethynylureas **1a-1f** were tested for their regioselective cyclization in the presence of the two evolved chimeric HAMases, **Table 2** and **SI Table 7**. In some cases, the limited solubility and water-stability of these aromatic ureas proved challenging. Nevertheless, both chimeras afforded preferentially either the quinazolinone- (Sav-SOD T-A-SFG) or the indole products (Sav-SOD N-SN-GGG).

**Table 2** Substrate scope using the fourth generation of **biot-Au 2** · Sav-SOD mutants obtained with the optimized reaction conditions for either 5-endo-dig<sup>a</sup> or 6-exo-dig<sup>b</sup> products.

Substrate						
Mutant	<b>1a</b>	<b>1b</b>	<b>1c</b>	<b>1d</b>	<b>1e</b>	<b>1f</b>
Sav-SOD S112N T114S T115N N118G K121G S122G <sup>a</sup>	45.9±1.6 (7:93)	35.9±0.1 (19:81)	22.0±1.0 (15:85)	15.3±0.3 (1:99)	5.2±0.1 (4:96)	6.9±0.3 (50:50)
Sav-SOD S112T T115A N118S K121F S122G <sup>b</sup>	104.7±5.9 (96:4)	35.3±3.4 (97:3)	41.7±2.5 (97:3)	26.0±3.5 (97:3)	16.7±1.1 (85:15) <sup>c</sup>	6.0±0.9 (96:4) <sup>c</sup>

The experiments were carried out in duplicate. The combined turnover for both products is displayed in relation to [**biot-Au 2**] as well as the quinazolinone:indole ratio (**3:2**). <sup>a</sup>Optimized reaction conditions 5-endo-dig: V<sub>tot</sub> 100 μL (V<sub>MES</sub> 45 μL, V<sub>DMSO</sub> 20 μL), [Sub] 15 mM, [Diamide] 15 mM, [**biot-Au 2**] 100 μM, [Sav] 200 μM, [MES-buffer] 50 mM, pH 5, 37 °C for 24 h; <sup>b</sup>Optimized reaction conditions 6-exo-dig: V<sub>tot</sub> 400 μL (V<sub>MES</sub> 365 μL, V<sub>DMSO</sub> 12 μL) [Sub] 2.5 mM, [**biot-Au 2**] 6.25 μM, [Sav] 12.5 μM, [MES-buffer] 50 mM, pH 5, 39 °C for 48 h; <sup>c</sup> with following changes: [**biot-Au 2**] 2.5 μM, [Sav] 5 μM, for 24 h. For a summary of results using the unoptimized reaction conditions used in Table 1, see **SI Table 7**.

### 3.4 Conclusion

Natural metalloenzymes often rely on dual-catalysis to functionalize challenging substrates. Capitalizing on the unique topology of the biotin-binding vestibule of streptavidin, we designed an artificial hydroaminase that proceeds via a  $\sigma,\pi$ -activation of a terminal alkyne by two biotinylated gold cofactors. To ensure the positioning of the two gold moieties, streptavidin's biotin-binding vestibule was equipped with a hydrophobic lid, borrowed from superoxide dismutase c.<sup>111</sup> *In silico* modelling of the resulting chimeric HAMase provided insight into the two mechanistic manifolds, and revealed close-lying amino-acid residues to target by directed evolution, to favor the preferential formation of the anti-Markovnikov product indole **2** over the

Markovnikov product quinazolinone **3**. These two products result from the dual-gold  $\sigma,\pi$ -activation and the single gold  $\pi$ -activation reaction manifolds respectively. Thus far, optimization of ArMs'-performance was mostly focused on optimizing enantioselectivity.<sup>77</sup> In addition to displaying remarkable levels of enantiocontrol, enzymes excel at imposing catalyst control to address regioselectivity challenges. Herein, we combined protein engineering and directed evolution to fine-tune the second coordination sphere around the abiotic cofactor to control the regioselectivity of the hydroamination reaction. Despite its pronounced thiophylicity, the biotinylated cofactor **biot-Au 2** could be used in the presence of *E. coli* cell free extracts, thus significantly simplifying the directed evolution campaign. We tentatively assign this feature to the cofactor's insolubility in the reaction medium. Upon solubilization resulting from binding to Sav, the cofactor is partially shielded from thiols thus affording biocompatible, active and selective artificial hydroaminases. Current efforts are aimed at integrating this versatile dual-activation reaction *in vivo* to complement the natural metabolism.

### 3.5 Appendix: Mechanistic Studies

Asensio and co-workers initially explored the alternative reaction pathways from the metal-catalyzed hydroamination of these aromatic ethynylureas by combining deuteration experiments and x-ray diffraction.<sup>96</sup> They were successful in preparing and crystallizing  $\sigma$ -coordinated gold-acetylide complexes from the trimethylsilane adduct in stoichiometric amounts of gold complex. In the presence of additional gold complexes, these  $\sigma$ -coordinated complexes regioselectively reacted to form aurated indoles. In contrast, the same gold complexes catalyzed the conversion of urea **1** to quinazolinone in the absence of base, while in the presence of base, indole was formed, **Figure 6**. In the 5-endo dig cyclization leading to the corresponding indole, the preformation of a  $\sigma$ -coordinated complex was determined to be a crucial factor for the regioselectivity of the reaction. The formation of this intermediate can occur either in the presence of a strong base (e.g. triethylamine) or via  $\sigma,\pi$ -coordination of two gold species.

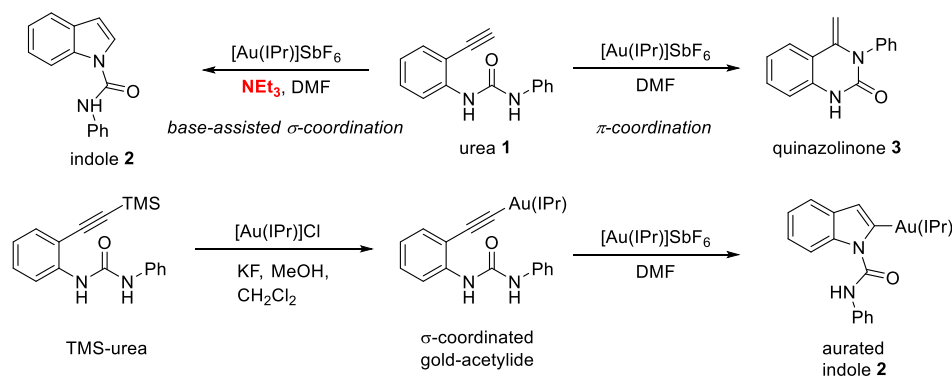


**Figure 6** Gold(I)-catalyzed hydroamination of urea **1** and its corresponding gold-acetylide performed by

Asensio and co-workers.<sup>96</sup> Reprinted with permission from Springer Nature.<sup>73</sup>

In order to provide strong evidence, that the regioselectivity was indeed predominantly directed by the coordination mode of the gold cofactors and not by basic amino acids or other reagents, we conducted a set of deuteration experiments complementary to the experiments performed by Asensio and co-workers. Instead of following the fate of a deuterated alkyne in a sealed reaction at -30 °C which is not transposable to biorthogonal chemistry, **Figure 7**, we performed the opposite: we investigated the deuterium incorporation into the corresponding products (**2** and **3**) by performing the reaction in D<sub>2</sub>O, **Figure 8**. It did not allow us to monitor the incorporation of deuterium into the quinazolinone, as these methylene protons are too acidic and reversibly exchanged in water. This phenomenon was observed by Asensio and co-workers and forced them to conduct their experiments in a dry environment at low temperatures. However, by characterizing the indole from reactions ran in D<sub>2</sub>O we can determine whether the 5-endo dig product was formed via base-assisted  $\sigma$ -coordination (which should yield mono-deuterated indole) or via  $\sigma,\pi$ -coordination of two gold centers (which, upon protodeauration, would yield di-deuterated indole **2-d<sub>2</sub>**).

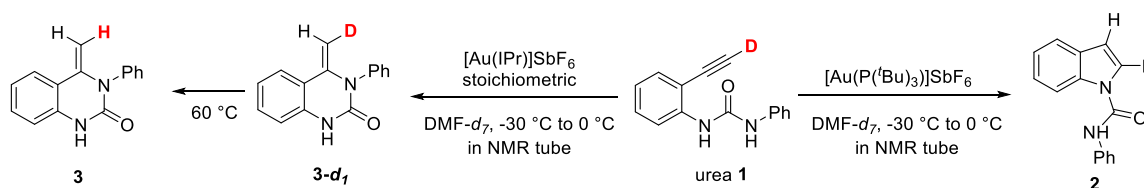


**Figure 7** Low-temperature deuteration experiments performed by Asensio and co-workers.<sup>96</sup>

Gratifyingly, we isolated di-deuterated indole **2-d<sub>2</sub>** with over 98% double-deuterium incorporation at the C1 and C2 positions. We further highlighted that no reversible proton-deuterium exchange occurs at these positions. Shaking a sample of indole **2-d<sub>2</sub>** in the presence of H<sub>2</sub>O (37 °C, 16 h) did not lead to any deuterium-hydronium-scrambling. Furthermore, shaking a sample of indole **2** in D<sub>2</sub>O did not lead to any deuterium incorporation in C1 and C2, **Figure 9**. We thus conclude, that the two deuterium detected on indole **2-d<sub>2</sub>** via <sup>1</sup>H NMR and HR-MS were a result of the dual-coordination of two gold-species in a  $\sigma,\pi$ -coordination and thus indole was produced via dual-gold coordination inside the chimeric protein.

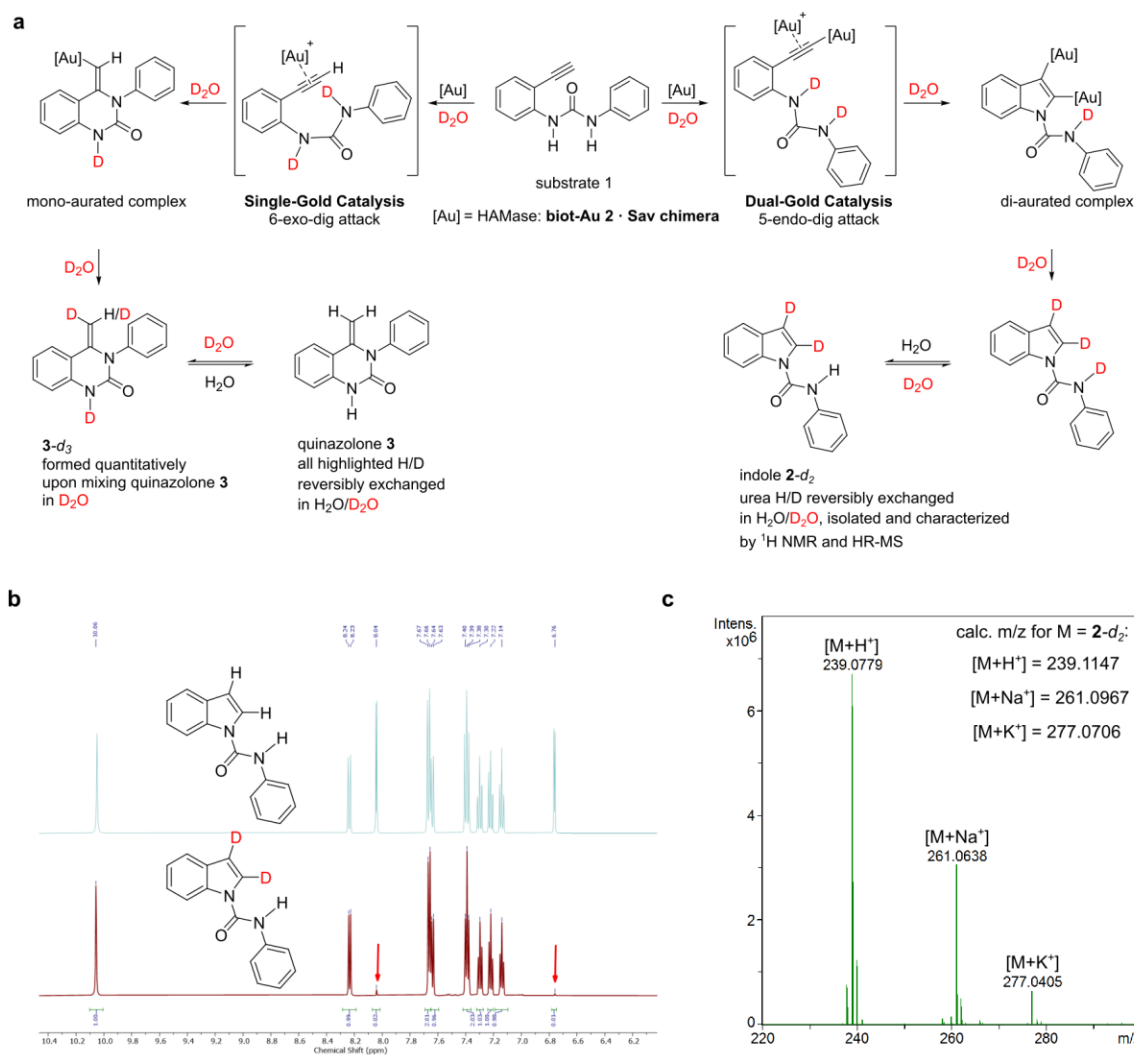


**Figure 8 Isotopic product-distribution of the HAMase biot-Au 2 · Sav-SOD N-SN-GGG carried out in  $D_2O$ .** **a** Deuteration profile of quinazolinone **3** and indole **2** resulting from the gold-catalyzed hydroamination. For the quinazolinone **3**, all highlighted protons/deuterons are readily exchanged in  $D_2O/H_2O$ ; **b**  $^1H$  NMR analysis of the indole **2-d<sub>2</sub>** isolated from preparative reactions in  $H_2O$  (top) and  $D_2O$  (bottom, the urea N–H is readily exchanged in the presence of traces of  $H_2O$ ) and **c** HR-MS analysis of **2-d<sub>2</sub>** resulting from the reaction performed in  $D_2O$ . Reprinted with permission from Springer Nature.<sup>73</sup>

We further highlighted, that spontaneous proton-deuterium exchange occurs on the methylene moiety of quinazolinone **3** through similar experiments via  $^1H$  NMR and HR-MS. In contrast to indole **2**, quinazolinone **3** revealed the incorporation of up to three deuterium in the presence of  $D_2O$  with rapid exchange of these deuteriums when put in a proton rich environment, **Figure 10-Figure 11**.

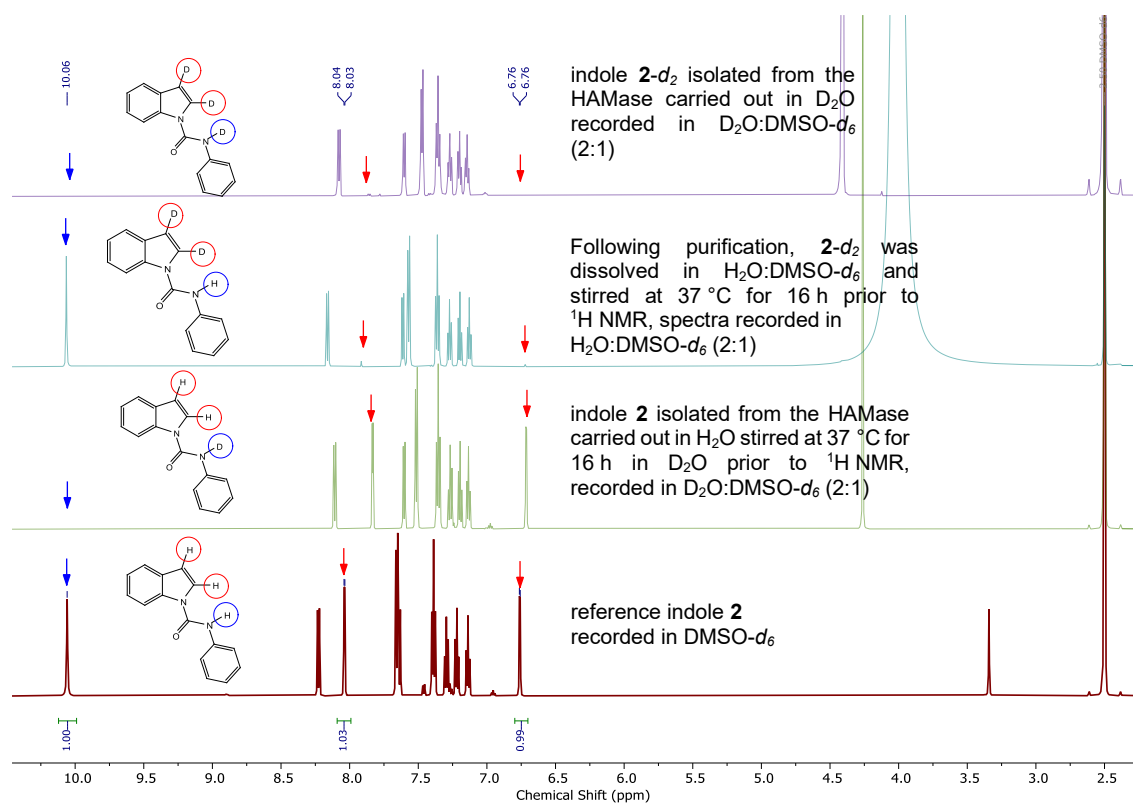


**Figure 9** Stacked <sup>1</sup>H NMR spectrum confirming the inertness of indole **2** and **2-d<sub>2</sub>** towards deuterium-proton exchange at the indole's C2 and C3 positions (highlighted in red). In contrast, the urea proton (blue) is readily exchanged. Reprinted with permission from Springer Nature.<sup>73</sup>

We further tried to crystallize the acetylide gold-complex in the protein by adding urea **1** or the corresponding N,N-dimethylated urea to crystal samples of various **biot-Au 2** Sav chimera without success. We hypothesize that by methylating the urea moiety, the substrate may still coordinate with the acetyl moiety to the gold cofactors but resist intramolecular hydroamination. Unfortunately, most crystals dissolved upon addition of substrate. The few that survived did yield an X-ray diffraction pattern, but with no electron density corresponding to any substrate derivative.

gr\_ward\_cryo+.523.1.fid  
NatRev-FC-quinnw  
\_Proton.dh DMSO /opt/nmrdata gr\_ward\_600R 8

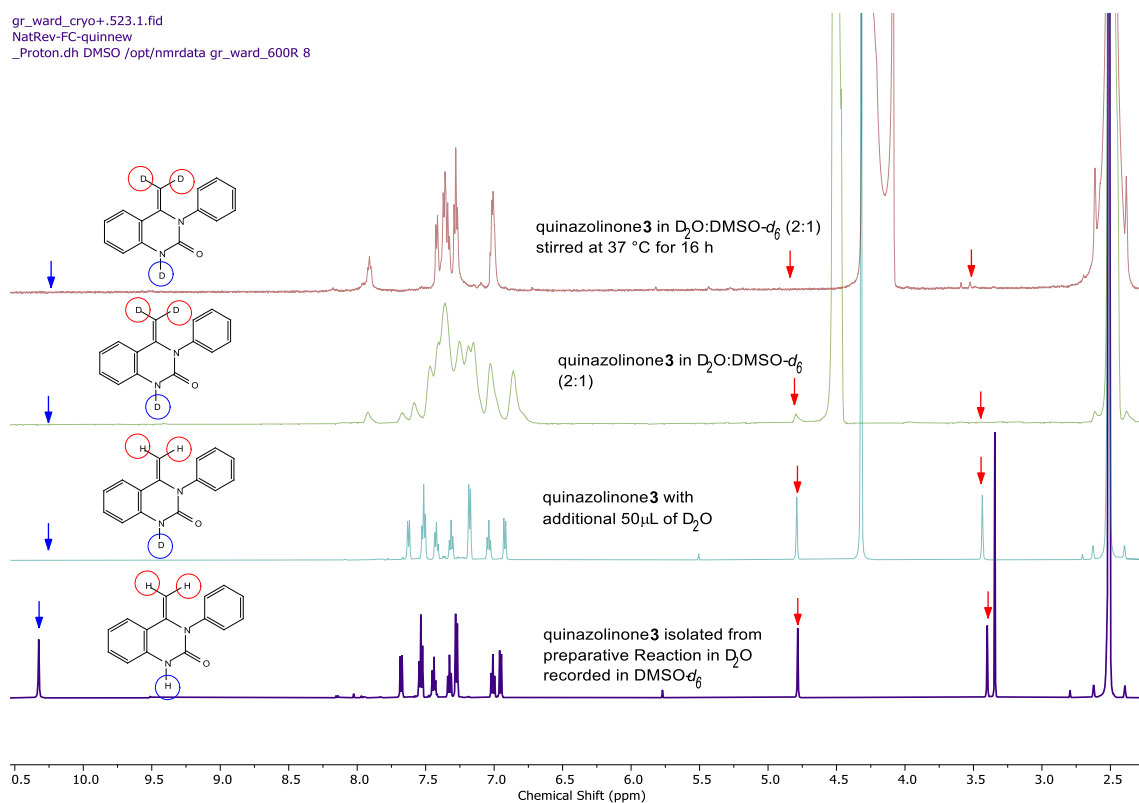


**Figure 10** Stacked <sup>1</sup>H NMR spectrum displaying the autodeuteration of quinazolinone **3** in D<sub>2</sub>O on the terminal alkene. Such a rapid H-D exchange in quinazolinone **3** was already reported by Asensio and co-workers<sup>96</sup>. Reprinted with permission from Springer Nature.<sup>73</sup>

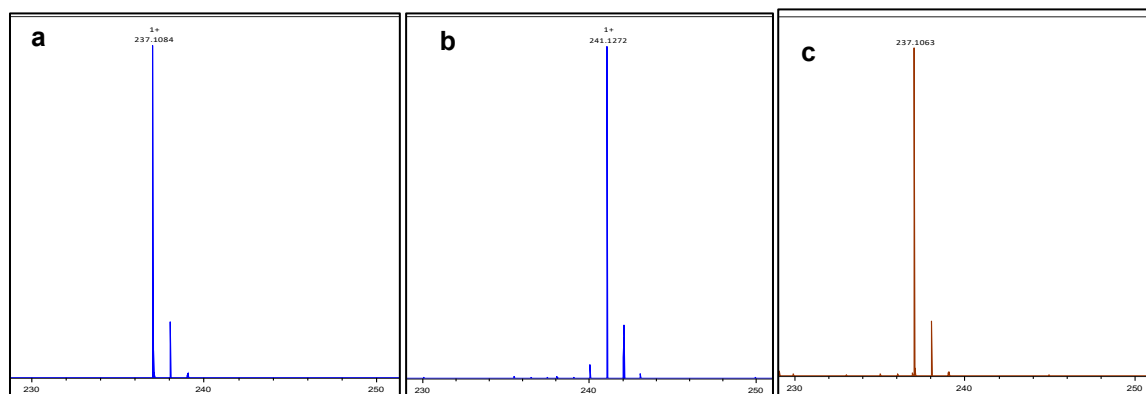


**Figure 11** HR-MS Spectrum of quinazolinone **3** injected (a) from H<sub>2</sub>O:MeCN (1:1) over direct injection (DI), (b) from D<sub>2</sub>O:MeCN (1:1) over DI and (c) from D<sub>2</sub>O:MeCN (1:1) over HPLC into HR-MS displaying the autodeuteration of quinazolinone **3** in D<sub>2</sub>O and the subsequent proton/deuterium exchange when submitted to HPLC. Reprinted with permission from Springer Nature.<sup>73</sup>



### 3.6 Appendix: Cooperativity Studies

Our best ArM **biot-Au 2** · Sav-SOD N-SN-GGG yielded 96% of 5-endo dig indole **2** as a result of optimized dual-gold catalysis. Such high 5-endo dig selectivities through the stochastic assembly of two monomeric gold species into two adjacent catalytic pockets would be improbable for a tetrameric scaffold. Under normal conditions, the side-by-side pattern occurs in three out of six (seven, if one counts the empty Sav) different assembly patterns of the ArM, **Figure 12**. This leaves three other patterns with only one bound cofactor, capable of only performing single-gold catalysis. In the best case scenario, where side-by-side incorporation always produces the 5-endo dig product at similar reaction rates, we would anticipate a maximum of 50% of dual gold catalysis leading to a maximum of 50% 5-endo dig indole **2**.

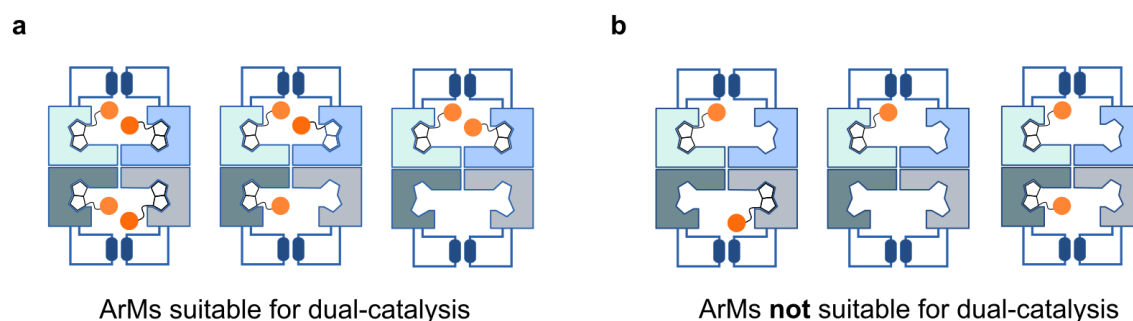


**Figure 12 Incorporation pattern for Sav-SOD-based ArMs.** **a** Incorporation pattern allowing for dual-catalysis due to the side-by-side incorporation of two cofactors. **b** Incorporation pattern with only 1 cofactor per dimeric unit only capable of single-catalysis.

We hypothesized that for our best 5-endo dig ArMs, there could be two additional factors contributing to such high regioselectivity outside of chemogenetic optimization: (i) the reaction rate of the single-gold site could be drastically reduced by selected amino acid residues, thus mono-occupied sites are “turned off” and (ii) the cofactor could be preferentially incorporated as a dimer (cooperativity) suggesting that the cofactor in solution may dimerize or agglomerate. There is some evidence for (i) and substantial evidence for (ii), it may well be a mixture of both.

When evaluating the evolutionary trajectory of our ArMs, we can observe that from Sav-SOD GGG towards N-SN-GGG an increase in regioselectivity is predominantly achieved by decreasing the amount of 6-exo dig product and not by increasing the turnover of 5-endo dig product, **Figure 5**. This may be a small hint towards (i) but further evidence would be needed to validate this hypothesis.

For our second hypothesis (ii), we gathered substantial evidence from HR-MS experiments, Diffusion Ordered Spectroscopy (DOSY) and X-ray diffraction patterns. When investigating X-ray data of the ArM, we could observe full occupation of all biotin bindings sites by at least the ligand, some gold(I) may decompose under irradiation. This, in combination with HABA

titrations highlights, that the ArM can be fully loaded with up to four cofactors. When investigating the free cofactors (**biot-Au 1-5**) in CD<sub>2</sub>Cl<sub>2</sub> and the corresponding non-biotinylated gold complex analogues via DOSY, we could observe a significantly lower diffusion constant even considering the molecular weight difference, **Figure 13, SI Table 8**. Rough estimates, derived from the diffusion coefficients, suggest a predominantly dimeric nature of **biot-Au 1-5** in CD<sub>2</sub>Cl<sub>2</sub>.

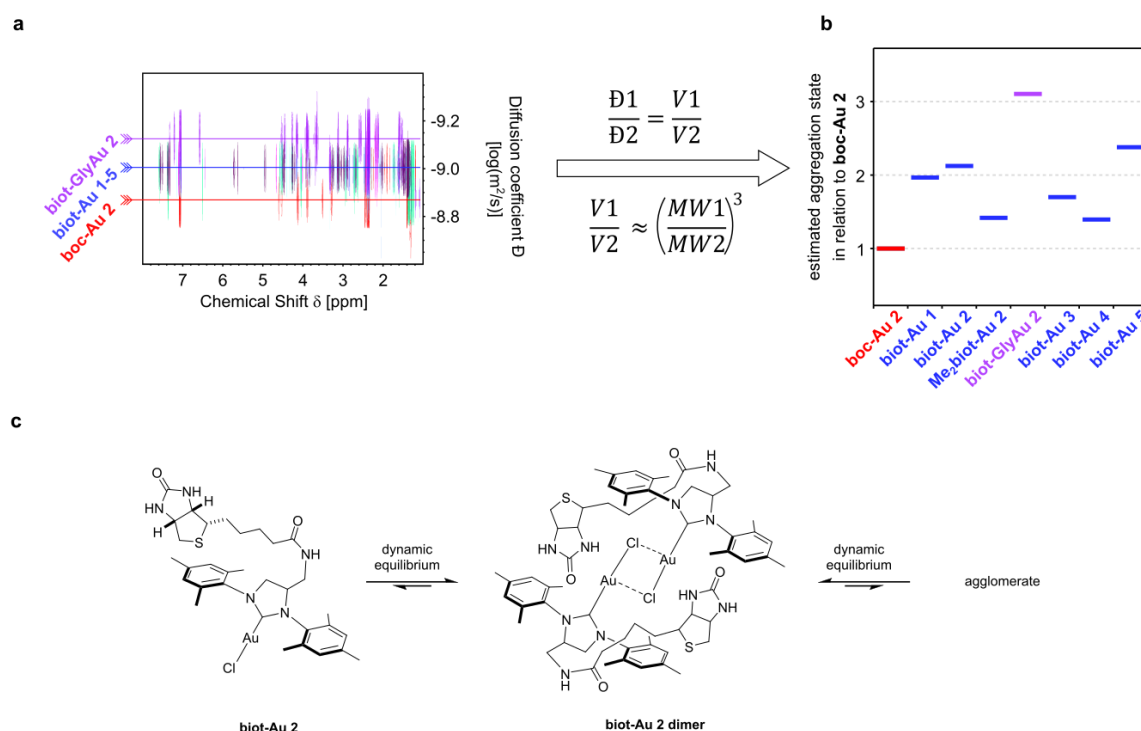


**Figure 13 Aggregation of biotinylated gold complexes.** (a) Overlay of recorded DOSY spectra for various gold complexes (b) Graphical representation of the estimated aggregation states calculated from the corresponding diffusion coefficients and adjusted to the molecular weight of the corresponding complex in relation to **boc-Au 2**. (c) Dynamic equilibrium of **biot-Au 2** in solution

HPLC into HR-MS spectra of **biot-Au 1-5** display clear patterns for dimeric aqua-complexes with the corresponding isotope patterns resulting from the same HPLC peak, **Figure 14 a-b**. While recording native MS spectra of **biot-Au 2** in different Sav at high cone voltages a large peak at  $m/z=1551$  arose which may indicate the release of dimeric **biot-Au 2** under such harsh conditions, **Figure 14 c**. This pattern is identical to dimeric isotope patterns recorded from direct injection into HR-MS, **Figure 14 d**.

Catalytic experiments were conducted where: (i) the ratio of cofactor to BBS was varied and (ii) the ArM was titrated with biotin, **Figure 15** and **Figure 16**. Interestingly, Sav-SOD N-SN-GGG displays a completely different reactivity- and selectivity pattern compared to Sav-SOD T-A-SFG: While for T-A-SFG the amount of 5-endo dig product seems to increase almost

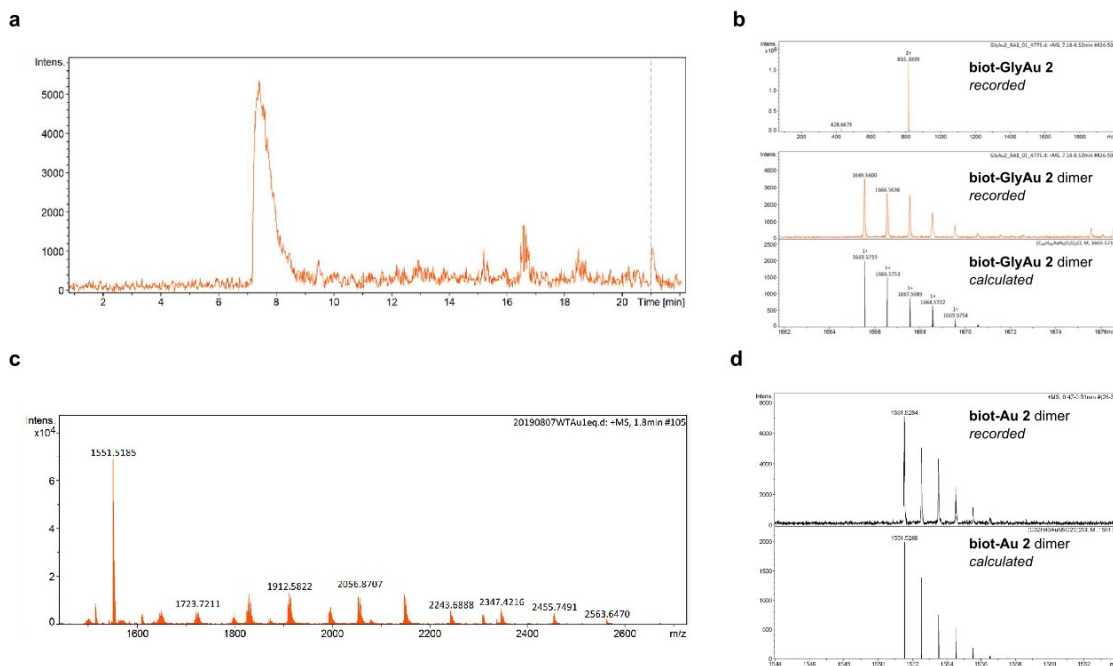


**Figure 14 HR-MS spectrum of dimeric gold complexes.** **a** HPLC chromatogram of **biot-GlyAu 2** indicating a single peak with, **b** two species recorded on the connected HR-MS: the monomer and the dimer. **c** Native-MS spectrum at maximum cone-voltage displaying the release of **biot-Au 2**-aquadimer complex in aqueous solution from streptavidin wild type soaked with the gold complex. **d** HR-MS (DI) spectrum of **biot-Au 2** with the recorded dimeric species.

linearly with higher cofactor:BBS ratio at low levels. For N-SN-GGG the ratio increases from 0.125 to 0.75 cofactor:BBS drastically and then remains constant. It must be pointed out, that even at such low cofactor:BBS ratios as 0.125, quinazolinone is still produced with >40% selectivity. This kind of behavior again hints towards the incorporation of two **biot-Au 2** simultaneously. However, we know that in the case of biotin to Sav titration, no cooperative effect occurs. Therefore, we titrated the protein with biotin before addition of the cofactor. We maintained standard reaction conditions using 0.5 eq of cofactor per BBS. As biotin is

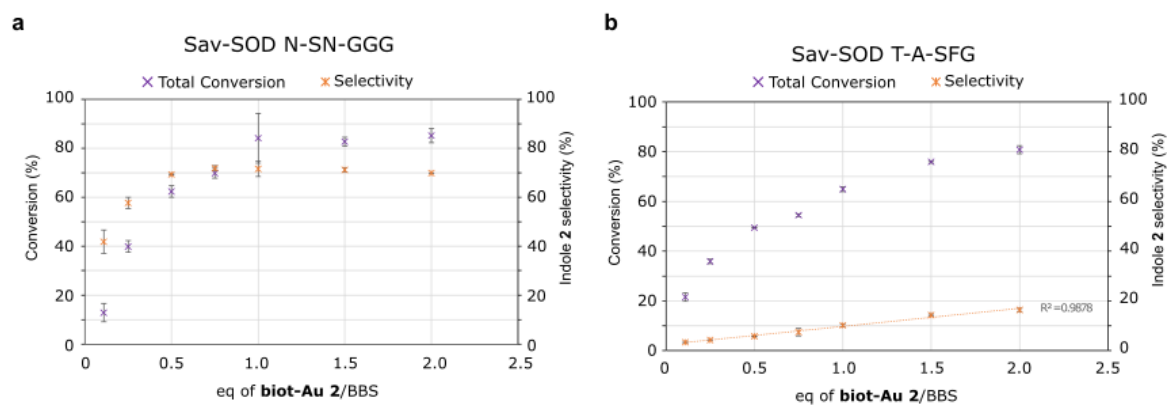


**Figure 15 The influence of different cofactor/BBS ratio on the catalytic performance of the ArM.** **a** Catalytic experiments with Sav-SOD N-SN-GGG displaying saturation in selectivity at 0.5 eq of cofactor/BBS and in reactivity at 1.0 eq of cofactor/BBS. **b** Catalytic experiments with Sav-SOD T-A-SFG displaying continues increase in reactivity and linear increase in indole **2** at low levels with increasing amounts of cofactor.

incorporated randomly, it would stochastically block BBS and drastically reduce the

incorporation of **biot-Au 2**-dimer in a side-by-side manner. The catalytic results support this hypothesis. For N-SN-GGG, the reactivity is completely shut down by adding only 0.5 eq of biotin per BBS. This means, when half the BBS are available the ArM is almost incapable of performing 5-endo dig cyclization. The ArM does not switch towards single-gold catalysis when the other binding sites are blocked by biotin. This is not true for the single gold 6-exo dig cyclization reaction: Titration T-A-SFG with biotin has almost no effect up to a ratio of 1 biotin/BBS. Afterwards the reactivity steadily decreases but is still maintained at lower levels even after addition of 4 biotin/BBS.

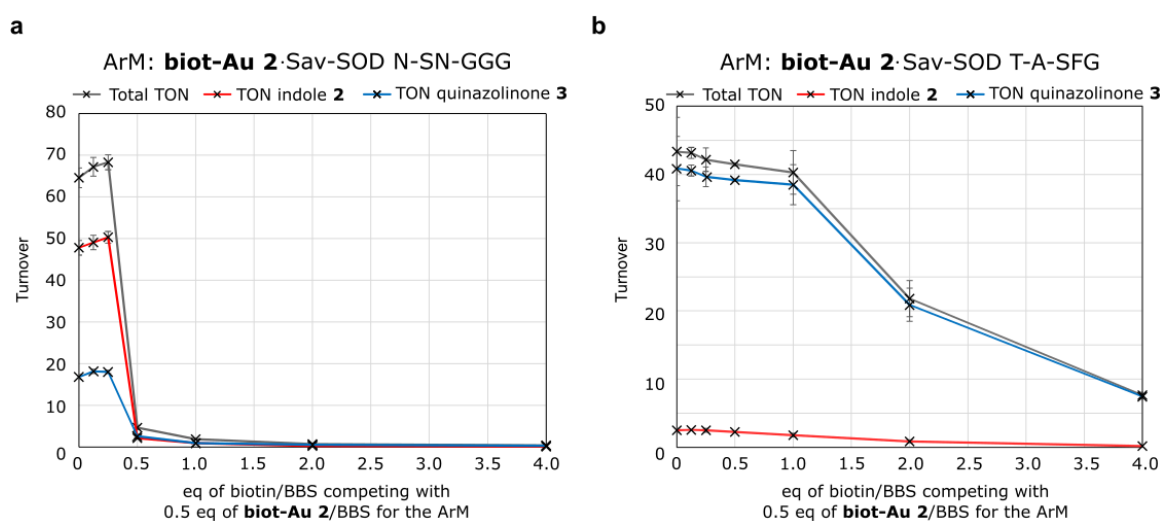


**Figure 16 Biotin titration experiment.** **a** Titrating **biot-Au 2** · Sav-SOD N-SN-GGG with biotin causing an almost complete shutdown in reactivity at 0.5 eq biotin/BBS. **b** Titrating **biot-Au 2** · Sav-SOD T-A-SFG with biotin causing slow and steady decrease in reactivity.

All these results lead us to the conclusions that the biotinylated gold complexes are likely to dimerize and/or agglomerate. This may favour the cooperative incorporation of dimers into the protein in a side-by-side manner which is crucial for dual-gold catalysis. This behavior may increase the stability of these gold complexes in aqueous media. Furthermore, optimized dual-gold ArMs may contain crucial AA that reduce the reactivity towards single-gold catalysis.

### 3.7 Appendix: Linker Studies

To improve dual-gold catalysis in the ArM, we hypothesized that a longer linker may position the gold centers in closer proximity, facilitating 5-endo dig cyclization. In a first attempt, we planned to extend biotin with an additional glycine residue, then couple it to the ligand and finally add gold, **Figure 17**. Glycine was coupled to biotin via either NHS-ester or peptide coupling to yield **biot-Gly**. A second peptide coupling allowed the addition of **biot-Gly** to the SIMes ligand in good yield (83%). Unfortunately, we were not able to introduce gold to this biotinylated ligand as the ligand decomposed and gold precipitated on the surface of the vial. Coupling **biot-Gly** to auroated SIMes **boc-Au 2** was unsuccessful and yielded a complex mixture.

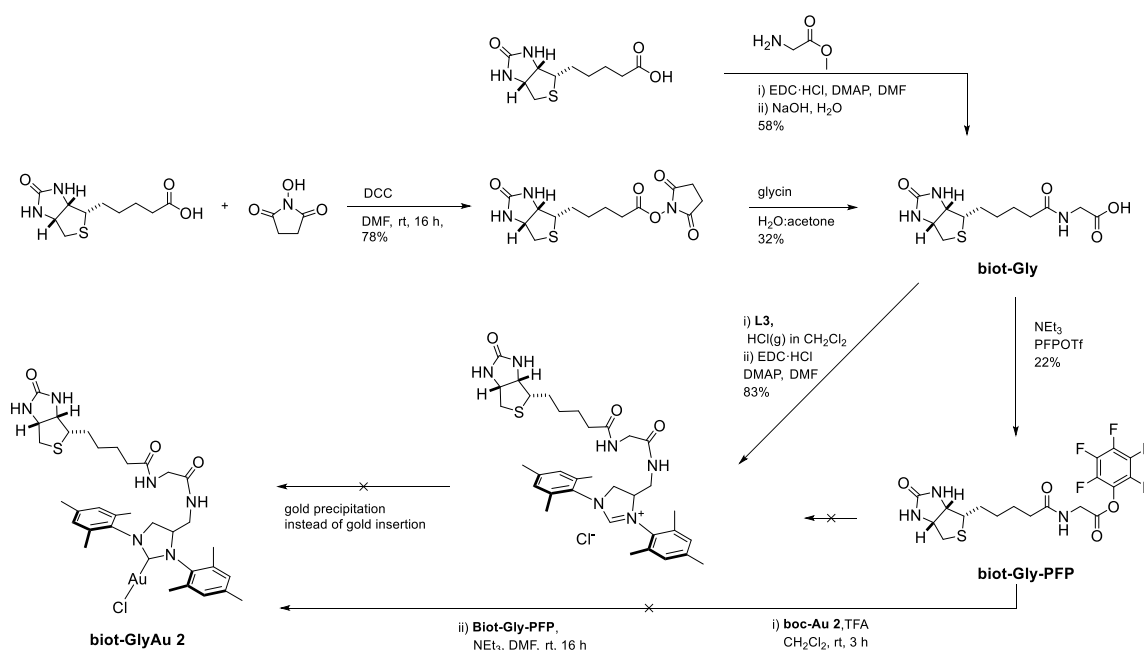


**Figure 17 Failed synthesis route of biot-GlyAu 2.** This route is based on the pre-functionalization of the NHC-ligand with extended biotin and subsequent gold insertion. However, the insertion of gold on the biotinylated ligand was unsuccessful and led to precipitation.

As a result, another strategy was pursued in which the ligand was first extended by boc-protected glycine, followed by gold insertion and subsequent biotinylation, **Figure 18**. Gratifyingly, **biot-GlyAu 2** was obtained in 24% yield over these three steps. Again, biotinylation proved challenging and drastically reduced the yield of the final product. Nonetheless, enough cofactor was obtained for characterization and a limited screening of Sav mutants.

As expected, **biot-GlyAu 2** did exceedingly well in producing the 5-endo dig indole **2**, **Figure 19a**. Over a set of 11 different Sav and Sav-SOD mutants, a rather consistent 60% to 80% of the product was indole **2**. Thus, **biot-GlyAu 2** did outperform **biot-Au 2** in terms of regioselectivity towards indole **2** for this set of mutants. However, the fact that the

regioselectivity was only moderately influenced by the Sav isoform, over a very diverse set of mutants was concerning. While for **biot-Au 2**-based ArMs, both reactivity and selectivity could be markedly varied through genetic optimization of the scaffold, this may not be the case for **biot-GlyAu 2**, **Figure 19 a-b**.

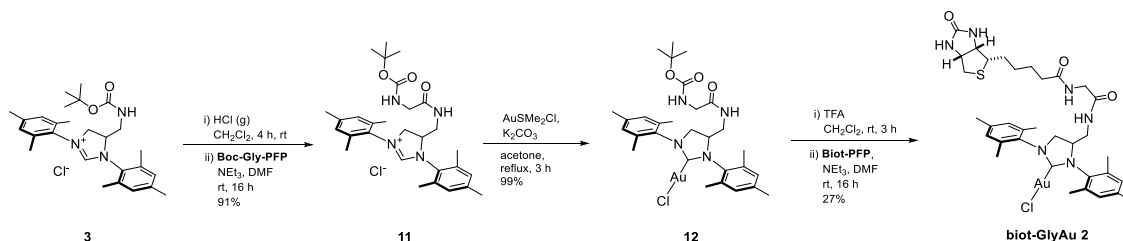


**Figure 18 Synthetic route to biot-GlyAu 2.** This route is based on the extension of the NHC-ligand with protected glycine followed by gold coordination and final biotinylation.

Computational insight of the binding of both cofactors to Sav revealed, that **biot-Au 2** is located closer to the surface of the binding vestibule due to the smaller linker length, **Figure 20 a**. When engaging in dual-gold catalysis, the transition state is again forced to be located closer to the protein surface, **Figure 20 b**. Interactions between the amino acids and the ligand as well as the substrate are frequent. In the case of **biot-GlyAu 2**, the cofactor is located further away from the protein surface, **Figure 20 c**. Extensive interactions between amino acid residues and glycine can be computed with only limited interaction of amino acids to the ligand. As a result, we concluded that although **biot-GlyAu 2** performs well in 5-endo dig cyclization, it is not suitable for ArM-design as in our experiments it displayed limited sensitivity to genetic optimization. Accordingly, directed evolution on this ArM may be challenging.

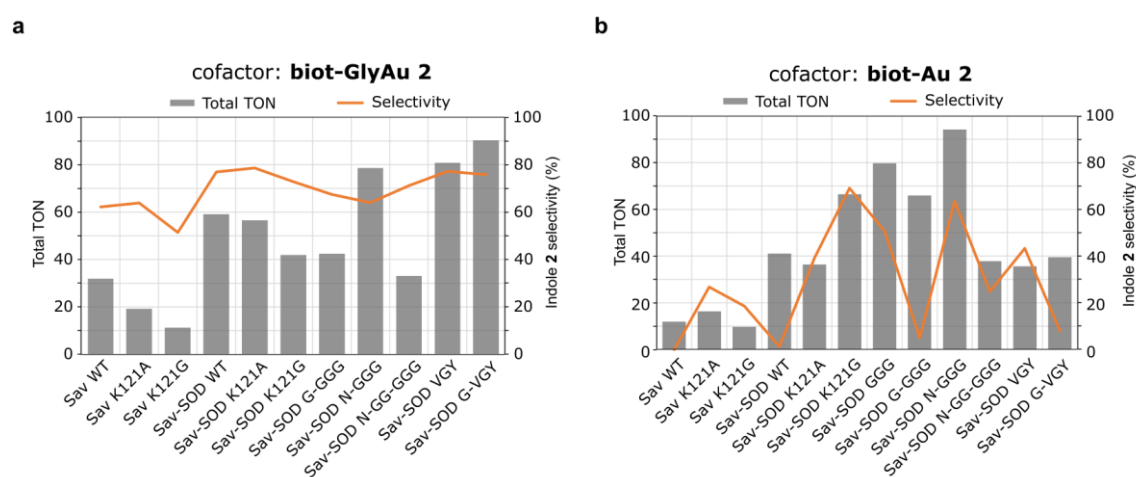


**Figure 19 Sav and Sav-SOD mutant screening with biot-Au 2 and biot-GlyAu 2.** **a** While proteinogenic variation of the Sav and Sav-SOD constructs had limited effect on the regioselectivity of **biot-GlyAu 2**-base ArMs, **b** large variations were observed for **biot-Au 2**-based ArMs.



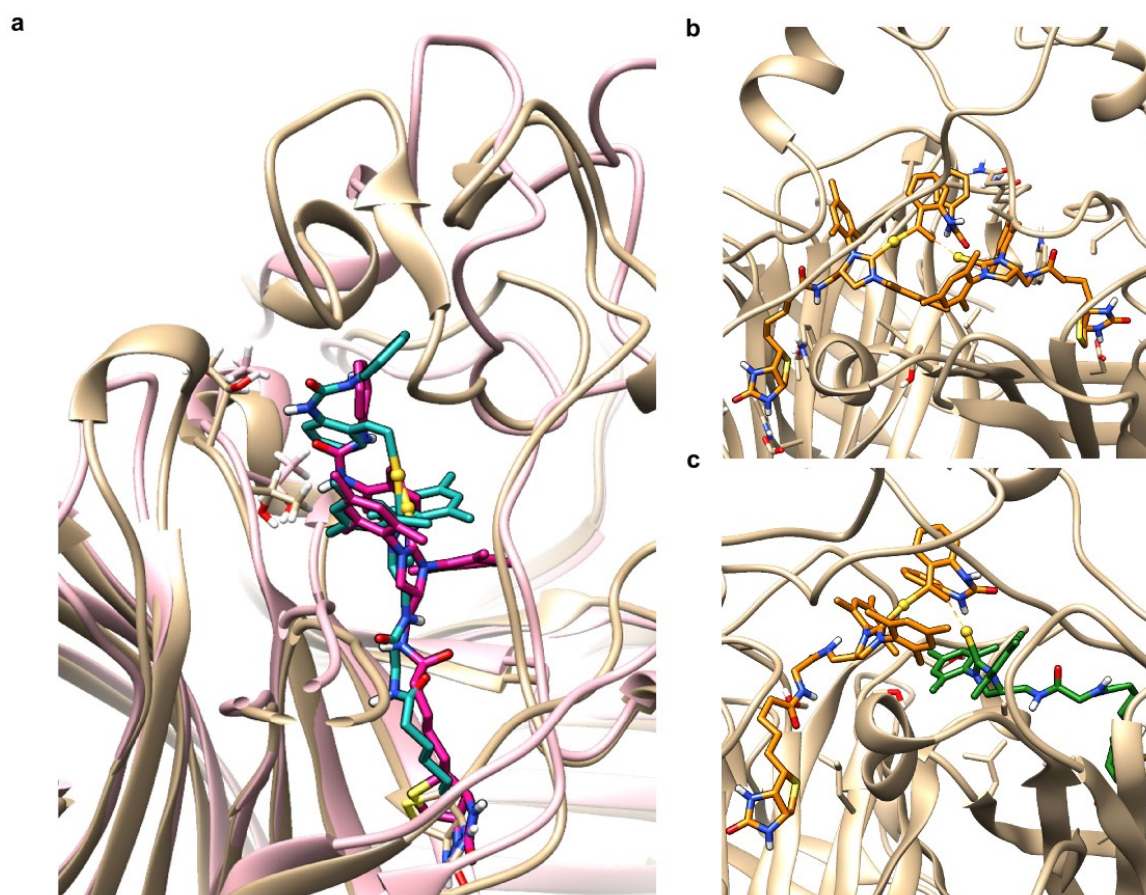


**Figure 20 Comparison of biot-Au 2- and biot-GlyAu 2-based ArMs and transition states via molecular modelling. a** Comparison of the incorporation depth of **biot-Au 2** (pink) and **biot-GlyAu 2** (cyan) into the biotin binding pocket. **b** Dual-gold transition state of two **biot-Au 2**. **c** Dual-gold transition state of two **biot-GlyAu 2**.

### 3.8 Appendix: Unreactive Substrates for Dual-Gold Catalysis

Would it be possible to translate our dual-gold catalysis system towards alkenes? The group of Hartwig has developed interesting rhodium-based catalysts capable of catalyzing the regioselective intramolecular hydroamination of vinyl arenes, however with no enantioselectivity, **Figure 21**.<sup>130,131</sup> Our plan was to utilize the regioselectivity of our dual-gold system and combine it with potential enantioselectivity directed from the protein itself to optimize the enantioselective intramolecular hydroamination of vinyl arenes **13** enantioselectively towards the desired regioisomer. We followed the synthetic procedure of Hartwig and co-workers and prepared vinyl arene **13** in four steps from phenyl butanoic acid **16**, **Figure 22**. Unfortunately, we could not detect any of the desired reaction products when screening a small set of Sav-SOD constructs with **biot-Au 2** (MES buffer pH 5, 37 °C, 24 h). For this reason, we did not further pursue this hydroamination reaction.

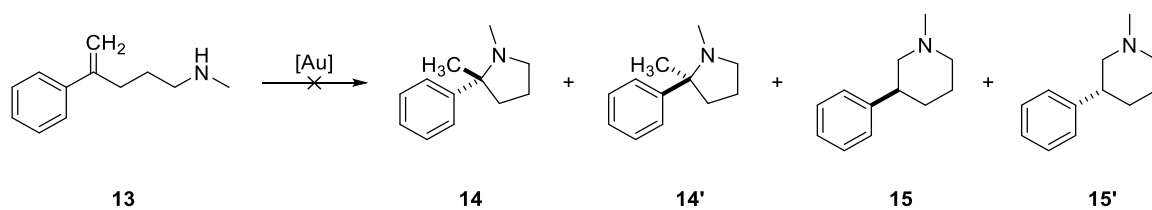


**Figure 21** The gold-catalyzed hydroamination of vinyl arene **13** may lead to various regio- and/or enantiomers.

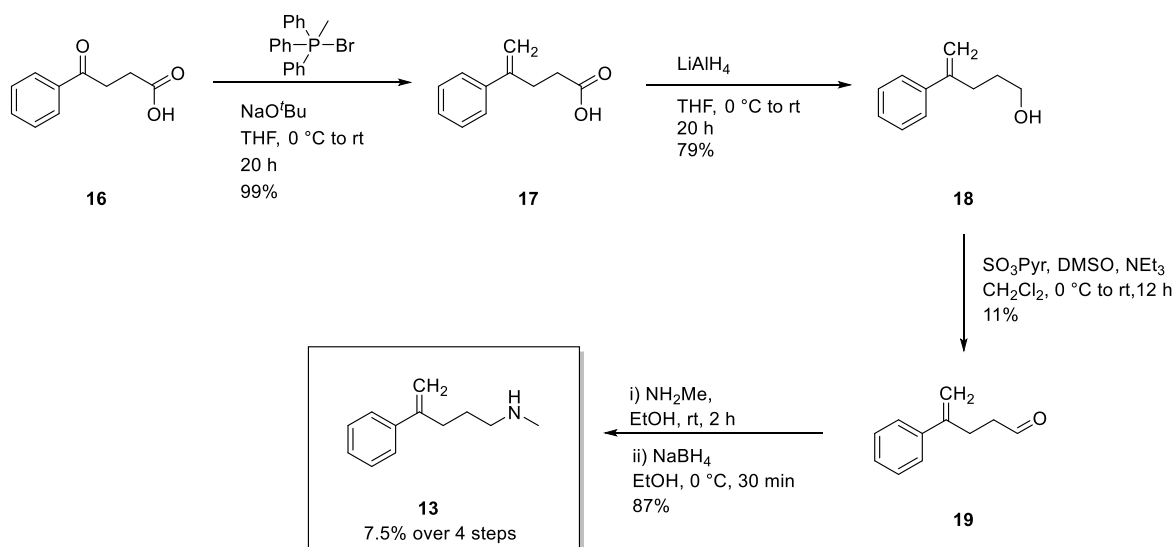


**Figure 22** The synthesis of vinyl arene **13** over four steps from phenyl butanoic acid **16** following Hartwig's procedure.<sup>130</sup>



## 4. Chapter 2: Systematic Screening of Gold-based ArMs

---

Vornholt, T., **Christoffel, F.**, Pellizzoni, M., Panke, S., Ward, T. R. & Jeschek, M. Systematic Engineering of Artificial Metalloenzymes for New-to-Nature Reactions. *Sci. Adv.* **7**, eabe4208 (2021).  
&  
*unpublished results*

### 4.1 Outline of the Authors Contribution

MJ and TRW conceived and supervised the study. S.P. advised the project. FC and MMP developed the gold-catalyzed indole and coumarin cyclization *in vitro*. FC synthesized the corresponding substrates and cofactors. TV prepared the Sav library and carried out the biological systematic screening experiments as well as the machine learning studies. TV designed the original versions of **Figure 25-26**, which were modified by FC and reprinted with permission from TV and the publisher AAAS.

### 4.2 Introduction

ArMs can display remarkable performance for biorthogonal reactions under mild reaction conditions while protecting the cofactor from poisoning by biomolecules. These features allowed several groups to utilize ArM technology for *in vivo* applications.<sup>67,125,126,132</sup> The possibility of performing abiotic reactions *in vivo* may be translated to enable the on-site synthesis of crucial metabolites and/or derivatives thereof in an organism. The potential of substituting, complementing and/or diversifying the natural metabolism opens the door for a wide field of applications including (i) the continuous evolution of ArMs in a Darwinian spirit through selection pressure to optimize catalytic efficiency, (ii) the treatment of metabolic disease through the substitution of defective metabolic routes via ArM cascades, (iii) the adaptation of microorganisms to synthetic metabolites (xeno-nutrients)<sup>133</sup>, and (iv) the regulation of microorganism behavior through incorporation of artificial metabolism sensitive to physical or chemical properties such as light, pH, etc.

In order to investigate these ambitious metabolistic challenges, a catalytic system would be required that displays a strong (chemical) signal over a noisy (biochemical) background present in a living cell. A strong signal can be achieved by utilizing an efficient catalysts with high TONs and by focusing on metabolites that already have a large impact when present at low quantities such as tryptophan and/or proline.<sup>134</sup> A way of reducing the background is the design of auxotroph organisms. Crucial metabolites will be delivered through the medium and

gradually decreased with the increase in efficiency of the ArM. Specifically, when utilizing ArM technology, it must be assured that the free cofactor does not significantly contribute to the biochemical background of the system. Sav-technology turns out to be a promising system, due to the strong binding of the cofactor and the capability of accelerated catalysis through assembly of the ArM (i.e. protein-acceleration catalysis). An optimal case would be, if the cofactor employed is only activate once incorporated into the ArM.

Our newly designed Au(I)-Sav system displayed many desired features required for the implementation into artificial metabolism: (i) the ArM proved stable under physiological conditions, (ii) the ArM performed biorthogonal reactions, (iii) the free cofactor was significantly less active than the ArM and finally (iv) the catalytic activity and selectivity could be improved by genetic optimization of the protein. As a result, we investigated the competence of Au(I)-Sav systems to catalyze the production of key metabolites including indole (for Trp) and dehydro-L-proline (for Pro). Furthermore, we explored the possibility of preparing key API-building blocks and fluorescent molecules with this system.

### 4.3 Results and Discussion

For our first project, the synthesis of indole **2** via hydroamination of 2-ethynylaniline **1**, we started by screening biotinylated cofactors **biot-Au 1-2** in MES buffer, **Figure 23**. Initial experiments were promising, as indole was detected, albeit with moderate TON. This was not such a big concern, as the free cofactors displayed a much lower activity. However, all samples contained significant amounts of side products. We verified, that the first side product was the hydrated substrate aminoacetophenone **3** and hypothesized that the second side product may be the dimerized hydrated substrate **4**. Fortunately, the hydration was a slow side reaction occurring in the background even in the absence of cofactor. With mutants displaying higher TONs towards indole, the ratio of indole/**3** increased steadily. The same behavior was not observed for the dimeric side product, which only occurred in the presence of ArM. Higher TON of indole yielded higher amounts of dimer **4**, albeit in such low quantity that we did not investigate the problem further. We were pleased to see, that such low concentrations of **3** would not harm *E. Coli* and thus not prevent the system from being applied *in vivo*.

From a small screening of all single mutants Sav K121X and Sav S112X, as well as some Sav L124X mutants, **biot-Au 1** · Sav K121L was determined to be the most effective ArM (~30 TON) for this reaction. In contrast to the previous chapter, **biot-Au 1** clearly outperformed **biot-Au 2** over almost all Sav mutants and was thus selected for the systematic screening campaign.

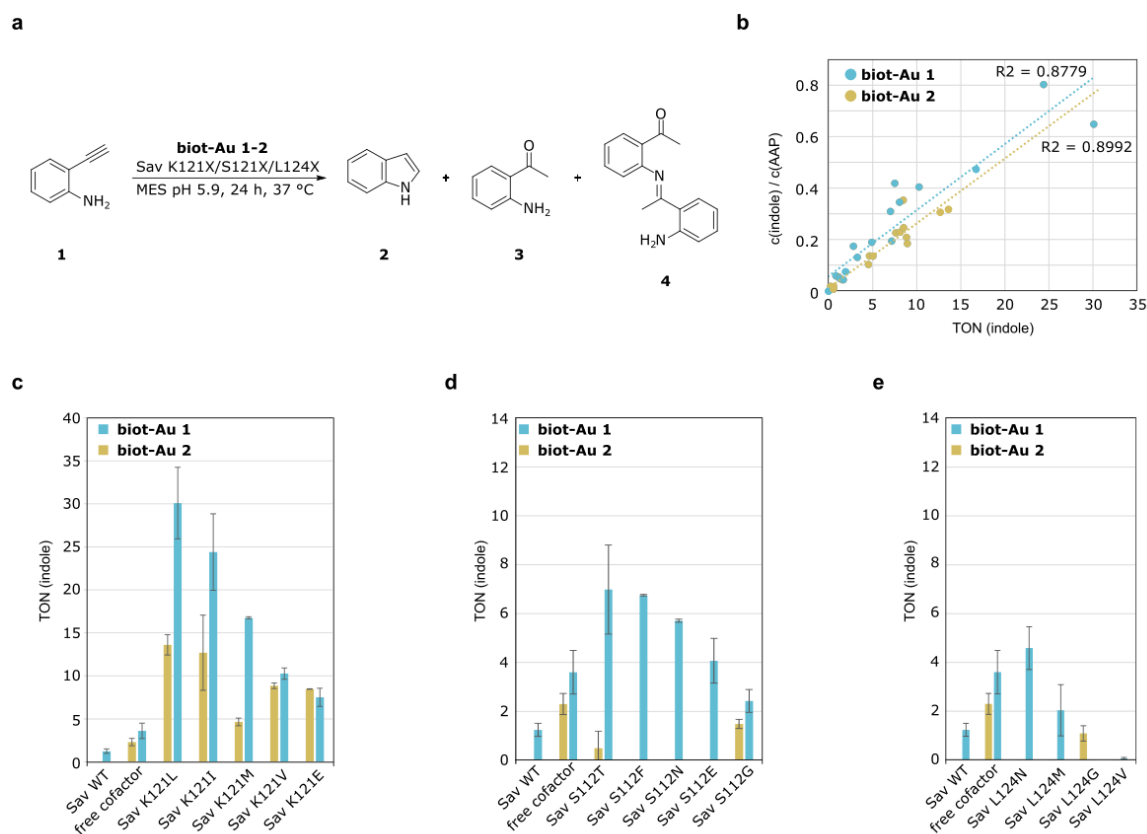


**Figure 23** *In vitro* optimization of the hydroamination of 2-ethynylaniline. **a** The reaction of 2-ethynylaniline leads to the formation of indole, aminoacetophenone (AAP) and a dimeric species of AAP. **b** With increasing activity of the ArM the ratio of indole/AAP changes in favor of indole. **c** Display of the five best Sav K121X single mutants. **d** Display of the best S112X single mutants. **e** Display of the four best L124X single mutants. Reaction conditions: [biot-Au] = 10  $\mu$ M; [Sav] = 20  $\mu$ M; [Sub] = 1 mM; in 200  $\mu$ L, 37  $^{\circ}$ C for 24 h

As we were not only interested in complementing the natural metabolism in *E. coli* but also in designing simpler methods to optimize ArMs, we started investigating fluorescent reactions in parallel to the hydroamination. HPLC analysis is often the bottleneck of directed evolution. Samples need to be purified (centrifugation, filtration), diluted, and successively injected into an HPLC/UPLC. The analysis of a single 96-well plate can take up to  $\sim$ 10 h (UPLC with  $\sim$ 5 min method) to  $\sim$ 72 h (HPLC with  $\sim$ 40 min method). On the other hand, a Tecan plate reader can analyze a 96-well plate in under 5 min with no laborious purification steps prior to analysis. For this reason, we investigated the hydroarylation of coumarin derivatives, **Figure 24 a**. The aryl-phenylpropiolate **5** can be readily prepared from phenylpropiolic acid and 3-(diethylamino)phenol via a Steglich esterification. The corresponding product is non-

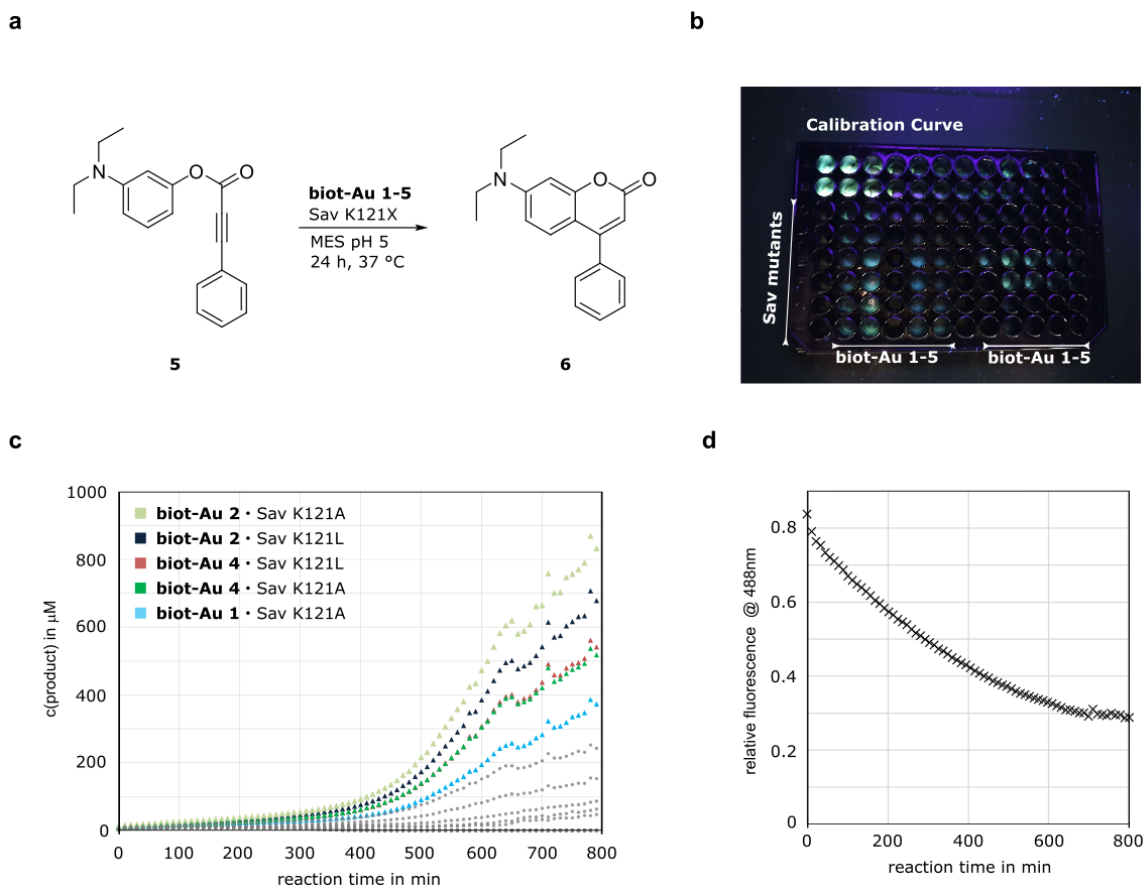


**Figure 24** *in vitro* optimization of the hydroarylation of phenylpropiolate **YY**. **a** The hydroamination of phenylpropiolate **YY** yields phenyl coumarin **XY**. **b** Dark 96 well screening plate under the UV lamp after 24 h of reaction time. **c** Screening results of the 96 well plate obtain via TECAN fluorescence measurement. Highlighted are the best performing ArMs. Reaction conditions: [biot-Au] = 10  $\mu$ M; [Sav] = 20  $\mu$ M; [Sub] = 1 mM; in 200  $\mu$ L, 37  $^{\circ}$ C for 24 h. **d** Average decrease in fluorescence of the most concentrated calibration Well A1 and B1 over time.

fluorescent. Upon gold-catalyzed hydroarylation, a green, fluorescent phenyl-coumarin derivative **6** is obtained. The strong fluorescence of the product allows to monitor the conversion via Tecan plate reader. We screened a selection of Sav mutants (Sav WT, Sav K121A, Sav K121L, Sav K121I) and cofactors (biot-Au 1-5) at two different ArM concentrations (10  $\mu$ M and 1  $\mu$ M). The first two rows of the plate contain a dilution line for the calibration curve in doublets. The other rows contain various Sav mutants, while the columns contain different cofactors, except the first column which contains the substrate with only the protein. The third and the ninth column contains ArMs with **biot-Au 2**. Already by eye, one can see, that **biot-Au 2** outperforms all other cofactors, **Figure 24 b**. Fluorescent read confirms the observation, **Figure 24 c**. Unfortunately, one can also see a very noisy fluorescent read. We could detect a decrease in fluorescence in the dilution line as well, indicating that the product either decomposes, auto-quenches or disappears (i.e. absorbed in plastic well-plate?), **Figure 24 d**. Nonetheless, **biot-Au 2** · Sav K121A and **biot-Au 2** · Sav K121A clearly outperform ArMs based on other cofactors over the whole reaction timeline. We decided to proceed with **biot-**

**Au 2** for the systematic screening of further Sav isoforms for the hydroarylation. Despite the noisy background, the performance order of the ArMs is consistent over the whole reaction time.

Having determined the optimal cofactors for hydroamination (**biot-Au 1**) and hydroarylation (**biot-Au 2**) we systematically screened Sav S112X-K121X double mutants via a periplasmic expression system.<sup>95</sup> An universal and automated screening protocol on a robotic platform was developed by TV and MJ that facilitated the screening of improved ArMs (Ruthenium- and Gold-based) for diverse reactions (metathesis, coumarin-deallylation, indole-deallylation, hydroamination and hydroarylation), **Figure 25 a**. However, herein we will only focus on the hydroamination (I) and the hydroarylation (II), **Figure 25 b-d**.

In order to achieve a good trade-off between accessibility to the cofactor, expression levels, and compatibility of the reaction a periplasmic expression system was implemented. Therein, a signal peptide of the outer membrane protein A (OmpA) was N-terminally fused to T7-tagged streptavidin.<sup>30</sup>

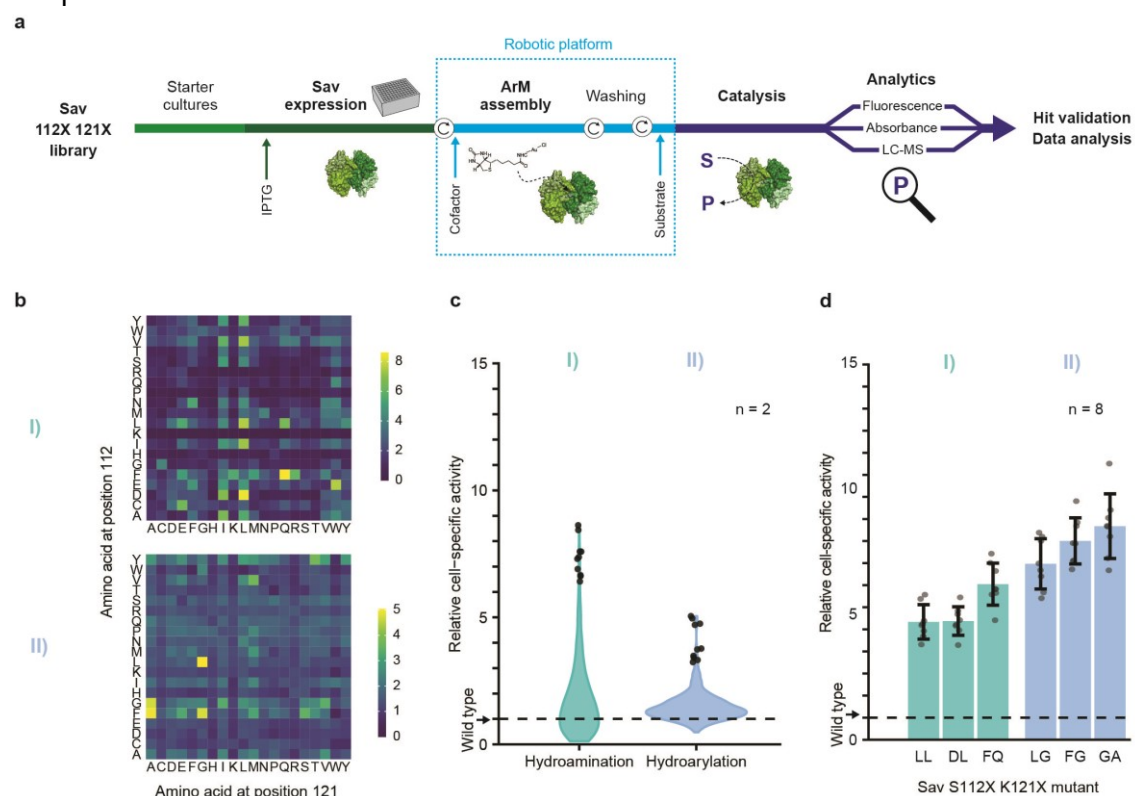


**Figure 25 Systematic screening of gold-based hydroaminases and hydroarylases. a.** Overview of the screening workflow. Circular arrows represent centrifugation steps for buffer exchange. **b** Cell-specific activity of 400 ArMs mutated at Sav positions 112 and 121 normalized to the activity of wild-type Sav (S112 K121). The displayed activities are product concentrations after 20 hours of reaction (mean of biological duplicates). Note that the screenings for reactions II was performed using robotics. **c** Activity distribution in the Sav mutant library for the two ArM reactions. Violins comprise 400 double mutants with the 10 most active ArMs depicted as circles. **d** Validation of hits from the 400 mutant screens. Bars are mean activity of eight biological replicates with SD (error bars) and individual replicates (circles). Mutants are designated by the amino acids in positions 112 and 121. Modified and reprinted with permission from TV and AAAS.<sup>95</sup>

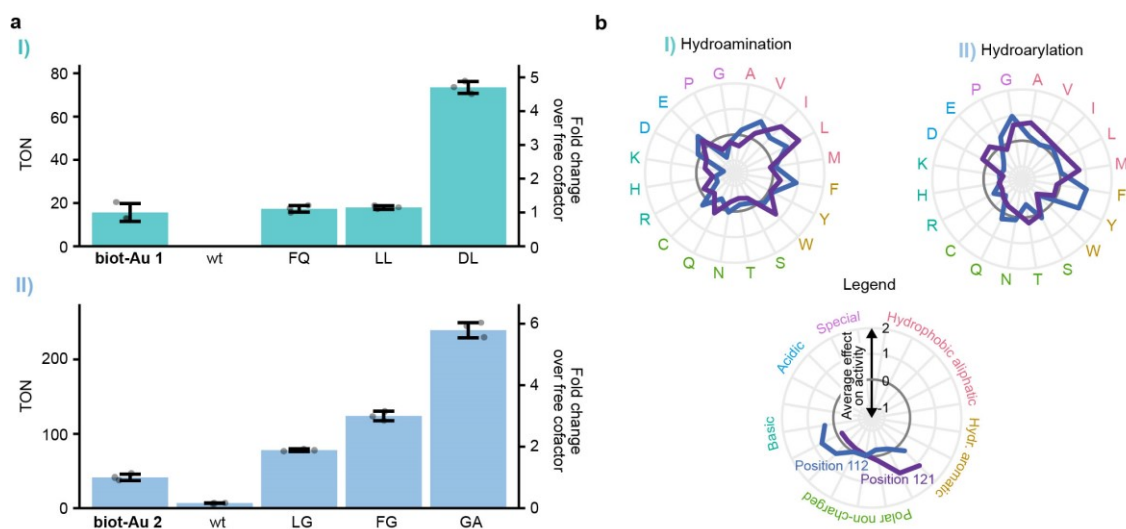


**Figure 26 Amino acid effects and implications for future ArM engineering.** **a** In vitro turnover number of ArM variants identified in the periplasmic screening. For each reaction, the three most active variants identified in the whole-cell screening were purified, and their TON was determined. Reactions were carried out at 37 °C and 200 rpm for 20 hours. Bars represent mean TONs of technical triplicate reactions with SD as error bars and individual replicates as circles. For comparison, the free cofactor and wild-type Sav variant (wt) were included. Mutants are designated by the amino acids in positions 112 and 121. **b** Effect of amino acids on ArM activity. Points outside and inside the dark gray circles indicate a positive and negative effect, respectively. Values were standardized by subtracting the mean activity of all 400 mutants and dividing by the corresponding SD. The mean across all 20 variants harboring the respective amino acid is shown. Modified and reprinted with permission from TV and AAAS.<sup>95</sup>

Then, a full factorial and sequence-verified library consisting of all 400 double-mutants of Sav S112X-K121X (X representing all 20 canonical amino acids) was prepared. This allowed for a systematic sequence-activity landscape for the two gold-catalyzed reactions, **Figure 25 b**. A substantial variation of the activity pattern was observed between the two gold-catalyzed reactions indicating the existence of distinct interactions between cofactor, protein and substrate. Interestingly, the most promising mutations from the initial *in vitro* screen, namely K121L for the hydroamination and K121A for the hydroarylation are also present in the top three of the whole-cell screening, **Figure 25 c-d**. For a final validation, the three most-active double-mutants for the hydroamination (Sav S112F K121Q, Sav S112L K121L and Sav S112D K121L) and the hydroarylation (Sav S112L K121G, Sav S112F K121G and S112G K121A) were purified and tested *in vitro*, **Figure 26 a**. Substantial improvement of up to 7-to 10 fold was recorded over Sav WT and/or free cofactor. However, the ranking of corresponding Sav hits changed from *in vivo* to *in vitro*, likely due to the change in reaction conditions.

A further benefit of using sequence-verified libraries is the exploration of the relation between biophysical properties and catalytic activity. Corresponding spider graphs are an effective way to simultaneously visualize the effect of individual amino acids and biophysical properties for different positions. Herein, positive deviations from zero indicate a beneficial effect on catalysis by the individual amino acid and vice versa. Amino acids are clustered by biophysical

properties. A general trend emerges, where hydrophobic and aromatic amino acids provide a positive effect, while basic amino acids seem to be rather detrimental, **Figure 26 b**.

## 4.4 Conclusion

In the first chapter, randomized iterative saturation mutagenesis was used to obtain efficient and selective hexa Sav-SOD mutants for the hydroamination of aromatic ureas. Some advantages of this method include a simple library preparation (NDT-VMA codons), low sequencing cost (only ~3% of the wells were sequenced) and rapid exploration of multiple positions (6 positions). Even with an automation setup, it would be challenging to screen so many positions in a full-factorial library (64 000 000 reactions). In the near future, this may however not be necessary. Full-factorial libraries do not only allow detecting mutants that are the result of synergistic interactions (which can not be detected by iterative approaches), but they provide a full activity landscape of the ArM. This activity landscape can form a strong test set for machine learning approaches and guide directed evolution with yet unknown efficiency.

Furthermore, this approach does not require any oversampling which drastically reduces the amount of catalyst and substrate required for the same number of positions. Herein, the two gold catalyzed reactions were significantly optimized and validated *in vitro*. The hit **biot-Au 1** · Sav S112D K121L afforded indole with ~80 TON and may provide a good starting point for the directed evolution of Trp-deficient *E. Coli* in a Darwinian manner.

## 4.5 Appendix: Unreactive Substrates & Proline Metabolism

Other substrates were explored that upon reaction with gold-based ArMs could lead to crucial metabolites for *E. Coli*. As previous reports on the directed evolution of allylic deallylase of fluorogenic allyl-carbamate-protected coumarins gave promising TONs of up to 150 and could later be translated to the uncaging of indole with almost 600 TON, we hypothesized that we may be able to utilize gold-based ArMs to deprotect tert-butylcarbamate indole **7**, **Figure 27 a**.<sup>32,85,95,135</sup> We could detect a modest increase (up to 50%) in the deprotection of tert-butylcarbamate indole **7** in the presence of gold-ArMs compared to the background deprotection of the solvent, **Figure 27 b**. The improvement was marginal, and the background deprotection too significant. Such strong background reactions are not viable for *in vivo* design as they overshadow the catalytic activity of the ArM crucial for reliable evolution attempts.

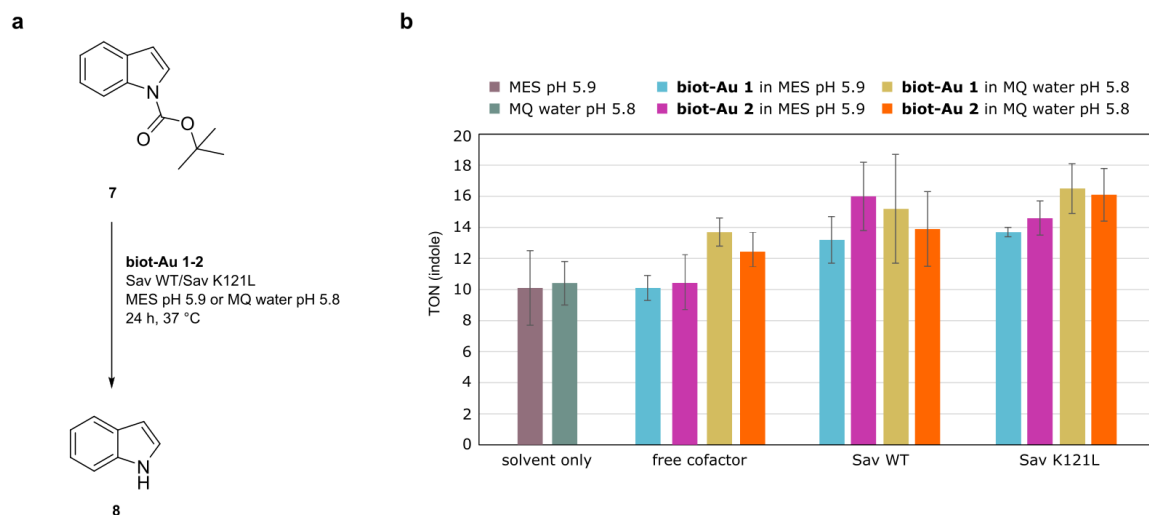


**Figure 27 Gold-catalyzed deprotection of indole carbamates.** **a** tert-butyl carbamate indole **7** is subjected to gold-catalyzed deprotection screening in aqueous conditions. **b** Screening results of tert-butyl carbamate indole **7** displaying a strong background reaction with minor improvement in Sav WT and Sav K121L. Reaction conditions: [Au] = 5  $\mu$ M; [Sav] = 10  $\mu$ M; [Sub] = 5 mM; 37 °C for 24 h; analyzed via UPLC-MS.

In a second attempt, we explored the hydroamination of 2-aminopent-3-ynoic acid **9** to dihydroproline **10** which upon reduction through Ec-proC could yield *L*-proline **11**, **Figure 28**. Interestingly, the corresponding pro-dihydroproline could be synthesized stereoselectively from proline in five steps, **Figure 29**.<sup>136</sup> Unfortunately, we were not able to detect any product from the reaction of various gold-based ArMs with the pro-hydroproline substrate.

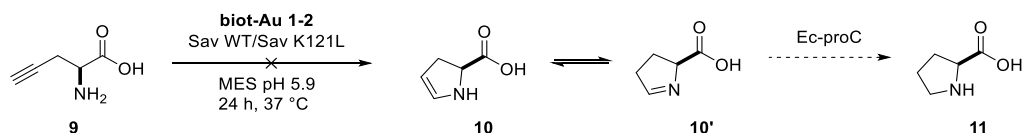


**Figure 28 Hydroamination of 2-aminopent-4-ynoic acid 9 to 2,3-dihydroproline 10 with subsequent tautomerization and enzymatic conversion to *L*-proline 11.**



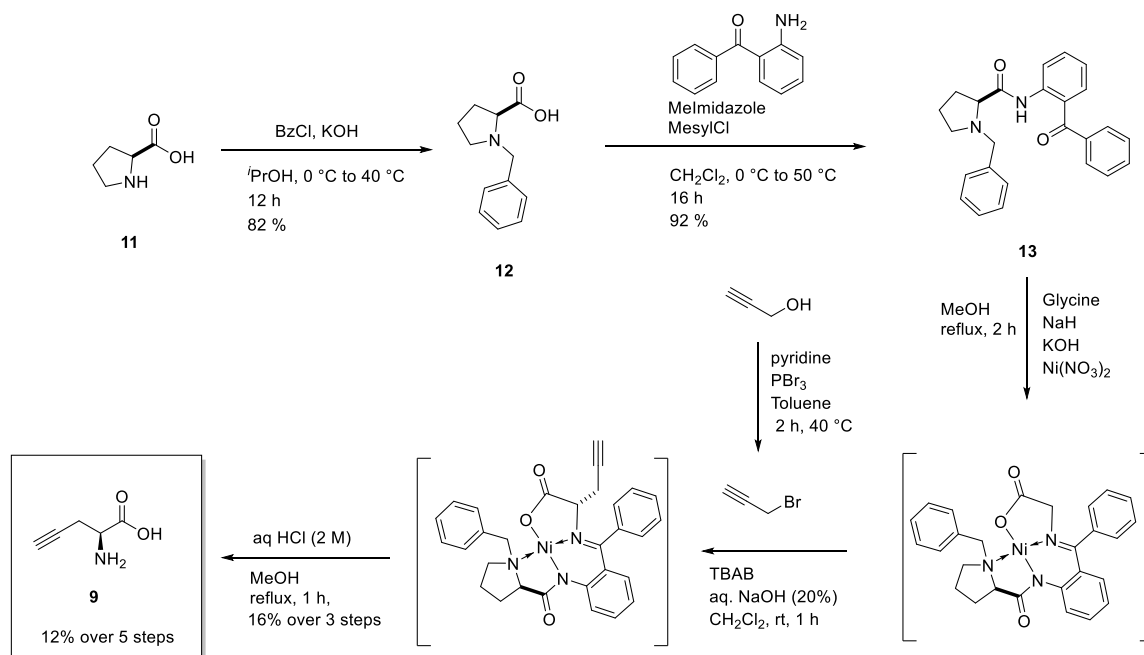


**Figure 29 Stereoselective synthesis of (S)-2-aminopent-4-ynoic acid from proline over five steps.**<sup>136</sup>

## 5. Chapter 3: Intramolecular Heck Reaction

---

**Christoffel, F.** & Ward, T. R. Palladium-Catalyzed Heck Cross-Coupling Reactions in Water: A Comprehensive Review. *Catal. Letters* **148**, 489–511 (2018).  
&  
*unpublished results*

### 5.1 Outline of the Authors Contribution

TRW and FC conceived and designed the study. FC synthesized and characterized the substrates and the palladium complexes. FC conducted the catalytic experiments.

### 5.2 Introduction

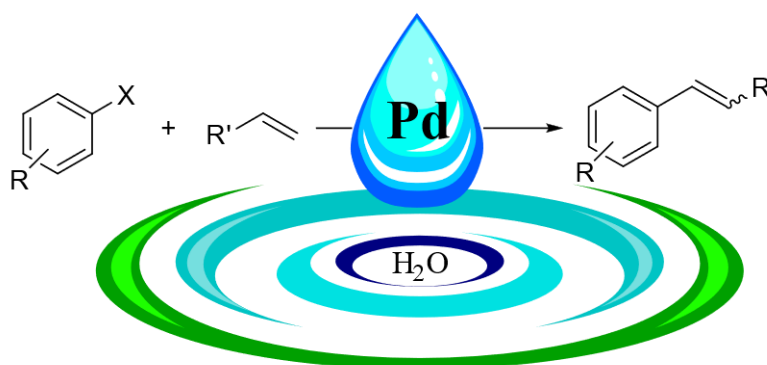


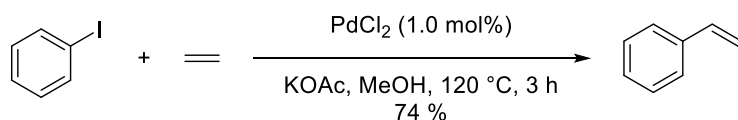
**Figure 30** Graphical abstract depicting a standard Heck cross-coupling reaction. Reprinted with permission from Springer Nature.<sup>137</sup>

Palladium-catalyzed cross-coupling reactions have emerged as one of the most versatile tools in organic chemistry. Extensive efforts were made to adapt these reactions to aqueous media, not only for the purpose of environmental concerns but also to expand the scope, increase the efficiency and implement bio-compatible protocols. Among different palladium cross-coupling reactions, the Heck reaction turned out to be the most challenging in an aqueous environment, **Figure 30**. This led to various original developments in catalyst design.

The Heck cross-coupling reaction (HCR hereafter) was discovered independently by T. Mizoroki in 1971 and R. F. Heck in 1972 and is generally referred to as the palladium-catalyzed arylation of olefins. In the presence of catalytic amounts of palladium, an aryl (pseudo)halide reacts with an alkene in the presence of a base to afford the corresponding arylated alkene, **Figure 31**.<sup>138,139</sup> What first started as a method for the synthesis of stilbenes from styrenes

quickly developed into one of the most versatile and efficient reactions to synthesize substituted olefins both in academia and in industry. Together with Ei-ichi Negishi and Akira Suzuki, Richard F. Heck was awarded the Nobel Prize in Chemistry in 2010 “for palladium-catalyzed cross-couplings in organic synthesis”.<sup>140</sup> Among the reviews covering Pd-catalyzed cross-coupling reactions,<sup>141–144</sup> one should mention the one by Beletskaya and co-workers<sup>145</sup> as it covers some of the most unique properties of the HCR.

#### Mizoroki 1971



#### Heck 1972

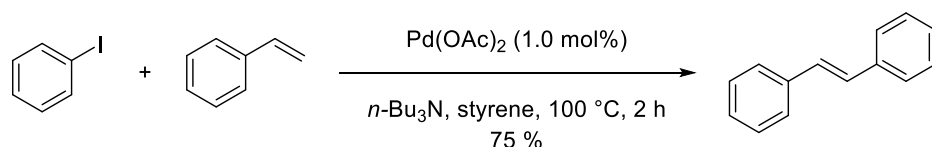
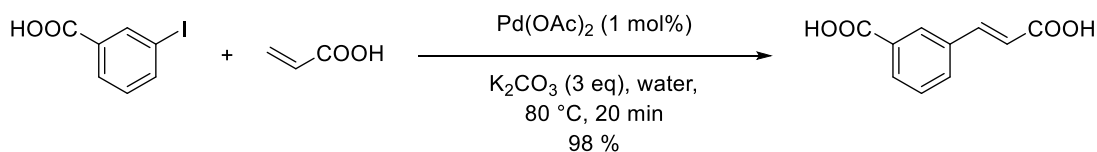


**Figure 31** The Heck-Mizoroki cross-coupling reaction reported in the early 70s.<sup>138,139</sup> Reprinted with permission from Springer Nature.<sup>137</sup>

Beside minimizing organic waste and avoiding hazardous reaction conditions, running Pd-catalyzed cross-coupling reactions in water presents many benefits. Indeed, the use of water as a solvent offers the following attractive features: i) it may simplify the purification of the product; ii) it allows for an easy recovery and recycling of the catalyst iii) as water is one of the most polar solvents, it can accelerate catalysis by promoting the migratory insertion and protecting the catalyst by displacing labile ligands from its coordination sphere; iv) the use of water may invert the selectivity of intramolecular HCR and provide an environment for protective-group free synthesis of complex building blocks; v) Finally, efficient and robust aqueous Pd-catalyzed cross-coupling reactions have found use in bioorthogonal chemistry *in vivo*.<sup>10,126,132,146–151</sup>

In 1988, Beletskaya and co-workers discovered a ligand-free Pd(OAc)<sub>2</sub>-catalyzed reaction of water soluble arylhalides with acrylic acid in water in the presence of K<sub>2</sub>CO<sub>3</sub> as base. High yields (> 95 %) were obtained using moderate reaction conditions (50-100 °C) which, at that time, were comparable to reactions performed under anhydrous conditions in polar aprotic solvents including MeCN, DMF, DMA, NMP, etc.<sup>152</sup> Calabrese and co-workers reported in 1990 the use of a sulfonated water-soluble phosphine ligand for aqueous Pd-catalyzed HCR, **Figure 32**.<sup>153</sup> Since 2000, many sophisticated Pd-based catalysts were developed for the aqueous Suzuki-Miyaura cross-coupling (SMC). However, their use in aqueous HCR remains limited.<sup>154–156</sup>

### Beletskaya 1988



### Calabrese 1990

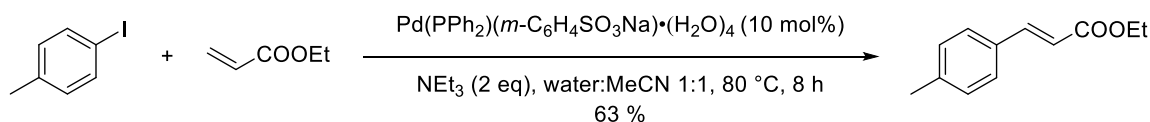


**Figure 32 First reports on aqueous homogeneous Heck reactions.**<sup>152,153</sup> Reprinted with permission from Springer Nature

Previous efforts in transferring palladium catalysis towards biorthogonal chemistry via ArM technology were successful. These artificial Suzukiases<sup>149</sup> and Heckases<sup>157</sup> displayed remarkable stereo- and enantioselectivity but only limited stability with regards to the palladium cofactor. An oxygen-free environment and/or the addition of up to 75% organic solvent (DMF, DMSO, ethylene glycol) were required which restricts the use of such systems towards *in vitro* chemistry. With the goal to push ArM-based palladium chemistry *in vivo* and complement the natural metabolism, we set out to design an artificial Heckase based on the biotin-streptavidin technology and integrate it toward *in vivo*-production of tryptophan.

## 5.3 Results and Discussion

The goal of this project was to develop an artificial Heckase to prepare indole *in vivo*. Therefore, we needed to design (i) a biocompatible Heck reaction to yield indole, (ii) a biocompatible Palladium catalyst capable of binding to Sav, and finally (iii) integrate the corresponding Heckase into the *in vivo*-production of tryptophan. Unfortunately, we did not succeed with the first two targets and were thus not able to design an artificial Heckase for indole production. This chapter summarizes the challenges faced during this project in tackling pro-indole substrate synthesis, biotinylated Pd-NHC synthesis and the biostability of substrates and catalysts.

The first attempt was to synthesize 2-iodo-N-vinylaniline from 2-iodo aniline. Interestingly, this rather simple small molecule was not commercially available and there were no reports on its synthesis, **Figure 33 a**. Nucleophilic substitution of vinyl halides with the aniline was not successful. It was quickly clear that the aniline had to be protected. During this project, we prepared boc-protected, formyl-protected, acetyl-protected, tosyl-protected and nosyl-protected 2-iodo anilines, **Figure 33 b**.

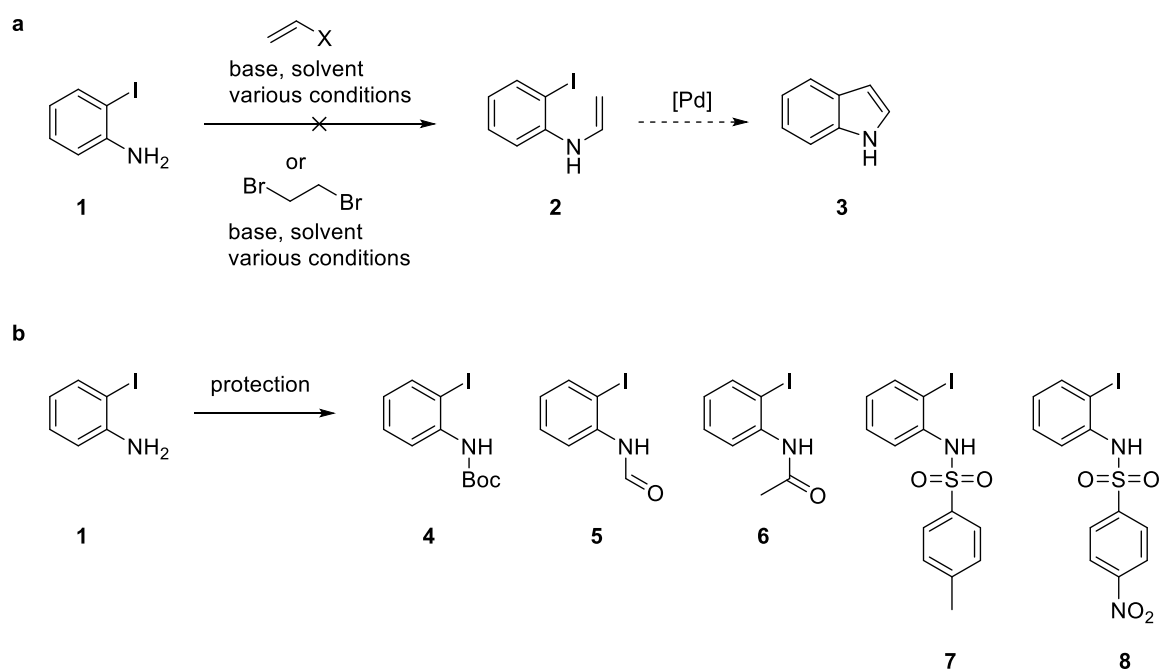


**Figure 33 Substrate synthesis for the Heckase project.** **a** The synthesis of indole via artificial Heckase from 2-iodo-N-vinylaniline. **b** The protection of 2-iodo aniline with boc, formyl, acetyl, tosyl and nosyl groups.

Our next substrate attempt focused on boc-protected 2-iodo aniline **4**, which was acetylated in very good yield to acetyl aniline **9**, **Figure 34**. We hypothesized that upon reduction of **9**, trapping of hemiaminal with TMS to yield **10** followed by elimination would yield boc-protected vinyl aniline **11**. Unfortunately, TMS-protected hemiaminal **10** decomposed into a mixture of compounds. No vinyl aniline **11** was detected.

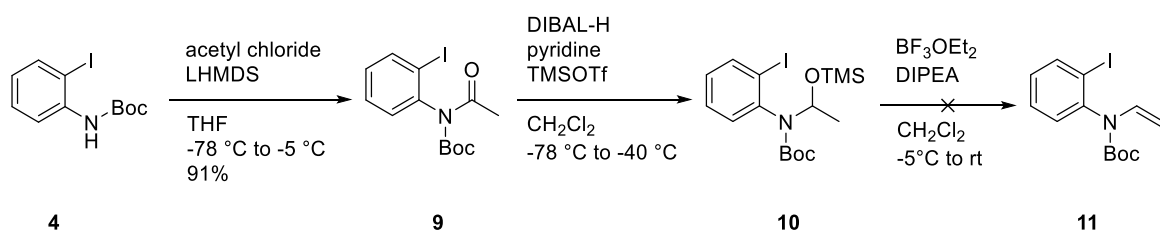


**Figure 34 Synthesis route towards boc-protected pro-indole 11.**

Another attempt focused on the olefination of formyl aniline **5** with the petasis titanocene **13**, which can be readily prepared from titanocene **14**, **Figure 35**. The reactions were not successful. We further attempted to couple dibromoethane to formyl aniline **5** unsuccessfully.

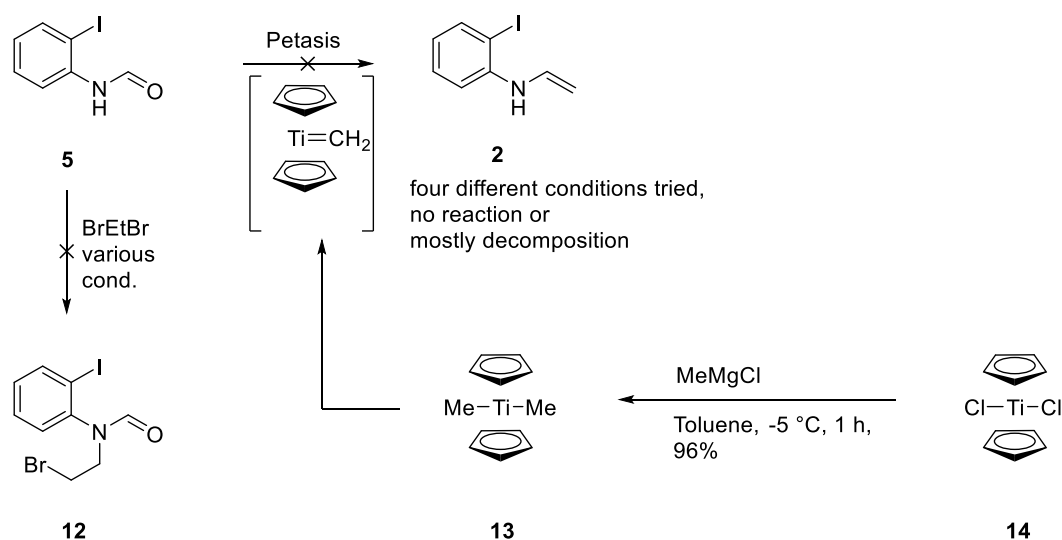


**Figure 35** Synthesis route towards pro-indole **2** via petasis olefination.

Next, we started from acetyl aniline **6**, in the hope it would be less prone to decomposition compared to formyl aniline **5**, **Figure 36**. We pursued two routes which both relied on the nucleophilic substitution of halides to aniline **6**. We were again not able to couple dibromoethane, but traces of vinyl-acetyl aniline **15** could be detected. Unfortunately, we could not improve the nucleophilic substitution of vinyl bromide to aniline **6** to provide useful yields of **15**.

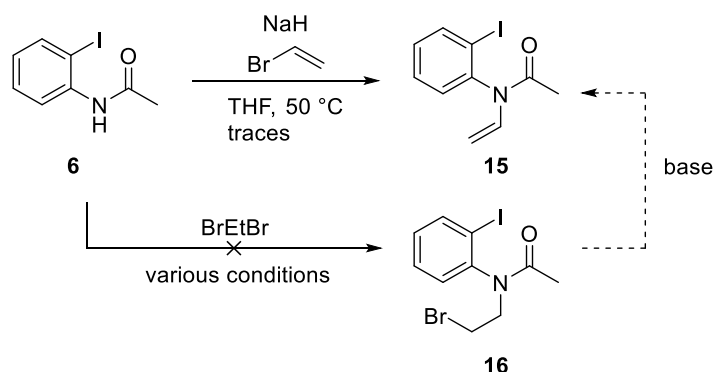


**Figure 36** Synthesis route towards acetyl-protected pro-indole **15**.

Our final attempts relied on the use of sulfonamide protecting groups, **Figure 37**. We protected 2-iodo aniline with tosyl and nosyl groups to yield **7** and **8** in very good yields. Attempts to directly couple vinyl bromide were not successful. However, upon reaction with dibromoethane we could generate bromoethyl anilines **17** and **19** in very good yields. Subsequent nucleophilic elimination with KO<sup>t</sup>Bu yielded the sulfonamide-protected vinyl anilines **18** and **20** in moderate to good yields.

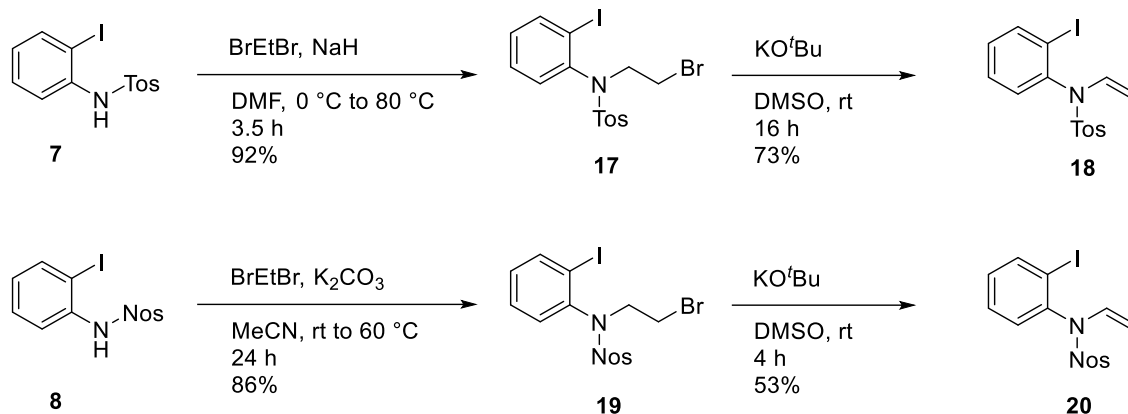


**Figure 37** Synthesis route towards tosyl- and nosyl-protected pro-indole **18** and **20**.

Various attempts in deprotecting the sulfonamide without losing or destroying the vinyl moiety were not successful, **Figure 38**. Nosyl vinyl aniline **20** could be deprotected in the presence of HF and pyridine, the product isolated was however acetyl aniline **6**. As a result, we decided to screen our Heck reactions with the corresponding sulfonamides **18** and **20**. We hoped that eventually we could find a way to deprotect the corresponding sulfonamide indoles e.g. through thiols that can be found in *E. Coli*.

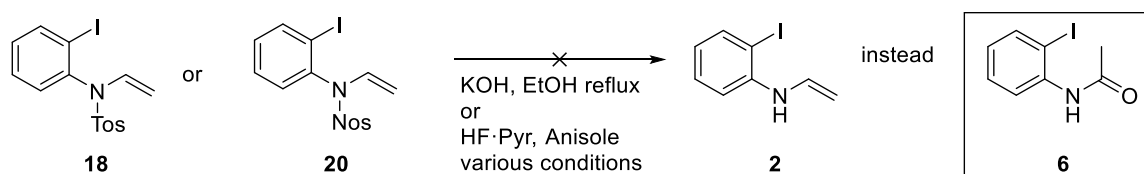


**Figure 38** Attempts to deprotect tosyl- and nosyl-vinyl anilines **18** and **20** to get pro-indole **2** yielded acetyl aniline **6**.

We first screened various commercial palladium sources and ligands and quickly realized, that in pure degassed DMF, at 120 °C the intramolecular Heck reaction of tosyl vinyl aniline **18** worked very well, **Figure 39**. However, upon addition of water most commercial sources did not perform at all. For this reason, we synthesized five different palladium complexes, four of them containing NHC ligands to test for aqueous intramolecular Heck reactions, **Figure 40**.<sup>149,158–162</sup>

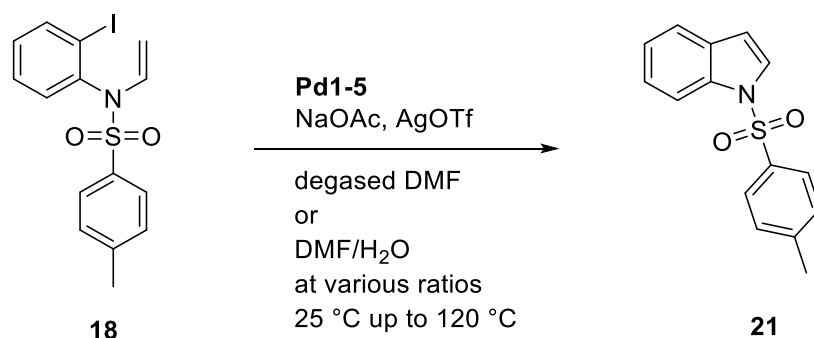


**Figure 39** Reaction screening for the intramolecular Heck reaction of tosyl-protected vinyl aniline **18** to yield tosyl-indole **21**.

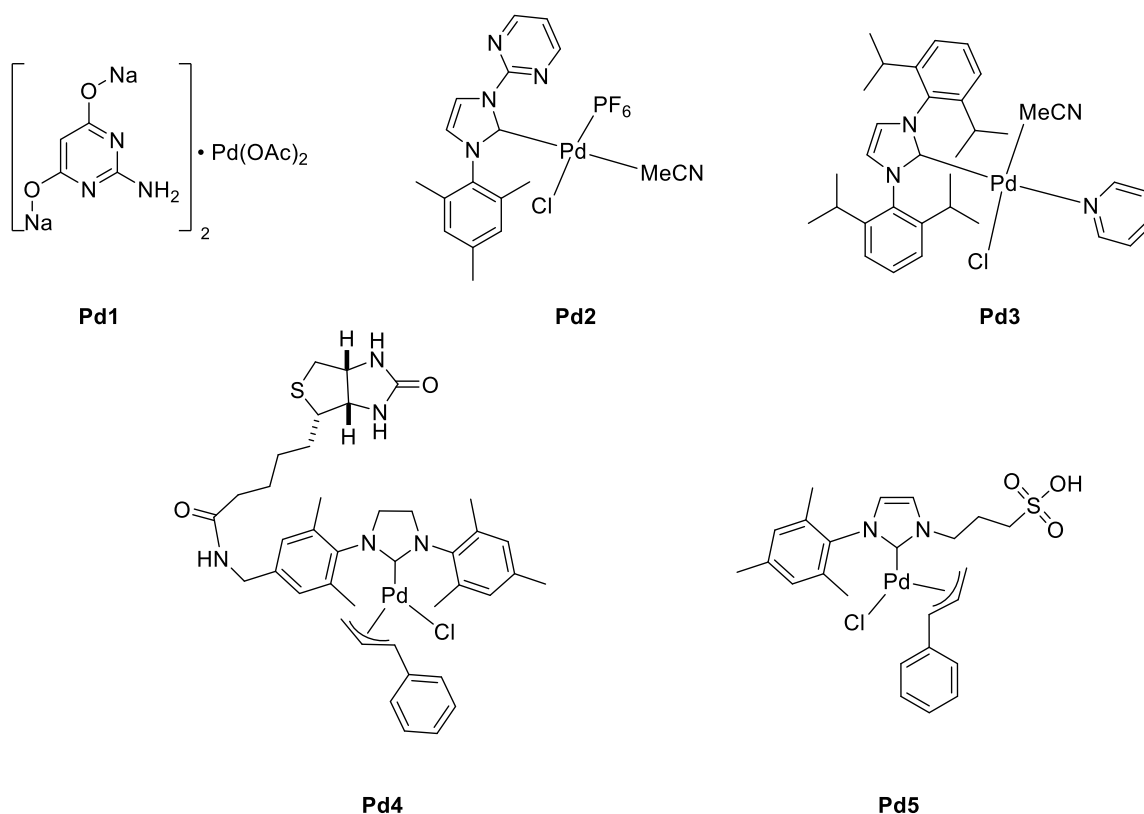


**Figure 40** Various Palladium complexes were prepared according to literature procedures.<sup>149,158–163</sup>

The corresponding Pd complexes performed very differently in 1:1 mixtures of DMF and water at 80 °C. While the three Pd-NHC complexes **Pd2**, **Pd3** and **Pd5** catalyzed the reaction rather well, **Pd1** and biotinylated complex **Pd4** did not display any activity, **Table 3** entry 1-5. The addition of Sav WT to **Pd4** did not improve catalysis. Next, we investigated more biocompatible reaction conditions (40 °C and 2:8 DMF:water) **Table 3** entry 6-10. Sulfonated complex **Pd5** performed best with 90% conversion. However, in the absence of organic solvent (DMF) or base (NaOAc), **Pd5** was inactive. We were planning to design a sulfonated and biotinylated Pd-NHC complex that would retain the activity of **Pd5** but be susceptible to protein engineering on Sav. However, before starting such a synthetic endeavour, we wanted to make sure that we could cleave of the protecting group to release the crucial metabolite indole *in vivo*.

Unfortunately, we could not detect clean conversion of the nosyl substrate **20** to the corresponding indole. Upon catalysis a complex mixture of various products was obtained. Thus, we did not pursue the synthesis of more thiol-labile dinitrogenated substrates. We hypothesized that, thiols such as cysteine or glutathione that can be present in rather high concentrations *in vivo* may support the deprotection of the sulfonamide from the corresponding indole. However, we were unable to deprotect tosyl- or nosyl indole under biocompatible reaction conditions, **Figure 41**.



**Table 3** Selected Results of Pd-catalyzed intramolecular Heck coupling of tosyl-protected 2-iodo-N-vinyl aniline with **Pd1-5** in aqueous degassed DMF.

Entry	Palladium Catalyst	Temperature	Water content	Conversion <sup>a</sup>
0	-	80°C	50%	0%
1	<b>Pd1</b>	80°C	50%	0%
2	<b>Pd2</b>	80°C	50%	53%
3	<b>Pd3</b>	80 C	50%	83% (27% <sup>b</sup> )
4	<b>Pd4</b>	80°C	50%	0% (0% <sup>c</sup> )
5	<b>Pd5</b>	<b>80°C</b>	<b>50%</b>	<b>99%</b>
6	<b>Pd1</b>	40°C	80%	0%
7	<b>Pd2</b>	40°C	80%	24%
8	<b>Pd3</b>	40°C	80%	30%
9	<b>Pd4</b>	40°C	80%	0%
10	<b>Pd5</b>	<b>40°C</b>	<b>80%</b>	<b>90%(0%<sup>d</sup>)</b>

<sup>a</sup>The analytical experiments were carried out in duplicates with the following reaction conditions:  $V_{\text{tot}}$  400  $\mu\text{L}$ , [Sub] 10 mM, [Pdcat] 2 mM, [NaOAc] 4 mM, [AgOTf] 4 mM, 40 °C or 80 °C for 24 h. <sup>b</sup> In the absence of AgOTf. <sup>c</sup> In the presence of 2 eq Sav WT no improvement was detected. <sup>d</sup> No conversion in the absence of DMF, or NaOAc. Reactions run with other bases such as triethylamine gave lower conversion.

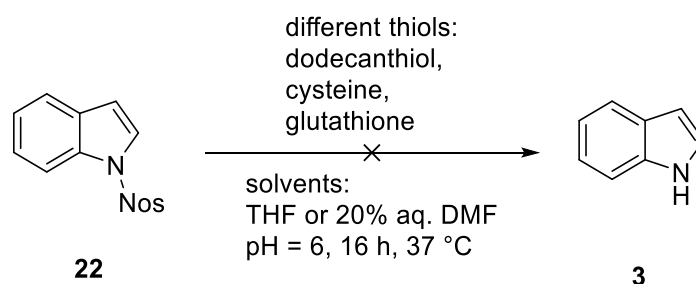


**Figure 41** Deprotection attempts of nosyl-protected indole **22** in the presence of various thiols.

## 5.4 Conclusion

In conclusion, we designed an intramolecular Heck reaction to yield protected indoles in aqueous mixtures at moderate temperatures. We faced synthetic challenges when designing unprotected enamine **2**. Analogues thereof with labile protecting groups either decomposed or were synthetically challenging, while analogues bearing stable protecting groups generated indoles that couldn't be deprotected under biocompatible conditions. These challenges, combined with the difficulty of preparing biotinylated Pd complexes, lead us to pursue the gold-catalyzed hydroamination: commercial substrates could be converted to indoles without the need for additives, bases and/or degassed solvents. Furthermore, the biotinylated gold complexes were synthetically easier to prepare and proved highly stable.

## 6. Chapter 4: Gold-triggered Drug-Release Systems

---

**Christoffel, F.**, Igareta, N. V., Lozhkin, B., Meyer, P., Sabatino, V., Ward, T. R.  
*unpublished results*

### 6.1 Outline of the Authors Contribution

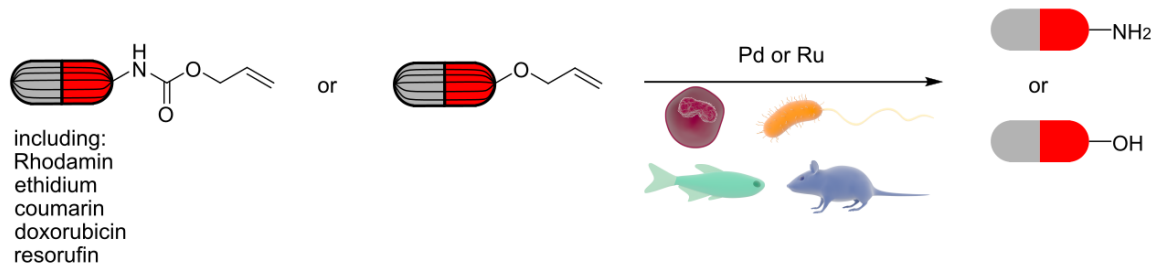
TRW, VS and FC conceived and designed the study. FC and VS developed the gold-catalyzed “close-to-release” cyclization of pro-furan substrates. FC and PM developed the gold-catalyzed “close-to-release” cyclization in “4.6 Appendix: Unreactive Substrates”. NVI and FC prepared the Sav isoforms. NVI and BL prepared the LM3 and the TATE peptide on rink amide and trityl resin, respectively. FC and NVI developed the peptide functionalization with gold-NHC complexes. BL synthesized the sulfimidated NHC ligands and FC the gold complexes thereof.

### 6.2 Introduction

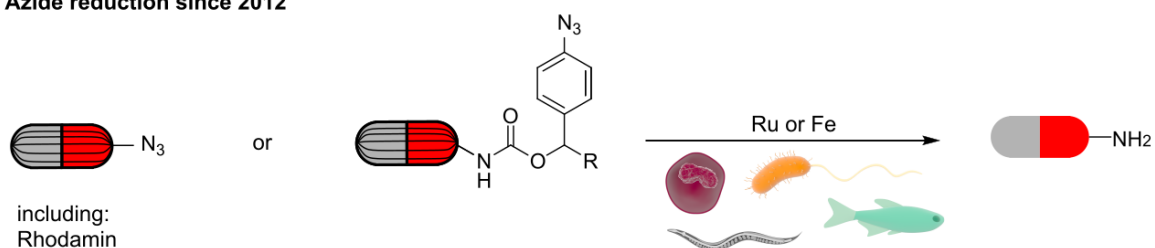
The work on aqueous transition metal catalysis laid the foundation for bioorganometallic chemistry and subsequent biorthogonal, metal-based uncaging reactions. Such an uncaging reaction is commonly referred to a reaction where a protecting moiety is cleaved of a probe in the presence of a catalyst to release an active payload.<sup>137,164,165</sup> Cellular mechanisms rely heavily on metalloproteins containing first-row transition metals such as iron, copper and zinc. In contrast, second row transition metals are rarely found in natural metalloproteins.<sup>166,167</sup> For this reason, biocompatible second row transition metals form an interesting source of biorthogonal catalysts with promising applications in the uncaging of active ingredients *in vivo*.<sup>168</sup>

Over the last decades, ruthenium and palladium were extensively used in various biorthogonal reactions including the uncaging of allenes,<sup>169</sup> allyls,<sup>170,171</sup> propargyls,<sup>85,172–178</sup> propargyloxycarbonyls (Proc),<sup>179–185</sup> allyloxycarbonyls (Alloc),<sup>32,132,194,195,186–193</sup> azides<sup>189,196</sup> and naphthyls,<sup>197</sup> **Figure 42**. Initial developments of these reactions usually rely on the uncaging of fluorescent molecules such as rhodamine and/or coumarin. These fluorescent probes facilitate reaction control *in vitro* as well as *in vivo* and allow the detection of products at very low concentrations. As a result, fluorescent probes were widely uncaged in living systems including various cell types, bacteria, *C. elegans*, zebrafish and mice. One of the first reports of such biorthogonal uncaging in living systems relied on the ruthenium-catalyzed Alloc-cleavage of rhodamine 110 in HeLa cells by Meggers and co-workers in 2006.<sup>188</sup> The same reaction was further expanded to other organisms.<sup>32,132,194,195,186–193</sup>

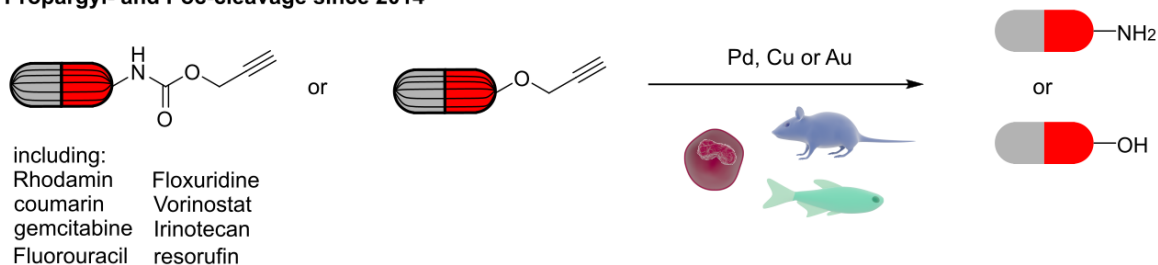
### Alloc-cleavage since 2006



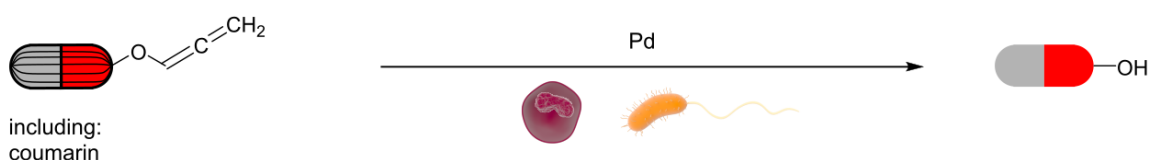
### Azide reduction since 2012



### Propargyl- and Poc-cleavage since 2014



### Allene-cleavage since 2016



### Close-to-release since 2019

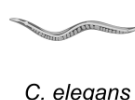
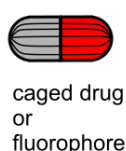
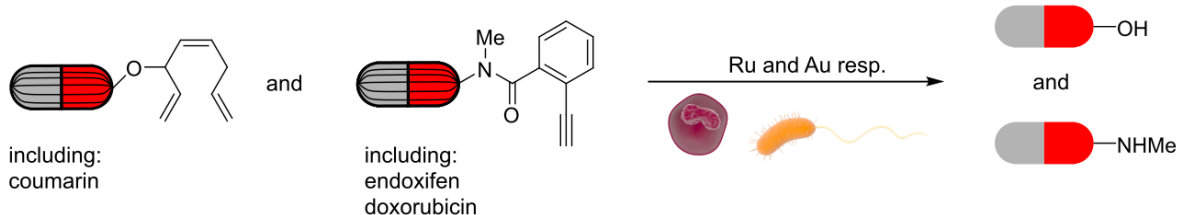


**Figure 42 Biorthogonal, transition-metal-catalyzed uncaging reactions in living systems.** Various payloads including fluorophores and active pharmaceuticals were protected with transition-metal cleavable moieties. The corresponding protected ingredients could be uncaged in various living systems including cells, bacteria, *C. elegans*, zebrafish and mice.<sup>170,171,180–189,172,190–197,173–179</sup>

In contrast to the many uncaging reactions catalyzed by Ru and Pd applied in various organisms, Au-catalyzed uncaging has been undeservingly underrepresented. In fact, Au-catalysts display remarkable biocompatibility, low toxicity, good reactivity at room temperature and a propensity to coordinate alkynes, the most widely used biorthogonal functional group. Thiols such as cysteine or glutathione are known to poison gold-catalysts and are present at significant concentrations in cells. However, smart catalyst design can protect the corresponding gold-complex from harmful metabolites while simultaneously increasing the reactivity towards the desired reaction, see chapter 1. In 2017, the groups of Tanaka and Unciti-Broceta recognized this potential and developed the first gold-catalyzed propargyl and POC-uncaging reactions in living systems and/or in biological medium.<sup>67,68</sup>

A common disadvantage of these simple uncaging reactions is the cleaved moiety which consists of a simple unsaturated ether or carbonyl group with no possibilities for further functionalization. Especially for medical applications, it would be useful to modulate the chemical and physiological properties of the prodrug to be very different to the active drug. For this reason, in 2020, the group of Tanaka developed the uncaging of large 2-alkynylbenzamides to release substituted amines in the presence of gold.<sup>198</sup> This allowed, to drastically change the hydrophilicity of the prodrug, preventing it to enter healthy cells, while upon uncaging, the corresponding chemotherapeutic could easily penetrate into the HeLa cell. Unfortunately, the reaction does require equimolar amounts of catalyst to proceed *in vivo*.

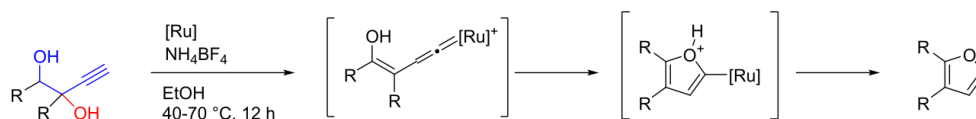
## 6.3 Results and Discussion

Driven by our progress in designing highly active gold ArMs including hydroarylates and hydroaminases, we were interested in utilizing them for biorthogonal uncaging. The driving force of generating aromatic intermediates proved to be an efficient tool to design “close-to-release” probes.<sup>197,198</sup> A Report on intramolecular cyclizations of substituted 3-butyne-1,2-diols into furans with the elimination of water in the presence of ruthenium encouraged us to design a novel “close-to-release” protocol based on profuran substrates, **Figure 43**.<sup>199</sup> We decided to utilize umbelliferone as the payload, as coumarin-based fluorophores have a large difference in fluorescence intensity upon release.<sup>200</sup> Furthermore, various active pharmaceutical ingredients (API) contain coumarin moieties.<sup>201–204</sup> From glycerol, we could synthesize TMS-

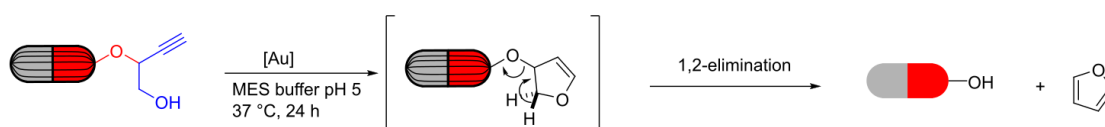
**Figure 43 Modification of the ruthenium-catalyzed dehydrative intramolecular cyclization to a gold-catalyzed “close-to-release” reaction.**<sup>205</sup>

protected profuran **3** in two steps with 80% overall yield, **Figure 44**. Following a Mitsunobu reaction with triphenylphosphine beads, umbelliferone was coupled to profuran **3** and after filtration subsequently deprotected in TBAF to yield protected umbelliferone **4**. Initial

experiments in aqueous buffers with different ruthenium-catalysts including biotinylated Nishibayashi and co-workers in 2008:



this work:



Grubbs-Hoveyda 2<sup>nd</sup> generation catalyst<sup>197</sup> were not successful in cleaving the butynol moiety from umbelliferone and releasing the payload. However, it was also reported that gold complexes can perform similar dehydrative intramolecular cyclizations to yield furan derivatives.<sup>205</sup> This motivated us to investigate the capability of our gold-ArMs from chapter 1 and 2 to catalyze this intramolecular cyclization with subsequent 1,2-elimination under aqueous conditions. To our delight, we could detect a clear blue fluorescence of the previously clear reaction vial upon exposure to UV-light already after two hours of reaction time. A simple pre-screening to evaluate the optimal cofactor and Sav-system followed. A dark 96 well plate was loaded with different biotinylated gold complexes **biot-Au 1-5** and Sav as well as Sav-SOD mutants similar to the hydroarylation screening in chapter 2, **Figure 24**. The results show a clear preference for **biot-Au 2** as the optimal cofactor and Sav-SOD K121A as the optimal Sav construct, **Figure 45**. In three hours, this ArM achieved 68% conversion of caged umbelliferone **4**.

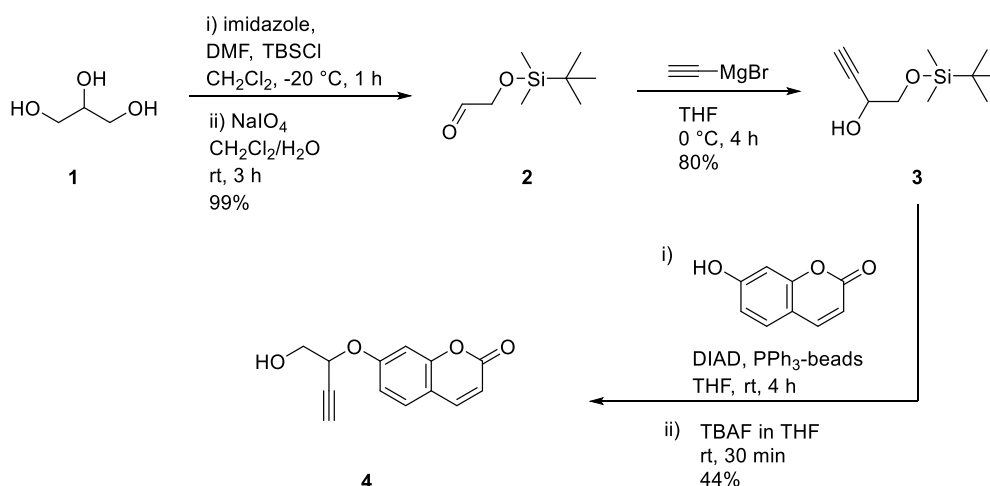


**Figure 44** Synthesis of caged umbelliferone **4** from glycerol.

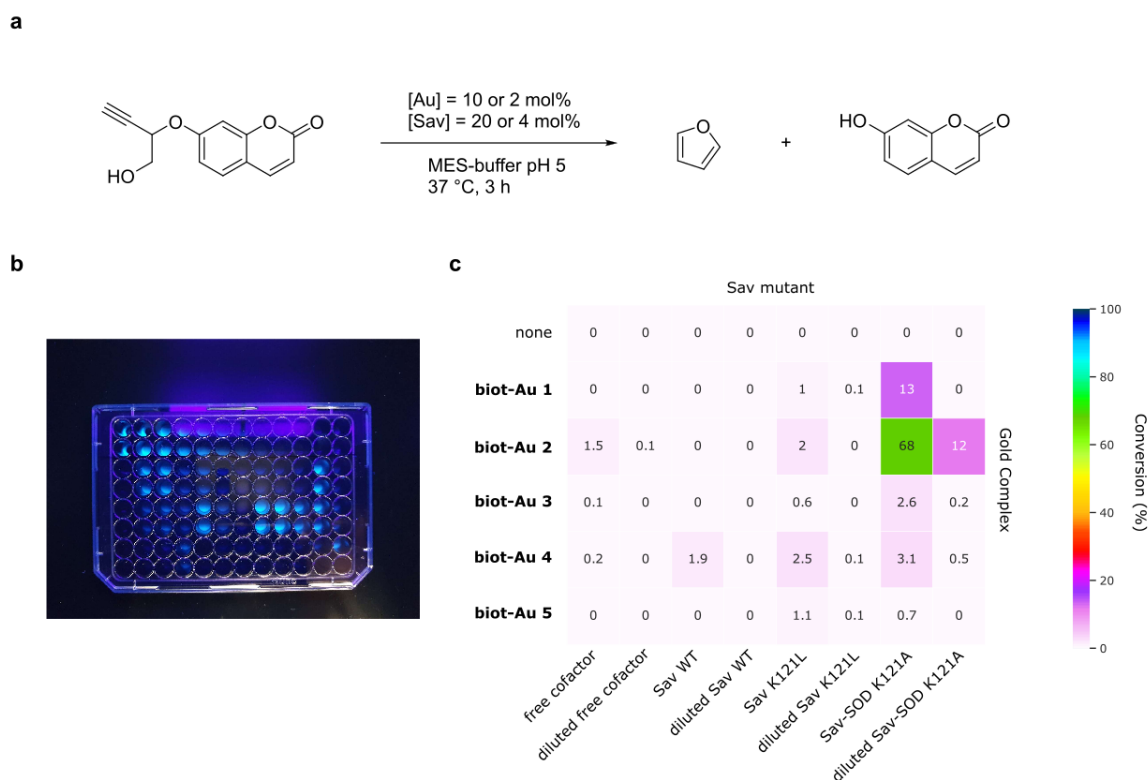


**Figure 45 Fluorescence Screening of caged umbelliferone 4.** **a** The “close-to-release” reaction of caged umbelliferone **4** to furane and umbelliferone in MES buffer was screened at concentrated (10 mol%) and dilute (5 mol%) catalyst loadings. **b** The dark 96-well plate after 24 h of reaction time. **c** Heatmap displaying the catalytic results of the screening after 3 h of reaction time.

Despite the promising initial results, the turnover of the best-performing system is still moderate (6-7 TON). Follow up screenings at lower catalyst loadings (2 mol%) yielded even lower TONs (>3). Nevertheless, Sav-SOD K121A · biot-Au 2 would be an ideal starting point for a systematic optimization protocol as detailed in chapter 2.<sup>95</sup>

In order to broaden the spectrum of our newly designed close-to-release reactions towards smaller gold catalysts, we collaborated with the Fani Group from the University Hospital of Basel. With their assistance, cancer-targeting cyclic peptides p-Cl-Phe-cyclo(D-Cys-Tyr-D-4-amino-Phe(carbamoyl)-Lys-Thr-Cys)D-Tyr-NH<sub>2</sub> (LM3) and H-D-Phe-Cys-Phe-D-Trp-Lys-Thr-Cys-Thr-OH (TATE) were prepared, **Figure 46**.<sup>206,207</sup> These peptides are known tumor-targeting somatostatin analogues and act as either agonist (TATE) or antagonist (LM3). Simplified, antagonists (commonly referred to as “blockers”) are compounds that upon binding to the target-receptor block the binding site (directly or indirectly) for potential agonists, the activity of the system is reduced or completely inhibited. Antagonists such as beta-blockers, antihistamines, etc. are widely used as APIs. On the other hand, agonists are compounds (peptides, hormones, neurotransmitter, etc.) that upon binding to the target-receptor induce an active response by the cell. Common agonists are insulin,

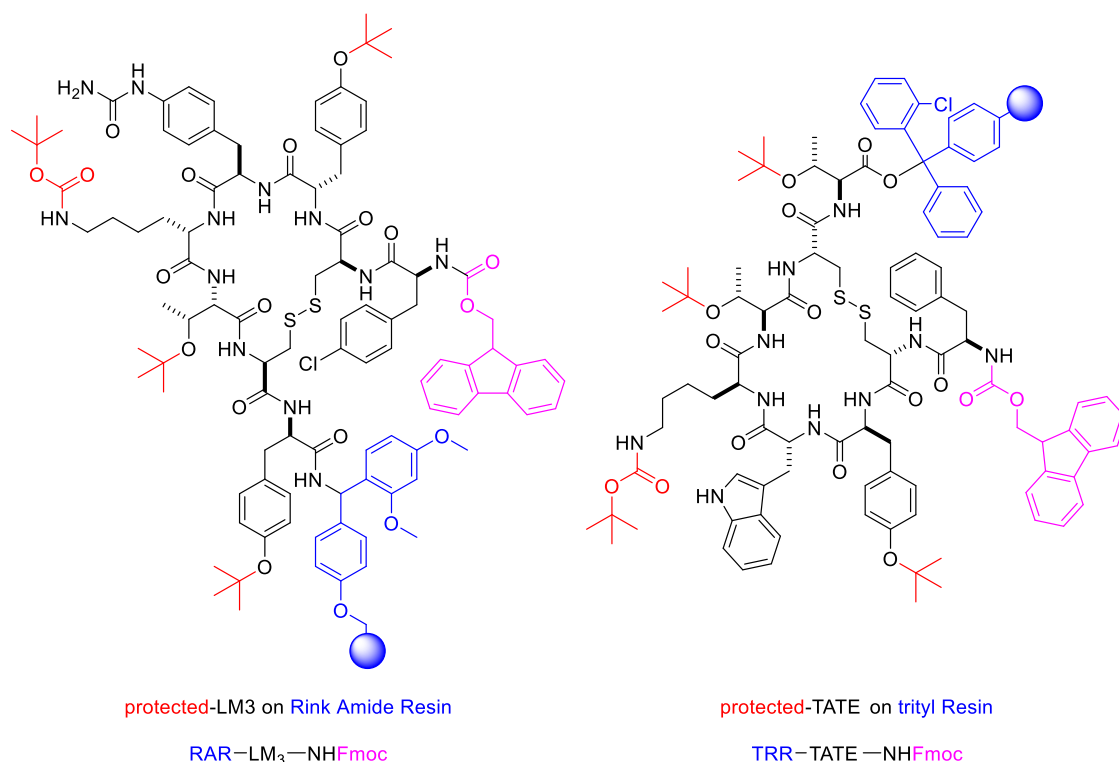


**Figure 46 Protected cancer-targeting peptides LM3 and TATE.**

calcitonin or oxytocin.<sup>208</sup> Somastotatin agonists usually internalize upon binding to the target-receptor allowing for an attached cargo to be delivered into the cell. In contrast, somastotatin antagonists display very low internalization rates and remain primarily on the cell surface. This may be a result of the fact, that antagonists usually bind to a larger population of binding sites.<sup>209</sup> Both properties can be advantageous when designing targeted treatments and have been successfully used in the clinics. In a field referred to as Theranostics (Therapy & Diagnostics), a radioactive drug is attached to the cancer-targeting peptide. The peptide delivers the radioactive moiety into the desired target cell, and allows for targeted radiotherapy at the tumors even at highly metastatic stages.<sup>210</sup>

Our plan was, to functionalize these peptides with gold to obtain cancer-targeting gold catalysts. In contrast to Sav-based ArMs, they could easily distribute around the body and selectively cover the surface of the desired cancer cells. In a further step, protected and thus less active chemotherapeutics would be added. These unreactive drugs would circulate in the blood before being selectively cleaved at the desired location to release the active therapeutic on/in the cancer cell. Obvious advantages would include the selective and catalytic release of active ingredients at the target location which would increase the therapeutic effect on the tumor while simultaneously reducing burden on healthy cells. For obvious reasons, we would first experiment with our caged umbelliferone in order to test our system for this specific close-to-release reaction.

The first step of this plan was to efficiently functionalize the peptides with gold. We decided, to follow a similar approach as with the Sav-projects. We utilized amino functionalized NHC ligands, which would be first transformed to the desired gold complex. Afterwards, the boc-group was cleaved with gaseous hydrochloric acid and the unprotected gold complex was coupled to the carboxylic acid moiety of with succinic acid modified LM3 and TATE, **Figure 47**. The gold-functionalized peptides were washed, cleaved from the resin and precipitated by addition of cold diethyl ether. Reaction control was performed using a standard three step Kaiser test which revealed the presence of free amines through the formation of a purple chromophore, **Figure 48**. A mild and a harsh cleaving protocol were tested. By only using 5% TFA, we could cleave TATE without removing the permanent protecting groups, while with 95% TFA we would cleave **TATE-Au** and simultaneously remove all protecting groups on the peptide, **Figure 49**. In contrast, HR-MS spectrum of **LM3-Au** did not display the presence of the desired compound, but a pattern slightly lower in *m/z* indicating the potential decomposition of the urea moiety on the D-4-amino-Phe(carbamoyl) fragment.

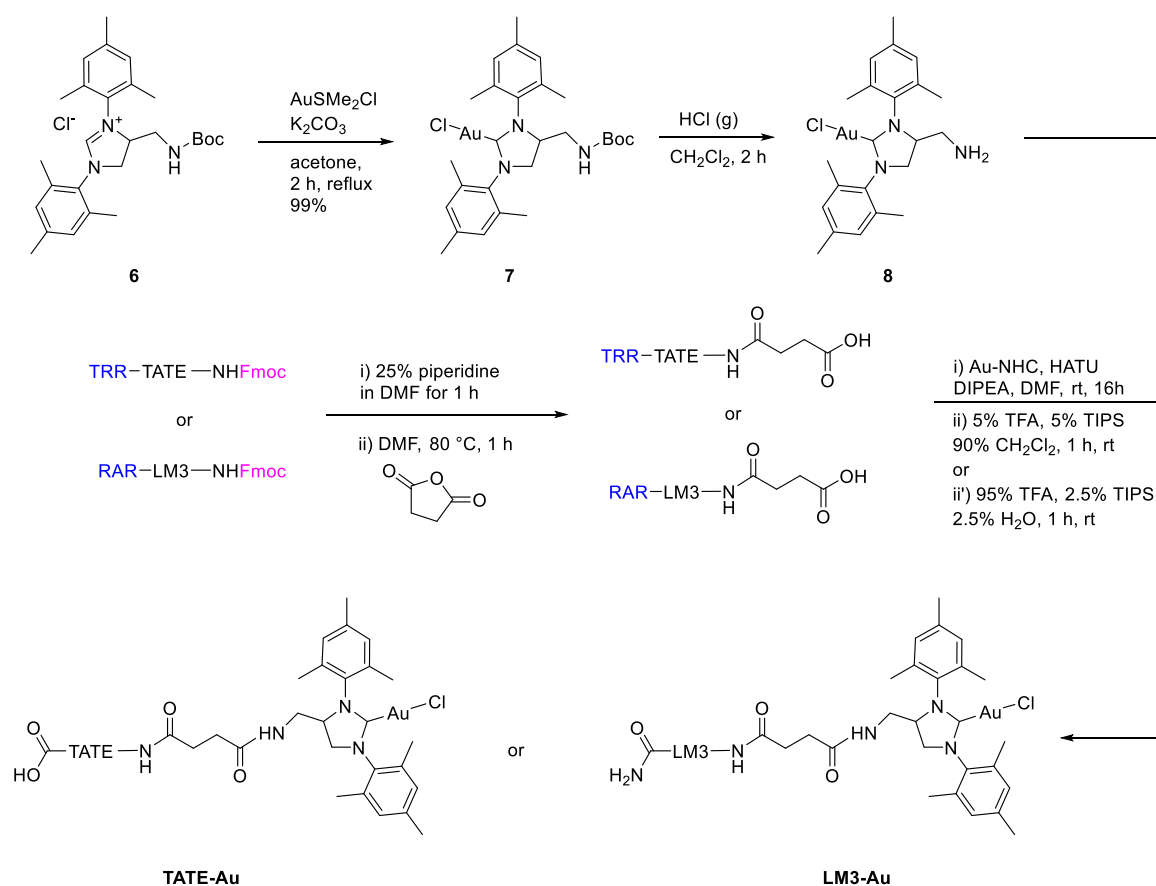


**Figure 47 Synthesis of TATE-Au and LM3-Au on trityl resin and rink amide resin, respectively.** *Ad hoc* reaction control was done via Kaiser test and later verified via HPLC into HR-MS. Yields of the gold-functionalized peptides were around 1 mg and could not be determined exactly as the reactions were performed on analytical scale.



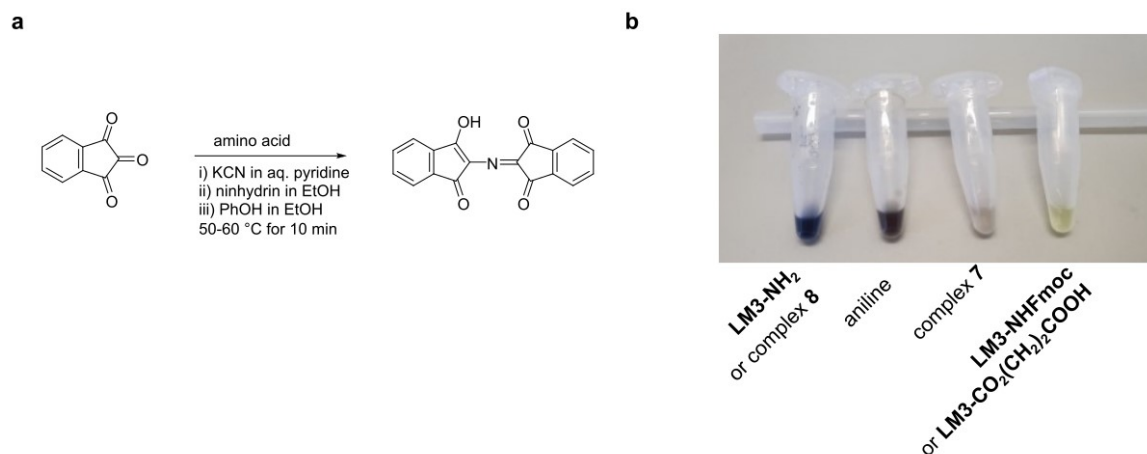


**Figure 48 Kaiser Test.** **a** The reaction of ninhydrin with amino acids leads to a complex reaction resulting in the formation of Ruhemanns Purple a strong purple chromophore. **b** Eppendorf tubes displaying common color patterns appearing in the Kaiser Test.

Before upscaling the synthesis of the most promising peptide and improving on the purification, we tested the available samples of **TATE-Au** and **LM3-Au** on the hydroarylation of pro-coumarin **9** and the close-to-release reaction of pro-furan **4** while comparing it to the performance of **biot-Au 2 · Sav-SOD K121A**, **Figure 50**. First screenings in MeCN:H<sub>2</sub>O (1:1) highlighted the capability of both gold-functionalized peptides to catalyze the hydroarylation of pro-coumarin **9** almost quantitatively, clearly outperforming the ArM under these conditions, **Error! Reference source not found.** entry 6-11.

**Figure 49 HPLC into HR-MS Spectrum of TATE-COOH<sup>+</sup> and TATE-Au<sup>2+</sup>.**

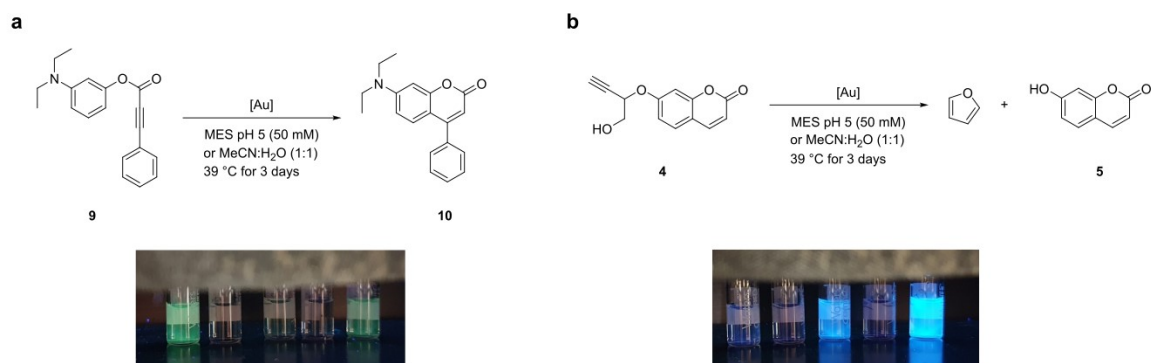


**Figure 50 Screening the gold-functionalized peptides for the intramolecular hydroarylation and the close-to-release reaction.**

In contrast, the close-to-release reaction did not proceed in aqueous acetonitrile. However, when run in MES buffer (50 mM, pH 5), the ArM displays quantitative conversion. The two peptides also catalyze the reaction, albeit in much lower conversions (11% for **LM3-Au** and 7% for **TATE-Au**). The reaction conditions seem to have a large influence on these reactions. Interestingly, while MES buffer was crucial for the close-to-release, it proved detrimental for the hydroarylation, **Table 4** entry 3 vs 4 and entry 9 vs 10. Further reaction improvement may be possible through careful tuning of the reaction conditions and/or by utilizing HPLC-purified peptide analogues which both require larger amounts of gold-functionalized peptides **LM3-Au** and **TATE-Au**. The coupling of succinic anhydride with **LM3** gave better results compared to the sequential coupling of protected succinic acid followed by deprotection and second coupling, **Table 4** entry 3 vs 3<sup>b</sup> and entry 4 vs 4<sup>b</sup>.

**Table 4** Selected Results of **LM3-Au** and **TATE-Au**-catalyzed intramolecular cyclization reactions.

Entry	Au-Catalyst	Substrate	Solvent	Conversion <sup>a</sup>
0	-	<b>4</b>	MES pH 5	0%
1	-	<b>4</b>	MeCN:H <sub>2</sub> O (1:1)	0%
2	<b>biot-Au 2</b> · Sav-SOD K121A	<b>4</b>	MES pH 5	99%
3	<b>LM3-Au</b>	<b>4</b>	MeCN:H <sub>2</sub> O (1:1)	1% (0% <sup>b</sup> )
4	<b>LM3-Au</b>	<b>4</b>	MES pH 5	11% (0% <sup>b</sup> )
5	<b>TATE-Au</b>	<b>4</b>	MES pH 5	7% (1% <sup>c</sup> )
6	-	<b>9</b>	MES pH 5	0%
7	-	<b>9</b>	MeCN:H <sub>2</sub> O (1:1)	0%
8	<b>biot-Au 2</b> · Sav-SOD K121A	<b>9</b>	MeCN:H <sub>2</sub> O (1:1)	37%
9	<b>LM3-Au</b>	<b>9</b>	MES pH 5	0%
10	<b>LM3-Au</b>	<b>9</b>	MeCN:H <sub>2</sub> O (1:1)	97%
11	<b>TATE-Au</b>	<b>9</b>	MeCN:H <sub>2</sub> O (1:1)	99% (96% <sup>c</sup> )

<sup>a</sup>The conversion was determined via UPLC-MS at 321 nm. Reaction condition  $V_{\text{tot}}$  500  $\mu\text{L}$ , [Sub] 1 mM, [Au] 20  $\mu\text{M}$  and [Sav] 40  $\mu\text{M}$  (ArM) or ca 0.5 mg/mL (peptide), 39 °C for 3 days. <sup>b</sup> **LM3-Au** synthesized via sequential coupling of protected succinic acid followed by gold complex. <sup>c</sup> **TATE-Au** cleaved under mild conditions (5% TFA, 5% TIPS in CH<sub>2</sub>Cl<sub>2</sub>)

## 6.4 Conclusion

A new close-to-release reaction was developed in which an intramolecular cyclization of butynol followed by a 1,2-elimination forms furan and releases umbelliferone. This reaction was catalyzed by chimeric ArM **biot-Au 2** · Sav-SOD K121A to yield quantitative conversion. Further studies in transferring the system *in vivo* could allow for the design of highly efficient close-to-release ArMs by utilizing the developed systematic screening protocol from chapter 2.

To facilitate the medical application of the newly designed close-to-release reaction, the system was expanded to enable gold-catalysis on cancer-targeting peptides. Gold-functionalized peptides **LM3-Au** and **TATE-Au** were synthesized in small quantities to test the highly-efficient hydroarylation of pro-coumarin substrate **9**. These peptides were also capable of releasing umbelliferone from pro-furan substrate **4** albeit in lower conversion. We discovered a large influence of the solvent which may complicate *in vivo* applications. Further attempts in designing more efficient close-to-release probes were of limited success, see appendix below. Nevertheless, we could establish the first proof-of-concept of gold-catalysis on cancer-targeting peptides by utilizing a newly designed, biorthogonal close-to-release reaction. We believe that this could be a significant step towards utilizing biorthogonal transition-metal-chemistry for targeted therapy, with an immense potential against highly metastatic cancer.

## 6.5 Appendix: Unreactive Substrates

As the optimization of reaction conditions is not a viable solution for improving a system aiming to function *in vivo*, we investigated other candidates for the gold-catalyzed close-to-release strategy. We experimented with substrates that after gold-catalyzed intramolecular cyclization could spontaneously undergo elimination or self-immolation to release a cargo. As we designed artificial hydroaminases capable of transforming 2-ethynylaniline to indole, we hypothesized that we could utilize this aromatization to force a self-immolation in para-position. We thus prepared alcohol **15** from methyl ester **11** in four steps and coupled it via a Mitsunobu reaction to umbelliferone, **Figure 51**. The corresponding substrate **16** did not react to release umbelliferone in the presence of **biot-Au 2** · Sav-SOD K121A. No diagnostic fluorescence was observed. UPLC-MS analysis revealed the presence of only the substrate in the reaction mixture, **Figure 52**.

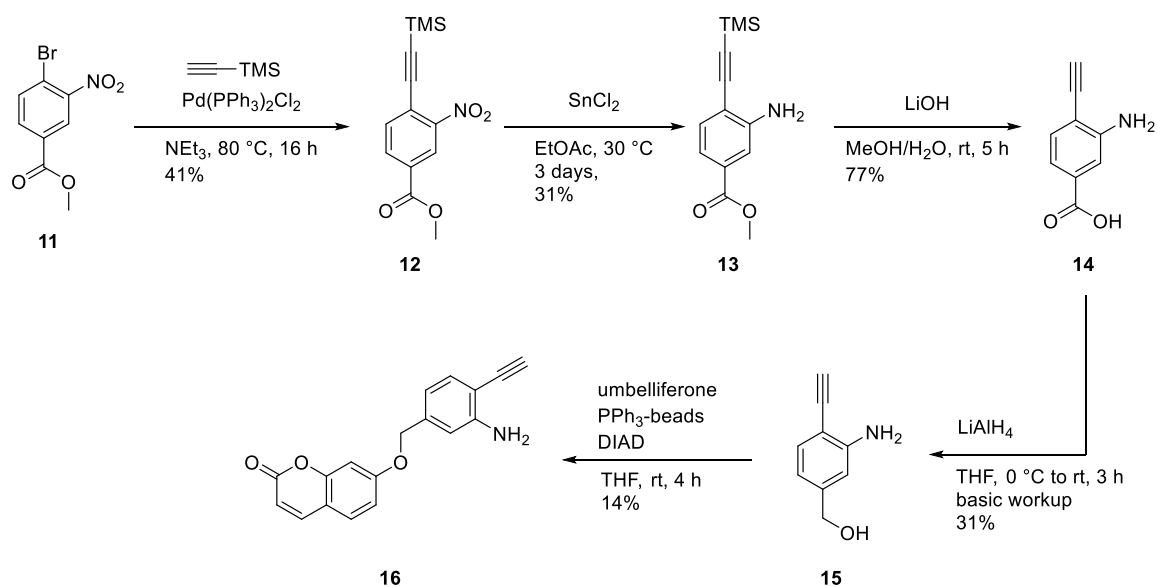


**Figure 51** The synthesis of 2-ethynylaniline-derived “close-to-release” probes.

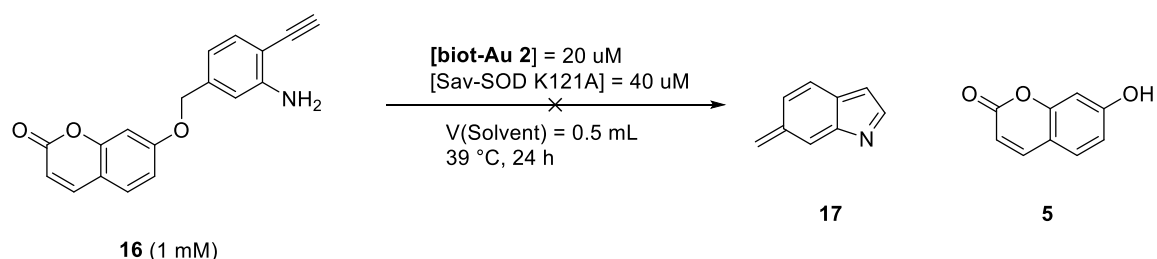


**Figure 52** A self-immolative substrate for the gold-catalyzed uncaging of umbelliferone. No conversion of **16** was detected in the presence of **biot-Au 2** · Sav-SOD K121A, only the substrate **16** was detected after UPLC-MS analysis of the reaction mixture.

Another approach was based on the synthesis of pro-naphthalene substrates that proved efficient when combined with ring-closing metathesis to release a cargo following spontaneous 1,4-elimination.<sup>197</sup> Upon zinc-coupling of propargyl bromide, mono- or dimethoxy aldehydes **18** and **19** respectively were converted into the corresponding aromatic butynol **20** and **21**, **Figure 53**. Umbelliferone was again coupled to the close-to-release substrate via a Mitsunobu reaction. The corresponding alkyne could be extended via Sonogashira coupling to yield product **24**, **Figure 54**. An interesting perk of this approach was, the electronics of the substrate could be modulated through the incorporation of functional groups on the aromatic moiety which eventually could allow to improve the spontaneous elimination. Substrates **22**, **23** and **26** were tested in the presence of a selection of ArMs, **Figure 55**. Unfortunately, we could not achieve the large improvement in cargo-release that we hoped for. We only detected little umbelliferone in the reaction media with the uncaging of **22** and **23** while no product at all with **26**.

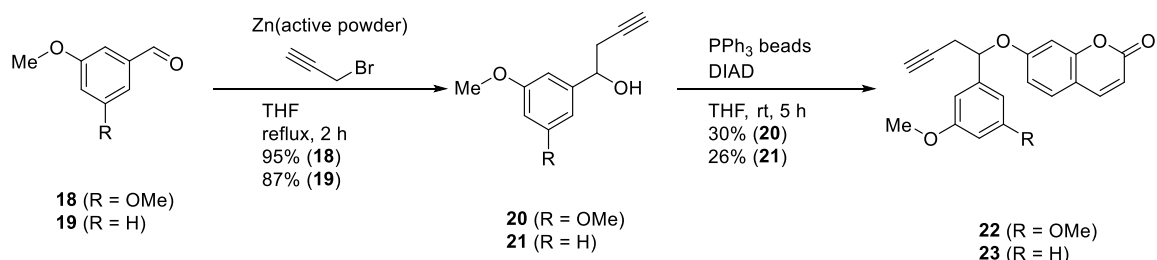


**Figure 53** The synthesis of pro-naphthalene-derived “close-to-release” substrates **22** and **23**.

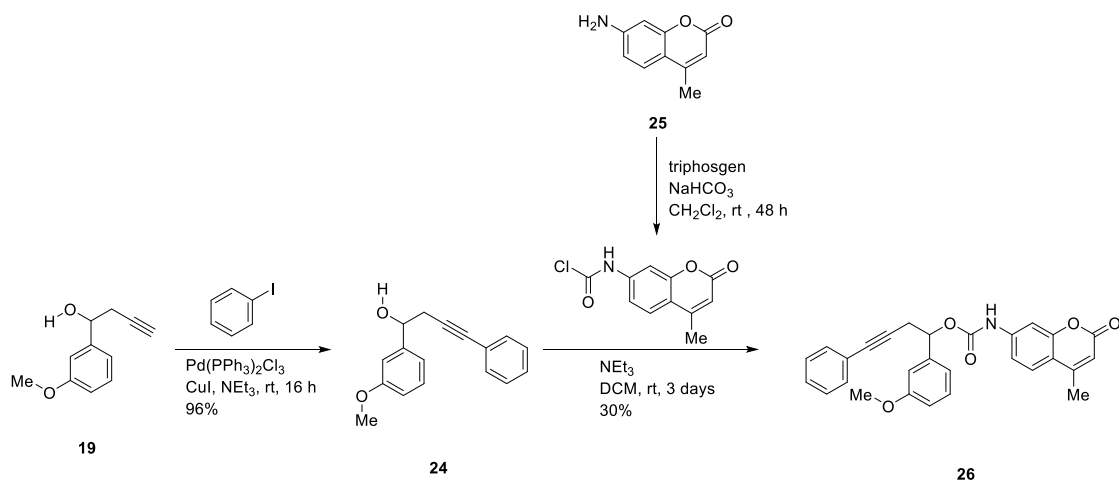


**Figure 54** The synthesis of carbamate **26** for the gold-catalyzed “close-to-release” reaction.

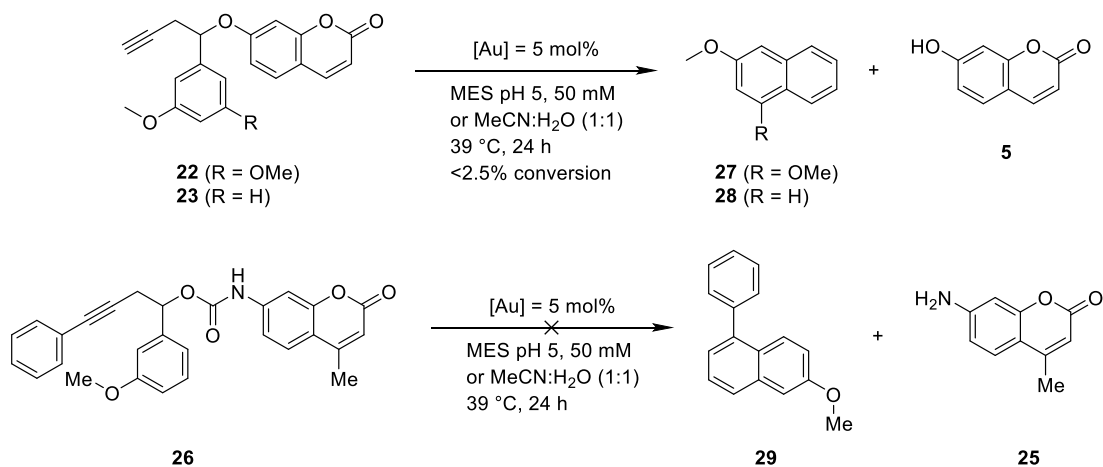


**Figure 55** Gold-catalyzed “close-to-release” reaction of pro-naphthalene in the presence of gold complexes.

## 6.6 Appendix: Sulfimide Gold-NHC complex

In order to expand the scope of ArMs towards new hosts, we set out to evaluate new protein scaffolds, thus requiring new ligand/cofactor designs. Instead of coupling a highly polar moiety such as biotin or sulfonamide over a linker to a ligand, we thought about designing an all-in-one solution: a ligand with polar moieties in the back that would simultaneously function as the binding moiety to the protein. As part of this thesis, I designed an experimental procedure to generate stable gold-complexes from the rather exotic ligands prepared by BL. The challenges herein were the protecting groups on the sulfimide moiety. They were crucial for the NHC

synthesis, but often proved difficult to cleave. Our first attempts with benzyl-protected ligand **30** were thus unsuccessful as we could not cleave the benzyl group from the gold complex **31**, **Figure 56**.

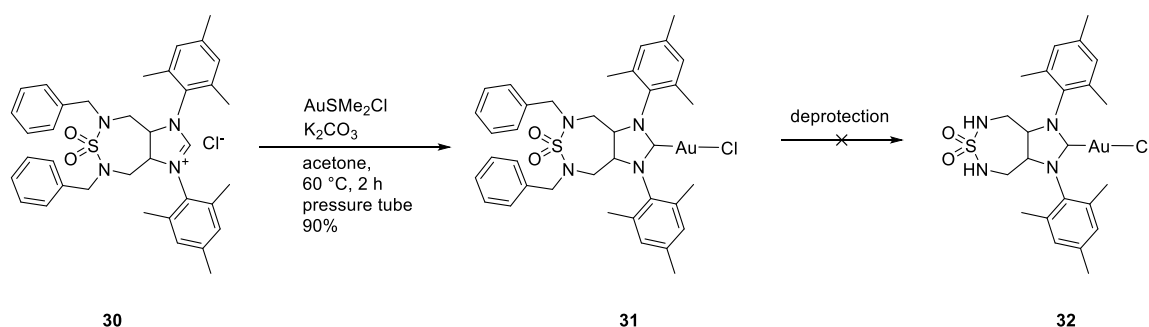


**Figure 56** No deprotection of benzyl-protected sulfimide-NHC complex **31** achieved.

As a result, a boc-protected analogue was prepared **33**, **Figure 57**. The boc-protected ligand was easily deprotected in the presence of trifluoroacetic acid in  $\text{CH}_2\text{Cl}_2$  to yield **34**. Subsequent gold insertion in the presence of an inorganic base in acetone yielded the corresponding gold complex **35**. The formation of the desired complex was confirmed by LC-MS and HR-MS, **Figure 58**. Very clean spectra displaying only the expected masses were obtained. Unfortunately,  $^1\text{H-NMR}$  analysis was ambiguous, **Figure 59**. A rather messy spectrum was obtained which, however clearly highlighted the functionalization of the ligand on the imidazolidene moiety, as no imidazolidene peak was detected. Further experiments are needed to unambiguously describe the nature of the complex and prepare preparative quantities of the complex. This should not constitute a big challenge, as a simple synthetic protocol for the complex was developed.

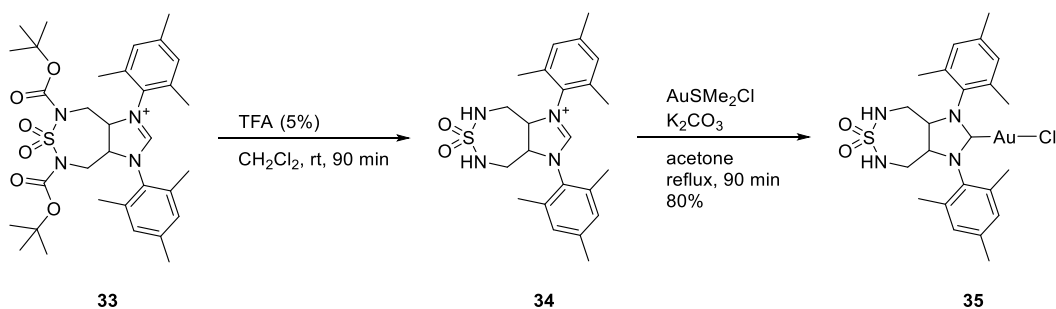
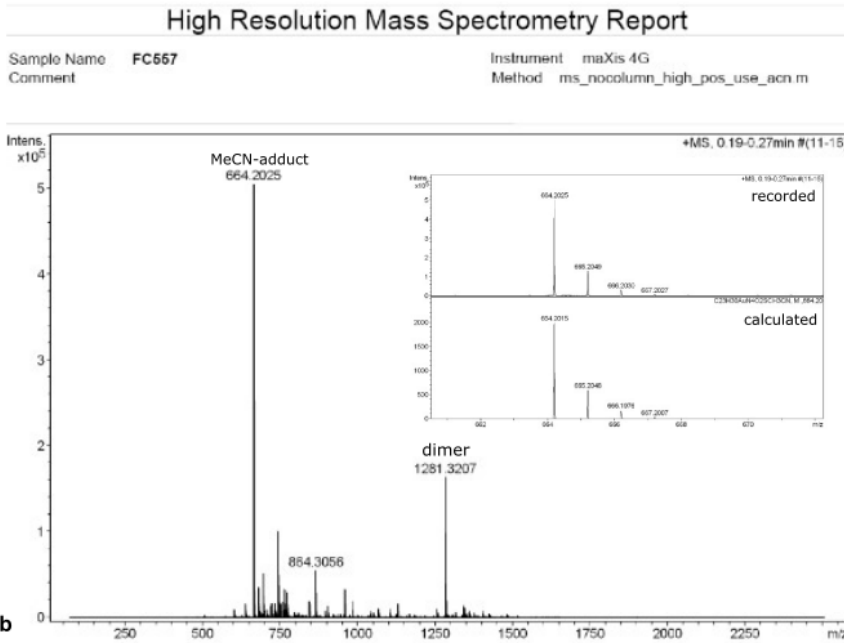


**Figure 57** The synthesis of sulfimide gold complex **35** via boc-protected sulfimide-NHC ligand **33**.

a



b

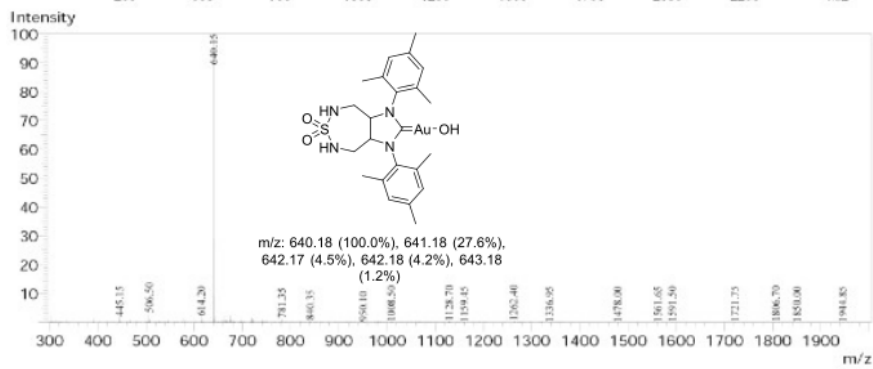


**Figure 58 HR-MS and ESI-MS spectrum of sulfimide gold complex 35. a** HR-MS spectrum after HPLC. **b** ESI-MS spectrum from direct-injection.

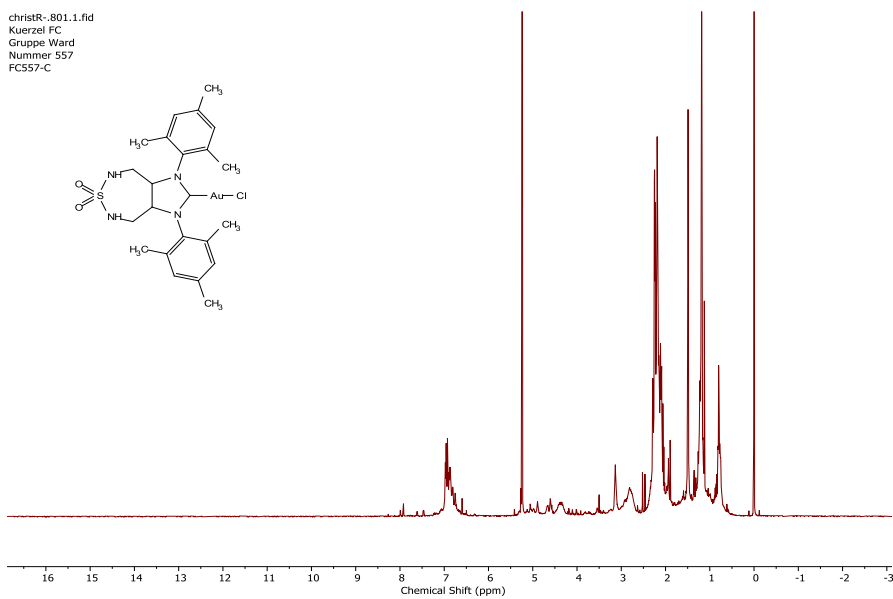


**Figure 59  $^1\text{H}$  NMR spectrum of sulfimide gold complex 35.**

## 7. Final Conclusion and Outlook

---

In the past, precious metals including palladium, ruthenium, iridium and rhodium were introduced to Sav utilizing phosphine ligands, N-heterocyclic carbenes, piano-stool complexes and sulfonamides. The repertoire of ArMs was now extended by the addition of gold(I) via biotinylated N-heterocyclic carbenes. The initial hypothesis that gold would be an ideal catalyst for biorthogonal and biocompatible reactions led to the development of gold-based hydroaminases and hydroarylates based on the biotin-streptavidin technology. These ArMs proved highly efficient (TONs > 350) and robust, displaying good activity in the periplasm of *E. coli* as well as in cell-free-extracts. As a result, screening protocols allowing for the systematic screening of Sav double-mutants (periplasm) or the directed evolution of chimeric Sav (cell-free-extracts) were established. We utilized the unique property of gold to engage in dual-gold-catalysis by designing a chimeric Sav variant where a protein fragment from superoxide dismutase shields the solvent-exposed binding pocket. The presence of two close-lying gold moieties leads to a shift in regioselectivity, giving access to a new set of products. The chimeric ArM was evolved to produce either the anti-Markovnikov product, an aromatic quinazolinone, or the Markovnikov product, an indole. Nonchimeric analogues were used for the optimization of hydroarylates and hydroaminases. The latter catalyzed the transformation of 2-ethynyl aniline to indole, a crucial metabolite in the tryptophan synthase pathway. Similar approaches to access indole via palladium-based ArMs were not successful due to synthetic challenges around the substrate and a lack of biostability of the cofactor.

Bioorthogonal gold(I) catalysis was extended beyond ArM technology, by functionalizing somastotatin analogues LM3 and TATE with gold(I) N-heterocyclic carbene complexes. The corresponding gold peptides were stable and catalytically active. Coumarin analogues were obtained quantitatively via hydroarylation induced by gold-functionalized peptides without the need of base or additives. Furthermore, we designed a new close-to-release protocol allowing for the release of umbelliferone by the addition of gold-functionalized ArMs or peptides. Therein, pro-furan moieties are used to temporarily protect hydroxyl groups. In the presence of gold ArMs or gold peptides this group is cleaved after intramolecular cyclization followed by 1,2-elimination to release the alcohol and furan.

In the course of this thesis, the first systematic screening of gold ArMs, the first dual-gold ArMs and the first gold-functionalized somastotatin analogues were designed, optimized and successfully implemented in gold catalysis. The remarkable acceleration in catalytic performance of the gold cofactor upon incorporation into Sav and the remarkable biostability makes these gold ArMs privileged catalyst for biorthogonal catalysis. As the field of gold catalysis is steadily expanding, there will be more and more reactions available for gold-ArM



technology where genetic optimization allows for exceptional activity and stereoselectivity. As part of this study, the gold-ArMs were limited to alkynes, as other substrates were unreactive. Alternative ligand design may allow to expand this reactivity towards alkenes or allenes. N,O-ligands have shown good activity in aqueous solvent coordinating and stabilizing Au(III), after biotinylation they may allow to expand the substrate scope beyond alkynes.<sup>211-214</sup>

In parallel to these projects, a novel “close-to-release” reaction was developed which is compatible with the gold ArMs and gold peptides from our now established repertoire. So far, umbelliferone was efficiently uncaged in MES buffer. Substrate derivatization proved challenging but could give access to promising pro-drugs. Especially for metastatic cancer, the targeted release of chemotherapeutics could drastically mitigate side effects. The synthesis of pro-furan-protected doxorubicin or endoxifen could give a good starting point to investigate the therapeutic feasibility of this novel reaction. Furthermore, preparation, purification and characterization of the gold-peptides must be improved before further investigation of its utility in prodrug activation.

## 8. Experimental and Supplementary Information

---

### 8.1 General Methods:

Procedures for the synthesis of the gold complexes were carried out in oven-dried glassware under a dry nitrogen atmosphere with rigorous exclusion of moisture and oxygen from reagents and glassware using standard Schlenk techniques or a MBraun Labstar glove box workstation. Dry solvents were directly purchased from Acros Organics and used without further purification. Water used for molecular biology and in the catalytic reactions was purified by Milli-Q Advantage system. Degassed solvents were prepared via three freeze-pump-thaw cycles.

Chemicals were purchased from Sigma Aldrich, Acros Organics, Alfa Aesar or Fluorochem and used without further purification. All catalytic reactions were carried out with non-degassed solvents under air. Temperature was maintained using Thermowatch-controlled heating blocks. Analytical thin-layer chromatography (TLC) was performed on pre-coated Merck silica gel 60 F<sub>254</sub> plates (0.25 mm) and visualized using UV light. Flash column chromatography was carried out on a Biotage Isolera using *Silicycle* SiliaFlash P60 (230-400 mesh) filled KP-Sil columns unless stated otherwise. Concentration refers to the removal of volatile solvents via distillation using a rotary evaporator Büchi R-300HL equipped with a thermostated bath B-300, a vacuum regulator CVC-3000, followed by residual solvent removal under high vacuum.

<sup>1</sup>H NMR (500 MHz) and <sup>13</sup>C NMR (126 MHz) spectra were recorded at room temperature on a Bruker 500 MHz or 600 MHz spectrometer. Data are summarized with the coupling constants described as follows: chemical shift, multiplicity (s = singlet, d = doublet, t = triplet, q = quartet, m = multiplet, br = broad signal, bs = broad singlet, dd = doublet doublets, dt = doublet triplets, dq = doublet quartets, td = triplet doublets, ddd = doublet of doublet of doublets, ddt = doublet of doublet of triplets, dtd = doublet of triplet of doublets, dddd = doublet of doublet of doublet of doublets), coupling constants in Hertz (Hz). Chemical shifts ( $\delta$ ) are reported in ppm relative to the residual solvent peak. Peaks were fully assigned using 2D-NMR spectroscopy including COSY, NOESY, HMBC and HMQC. The NMR spectra were analyzed using MestreNova© NMR data processing software.

GC-MS analysis was performed on a Shimadzu GCMS-QP2010S equipped with Agilent HP1-1MS (length: 30 m; Diameter: 0.25 mm; Film: 0.25  $\mu$ M). GC column flow 2.05 mL/min Helium.

High-resolution mass spectrometry (HR-MS) was performed by the analytical facility of the chemistry department of the University of Basel on a Bruker maXis 4G QTOF ESI mass

spectrometer coupled to a Shimadzu LC. Prior to HR-MS submission, all samples were characterized via direct injection or LC from solutions in MeOH (gold complex synthesis) or MeCN (substrate synthesis) on a Shimadzu LCMS-2020. Native-MS was performed via direct injection (aqueous buffer) to a Bruker maXis 4G QTOF ESI mass spectrometer.

Fluorescence assays were recorded on a Tecan fluorimeter Infinite M1000Pro. Samples were prepared on a clear 96-well plate. Measurements settings for Fluorescence Top Reading: Excitation Wavelength 485 nm, Emission Wavelength 520 nm, Excitation Bandwidth 5 nm, Emission Bandwidth 5 nm, Gain 94 (100%), Number of slashes 10, Flash frequency 400 Hz, Integration time 20  $\mu$ s, Lag time 0 s, Settle Time 100 ms.

UPLC experiments were performed on an Acquity UPLC-H Class Bio from Waters equipped with a PDA set to 254 nm and a SQ detector 2 with the following column: ACQUITY UPLC, HSS T3 1.8  $\mu$ m, 2.1  $\times$  100 mm. Solvents for UPLC analysis were Milli-Q water and LC-MS grade acetonitrile, each containing 0.1% formic acid, later on referred to as (C) and (D). The flow rate was set to 0.60 ml/min and the column temperature was maintained at 40  $^{\circ}$ C. The method used includes the following parameters:  $t_{\text{total}}$  = 9.00 min with 0.00 min – 90% C; 0.60 min – 60% C; 6.95 min – 42% C; 7.20 min – 10% C; 7.80 min 10% C; 8.00 min – 90% C; 8.50 min – 90% C end. Mass detection was performed in scan mode for positive ions (cone voltage 40 V, desolvation temperature: 600  $^{\circ}$ C) and SIR ( $m/z$  = corresponding substrate & products). Determined TONs and yields for catalysis are a mean of multiple sets of runs determined in relation to an internal standard (phthalane) at 254 nm processed with Waters TargetLynx unless stated otherwise. The standard deviation is displayed as error bars.

Molecular biology reagents were purchased from New England Biolabs (NEB), Integrated DNA Technologies (IDT), and Macherey-Nagel and were used as described in the accompanying protocols.

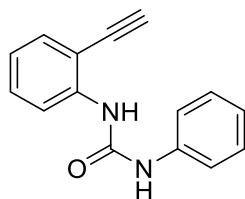
## 8.2 Chapter 1: Dual-Gold-based chimeric ArMs

### Substrate Synthesis

#### **General procedure A: urea substrates 1 and 1a-1f:**

The urea bearing substrates **1-1f** were prepared according to a modified procedure of Medio-Simon and co-workers.<sup>96</sup> A 10 mL pressure tube equipped with a stirring bar was charged with the corresponding 2-alkynylaniline (1 eq) and the phenyl isocyanate (1 eq). The tube was sealed after the addition of CH<sub>2</sub>Cl<sub>2</sub> (2 mL/mmol) and placed in a heating block at 80 °C. After 5 h, the heating was stopped and the mixture was stirred until it reached room temperature. The urea precipitated as a white solid and was collected on a ground-glass frit. The white solid was washed by adding small portions of cold CH<sub>2</sub>Cl<sub>2</sub> (2 mL). The precipitate was dried *in vacuo* yielding the urea as a white solid.

#### **Substrate 1**



The product was prepared according to the general procedure A and isolated as a white solid (1.20 g, 5.10 mmol, 99%). The spectra are in agreement with literature data.<sup>96</sup>

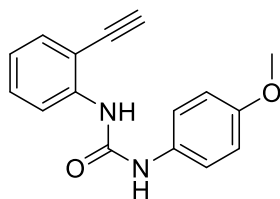
<sup>1</sup>H NMR (500 MHz, DMSO-*d*<sub>6</sub>) δ 9.57 (s, 1H), 8.19 (s, 1H), 8.13 (d, *J* = 8.4 Hz, 1H), 7.52 – 7.45 (m, 2H), 7.43 (dd, *J* = 7.7, 1.6 Hz, 1H), 7.35 (td, *J* = 8.5, 7.9, 1.6 Hz, 1H), 7.30 (t, *J* = 7.9 Hz, 2H), 6.99 (td, *J* = 7.5, 1.3 Hz, 2H), 4.65 (s, 1H).

<sup>13</sup>C NMR (126 MHz, DMSO-*d*<sub>6</sub>) δ 152.18, 140.93, 139.52, 132.48, 129.65, 128.89, 122.12, 121.94, 119.24, 118.29, 110.55, 87.46, 79.53.

UPLC-MS: *T*<sub>R</sub> = 4.21 min; MS (ESI, pos) *m/z*: 237.24 [100 %, M+H]<sup>+</sup>.

HR-MS (ESI, pos): *m/z* calcd. for C<sub>15</sub>H<sub>12</sub>N<sub>2</sub>ONa<sup>+</sup> 259.0842 found 259.0841 [M+Na]<sup>+</sup>.

### Substrate 1a



The product was prepared according to the general procedure A and isolated as a white solid (439 mg, 1.65 mmol, 82%).  $R_f$  0.57 (cyclohexane:ethyl acetate 80:20)

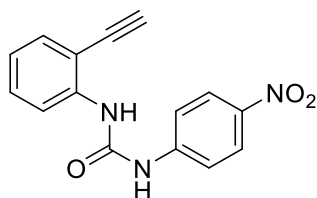
$^1\text{H}$  NMR (500 MHz,  $\text{DMSO-}d_6$ )  $\delta$  9.40 (s, 1H), 8.13 (d,  $J = 8.4$  Hz, 1H), 8.10 (s, 1H), 7.42 (dd,  $J = 7.7, 1.6$  Hz, 1H), 7.37 (d,  $J = 9.0$  Hz, 2H), 7.33 (t,  $J = 7.6$  Hz, 1H), 6.97 (t,  $J = 7.5$  Hz, 1H), 6.88 (d,  $J = 8.9$  Hz, 2H), 4.65 (s, 1H), 3.72 (s, 3H).

$^{13}\text{C}$  NMR (126 MHz,  $\text{DMSO-}d_6$ )  $\delta$  154.63, 152.29, 141.12, 132.49, 132.42, 129.61, 121.67, 120.08, 119.00, 114.08, 110.29, 87.41, 79.53, 55.17.

UPLC-MS:  $T_R = 3.97$  min; MS (ESI, pos)  $m/z$ : 266.83 [100 %,  $\text{M}+\text{H}$ ] $^+$ .

HR-MS (ESI, pos):  $m/z$  calcd. for  $\text{C}_{16}\text{H}_{14}\text{N}_2\text{O}_2\text{Na}^+$  289.0947 found 289.0947 [ $\text{M}+\text{Na}$ ] $^+$ .

### Substrate 1b



The product was prepared according to the general procedure A and isolated as a pale yellow solid (445 mg, 1.58 mmol, 79%).  $R_f$  0.44 (cyclohexane:ethyl acetate 80:20)

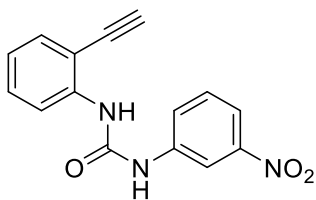
$^1\text{H}$  NMR (500 MHz,  $\text{DMSO-}d_6$ )  $\delta$  10.26 (s, 1H), 8.40 (s, 1H), 8.21 (d,  $J = 9.2$  Hz, 2H), 8.11 (d,  $J = 8.4$  Hz, 1H), 7.71 (d,  $J = 9.1$  Hz, 2H), 7.47 (dd,  $J = 7.8, 1.6$  Hz, 1H), 7.42 – 7.35 (m, 1H), 7.05 (t,  $J = 7.5$  Hz, 1H), 4.70 (s, 1H).

$^{13}\text{C}$  NMR (126 MHz,  $\text{DMSO-}d_6$ )  $\delta$  151.73, 146.12, 141.24, 140.16, 132.59, 129.72, 125.22, 122.69, 119.61, 117.59, 111.22, 87.68, 79.33.

UPLC-MS:  $T_R = 5.30$  min; MS (ESI, pos)  $m/z$ : 282.15 [100 %,  $\text{M}+\text{H}$ ] $^+$ .

HR-MS (ESI, pos):  $m/z$  calcd. for  $\text{C}_{15}\text{H}_{11}\text{N}_3\text{O}_3\text{H}^+$  282.0873 found 282.0876 [ $\text{M}+\text{H}$ ] $^+$ .

### Substrate 1c



The product was prepared according to the general procedure A and isolated as a white solid (535 mg, 1.90 mmol, 95%).  $R_f$  0.43 (cyclohexane:ethyl acetate 80:20)

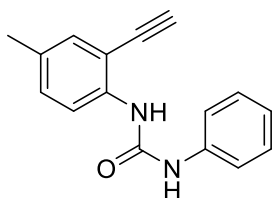
$^1\text{H}$  NMR (500 MHz,  $\text{DMSO-}d_6$ )  $\delta$  10.09 (s, 1H), 8.59 – 8.52 (m, 1H), 8.29 (s, 1H), 8.14 (d,  $J$  = 8.4 Hz, 1H), 7.85 (dd,  $J$  = 8.2, 2.3 Hz, 1H), 7.73 – 7.68 (m, 1H), 7.59 (t,  $J$  = 8.1 Hz, 1H), 7.46 (dd,  $J$  = 7.7, 1.5 Hz, 1H), 7.42 – 7.34 (m, 1H), 7.04 (t,  $J$  = 7.5 Hz, 1H), 4.70 (s, 1H).

$^{13}\text{C}$  NMR (126 MHz,  $\text{DMSO-}d_6$ )  $\delta$  152.09, 148.18, 140.82, 140.37, 132.53, 130.23, 129.72, 124.21, 122.45, 119.44, 116.55, 112.11, 110.97, 87.62, 79.36.

UPLC-MS:  $T_R$  = 5.20 min; MS (ESI, pos)  $m/z$ : 281.96 [100 %,  $\text{M}+\text{H}$ ] $^+$ .

HR-MS (ESI, pos):  $m/z$  calcd. for  $\text{C}_{15}\text{H}_{11}\text{N}_3\text{O}_3\text{H}^+$  282.0873 found 282.0876 [ $\text{M}+\text{H}$ ] $^+$ .

### Substrate 1d



The product was prepared according to the general procedure A and isolated as a white solid (219 mg, 0.875 mmol, 83%).

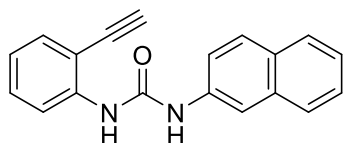
$^1\text{H}$  NMR (500 MHz,  $\text{DMSO-}d_6$ )  $\delta$  9.49 (s, 1H), 8.11 (s, 1H), 7.99 (d,  $J$  = 8.5 Hz, 1H), 7.45 (d,  $J$  = 8.4 Hz, 2H), 7.29 (t,  $J$  = 7.9 Hz, 2H), 7.25 (d,  $J$  = 2.1 Hz, 1H), 7.16 (dd,  $J$  = 8.7, 2.1 Hz, 1H), 6.98 (t,  $J$  = 7.3 Hz, 1H), 4.60 (s, 1H), 2.23 (s, 3H).

$^{13}\text{C}$  NMR (126 MHz,  $\text{DMSO-}d_6$ )  $\delta$  152.25, 139.62, 138.49, 132.48, 131.00, 130.33, 128.86, 122.00, 119.43, 118.22, 110.60, 86.98, 79.71, 19.95.

UPLC-MS:  $T_R$  = 5.28 min; MS (ESI, pos)  $m/z$ : 250.91 [100 %,  $\text{M}+\text{H}$ ] $^+$ .

HR-MS (ESI, pos):  $m/z$  calcd. for  $\text{C}_{16}\text{H}_{14}\text{N}_2\text{ONa}^+$  273.0998 found 273.0999 [ $\text{M}+\text{Na}$ ] $^+$ .

### Substrate 1e



The product was prepared according to the general procedure A and isolated as a white solid (390 mg, 1.362 mmol, 68%).

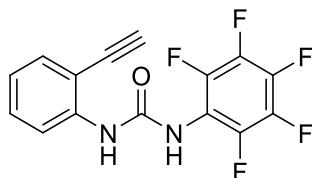
$^1\text{H}$  NMR (500 MHz,  $\text{DMSO-}d_6$ )  $\delta$  9.81 (s, 1H), 8.29 (s, 1H), 8.19 (dd,  $J = 8.5, 1.1$  Hz, 1H), 8.14 (d,  $J = 2.1$  Hz, 1H), 7.85 (m, 2H), 7.80 (m, 1H), 7.50 (dd,  $J = 8.8, 2.2$  Hz, 1H), 7.46 (m, 2H), 7.37 (m, 2H), 7.01 (td,  $J = 7.5, 1.2$  Hz, 1H), 4.69 (s, 1H).

$^{13}\text{C}$  NMR (126 MHz,  $\text{DMSO-}d_6$ )  $\delta$  152.25, 140.86, 137.15, 133.70, 132.50, 129.64, 129.18, 128.50, 127.45, 127.03, 126.38, 124.08, 121.99, 119.55, 119.25, 113.63, 110.61, 87.51, 79.51.

UPLC-MS:  $T_R = 7.55$  min; MS (ESI, pos)  $m/z$ : 287.24 [100 %,  $\text{M}+\text{H}$ ] $^+$ .

HR-MS (ESI, pos):  $m/z$  calcd. for  $\text{C}_{19}\text{H}_{14}\text{N}_2\text{OH}^+$  287.1179 found 287.1174 [ $\text{M}+\text{H}$ ] $^+$ ;  $m/z$  calcd. for  $\text{C}_{19}\text{H}_{14}\text{N}_2\text{ONa}^+$  309.0998 found 309.0995 [ $\text{M}+\text{Na}$ ] $^+$ ;

### Substrate 1f



The product was prepared according to the general procedure A and isolated as a white solid (990 mg, 3.03 mmol, 99%).

$^1\text{H}$  NMR (500 MHz,  $\text{DMSO-}d_6$ )  $\delta$  9.50 (s, 1H), 8.51 (s, 1H), 8.07 (dd,  $J = 8.5, 1.1$  Hz, 1H), 7.46 (dd,  $J = 7.8, 1.6$  Hz, 1H), 7.36 (ddd,  $J = 8.7, 7.4, 1.7$  Hz, 1H), 7.03 (td,  $J = 7.6, 7.5, 1.2$  Hz, 1H), 4.69 (s, 1H).

$^{13}\text{C}$  NMR (126 MHz,  $\text{DMSO-}d_6$ )  $\delta$  151.58, 140.34, 132.51, 129.74, 122.53, 119.11, 110.89, 87.67, 79.22.

UPLC-MS:  $T_R = 5.38$  min; MS (ESI, pos)  $m/z$ : 326.26 [100 %,  $\text{M}+\text{H}$ ] $^+$ .

HR-MS (ESI, pos):  $m/z$  calcd. for  $\text{C}_{15}\text{H}_7\text{F}_5\text{N}_2\text{ONa}^+$  349.0371 found 349.0366 [ $\text{M}+\text{Na}$ ] $^+$ .

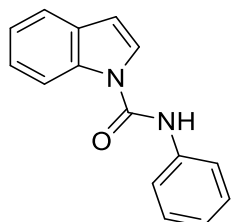
### General procedure B: indole products 2 and 2a-2f

Procedure B1: Indole (1 eq) as a solution in dry THF (5 mL/mmol) was added dropwise to a solution of sodium (1.3 eq, cut in small pieces) in dry THF (5 mL/mmol). The mixture was

stirred under reflux for 16 h and then cooled to room temperature. The selected isocyanate (1 eq) as a solution in dry THF (5 mL/mmol) was added dropwise and the mixture was stirred for 5 h at room temperature. The mixture was cooled to 0 °C before quenching the reaction with water (15 mL). The solution was diluted with ethyl acetate (15 mL), transferred to a separating funnel and extracted with ethyl acetate (3x10 mL). The combined organic phases were washed with brine (10 mL), dried over magnesium sulfate and the solvent was removed *in vacuo*. The product was recrystallized from a mixture of petroleum ether and diethyl ether.

Procedure B2: Indole (1 eq) as a solution in dry THF (5 mL/mmol) was added dropwise to an ice-cold suspension of NaH (1.3 eq as a 60% suspension in mineral oil) in dry THF (5 mL/mmol). The solution was stirred for 30 min at 0 °C. Then, the selected isocyanate (1 eq) was added dropwise as a solution in dry THF (5 mL/mmol) upon which the solution turned red. The mixture was allowed to warm to room temperature and stirred for 16 h. The mixture was cooled to 0 °C and then quenched with water (15 mL). The solution was diluted with ethyl acetate (15 mL), transferred to a separating funnel and extracted with ethyl acetate (3x10 mL). The combined organic phases were washed with brine (10 mL), dried over magnesium sulfate and the solvent was removed *in vacuo*. The crude was purified via flash column chromatography (KP-Sil 50 g, linear gradient of 10% to 20% ethyl acetate in cyclohexane).

## Product 2



The indole **2** was prepared according to the general procedure B1 and isolated as white crystals (752 mg, 3.18 mmol, 32%).

<sup>1</sup>H NMR (500 MHz, DMSO-*d*<sub>6</sub>) δ 10.05 (s, 1H), 8.23 (d, *J* = 8.2 Hz, 1H), 8.04 (d, *J* = 3.6 Hz, 1H), 7.70 – 7.59 (m, 3H), 7.39 (dd, *J* = 8.5, 7.3 Hz, 2H), 7.30 (ddd, *J* = 8.3, 7.1, 1.4 Hz, 1H), 7.24 – 7.20 (m, 1H), 7.14 (td, *J* = 7.4, 1.1 Hz, 1H), 6.76 (d, *J* = 3.6 Hz, 1H).

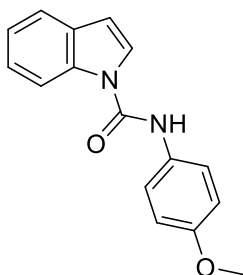
<sup>13</sup>C NMR (126 MHz, DMSO-*d*<sub>6</sub>) δ 149.85, 138.39, 135.40, 129.70, 128.75, 125.58, 123.88, 123.75, 122.23, 120.85, 118.17, 115.04, 106.41.

UPLC-MS: T<sub>R</sub> = 5.09 min; MS (ESI, pos) *m/z*: 237.17 [100 %, M+H]<sup>+</sup>.

HR-MS (ESI, pos): *m/z* calcd. for C<sub>15</sub>H<sub>12</sub>N<sub>2</sub>ONa<sup>+</sup> 259.0842 found 259.0840 [M+Na]<sup>+</sup>.



## Product 2a



The indole **2a** was prepared according to the general procedure B2 and isolated as a white solid (232 mg, 0.871 mmol, 87%).  $R_f$  0.36 (cyclohexane:ethyl acetate 80:20)

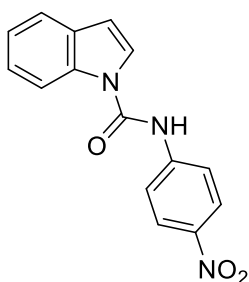
$^1\text{H}$  NMR (500 MHz,  $\text{DMSO-}d_6$ )  $\delta$  9.90 (s, 1H), 8.22 (d,  $J = 8.3$  Hz, 1H), 8.01 (d,  $J = 3.6$  Hz, 1H), 7.63 (d,  $J = 7.7$  Hz, 1H), 7.54 (d,  $J = 8.9$  Hz, 2H), 7.28 (t,  $J = 7.7$  Hz, 1H), 7.21 (t,  $J = 7.4$  Hz, 1H), 6.96 (d,  $J = 8.9$  Hz, 2H), 6.74 (d,  $J = 3.6$  Hz, 1H), 3.76 (s, 3H).

$^{13}\text{C}$  NMR (126 MHz,  $\text{DMSO-}d_6$ )  $\delta$  155.88, 149.93, 135.39, 131.10, 129.60, 125.42, 123.65, 122.78, 122.08, 120.79, 115.01, 113.91, 106.26, 55.23.

UPLC-MS:  $T_R = 4.94$  min; MS (ESI, pos)  $m/z$ : 267.23 [100 %,  $\text{M}+\text{H}^+$ ].

HR-MS (ESI, pos):  $m/z$  calcd. for  $\text{C}_{16}\text{H}_{14}\text{N}_2\text{O}_2\text{H}^+$  267.1128 found 267.1125 [ $\text{M}+\text{H}^+$ ].

## Product 2b



The indole **2b** was prepared according to the general procedure B2 and isolated as a pale yellow solid (221 mg, 0.786 mmol, 79%).  $R_f$  0.18 (cyclohexane:ethyl acetate 80:20)

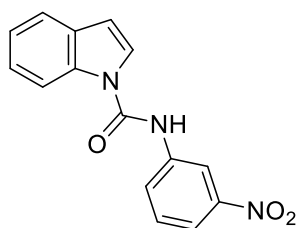
$^1\text{H}$  NMR (500 MHz,  $\text{DMSO-}d_6$ )  $\delta$  10.60 (s, 1H), 8.30 (d,  $J = 9.2$  Hz, 2H), 8.23 (d,  $J = 8.3$  Hz, 1H), 8.06 (d,  $J = 3.7$  Hz, 1H), 7.95 (d,  $J = 9.2$  Hz, 2H), 7.66 (d,  $J = 7.7$  Hz, 1H), 7.33 (t,  $J = 7.7$  Hz, 1H), 7.25 (t,  $J = 7.4$  Hz, 1H), 6.81 (d,  $J = 3.7$  Hz, 1H)

$^{13}\text{C}$  NMR (126 MHz,  $\text{DMSO-}d_6$ )  $\delta$  149.56, 145.09, 142.53, 135.34, 129.86, 125.66, 124.84, 124.06, 122.68, 121.00, 119.93, 115.09, 107.09.

UPLC-MS:  $T_R = 6.10$  min; MS (ESI, pos)  $m/z$ : 282.22 [100 %,  $\text{M}+\text{H}^+$ ].

HR-MS (ESI, neg):  $m/z$  calcd. for  $C_{15}H_{10}N_3O_3^-$  280.0728 found 280.0731  $[M-H]^-$ .

### Product 2c



The indole **2c** was prepared according to the general procedure B2 and isolated as a pale yellow solid (271 mg, 0.963 mmol, 96%).  $R_f$  0.23 (cyclohexane:ethyl acetate 80:20)

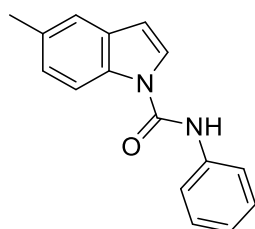
$^1H$  NMR (500 MHz,  $DMSO-d_6$ )  $\delta$  10.47 (s, 1H), 8.65 (t,  $J = 2.3$  Hz, 1H), 8.26 (d,  $J = 8.3$  Hz, 1H), 8.15 – 8.10 (m, 1H), 8.06 (d,  $J = 3.6$  Hz, 1H), 7.99 (dd,  $J = 8.2, 2.3$  Hz, 1H), 7.69 (t,  $J = 8.2$  Hz, 1H), 7.65 (d,  $J = 7.7$  Hz, 1H), 7.32 (dd,  $J = 8.4, 7.0$  Hz, 1H), 7.25 (t,  $J = 7.4$  Hz, 1H), 6.81 (d,  $J = 3.6$  Hz, 1H).

$^{13}C$  NMR (126 MHz,  $DMSO-d_6$ )  $\delta$  149.79, 147.97, 139.85, 135.36, 130.19, 129.79, 126.44, 125.44, 124.00, 122.55, 120.96, 118.19, 115.11, 114.58, 107.00.

UPLC-MS:  $T_R = 5.95$  min; MS (ESI, pos)  $m/z$ : 282.15 [100 %,  $M+H$ ] $^+$ .

HR-MS (ESI, neg):  $m/z$  calcd. for  $C_{15}H_{10}N_3O_3^-$  280.0728 found 280.0732  $[M-H]^-$ .

### Product 2d



The indole **2d** was prepared according to the general procedure B1 and isolated as golden crystals (230 mg, 0.918 mmol, 46%).

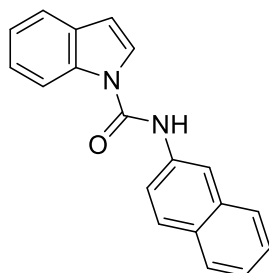
$^1H$  NMR (500 MHz,  $DMSO-d_6$ )  $\delta$  9.97 (s, 1H), 8.10 (d,  $J = 8.4$  Hz, 1H), 7.99 (d,  $J = 3.7$  Hz, 1H), 7.65 (dd,  $J = 8.3, 1.4$  Hz, 2H), 7.39 (dd,  $J = 15.6, 7.6$  Hz, 3H), 7.18 – 7.07 (m, 2H), 6.67 (d,  $J = 3.6$  Hz, 1H), 2.40 (s, 3H).

$^{13}C$  NMR (126 MHz,  $DMSO-d_6$ )  $\delta$  149.79, 138.40, 133.67, 131.05, 129.91, 128.71, 125.50, 125.11, 123.78, 120.77, 120.55, 114.72, 106.14, 20.94.

UPLC-MS:  $T_R = 6.48$  min; MS (ESI, pos)  $m/z$ : 251.18 [100 %,  $M+H$ ] $^+$ .

HR-MS (ESI, pos): m/z calcd. for C<sub>16</sub>H<sub>14</sub>N<sub>2</sub>ONa<sup>+</sup> 273.0998 found 273.0995 [M+Na]<sup>+</sup>

### Product 2e



The indole **2e** was prepared according to the general procedure B1 and isolated as a white solid (210 mg, 0.733 mmol, 73%).

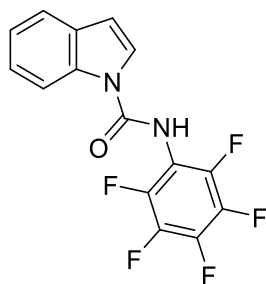
<sup>1</sup>H NMR (500 MHz, DMSO-*d*<sub>6</sub>) δ 10.25 (s, 1H), 8.28 (dd, *J* = 8.2, 1.0 Hz, 1H), 8.26 (d, *J* = 2.2 Hz, 1H), 8.10 (d, *J* = 3.7 Hz, 1H), 7.94 (d, *J* = 8.8 Hz, 1H), 7.90 (m, 2H), 7.78 (dd, *J* = 8.8, 2.1 Hz, 1H), 7.66 (dt, *J* = 7.7, 1.0 Hz, 1H), 7.51 (ddd, *J* = 8.0, 6.8, 1.3 Hz, 1H), 7.45 (ddd, *J* = 8.2, 6.8, 1.3 Hz, 1H), 7.32 (ddd, *J* = 8.4, 7.1, 1.3 Hz, 1H), 7.24 (ddd, *J* = 8.1, 7.2, 1.1 Hz, 1H), 6.79 (dd, *J* = 3.7, 0.8 Hz, 1H).

<sup>13</sup>C NMR (126 MHz, DMSO-*d*<sub>6</sub>) δ 149.93, 136.04, 135.42, 133.30, 130.04, 129.72, 128.31, 127.50, 127.36, 126.49, 125.59, 124.93, 123.80, 122.28, 121.20, 120.87, 116.97, 115.07, 106.53.

UPLC-MS: T<sub>R</sub> = 8.20 min; MS (ESI, pos) m/z: 287.24 [100 %, M+H]<sup>+</sup>.

HR-MS (ESI, pos): m/z calcd. for C<sub>19</sub>H<sub>14</sub>N<sub>2</sub>OH<sup>+</sup> 287.1179 found 287.1175 [M+H]<sup>+</sup>; m/z calcd. for C<sub>19</sub>H<sub>14</sub>N<sub>2</sub>ONa<sup>+</sup> 309.0998 found 309.0999 [M+Na]<sup>+</sup>.

### Product 2f



The indole **2f** was prepared according to the general procedure B2 and isolated as a white solid (305 mg, 0.935 mmol, 94%).

$^1\text{H}$  NMR (500 MHz,  $\text{DMSO-}d_6$ )  $\delta$  10.36 (s, 1H), 8.21 (dd,  $J$  = 8.2, 1.0 Hz, 1H), 8.02 (d,  $J$  = 3.7 Hz, 1H), 7.66 (dt,  $J$  = 7.7, 0.9, 0.9 Hz, 1H), 7.32 (ddd,  $J$  = 8.3, 7.1, 1.4 Hz, 1H), 7.26 (td,  $J$  = 7.4, 7.3, 1.2 Hz, 1H), 6.84 (d,  $J$  = 3.6 Hz, 1H).

$^{19}\text{F}$  NMR (471 MHz,  $\text{DMSO-}d_6$ )  $\delta$  -144.61 – -146.83 (m), -156.79, -160.53 – -164.73 (m).

$^{13}\text{C}$  NMR (126 MHz,  $\text{DMSO-}d_6$ )  $\delta$  149.66, 135.42, 129.70, 125.01, 124.34, 122.87, 121.06, 115.05, 107.97.

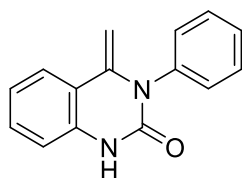
UPLC-MS:  $T_R$  = 6.61 min; MS (ESI, pos)  $m/z$ : 326.24 [100 %,  $\text{M}+\text{H}$ ] $^+$ .

HR-MS (ESI, pos):  $m/z$  calcd. for  $\text{C}_{15}\text{H}_7\text{F}_5\text{N}_2\text{ONa}^+$  349.0371 found 349.0373 [ $\text{M}+\text{Na}$ ] $^+$ .

### General procedure C: quinazolinone products 3 and 3a-3f

Prepared according to a modified procedure of Asensio and co-workers.<sup>52</sup> An oven dried resealable test tube with a Teflon stirring bar was charged with the urea substrate (0.2 mmol or 0.4 mmol),  $[\text{AuCl}(\text{IPr})]$  (5 mol%) and Silver hexafluoroantimonate(V) (7.5 mol%). The tube was flushed and backfilled with nitrogen three times before the addition of degassed DMF (1 mL/mmol). The tube was sealed with a Teflon screw-cap and placed in a heating block at 60 °C for 5 h. Then, the heating was stopped and the mixture was stirred until it reached room temperature. The crude was diluted with  $\text{CH}_2\text{Cl}_2$  (2-3 mL), and filtrated over a plug of celite. The solvent was removed under reduced pressure. The products were purified via flash column chromatography (KP-Sil 25 g, linear gradient of 15% to 25% ethyl acetate in cyclohexane).

### Product 3



The quinazolinone **3** was prepared according to the general procedure C and isolated as white solid (43 mg, 0.182 mmol, 46%). The spectra are in agreement with literature data.<sup>52</sup>

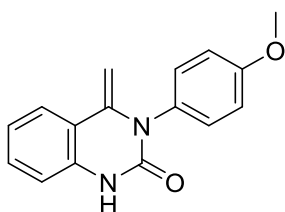
$^1\text{H}$  NMR (500 MHz,  $\text{DMSO-}d_6$ )  $\delta$  10.30 (s, 1H), 7.69 – 7.64 (m, 1H), 7.52 (dd,  $J$  = 8.3, 7.2 Hz, 2H), 7.46 – 7.39 (m, 1H), 7.32 (ddd,  $J$  = 8.4, 7.3, 1.3 Hz, 1H), 7.29 – 7.25 (m, 2H), 7.00 (ddd,  $J$  = 8.3, 7.3, 1.2 Hz, 1H), 6.95 (dd,  $J$  = 8.1, 1.2 Hz, 1H), 4.77 (d,  $J$  = 1.9 Hz, 1H), 3.40 (d,  $J$  = 1.9 Hz, 1H).

$^{13}\text{C}$  NMR (126 MHz,  $\text{DMSO-}d_6$ )  $\delta$  149.24, 143.32, 138.66, 135.88, 130.41, 129.70, 129.37, 127.99, 124.10, 122.14, 116.12, 114.77, 85.89.

UPLC-MS:  $T_R$  = 2.58 min; MS (ESI, pos)  $m/z$ : 236.91 [100 %,  $\text{M}+\text{H}$ ] $^+$ .

HR-MS (ESI, pos):  $m/z$  calcd. for  $\text{C}_{15}\text{H}_{12}\text{N}_2\text{O}\text{H}^+$  237.1022 found 237.1020 [ $\text{M}+\text{H}$ ] $^+$ ;  $m/z$  calcd. for  $\text{C}_{15}\text{H}_{12}\text{N}_2\text{O}\text{Na}^+$  259.0842 found 259.0839 [ $\text{M}+\text{Na}$ ] $^+$ .

### Product 3a



The quinazolinone **3a** was prepared according to the general procedure C and isolated as a white solid (12 mg, 0.045 mmol, 23%). The spectra are in agreement with literature data.<sup>52</sup>

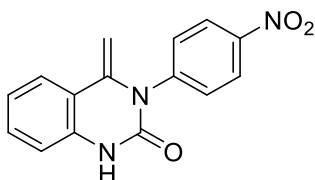
$^1\text{H}$  NMR (500 MHz,  $\text{DMSO-}d_6$ )  $\delta$  10.24 (s, 1H), 7.65 (dd,  $J$  = 8.2, 1.4 Hz, 1H), 7.35 – 7.25 (m, 1H), 7.16 (d,  $J$  = 8.8 Hz, 1H), 7.05 (d,  $J$  = 8.9 Hz, 2H), 6.99 (ddd,  $J$  = 8.2, 7.3, 1.2 Hz, 1H), 6.93 (dd,  $J$  = 8.1, 1.2 Hz, 1H), 4.76 (d,  $J$  = 1.7 Hz, 1H), 3.80 (s, 3H), 3.45 (d,  $J$  = 1.8 Hz, 1H).

$^{13}\text{C}$  NMR (126 MHz,  $\text{DMSO-}d_6$ )  $\delta$  158.57, 149.42, 143.55, 130.35, 130.30, 124.12, 122.07, 116.12, 114.86, 114.71, 85.73, 55.33.

UPLC-MS:  $T_R$  = 2.57 min; MS (ESI, pos)  $m/z$ : 267.16 [100 %,  $\text{M}+\text{H}$ ] $^+$ .

HR-MS (ESI, pos):  $m/z$  calcd. for  $\text{C}_{16}\text{H}_{14}\text{N}_2\text{O}_2\text{Na}^+$  289.0947 found 289.0948 [ $\text{M}+\text{Na}$ ] $^+$ .

### Product 3b



The quinazolinone **3b** was prepared according to the general procedure C and isolated as a yellow solid (11 mg, 0.039 mmol, 10%).

$^1\text{H}$  NMR (500 MHz,  $\text{DMSO-}d_6$ )  $\delta$  10.46 (s, 1H), 8.41 – 8.32 (m, 2H), 7.94 (d,  $J$  = 9.2 Hz, 1H), 7.70 (dd,  $J$  = 8.1, 1.4 Hz, 1H), 7.65 – 7.57 (m, 2H), 7.34 (ddd,  $J$  = 8.2, 7.3, 1.3 Hz, 1H), 7.03

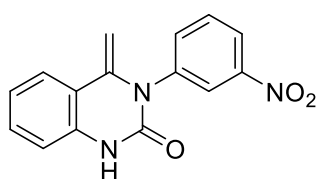
(ddd,  $J = 8.2, 7.3, 1.2$  Hz, 1H), 6.97 (dd,  $J = 8.1, 1.2$  Hz, 1H), 4.85 (d,  $J = 2.4$  Hz, 1H), 3.43 (d,  $J = 2.4$  Hz, 1H).

$^{13}\text{C}$  NMR (126 MHz,  $\text{DMSO-}d_6$ )  $\delta$  148.87, 146.87, 144.76, 142.86, 135.67, 131.25, 130.61, 125.06, 124.14, 122.37, 116.05, 114.94, 86.66.

UPLC-MS:  $T_R = 2.94$  min; MS (ESI, pos)  $m/z$ : 282.15 [100 %,  $\text{M}+\text{H}^+$ ].

HR-MS (ESI, pos):  $m/z$  calcd. for  $\text{C}_{15}\text{H}_{11}\text{N}_3\text{O}_3\text{H}^+$  282.0873 found 282.0870 [ $\text{M}+\text{H}^+$ ].

### Product 3c



The quinazolinone **3c** was prepared according to the general procedure C and isolated as a pale yellow solid (43 mg, 0.153 mmol, 76%).

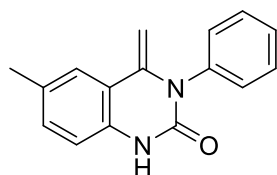
$^1\text{H}$  NMR (500 MHz,  $\text{DMSO-}d_6$ )  $\delta$  10.45 (s, 1H), 8.31 (dt,  $J = 7.0, 2.4$  Hz, 1H), 8.20 (t,  $J = 1.6$  Hz, 1H), 7.84 – 7.79 (m, 2H), 7.71 (dd,  $J = 8.1, 1.3$  Hz, 1H), 7.34 (ddd,  $J = 8.4, 7.4, 1.3$  Hz, 1H), 7.03 (td,  $J = 7.7, 1.2$  Hz, 1H), 6.97 (dd,  $J = 8.1, 1.2$  Hz, 1H), 4.85 (d,  $J = 2.4$  Hz, 1H), 3.42 (d,  $J = 2.4$  Hz, 1H).

$^{13}\text{C}$  NMR (126 MHz,  $\text{DMSO-}d_6$ )  $\delta$  149.09, 148.85, 143.06, 139.75, 136.86, 135.72, 131.18, 130.56, 124.92, 124.17, 123.14, 122.31, 116.11, 114.93, 86.50.

UPLC-MS:  $T_R = 2.92$  min; MS (ESI, pos)  $m/z$ : 282.29 [100 %,  $\text{M}+\text{H}^+$ ].

HR-MS (ESI, pos):  $m/z$  calcd. for  $\text{C}_{15}\text{H}_{11}\text{N}_3\text{O}_3\text{H}^+$  282.0873 found 282.0869 [ $\text{M}+\text{H}^+$ ].

### Product 3d



The quinazolinone **3d** was prepared according to the general procedure C and isolated as a bone white solid (17 mg, 0.068 mmol, 34%). The spectra are in agreement with literature data.<sup>52</sup>

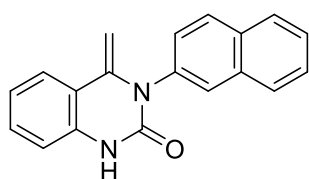
$^1\text{H}$  NMR (500 MHz,  $\text{DMSO-}d_6$ )  $\delta$  10.21 (s, 1H), 7.52 (t,  $J = 7.7$  Hz, 2H), 7.48 (d,  $J = 1.9$  Hz, 1H), 7.45 – 7.37 (m, 1H), 7.28 – 7.22 (m, 2H), 7.14 (dd,  $J = 8.2, 1.8$  Hz, 1H), 6.85 (d,  $J = 8.1$  Hz, 1H), 4.75 (d,  $J = 1.8$  Hz, 1H), 3.37 (d,  $J = 1.8$  Hz, 1H), 2.27 (s, 3H).

$^{13}\text{C}$  NMR (126 MHz,  $\text{DMSO-}d_6$ )  $\delta$  149.25, 143.40, 138.77, 133.55, 131.17, 131.05, 129.67, 129.38, 127.92, 124.06, 115.90, 114.70, 85.62, 20.42.

UPLC-MS:  $T_R = 3.18$  min; MS (ESI, pos)  $m/z$ : 251.04 [100 %,  $\text{M}+\text{H}$ ] $^+$ .

HR-MS (ESI, pos):  $m/z$  calcd. for  $\text{C}_{16}\text{H}_{14}\text{N}_2\text{ONa}^+$  273.0998 found 273.1000 [ $\text{M}+\text{Na}$ ] $^+$ .

### Product 3e



The quinazolinone **3e** was prepared according to the general procedure C and isolated as a white solid (49 mg, 0.171 mmol, 86%).

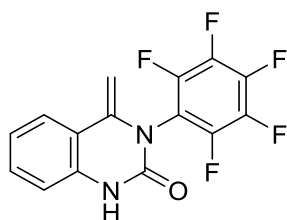
$^1\text{H}$  NMR (500 MHz,  $\text{DMSO-}d_6$ )  $\delta$  10.38 (s, 1H), 8.07 (d,  $J = 8.6$  Hz, 1H), 8.00 (ddd,  $J = 11.8, 7.0, 2.0$  Hz, 2H), 7.88 (d,  $J = 2.0$  Hz, 1H), 7.70 (dd,  $J = 8.2, 1.4$  Hz, 1H), 7.58 (ddd,  $J = 7.6, 5.6, 1.6$  Hz, 2H), 7.39 (dd,  $J = 8.6, 2.1$  Hz, 1H), 7.34 (ddd,  $J = 8.3, 7.3, 1.3$  Hz, 1H), 7.03 (td,  $J = 7.7, 1.2$  Hz, 1H), 6.98 (dd,  $J = 8.0, 1.3$  Hz, 1H), 4.82 (d,  $J = 2.0$  Hz, 1H), 3.45 (d,  $J = 2.0$  Hz, 1H).

$^{13}\text{C}$  NMR (151 MHz,  $\text{DMSO-}d_6$ )  $\delta$  149.45, 143.36, 136.02, 135.91, 133.66, 132.31, 130.49, 129.49, 128.06, 127.87, 127.68, 127.37, 126.64, 126.37, 124.16, 122.22, 116.19, 114.84, 86.26.

UPLC-MS:  $T_R = 5.41$  min; MS (ESI, pos)  $m/z$ : 287.24 [100 %,  $\text{M}+\text{H}$ ] $^+$ .

HR-MS (ESI, pos):  $m/z$  calcd. for  $\text{C}_{19}\text{H}_{14}\text{N}_2\text{ONa}^+$  309.0998 found 309.0997 [ $\text{M}+\text{Na}$ ] $^+$ .

### Product 3f



The quinazolinone **3f** was prepared according to the general procedure C and isolated as a white solid (59 mg, 0.181 mmol, 90%).

$^1\text{H}$  NMR (500 MHz, DMSO- $d_6$ )  $\delta$  10.75 (s, 1H), 7.75 (dd,  $J$  = 8.1, 1.3 Hz, 1H), 7.38 (ddd,  $J$  = 8.3, 7.3, 1.3 Hz, 1H), 7.07 (ddd,  $J$  = 8.2, 7.3, 1.2 Hz, 1H), 6.99 (dd,  $J$  = 8.1, 1.2 Hz, 1H), 4.99 (d,  $J$  = 3.2 Hz, 1H), 3.97 (d,  $J$  = 3.2 Hz, 1H).

$^{13}\text{C}$  NMR (126 MHz, DMSO- $d_6$ )  $\delta$  148.23, 140.31, 135.06, 131.01, 124.37, 122.98, 115.33, 115.25, 86.69.

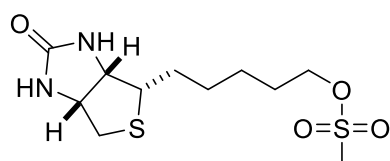
$^{19}\text{F}$  NMR (471 MHz, DMSO- $d_6$ )  $\delta$  -144.61 – -149.11 (m), -153.31, -161.92 (d,  $J$  = 4.7 Hz).

UPLC-MS:  $T_R$  = 2.79 min; MS (ESI, pos)  $m/z$ : 326.31 [100 %,  $\text{M}+\text{H}$ ] $^+$ .

HR-MS (ESI, pos):  $m/z$  calcd. for  $\text{C}_{15}\text{H}_7\text{F}_5\text{N}_2\text{O}\text{Na}^+$  349.0371 found 349.0371 [ $\text{M}+\text{Na}$ ] $^+$ .

## Synthesis of biotin analogues

### Biotin mesylate: BiotMs



An oven-dried flask was charged with biotinol<sup>215</sup> 691 mg, 3.00 mmol, 1 eq), dry  $\text{CH}_2\text{Cl}_2$  (30 mL), pyridine (10 mL) and diisopropylethylamine (1.24 mL, 7.50 mmol, 2.5 eq). The mixture was cooled to 0 °C before slowly adding mesyl chloride (0.69 mL, 9.0 mmol, 3 eq). The clear yellow solution was stirred (3 h at 0 °C) before quenching the mixture with the addition of water (30 mL). The solution was extracted with  $\text{CH}_2\text{Cl}_2$  (3x30 mL), dried over magnesium sulfate and concentrated *in vacuo*. The product was precipitated from  $\text{CH}_2\text{Cl}_2$  by the addition of diethylether to yield biotin mesylate (**BiotMs**) as a pale yellow solid (749 mg, 2.43 mmol, 81%).

$^1\text{H}$  NMR (500 MHz, Chloroform- $d$ )  $\delta$  4.54 (dd,  $J$  = 7.9, 4.9 Hz, 1H), 4.34 (dd,  $J$  = 7.8, 4.6 Hz, 1H), 4.24 (t,  $J$  = 6.4 Hz, 2H), 3.16 (ddd,  $J$  = 8.0, 6.4, 4.5 Hz, 1H), 3.02 (s, 3H), 2.93 (dd,  $J$  = 12.9, 5.0 Hz, 1H), 2.77 (d,  $J$  = 12.8 Hz, 1H), 1.77 (m, 2H), 1.70 (m, 2H), 1.47 (m, 4H).

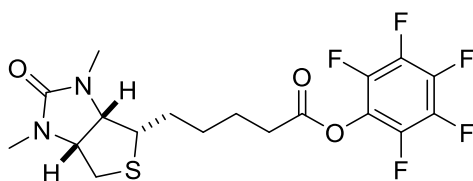
$^{13}\text{C}$  NMR (126 MHz, DMSO- $d_6$ )  $\delta$  162.70, 70.40, 60.99, 59.18, 55.39, 36.54, 28.32, 28.15, 28.00, 24.96.

UPLC-MS:  $T_R$  = 2.43 min; MS (ESI, pos)  $m/z$ : 309.27 [100%,  $\text{M}+\text{H}$ ] $^+$ ; 331.03 [21%,  $\text{M}+\text{Na}$ ] $^+$ .

HR-MS (ESI, pos):  $m/z$  calcd. for  $\text{C}_{11}\text{H}_{20}\text{N}_2\text{O}_4\text{S}_2\text{H}^+$  309.0937 found 309.0937 [ $\text{M}+\text{H}$ ] $^+$ .



### ***N,N*-dimethyl biotin pentafluorophenyl ester**



*N,N*-dimethyl biotin was prepared according to a modified procedure of Dorofeeva and co-workers.<sup>216</sup> An oven-dried flask equipped with a reflux condenser was charged with D(+)-biotin (5.00 g, 20.5 mmol, 1 eq), aq. formaldehyde (9.17 mL, 37%, 123 mmol, 6 eq) and formic acid (30 mL). The mixture was refluxed for two days. The formic acid was removed *in vacuo* and the crude was dissolved in aq. NaOH (50 mL, 0.5 M). The aqueous mixture was filtered and acidified with aq. HCl (2 M) until the product precipitated. The filter cake was washed with water and diethyl ether to yield the dimethylated product as white flakes (4.68 g, 17.2 mmol, 84%). The spectra are in agreement with the literature data.

*N,N*-dimethyl biotin pentafluorophenyl was prepared according to a modified procedure of Ward and co-workers.<sup>103</sup> *N,N*-dimethyl biotin (300 mg, 1.10 mmol, 1 eq) was dissolved in dry DMF and triethylamine was added (0.27 mL, 1.93 mmol, 1.75 eq). After complete dissolution, pentafluorophenyl trifluoroacetate (0.28 mL, 1.65 mmol, 1.5 eq) was added dropwise. The mixture was stirred (90 min) before removing the solvent *in vacuo*. The crude was purified via flash column chromatography (KP-Sil 50 g, gradient of 2% to 15% methanol in CH<sub>2</sub>Cl<sub>2</sub>) to yield the product as a white solid (482 mg, 1.1 mmol, 99%).

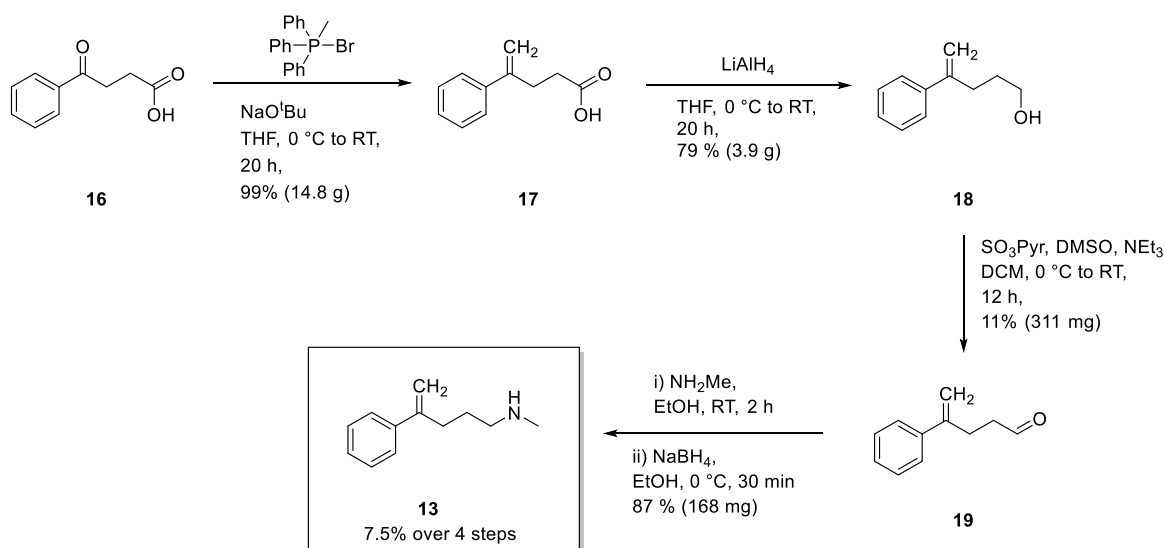
<sup>1</sup>H NMR (500 MHz, CD<sub>2</sub>Cl<sub>2</sub>) δ 4.15 (dq, J = 8.5, 4.3 Hz, 1H), 3.93 (dd, J = 8.8, 5.2 Hz, 1H), 3.31 – 3.21 (m, 1H), 2.88 – 2.85 (m, 2H), 2.83 (s, 3H), 2.73 (s, 3H), 2.72 – 2.67 (m, 2H), 1.85 – 1.73 (m, 2H), 1.73 – 1.58 (m, 2H), 1.57 – 1.48 (m, 2H).

<sup>19</sup>F NMR (471 MHz, CD<sub>2</sub>Cl<sub>2</sub>) δ -153.41, -159.23, -163.35.

<sup>13</sup>C NMR (126 MHz, CD<sub>2</sub>Cl<sub>2</sub>) δ 176.39, 169.90, 162.18, 162.15, 67.20, 64.74, 56.22, 56.09, 35.80, 33.67, 33.11, 29.65, 29.62, 29.26, 29.22, 25.13.

HR-MS (ESI, pos): m/z calcd. for C<sub>18</sub>H<sub>19</sub>F<sub>5</sub>N<sub>2</sub>O<sub>3</sub>SNa<sup>+</sup> 461.0929 found 461.0922 [M+Na]<sup>+</sup>.

## Hartwig Substrate Synthesis



Vinylarene **13** was prepared according to the procedure of Hartwig and co-workers.<sup>130,131</sup> The spectra are in agreement with literature data:

Acid **17**:  $^1\text{H NMR}$  (500 MHz,  $\text{CDCl}_3$ )  $\delta$  7.40 (s, 2H), 7.34 (s, 2H), 7.28 (s, 1H), 5.32 (d,  $J = 1.0$  Hz, 2H), 5.11 (d,  $J = 1.3$  Hz, 2H), 2.88 – 2.81 (m, 1H), 2.58 – 2.51 (m, 1H).

Alcohol **18**:  $^1\text{H NMR}$  (500 MHz,  $\text{CDCl}_3$ )  $\delta$  7.33 (s, 2H), 7.25 (s, 2H), 7.19 (s, 1H), 5.22 (d,  $J = 1.5$  Hz, 1H), 5.02 (d,  $J = 1.4$  Hz, 1H), 3.58 (t,  $J = 6.4$  Hz, 2H), 2.53 (td,  $J = 7.5, 1.3$  Hz, 2H), 1.69 – 1.60 (m, 2H), 1.53 (s, 1H).

Aldehyde **19**:  $^1\text{H NMR}$  (500 MHz,  $\text{CDCl}_3$ )  $\delta$  9.79 (s, 1H), 7.38 (s, 2H), 7.34 (s, 2H), 7.29 (s, 1H), 5.33 (s, 1H), 5.10 (d,  $J = 1.3$  Hz, 1H), 2.85 (td,  $J = 7.4, 1.3$  Hz, 2H), 2.61 (td,  $J = 7.5, 1.5$  Hz, 2H).

Methylamine **13**:  $^1\text{H NMR}$  (600 MHz,  $\text{DMSO-}d_6$ )  $\delta$  8.37 (d,  $J = 1.4$  Hz, 1H), 7.51 – 7.42 (m, 2H), 7.40 – 7.34 (m, 2H), 7.33 – 7.25 (m, 1H), 5.35 (s, 1H), 5.10 (d,  $J = 1.8$  Hz, 1H), 2.72 (d,  $J = 7.5$  Hz, 2H), 2.54 (s, 2H), 2.41 (d,  $J = 1.3$  Hz, 3H), 1.64 (s, 2H).

$^{13}\text{C NMR}$  (151 MHz,  $\text{DMSO-}d_6$ )  $\delta$  165.34, 146.88, 140.02, 128.47, 127.64, 125.84, 112.64, 54.96, 48.73, 33.44, 31.60, 25.35.

Piperidine **15**:  $^1\text{H NMR}$  (500 MHz,  $\text{CD}_2\text{Cl}_2$ )  $\delta$  7.27 (d,  $J = 7.3$  Hz, 2H), 7.25 – 7.21 (m, 2H), 7.18 (s, 1H), 2.92 – 2.86 (m, 1H), 2.82 (d,  $J = 3.7$  Hz, 1H), 2.79 (s, 1H), 2.24 (s, 3H), 1.94 (d,  $J = 11.2$  Hz, 1H), 1.91 – 1.84 (m, 2H), 1.74 (dd,  $J = 4.2, 2.9$  Hz, 1H), 1.73 – 1.59 (m, 2H), 1.41 (dd,  $J = 12.4, 4.3$  Hz, 1H).

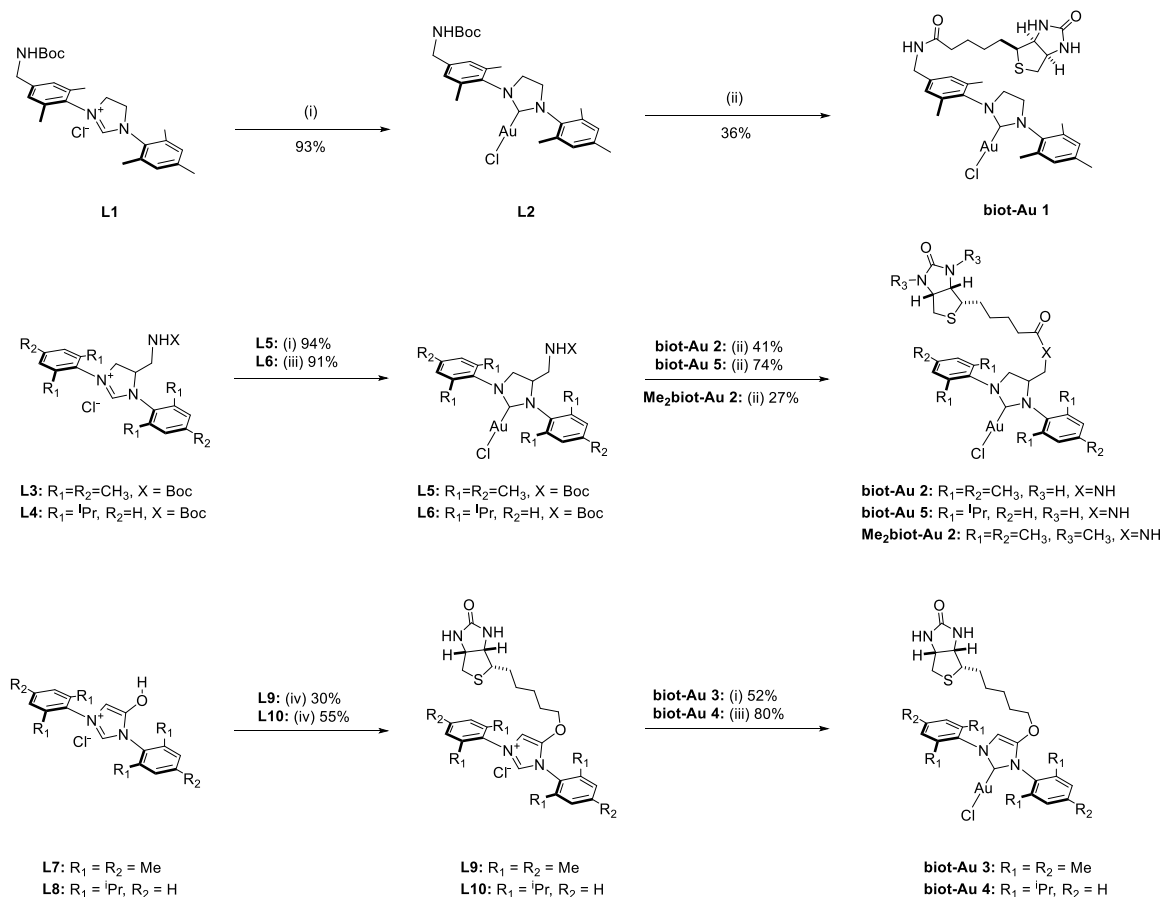
## Synthesis of gold complexes

### **General procedures D1 & D2: coordination to gold**

D1: An oven-dried flask was charged with the corresponding NHC salt (1 eq), Silver(I)oxide (0.6 eq) and degassed  $\text{CH}_2\text{Cl}_2$  (10 mL/mmol). The mixture was stirred (4 h) at room temperature in the dark. The mixture was filtered through a plug of celite into a tube containing chloro(dimethylsulfide) gold(I) (1 eq). The resulting mixture was stirred for (16 h). The mixture was filtered through a plug of celite and the solvent was removed *in vacuo*.

D2: Carried out according to a modified procedure of Nolan and co-workers:<sup>101</sup> An oven-dried pressure tube was charged with the corresponding NHC salt (1 eq), chloro(dimethylsulfide) gold(I) (1 eq), potassium carbonate (2 eq) and acetone (5 mL, HPLC-grade). The tube was sealed and stirred (2 h at 65 °C). The mixture was cooled to room temperature and the solvent was removed *in vacuo*. Dry  $\text{CH}_2\text{Cl}_2$  (10 mL) was added before filtering the crude through a plug of celite. The solvent was removed *in vacuo*.

Purification: Dry  $\text{CH}_2\text{Cl}_2$  (0.5 mL) was added to dissolve the crude from either protocols D1 or D2. Upon addition of dry hexane (4 mL) the corresponding gold complex precipitated as white crystals which were collected by carefully removing the solvent via syringe. Boc-protected gold complexes tend to be less stable than the corresponding biotinylated gold complexes. It is thus recommended, to promptly continue with the biotin coupling step.



**SI Figure 1** Synthesis of biotinylated gold complexes: (i)  $Ag_2O$ ,  $CH_2Cl_2$ , rt, 4 h then  $(CH_3)_2SAuCl$ ,  $CH_2Cl_2$ , rt, 16 h, (ii) TFA,  $CH_2Cl_2$ , rt, 2 h, then biotin pentafluorophenyl ester,  $NEt_3$ , DMF, rt, 16 h, (iii)  $(CH_3)_2SAuCl$ ,  $K_2CO_3$ , acetone, 65 °C, 90 min, (iv) biotin mesylate, KI,  $K_2CO_3$ , acetone, reflux, 2 days, (v)  $HCl(g)$ ,  $CH_2Cl_2$ , rt, 4 h then Boc-Gly pentafluorophenyl ester,  $NEt_3$ , DMF, rt, 16 h.

## General procedures E1 & E2: biotin coupling

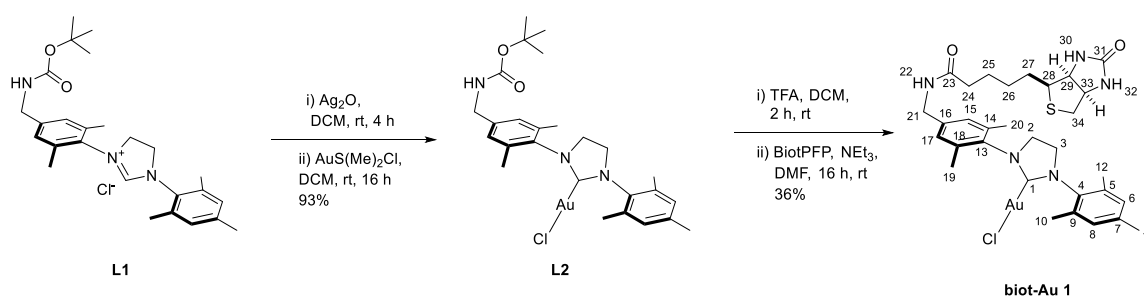
**E1:** An oven-dried flask was charged with the corresponding imidazolium salt or NHC complex (1 eq), degassed  $CH_2Cl_2$  (2 mL) and trifluoroacetic acid (20 eq). The mixture was stirred at room temperature in the dark until full deprotection of the boc group (reaction control via ninhydrin-stained TLC after ca. 3 hours). The solvent and the trifluoroacetic acid were removed via high vacuum while gently heating the flask with the heat gun (<50 °C!). It is essential to remove all TFA before proceeding. The dried crude was dissolved in degassed DMF (2 mL). Pentafluorophenylbiotin (1 eq) and trimethylamine (20 eq) were added. The mixture was stirred (16 h) at room temperature in the dark. The solvent and the base were removed via high vacuum overnight to yield a yellow crude product.

**E2:** According to a modified procedure of Plenio and co-workers:<sup>217</sup> An oven-dried pressure tube was charged with the corresponding NHC salt (1 eq), potassium iodide (1.1 eq), biotin mesylate (1 eq), potassium carbonate (2 eq) and acetone (7 mL). The tube was sealed and

heated (65 °C for 2 days). The mixture was filtered through a plug of celite and the solvent was removed *in vacuo*.

Purification: After careful removal of the solvents, the crude from either protocols E1 or E2 was purified via flash column chromatography (KP-Sil 10 g, gradient of 3% to 20% methanol in CH<sub>2</sub>Cl<sub>2</sub>). The product was diluted in dry CH<sub>2</sub>Cl<sub>2</sub> (>1 mL) and precipitated by the addition of dry hexane. The purified biotinylated gold complexes were air- and moisture stable. Stock solutions of 2 mM in DMSO could be stored for months in the fridge without significant degradation of the biotinylated gold complexes (as revealed by HR-MS) or any inhibition of catalytic activity.

### Synthesis of the gold complex biot-Au 1



Imidazolium salt **L1** was prepared according to the procedure of Ward and co-workers in 6 steps.<sup>103</sup>

The gold complex **L2** was prepared following the general procedure D1 yielding the product as a white solid (220 mg, 0.336 mmol, 93%):

<sup>1</sup>H NMR (500 MHz, CD<sub>2</sub>Cl<sub>2</sub>) δ 7.11 (s, 2H), 7.02 (s, 2H), 5.04 (s, 1H), 4.28 (d, *J* = 6.2 Hz, 2H), 4.02 (s, 4H), 2.37 (s, 6H), 2.34 (s, 6H), 2.33 (s, 3H), 1.46 (s, 9H).

<sup>13</sup>C NMR (126 MHz, CD<sub>2</sub>Cl<sub>2</sub>) δ 195.34, 140.97, 139.74, 136.94, 136.76, 136.28, 135.23, 130.19, 128.14, 51.32, 51.23, 28.68, 21.43, 18.47, 18.32.

HR-MS (ESI, pos): *m/z* calcd. for C<sub>26</sub>H<sub>35</sub>AuClN<sub>3</sub>O<sub>2</sub>Na<sup>+</sup> 676.1976 found 676.1970 [M+Na]<sup>+</sup>.

The biotinylated gold complex **biot-Au 1** was prepared following the general procedure E1 yielding the product as a white solid (67 mg, 0.086 mmol, 36%): R<sub>f</sub> 0.52 (MeOH: CH<sub>2</sub>Cl<sub>2</sub> 5:95)

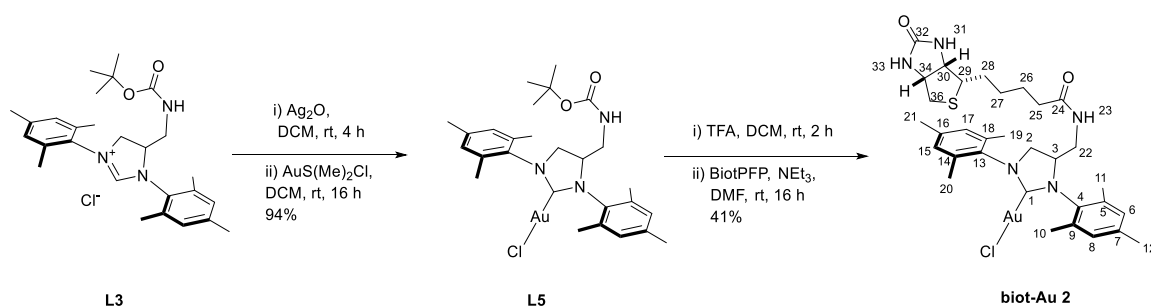
<sup>1</sup>H NMR (500 MHz, CD<sub>2</sub>Cl<sub>2</sub>) δ = 7.11 (s, 2H, C17H, C15H), 7.02 (s, 2H, C8H, C6H), 6.29 (s, 1H, N22H), 5.50 (s, 1H, N30H), 4.77 (s, 1H, N32H), 4.49 (dd, *J* = 8.0, 4.5 Hz, 1H, C33H), 4.38 (d, *J* = 6.0 Hz, 2H, C21H), 4.29 (dd, *J* = 7.9, 4.7 Hz, 1H, C29H), 4.01 (s, 4H, C2H<sub>2</sub>, C3H<sub>2</sub>), 3.17 (td, *J* = 7.5 Hz, 4.4, 2H, C28H), 2.92 (m, 1H, C34H), 2.68 (t, *J* = 12.2 Hz, 1H, C34H), 2.37 (s,

$^1\text{H}$  NMR (500 MHz,  $\text{CD}_2\text{Cl}_2$ )  $\delta$  7.05 (s, 1H, C19H<sub>3</sub>/C20H<sub>3</sub>), 7.04 (s, 1H, C19H<sub>3</sub>/C20H<sub>3</sub>), 7.02 (s, 2H, C19H<sub>3</sub>/C20H<sub>3</sub>), 4.53 (m, 1H, C24H<sub>2</sub>), 4.49 (m, 1H, C24H<sub>2</sub>), 4.10 (t,  $J = 11.4$  Hz, 1H, C24H<sub>2</sub>), 3.94-3.81 (m, 1H, C24H<sub>2</sub>), 3.47 (m, 1H, C24H<sub>2</sub>), 3.26 (m, 1H, C24H<sub>2</sub>), 2.41 (s, 3H, C26H<sub>2</sub>), 2.36 (s, 4H, C25H<sub>2</sub>, C27H<sub>2</sub>), 2.34 (s, 4H, C25H<sub>2</sub>, C27H<sub>2</sub>), 2.33 (s, 3H, C26H<sub>2</sub>), 2.32 (s, 4H, C25H<sub>2</sub>, C27H<sub>2</sub>), 2.31 (s, 3H, C26H<sub>2</sub>), 1.36 (s, 9H, C26H<sub>2</sub>).

$^{13}\text{C}$  NMR (101 MHz,  $\text{CD}_2\text{Cl}_2$ )  $\delta$  195.01 (C1), 173.78 (C23), 164.60 (C31), 140.70 (C16), 139.68 (C4), 136.83 (C18, C14), 136.69 (C13), 136.27 (C5, C9), 135.24 (C7), 130.15 (C6, C8), 128.49 (C15/C17), 128.47 (C17/C15), 62.21 (C29), 60.81 (C33), 56.13 (C28), 51.32 (C3/C2), 51.27 (C2/C3), 43.15 (C21), 41.11 (C34), 36.40 (C24), 28.70 (C25, C26, C27), 21.42 (C11), 18.51 (C20/C19), 18.47 (C19/C20), 18.35 (C10, C12).

HR-MS (ESI, pos):  $m/z$  calcd. for  $\text{C}_{31}\text{H}_{41}\text{AuN}_5\text{O}_2\text{S}^+$  744.2641 found 744.2651  $[\text{M}-\text{Cl}]^+$ .

### Synthesis of the gold complex biot-Au 2



Imidazolium salt **L3** was prepared according to the procedure of Grubbs and co-workers in 4 steps by Boris Lozhkin.<sup>104</sup> The gold complex **L5** was prepared following the general procedure D1 yielding the product as a white solid (126 mg, 0.189 mmol, 94%):

$^1\text{H}$  NMR (500 MHz,  $\text{CD}_2\text{Cl}_2$ )  $\delta$  7.05 (s, 1H), 7.04 (s, 1H), 7.02 (s, 2H), 4.53 (m, 1H), 4.49 (m, 1H), 4.10 (t,  $J = 11.4$  Hz, 1H), 3.94-3.81 (m, 1H), 3.47 (m, 1H), 3.26 (m, 1H), 2.41 (s, 3H), 2.36 (s, 4H), 2.34 (s, 4H), 2.33 (s, 3H), 2.32 (s, 4H), 2.31 (s, 3H), 1.36 (s, 9H).

$^{13}\text{C}$  NMR (126 MHz,  $\text{CD}_2\text{Cl}_2$ )  $\delta$  196.01, 139.81, 136.78, 136.16, 130.75, 130.53, 130.23, 130.19, 63.81, 32.16, 28.47, 23.22, 21.43, 21.37, 19.53, 18.52, 18.38, 18.35, 14.44.

HR-MS (ESI, neg):  $m/z$  calcd. for  $\text{C}_{27}\text{H}_{36}\text{AuClN}_3\text{O}_2^-$  666.2156 found 666.2177  $[\text{M}-\text{H}]^-$ ; for  $\text{C}_{27}\text{H}_{37}\text{AuClN}_3\text{O}_2\text{HCOO}^-$  712.2211 found 712.2233  $[\text{M}+\text{HCOO}]^-$ .

The biotinylated gold complex **biot-Au 2** was prepared following the general procedure E1 yielding the product as a white solid (18 mg, 0.023 mmol, 41%):

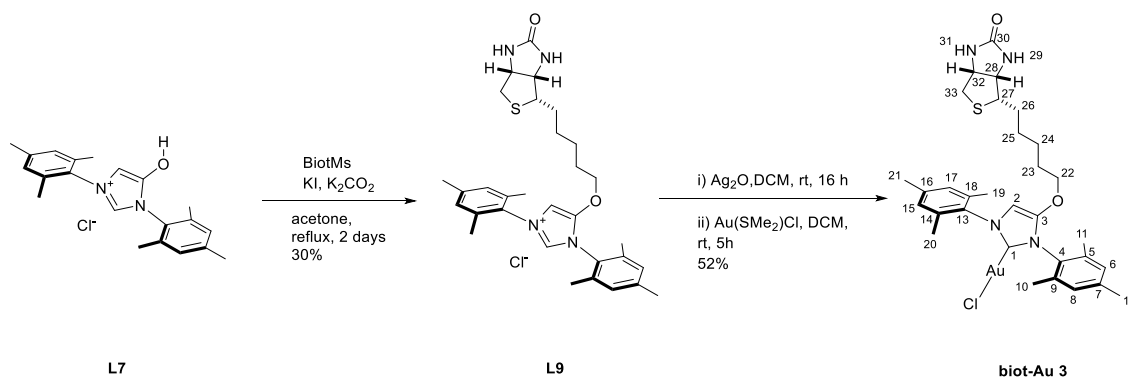
$^1\text{H}$  NMR (500 MHz,  $\text{CD}_2\text{Cl}_2$ )  $\delta$  7.06 (s, 1H, C8H/C6H), 7.04 (s, 1H, C6H/C8H), 7.01 (s, 2H, C15H, C17H), 5.71 (d,  $J = 6.1$  Hz, 1H, N23H), 5.38 (s, 1H, N31H), 4.76 (d,  $J = 5.3$  Hz, 1H,

<sup>1</sup>H NMR (500 MHz, CD<sub>2</sub>Cl<sub>2</sub>) δ 8.92 (d, *J* = 1.9 Hz, 1H), 7.26 (d, *J* = 1.9 Hz, 1H), 7.12 (d, *J* = 6.2 Hz, 4H), 5.01 (s, 1H), 4.74 (s, 1H), 4.52 – 4.44 (m, 1H), 4.31 (t, *J* = 6.6 Hz, 2H), 4.28 (m, 1H), 3.41 (d, *J* = 4.3 Hz, 1H), 3.12 (ddd, *J* = 8.6, 6.1, 4.5 Hz, 1H), 2.90 (dd, *J* = 12.8, 5.0 Hz, 1H), 2.70 (d, *J* = 12.8 Hz, 1H), 2.39 (d, *J* = 4.7 Hz, 6H), 2.24 (s, 6H), 2.17 (s, 6H), 1.77 (m, 2H), 1.66 (m, 1H), 1.54 (m, 1H), 1.39 (m, 4H).

<sup>13</sup>C NMR (126 MHz, CD<sub>2</sub>Cl<sub>2</sub>) δ 196.04 (C1), 173.90 (C24), 163.61 (C32), 139.80 (C7, C16), 136.82 (C4), 136.36 (C13), 135.13 (C14, C18), 134.41 (C9, C5), 130.76 (C8/C6), 130.53 (C6/C8), 130.16 (C15, C17), 63.40 (C3), 62.25 (C30), 60.60 (C34), 55.91 (C29), 55.36 (C2), 42.47 (C22), 41.15 (C35), 36.00 (C25), 28.58 (C27/C28), 28.51 (C28/C27), 25.68 (C26), 21.43 (C12, C21), 19.59 (C10/C11), 18.53 (C19/C20), 18.38 (C11/C10), 18.34 (C20/C19).

HR-MS (ESI, pos): *m/z* calcd. for C<sub>32</sub>H<sub>43</sub>AuN<sub>5</sub>O<sub>2</sub>S<sup>+</sup> 758.2803 found 758.2794 [M-Cl]<sup>+</sup>; for C<sub>32</sub>H<sub>43</sub>AuClN<sub>5</sub>O<sub>2</sub>SNa<sup>+</sup> 816.2384 found 816.2384 [M+Na]<sup>+</sup>.

### Synthesis of the gold complex biot-Au 3



The imidazolium salt **L7** was prepared according to the procedure of Lavigne and co-workers in three steps.<sup>105</sup>

The biotinylated imidazolium salt **L9** was prepared following the general procedure E2 yielding the product as a pale orange solid (107 mg, 0.201 mmol, 54%):

<sup>1</sup>H NMR (500 MHz, CD<sub>2</sub>Cl<sub>2</sub>) δ 8.92 (d, *J* = 1.9 Hz, 1H), 7.26 (d, *J* = 1.9 Hz, 1H), 7.12 (d, *J* = 6.2 Hz, 4H), 5.01 (s, 1H), 4.74 (s, 1H), 4.52 – 4.44 (m, 1H), 4.31 (t, *J* = 6.6 Hz, 2H), 4.28 (m, 1H), 3.41 (d, *J* = 4.3 Hz, 1H), 3.12 (ddd, *J* = 8.6, 6.1, 4.5 Hz, 1H), 2.90 (dd, *J* = 12.8, 5.0 Hz, 1H), 2.70 (d, *J* = 12.8 Hz, 1H), 2.39 (d, *J* = 4.7 Hz, 6H), 2.24 (s, 6H), 2.17 (s, 6H), 1.77 (m, 2H), 1.66 (m, 1H), 1.54 (m, 1H), 1.39 (m, 4H).

$^{13}\text{C}$  NMR (126 MHz,  $\text{CD}_2\text{Cl}_2$ )  $\delta$  163.53, 148.32, 142.42, 142.27, 135.59, 134.87, 131.44, 131.23, 130.40, 130.36, 127.36, 102.73, 75.39, 62.28, 60.59, 56.08, 41.16, 29.10, 29.03, 28.72, 25.98, 21.55, 21.50, 18.19, 18.13.

HR-MS (ESI, pos):  $m/z$  calcd. for  $\text{C}_{31}\text{H}_{41}\text{N}_4\text{O}_2\text{S}^+$  533.2945 found 533.2944  $[\text{M}-\text{Cl}]^+$ .

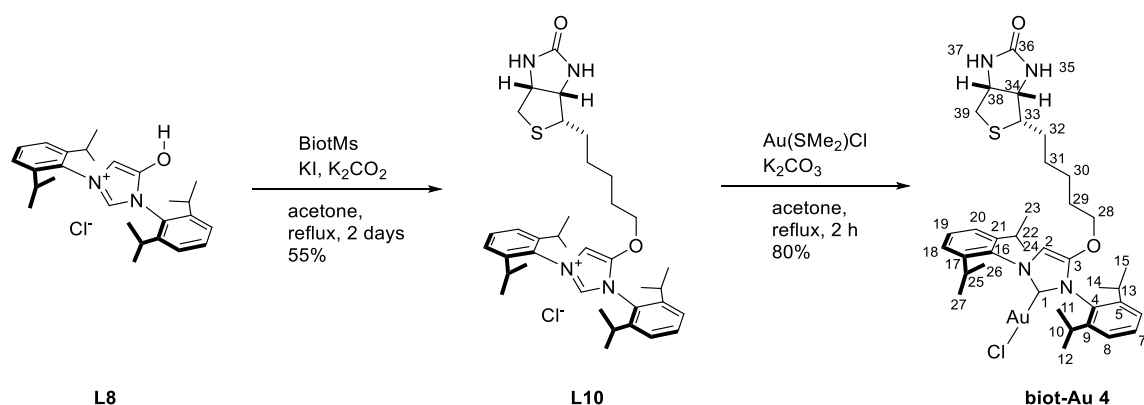
Biotinylated gold complex **biot-Au 3** was prepared following the general procedure D1 yielding the product as a golden solid (38 mg, 0.050 mmol, 50%):

$^1\text{H}$  NMR (500 MHz,  $\text{CD}_2\text{Cl}_2$ )  $\delta$  7.06 (d,  $J$  = 6.4 Hz, 4H, C8H, C6H, C15H, C17H), 6.40 (s, 1H C2H), 4.63 (s, 2H, N29H, N31H), 4.48 (m, 1H, C32H), 4.25 (ddd,  $J$  = 7.7, 4.5, 1.6 Hz, 1H, C28H), 3.98 (t,  $J$  = 6.4 Hz, 2H, C22H<sub>2</sub>), 3.09 (ddd,  $J$  = 9.1, 5.9, 4.6 Hz, 1H, C27H), 2.90 (dd,  $J$  = 12.9, 5.0 Hz, 1H, C33H<sub>2</sub>), 2.69 (d,  $J$  = 12.8 Hz, 1H, C33H<sub>2</sub>), 2.38 (s, 3H, C21H<sub>3</sub>/C12H<sub>3</sub>), 2.37 (s, 3H, C12H<sub>3</sub>/C21H<sub>3</sub>), 2.17 (s, 6H, C10H<sub>3</sub>, C11H<sub>3</sub>), 2.12 (s, 6H, C19H<sub>3</sub>, C20H<sub>3</sub>), 1.69 (m, 2H, C23H<sub>2</sub>), 1.59 (m, 2H, C26H<sub>2</sub>), 1.35 (m, 2H, C24H<sub>2</sub>), 1.26 (m, 2H, C25H<sub>2</sub>).

$^{13}\text{C}$  NMR (126 MHz,  $\text{CD}_2\text{Cl}_2$ )  $\delta$  168.13 (C1), 163.01 (C30), 148.35 (C3), 140.51-140.40 (C7, C16), 136.16 (C14, C18), 136.01 (C4), 135.59 (C9, C5), 131.78 (C9), 129.84-129.80 (C8, C6, C15, C17), 99.21 (C2), 73.41 (C22), 62.39 (C28), 60.59 (C32), 55.98 (C27), 41.16 (C33), 29.18-29.14 (C25, C26), 28.89 (C23), 26.17 (C24), 21.59-21.50 (C12, C21), 18.28 (C19, C20), 18.03 (C10, C11).

HR-MS (ESI, neg):  $m/z$  calcd. for  $\text{C}_{31}\text{H}_{39}\text{AuClN}_4\text{O}_2\text{S}^-$  763.2142 found 763.2154  $[\text{M}-\text{H}]^-$ ; for  $\text{C}_{31}\text{H}_{40}\text{AuClN}_4\text{O}_2\text{SHCOO}^-$  809.2197 found 809.2201  $[\text{M}+\text{HCOO}]^-$ .

### Synthesis of the gold complex **biot-Au 4**



The imidazolium salt **L8** was prepared according to the procedure of Lavigne and co-workers in 3 steps.<sup>105</sup>

The biotinylated NHC salt **L10** was prepared following the general procedure E2 yielding the product as a yellow solid (122 mg, 0.187 mmol, 55%):



$^1\text{H}$  NMR (500 MHz,  $\text{CD}_2\text{Cl}_2$ )  $\delta$  8.72 (d,  $J = 1.9$  Hz, 1H), 7.65 (m, 1H), 7.62 (m, 2H), 7.41 (dd,  $J = 7.8, 2.4$  Hz, 4H), 4.97 (s, 1H), 4.69 (s, 1H), 4.48 (m, 1H), 4.39 (t,  $J = 6.6$  Hz, 2H), 4.29 (m, 1H), 3.12 (m, 1H), 2.90 (dd,  $J = 12.8, 5.0$  Hz, 1H), 2.69 (d,  $J = 12.8$  Hz, 1H), 2.53 (dt,  $J = 12.7, 6.6$  Hz, 1H), 2.44 (pd,  $J = 6.8, 2.8$  Hz, 2H), 2.00 (s, 1H), 1.78 (s, 2H), 1.65 (s, 1H), 1.53 (s, 1H), 1.40 (s, 4H), 1.36 (d,  $J = 6.8$  Hz, 6H), 1.28 (dd,  $J = 6.7, 1.0$  Hz, 6H), 1.24 (dd,  $J = 6.9, 3.8$  Hz, 12H).

$^{13}\text{C}$  NMR (126 MHz,  $\text{CD}_2\text{Cl}_2$ )  $\delta$  163.22, 149.20, 146.34, 145.74, 132.94, 132.84, 131.27, 130.62, 126.50, 125.42, 104.13, 75.76, 62.24, 60.57, 55.98, 41.16, 30.02, 29.74, 29.08, 28.83, 25.97, 25.26, 24.63, 24.31, 23.86.

HR-MS (ESI, pos):  $m/z$  calcd. for  $\text{C}_{37}\text{H}_{53}\text{N}_4\text{O}_2\text{S}^+$  617.3884 found 617.3893 [M-Cl] $^+$ .

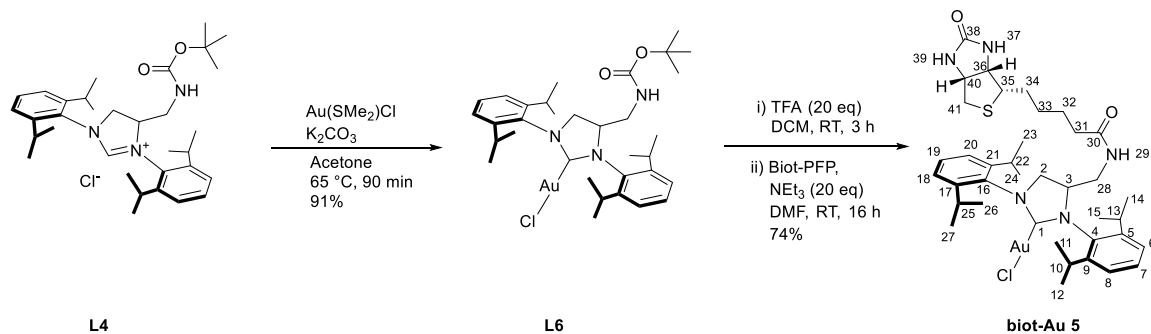
The biotinylated gold complex **biot-Au 4** was prepared following the general procedure D1 yielding the product as a white solid (24 mg, 0.028 mmol, 80%):

$^1\text{H}$  NMR (600 MHz,  $\text{CD}_2\text{Cl}_2$ )  $\delta$  7.54 (q,  $J = 8.3$  Hz, 2H, C7H, C19H), 7.33 (d,  $J = 2.8$  Hz, 4H, C8H, C6H, C18H, C20H), 6.46 (s, 1H, C2H), 4.71 (s, 2H, N35H, N37H), 4.47 (t,  $J = 6.4$  Hz, 1H, C38H), 4.23 (t,  $J = 6.2$  Hz, 1H, C34H), 4.01 (t,  $J = 6.4$  Hz, 2H, C28H<sub>2</sub>), 3.06 (s, 1H, C33H), 2.89 (dd,  $J = 13.0, 5.0$  Hz, 1H, C39H), 2.69 (m, 1H, C39H), 2.67 (m, 2H, C22H, C25H), 2.61 (p,  $J = 6.5, 6.0$  Hz, 2H, C10H, C23H), 1.69 (t,  $J = 6.8$  Hz, 2H, C29H<sub>2</sub>), 1.53 (m, 2H, C32H<sub>2</sub>), 1.38 (m, 4H, C30H<sub>2</sub>, C31H<sub>2</sub>), 1.34 (d,  $J = 6.8$  Hz, 6H, C24H<sub>3</sub>, C27H<sub>2</sub>), 1.32 (d,  $J = 7.0$  Hz, 6H, C12H<sub>3</sub>, C14H<sub>3</sub>), 1.25 (d,  $J = 7.0$  Hz, 6H, C26H<sub>3</sub>, C23H<sub>3</sub>), 1.21 (d,  $J = 6.9$  Hz, 6H, C11H<sub>3</sub>, C15H<sub>3</sub>).

$^{13}\text{C}$  NMR (151 MHz,  $\text{CD}_2\text{Cl}_2$ )  $\delta$  179.96 (C1), 163.10 (C36), 148.98 (C3), 146.94 (C5, C9), 146.47 (C17, C21), 135.17 (C16), 131.11 (C7/C19), 131.02 (C19/C7), 130.89 (C4), 124.67-124.55 (C6, C8, C18, C20), 99.83 (C2), 73.17 (C28), 62.33 (C34), 60.52 (C38), 55.94 (C33), 41.16 (C39), 29.54 (C10, C23), 29.25 (C22, C25), 29.20-29.00 (C29, C31, C32), 26.19 (C30), 24.96 (C26, C23), 24.39 (C11, C15), 23.95 (C12, C14).

HR-MS (ESI, pos):  $m/z$  calcd. for  $\text{C}_{37}\text{H}_{52}\text{AuN}_4\text{O}_2\text{S}^+$  813.3476 found 813.3458 [M-Cl] $^+$ ;  $\text{C}_{37}\text{H}_{52}\text{AuN}_4\text{O}_2\text{SCH}_3\text{CN}^+$  854.3742 found 854.3718 [M-Cl+CH<sub>3</sub>CN] $^+$ .

## Synthesis of the gold complex biot-Au 5



The imidazolium salt **L4** was prepared according to the procedure of Ward and co-workers in four steps by Boris Lozhkin.<sup>218</sup>

The gold complex **L6** was prepared following the general procedure D1 yielding the product as a white solid (127 mg, 0.182 mmol, 91%):

<sup>1</sup>H NMR (600 MHz, CD<sub>2</sub>Cl<sub>2</sub>) δ 7.48 (dd, *J* = 19.4, 7.7 Hz, 2H), 7.33 – 7.27 (m, 4H), 4.48 (t, *J* = 6.4, 6.4 Hz, 1H), 4.44 – 4.33 (m, 1H), 4.17 (t, *J* = 11.4, 11.4 Hz, 1H), 3.90 (t, *J* = 10.8, 10.8 Hz, 1H), 3.60 – 3.50 (m, 1H), 3.29 – 3.22 (m, 1H), 3.17 (dt, *J* = 12.5, 5.7, 5.7 Hz, 1H), 3.08 (p, *J* = 7.0, 7.0, 6.9, 6.9 Hz, 1H), 3.02 (dt, *J* = 12.9, 6.3, 6.3 Hz, 1H), 2.95 (hept, *J* = 6.9, 6.9, 6.5, 6.5, 6.5, 6.5 Hz, 1H), 1.46 (d, *J* = 6.8 Hz, 3H), 1.42 (d, *J* = 6.8 Hz, 3H), 1.39 – 1.36 (m, 12H), 1.35 (s, 9H), 1.34 (s, 6H).

<sup>13</sup>C NMR (151 MHz, CD<sub>2</sub>Cl<sub>2</sub>) δ 196.78, 155.86, 147.50, 146.68, 130.33, 130.16, 125.29, 124.94, 124.84, 124.65, 80.19, 65.88, 57.61, 42.60, 31.73, 29.29, 29.09, 29.02, 28.90, 28.06, 25.88, 25.24, 24.99, 24.85, 24.20, 23.80, 23.37, 22.80, 14.03.

HR-MS (ESI, pos): *m/z* calcd. for C<sub>33</sub>H<sub>49</sub>AuClN<sub>3</sub>O<sub>2</sub>Na<sup>+</sup> 774.3071 found 774.3057 [M+Na]<sup>+</sup>.

The biotinylated gold complex **biot-Au 5** was prepared following the general procedure E1 yielding the product as a white solid (117 mg, 0.133 mmol, 74%):

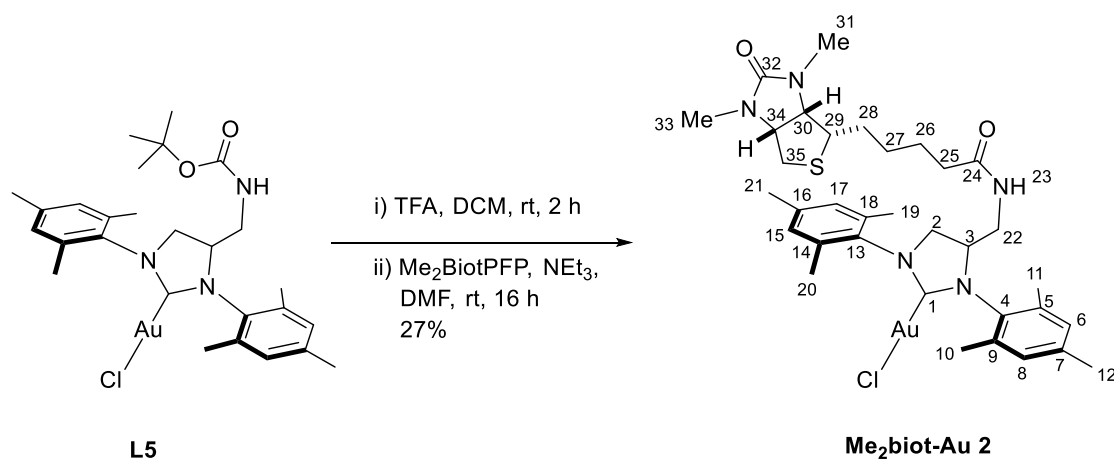
<sup>1</sup>H NMR (500 MHz, CD<sub>2</sub>Cl<sub>2</sub>) δ 7.52 (td, *J* = 7.8, 1.1 Hz, 1H, C7H/C19H), 7.47 (t, *J* = 7.8 Hz, 1H, C19H/C7H), 7.33 (td, *J* = 7.6, 1.2 Hz, 2H, (C8H, C6H)/(C18H, C20H)), 7.28 (dd, *J* = 7.8, 1.2 Hz, 2H, (C18H, C20H)/(C8H, C6H)), 5.56-5.47 (m, 1H, N29H), 5.23 (s, 1H, N37H), 4.70 (d, *J* = 10.9 Hz, 1H, N39H), 4.52-4.42 (m, 2H, C40H, C3H), 4.24 (dd, *J* = 4.8, 2.3 Hz, 1H, C36H), 4.17 (t, *J* = 11.4 Hz, 1H, C2H), 3.92-3.82 (m, 1H, C2H), 3.85-3.76 (m, 1H, C28H), 3.25 (m, 1H, C28H), 3.22 (m, 1H, C22H/C25H), 3.11 (m, 1H, C10H/C13H), 3.08 (m, 1H, C35H), 3.04-2.99 (m, 1H, C25H/C22H), 2.98-2.92 (m, 1H, C13H/C10H), 2.88 (ddd, *J* = 12.9, 5.0, 2.8 Hz, 1H, C41H), 2.66 (dd, *J* = 12.8, 2.4 Hz, 1H, C41H), 1.98 (m, 2H, C31H<sub>2</sub>), 1.65-1.60 (m, 2H,

C34H<sub>2</sub>), 1.53-1.49 (m, 2H, C32H<sub>2</sub>), 1.47 (d, *J* = 6.8 Hz, 3H, CH<sub>3</sub>), 1.43 (d, *J* = 6.8 Hz, 3H, CH<sub>3</sub>), 1.35 (m, 18H, 4xCH<sub>3</sub>), 1.29-1.21 (m, 2H, C33H<sub>2</sub>).

<sup>13</sup>C NMR (126 MHz, CD<sub>2</sub>Cl<sub>2</sub>) δ 197.24 (C1), 173.63 (C30), 163.35 (C38), 147.94-147.09 (C9, C5, C17, C21), 134.55 (C4/C16), 133.41 (C16/C4), 130.88-130.61 (C7, C19), 125.85-125.07 (C8, C6, C18, C20), 65.84 (C3), 62.24 (C36), 60.59 (C40), 58.35 (C2), 55.87 (C35), 42.24 (C28), 41.12 (C41), 36.06 (C31), 29.72-29.37 (C22, C25, C10, C13), 28.69-28.66 (C32, C34), 26.38 (CH<sub>3</sub>), 25.66 (C33), 25.42(CH<sub>3</sub>), 25.31(CH<sub>3</sub>), 24.65 (CH<sub>3</sub>), 24.29 (CH<sub>3</sub>), 23.86 (CH<sub>3</sub>).

HR-MS (ESI, pos): *m/z* calcd. for C<sub>38</sub>H<sub>55</sub>AuCIN<sub>5</sub>O<sub>2</sub>SH<sup>+</sup> 878.3503 found 878.3506 [M+H]<sup>+</sup>; C<sub>38</sub>H<sub>55</sub>AuCIN<sub>5</sub>O<sub>2</sub>SNa<sup>+</sup> 900.3323 found 900.3325 [M+Na]<sup>+</sup>.

### Synthesis of the gold complex Me<sub>2</sub>biot-Au 2



The biotinylated gold complex **Me<sub>2</sub>biot-Au 2** was prepared following the general procedure E1 yielding the product as a white solid (11 mg, 0.013 mmol, 27%):

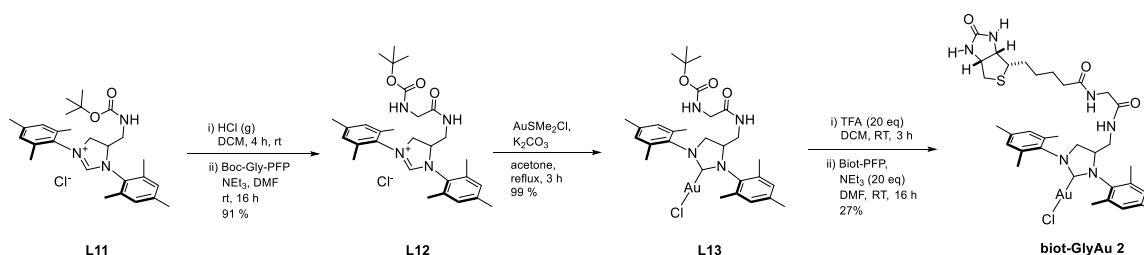
<sup>1</sup>H NMR (500 MHz, CD<sub>2</sub>Cl<sub>2</sub>) δ 7.06 (s, 1H, C8H/C6H), 7.04 (s, 1H, C6H/C8H), 7.01 (s, 2H, C15H, C17H), 5.44 (t, *J* = 6.3 Hz, 1H, N23H), 4.51 (ddd, *J* = 12.9, 8.5, 6.0 Hz, 1H, C3H), 4.16 – 4.10 (m, 1H, C34H), 4.11 (q, *J* = 12.0, 11.4 Hz, 1H, C2H), 3.88 (dd, *J* = 8.8, 5.1 Hz, 1H, C30H), 3.83 (ddd, *J* = 11.7, 8.7, 4.8 Hz, 1H, C2H), 3.81 – 3.72 (m, 1H, C22H), 3.23 (m, 1H, C22H), 3.20 (m, 1H, C29H), 2.82 (d, *J* = 4.1 Hz, 2H, C35H<sub>2</sub>), 2.79 (s, 3H, C31H), 2.71 (d, *J* = 2.2 Hz, 3H, C33H), 2.43 (s, 3H, C10H<sub>3</sub>/C11H<sub>3</sub>), 2.37 (s, 3H, C19H<sub>3</sub>/C20H<sub>3</sub>), 2.35 (s, 3H, C12H<sub>3</sub>), 2.33 (s, 3H, C21H<sub>3</sub>), 2.31 (s, 6H, C11H<sub>3</sub>/C10H<sub>3</sub>, C20H<sub>3</sub>/C19H<sub>3</sub>), 2.07 – 1.89 (m, 2H, C25H<sub>2</sub>), 1.67 (m, 2H, C28H<sub>2</sub>), 1.45 (m, 2H, C26H<sub>2</sub>), 1.31 (s, 1H, C27H<sub>2</sub>).

<sup>13</sup>C NMR (126 MHz, CD<sub>2</sub>Cl<sub>2</sub>) δ 196.10 (C1), 173.63 (C24), 162.10 (C32), 139.85-139.82 (C7, C16), 136.80 (C4), 136.33 (C13), 136.14 (C5/C9), 135.13 (C14, C18), 134.39 (C9/C5), 130.78 (C8/C6), 130.54 (C6/C8), 130.22 (C15, C17), 130.17 (C15, C17), 67.18 (C3), 64.74

(C30), 63.52 (C34), 56.26 (C29), 55.33 (C2), 42.40 (C22), 36.48 (C25), 35.75 (C35), 33.14 (C31), 32.15 (C27), 29.63 (C33), 29.56-29.33 (C26), 25.67 (C28), 21.42 (C12, C21), 19.57 (C10/C11), 18.53 (C19/C20), 18.36 (C11/C10), 18.33 (C20/C19).

HR-MS (ESI, pos):  $m/z$  calcd. for  $C_{34}H_{47}AuN_5O_2S^+$  786.3116 found 786.3104  $[M-Cl]^+$ ;  
 $C_{34}H_{47}AuClN_5O_2S Na^+$  844.2697 found 844.2682  $[M+Na]^+$ .

### Synthesis of the gold complex biot-GlyAu2



In a dried, nitrogen-flushed, two-headed flask equipped with a gas outlet and a septum, boc-protected NHC **L11** (100 mg, 0.212 mmol, 1 eq) was dissolved in dry  $CH_2Cl_2$  (4 mL). The mixture was stirred at room temperature (2 h) under consistent HCl-gas flow. The HCl-gas was prepared through dropwise addition of concentrated sulfuric acid to ammonium chloride powder and introduced to the reaction mixture via cannula. After two hours, the cannula was removed and the mixture was stirred at room temperature (2 h) before evaporating the solvent (reaction control with ninhydrin-stained TLC). The crude was dissolved in dry DMF (3 mL) and transferred to a vial containing PFP Boc-glycinate (72.3 mg, 0.212 mmol, 1 eq) before adding trimethylamine (0.60 mL, 4.24 mmol, 20 eq). The mixture was stirred at room temperature (16 h). Silica was added to the mixture and the solvent was removed *in vacuo*. The crude was purified via flash column chromatography (KP-Sil 25 g, gradient of 3% to 25% methanol in  $CH_2Cl_2$ ) to yield NHC **L12** as a white solid (102 mg, 0.193 mmol, 91%):

$^1H$  NMR (600 MHz,  $DMSO-d_6$ )  $\delta$  9.10 (s, 1H), 8.16 (t,  $J = 6.0$  Hz, 1H), 7.10 (m, 4H), 7.03 (t,  $J = 6.0$  Hz, 1H), 4.96 – 4.86 (m, 1H), 4.59 (t,  $J = 11.7$  Hz, 1H), 4.25 (dd,  $J = 12.1, 7.4$  Hz, 1H), 3.59 – 3.52 (m, 1H), 3.41 (d,  $J = 5.4$  Hz, 2H), 3.26 (dt,  $J = 12.9, 5.0$  Hz, 1H), 2.39 (s, 3H), 2.36 (s, 3H), 2.31 (s, 3H), 2.31 – 2.27 (m, 9H), 1.34 (s, 9H).

$^{13}C$  NMR (151 MHz,  $DMSO-d_6$ )  $\delta$  170.54, 160.39, 155.79, 139.86, 139.54, 135.45, 135.40, 135.36, 78.20, 61.92, 54.43, 45.43, 43.39, 28.13, 20.60, 20.54, 18.14, 17.78, 17.38, 17.14.

HR-MS (ESI, pos):  $m/z$  calcd. for  $C_{29}H_{41}N_4O_3^+$  493.3173 found 493.3169  $[M-Cl]^+$ .

Gold complex **L13** was prepared following the general procedure D2 yielding the product as a golden solid (70 mg, 0.096 mmol, 99%):

$^1\text{H}$  NMR (500 MHz, Methylene Chloride- $d_2$ )  $\delta$  7.06 (d,  $J$  = 12.0 Hz, 2H), 7.01 (s, 2H), 6.09 (s, 1H), 4.76 (s, 1H), 4.61 – 4.47 (m, 1H), 4.09 (t,  $J$  = 11.4 Hz, 1H), 3.81 (dd,  $J$  = 11.6, 8.7 Hz, 1H), 3.79 – 3.71 (m, 1H), 3.58 (qd,  $J$  = 17.0, 6.1 Hz, 2H), 3.29 (dt,  $J$  = 13.8, 5.4 Hz, 1H), 2.43 (s, 3H), 2.36 (d,  $J$  = 3.9 Hz, 6H), 2.33 (s, 3H), 2.31 (s, 6H), 1.42 (s, 9H).

$^{13}\text{C}$  NMR (126 MHz, Methylene Chloride- $d_2$ )  $\delta$  196.28, 139.86, 136.87, 136.27, 136.23, 136.08, 135.05, 134.41, 130.78, 130.62, 130.22, 130.19, 63.29, 55.25, 42.28, 28.54, 21.43, 21.41, 19.55, 18.50, 18.36, 18.31.

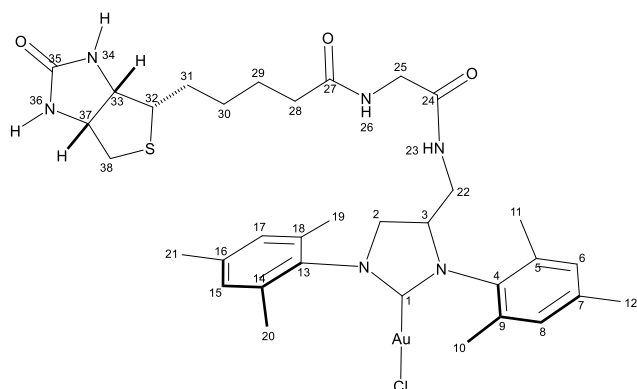
HR-MS (ESI, pos):  $m/z$  calcd. for  $\text{C}_{29}\text{H}_{40}\text{AuN}_4\text{O}_3\text{NH}_3^+$  706.3026 found 706.3033  $[\text{M}+\text{NH}_3-\text{Cl}]^+$ .

Biotinylated gold complex **biot-GlyAu 2** was prepared following the general procedure E1 yielding the product as a white solid (8 mg, 0.018 mmol, 27%):

$^1\text{H}$  NMR (500 MHz, Methylene Chloride- $d_2$ )  $\delta$  7.39 (d,  $J$  = 6.2 Hz, 1H, N23H), 7.21 (s, 1H, N26H), 7.02 (m, 2H, C6H, C8H), 7.00 (s, 2H, C15H, C17H), 6.54 (d,  $J$  = 5.1 Hz, 1H, N34H), 5.22 (d,  $J$  = 40.6 Hz, 1H, N36H), 4.50 (m, 1H, C3H), 4.41 (q,  $J$  = 7.1 Hz, 1H, C37H), 4.22 (p,  $J$  = 4.6, 4.2 Hz, 1H, C33H), 4.10 (td,  $J$  = 11.3, 5.1 Hz, 1H, C2H<sub>2</sub>), 3.89 – 3.81 (m, 2H, C2H<sub>2</sub>, C25H<sub>2</sub>), 3.70 – 3.60 (m, 2H, C25H<sub>2</sub>, C22H<sub>2</sub>), 3.29 (d,  $J$  = 10.0 Hz, 1H, C22H<sub>2</sub>), 3.07 (q,  $J$  = 7.3, 6.2 Hz, 1H, C32H), 2.85 (dt,  $J$  = 12.9, 4.5 Hz, 1H, C38H<sub>2</sub>), 2.57 (t,  $J$  = 13.6 Hz, 1H, C38H<sub>2</sub>), 2.39 (s, 3H, C10H<sub>3</sub>/C11H<sub>3</sub>), 2.36 (s, 3H, C19H<sub>3</sub>/C20H<sub>3</sub>), 2.33 (s, 3H, C12H<sub>3</sub>), 2.32 (s, 3H, C21H<sub>3</sub>), 2.31 (s, 3H, C11H<sub>3</sub>/C10H<sub>3</sub>), 2.30 (m, 3H, C20H<sub>3</sub>/C19H<sub>3</sub>), 2.22 – 2.07 (m, 2H, C28H<sub>2</sub>), 1.63 – 1.52 (m, 4H, C31H<sub>2</sub>, C29H<sub>2</sub>), 1.32 – 1.28 (m, 2H, C30H<sub>2</sub>).

$^{13}\text{C}$  NMR (126 MHz, Methylene Chloride- $d_2$ )  $\delta$  195.87 (C1), 174.60 (C27), 171.14-171.05 (C24), 164.42 (C35), 139.76-139.64 (C7, C16), 137.12 (C4), 136.41-136.18 (C13), 63.16 (C3), 62.33 (C33), 60.68 (C37), 56.10-55.57 (C2), 46.59 (C32), 43.65 (C25), 42.13 (C22), 41.16-41.01 (C38), 35.38 (C28), 28.58 (C29/C31), 28.25-28.13 (C30), 25.72-25.57 (C31/C29), 21.43 (C12, C21), 19.64 (C10), 18.52 (C11/C19), 18.38 (C20).

HR-MS (ESI, pos):  $m/z$  calcd. for  $\text{C}_{34}\text{H}_{46}\text{AuN}_6\text{O}_3\text{S}^+$  815.3012, 816.3045, 817.3076 found 815.3010, 816.3032, 817.3031  $[\text{M}-\text{Cl}]^+$ ,  $(\text{C}_{34}\text{H}_{46}\text{AuN}_6\text{O}_3\text{S})_2^{2+}$  815.3012, 815.8028, 816.3043, 816.8012 found 815.3010, 815.8026, 816.3032, 816.8030  $[\text{M}-\text{Cl}]_2^{2+}$ ,



## Hydroamination screening & reaction optimization

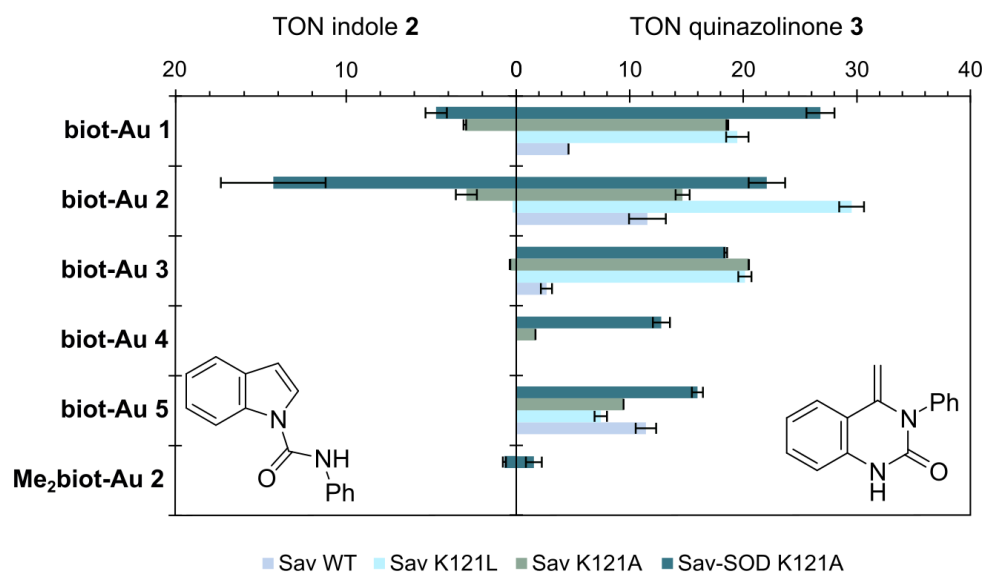
### Cofactor screening

	Cofactor only		Sav WT		Sav K121L		Sav K121A		Sav-SOD K121A	
	TON quinazolinone <b>3</b>	TON indole <b>2</b>	TON quinazolinone <b>3</b>	TON indole <b>2</b>	TON quinazolinone <b>3</b>	TON indole <b>2</b>	TON quinazolinone <b>3</b>	TON indole <b>2</b>	TON quinazolinone <b>3</b>	TON indole <b>2</b>
<b>biot-Au 1</b>	0	0	4.6 ± 0.0	0	19.5 ± 1.0	0	18.6 ± 0.1	3.0 ± 0.1	26.8 ± 1.2	4.7 ± 0.6
<b>biot-Au 2</b>	0	0	11.6 ± 1.6	0	29.5 ± 1.1	0.2 ± 0.1	14.7 ± 0.5	2.9 ± 0.6	22.1 ± 1.6	14.3 ± 3.1
<b>biot-Au 3</b>	0	0	2.7 ± 0.5	0	20.1 ± 0.6	0	20.5 ± 0.8	0.4 ± 0.1	18.5 ± 0.1	0
<b>biot-Au 4</b>	0	0	0	0	0	0	1.7 ± 0.4	0	12.8 ± 0.8	0
<b>biot-Au 5</b>	0	0	11.4 ± 0.9	0	7.4 ± 0.5	0	9.5 ± 0.1	0	16.0 ± 0.5	0
<b>Me<sub>2</sub>biot-Au 2</b>	0	0	0	0	0	0	0	0	1.55 ± 0.7	0.7 ± 0.09

**SI  
Table  
1**

Tabulation of data displayed in **SI Figure 2**.

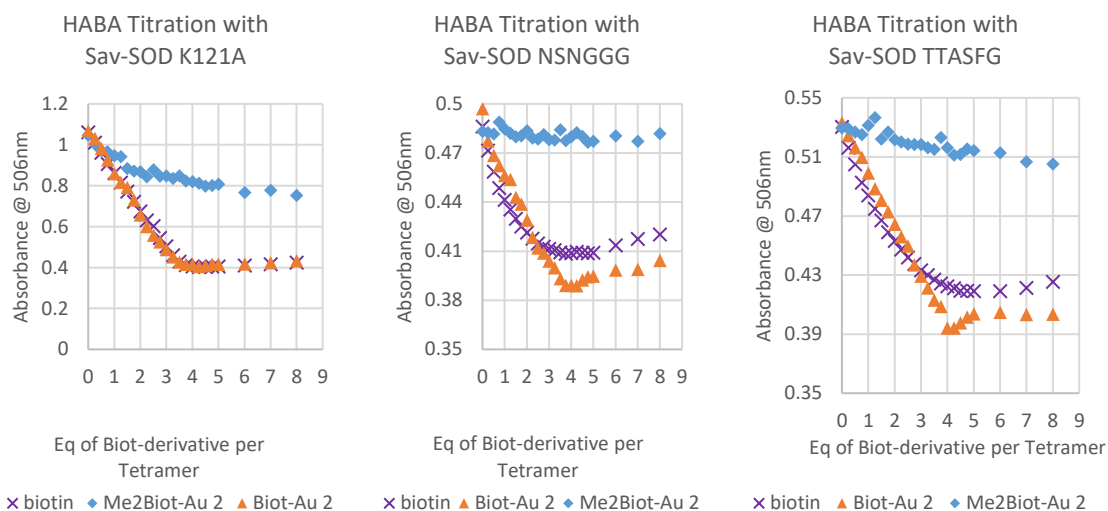
All experiments were conducted as duplicates. An Eppendorf tube (1500  $\mu$ L) was charged successively with MES-buffer (165  $\mu$ L, 50 mM, pH 5), purified protein (20  $\mu$ L of 1000  $\mu$ M BBS in MQ-water) and cofactor (5  $\mu$ L of 2 mM in DMSO). The tubes were incubated in a thermoshaker (20 min, 37  $^{\circ}$ C, 900 rpm). Afterwards, substrate 1 (10  $\mu$ L of 100 mM in DMSO) was added and the tubes were shaken in a thermoshaker for 24 hours. The reaction was quenched by the addition of methanol (200  $\mu$ L), followed by centrifugation (14'000 rpm, 10  $^{\circ}$ C, 10 min). In UPLC vials, the reaction mixture (20  $\mu$ L) was diluted in UPLC media (980  $\mu$ L, 1:1 MeCN:MQ-Water containing 20.4  $\mu$ M of phthalane) before UPLC-MS analysis.



**SI Figure 2** Cofactor screening using purified Sav samples: [**biot-Au 2**] = 1 mol%, [Sav] = 2 mol%, MES-buffer pH = 5, 37 °C and 24 h reaction time. All reactions were performed in duplicate.

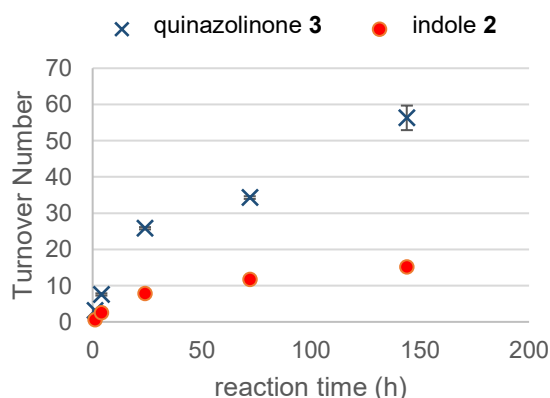
### Control experiments and reaction optimization

An Eppendorf tubes (1500  $\mu$ L) was charged successively with MES-buffer (165  $\mu$ L, 50 mM, pH 5) or a mixture of MES-buffer and cell lysate (BL21 *E. coli* with DNase and lysozyme in MQ water), purified protein (20  $\mu$ L of 1000  $\mu$ M BBS in MQ-water), additives (dissolved either in DMSO or MQ water) and cofactor (5  $\mu$ L of 2 mM in DMSO). All additives were freshly prepared prior to each run. The tubes were incubated in a thermoshaker (20 min, 37 °C, 900 rpm). Afterwards, substrate **1** (10  $\mu$ L of 100 mM in DMSO) was added and the tubes were shaken in a thermoshaker for the indicated reaction time at 37 °C. The reaction was quenched by the addition of methanol (200  $\mu$ L) followed by centrifugation (14'000 rpm, 10 °C, 10 min). In UPLC vials, the reaction mixture (20  $\mu$ L) was diluted in UPLC media (980  $\mu$ L, 1:1 MeCN:MQ-Water containing 40.8  $\mu$ M of phthalane) before UPLC-MS analysis.



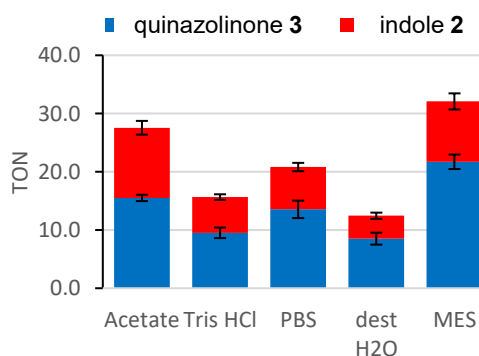
**SI Figure 3** HABA displacement titration of biotin and biotinylated cofactors **biot-Au 2** and **Me<sub>2</sub>biot-Au 2** in the presence of Sav-SOD K121A, Sav-SOD S112N T114S T115N N118G K121G S122G and Sav-SOD S112T T114T T115A N118S K121F S122G. For procedure see.<sup>219</sup>

Time (h)	TON quinazolinone <b>3</b>	TON indole <b>2</b>
1	3.7 ± 0.1	0.8 ± 0.0
3	8.0 ± 0.5	3.0 ± 0.1
6	11.9 ± 0.2	6.6 ± 0.2
24	22.1 ± 1.6	14.3 ± 3.1
72	33.1 ± 0.3	20.5 ± 0.1



**SI Figure 4** Timecourse of the HAMase conversion using **biot-Au 2** · Sav-SOD K121A: [**biot-Au 2**] 1 mol%, [Sav] = 2 mol%, MES-buffer pH 5, 37 °C.

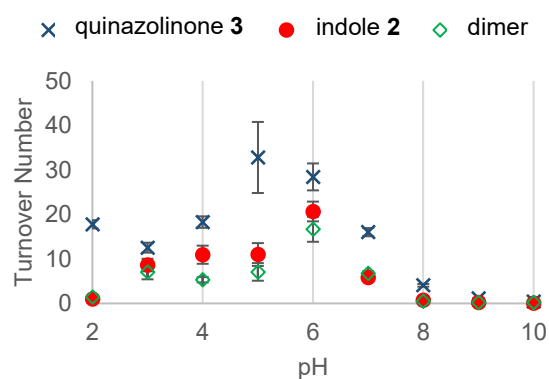
Buffer	TON quinazolinone <b>3</b>	TON indole <b>2</b>
Acetate	15.5 ± 0.5	12.0 ± 1.2
Tris HCl	9.5 ± 0.9	6.1 ± 0.5
PBS	13.5 ± 1.5	7.3 ± 0.7
MQ H <sub>2</sub> O	8.5 ± 1.0	3.9 ± 0.5
MES	21.7 ± 1.2	10.4 ± 1.4



**SI Figure 5** Reactivity of **biot-Au 2** · Sav-SOD K121A in different aqueous buffer: [**biot-Au 2**] 1 mol%, [Sav] 2 mol%, pH 5, 37 °C, 24 h reaction time.

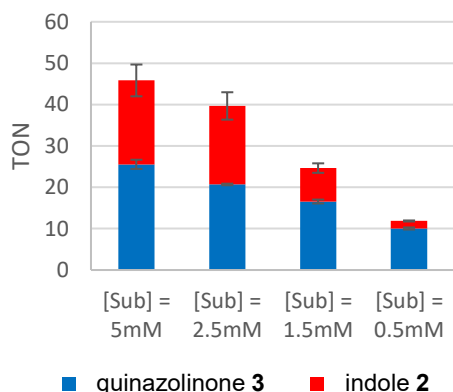


pH	TON quinazolinone 3	TON indole 2	TON dimer
2	17.8 ± 0.9	1.0 ± 0.0	1.4 ± 0.1
3	12.5 ± 1.1	8.6 ± 1.4	7.1 ± 1.7
4	18.3 ± 1.3	10.9 ± 2.0	5.3 ± 0.6
5	32.8 ± 8.0	11.0 ± 2.6	7.1 ± 2.0
6	28.4 ± 3.0	20.7 ± 2.2	16.7 ± 2.8
7	16.0 ± 0.9	5.8 ± 0.0	6.8 ± 0.4
8	4.1 ± 0.3	0.7 ± 0.0	0.5 ± 0.0
9	1.2 ± 0.1	0.2 ± 0.0	0.2 ± 0.0
10	0.5 ± 0.0	0.1 ± 0.0	0.2 ± 0.0



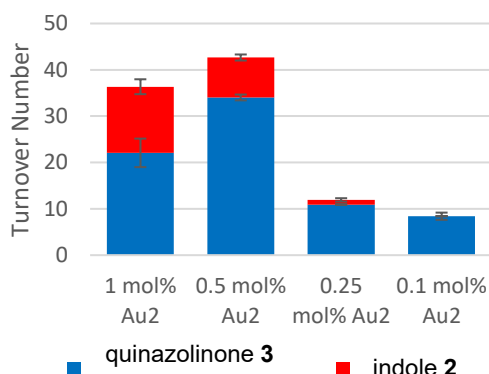
**SI Figure 6** Reactivity of **biot-Au 2** · Sav-SOD K121A at different pH in MES-Buffer: [**biot-Au 2**] 1 mol%, [Sav] 2 mol%, 37 °C and 72 h reaction time. All reactions were performed in duplicates.

[Sub 1] = mM	TON quinazolinone 3	TON indole 2
5	25.5 ± 1.1	20.3 ± 3.8
2.5	20.7 ± 0.2	19.0 ± 3.3
1.5	16.6 ± 0.5	8.1 ± 1.1
0.5	10.0 ± 0.3	1.8 ± 0.1

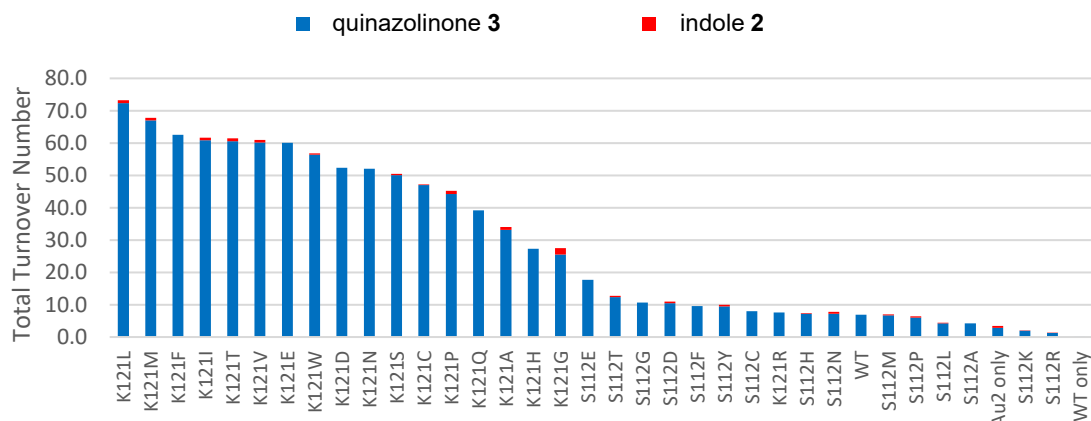


**SI Figure 7** Performance of chimeric streptavidin with different substrate concentrations. Reaction conditions: [**biot-Au 2**] = 1 mol%, [Sav] = 2 mol%, MES-buffer pH = 5, 37 °C and 28 h reaction time. All reactions were performed in duplicates.

c( <b>biot-Au 2</b> ) in mol%	TON quinazolinone 3	TON indole 2
1.00	22.1 ± 1.6	14.3 ± 3.1
0.50	34.0 ± 0.7	8.6 ± 0.6
0.25	10.9 ± 0.4	1.0 ± 0.1
0.10	8.4 ± 0.8	0



**SI Figure 8** Reactivity of **biot-Au 2** · Sav-SOD K121A with varying cofactor concentrations. Reaction conditions: [Sav] = 2x[**biot-Au 2**], MES-buffer pH = 5, 37 °C and 24 h reaction time. All reactions were performed in duplicates.



**SI Figure 9** Screening Sav mutants bearing mutations on position K121 or S112: [biot-Au 2] 1 mol%, [Sav] 2 mol%, MES-buffer pH 5, 37 °C and 5 days reaction time. All reactions were performed in duplicates.

**SI Table 2** Summary of the HAMase activity screening using Sav mutants: [biot-Au 2] 1 mol%, [Sav] 2 mol%, MES-buffer pH 5, 37 °C and 5 days reaction time. All reactions were performed in duplicates.

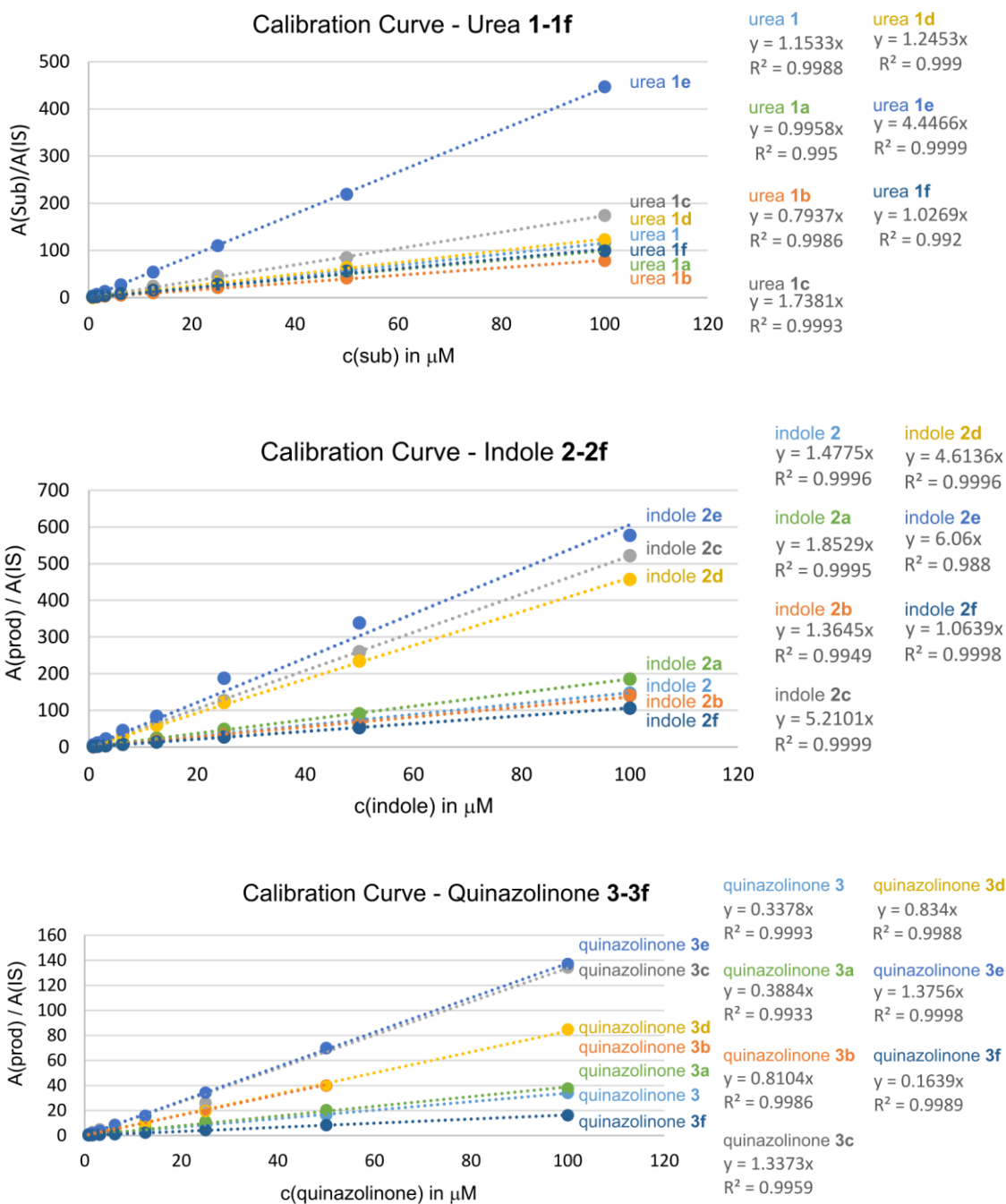
Sav Mutants	TON quinazolinone 3	TON indole 2
K121L	72.4 ± 2.0	0.8 ± 0.1
K121M	67.0 ± 0.4	0.8 ± 0.1
K121F	62.5 ± 0.7	0
K121I	60.8 ± 1.3	0.8 ± 0.1
K121T	60.6 ± 0.8	0.9 ± 0.2
K121V	60.1 ± 0.9	0.8 ± 0.1
K121E	60.1 ± 4.4	0
K121W	56.4 ± 0.7	0.4 ± 0.1
K121D	52.3 ± 0.8	0
K121N	52.1 ± 1.7	0
K121S	50.1 ± 0.8	0.4 ± 0.1
K121C	47.0 ± 1.2	0.2 ± 0.1
K121P	44.3 ± 0.9	0.9 ± 0.1
K121Q	39.2 ± 0.6	0
K121A	33.1 ± 0.5	0.9 ± 0.1
K121H	27.3 ± 0.8	0
K121G	25.5 ± 0.3	1.9 ± 0.1
S112E	17.7 ± 0.4	0
S112T	12.3 ± 0.2	0.4 ± 0.1
S112G	10.6 ± 0.4	0
S112D	10.5 ± 0.0	0.5 ± 0.1
S112F	9.6 ± 0.1	0
S112Y	9.5 ± 0.0	0.5 ± 0.1
S112C	8.0 ± 0.2	0
K121R	7.6 ± 0.9	0
S112H	7.2 ± 0.4	0.2 ± 0.1
S112N	7.2 ± 0.0	0.6 ± 0.1
WT	6.9 ± 0.1	0
S112M	6.7 ± 0.2	0.3 ± 0.1
S112P	6.0 ± 0.1	0.4 ± 0.1
S112L	4.2 ± 0.2	0.2 ± 0.1
S112A	4.2 ± 0.1	0
biot-Au 2 only	2.8 ± 0.1	0.6 ± 0.1
S112K	2.0 ± 0.0	0.1 ± 0.1
S112R	1.3 ± 0.2	0.1 ± 0.1
WT without biot-Au 2	0.1 ± 0.1	0

**SI Table 3** Evaluation of the reactivity and stability of various gold-complexes and gold-based ArM

Au-Complex	Mutant	Additives	TON quinazolinone 3	TON indole 2
(CH <sub>3</sub> ) <sub>2</sub> SAuCl	-	none	0	0.2 ± 0.0
AuSIMes	-	none	1.3 ± 0.5	0.6 ± 0.0
AuIMes	-	none	0.3 ± 0.3	0.2 ± 0.1
AuSIPr	-	none	0.2 ± 0.2	0.0 ± 0.0
AuIPr	-	none	0.3 ± 0.3	0.0 ± 0.0
<b>biot-Au 2</b>	-	none	1.3 ± 0.1	0.2 ± 0.0
AuSIMes	Sav K121L	none	0	0.3 ± 0.1
<b>biot-Au 2</b>	Sav K121L	none	47.5 ± 1.4	2.1 ± 0.0
<b>biot-Au 2</b>	Sav-SOD K121A	none	33.1 ± 0.3	20.5 ± 0.1
<b>biot-Au 2</b>	Sav-SOD K121A	10% cell lysate	14.7 ± 0.3	5.1 ± 0.1
<b>biot-Au 2</b>	Sav-SOD K121A	50% cell lysate	12.9 ± 0.3	2.3 ± 0.0
<b>biot-Au 2</b>	Sav-SOD K121A	2 mol% GSH red <sup>c</sup>	28.7 ± 0.7	9.5 ± 0.4
<b>biot-Au 2</b>	Sav-SOD K121A	20 mol% GSH red <sup>c</sup>	22.3 ± 1.1	6.2 ± 0.3
<b>biot-Au 2</b>	Sav-SOD K121A	100 mol% GSH red <sup>c</sup>	7.4 ± 0.1	1.2 ± 0.1
<b>biot-Au 2</b>	Sav-SOD K121A	100 mol% GSH red <sup>d</sup>	7.4 ± 0.5	1.4 ± 0.0
<b>biot-Au 2</b>	Sav-SOD K121A	100 mol% GSH ox <sup>d</sup>	33.6 ± 0.4	12.8 ± 0.4
<b>biot-Au 2</b>	Sav-SOD K121A	1 mol% biotin <sup>d</sup>	19.0 ± 0.5	10.2 ± 1.3
<b>biot-Au 2</b>	Sav-SOD K121A	2 mol% biotin <sup>d</sup>	12.0 ± 0.6	3.8 ± 0.3
<b>biot-Au 2</b>	Sav-SOD K121A	2 mol% biotin <sup>c</sup>	15.9 ± 0.3	3.7 ± 0.2
<b>biot-Au 2</b>	Sav-SOD K121A	4 mol% biotin <sup>d</sup>	6.7 ± 0.6	1.8 ± 0.2
<b>biot-Au 2</b>	Sav-SOD K121A	100 mol% Diamide <sup>d</sup>	20.2 ± 0.4	34.2 ± 0.0
<b>biot-Au 2</b>	-	100 mol% Diamide <sup>d</sup>	10.0 ± 0.8	3.4 ± 0.3

<sup>a</sup>Reaction conditions: V<sub>tot</sub> 200 μL (V<sub>DMSO</sub> 15 μL), [Sub] 5 mM, [**biot-Au 2**] 50 μM, [Sav] 100 μM, MES-buffer pH 5 + cell lysate, 37 °C for 72 h. The reactions were carried out in duplicates.  
<sup>b</sup>Turnover Number <sup>c</sup>Additive added before cofactor incubation <sup>d</sup>Additive added after cofactor incubation

## Calibration curves for UPLC-MS

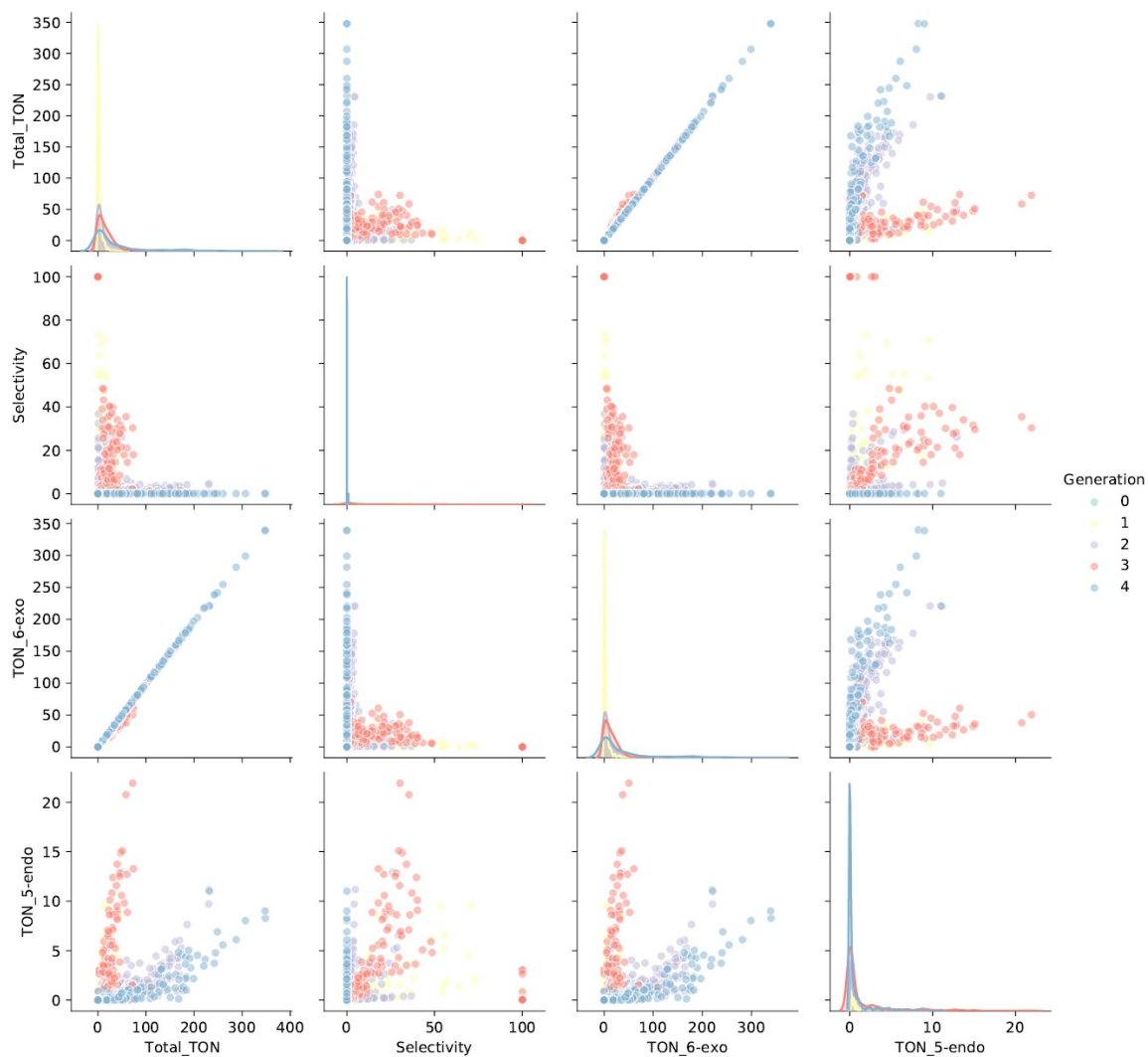


## Catalysis in cell-free extracts

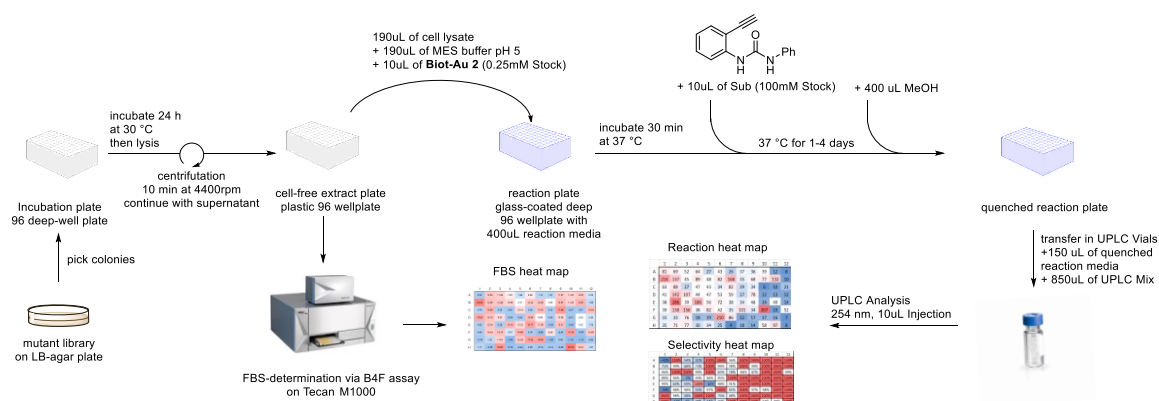
Each pipetting operation was followed by five mixing steps. In a glass 96-well plate, cell-free extracts (190  $\mu$ L) were mixed with MES buffer (190  $\mu$ L, pH 5, 50 mM). To the mixture, **biot-Au 2** (10  $\mu$ L, 0.25 mM in DMSO) was added, the plate was sealed with aluminum foil and shaken (30 min at 37 °C). Afterwards, the substrate (10  $\mu$ L, 100 mM in DMSO) was added, the plate was sealed and the mixture was shaken (4 days at 37 °C). The reaction was quenched by addition of MeOH (400  $\mu$ L, HPLC grade). In UPLC vials, the reaction mixture (150  $\mu$ L) was diluted in UPLC media (850  $\mu$ L, 1:1 MeCN:MQ-Water containing 40  $\mu$ M of phthalane and 0.1% formic acid) prior to UPLC-MS analysis. For the first round of directed evolution on position N118, K121 and S122, our hit selection was based on the measured activity and selectivity in relation to the B4F assay as the expression levels varied. Expression was optimized, thus for next rounds of directed evolution, hit selection was based solely on activity and selectivity.

**SI Table 4** Investigation of *E. coli* strains for cell-free extract catalysis with various ratios of MES buffer (pH 5, 50 mM) to cell-free extract (cfe) before directed evolution.

E.Coli Strain	Mutant	Amount of cfe (%)	TON quinazolinone <b>3</b>	TON indole <b>2</b>
BL21(DE3)	emptyV	100	0	0
BL21(DE3)	Sav_WT	100	0	0
BL21(DE3)	Sav_K121L	100	0	0
BL21(DE3)	emptyV	50	0	0
BL21(DE3)	Sav_WT	50	1	0
BL21(DE3)	Sav_K121L	50	11	0
BL21(DE3)	emptyV	30	0	0
BL21(DE3)	Sav_WT	30	2	0
BL21(DE3)	Sav_K121L	30	15	0
SHuffle-T7	emptyV	50	0	0
SHuffle-T7	Sav_WT	50	0	0
SHuffle-T7	Sav_K121L	50	0	0
SHuffle-T7	emptyV	30	0	0
SHuffle-T7	Sav_WT	30	0	0
SHuffle-T7	Sav_K121L	30	0	0



**SI Figure 10** Scatterplot of 2500 cell-free-extract experiments covering 4 Generations of chimeric streptavidin analyzed via UPLC-MS after preselection via B4F-assay displaying the two evolution trajectories of HAMase.



**SI Figure 11** Workflow for the directed evolution of Sav-SOD K121A using cell-free extracts for screening.

## Determination of the biotin-binding sites

First, a solution of B4F (1  $\mu$ M) in MOPS (50 mM, pH = 7.4) was prepared. Then, 200  $\mu$ L of this B4F solution was added to a clear micro wellplate, followed by 10  $\mu$ L of cell-free extract (cfe). The negative control contained 10  $\mu$ L of lysis buffer (LB). The positive control (Sav<sub>STD</sub>) contained 10  $\mu$ L of 40  $\mu$ M Sav as 100% saturation point. It should be noted that, the lysis buffer and protein components can alter the B4F fluorescence up to 10-20%. The fluorescence of each well was measured using a Tecan fluorimeter Infinite M1000Pro. The total concentration of Sav should be linear within this region and calculated using the following equation:

$$[\text{SAV}_{\text{CFE}}](\mu\text{M}) = [(F_{\text{CFE}} - F_{\text{SAVSTD}}) - (F_{\text{LB}} - F_{\text{SAVSTD}})] / (-F_{\text{LB}} - F_{\text{SAVSTD}}) * 20$$

$F_{\text{CFE}}$  = Fluorescence intensity of Cell free extract

$F_{\text{SAVSTD}}$  = Fluorescence intensity of Sav Standard to bind all free BF4

$F_{\text{LB}}$  = Fluorescence intensity of Lysis buffer

## Summary of key experiments using purified Sav

Under the general UPLC-conditions (General Information), the following retention times were obtained internal standard (phthalane) at ~2.11 min, the quinazolinone **3** at ~2.64 min, the urea **1** at ~4.19 min, the indole **2** at ~5.05 min and a dimeric side product at 6.40 min. Higher MeOH content changes the retention times (see optimized conditions **SI Table 5**). Standard reaction conditions:  $V_{\text{tot}}$  200  $\mu$ L ( $V_{\text{DMSO}}$  15  $\mu$ L), [Sub] 5 mM, [**biot-Au 2**] 50  $\mu$ M, [Sav] 100  $\mu$ M, MES-buffer pH 5, 37 °C for 24 h. The reactions were carried out in two sets of duplicates; The reactions were quenched with MeOH to a total volume of 800  $\mu$ L followed by centrifugation (14'000 rpm, 10 °C, 10 min). In UPLC vials, the reaction mixture (40  $\mu$ L) was diluted in UPLC media (960  $\mu$ L, 1:1 MeCN:MQ-Water containing 40.8  $\mu$ M of phthalane) before UPLC-MS analysis

**SI Table 5** Selected Results of evolved ArMs with and without SOD loop. <sup>a b</sup>

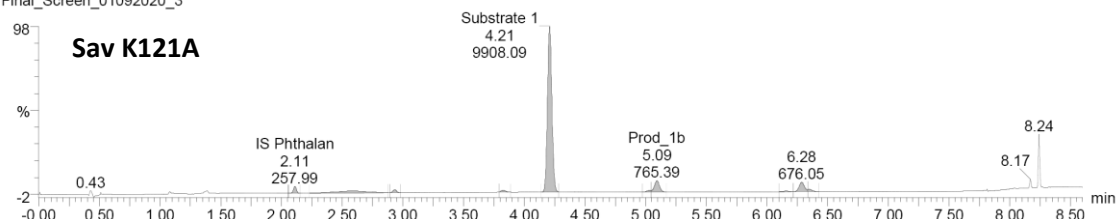
Mutant	TON quinazolinone <b>3</b>	TON indole <b>2</b>	TON Total	Selectivity for indole <b>2</b>
Sav K121A	17.95	3.52	21.48	16.4%
Sav K121A	17.00	3.91	20.91	18.7%
Sav K121A	18.72	3.99	22.71	17.6%
Sav K121A	17.60	3.29	20.89	15.8%
Sav-SOD K121A	25.49	16.18	41.67	38.8%
Sav-SOD K121A	24.08	16.09	40.17	40.1%
Sav-SOD K121A	24.73	12.38	37.11	33.4%
Sav-SOD K121A	23.64	15.48	39.12	39.6%
Sav-SOD N118G K121G S122G	27.52	33.92	61.44	55.2%
Sav-SOD N118G K121G S122G	25.50	30.19	55.68	54.2%
Sav-SOD N118G K121G S122G	26.97	34.72	61.68	56.3%

Sav-SOD N118G K121G S122G	23.95	28.01	51.96	53.9%
Sav-SOD N118S K121F S122G	38.59	0.38	38.97	1.0%
Sav-SOD N118S K121F S122G	37.89	0.45	38.34	1.2%
Sav-SOD N118S K121F S122G	37.34	0.36	37.70	1.0%
Sav-SOD N118S K121F S122G	39.64	0.45	40.10	1.1%
Sav_SOD S112N N118G K121G S122G	21.90	44.78	66.68	67.2%
Sav_SOD S112N N118G K121G S122G	20.92	44.67	65.59	68.1%
Sav_SOD S112N N118G K121G S122G	21.13	44.51	65.64	67.8%
Sav_SOD S112N N118G K121G S122G	20.19	41.77	61.96	67.4%
Sav_SOD S112T N118S K121F S122G	40.42	1.07	41.49	2.6%
Sav_SOD S112T N118S K121F S122G	42.50	1.23	43.73	2.8%
Sav_SOD S112T N118S K121F S122G	40.24	1.03	41.27	2.5%
Sav_SOD S112T N118S K121F S122G	40.80	1.14	41.94	2.7%
Sav_SOD S112N T114S T115N N118G K121G S122G	18.14	55.07	73.21	75.2%
Sav_SOD S112N T114S T115N N118G K121G S122G	17.59	46.04	63.63	72.3%
Sav_SOD S112N T114S T115N N118G K121G S122G	18.54	52.31	70.85	73.8%
Sav_SOD S112N T114S T115N N118G K121G S122G	17.61	46.49	64.10	72.5%
Sav_SOD S112T T115A N118S K121F S122G	41.48	2.90	44.38	6.5%
Sav_SOD S112T T115A N118S K121F S122G	41.69	3.08	44.77	6.9%
Sav_SOD S112T T115A N118S K121F S122G	42.98	3.53	46.51	7.6%
Sav_SOD S112T T115A N118S K121F S122G	41.02	2.98	44.00	6.8%

Name: Final\_Screen\_01092020\_3, Date: 01-Sep-2020, Time: 12:24:18, ID: , Description:

#	Name	Trace	RT	Area	IS Area	Response	Primar...	Conc.	%Dev
1	1 IS Phthalan	AN1	2.11	257.988		257.988	bb		
2	2 Substrate 1	AN1	4.21	9908.093		9908.093	bb		
3	3 Prod_1a	AN1	2.58	724.845		724.845	MM		
4	4 Prod_1b	AN1	5.09	765.393		765.393	db		
5	5 Unkn Product	AN1							
6	6 Dimer	AN1	6.35	118.390		118.390	db		

Final\_Screen\_01092020\_3

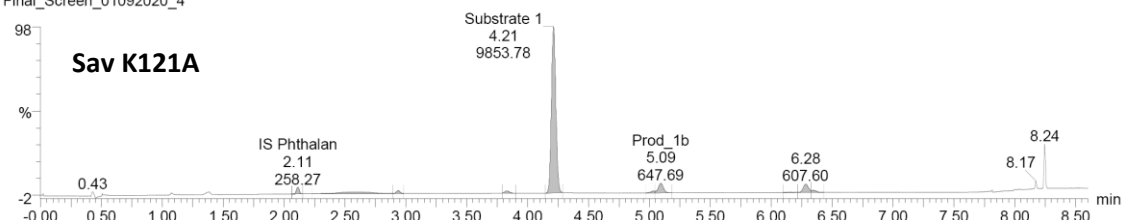




Name: Final\_Screen\_01092020\_4, Date: 01-Sep-2020, Time: 12:33:55, ID: , Description:

#	Name	Trace	RT	Area	IS Area	Response	Primar...	Conc.	%Dev
1	1 IS Phthalan	AN1	2.11	258.274		258.274	bb		
2	2 Substrate 1	AN1	4.21	9853.776		9853.776	bb		
3	3 Prod_1a	AN1	2.58	752.136		752.136	MM		
4	4 Prod_1b	AN1	5.09	647.686		647.686	db		
5	5 Unkn Product	AN1							
6	6 Dimer	AN1	6.35	140.270		140.270	db		

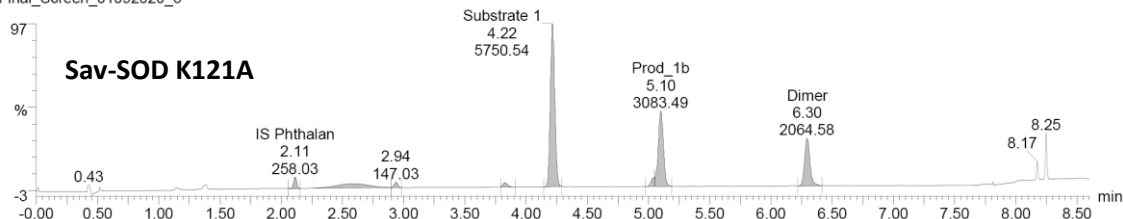
Final\_Screen\_01092020\_4



Name: Final\_Screen\_01092020\_5, Date: 01-Sep-2020, Time: 12:43:39, ID: , Description:

#	Name	Trace	RT	Area	IS Area	Response	Primar...	Conc.	%Dev
1	1 IS Phthalan	AN1	2.11	258.029		258.029	bb		
2	2 Substrate 1	AN1	4.22	5750.540		5750.540	bb		
3	3 Prod_1a	AN1	2.59	1035.922		1035.922	bd		
4	4 Prod_1b	AN1	5.10	3083.492		3083.492	db		
5	5 Unkn Product	AN1							
6	6 Dimer	AN1	6.30	2064.581		2064.581	bb		

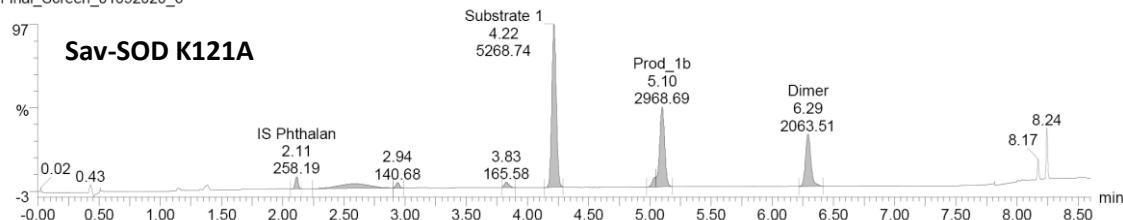
Final\_Screen\_01092020\_5



Name: Final\_Screen\_01092020\_6, Date: 01-Sep-2020, Time: 12:53:16, ID: , Description:

#	Name	Trace	RT	Area	IS Area	Response	Primar...	Conc.	%Dev
1	1 IS Phthalan	AN1	2.11	258.194		258.194	bb		
2	2 Substrate 1	AN1	4.22	5268.743		5268.743	bb		
3	3 Prod_1a	AN1	2.59	1017.084		1017.084	bd		
4	4 Prod_1b	AN1	5.10	2968.690		2968.690	db		
5	5 Unkn Product	AN1							
6	6 Dimer	AN1	6.29	2063.508		2063.508	bb		

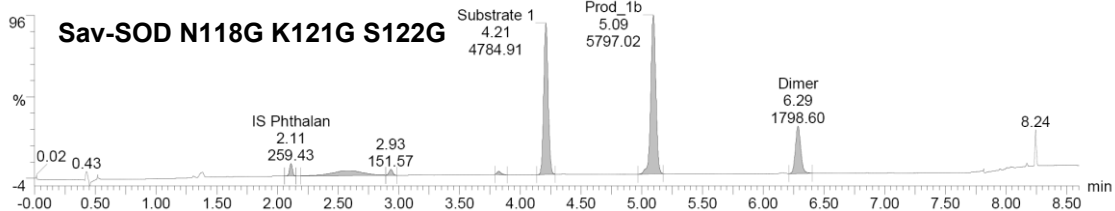
Final\_Screen\_01092020\_6



Name: Final\_Screen\_01092020\_9, Date: 01-Sep-2020, Time: 13:22:23, ID: , Description:

#	Name	Trace	RT	Area	IS Area	Response	Primar...	Conc.	%Dev
1	1 IS Phthalan	AN1	2.11	259.430		259.430	bb		
2	2 Substrate 1	AN1	4.21	4784.912		4784.912	bb		
3	3 Prod_1a	AN1	2.59	1104.106		1104.106	bd		
4	4 Prod_1b	AN1	5.09	5797.015		5797.015	bb		
5	5 Unkn Product	AN1							
6	6 Dimer	AN1	6.29	1798.598		1798.598	bb		

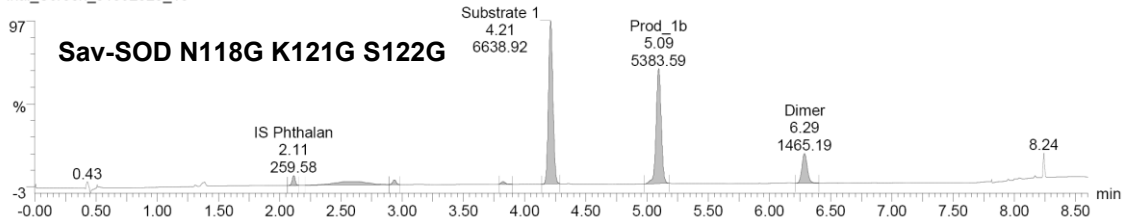
Final\_Screen\_01092020\_9



Name: Final\_Screen\_01092020\_10, Date: 01-Sep-2020, Time: 13:31:59, ID: , Description:

#	Name	Trace	RT	Area	IS Area	Response	Primar...	Conc.	%Dev
1	1 IS Phthalan	AN1	2.11	259.579		259.579	bb		
2	2 Substrate 1	AN1	4.21	6638.922		6638.922	bb		
3	3 Prod_1a	AN1	2.59	1036.340		1036.340	MM		
4	4 Prod_1b	AN1	5.09	5383.585		5383.585	bb		
5	5 Unkn Product	AN1							
6	6 Dimer	AN1	6.29	1465.192		1465.192	bb		

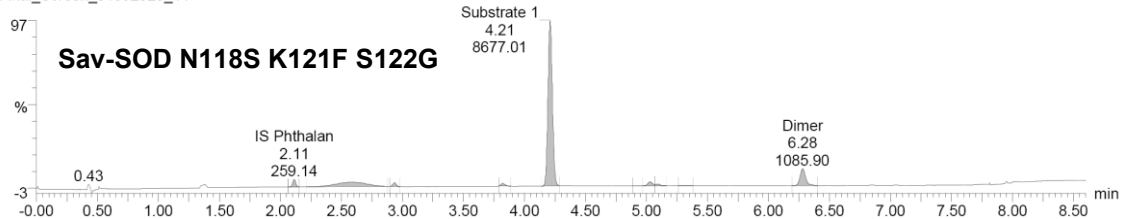
Final\_Screen\_01092020\_10



Name: Final\_Screen\_01092020\_11, Date: 01-Sep-2020, Time: 13:41:36, ID: , Description:

#	Name	Trace	RT	Area	IS Area	Response	Primar...	Conc.	%Dev
1	1 IS Phthalan	AN1	2.11	259.140		259.140	bb		
2	2 Substrate 1	AN1	4.21	8677.011		8677.011	bb		
3	3 Prod_1a	AN1	2.58	1649.260		1649.260	MM		
4	4 Prod_1b	AN1	5.09	106.861		106.861	db		
5	5 Unkn Product	AN1							
6	6 Dimer	AN1	6.28	1085.898		1085.898	bb		

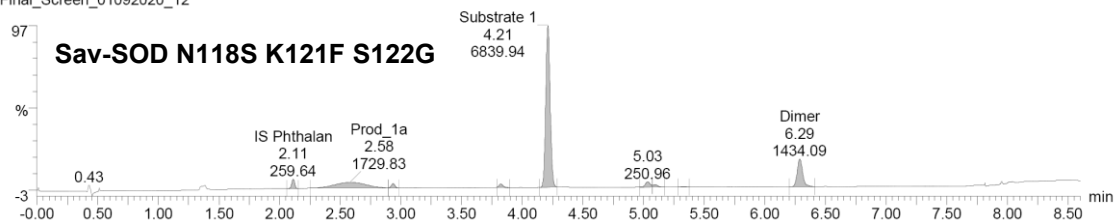
Final\_Screen\_01092020\_11



Name: Final\_Screen\_01092020\_12, Date: 01-Sep-2020, Time: 13:51:13, ID: , Description:

#	Name	Trace	RT	Area	IS Area	Response	Primar...	Conc.	%Dev
1	1 IS Phthalan	AN1	2.11	259.640		259.640	bb		
2	2 Substrate 1	AN1	4.21	6839.944		6839.944	bb		
3	3 Prod_1a	AN1	2.58	1729.834		1729.834	bd		
4	4 Prod_1b	AN1	5.09	108.089		108.089	db		
5	5 Unkn Product	AN1							
6	6 Dimer	AN1	6.29	1434.086		1434.086	bb		

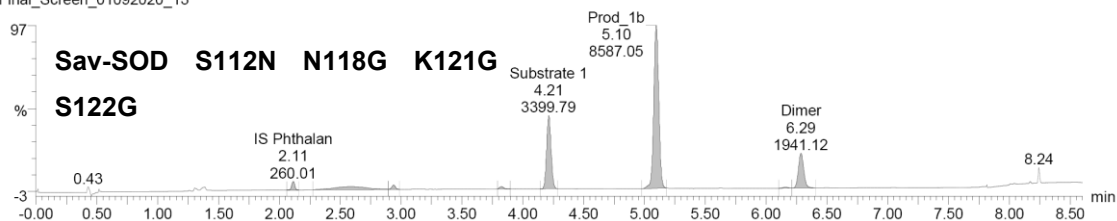
Final\_Screen\_01092020\_12



Name: Final\_Screen\_01092020\_13, Date: 01-Sep-2020, Time: 14:00:57, ID: , Description:

#	Name	Trace	RT	Area	IS Area	Response	Primar...	Conc.	%Dev
1	1 IS Phthalan	AN1	2.11	260.012		260.012	bb		
2	2 Substrate 1	AN1	4.21	3399.789		3399.789	bb		
3	3 Prod_1a	AN1	2.59	904.014		904.014	MM		
4	4 Prod_1b	AN1	5.10	8587.047		8587.047	bb		
5	5 Unkn Product	AN1							
6	6 Dimer	AN1	6.29	1941.123		1941.123	db		

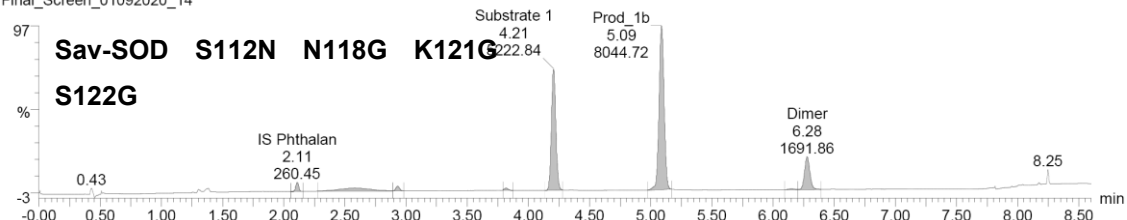
Final\_Screen\_01092020\_13



Name: Final\_Screen\_01092020\_14, Date: 01-Sep-2020, Time: 14:10:34, ID: , Description:

#	Name	Trace	RT	Area	IS Area	Response	Primar...	Conc.	%Dev
1	1 IS Phthalan	AN1	2.11	260.447		260.447	bb		
2	2 Substrate 1	AN1	4.21	5222.840		5222.840	bb		
3	3 Prod_1a	AN1	2.58	873.104		873.104	MM		
4	4 Prod_1b	AN1	5.09	8044.721		8044.721	bb		
5	5 Unkn Product	AN1							
6	6 Dimer	AN1	6.28	1691.863		1691.863	db		

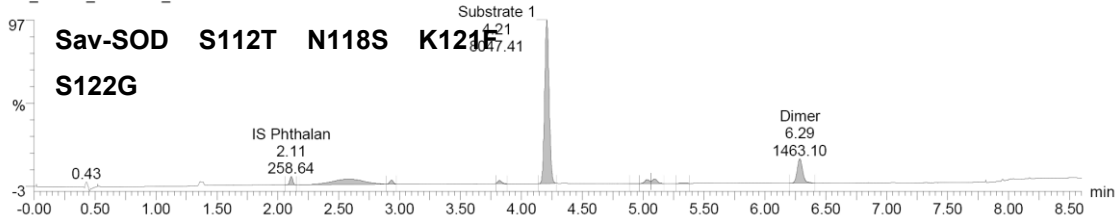
Final\_Screen\_01092020\_14



Name: Final\_Screen\_01092020\_15, Date: 01-Sep-2020, Time: 14:20:18, ID: , Description:

#	Name	Trace	RT	Area	IS Area	Response	Primar...	Conc.	%Dev
1	1 IS Phthalan	AN1	2.11	258.644		258.644	bb		
2	2 Substrate 1	AN1	4.21	8047.411		8047.411	bb		
3	3 Prod_1a	AN1	2.59	1848.910		1848.910	bd		
4	4 Prod_1b	AN1	5.09	255.844		255.844	db		
5	5 Unkn Product	AN1							
6	6 Dimer	AN1	6.29	1463.098		1463.098	bb		

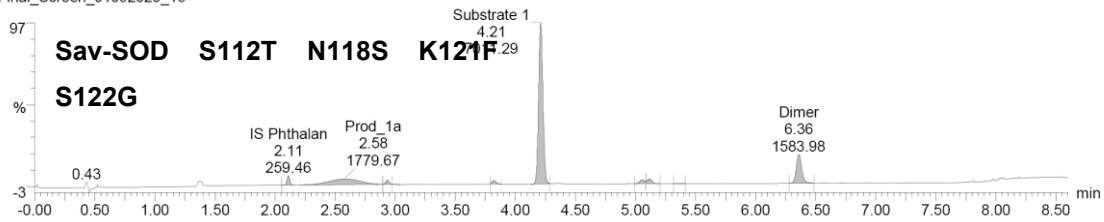
Final\_Screen\_01092020\_15



Name: Final\_Screen\_01092020\_16, Date: 01-Sep-2020, Time: 14:29:54, ID: , Description:

#	Name	Trace	RT	Area	IS Area	Response	Primar...	Conc.	%Dev
1	1 IS Phthalan	AN1	2.11	259.464		259.464	bb		
2	2 Substrate 1	AN1	4.21	7011.287		7011.287	bb		
3	3 Prod_1a	AN1	2.58	1779.672		1779.672	MM		
4	4 Prod_1b	AN1	5.11	239.868		239.868	db		
5	5 Unkn Product	AN1							
6	6 Dimer	AN1	6.36	1583.983		1583.983	bb		

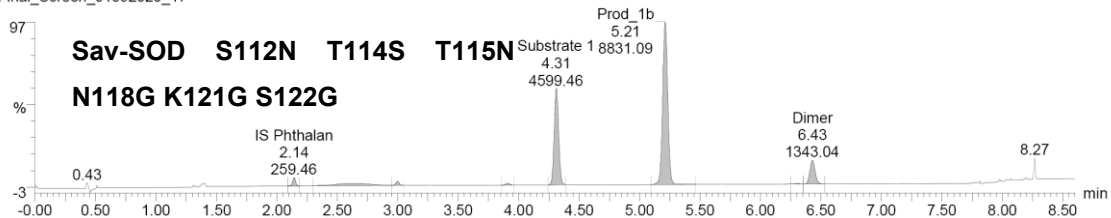
Final\_Screen\_01092020\_16



Name: Final\_Screen\_01092020\_17, Date: 01-Sep-2020, Time: 14:39:31, ID: , Description:

#	Name	Trace	RT	Area	IS Area	Response	Primar...	Conc.	%Dev
1	1 IS Phthalan	AN1	2.14	259.456		259.456	bb		
2	2 Substrate 1	AN1	4.31	4599.458		4599.458	bb		
3	3 Prod_1a	AN1	2.64	755.262		755.262	bd		
4	4 Prod_1b	AN1	5.21	8831.090		8831.090	MM		
5	5 Unkn Product	AN1	3.91	71.373		71.373	bb		
6	6 Dimer	AN1	6.43	1343.039		1343.039	db		

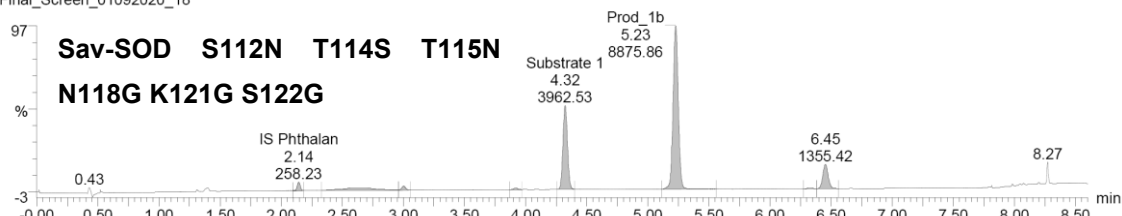
Final\_Screen\_01092020\_17



Name: Final\_Screen\_01092020\_18, Date: 01-Sep-2020, Time: 14:49:15, ID: , Description:

#	Name	Trace	RT	Area	IS Area	Response	Primar...	Conc.	%Dev
1	1 IS Phthalan	AN1	2.14	258.233		258.233	bb		
2	2 Substrate 1	AN1	4.32	3962.528		3962.528	bb		
3	3 Prod_1a	AN1	2.63	752.270		752.270	MM		
4	4 Prod_1b	AN1	5.23	8875.862		8875.862	MM		
5	5 Unkn Product	AN1	3.92	69.542		69.542	bb		
6	6 Dimer	AN1	6.33	38.108		38.108	bd		

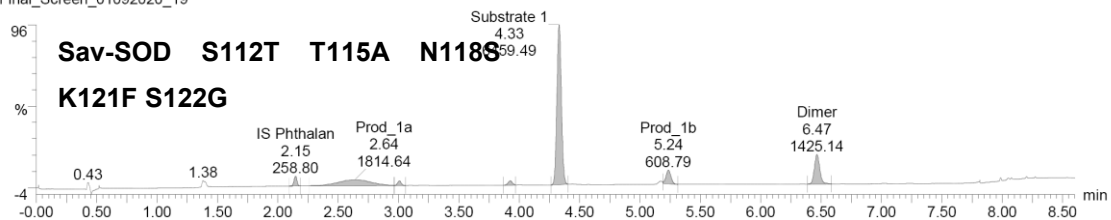
Final\_Screen\_01092020\_18



Name: Final\_Screen\_01092020\_19, Date: 01-Sep-2020, Time: 14:58:51, ID: , Description:

#	Name	Trace	RT	Area	IS Area	Response	Primar...	Conc.	%Dev
1	1 IS Phthalan	AN1	2.15	258.795		258.795	bb		
2	2 Substrate 1	AN1	4.33	6459.488		6459.488	bb		
3	3 Prod_1a	AN1	2.64	1814.644		1814.644	MM		
4	4 Prod_1b	AN1	5.24	608.787		608.787	MM		
5	5 Unkn Product	AN1	3.92	155.049		155.049	bb		
6	6 Dimer	AN1	6.47	1425.144		1425.144	bb		

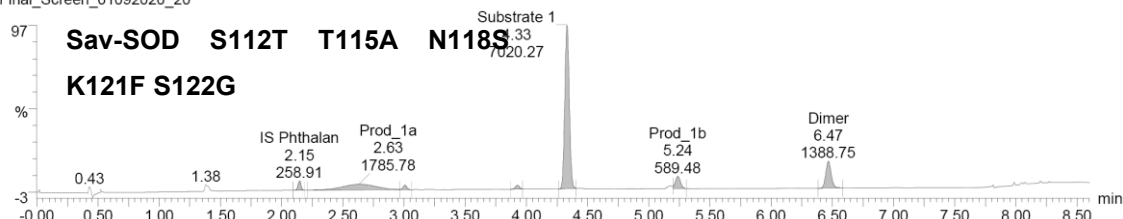
Final\_Screen\_01092020\_19



Name: Final\_Screen\_01092020\_20, Date: 01-Sep-2020, Time: 15:08:36, ID: , Description:

#	Name	Trace	RT	Area	IS Area	Response	Primar...	Conc.	%Dev
1	1 IS Phthalan	AN1	2.15	258.914		258.914	bb		
2	2 Substrate 1	AN1	4.33	7020.267		7020.267	bb		
3	3 Prod_1a	AN1	2.63	1785.775		1785.775	bd		
4	4 Prod_1b	AN1	5.24	589.483		589.483	MM		
5	5 Unkn Product	AN1							
6	6 Dimer	AN1	6.47	1388.747		1388.747	bb		

Final\_Screen\_01092020\_20



SI Table 6 Optimized Reaction Screening with top Hits in quadruplets.

Mutant	TON quinaz-	TON indole 2	TON Total	Selectivity for indole 2
--------	-------------	--------------	-----------	--------------------------

**olinone  
3**

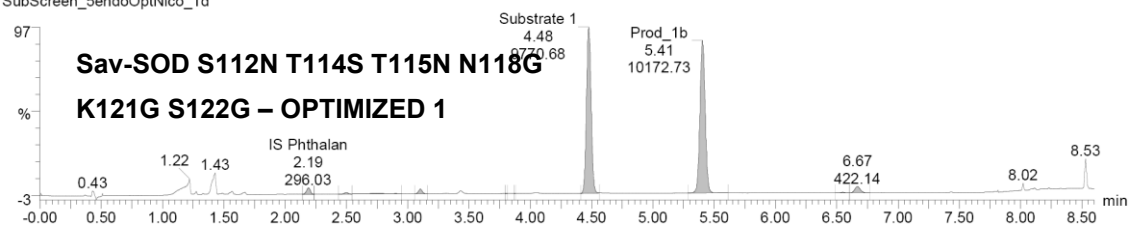
Sav-SOD S112N T114S T115N N118G K121G S122G – OPTIMIZED 1	1.78	46.51	48.30	96.3%
Sav-SOD S112N T114S T115N N118G K121G S122G – OPTIMIZED 2	1.65	47.17	48.83	96.6%
Sav-SOD S112N T114S T115N N118G K121G S122G – OPTIMIZED 3	2.07	53.86	55.86	96.3%
Sav-SOD S112N T114S T115N N118G K121G S122G – OPTIMIZED 4	1.93	49.84	51.77	96.3%
Sav-SOD S112T T115A N118S K121F S122G – OPTIMIZED 1	264.98	2.40	267.38	0.9%
Sav-SOD S112T T115A N118S K121F S122G – OPTIMIZED 2	308.30	2.73	311.03	0.9%
Sav-SOD S112T T115A N118S K121F S122G – OPTIMIZED 3	349.21	2.22	351.43	1.0%
Sav-SOD S112T T115A N118S K121F S122G – OPTIMIZED 4	397.26	3.83	401.09	0.6%

Optimized reaction conditions for quinazolinone **3**:  $V_{tot}$  400  $\mu$ L (365  $\mu$ L MES-buffer pH 5) [Sub] 2.5 mM, [biot-Au2] 2.5  $\mu$ M, [Sav] 5  $\mu$ M, 39  $^{\circ}$ C for 72 h and for indole **2**:  $V_{tot}$  100  $\mu$ L ( $V_{MES}$  45  $\mu$ L,  $V_{DMSO}$  20  $\mu$ L), [Sub] 15 mM, [Diamide] 15 mM, [biot-Au 2] 100  $\mu$ M, [SAV] 200  $\mu$ M, 37  $^{\circ}$ C for 72 h. Both sets of experiments were quenched with MeOH to a total volume of 800  $\mu$ L before UPLC MS analysis.

Name: SubScreen\_5endoOptNico\_1d, Date: 21-Sep-2020, Time: 18:49:12, ID: , Description:

#	Name	Trace	RT	Area	IS Area	Response	Primar...	Conc.	%Dev
1	IS Phthalan	AN1	2.19	296.034		296.034	MM		
2	Substrate 1	AN1	4.48	9770.684		9770.684	MM		
3	3 Prod_1a	AN1	2.78	89.121		89.121	MM		
4	4 Prod_1b	AN1	5.41	10172.733		10172.733	MM		
5	5 Unkn Product	AN1	3.87	0.092		0.092	bb		
6	6 Dimer	AN1	6.55	32.843		32.843	bd		

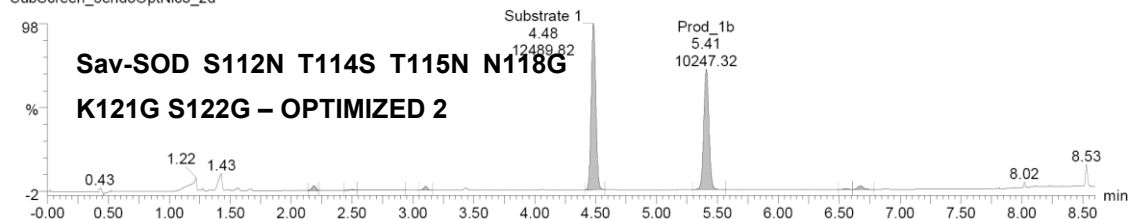
SubScreen\_5endoOptNico\_1d



Name: SubScreen\_5endoOptNico\_2d, Date: 21-Sep-2020, Time: 18:58:49, ID: , Description:

#	Name	Trace	RT	Area	IS Area	Response	Primar...	Conc.	%Dev
1	IS Phthalan	AN1	2.19	294.030		294.030	MM		
2	Substrate 1	AN1	4.48	12489.820		12489.820	MM		
3	3 Prod_1a	AN1	2.78	82.182		82.182	MM		
4	4 Prod_1b	AN1	5.41	10247.318		10247.318	MM		
5	5 Unkn Product	AN1							
6	6 Dimer	AN1	6.55	33.020		33.020	bd		

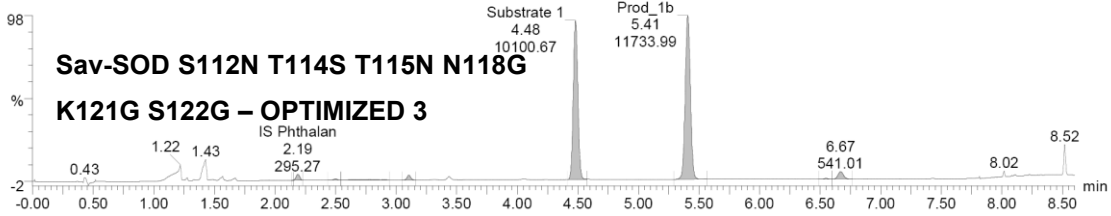
SubScreen\_5endoOptNico\_2d



Name: SubScreen\_5endoOptNico\_3d, Date: 21-Sep-2020, Time: 19:08:25, ID: , Description:

#	Name	Trace	RT	Area	IS Area	Response	Primar...	Conc.	%Dev
1	1 IS Phthalan	AN1	2.19	295.270		295.270	MM		
2	2 Substrate 1	AN1	4.48	10100.674		10100.674	MM		
3	3 Prod_1a	AN1	2.78	103.392		103.392	MM		
4	4 Prod_1b	AN1	5.41	11733.994		11733.994	MM		
5	5 Unkn Product	AN1							
6	6 Dimer	AN1	6.55	37.210		37.210	bd		

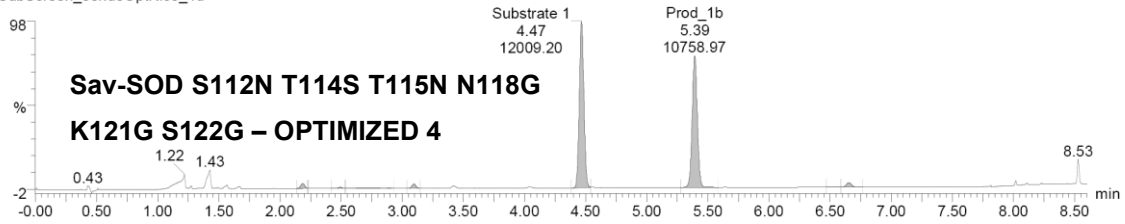
SubScreen\_5endoOptNico\_3d



Name: SubScreen\_5endoOptNico\_4d, Date: 21-Sep-2020, Time: 19:18:00, ID: , Description:

#	Name	Trace	RT	Area	IS Area	Response	Primar...	Conc.	%Dev
1	1 IS Phthalan	AN1	2.18	292.196		292.196	MM		
2	2 Substrate 1	AN1	4.47	12009.198		12009.198	MM		
3	3 Prod_1a	AN1	2.77	95.165		95.165	MM		
4	4 Prod_1b	AN1	5.39	10758.972		10758.972	MM		
5	5 Unkn Product	AN1							
6	6 Dimer	AN1	6.53	35.843		35.843	bd		

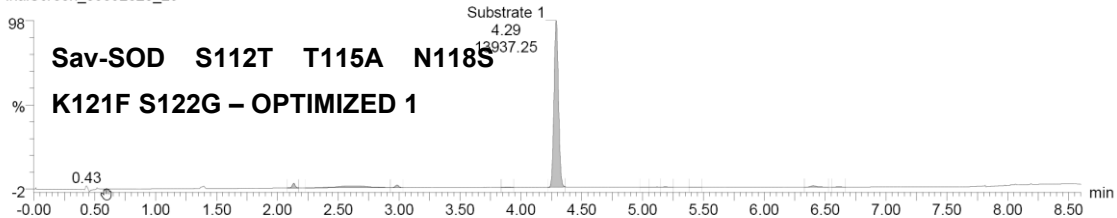
SubScreen\_5endoOptNico\_4d



Name: FinalScreen\_03092020\_29, Date: 03-Sep-2020, Time: 17:08:09, ID: , Description:

#	Name	Trace	RT	Area	IS Area	Response	Primar...	Conc.	%Dev
1	1 IS Phthalan	AN1	2.13	248.122		248.122	bb		
2	2 Substrate 1	AN1	4.29	13937.251		13937.251	bb		
3	3 Prod_1a	AN1	2.63	1110.630		1110.630	bd		
4	4 Prod_1b	AN1	5.19	43.966		43.966	db		
5	5 Unkn Product	AN1	3.89	45.051		45.051	bb		
6	6 Dimer	AN1	6.40	117.731		117.731	bb		

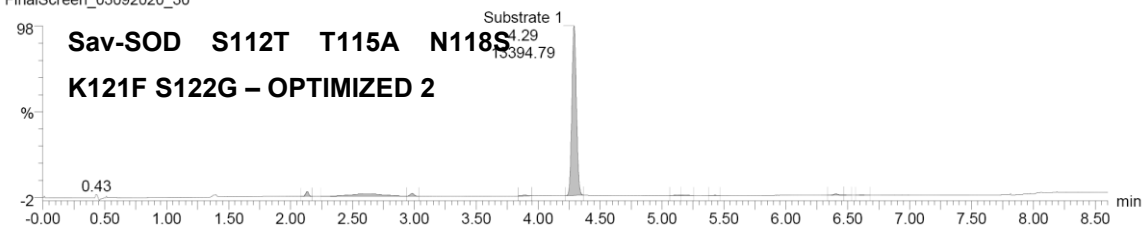
FinalScreen\_03092020\_29



Name: FinalScreen\_03092020\_30, Date: 03-Sep-2020, Time: 17:17:54, ID: , Description:

#	Name	Trace	RT	Area	IS Area	Response	Primar...	Conc.	%Dev
1	1 IS Phthalan	AN1	2.13	247.846		247.846	bb		
2	2 Substrate 1	AN1	4.29	13394.786		13394.786	bb		
3	3 Prod_1a	AN1	2.62	1290.762		1290.762	bd		
4	4 Prod_1b	AN1	5.19	49.984		49.984	db		
5	5 Unkn Product	AN1	3.89	52.997		52.997	bb		
6	6 Dimer	AN1	6.40	118.258		118.258	bd		

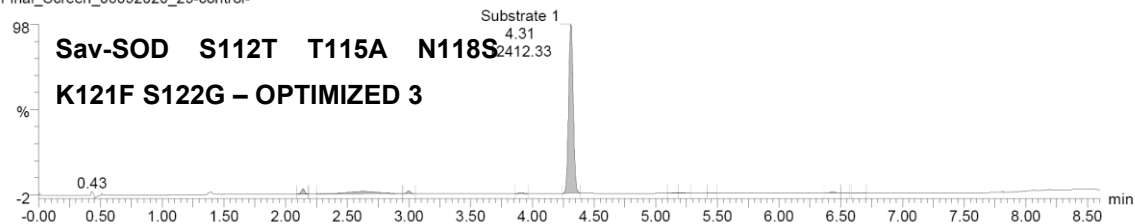
FinalScreen\_03092020\_30



Name: Final\_Screen\_06092020\_29-control-, Date: 07-Sep-2020, Time: 16:39:42, ID: , Description:

#	Name	Trace	RT	Area	IS Area	Response	Primar...	Conc.	%Dev
1	1 IS Phthalan	AN1	2.14	248.938		248.938	bb		
2	2 Substrate 1	AN1	4.31	12412.331		12412.331	bb		
3	3 Prod_1a	AN1	2.63	1174.785		1174.785	MM		
4	4 Prod_1b	AN1	5.15	32.678		32.678	bd		
5	5 Unkn Product	AN1	3.91	51.013		51.013	bb		
6	6 Dimer	AN1	6.43	89.735		89.735	bd		

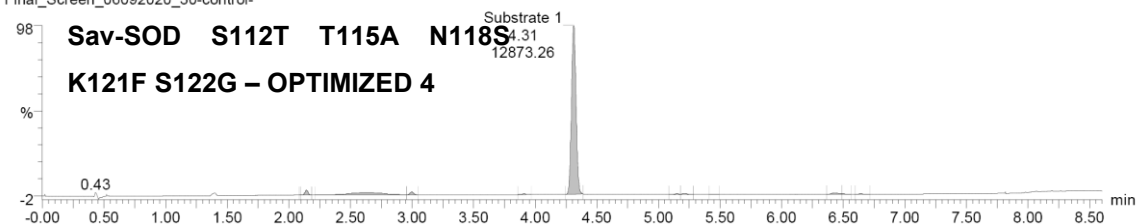
Final\_Screen\_06092020\_29-control-



Name: Final\_Screen\_06092020\_30-control-, Date: 07-Sep-2020, Time: 16:49:18, ID: , Description:

#	Name	Trace	RT	Area	IS Area	Response	Primar...	Conc.	%Dev
1	1 IS Phthalan	AN1	2.14	248.168		248.168	bb		
2	2 Substrate 1	AN1	4.31	12873.263		12873.263	bb		
3	3 Prod_1a	AN1	2.63	1332.312		1332.312	bd		
4	4 Prod_1b	AN1	5.21	56.188		56.188	db		
5	5 Unkn Product	AN1	3.91	58.028		58.028	bb		
6	6 Dimer	AN1	6.43	111.445		111.445	bd		

Final\_Screen\_06092020\_30-control-



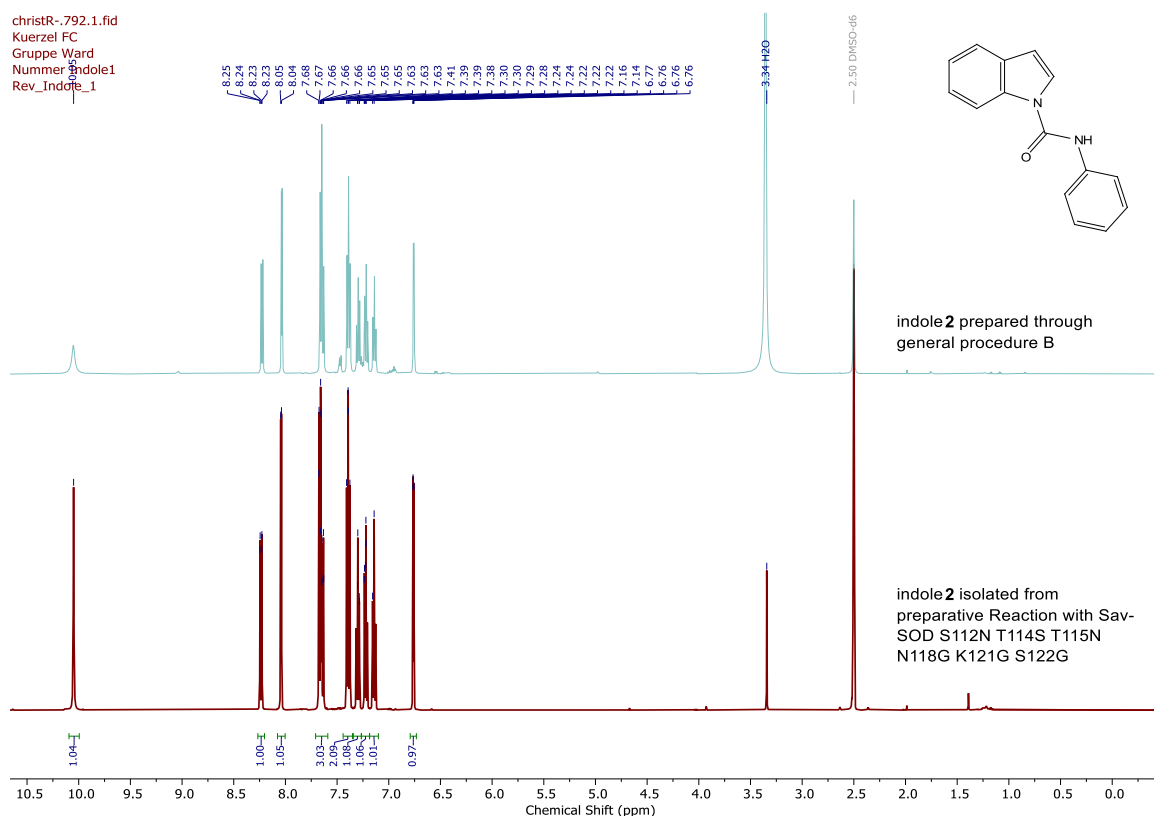


## Preparative reaction with purified Sav-SOD hits

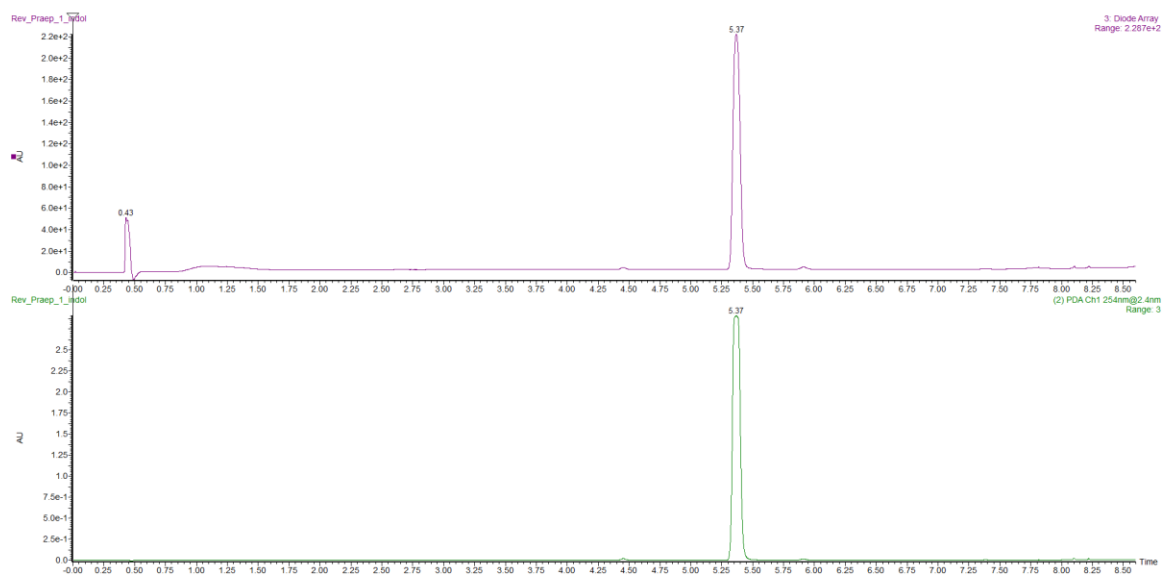
### Preparative reaction using Sav-SOD N-SN-GGG

To a 50 mL Falcon tube were added successively MES buffer (15 mL, 50 mM, pH 5), Sav-SOD S112N T114S T115N N118G K121G S122G (188 mg, 8  $\mu$ mol, 0.04 mol%), **biot-Au 2** (2 mL of 2 mM solution in DMSO, 4  $\mu$ mol, 0.02 mol%) and diamide (0.5 mL of 100 mM solution in H<sub>2</sub>O, 0.1 mmol, 50 mol%). The tube was closed, wrapped in aluminum foil and shaken (30 min at 37 °C in an incubator). Then, the substrate **1** (2 mL of 100 mM solution in DMSO, 0.2 mmol) was added, the tube was closed, sealed with parafilm, wrapped in aluminum foil and shaken (4 days at 37 °C in an incubator). The reaction mixture was diluted (80 mL) with a 1:1:1 mixture of brine, MQ water and sat. NH<sub>4</sub>Cl. The aqueous phase was extracted with EtOAc (5x50 mL), washed with brine (20 mL), dried over MgSO<sub>4</sub> and filtrated. The crude was taken up in silica and purified via flash column chromatography with a cyclohexane/EtOAc gradient to yield the following products in three fractions: indole **2** (34 mg, 0.14 mmol, 72%); quinazolinone **3** (3 mg, 13  $\mu$ mol, 6%); and sideproducts (10 mg, uncharacterisable).

The isolated ratio of indole **2** and quinazolinone **3** is 92:8 at a combined yield of 78%.



SI Figure 12 Stacked <sup>1</sup>H NMR spectra of isolated and the reference indole **2** in DMSO-*d*<sub>6</sub>.

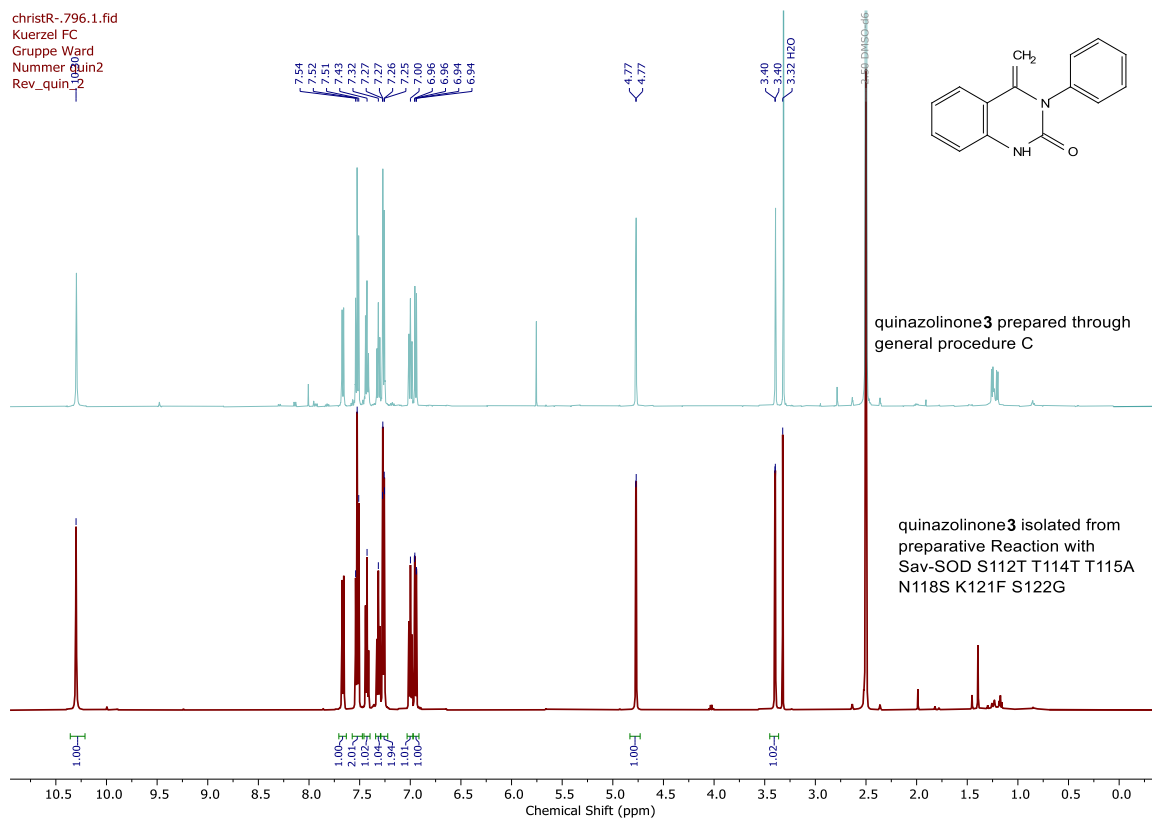


**SI Figure 13** UPLC-MS DAD (100-500 nm) and PDA (254 nm) Chromatogram of isolated indole **2** (5.37 min).

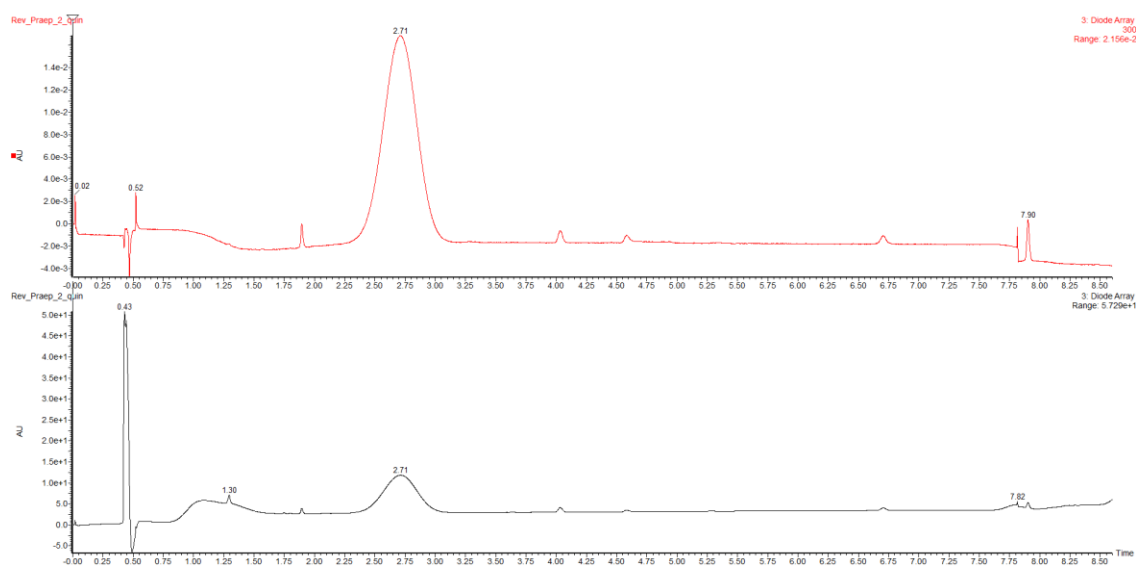
### Preparative reaction using Sav-SOD T-A-SFG

To a 100 mL tube were added successively MES buffer (80 mL, 50 mM, pH 5), Sav-SOD S112T T114T T115A N118S K121F S122G (47 mg, 2  $\mu$ mol, 0.01 mol%) and **biot-Au 2** (1 mL of 2 mM solution in DMSO, 1  $\mu$ mol, 0.005 mol%). The tube was closed, wrapped in aluminum foil and shaken (30 min at 37 °C in an incubator). Then, substrate **1** (1 mL of 100 mM solution in DMSO, 0.1 mmol) was added, the tube was closed, sealed with parafilm, wrapped in aluminum foil and shaken (4 days at 37 °C in an incubator). The reaction mixture was then diluted (80 mL) with a 1:1:1 mixture of brine, MQ water and sat.  $\text{NH}_4\text{Cl}$ . The aqueous phase was extracted with EtOAc (5x50 mL), washed with brine (20 mL), dried over  $\text{MgSO}_4$  and filtered. The crude was taken up in silica and purified via flash column chromatography with a cyclohexane/EtOAc gradient to yield the following products in three fractions: urea **1** (<1 mg, <4  $\mu$ mol, <4%); quinazolinone **3** (11 mg, 47  $\mu$ mol, 47%); and sideproducts (<1 mg, uncharacterisable).

The isolated ratio of quinazolinone **3** to indole **2** is >99:1 at a combined yield of 47% which corresponds to a total TON of 94. Indole **2** could not be isolated and is inferred from the chromatography purification trace.

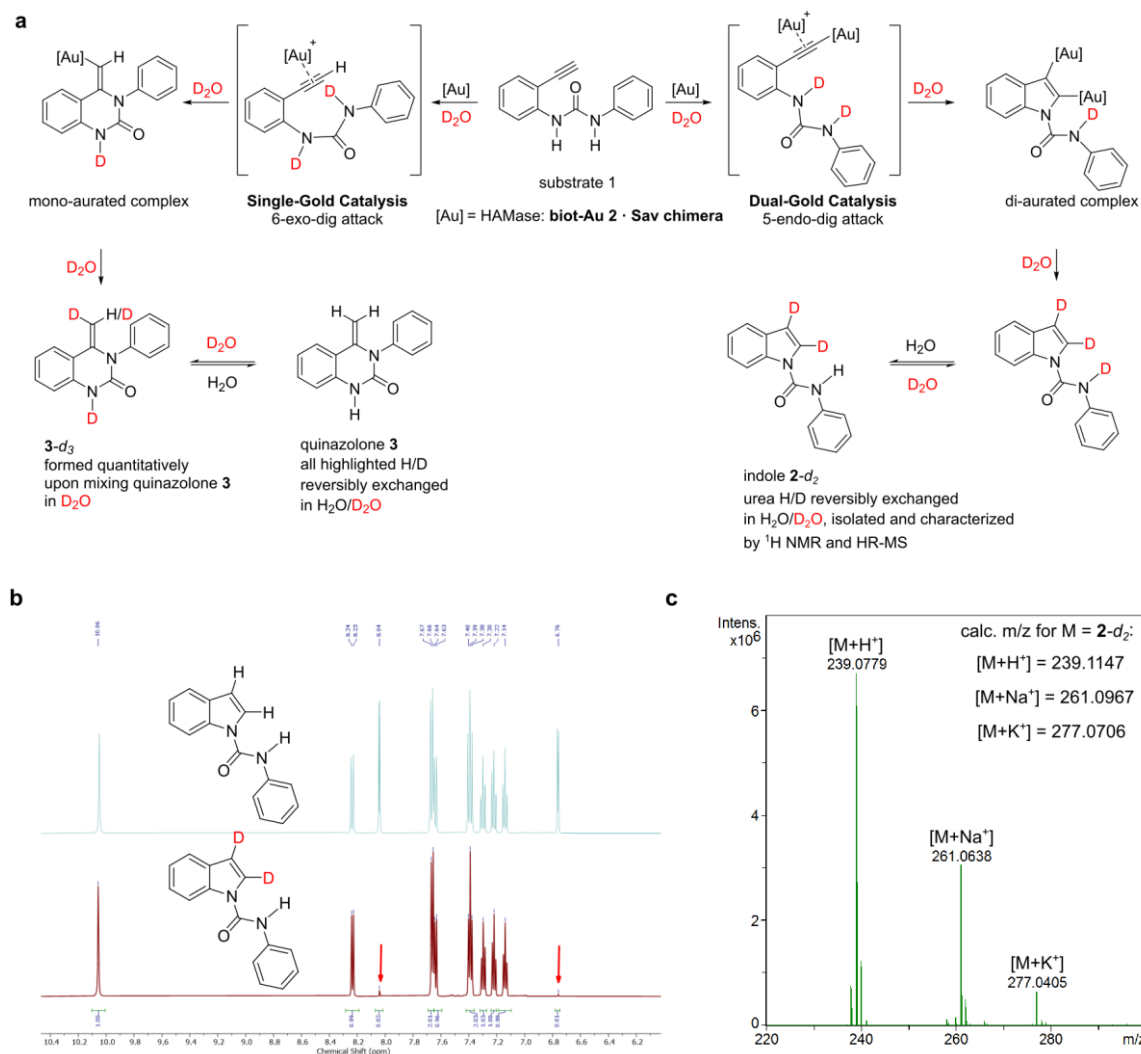


SI Figure 14 Stacked  $^1\text{H}$  NMR spectra of isolated and the reference quinazolinone **3** in  $\text{DMSO}-d_6$ .

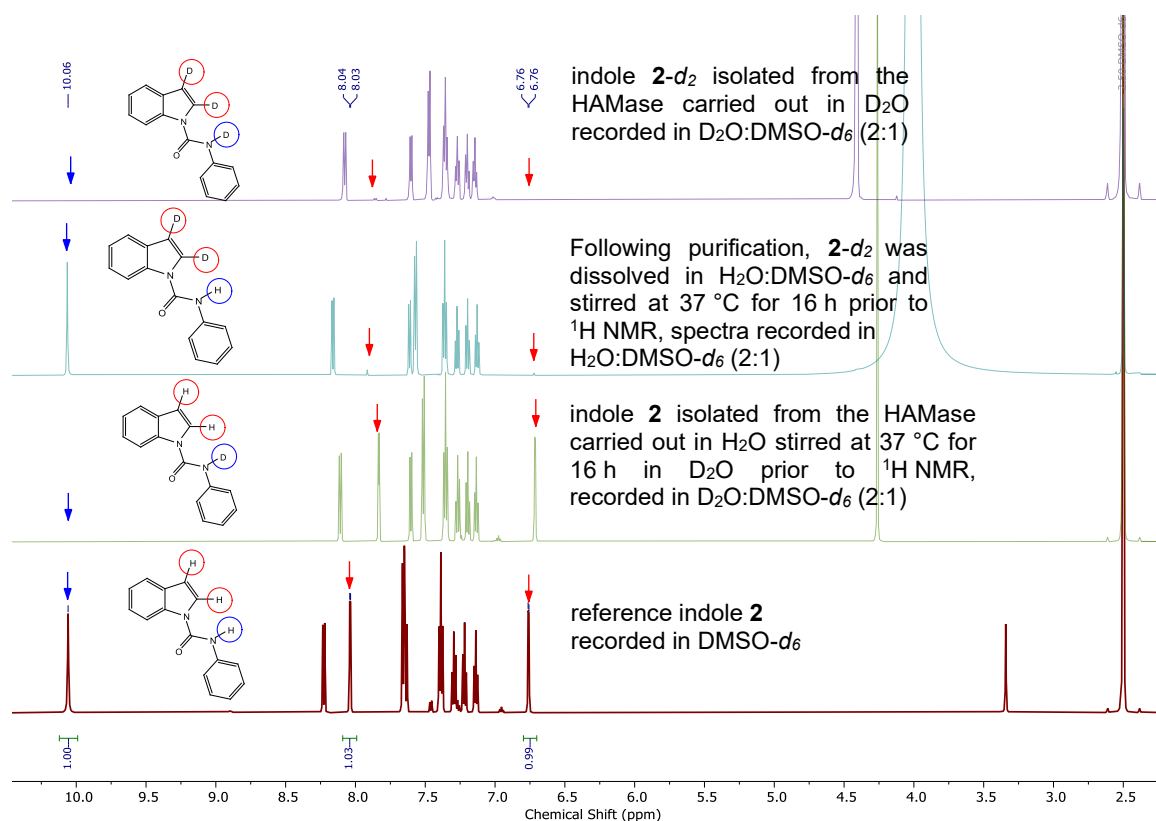


SI Figure 15 UPLC-MS DAD (100-500 nm) and DAD (300 nm) Chromatogram of isolated quinazolinone **3** (2.71 min).

## Experimental deuterium incorporation



**SI Figure 16 Isotopic product-distribution of the HAMase biot-Au 2 · Sav-SOD N-SN-GGG carried out in  $\text{D}_2\text{O}$ .** **a** Deuteration profile of quinazolinone **3** and indole **2** resulting from the gold-catalyzed hydroamination. For the quinazolinone **3**, all highlighted protons/deuterons are readily exchanged in  $\text{D}_2\text{O}/\text{H}_2\text{O}$ ; **b**  $^1\text{H}$  NMR analysis of the indole **2- $d_2$**  isolated from preparative reactions in  $\text{H}_2\text{O}$  (top) and  $\text{D}_2\text{O}$  (bottom, the urea N–H is readily exchanged in the presence of traces of  $\text{H}_2\text{O}$ ) and **c** HR-MS analysis of **2- $d_2$**  resulting from the reaction performed in  $\text{D}_2\text{O}$ .



**SI Figure 17** Stacked  $^1\text{H}$  NMR spectrum confirming the inertness of indole **2** and **2- $d_2$**  towards deuterium-proton exchange at the indole's C2 and C3 positions (highlighted in red). In contrast, the urea proton (blue) is readily exchanged.

### Preparative deuterium incorporation experiments Sav-SOD N-SN-GGG

To a 50 mL Falcon tube were added successively MES buffer (15 mL, 50 mM in  $\text{D}_2\text{O}$ , pH 5), Sav-SOD S112N T114S T115N N118G K121G S122G (188 mg, 8  $\mu\text{mol}$ , 0.04 mol%), **biot-Au 2** (2 mL of 2 mM solution in  $\text{DMSO-}d_6$ , 4  $\mu\text{mol}$ , 0.02 mol%) and diamide (0.5 mL of 100 mM solution in  $\text{D}_2\text{O}$ , 0.1 mmol, 50 mol%). The tube was closed, wrapped in aluminum foil and shaken (30 min at 37 °C in an incubator). Urea **1** (2 mL of 100 mM solution in  $\text{DMSO-}d_6$ , 0.2 mmol) was added, the tube was closed, sealed with parafilm, wrapped in aluminum foil and shaken (3 days at 37 °C in an incubator). Afterwards, the reaction mixture was diluted with  $\text{D}_2\text{O}$  (50 mL). The aqueous phase was extracted with EtOAc (5x50 mL), washed with NaCl in  $\text{D}_2\text{O}$  (20 mL), dried over  $\text{MgSO}_4$  and filtrated. The crude was taken up in silica and purified via flash column chromatography with a cyclohexane/EtOAc gradient to yield the following products in four fractions: deuterated indole **2- $d_2$**  (26 mg, 0.10 mmol, 53%); urea **1** (21 mg, 91  $\mu\text{mol}$ , 42%); traced of quinazolinone **3** (<1mg); and sideproducts (3 mg, uncharacterisable).

Deuterated Indole **2- $d_2$**  was isolated with twice >98% Deuterium intake in both the C2 and C3 position of the indole moiety.

## Preparative deuterium incorporation experiments Sav-SOD T-A-SFG

To a 100 mL tube were added successively MES buffer (80 mL, 50 mM in  $D_2O$ , pH 5), Sav-SOD S112T T114T T115A N118S K121F S122G (47 mg, 2  $\mu$ mol, 0.01 mol%) and **biot-Au 2** (1 mL of 2 mM solution in  $DMSO-d_6$ , 1  $\mu$ mol, 0.005 mol%). The tube was closed, wrapped in aluminum foil and shaken (30 min at 37 °C in an incubator). Urea **1** (1 mL of 100 mM solution in  $DMSO-d_6$ , 0.1 mmol) was added, the tube was closed, sealed with parafilm, wrapped in aluminum foil and shaken (4 days at 37 °C in an incubator). Afterwards, the reaction mixture was diluted with  $D_2O$  (50 mL). The aqueous phase was extracted with EtOAc (5x50 mL), washed with NaCl in  $D_2O$  (20 mL), dried over  $MgSO_4$  and filtrated. The crude was taken up in silica and purified via flash column chromatography with a cyclohexane/EtOAc gradient to yield the following products in four fractions: indole **2- $d_2$**  (<1 mg, <4  $\mu$ mol, <4%); urea **1** (11 mg, 40  $\mu$ mol, 40%); quinazolinone **3** (4 mg, 17  $\mu$ mol, 17%); and sideproducts (<1 mg, uncharacterisable).

Deuterated Indole **2- $d_2$**  was isolated with twice >99% Deuterium intake in both the C2 and C3 position of the indole moiety. Quinazolinone **3** was isolated with no detectable Deuterium intake.

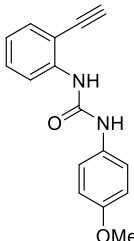
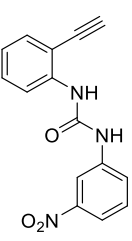
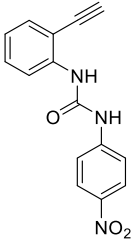
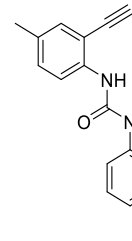
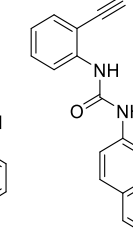
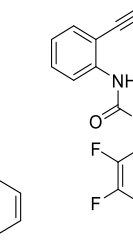
### Substrate screening

Procedure: An Eppendorf tube (1500  $\mu$ L) was charged successively with MES-buffer (50 mM, pH 5), purified protein (1000  $\mu$ M BBS in MQ-water), additives (100 mM, diamide dissolved in MQ water) and cofactor (2 mM in DMSO) were added. The tube was incubated in a thermoshaker (20 min, 37 °C, 900 rpm). Afterwards, urea **1** (100 mM in DMSO) was added and the tube was shaken in a thermoshaker. The reaction was quenched by the addition of methanol to a total volume of 800  $\mu$ L, followed by centrifugation (14'000 rpm, 10 °C, 10 min). In UPLC vials, the reaction mixture (40  $\mu$ L) was diluted in UPLC media (960  $\mu$ L, 1:1 MeCN:MQ-Water containing 40.8  $\mu$ M of phthalane) before UPLC-MS analysis.

Under optimized conditions, Sav-SOD NSNGGG<sup>b</sup> predominantly produces the 5-endo-dig product (indole) product most cases (**1a-1e**), while Sav-SOD TASFG<sup>c</sup> predominantly produces the quinazolinone products (**1a-1f**). Comparing the two mutants under standard reaction conditions<sup>a</sup> highlights the marked influence of the mutations on the regioselectivity for all substrates tested.

**SI Table 7** Substrate scope using the evolved **biot-Au 2** · Sav-SOD chimeras under standard reaction conditions<sup>a</sup> used for directed evolution and under reaction conditions optimized for 5-endo-dig<sup>b</sup> and 6-

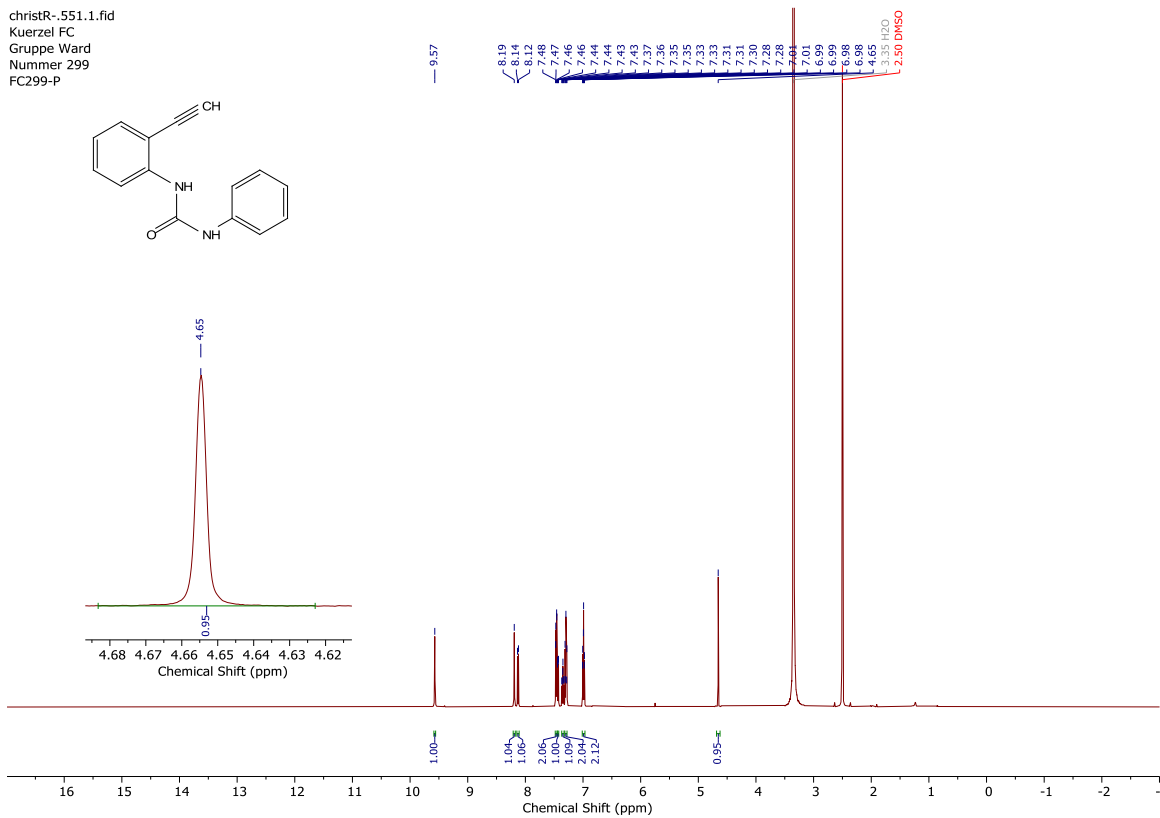
exo-dig<sup>c</sup> products.

Substrate Mutant						
	1a	1b	1c	1d	1e	1f
Sav-SOD	16.7±0.9	21.5±1.2	2.3±0.5	6.3±0.7	6.2±1.2	0 <sup>a</sup>
S112N T114S	(36:64) <sup>a</sup>	(16:84) <sup>a</sup>	(44:56) <sup>a</sup>	(32:68) <sup>a</sup>	(34:66) <sup>a</sup>	
T115N N118G	45.9±1.6	35.9±0.1	22.0±1.0	15.3±0.3	5.2±0.1	6.9±0.3
K121G S122G	(7:93) <sup>b</sup>	(19:81) <sup>b</sup>	(15:85) <sup>b</sup>	(1:99) <sup>b</sup>	(4:96) <sup>b</sup>	(50:50) <sup>b</sup>
Sav-SOD	13.2±1.3	10.2±1.6	4.0±0.5	3.9±0.1	7.3±0.9	1.5±0.1
S112T T115A	(93:7) <sup>a</sup>	(86:14) <sup>a</sup>	(97:3) <sup>a</sup>	(90:10) <sup>a</sup>	(91:9) <sup>a</sup>	(91:9) <sup>a</sup>
N118S K121F	104.7±5.9	35.3±3.4	41.7±2.5	26.0±3.5	16.7±1.1	6.0±0.9
S122G	(96:4) <sup>c</sup>	(97:3) <sup>c</sup>	(97:3) <sup>c</sup>	(97:3) <sup>c</sup>	(85:15) <sup>c,d</sup>	(96:4) <sup>c,d</sup>

The experiments were carried out in duplicate. The combined turnover for both products is displayed as well as the quinazolinone:indole ratio (**3:2**). <sup>a</sup>Standard Reaction conditions for directed evolution see **SI Table 5**; <sup>b</sup> Reaction conditions optimized for 5-endo-dig product:  $V_{\text{tot}}$  100  $\mu\text{L}$  ( $V_{\text{MES}}$  45  $\mu\text{L}$ ,  $V_{\text{DMSO}}$  20  $\mu\text{L}$ ), [Sub] 15 mM, [Diamide] 15 mM, [**biot-Au 2**] 100  $\mu\text{M}$ , [Sav] 200  $\mu\text{M}$ , [MES-buffer] 50 mM, pH 5, 37 °C for 24 h; <sup>c</sup> Reaction conditions optimized for 6-exo-dig product:  $V_{\text{tot}}$  400  $\mu\text{L}$  ( $V_{\text{MES}}$  365  $\mu\text{L}$ ,  $V_{\text{DMSO}}$  12  $\mu\text{L}$ ) [Sub] 2.5 mM, [**biot-Au 2**] 6.25  $\mu\text{M}$ , [Sav] 12.5  $\mu\text{M}$ , [MES-buffer] 50 mM, pH 5, 39 °C for 48 h; <sup>d</sup> with following changes: [**biot-Au 2**] 2.5  $\mu\text{M}$ , [Sav] 5  $\mu\text{M}$ , for 24 h.

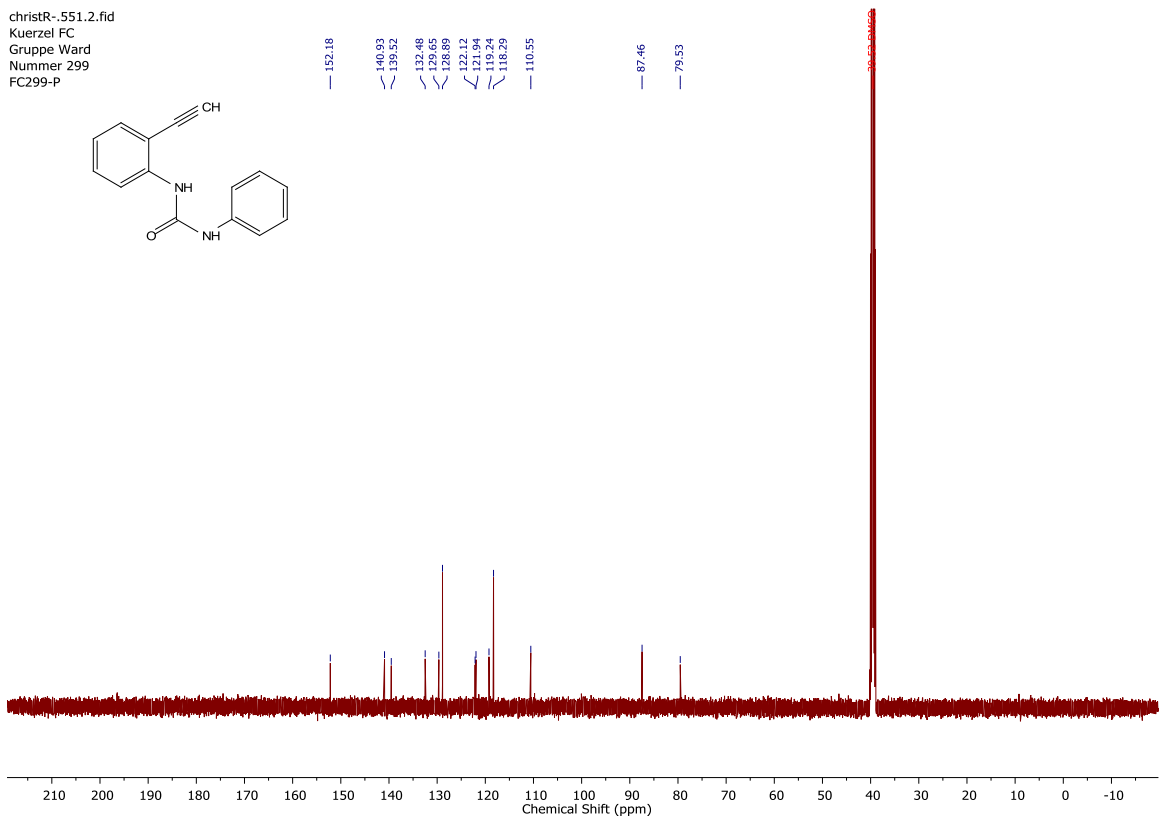
## NMR-Spectra

christR--551.1.fid  
Kuerzel FC  
Gruppe Ward  
Nummer 299  
FC299-P



## Spectrum 1 <sup>1</sup>H NMR Spectrum of urea 1 in DMSO-*d*<sub>6</sub>.

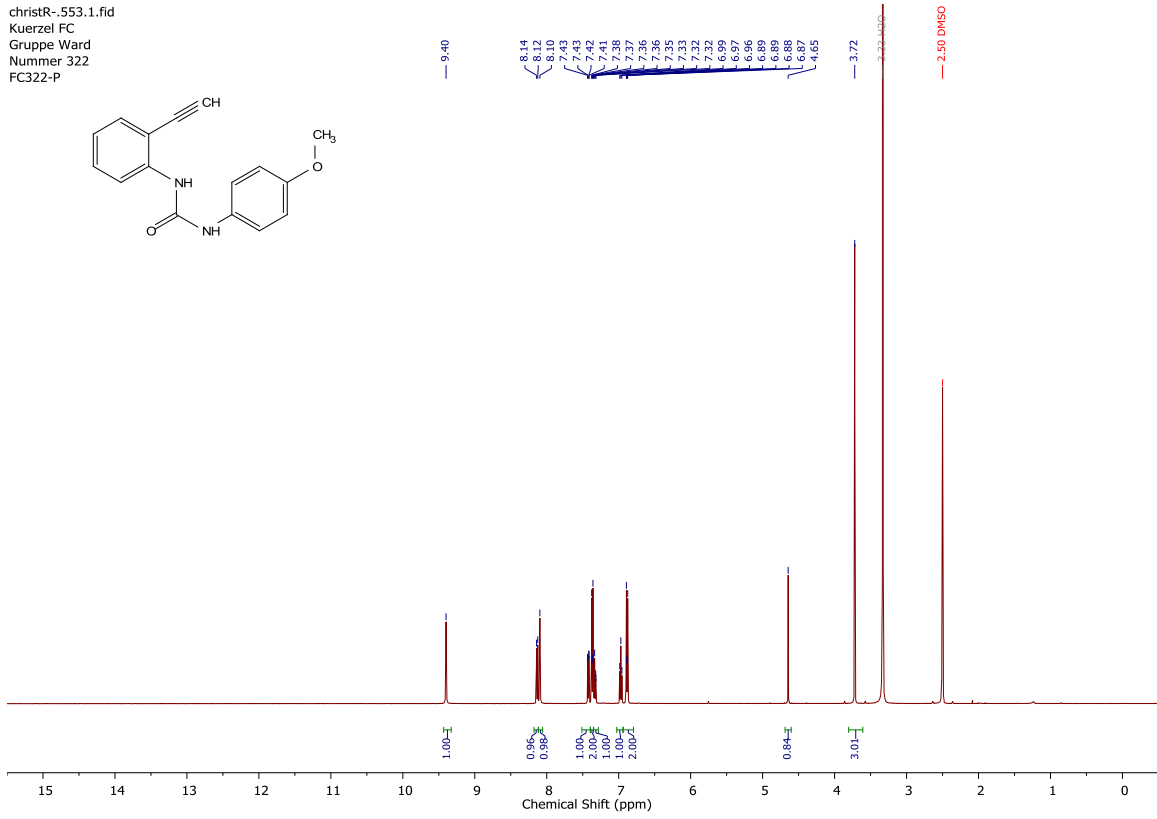
christR--551.2.fid  
Kuerzel FC  
Gruppe Ward  
Nummer 299  
FC299-P



## Spectrum 2 <sup>13</sup>C NMR Spectrum of urea 1 in DMSO-*d*<sub>6</sub>.

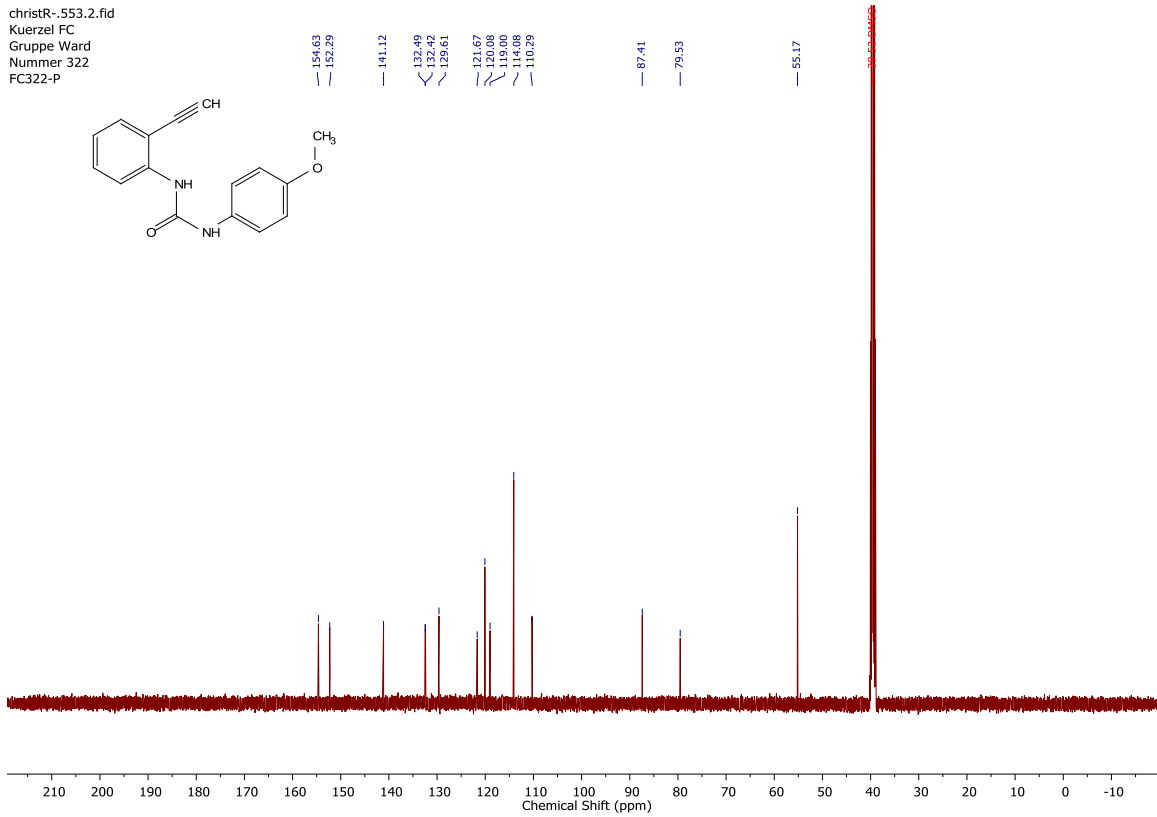


christR--553.1.fid  
 Kuerzel FC  
 Gruppe Ward  
 Nummer 322  
 FC322-P



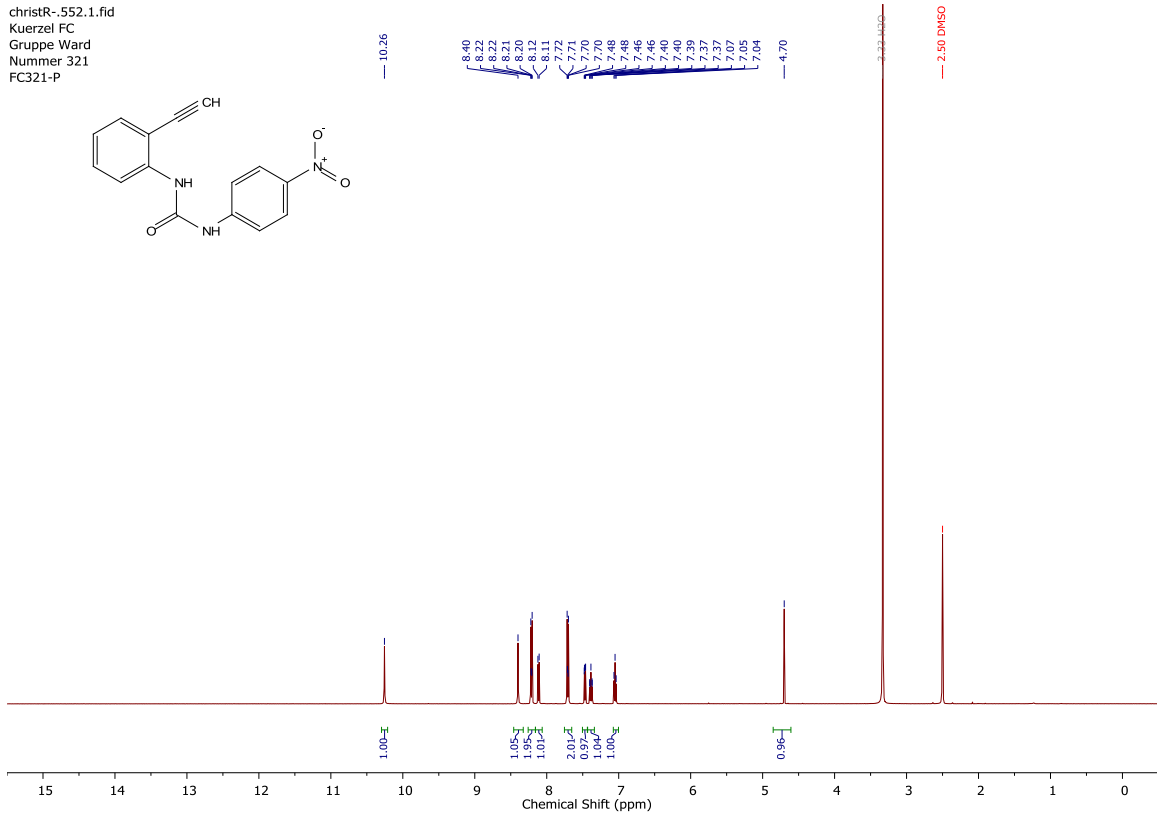
**Spectrum 3** <sup>1</sup>H NMR Spectrum of urea **1a** in DMSO-*d*<sub>6</sub>.

christR--553.2.fid  
 Kuerzel FC  
 Gruppe Ward  
 Nummer 322  
 FC322-P



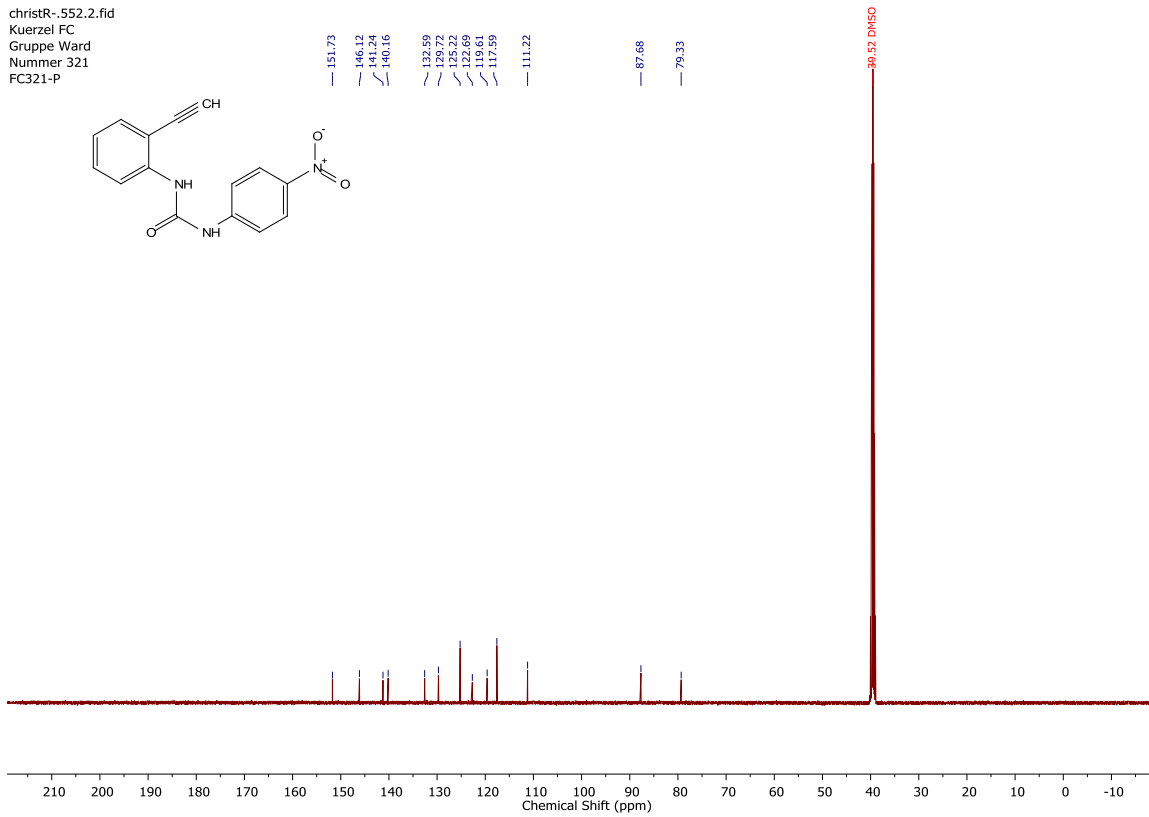
**Spectrum 4** <sup>13</sup>C NMR Spectrum of urea **1a** in DMSO-*d*<sub>6</sub>.

christR-.552.1.fid  
 Kuerzel FC  
 Gruppe Ward  
 Nummer 321  
 FC321-P



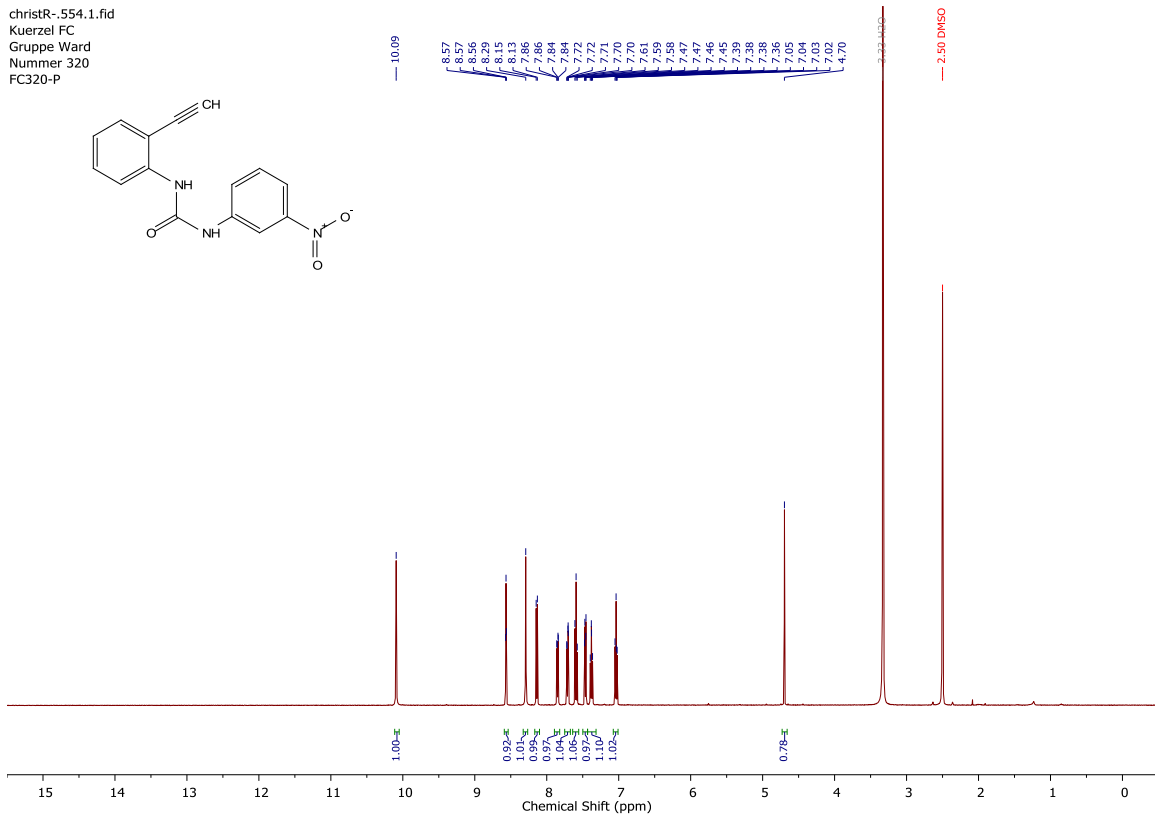
**Spectrum 5**  $^1\text{H}$  NMR Spectrum of urea **1b** in  $\text{DMSO-}d_6$ .

christR-.552.2.fid  
 Kuerzel FC  
 Gruppe Ward  
 Nummer 321  
 FC321-P



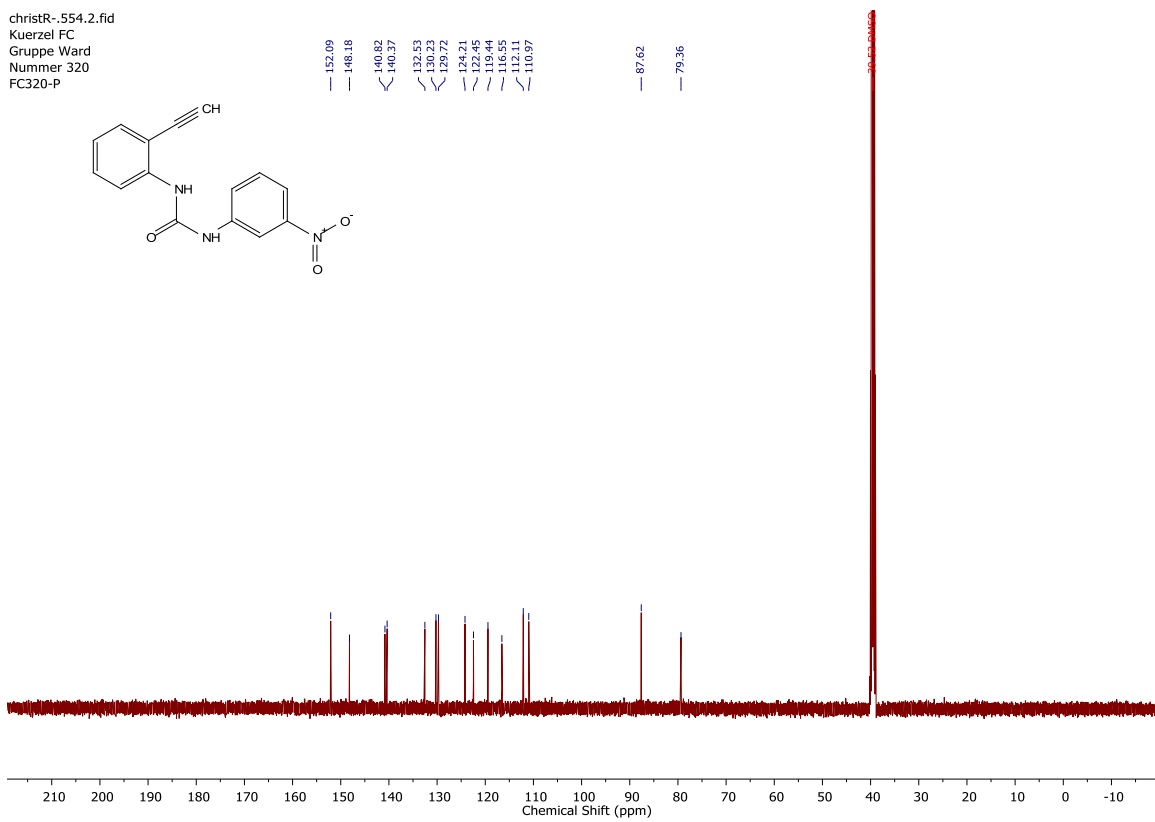
**Spectrum 6**  $^{13}\text{C}$  NMR Spectrum of urea **1b** in  $\text{DMSO-}d_6$ .

christR--554.1.fid  
 Kuerzel FC  
 Gruppe Ward  
 Nummer 320  
 FC320-P



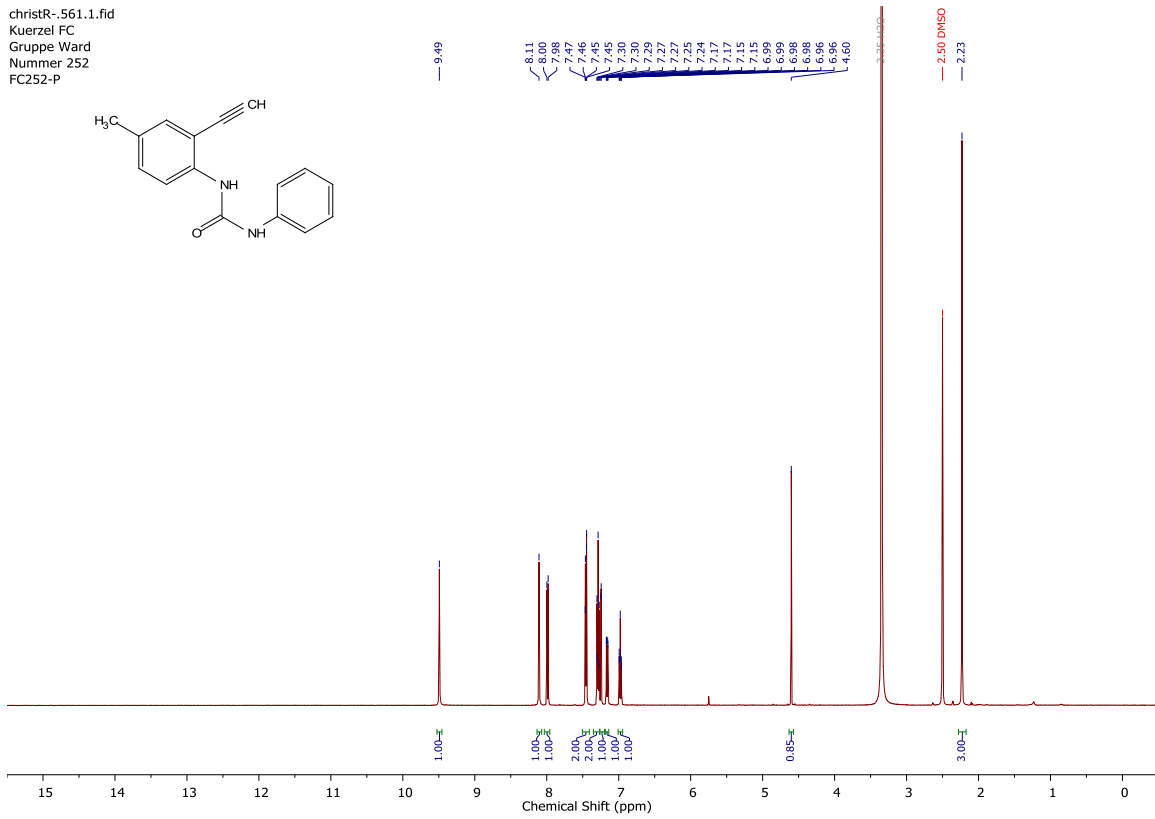
**Spectrum 7**  $^1\text{H}$  NMR Spectrum of urea **1c** in  $\text{DMSO-}d_6$ .

christR--554.2.fid  
 Kuerzel FC  
 Gruppe Ward  
 Nummer 320  
 FC320-P



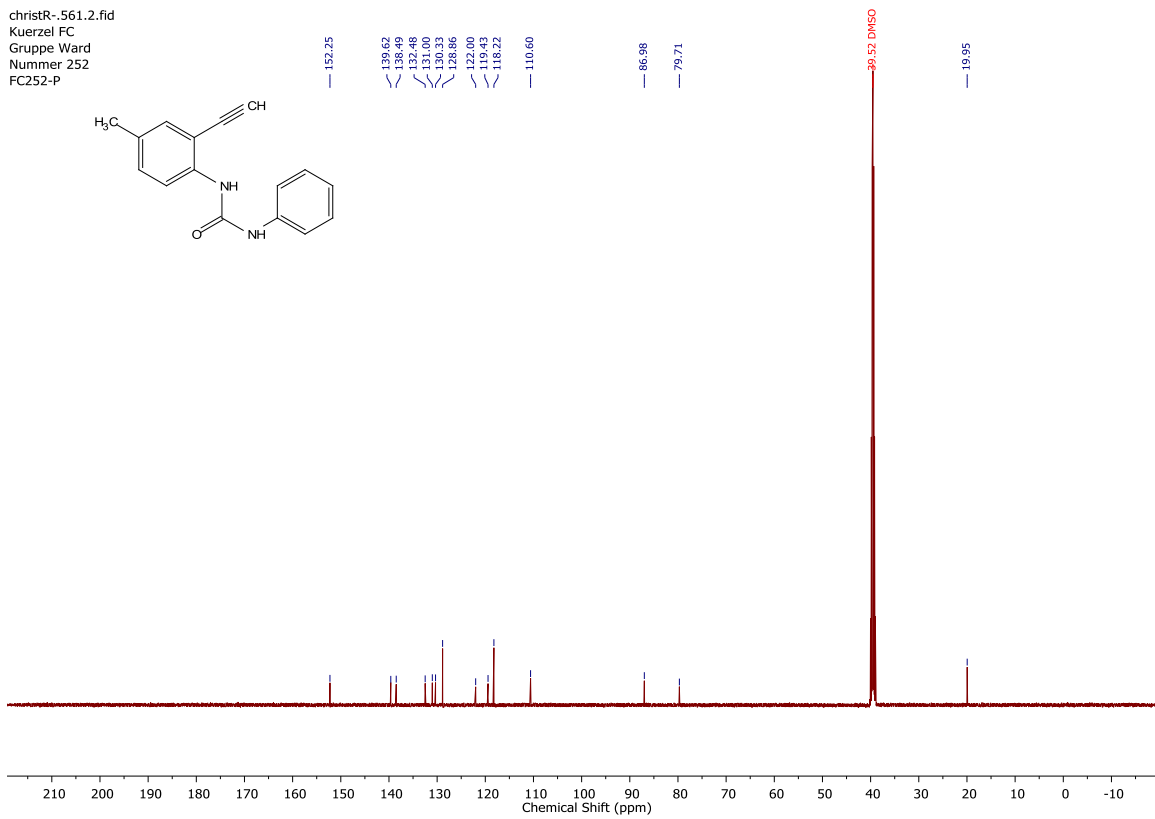
**Spectrum 8**  $^{13}\text{C}$  NMR Spectrum of urea **1c** in  $\text{DMSO-}d_6$ .

christR--561.1.fid  
 Kuerzel FC  
 Gruppe Ward  
 Nummer 252  
 FC252-P



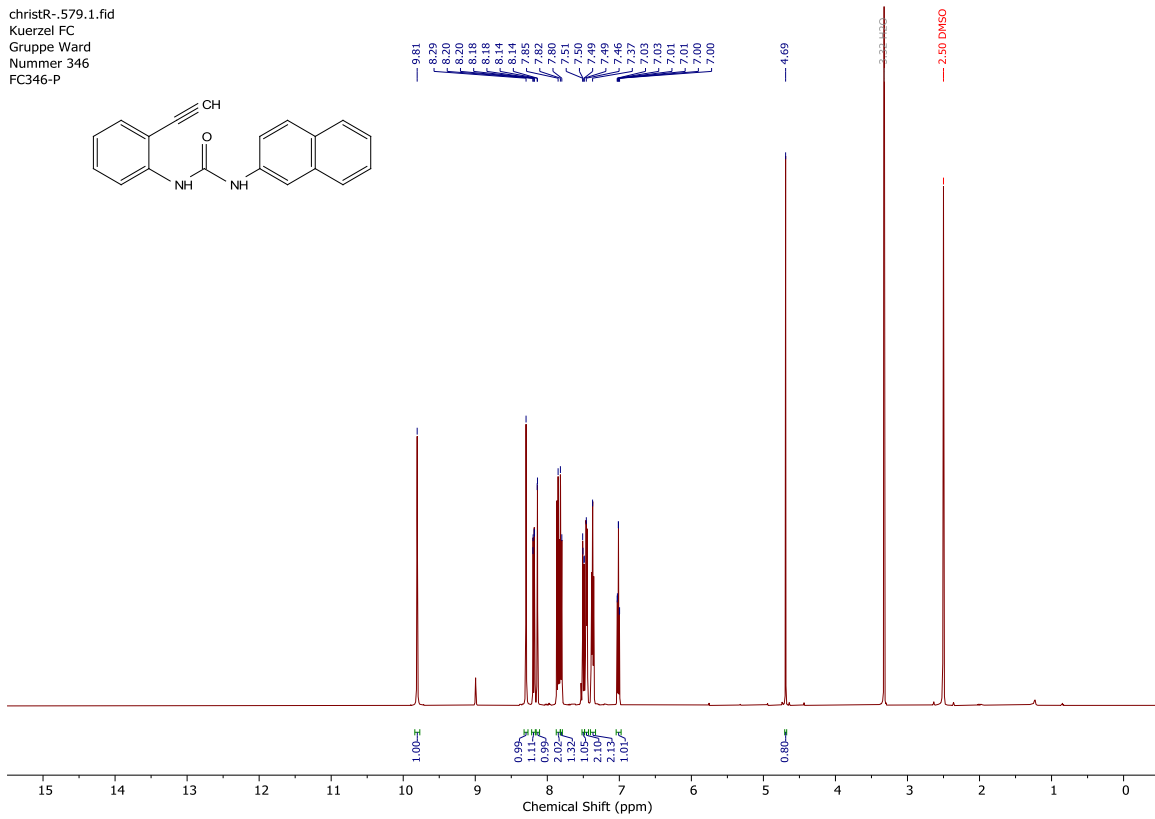
**Spectrum 9**  $^1\text{H}$  NMR Spectrum of urea **1d** in  $\text{DMSO-}d_6$ .

christR--561.2.fid  
 Kuerzel FC  
 Gruppe Ward  
 Nummer 252  
 FC252-P



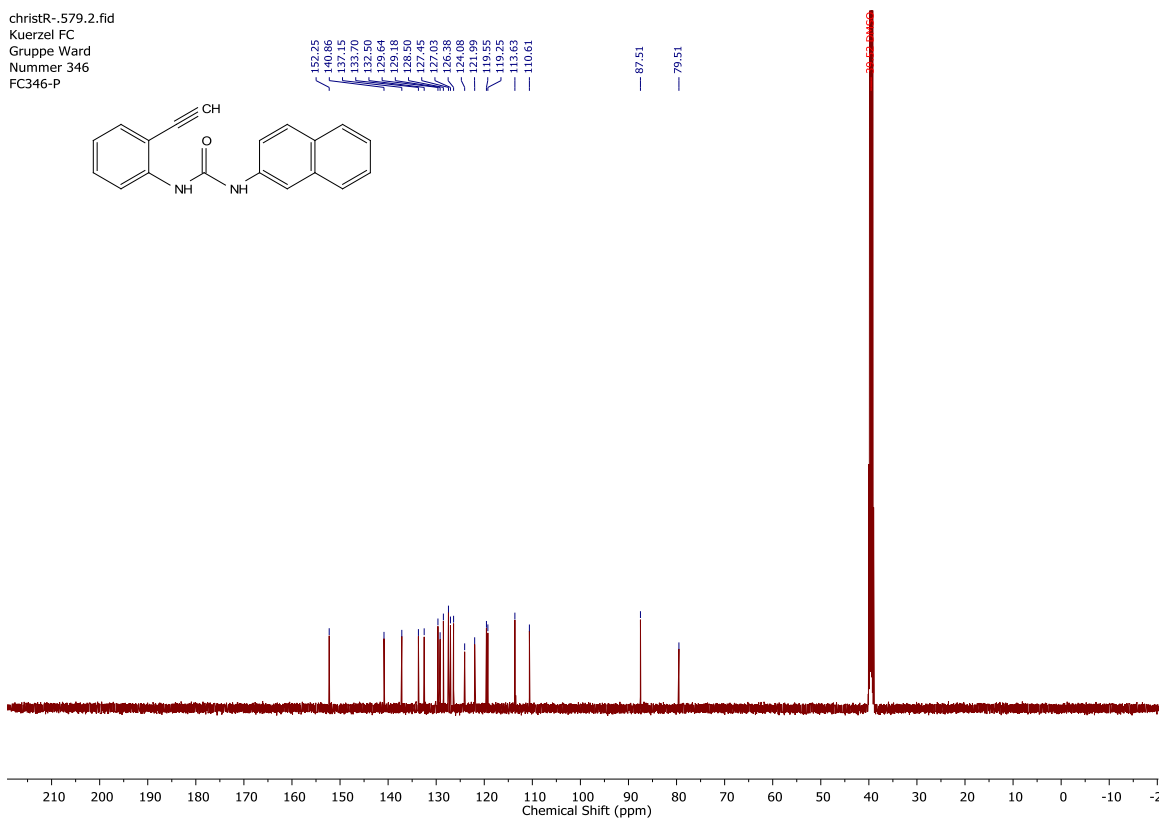
**Spectrum 10**  $^{13}\text{C}$  NMR Spectrum of urea **1d** in  $\text{DMSO-}d_6$ .

christR--579.1.fid  
Kuerzel FC  
Gruppe Ward  
Nummer 346  
FC346-P



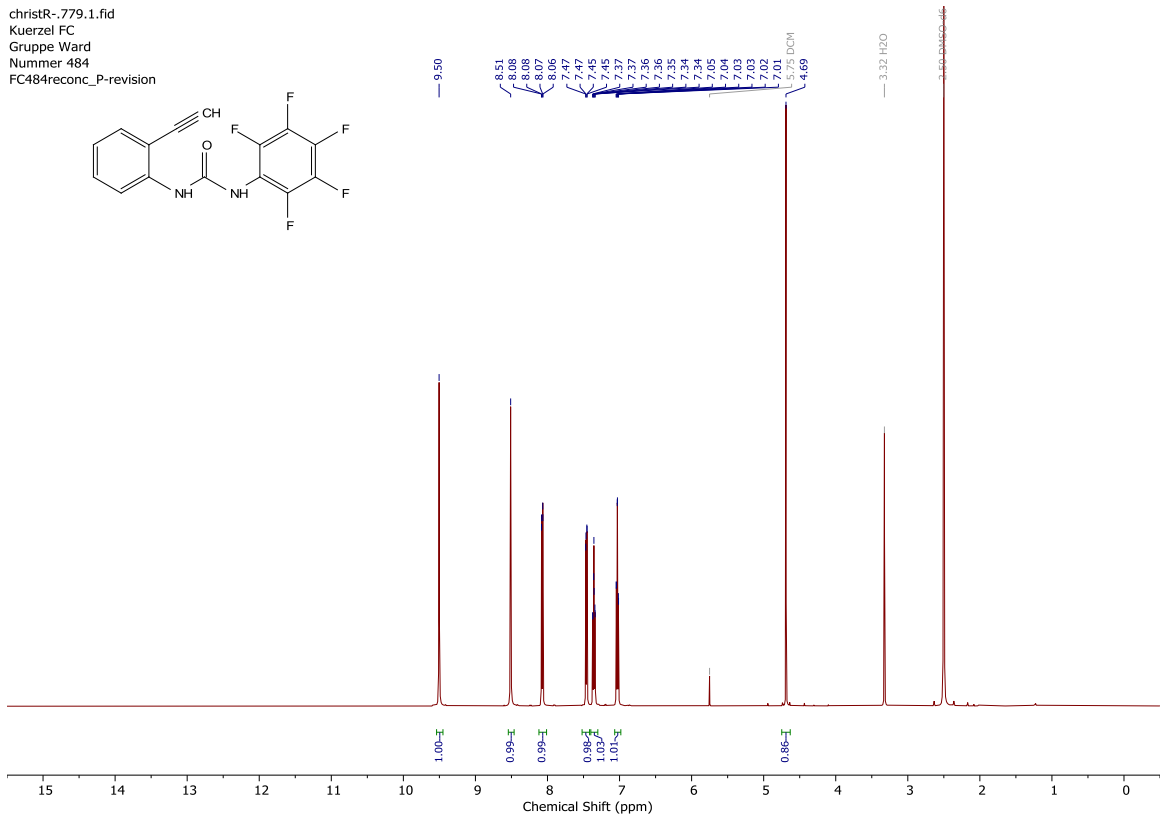
**Spectrum 11**  $^1\text{H}$  NMR Spectrum of urea **1e** in  $\text{DMSO-}d_6$ .

christR--579.2.fid  
Kuerzel FC  
Gruppe Ward  
Nummer 346  
FC346-P



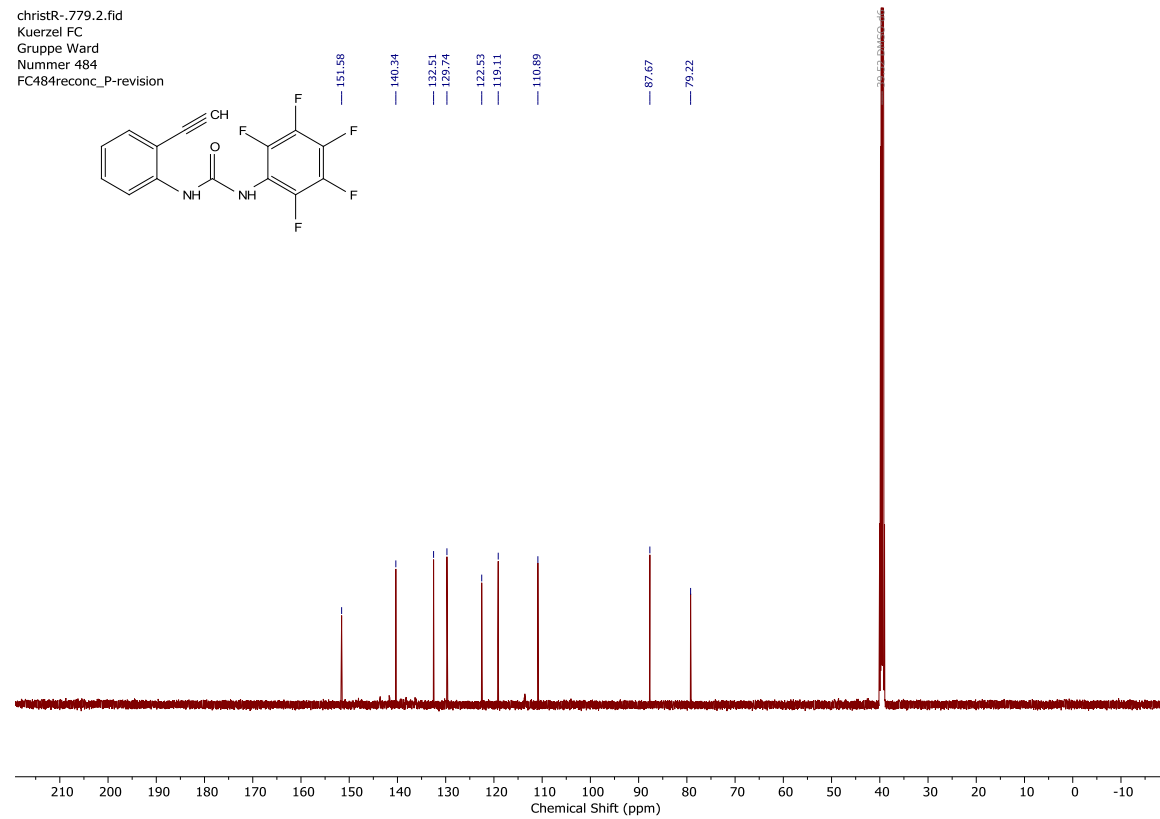
**Spectrum 12**  $^{13}\text{C}$  NMR Spectrum of urea **1e** in  $\text{DMSO-}d_6$ .

christR-.779.1.fid  
Kuerzel FC  
Gruppe Ward  
Nummer 484  
FC484reconc\_P-revision



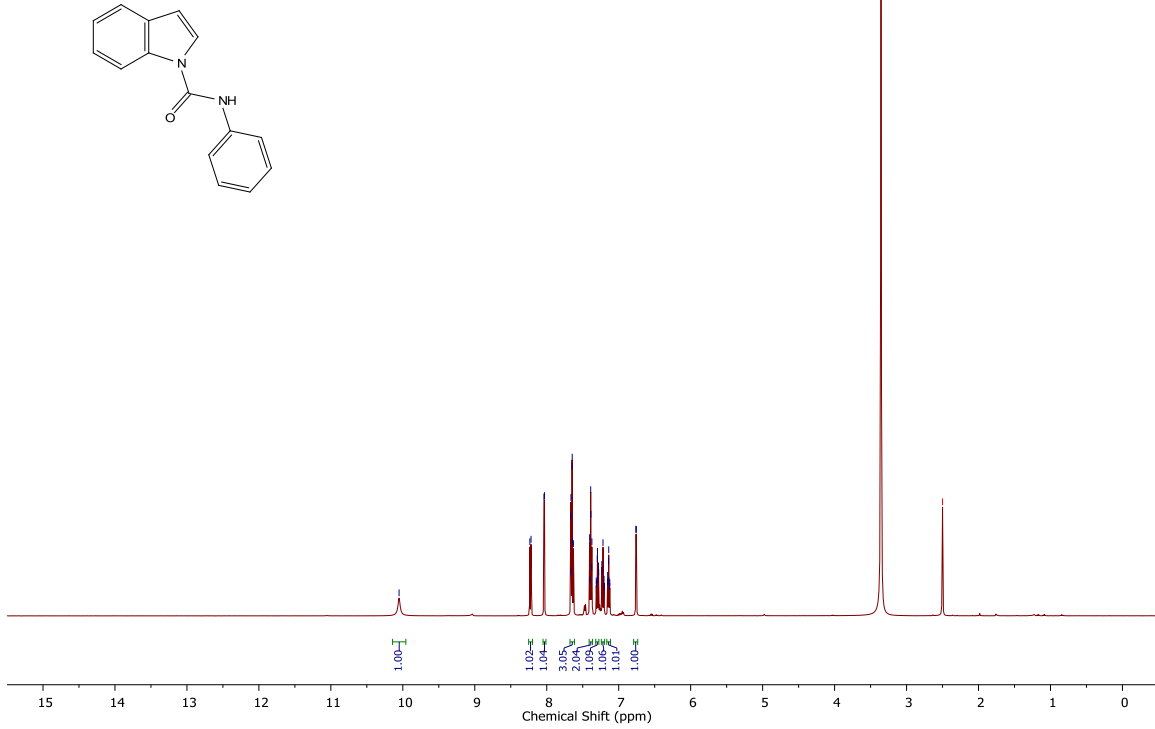
**Spectrum 13** <sup>1</sup>H NMR Spectrum of urea **1f** in DMSO-*d*<sub>6</sub>.

christR-.779.2.fid  
Kuerzel FC  
Gruppe Ward  
Nummer 484  
FC484reconc\_P-revision



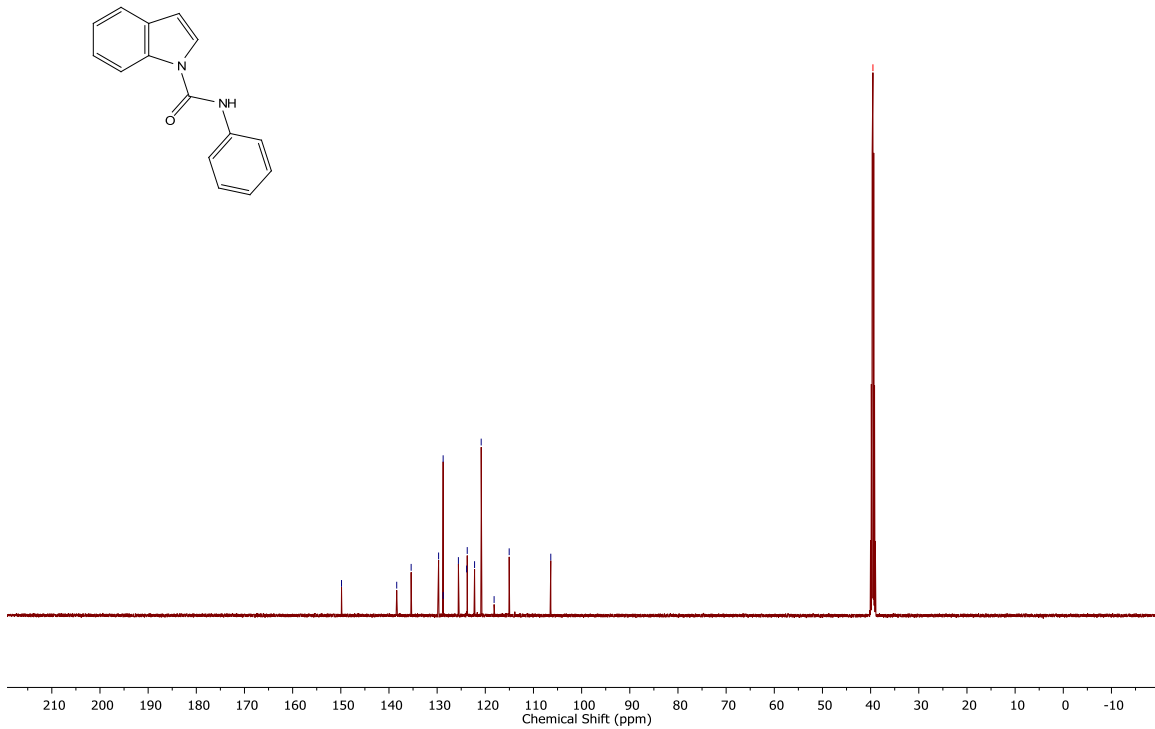
**Spectrum 14** <sup>13</sup>C NMR Spectrum of urea **1f** in DMSO-*d*<sub>6</sub>.

christR--562.1.fid  
Kuerzel FC  
Gruppe Ward  
Nummer 265  
FC265-P



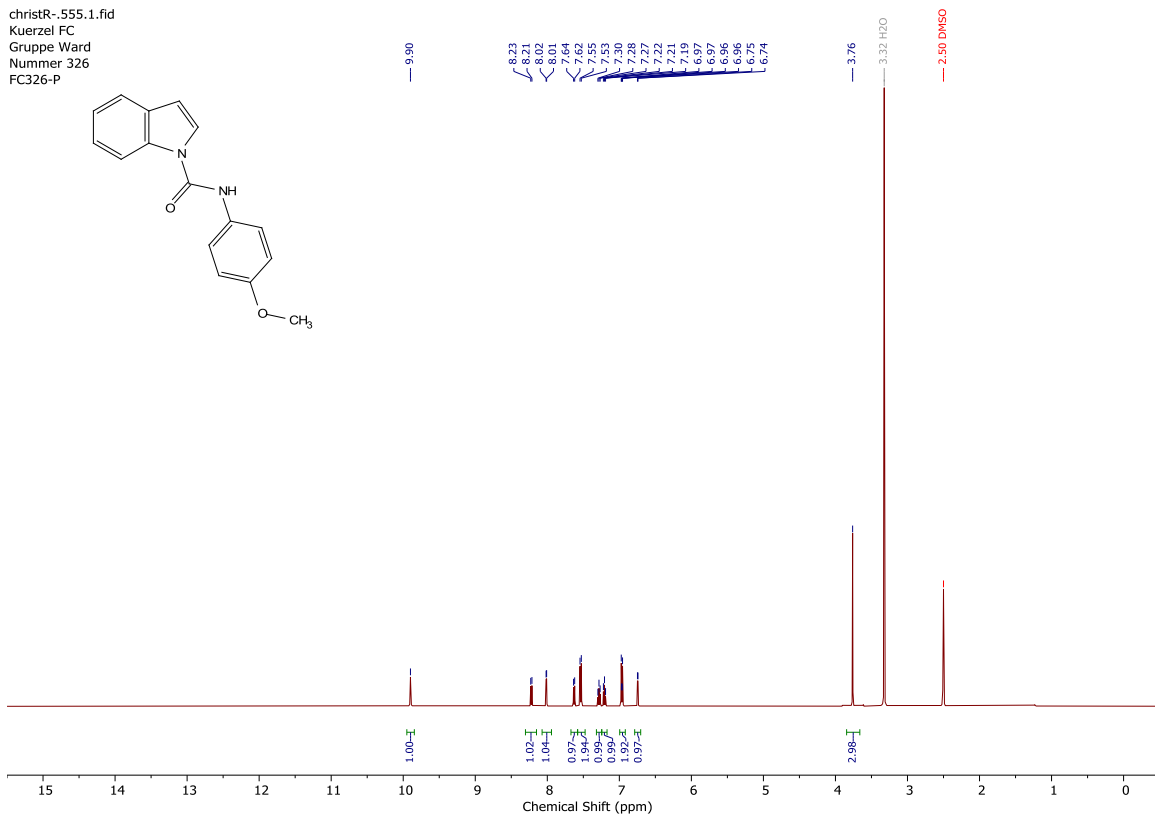
**Spectrum 15**  $^1\text{H}$  NMR Spectrum of indole **2** in  $\text{DMSO-}d_6$ .

christR--562.2.fid  
Kuerzel FC  
Gruppe Ward  
Nummer 265  
FC265-P



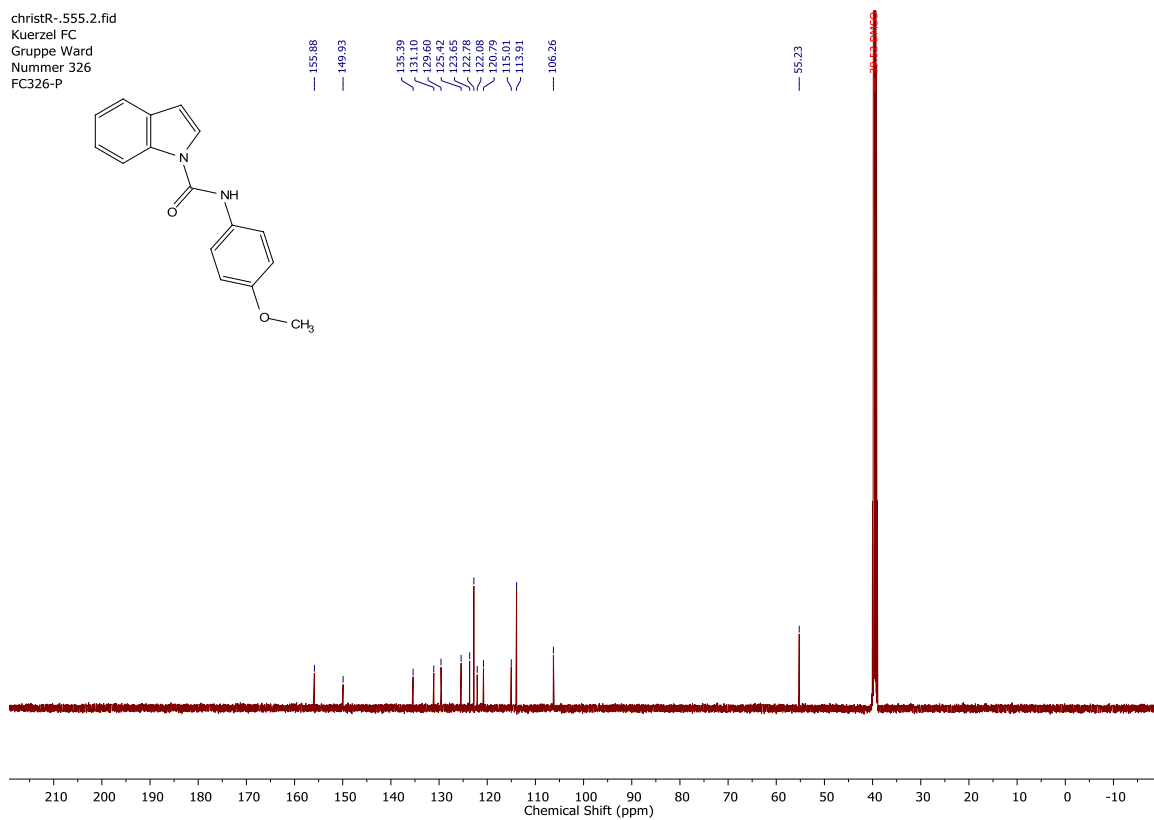
**Spectrum 16**  $^{13}\text{C}$  NMR Spectrum of indole **2** in  $\text{DMSO-}d_6$ .

christR-.555.1.fid  
Kuerzel FC  
Gruppe Ward  
Nummer 326  
FC326-P



**Spectrum 17** <sup>1</sup>H NMR Spectrum of indole **2a** in DMSO-*d*<sub>6</sub>.

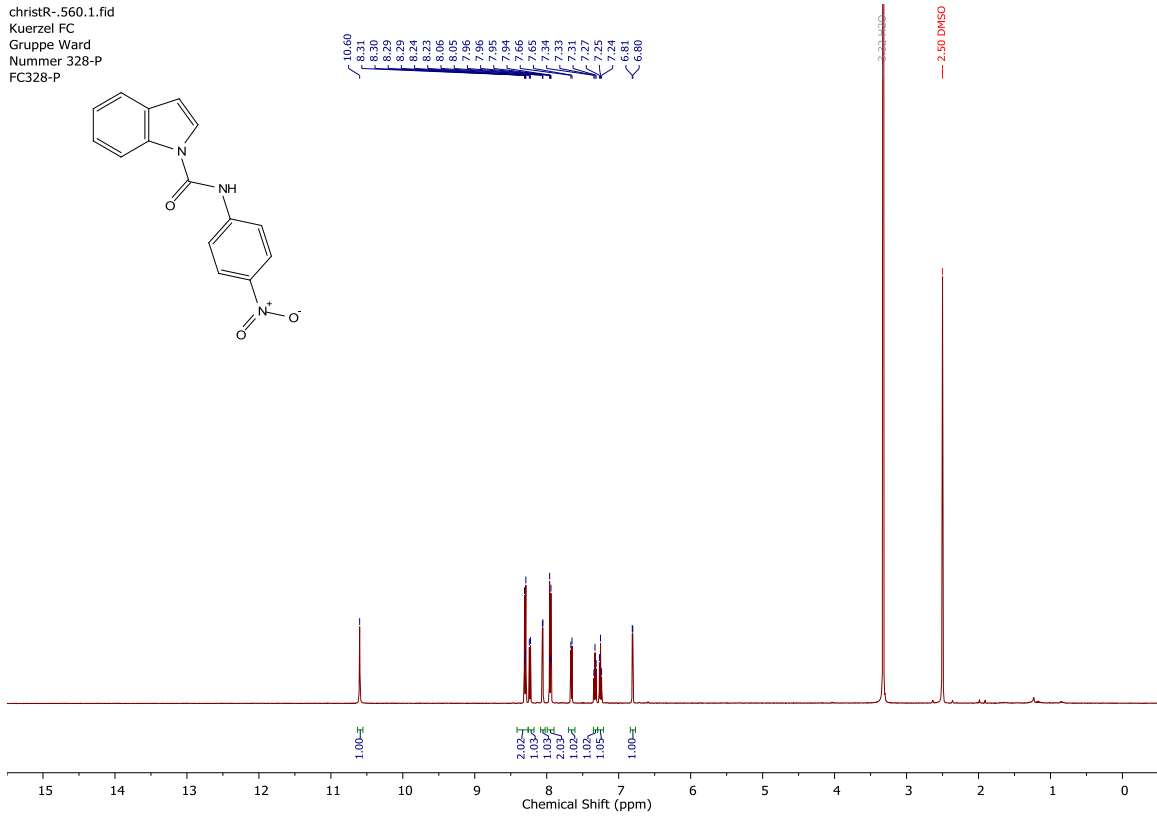
christR-.555.2.fid  
Kuerzel FC  
Gruppe Ward  
Nummer 326  
FC326-P



**Spectrum 18** <sup>13</sup>C NMR Spectrum of indole **2a** in DMSO-*d*<sub>6</sub>.

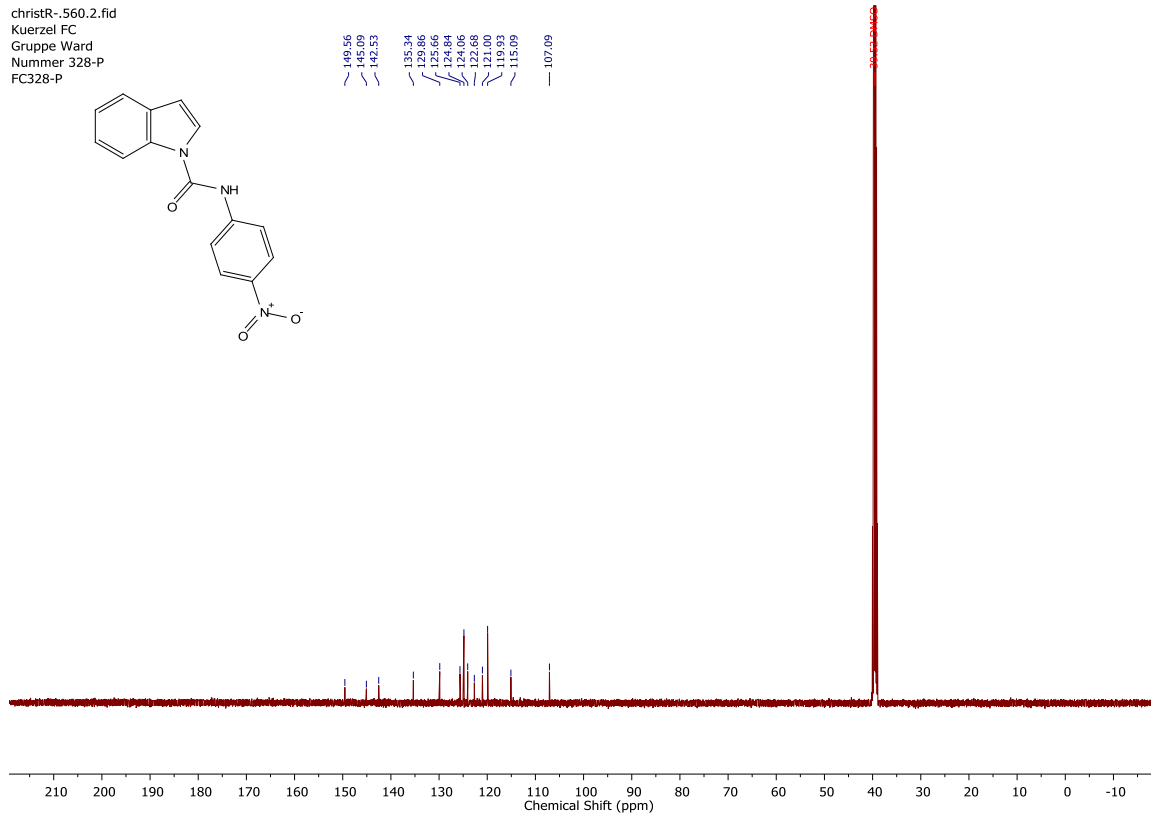


christR-.560.1.fid  
 Kuerzel FC  
 Gruppe Ward  
 Nummer 328-P  
 FC328-P



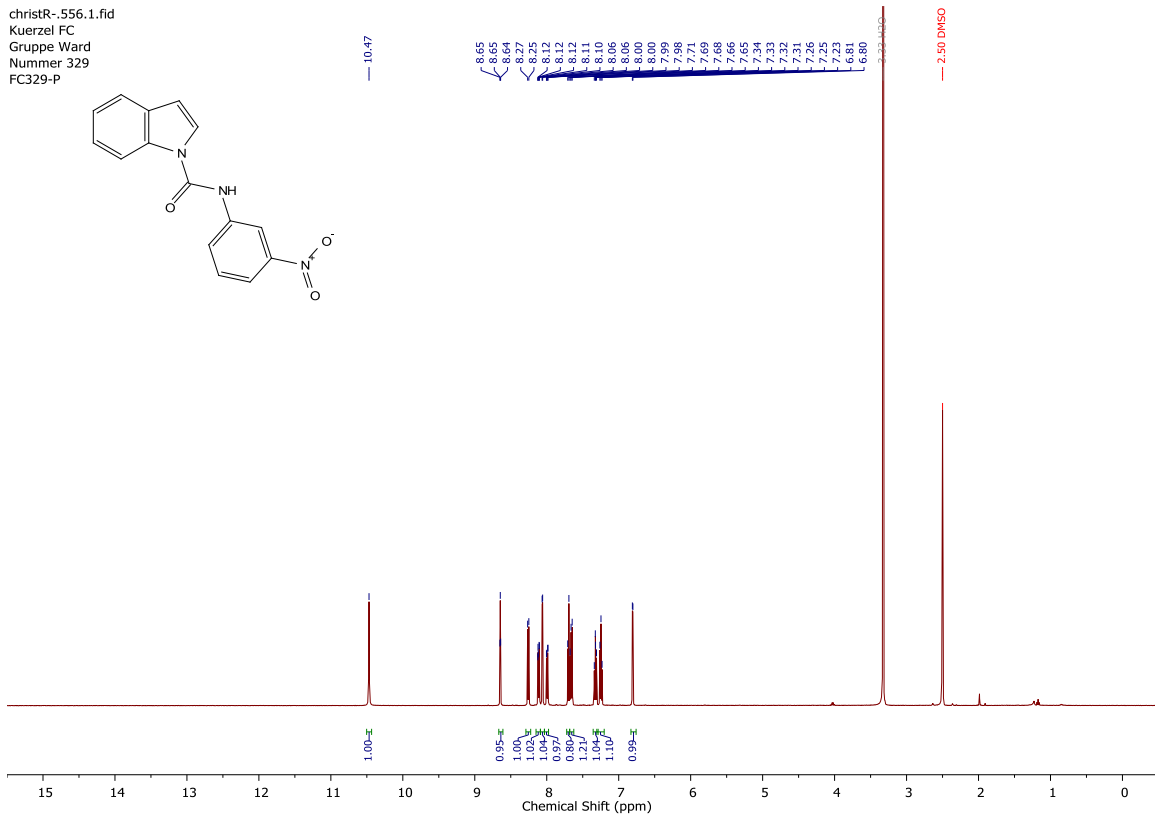
**Spectrum 19** <sup>1</sup>H NMR Spectrum of indole **2b** in DMSO-*d*<sub>6</sub>.

christR-.560.2.fid  
 Kuerzel FC  
 Gruppe Ward  
 Nummer 328-P  
 FC328-P



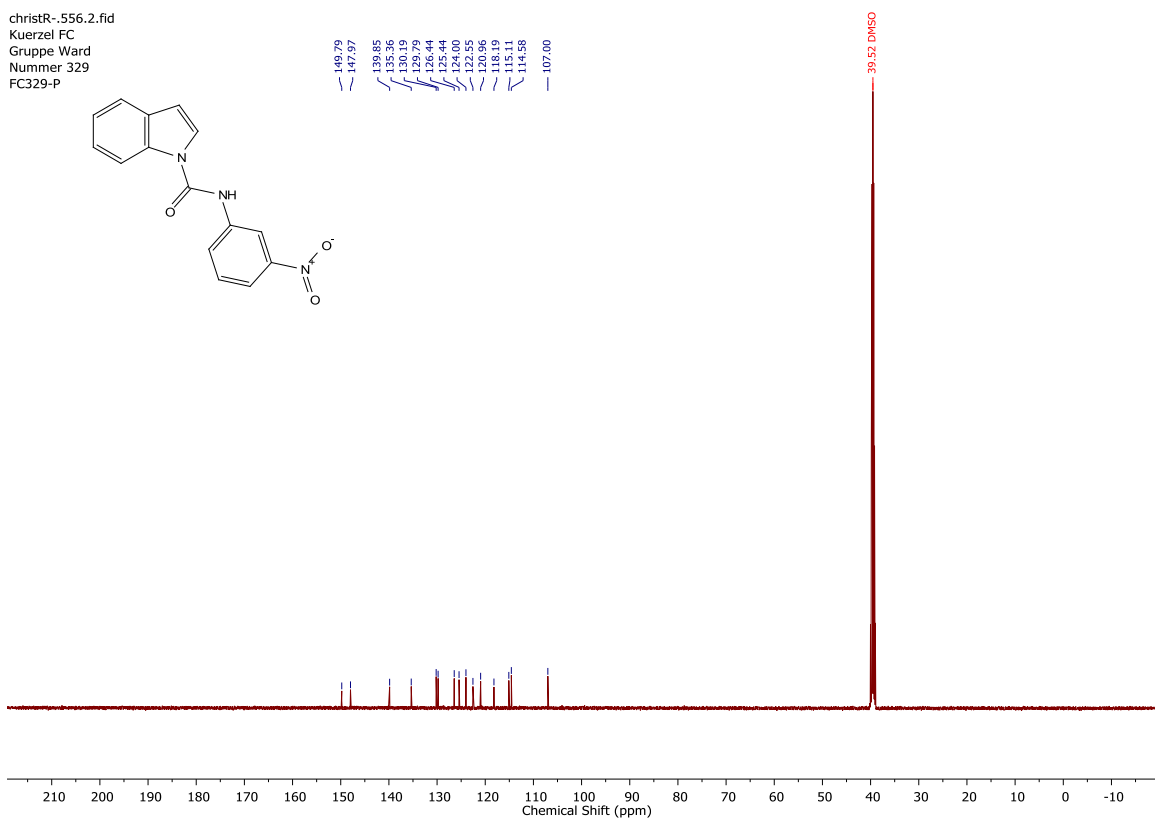
**Spectrum 20** <sup>13</sup>C NMR Spectrum of indole **2b** in DMSO-*d*<sub>6</sub>.

christR--556.1.fid  
Kuerzel FC  
Gruppe Ward  
Nummer 329  
FC329-P



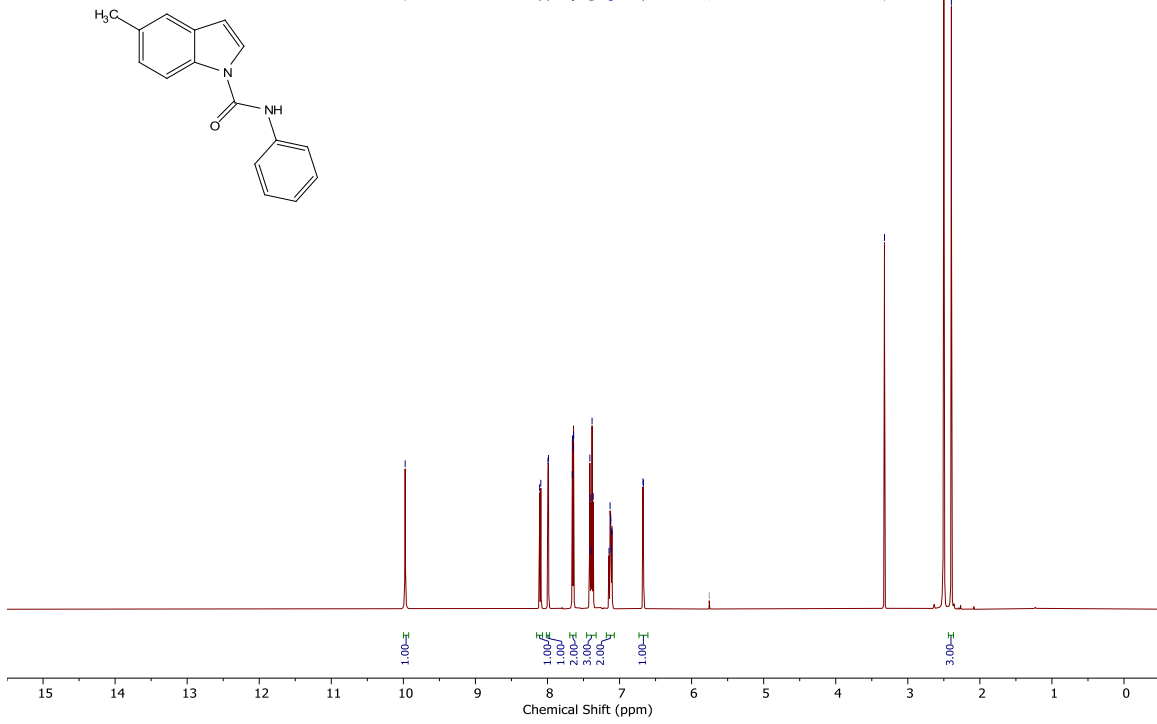
**Spectrum 21**  $^1\text{H}$  NMR Spectrum of indole **2c** in  $\text{DMSO-}d_6$ .

christR--556.2.fid  
Kuerzel FC  
Gruppe Ward  
Nummer 329  
FC329-P



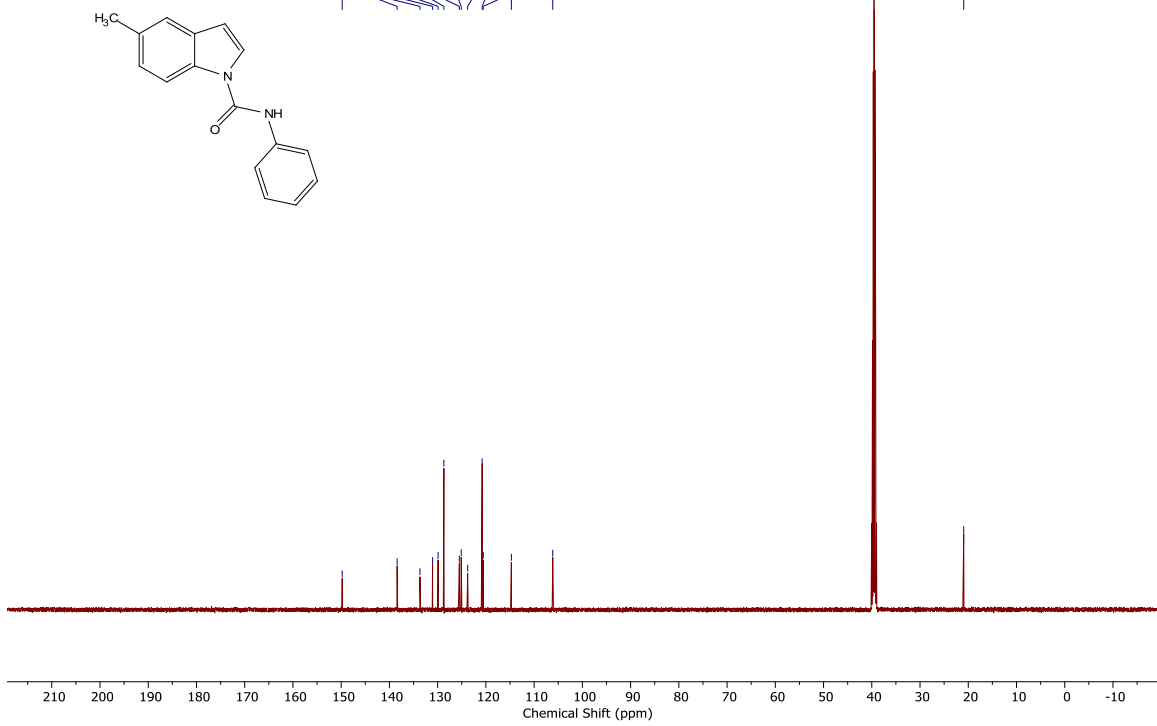
**Spectrum 22**  $^{13}\text{C}$  NMR Spectrum of indole **2c** in  $\text{DMSO-}d_6$ .

christR--781.2.fid  
Kuerzel FC  
Gruppe Ward  
Nummer 546  
FC546-P\_Revision

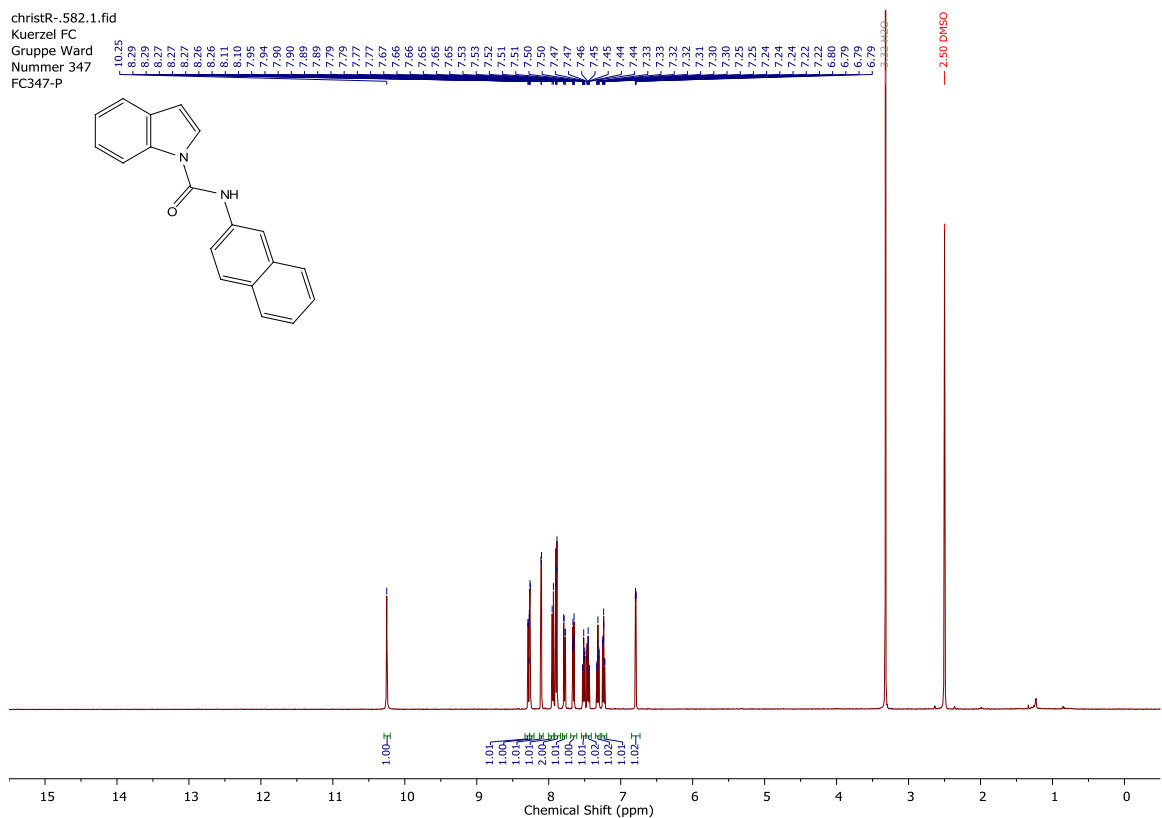


**Spectrum 23**  $^1\text{H}$  NMR Spectrum of indole **2d** in  $\text{DMSO-}d_6$ .

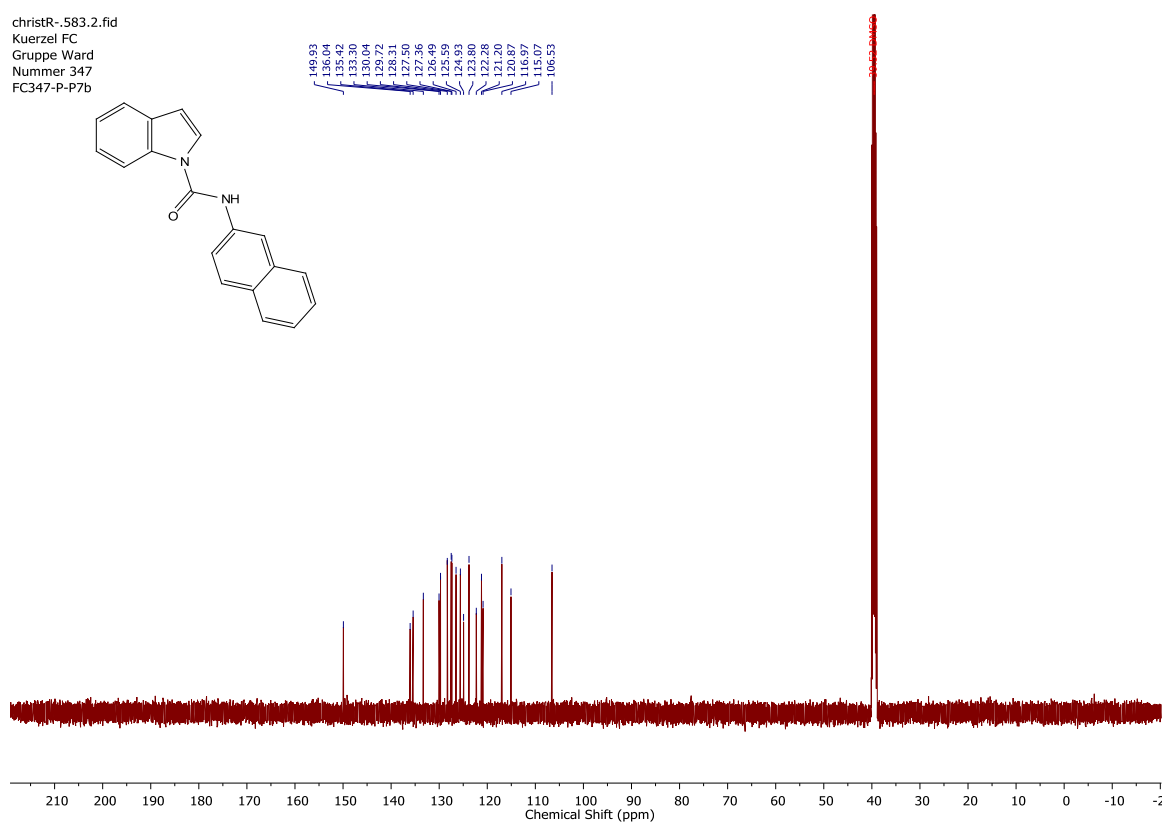
christR--781.3.fid  
Kuerzel FC  
Gruppe Ward  
Nummer 546  
FC546-P\_Revision



**Spectrum 24**  $^{13}\text{C}$  NMR Spectrum of indole **2d** in  $\text{DMSO-}d_6$ .

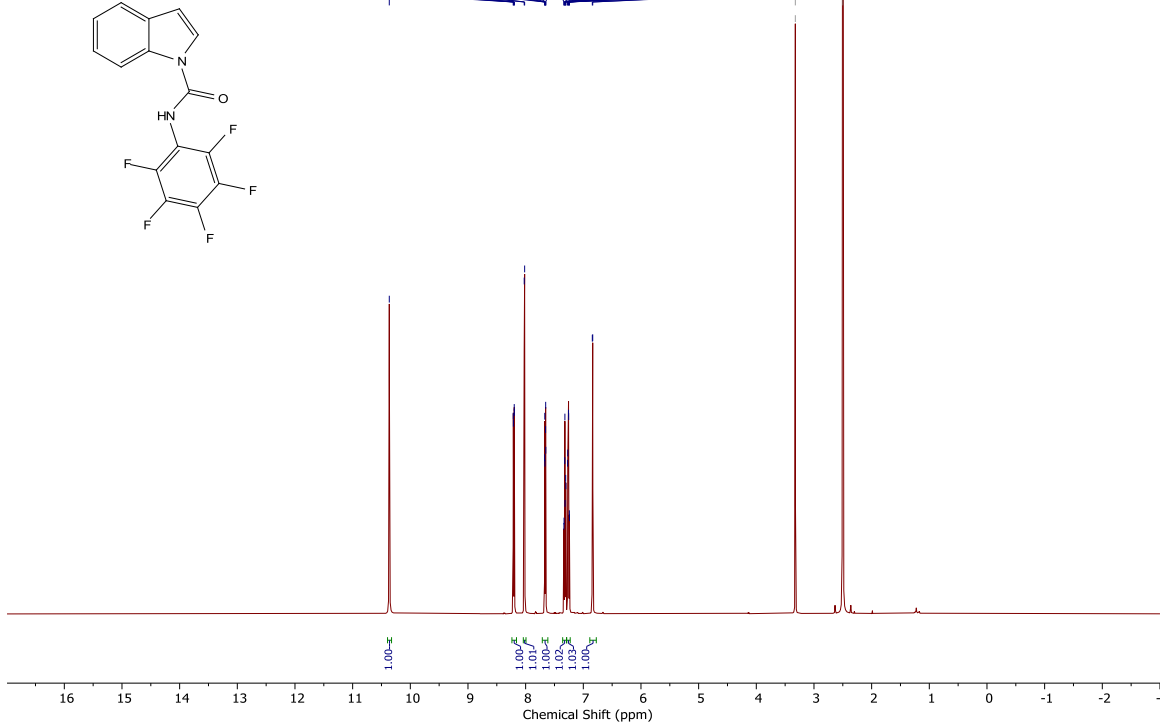


**Spectrum 25** <sup>1</sup>H NMR Spectrum of indole **2e** in DMSO-*d*<sub>6</sub>.



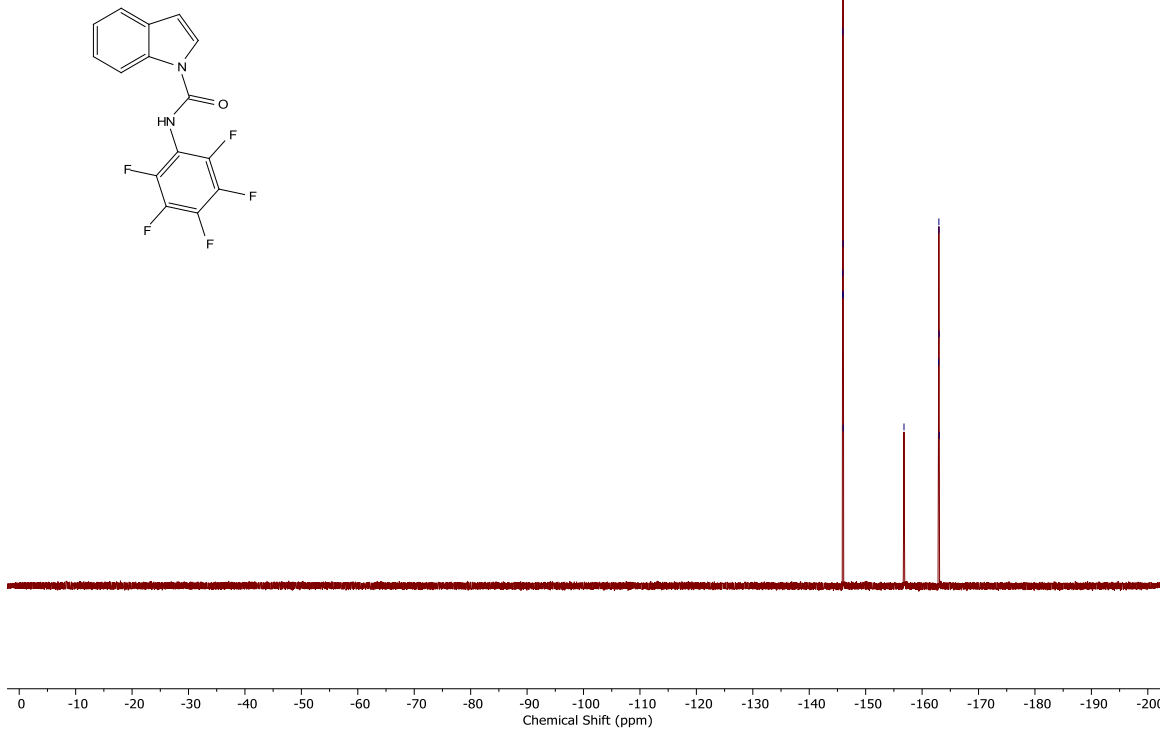
**Spectrum 26** <sup>13</sup>C NMR Spectrum of indole **2e** in DMSO-*d*<sub>6</sub>.

christR--780.1.fid  
Kuerzel FC  
Gruppe Ward  
Nummer 485  
FC485reconc\_P-revision



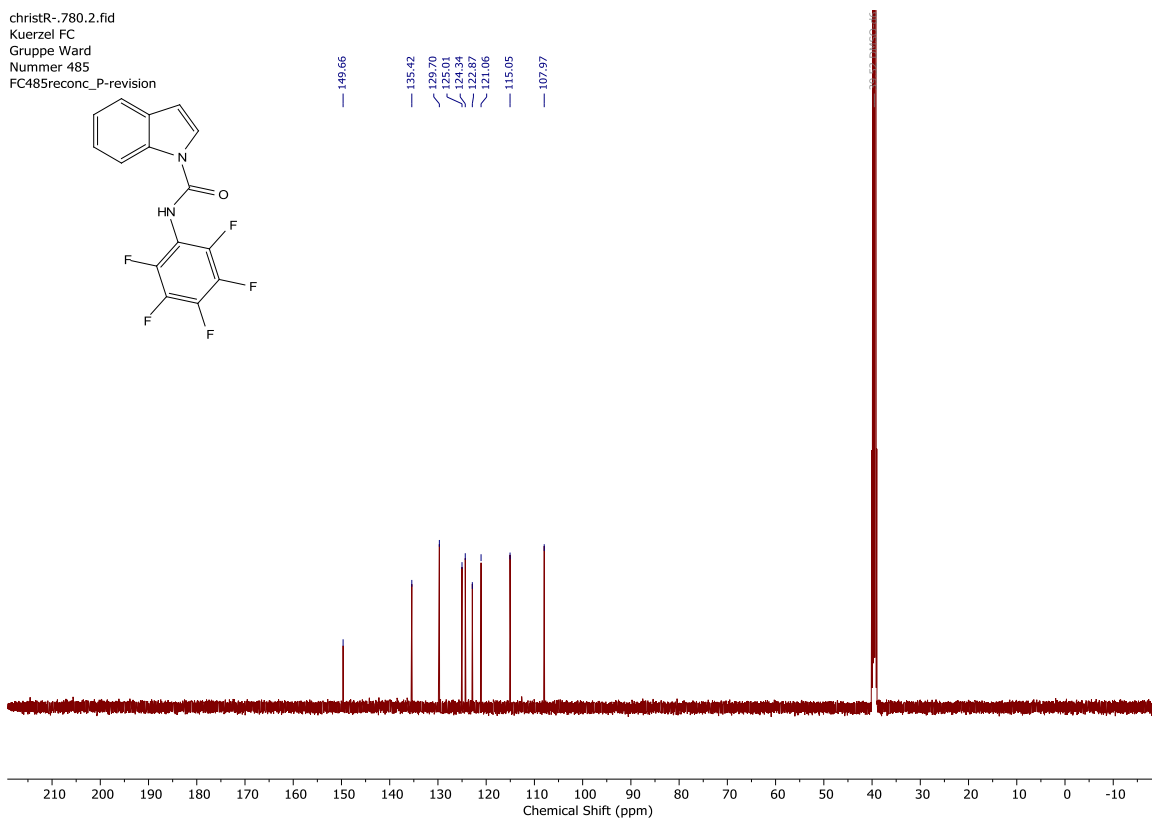
**Spectrum 27**  $^1\text{H}$  NMR Spectrum of indole **2f** in  $\text{DMSO-}d_6$ .

christR--723.2.fid  
Kuerzel FC  
Gruppe Ward  
Nummer 485  
FC485P



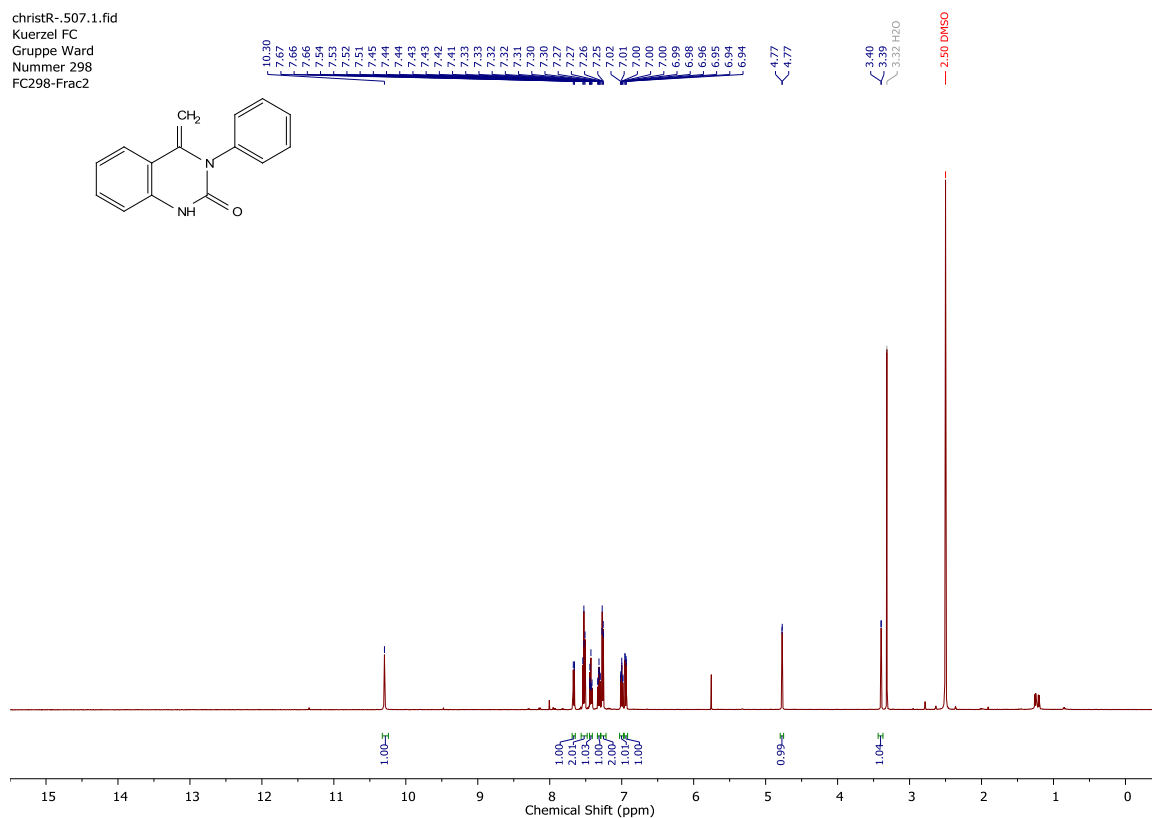
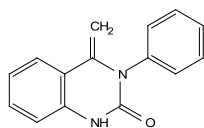
**Spectrum 28**  $^{19}\text{F}$  NMR Spectrum of indole **2f** in  $\text{DMSO-}d_6$ .

christR-.780.2.fid  
Kuerzel FC  
Gruppe Ward  
Nummer 485  
FC485reconc\_P-revision



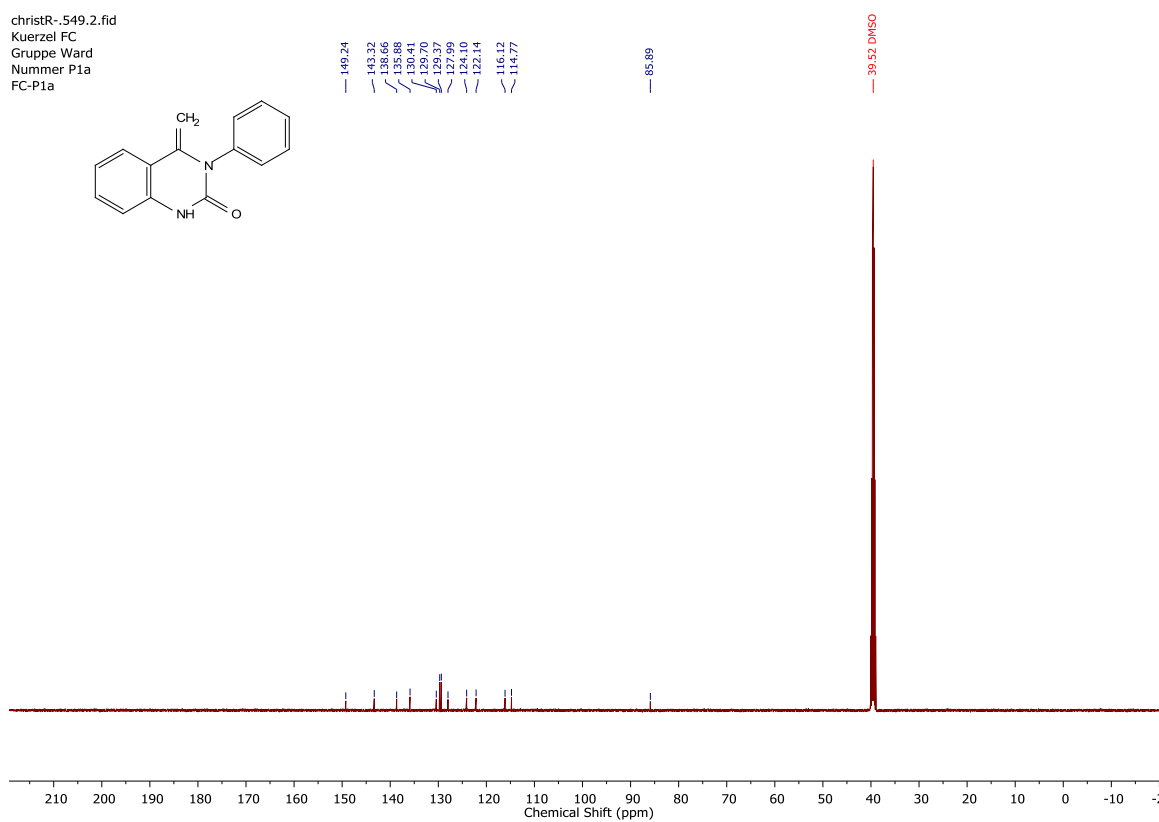
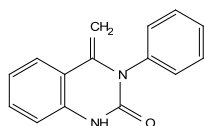
**Spectrum 29**  $^{13}\text{C}$  NMR Spectrum of indole **2f** in  $\text{DMSO-}d_6$ .

christR-.507.1.fid  
Kuerzel FC  
Gruppe Ward  
Nummer 298  
FC298-Frac2



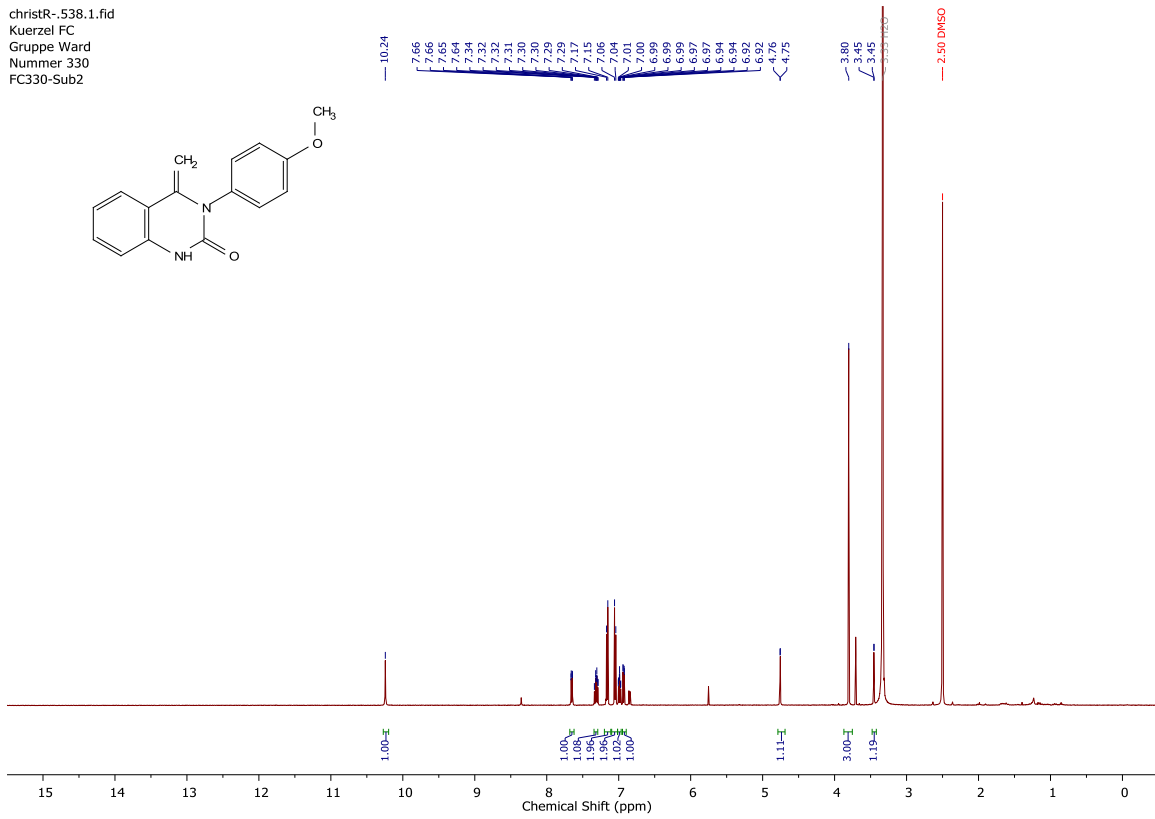
**Spectrum 30**  $^1\text{H}$  NMR Spectrum of quinazolinone **3** in  $\text{DMSO-}d_6$ .

christR-.549.2.fid  
Kuerzel FC  
Gruppe Ward  
Nummer P1a  
FC-P1a



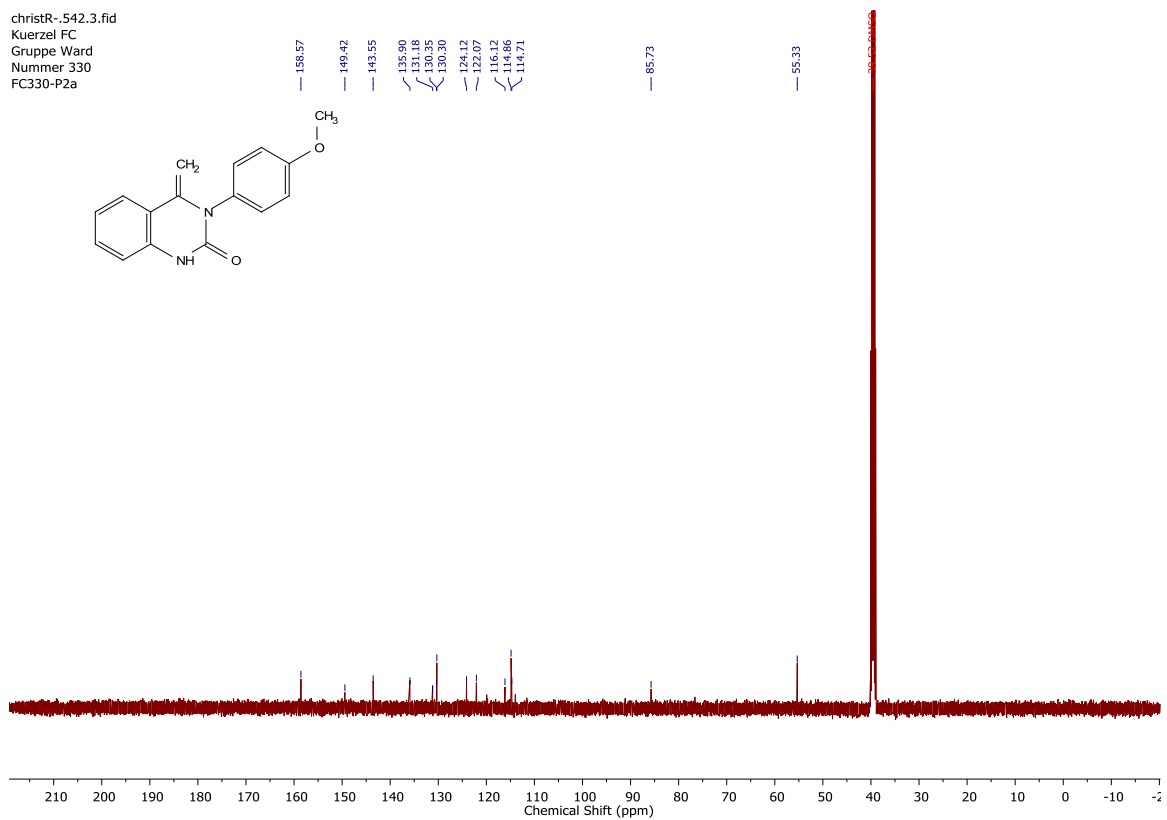
**Spectrum 31**  $^{13}\text{C}$  NMR Spectrum of quinazolinone **3** in  $\text{DMSO-}d_6$ .

christR-.538.1.fid  
 Kuerzel FC  
 Gruppe Ward  
 Nummer 330  
 FC330-Sub2



**Spectrum 32** <sup>1</sup>H NMR Spectrum of quinazolinone **3a** in DMSO-*d*<sub>6</sub>.

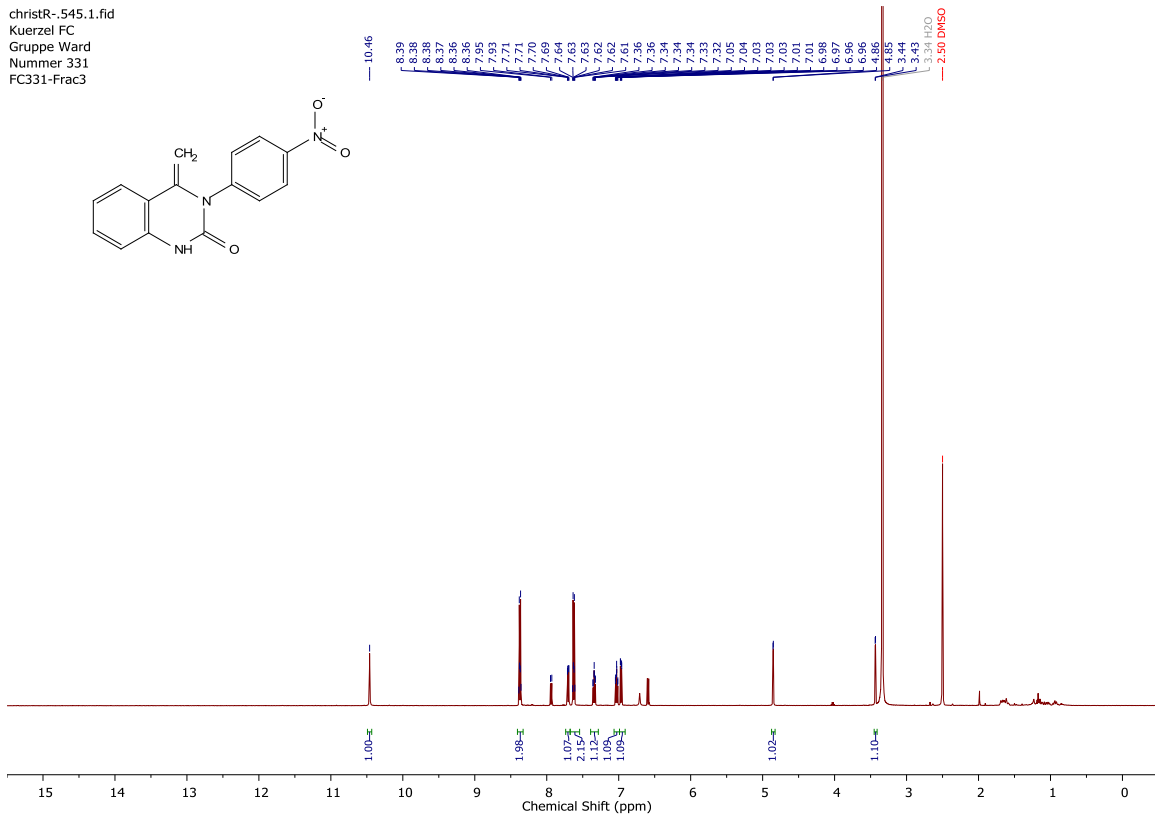
christR-.542.3.fid  
 Kuerzel FC  
 Gruppe Ward  
 Nummer 330  
 FC330-P2a



**Spectrum 33** <sup>13</sup>C NMR Spectrum of quinazolinone **3a** in DMSO-*d*<sub>6</sub>.

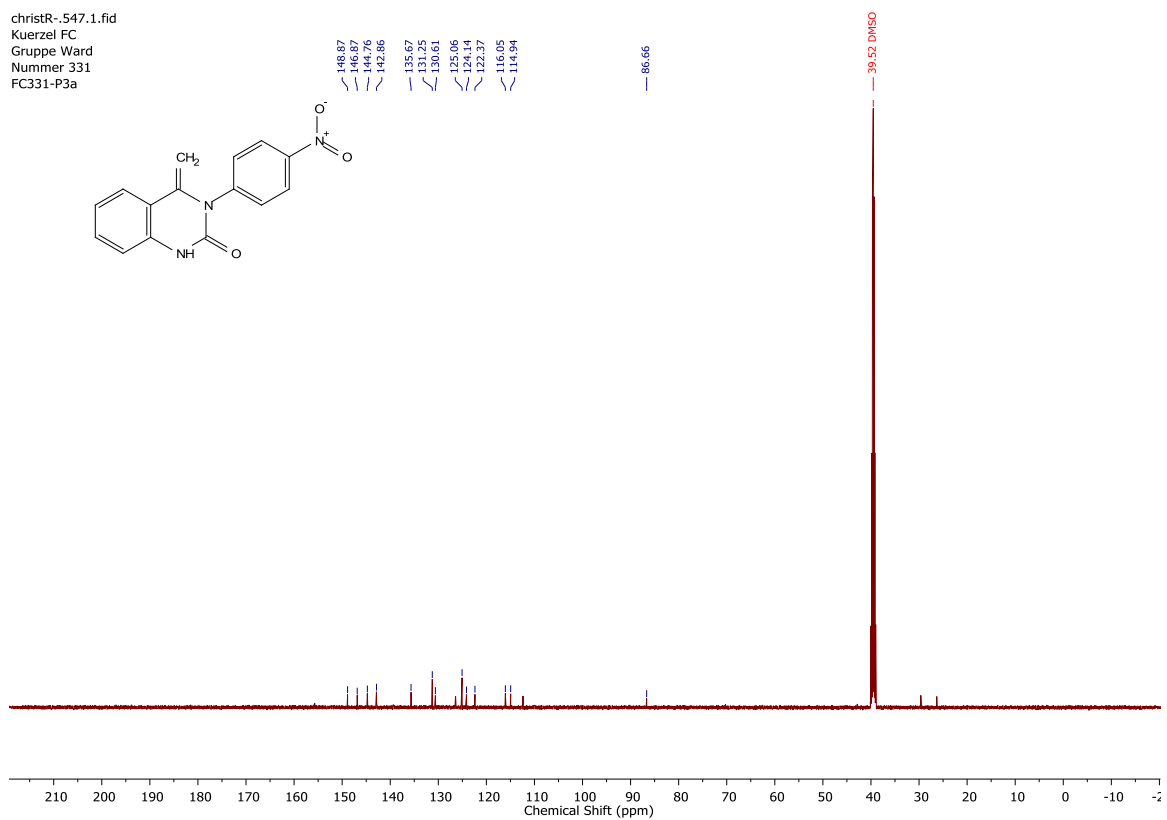


christR-.545.1.fid  
Kuerzel FC  
Gruppe Ward  
Nummer 331  
FC331-Frac3



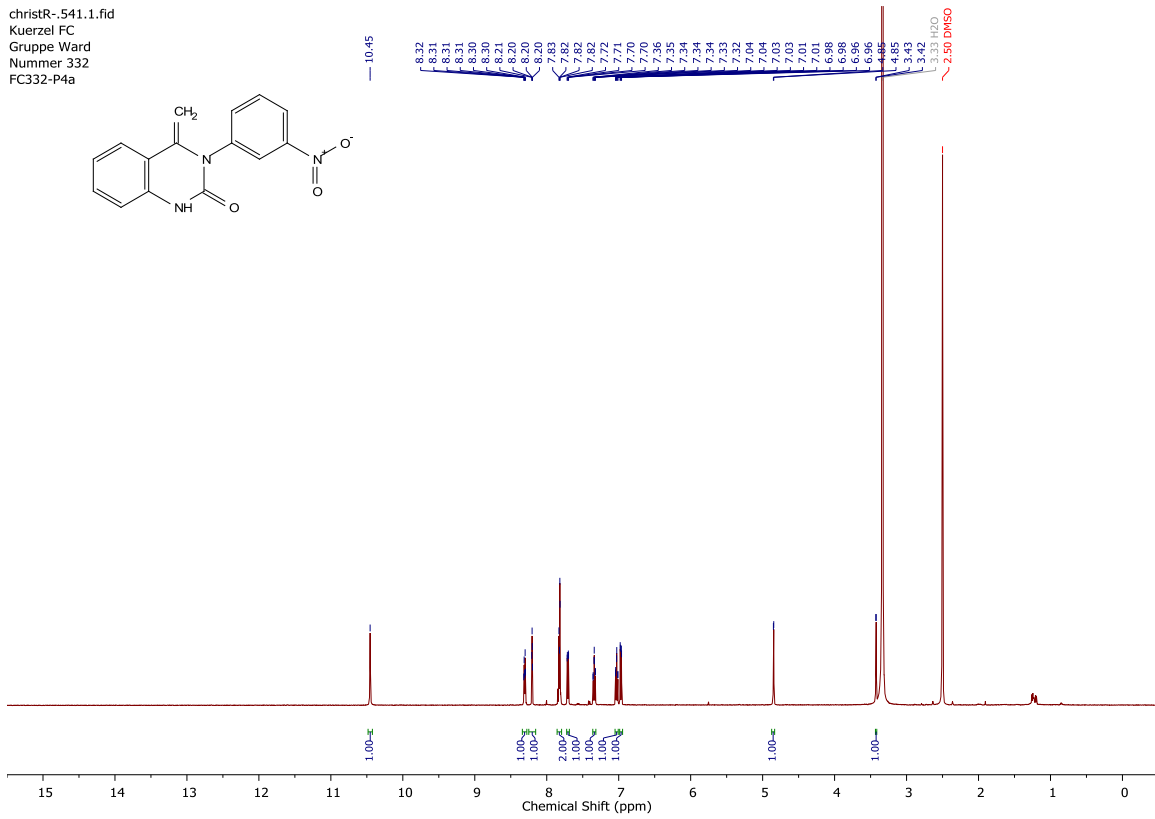
**Spectrum 34** <sup>1</sup>H NMR Spectrum of quinazolinone **3b** in DMSO-*d*<sub>6</sub>.

christR-.547.1.fid  
Kuerzel FC  
Gruppe Ward  
Nummer 331  
FC331-P3a



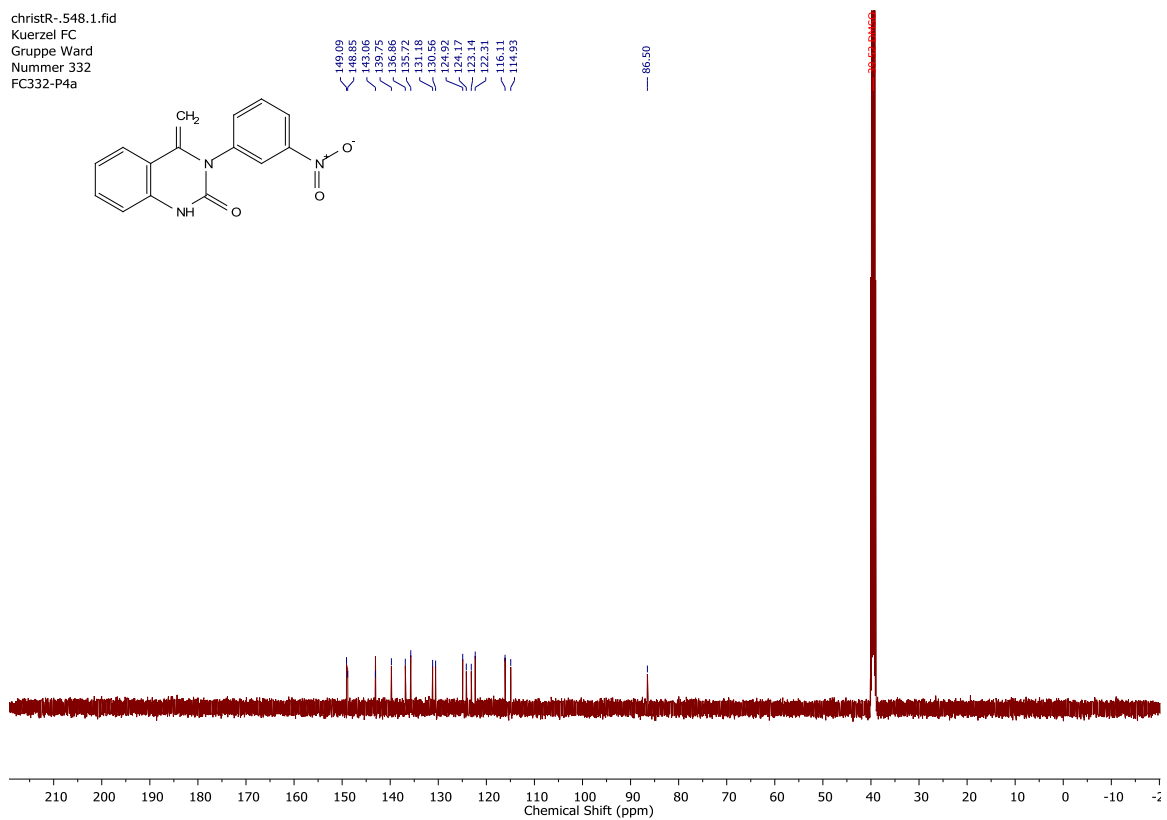
**Spectrum 35** <sup>13</sup>C NMR Spectrum of quinazolinone **3b** in DMSO-*d*<sub>6</sub>.

christR-.541.1.fid  
Kuerzel FC  
Gruppe Ward  
Nummer 332  
FC332-P4a



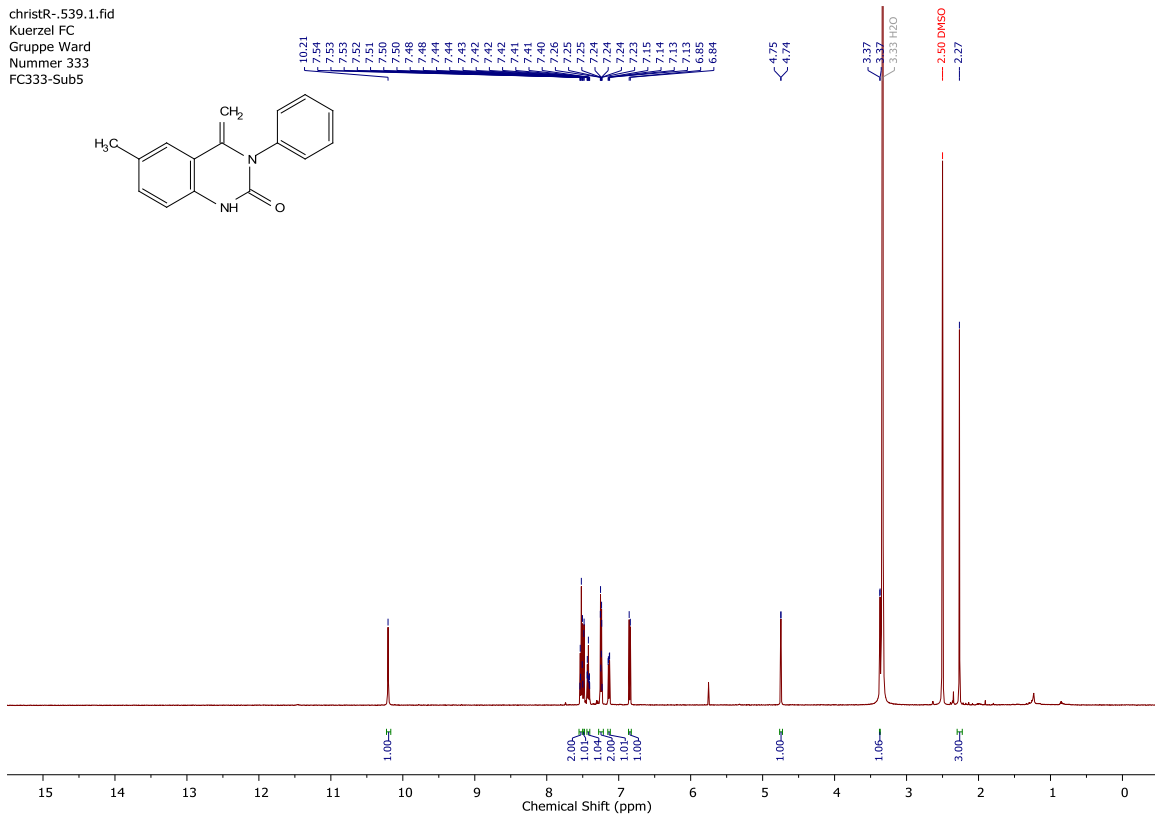
**Spectrum 36** <sup>1</sup>H NMR Spectrum of quinazolinone **3c** in DMSO-*d*<sub>6</sub>.

christR-.548.1.fid  
Kuerzel FC  
Gruppe Ward  
Nummer 332  
FC332-P4a



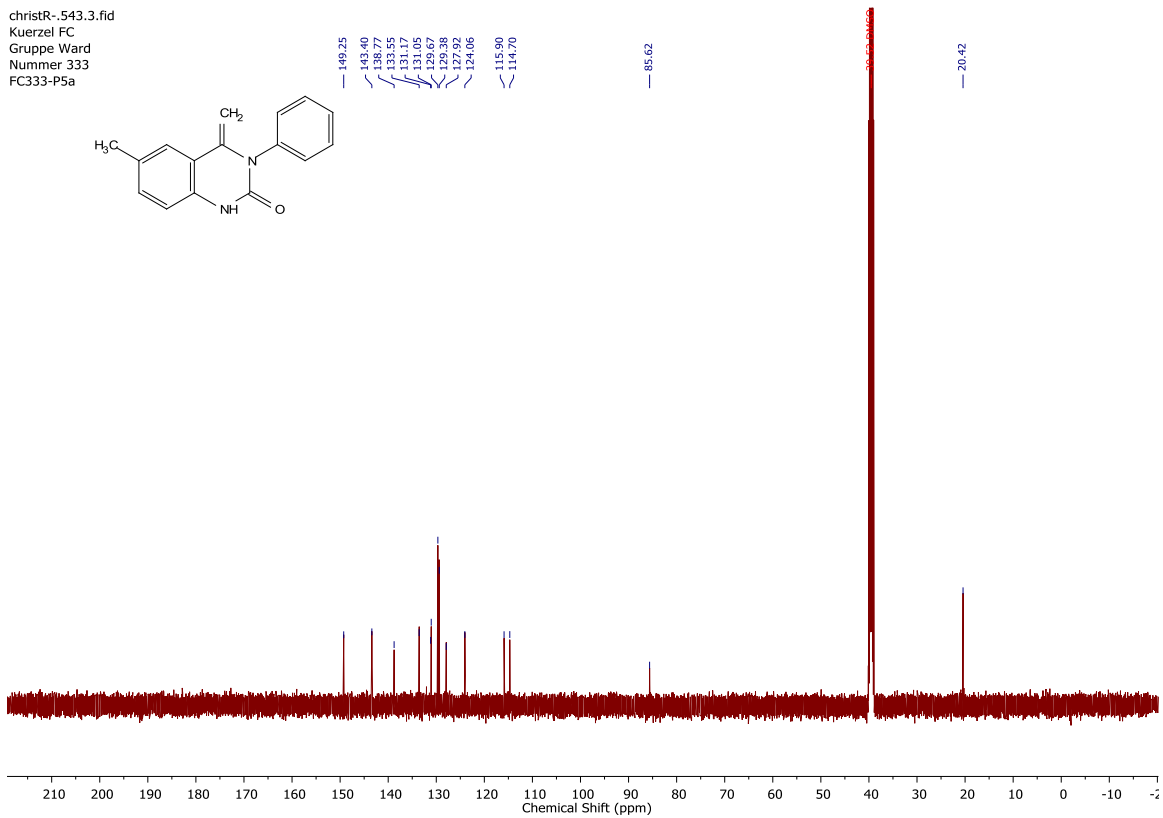
**Spectrum 37** <sup>13</sup>C NMR Spectrum of quinazolinone **3c** in DMSO-*d*<sub>6</sub>.

christR--539.1.fid  
Kuerzel FC  
Gruppe Ward  
Nummer 333  
FC333-Sub5



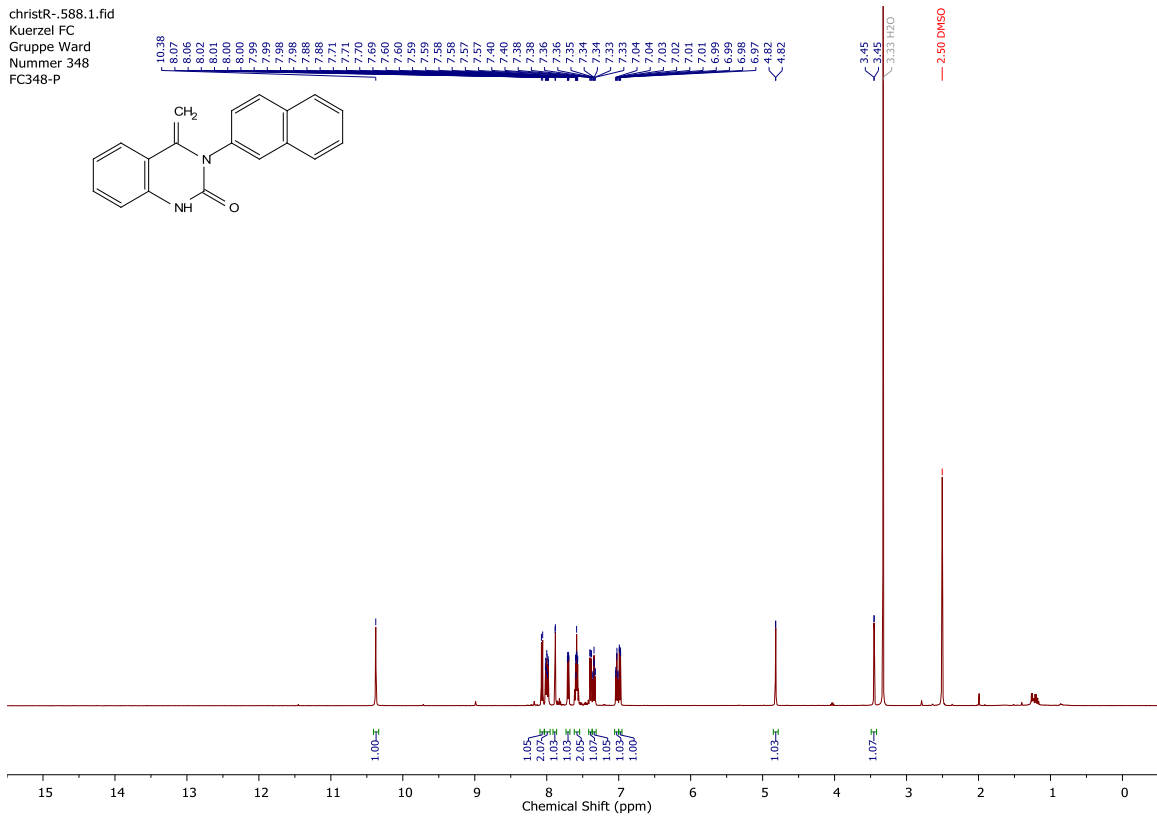
**Spectrum 38**  $^1\text{H}$  NMR Spectrum of quinazolinone **3d** in  $\text{DMSO-}d_6$ .

christR--543.3.fid  
Kuerzel FC  
Gruppe Ward  
Nummer 333  
FC333-P5a



**Spectrum 39**  $^{13}\text{C}$  NMR Spectrum of quinazolinone **3d** in  $\text{DMSO-}d_6$ .

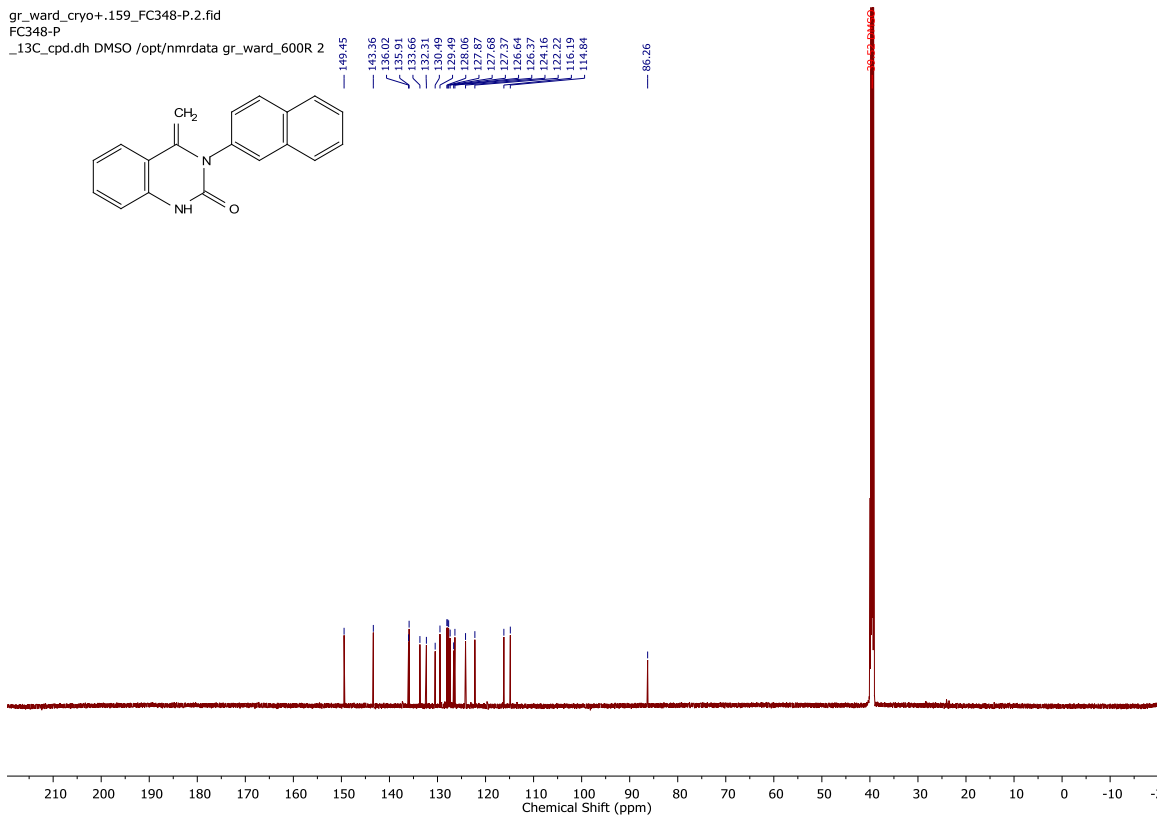
christR--588.1.fid  
 Kuerzel FC  
 Gruppe Ward  
 Nummer 348  
 FC348-P



**Spectrum 40** <sup>1</sup>H NMR Spectrum of quinazolinone **3e** in DMSO-*d*<sub>6</sub>.

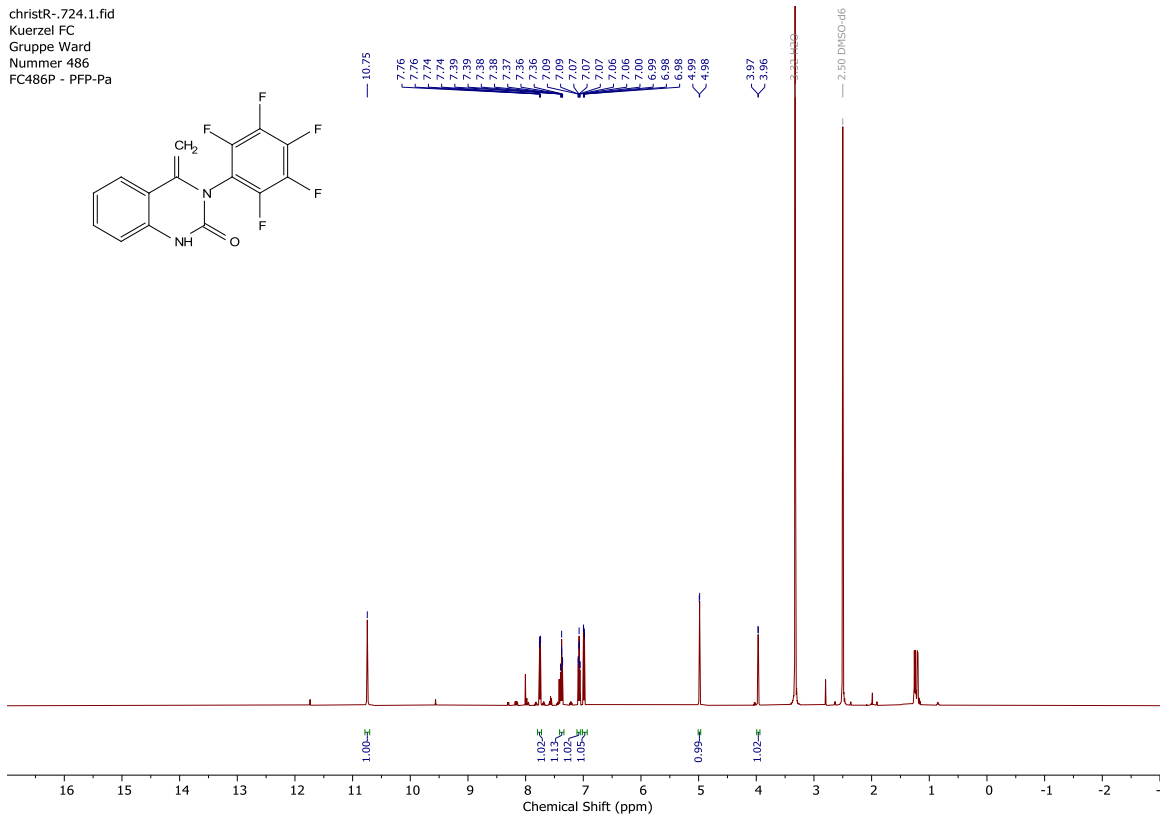
gr\_ward\_cryo+.159\_FC348-P.2.fid  
 FC348-P

\_13C\_cpd.dh DMSO /opt/nmrdata gr\_ward\_600R 2



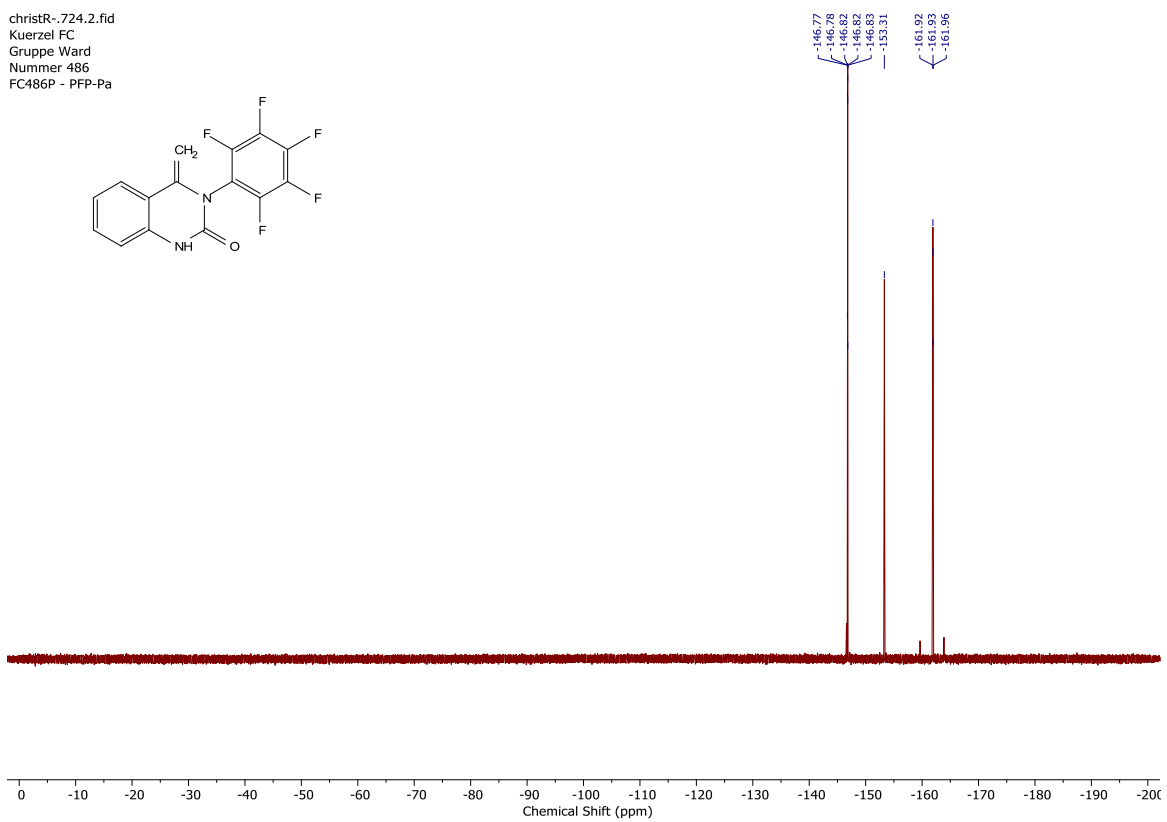
**Spectrum 41** <sup>13</sup>C NMR Spectrum of quinazolinone **3e** in DMSO-*d*<sub>6</sub>.

christR-.724.1.fid  
Kuerzel FC  
Gruppe Ward  
Nummer 486  
FC486P - PFP-Pa



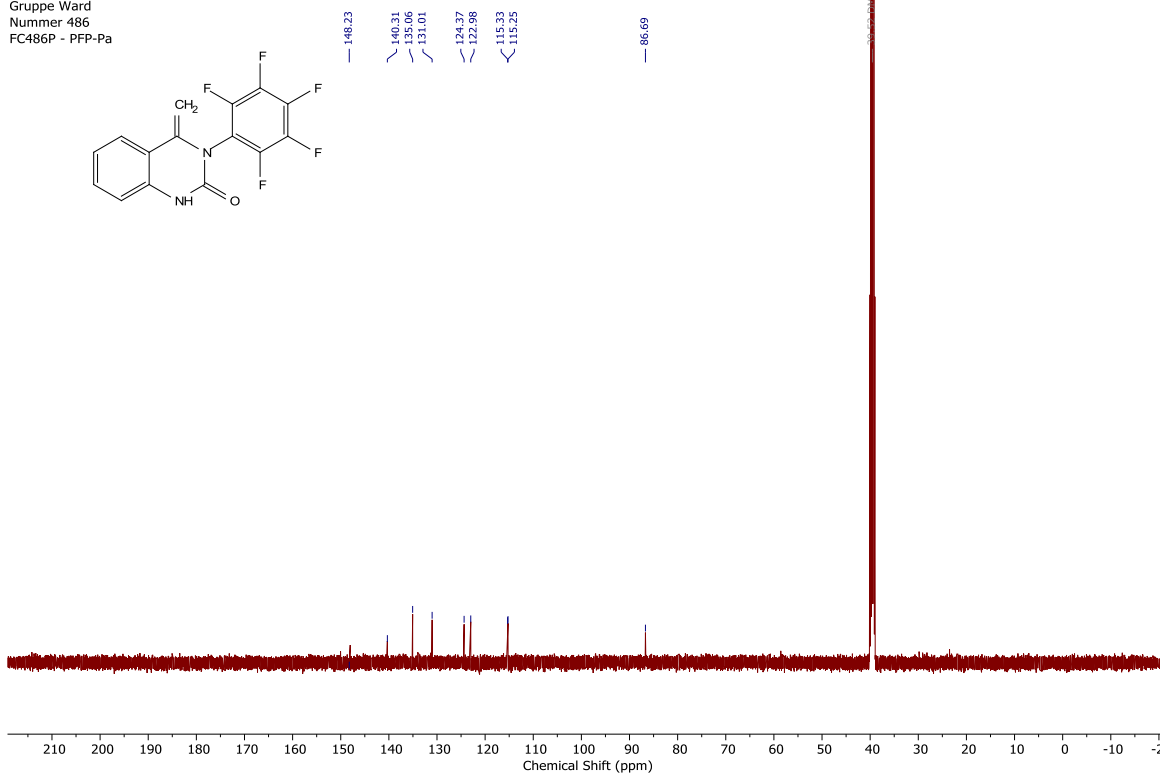
**Spectrum 42**  $^1\text{H}$  NMR Spectrum of quinazolinone **3f** in  $\text{DMSO-}d_6$ .

christR-.724.2.fid  
Kuerzel FC  
Gruppe Ward  
Nummer 486  
FC486P - PFP-Pa



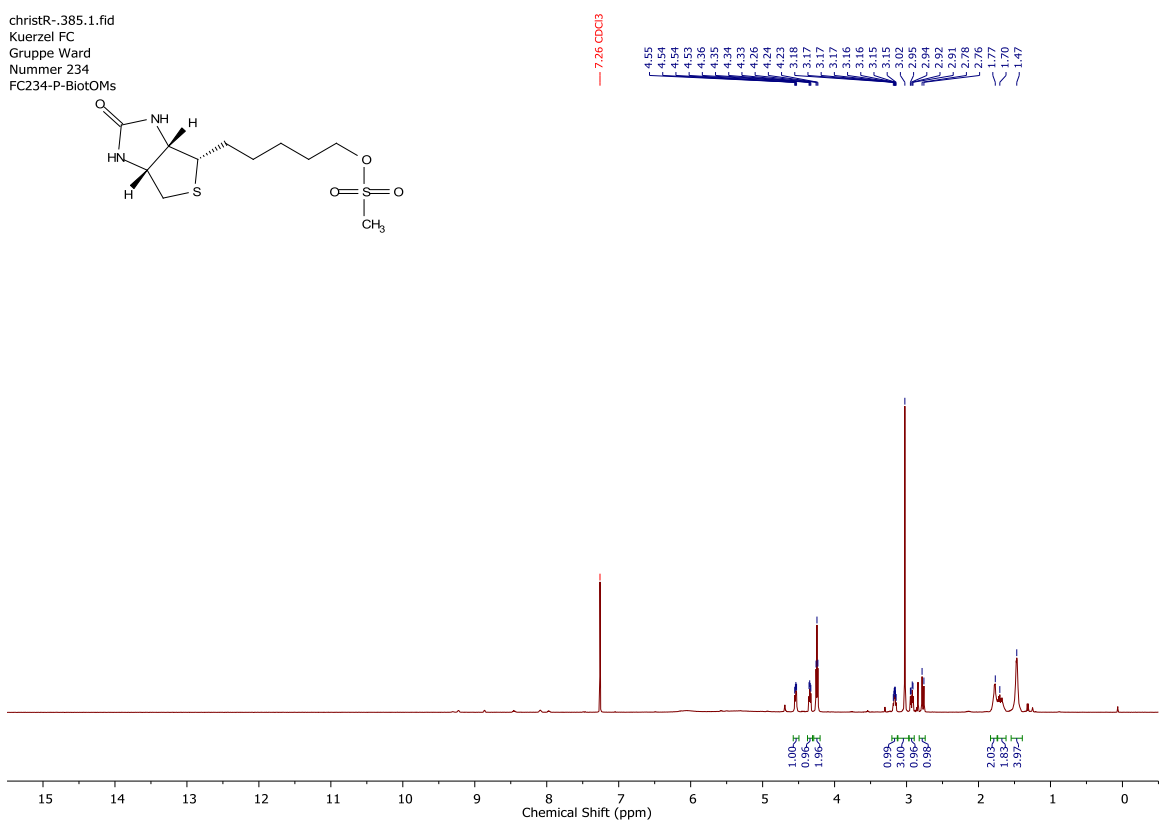
**Spectrum 43**  $^{19}\text{F}$  NMR Spectrum of quinazolinone **3f** in  $\text{DMSO-}d_6$ .

christR-.724.3.fid  
 Kuerzel FC  
 Gruppe Ward  
 Nummer 486  
 FC486P - PFP-Pa



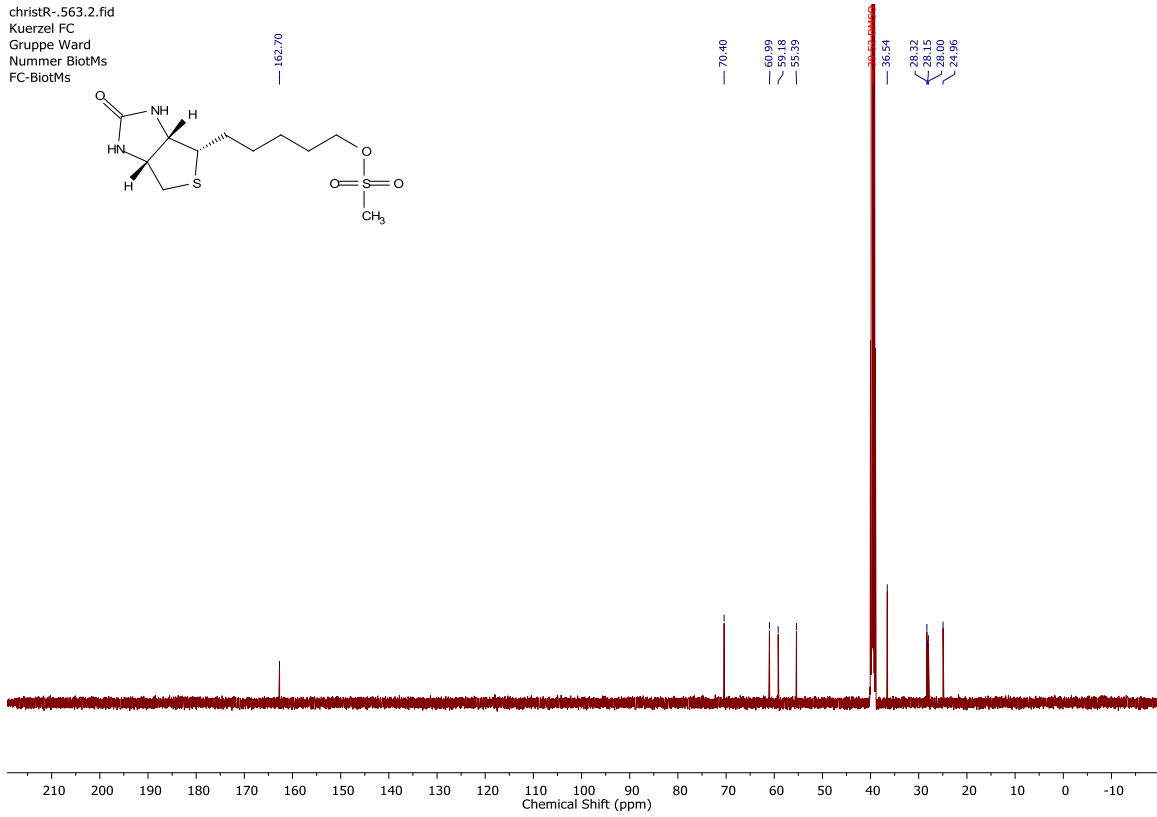
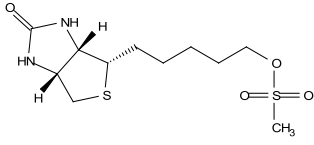
**Spectrum 44** <sup>13</sup>C NMR Spectrum of quinazolinone **3f** in DMSO-*d*<sub>6</sub>.

christR-.385.1.fid  
 Kuerzel FC  
 Gruppe Ward  
 Nummer 234  
 FC234-P-BiotOMs



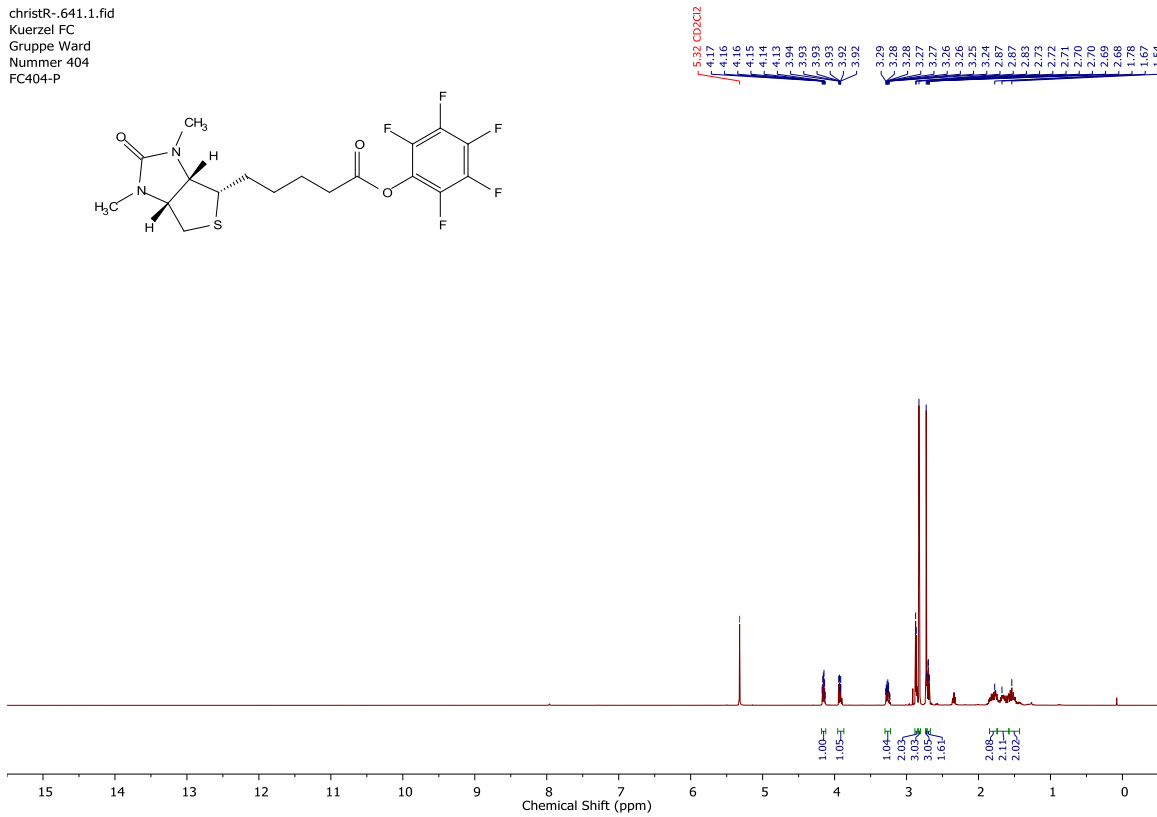
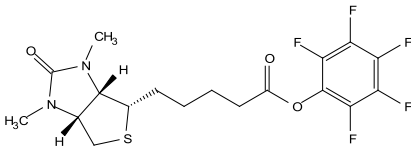
**Spectrum 45** <sup>1</sup>H NMR Spectrum of **BiotMS** in DMSO-*d*<sub>6</sub>.

christR--563.2.fid  
 Kuerzel FC  
 Gruppe Ward  
 Nummer BiotMs  
 FC-BiotMs



**Spectrum 46** <sup>13</sup>C NMR Spectrum of BiotMS in DMSO-*d*<sub>6</sub>.

christR--641.1.fid  
 Kuerzel FC  
 Gruppe Ward  
 Nummer 404  
 FC404-P



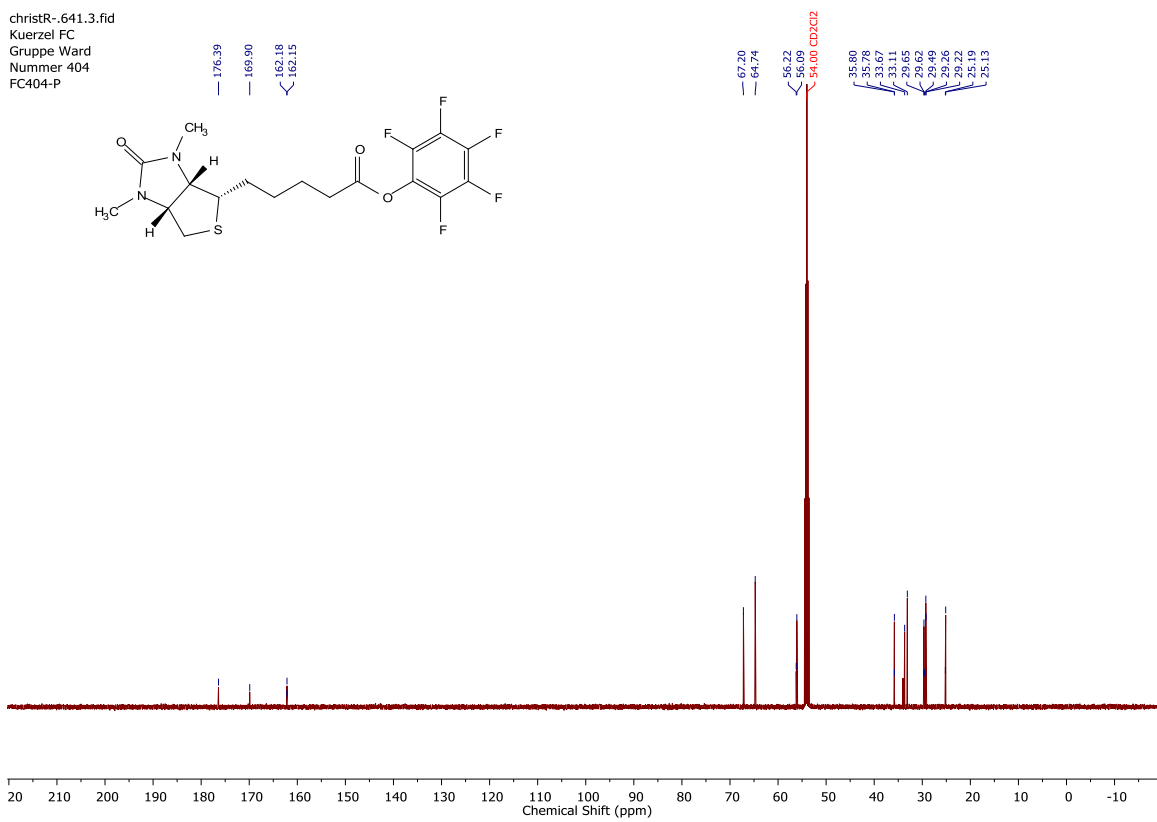
**Spectrum 47** <sup>1</sup>H NMR Spectrum of Me<sub>2</sub>BiotPFP in DMSO-*d*<sub>6</sub>.

christR-.641.2.fid  
Kuerzel FC  
Gruppe Ward  
Nummer 404  
FC404-P



**Spectrum 48** <sup>19</sup>F NMR Spectrum of Me<sub>2</sub>BiotPFP in DMSO-*d*<sub>6</sub>.

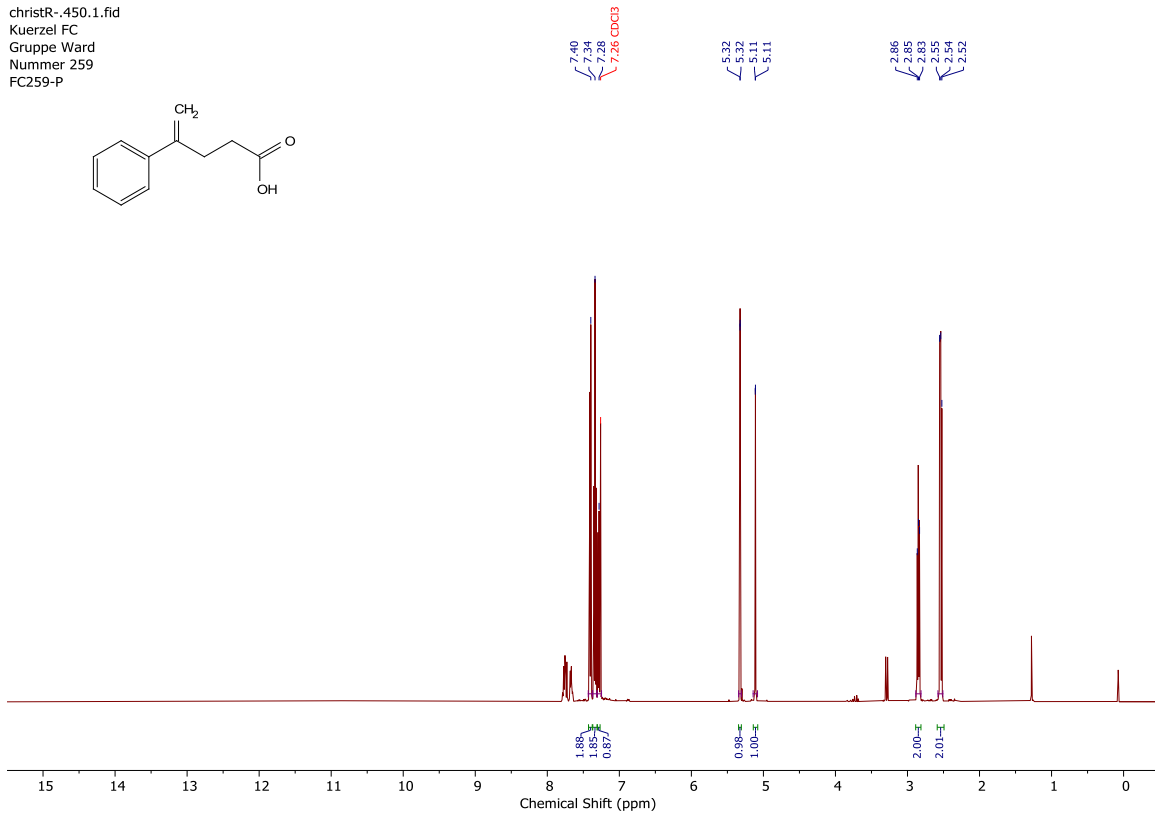
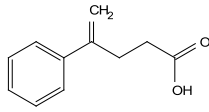
christR-.641.3.fid  
Kuerzel FC  
Gruppe Ward  
Nummer 404  
FC404-P



**Spectrum 49** <sup>13</sup>C NMR Spectrum of Me<sub>2</sub>BiotPFP in DMSO-*d*<sub>6</sub>.

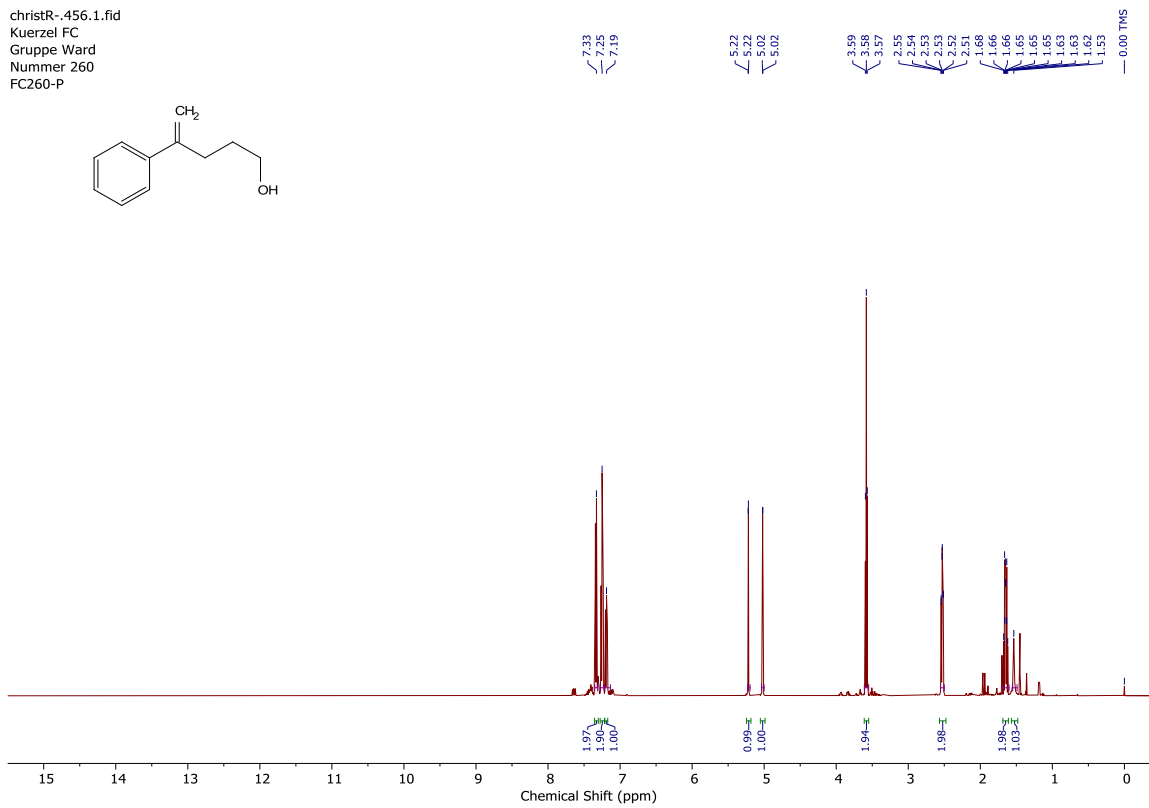
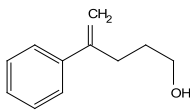


christR-.450.1.fid  
 Kuerzel FC  
 Gruppe Ward  
 Nummer 259  
 FC259-P



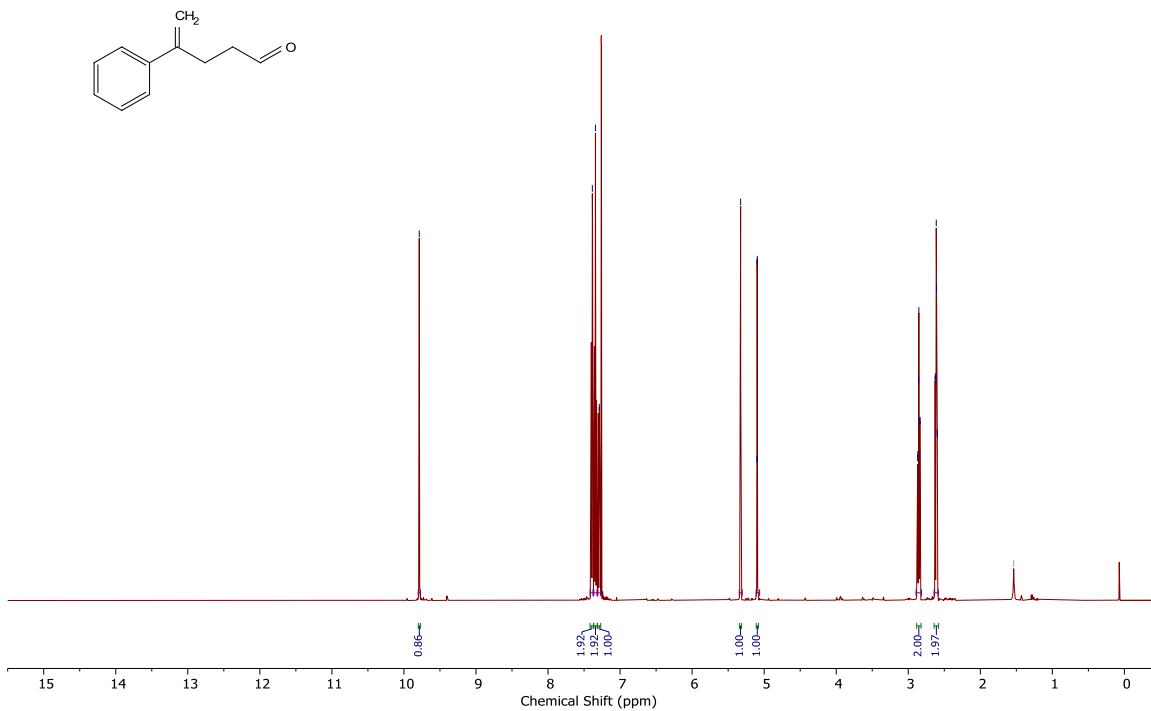
**Spectrum 50**  $^1\text{H}$  NMR spectrum of acid **17** in  $\text{CDCl}_3$ .

christR-.456.1.fid  
 Kuerzel FC  
 Gruppe Ward  
 Nummer 260  
 FC260-P



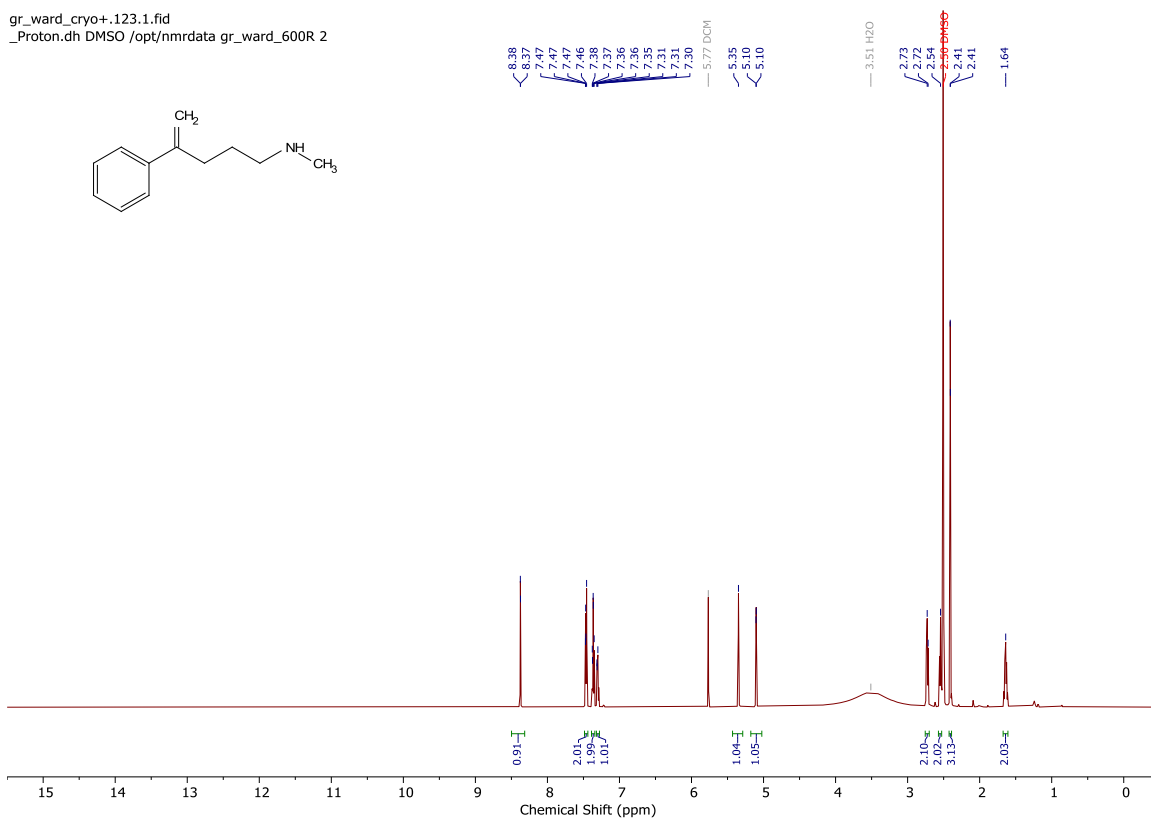
**Spectrum 51**  $^1\text{H}$  NMR spectrum of alcohol **18** in  $\text{CDCl}_3$ .

christR-.460.1.fid  
Kuerzel FC  
Gruppe Ward  
Nummer 262  
FC262-f;2

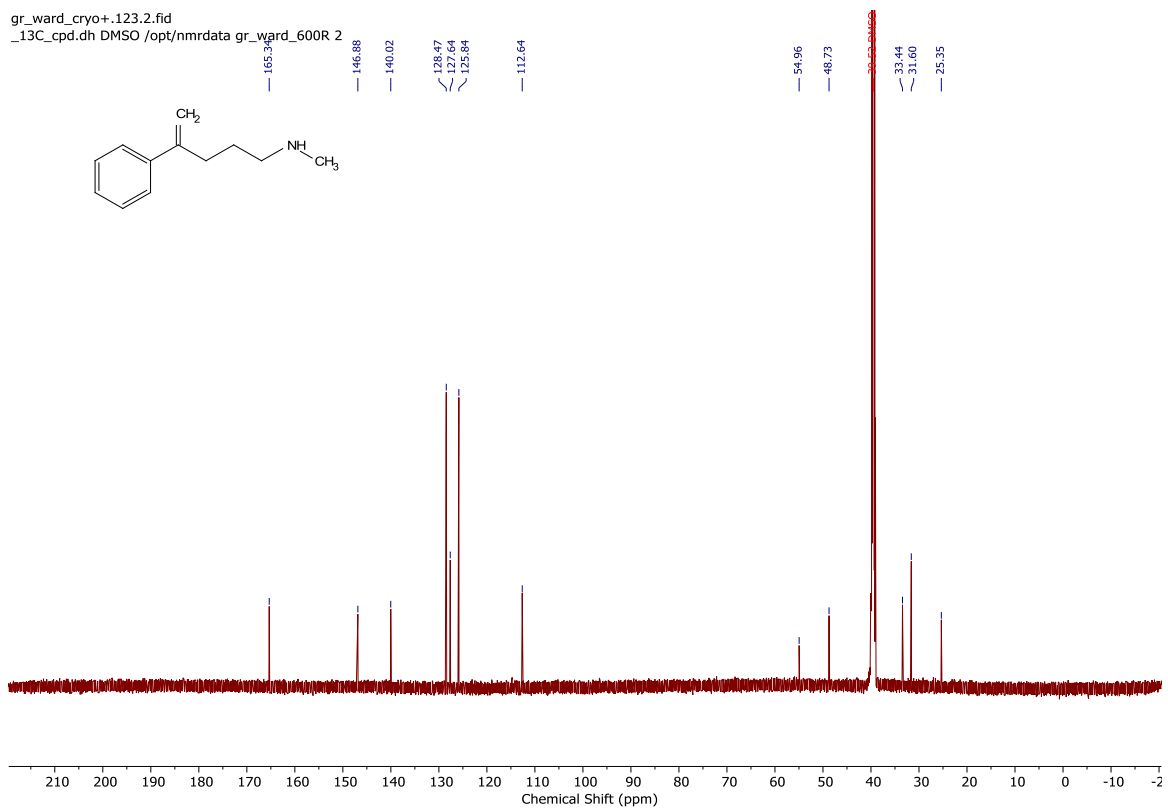


**Spectrum 52**  $^1\text{H}$  NMR spectrum of aldehyde **19** in  $\text{CDCl}_3$ .

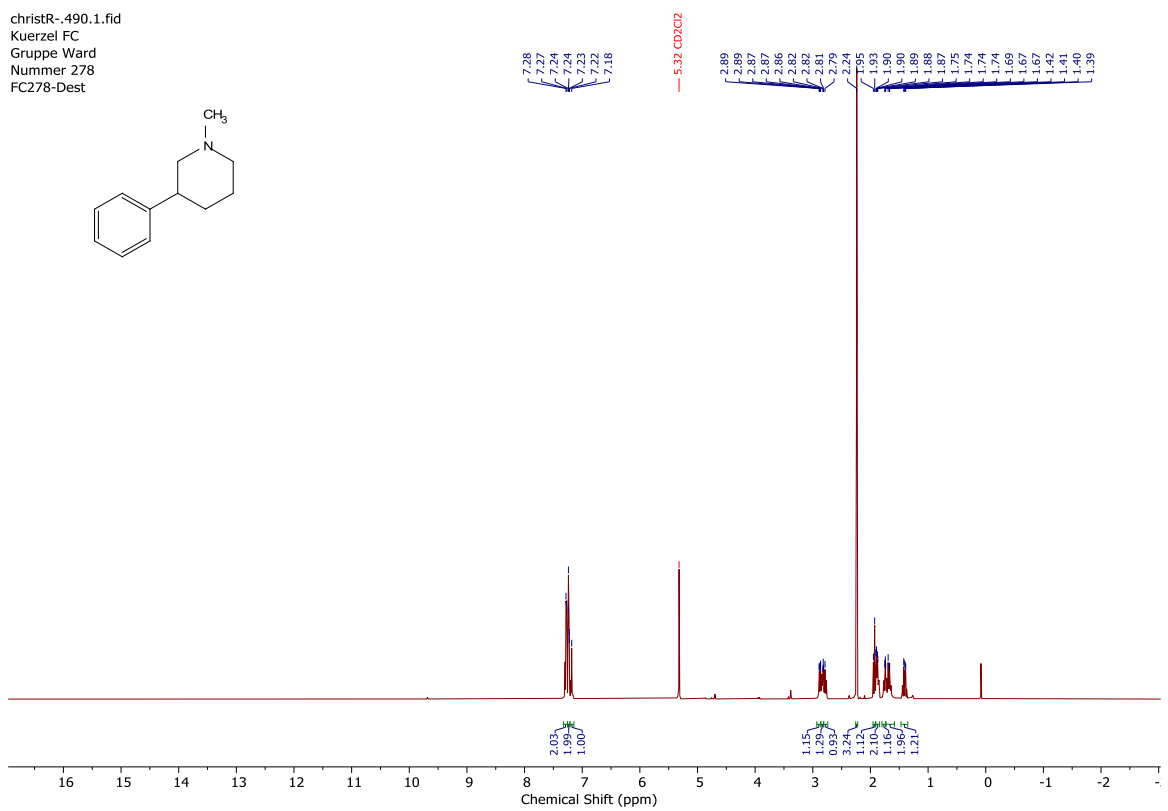
gr\_ward\_cryo+.123.1.fid  
\_Proton.dh DMSO /opt/nmrdata gr\_ward\_600R 2



**Spectrum 53**  $^1\text{H}$  NMR spectrum of amine **13** in  $\text{DMSO}-d_6$ .

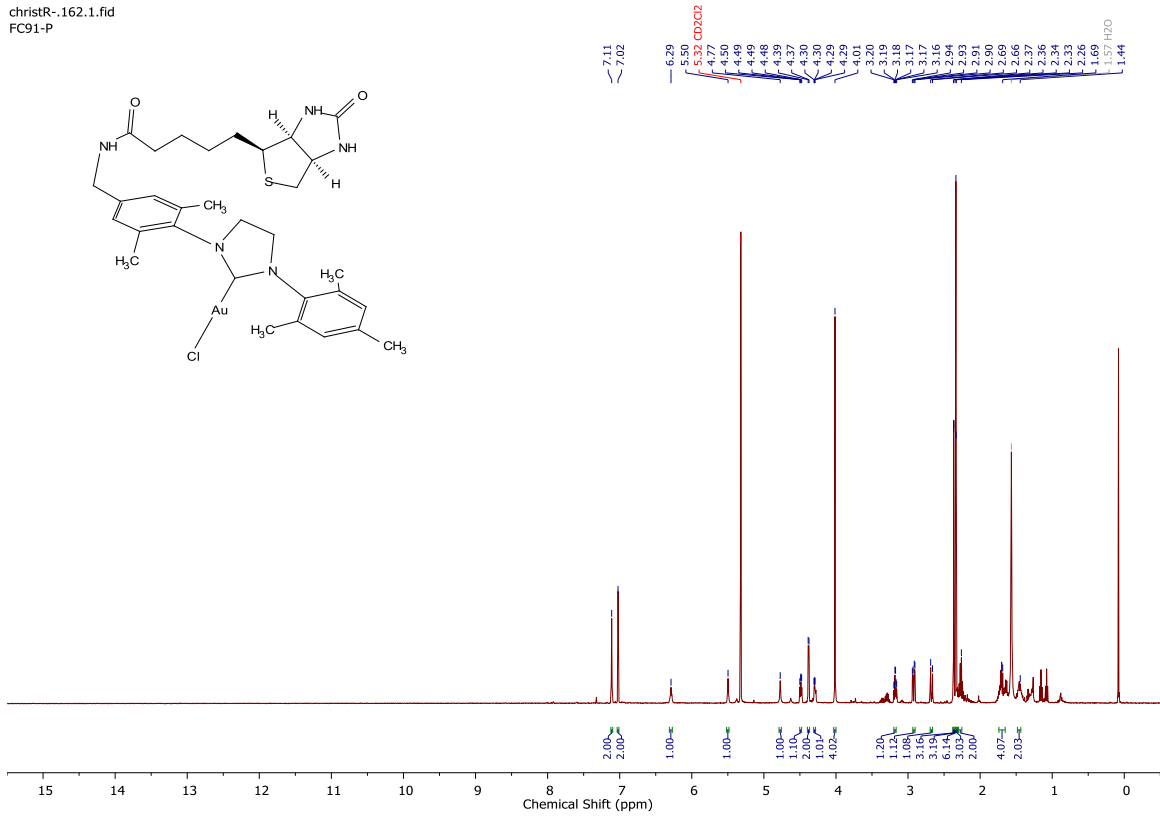


**Spectrum 54**  $^{13}\text{C}$  NMR spectrum of amine **13** in  $\text{DMSO-}d_6$ .

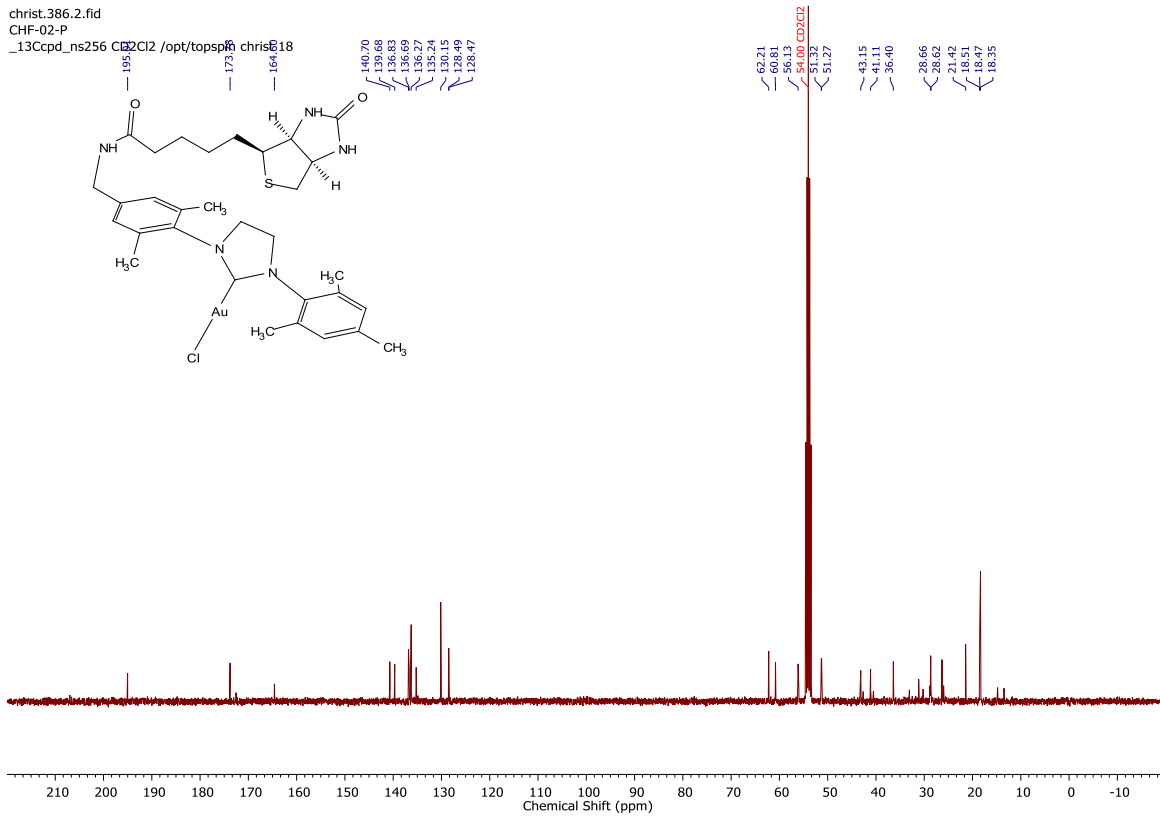


**Spectrum 55**  $^1\text{H}$  NMR spectrum of piperidine **15** in  $\text{CD}_2\text{Cl}_2$ .

christR-.162.1.fid  
FC91-P

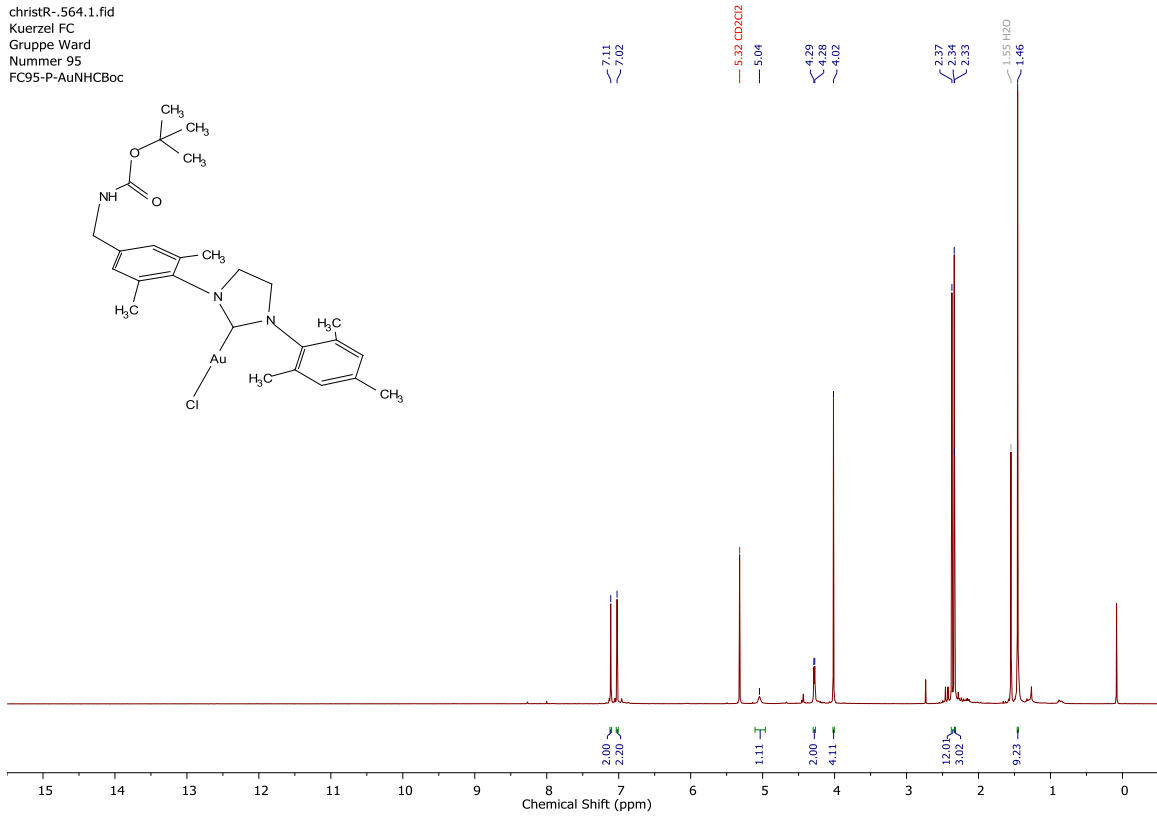


**Spectrum 56**  $^1\text{H}$  NMR Spectrum of biot-Au 1 in  $\text{CD}_2\text{Cl}_2$ .



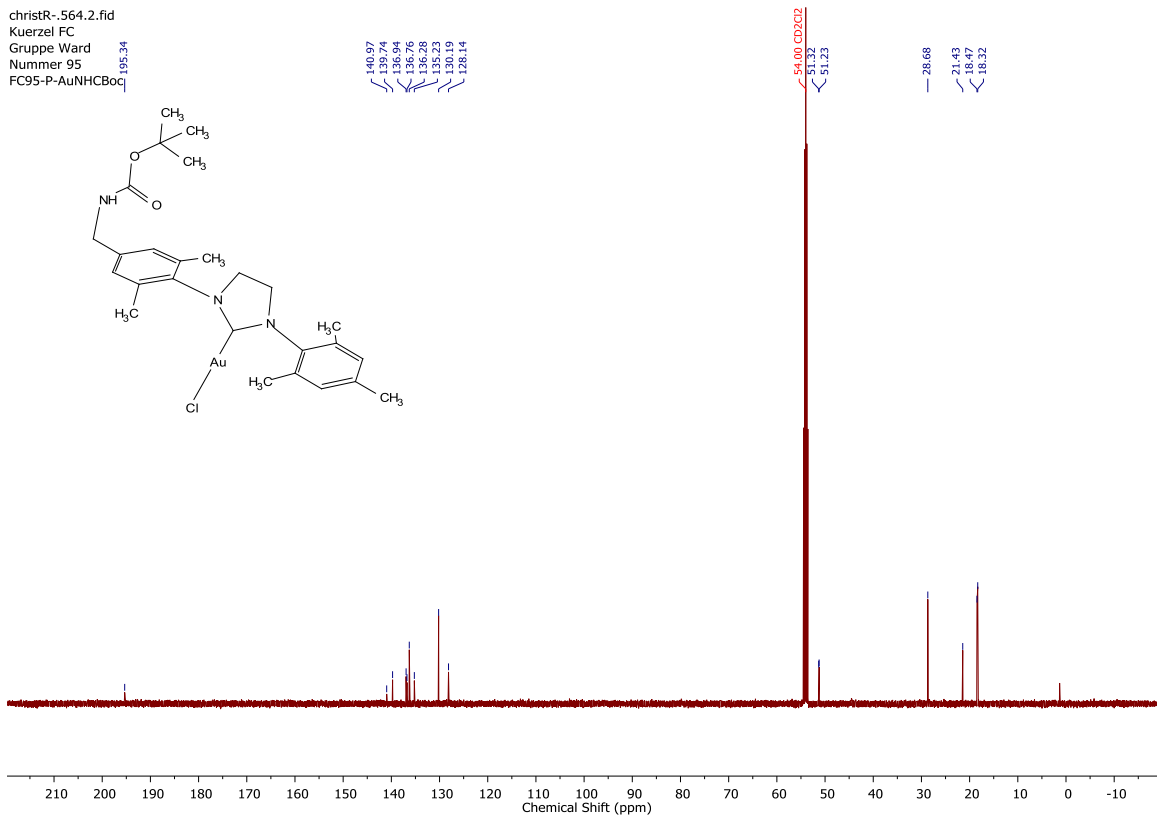
**Spectrum 57**  $^{13}\text{C}$  NMR Spectrum of biot-Au 1 in  $\text{CD}_2\text{Cl}_2$ .

christR--564.1.fid  
 Kuerzel FC  
 Gruppe Ward  
 Nummer 95  
 FC95-P-AuNHCBoc



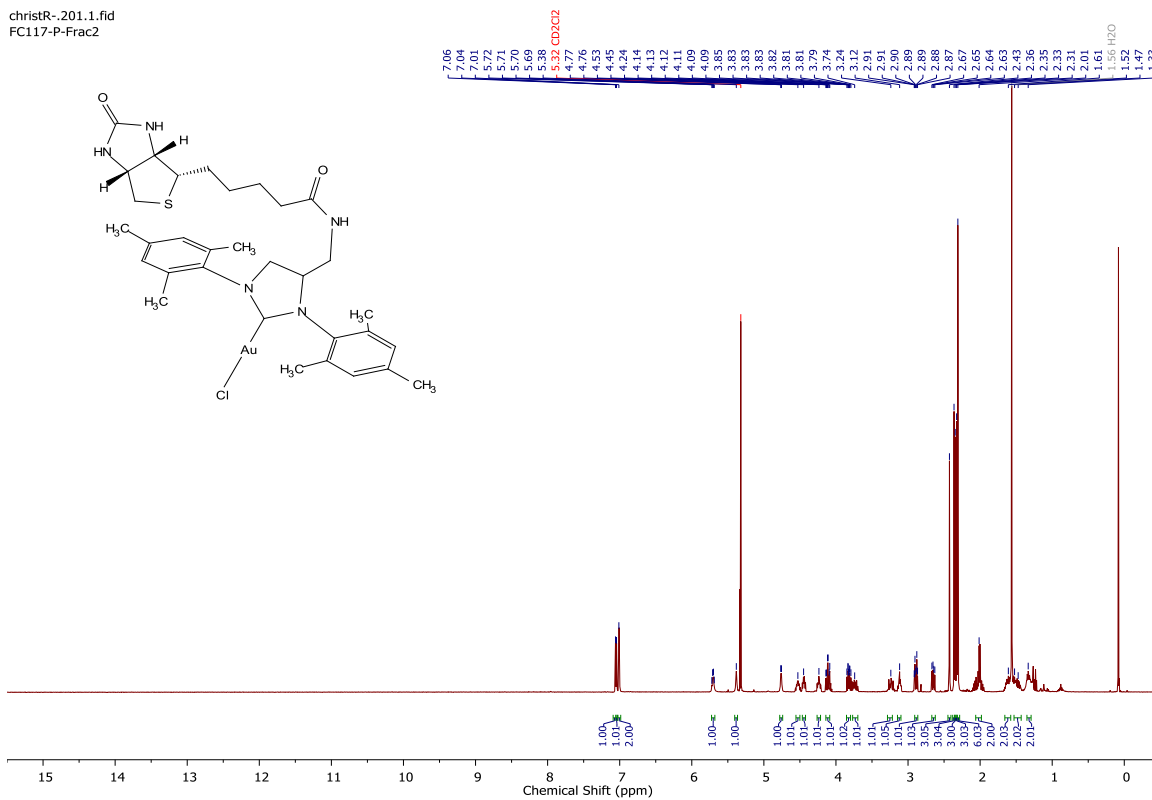
**Spectrum 58** <sup>1</sup>H NMR Spectrum of gold complex **L2** in CD<sub>2</sub>Cl<sub>2</sub>.

christR--564.2.fid  
 Kuerzel FC  
 Gruppe Ward  
 Nummer 95  
 FC95-P-AuNHCBoc



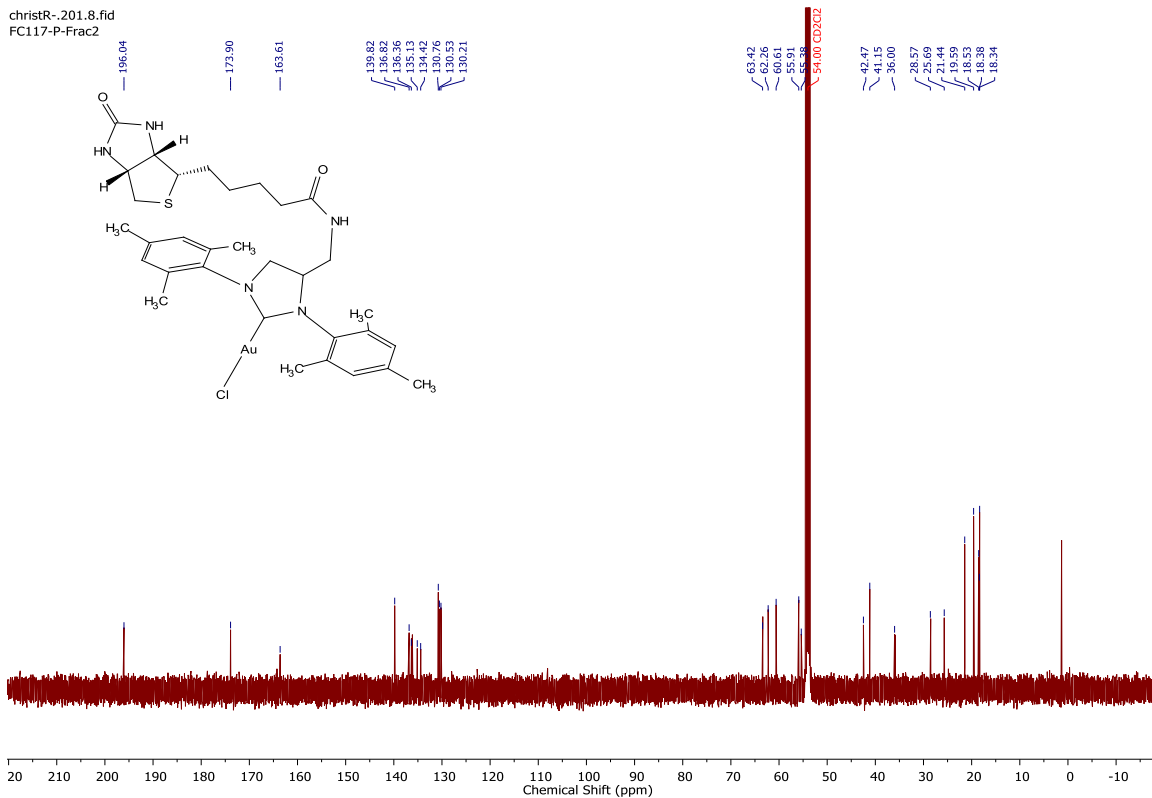
**Spectrum 59** <sup>13</sup>C NMR Spectrum of gold complex **L2** in CD<sub>2</sub>Cl<sub>2</sub>.

christR--201.1.fid  
FC117-P-Frac2



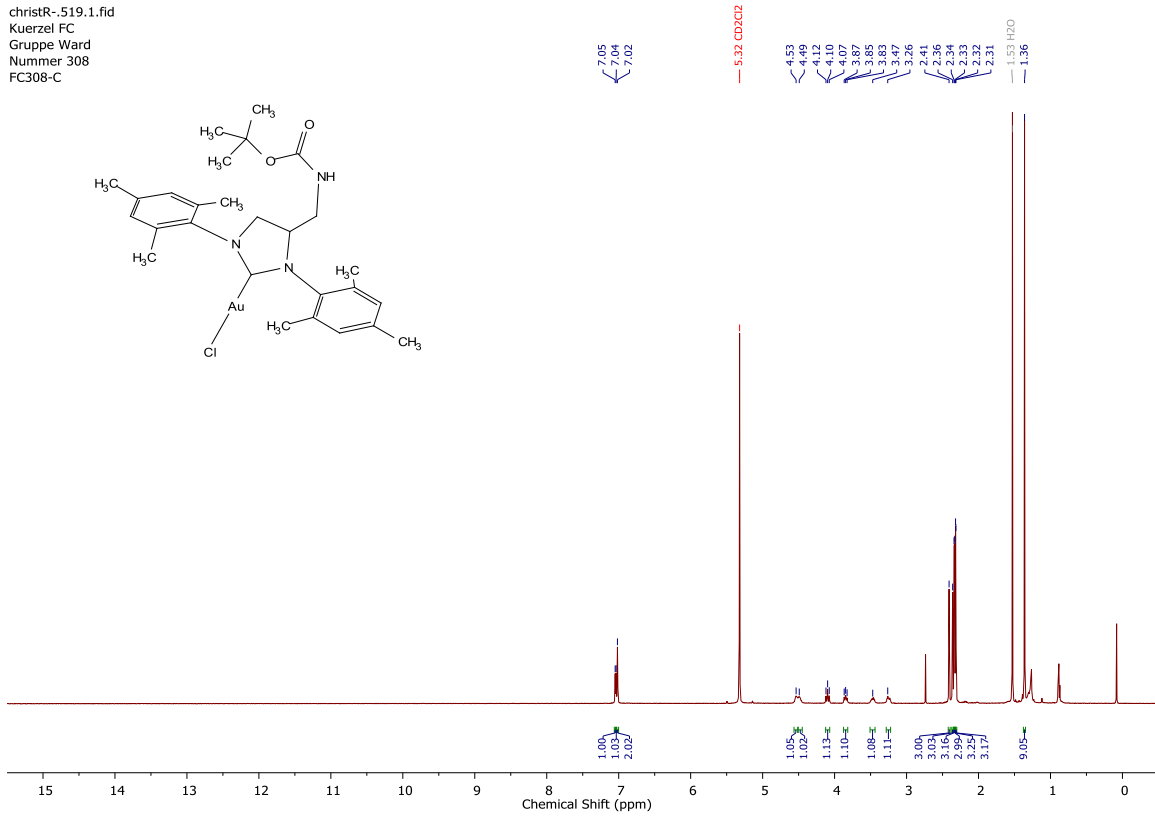
**Spectrum 60**  $^1\text{H}$  NMR Spectrum of biot-Au 2 in  $\text{CD}_2\text{Cl}_2$ .

christR--201.8.fid  
FC117-P-Frac2



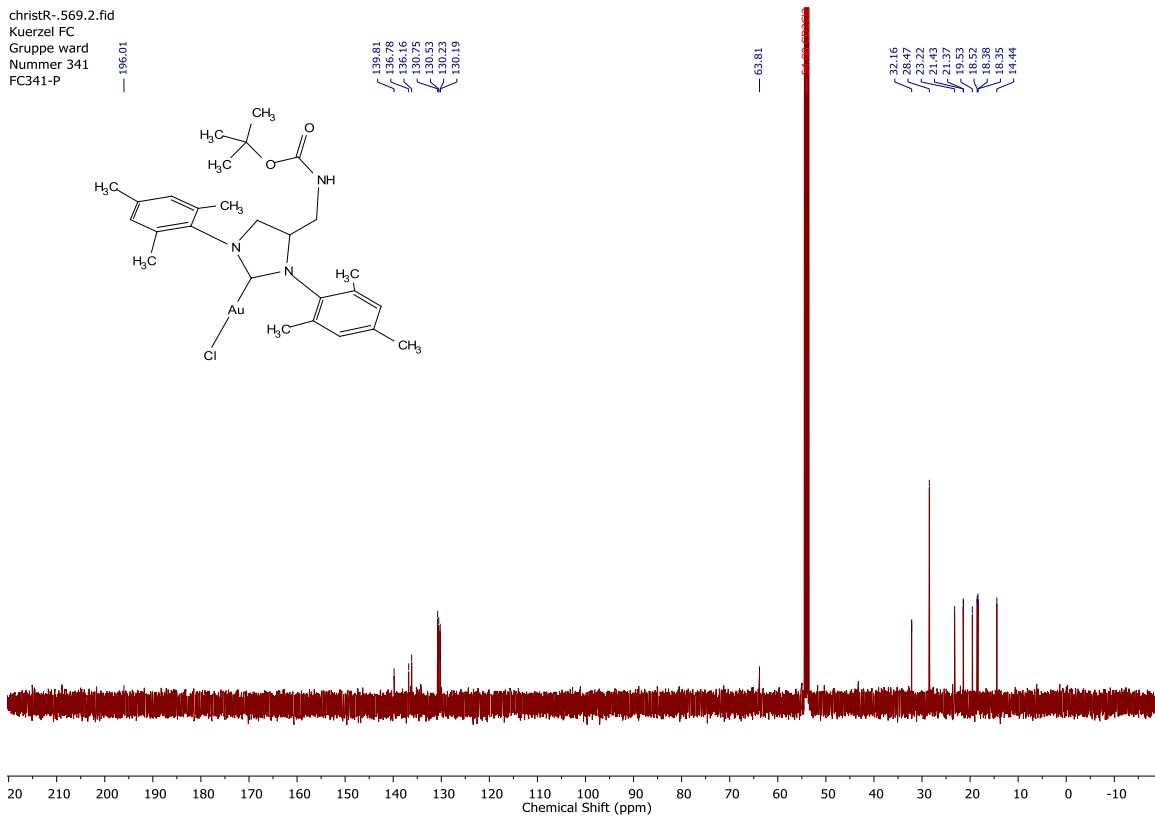
**Spectrum 61**  $^{13}\text{C}$  NMR Spectrum of biot-Au 2 in  $\text{CD}_2\text{Cl}_2$ .

christR--519.1.fid  
 Kuerzel FC  
 Gruppe Ward  
 Nummer 308  
 FC308-C



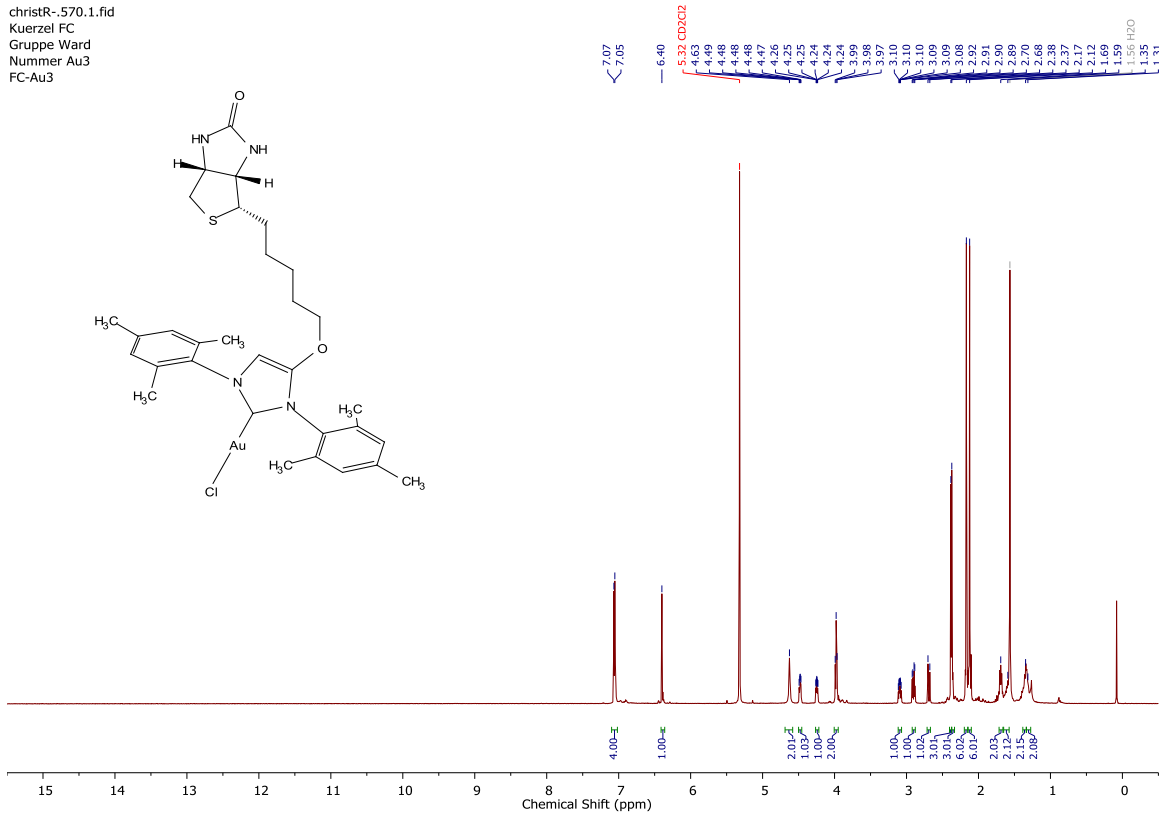
**Spectrum 62** <sup>1</sup>H NMR Spectrum of gold complex **L5** in CD<sub>2</sub>Cl<sub>2</sub>.

christR--569.2.fid  
 Kuerzel FC  
 Gruppe ward  
 Nummer 341  
 FC341-P



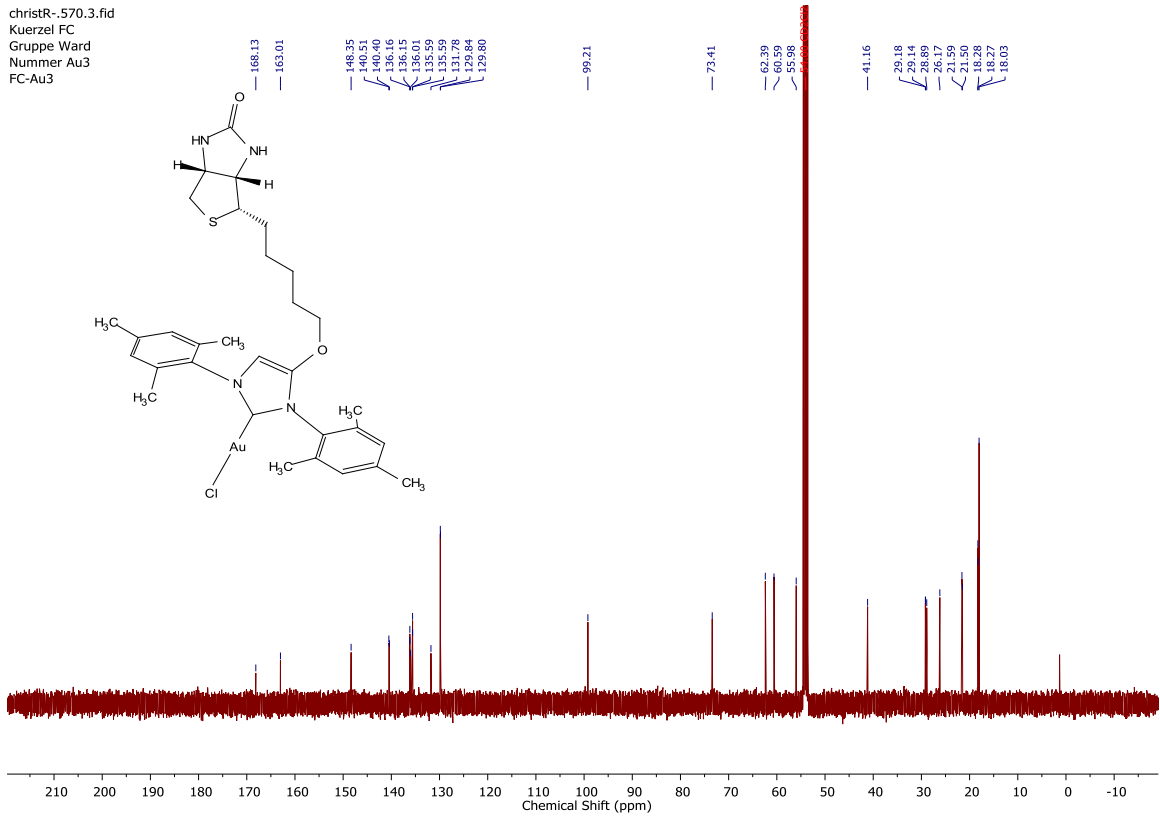
**Spectrum 63** <sup>13</sup>C NMR Spectrum of gold complex **L5** in CD<sub>2</sub>Cl<sub>2</sub>.

christR--570.1.fid  
 Kuerzel FC  
 Gruppe Ward  
 Nummer Au3  
 FC-Au3



**Spectrum 64** <sup>1</sup>H NMR Spectrum of **biot-Au 3** in CD<sub>2</sub>Cl<sub>2</sub>.

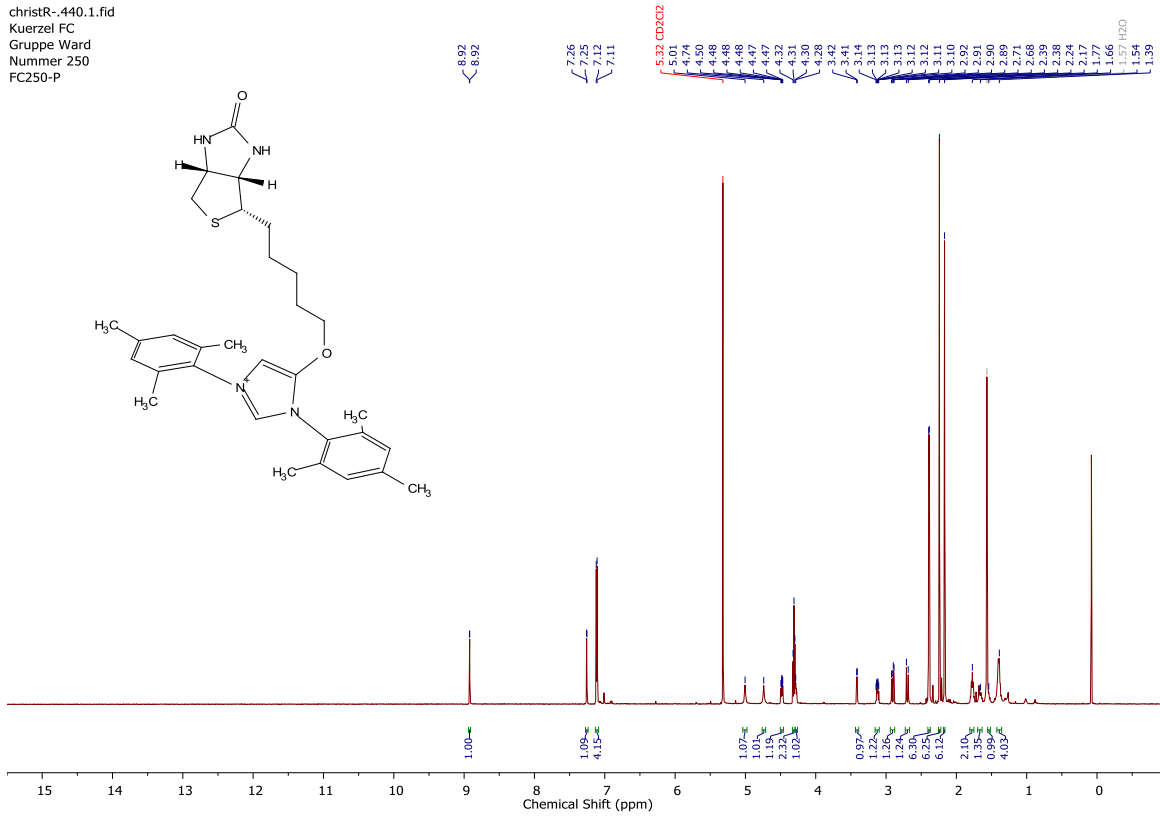
christR--570.3.fid  
 Kuerzel FC  
 Gruppe Ward  
 Nummer Au3  
 FC-Au3



**Spectrum 65** <sup>13</sup>C NMR Spectrum of **biot-Au 3** in CD<sub>2</sub>Cl<sub>2</sub>.

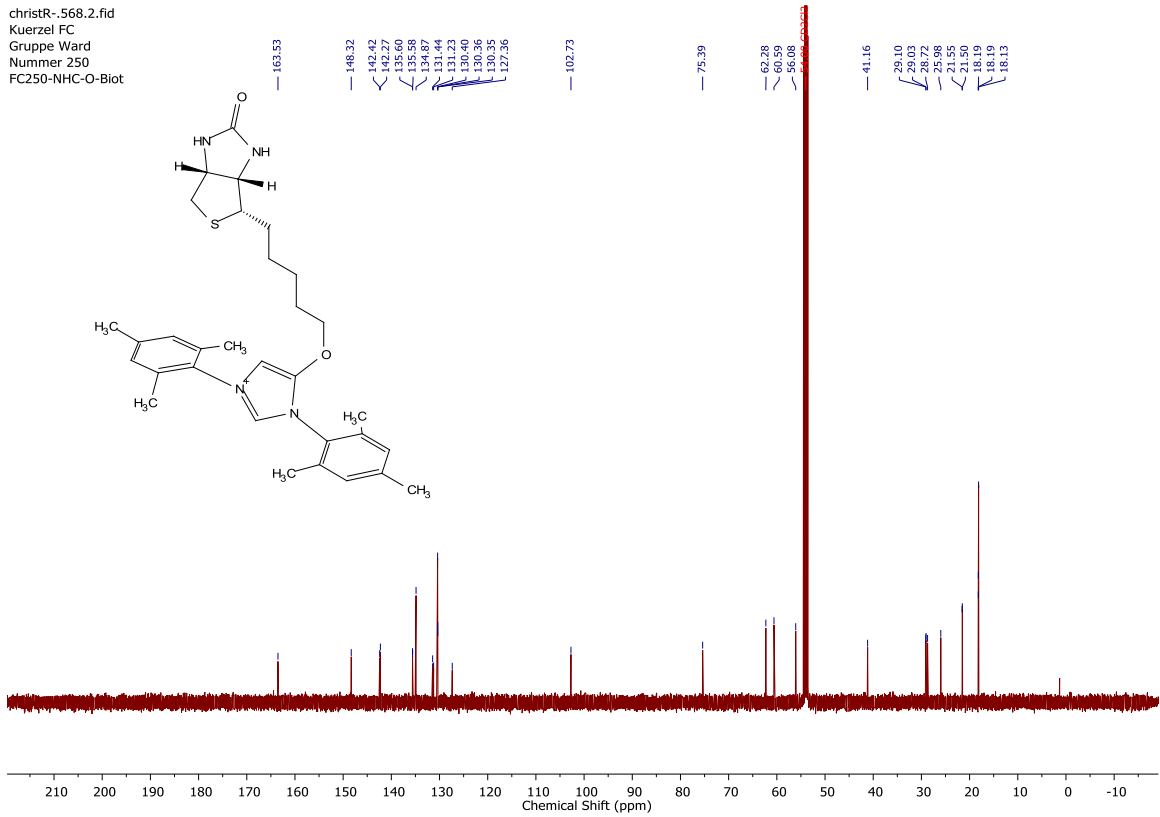


christR-.440.1.fid  
 Kuerzel FC  
 Gruppe Ward  
 Nummer 250  
 FC250-P



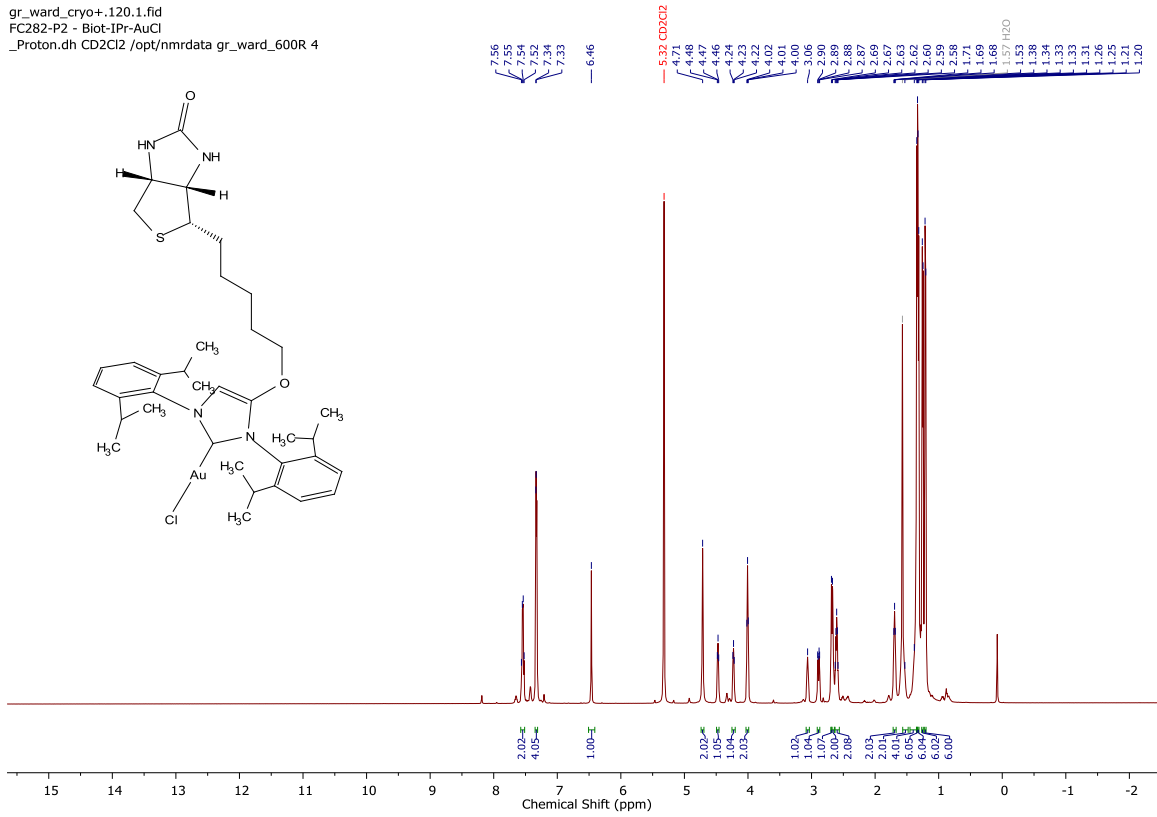
**Spectrum 66** <sup>1</sup>H NMR Spectrum of NHC salt L9 in CD<sub>2</sub>Cl<sub>2</sub>.

christR-.568.2.fid  
 Kuerzel FC  
 Gruppe Ward  
 Nummer 250  
 FC250-NHC-O-Biot

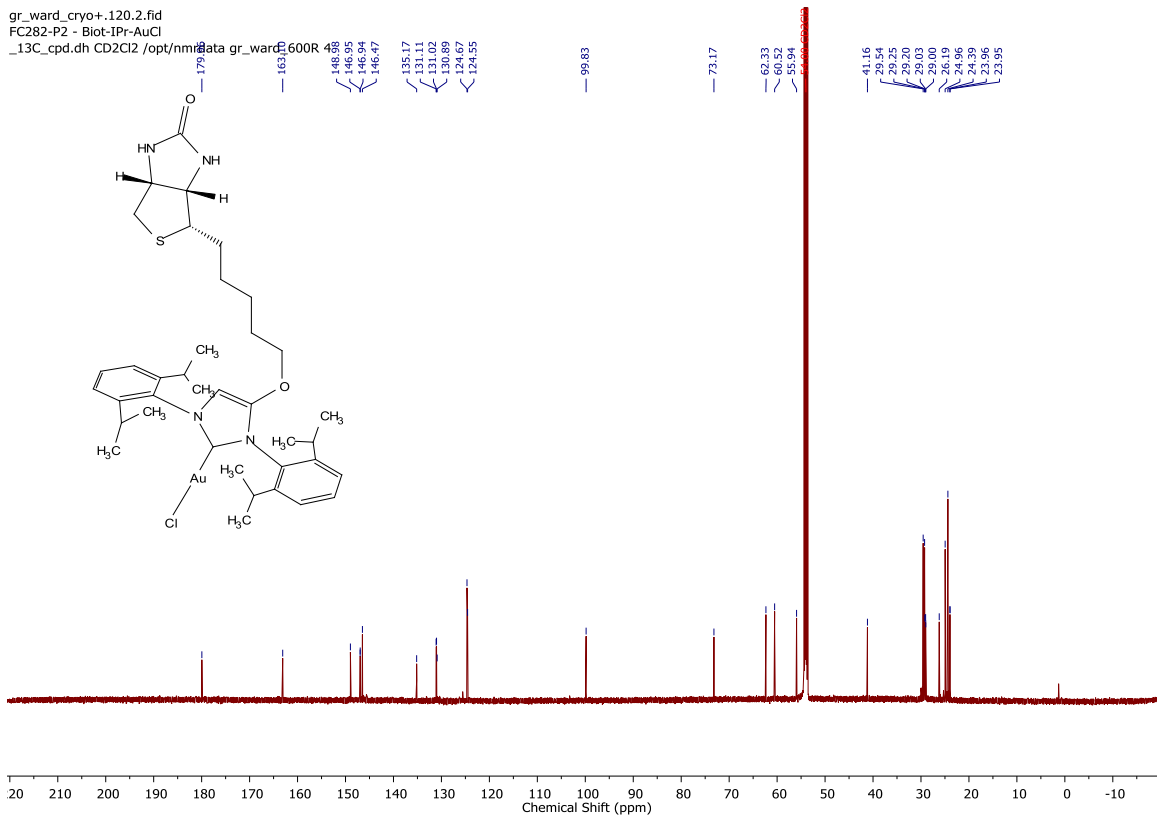


**Spectrum 67** <sup>13</sup>C NMR Spectrum of NHC salt L9 in CD<sub>2</sub>Cl<sub>2</sub>.

gr\_ward\_cryo+.120.1.fid  
 FC282-P2 - Biot-IPr-AuCl  
 \_Proton.dh CD2Cl2 /opt/nmrdata gr\_ward\_600R 4

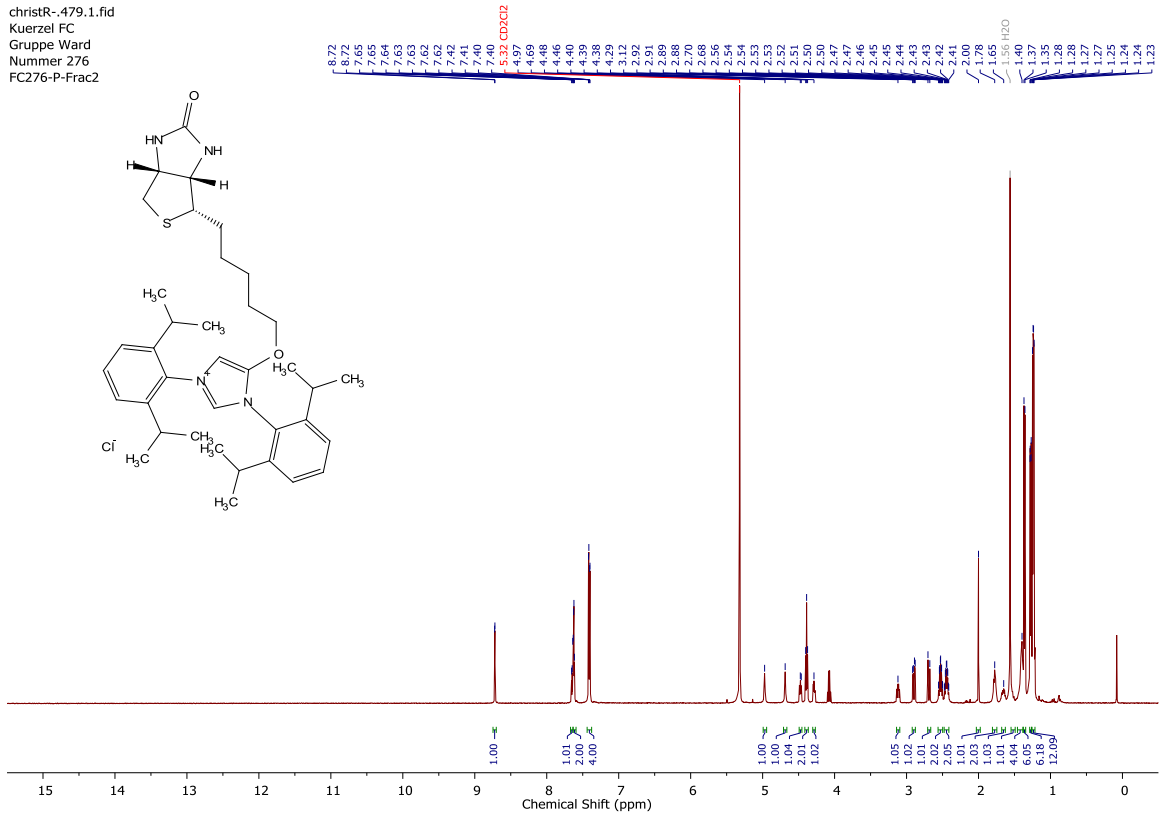


**Spectrum 68** <sup>1</sup>H NMR Spectrum of biot-Au 4 in CD<sub>2</sub>Cl<sub>2</sub>.

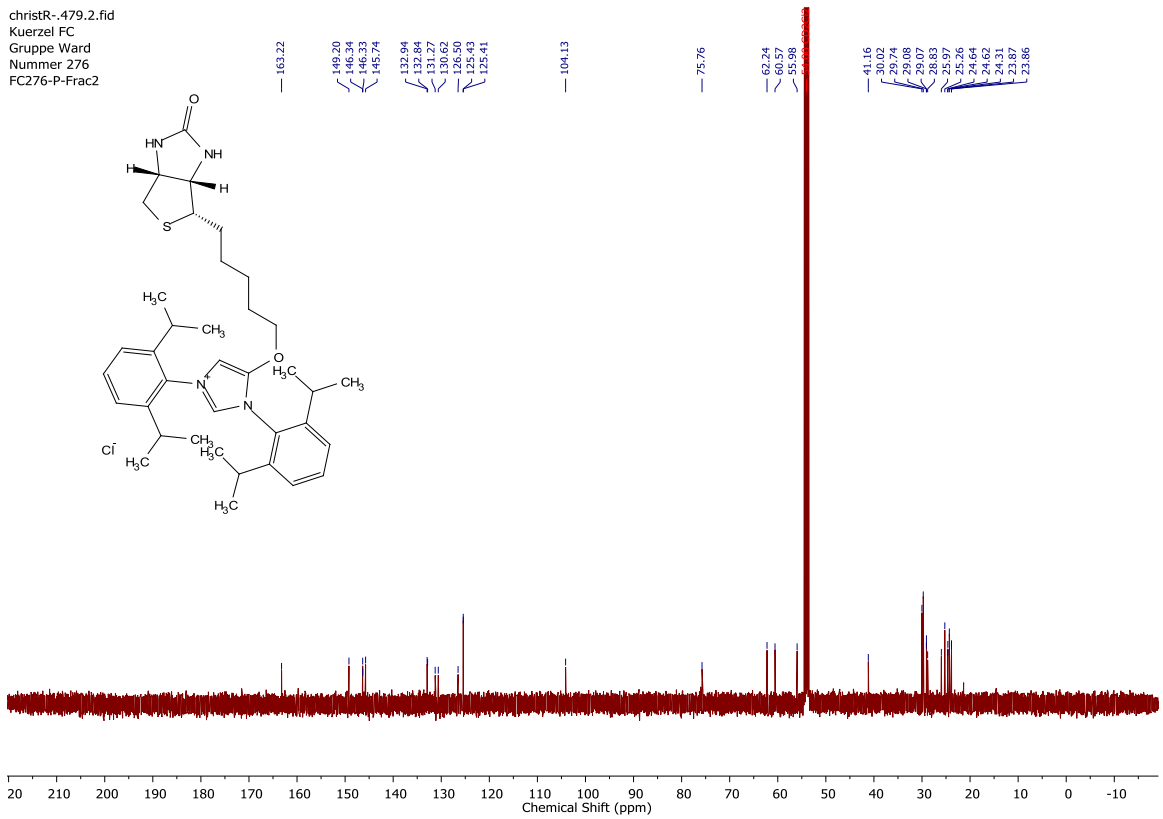


**Spectrum 69** <sup>13</sup>C NMR Spectrum of biot-Au 4 in CD<sub>2</sub>Cl<sub>2</sub>.

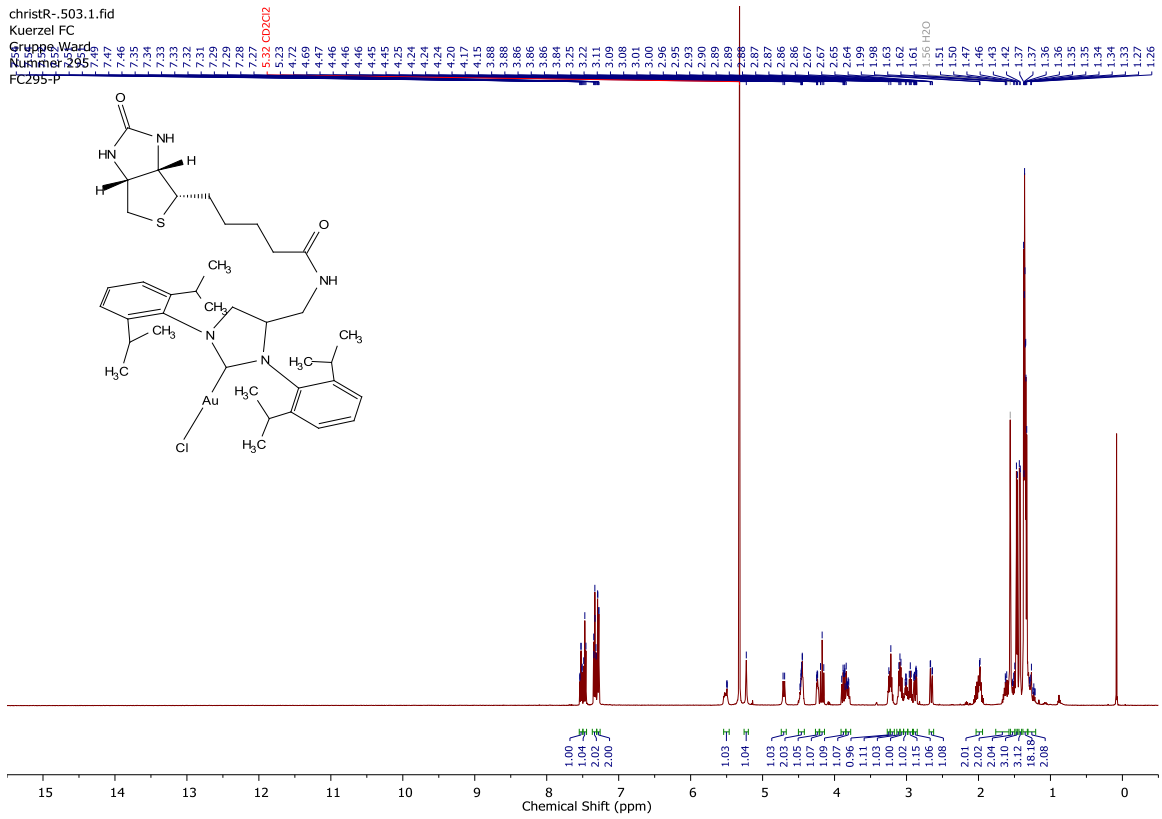
christR-.479.1.fid  
 Kuerzel FC  
 Gruppe Ward  
 Nummer 276  
 FC276-P-Frac2



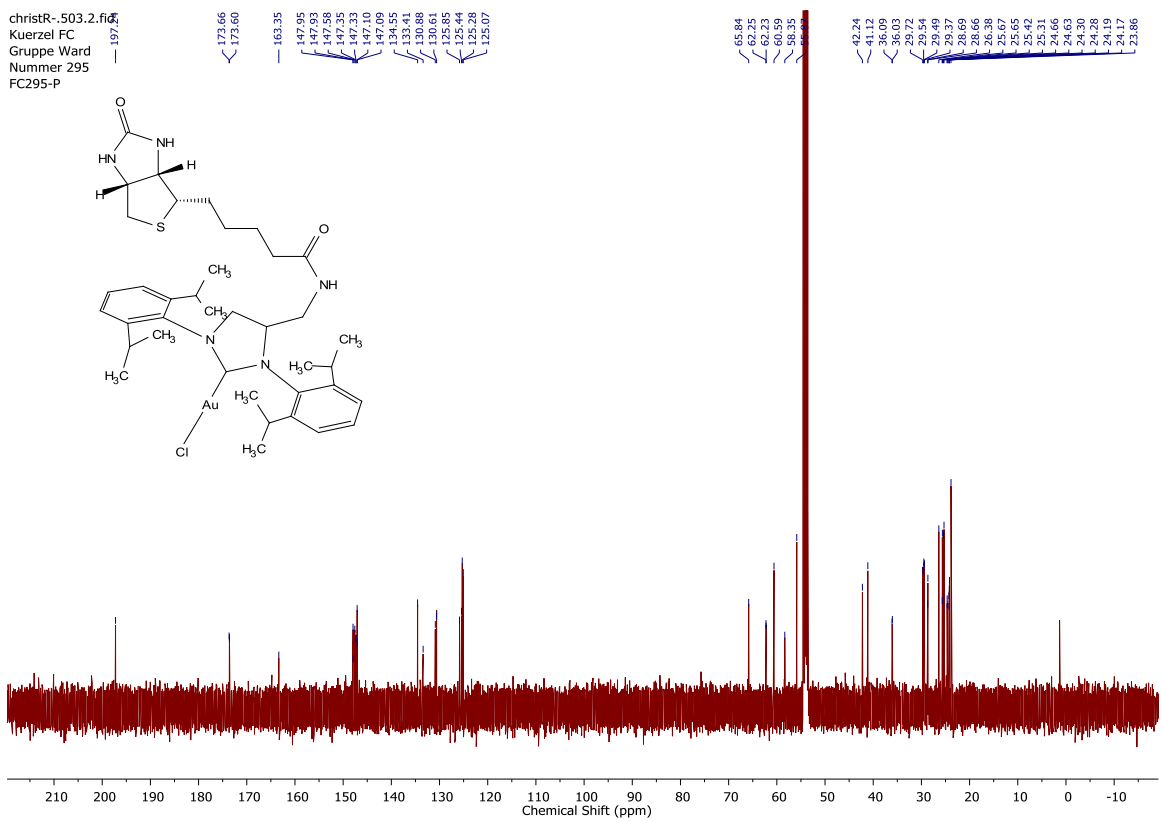
**Spectrum 70**  $^1\text{H}$  NMR Spectrum of NHC salt L10 in  $\text{CD}_2\text{Cl}_2$ .



**Spectrum 71**  $^{13}\text{C}$  NMR Spectrum of NHC salt L10 in  $\text{CD}_2\text{Cl}_2$ .



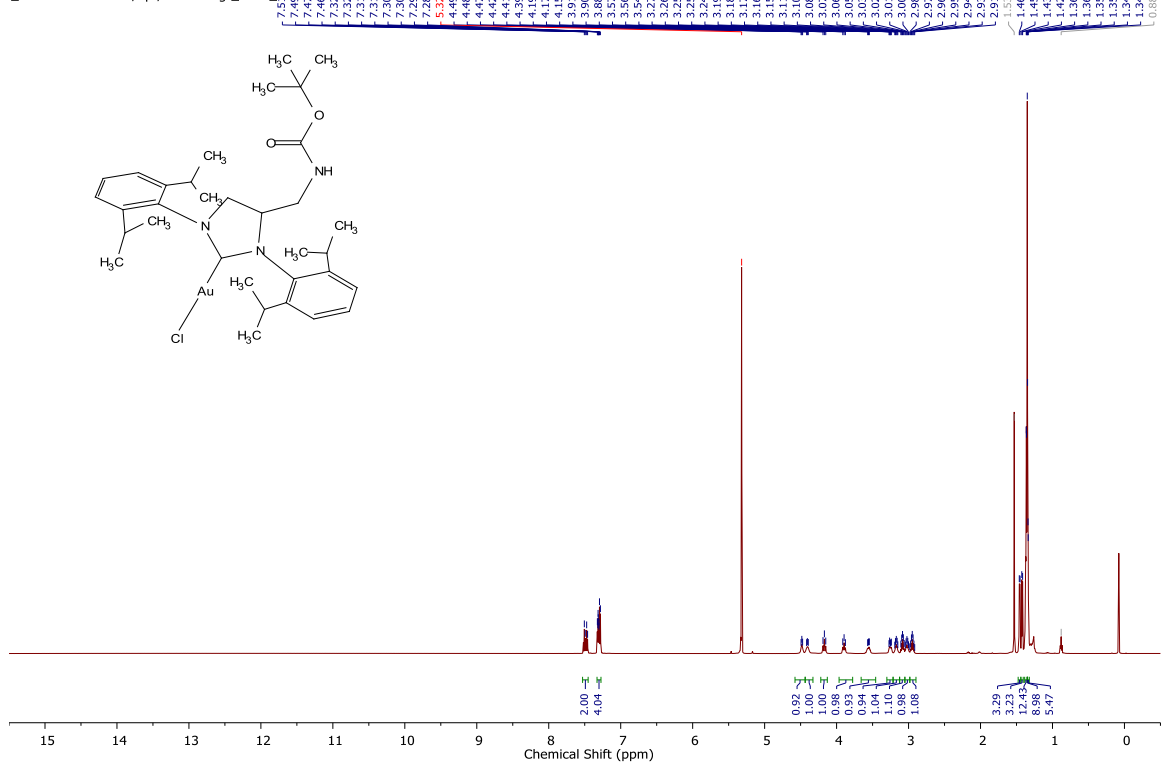
**Spectrum 72**  $^1\text{H}$  NMR Spectrum of **biot-Au 5** in  $\text{CD}_2\text{Cl}_2$ .



**Spectrum 73**  $^{13}\text{C}$  NMR Spectrum of **biot-Au 5** in  $\text{CD}_2\text{Cl}_2$ .

gr\_ward\_cryo+.124.1.fid  
FC283-P

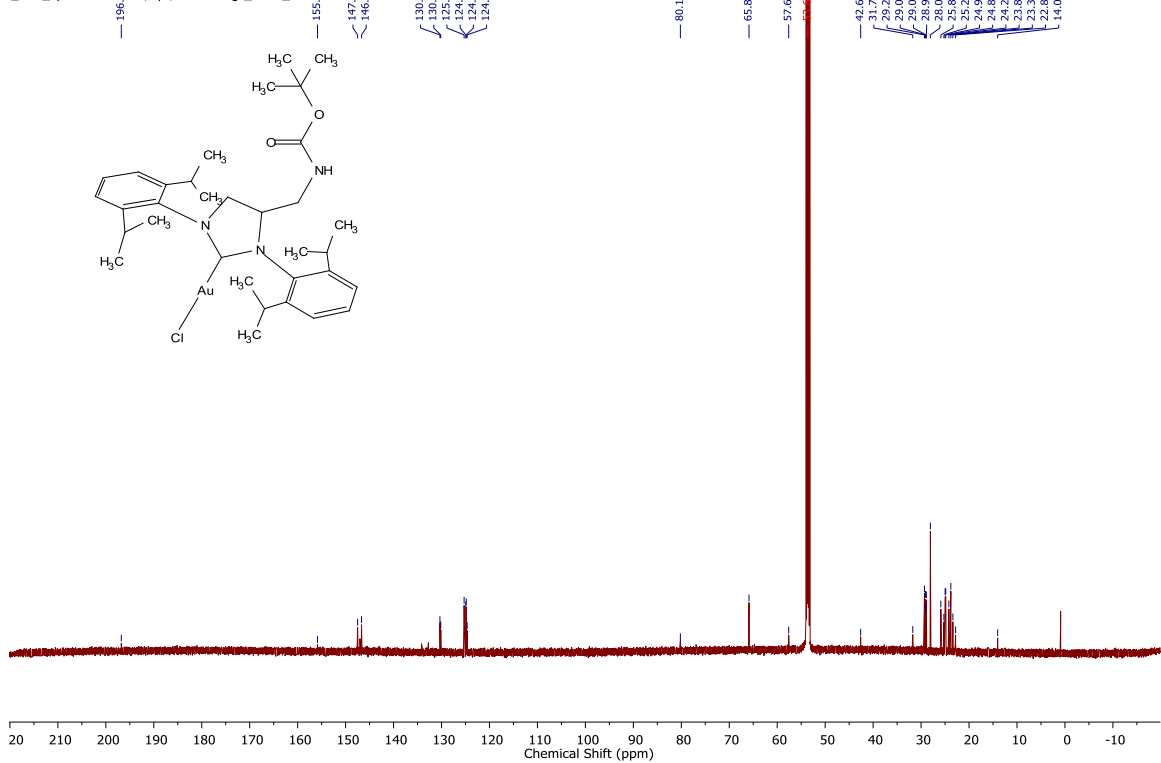
\_Proton.dh CD2Cl2 /opt/nmrdata gr\_ward\_600P



**Spectrum 74** <sup>1</sup>H NMR Spectrum of gold complex L6 in CD<sub>2</sub>Cl<sub>2</sub>.

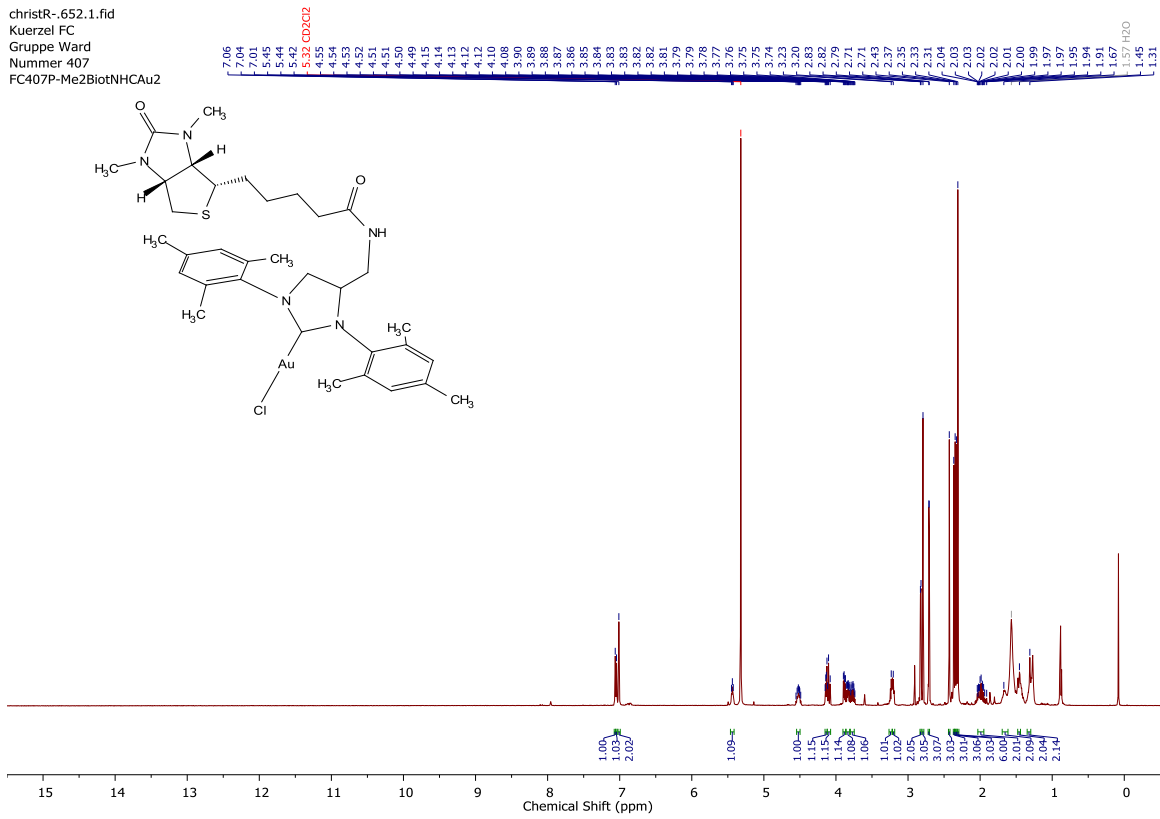
gr\_ward\_cryo+.124.2.fid  
FC283-P

\_13C\_cpd.dh CD2Cl2 /opt/nmrdata gr\_ward\_600P



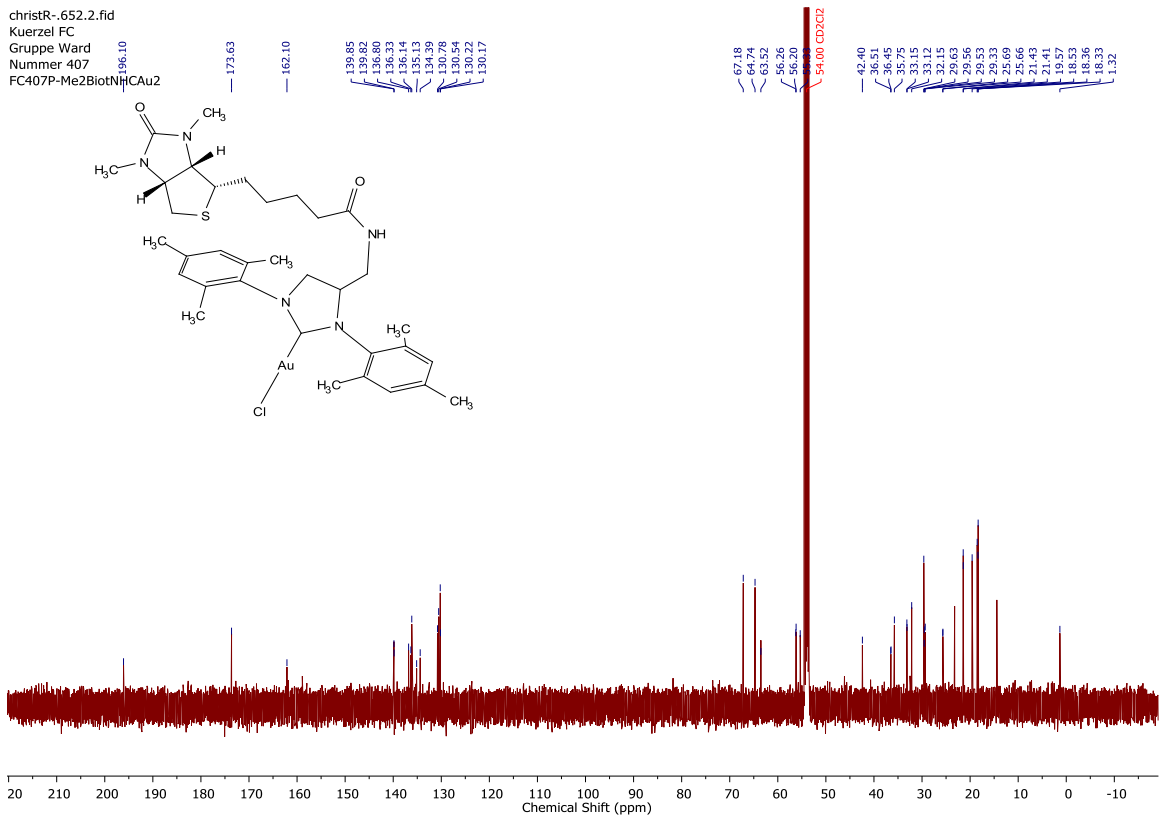
**Spectrum 75** <sup>13</sup>C NMR Spectrum of gold complex L6 in CD<sub>2</sub>Cl<sub>2</sub>.

christR-.652.1.fid  
 Kuerzel FC  
 Gruppe Ward  
 Nummer 407  
 FC407P-Me2BiotNHCAu2



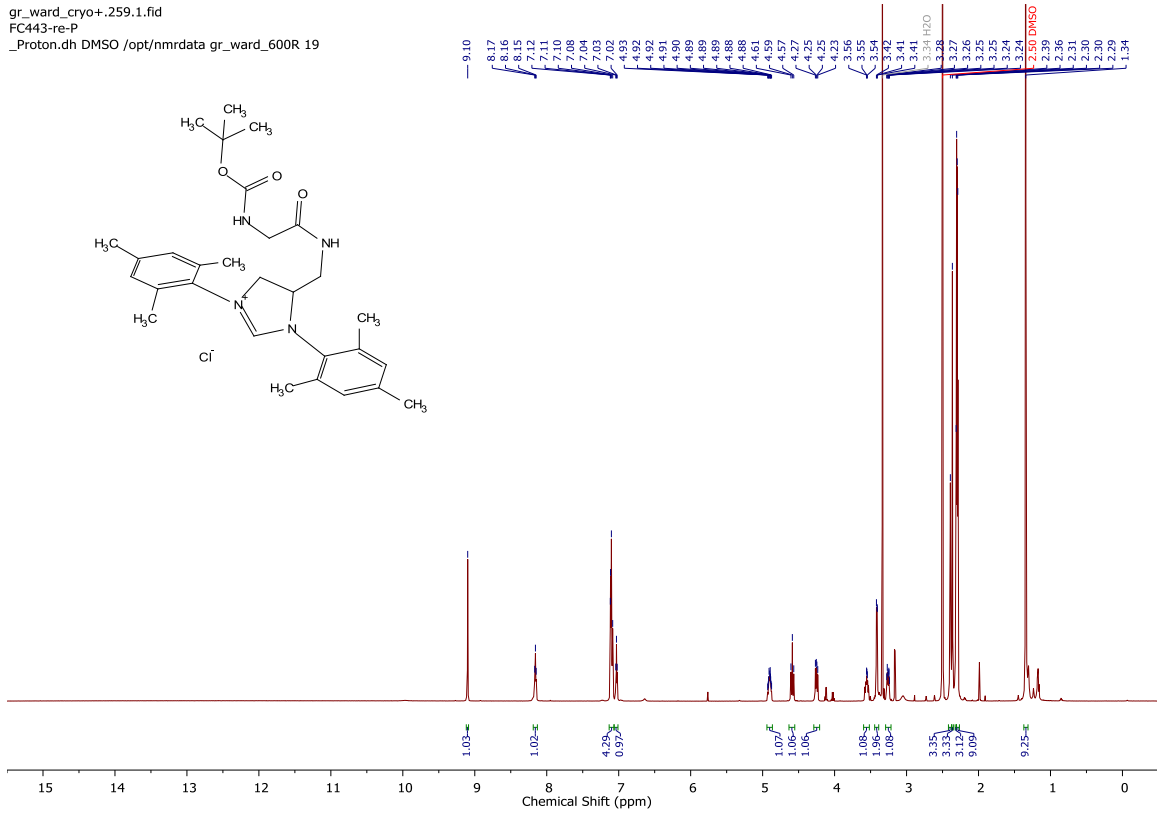
**Spectrum 76** <sup>1</sup>H NMR Spectrum of **Me<sub>2</sub>biot-Au 2** in CD<sub>2</sub>Cl<sub>2</sub>.

christR-.652.2.fid  
 Kuerzel FC  
 Gruppe Ward  
 Nummer 407  
 FC407P-Me2BiotNHCAu2

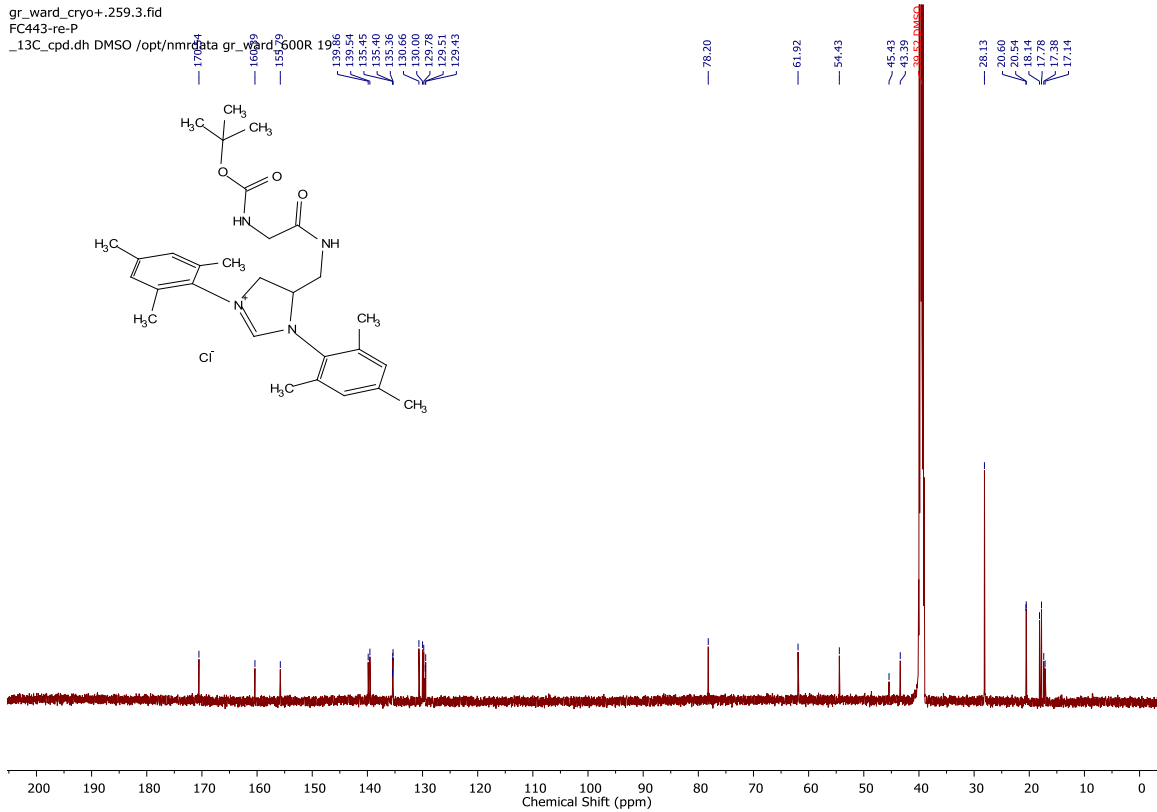


**Spectrum 77** <sup>13</sup>C NMR Spectrum of **Me<sub>2</sub>biot-Au 2** in CD<sub>2</sub>Cl<sub>2</sub>.

gr\_ward\_cryo+.259.1.fid  
 FC443-re-P  
 \_Proton.dh DMSO /opt/nmrdata gr\_ward\_600R 19

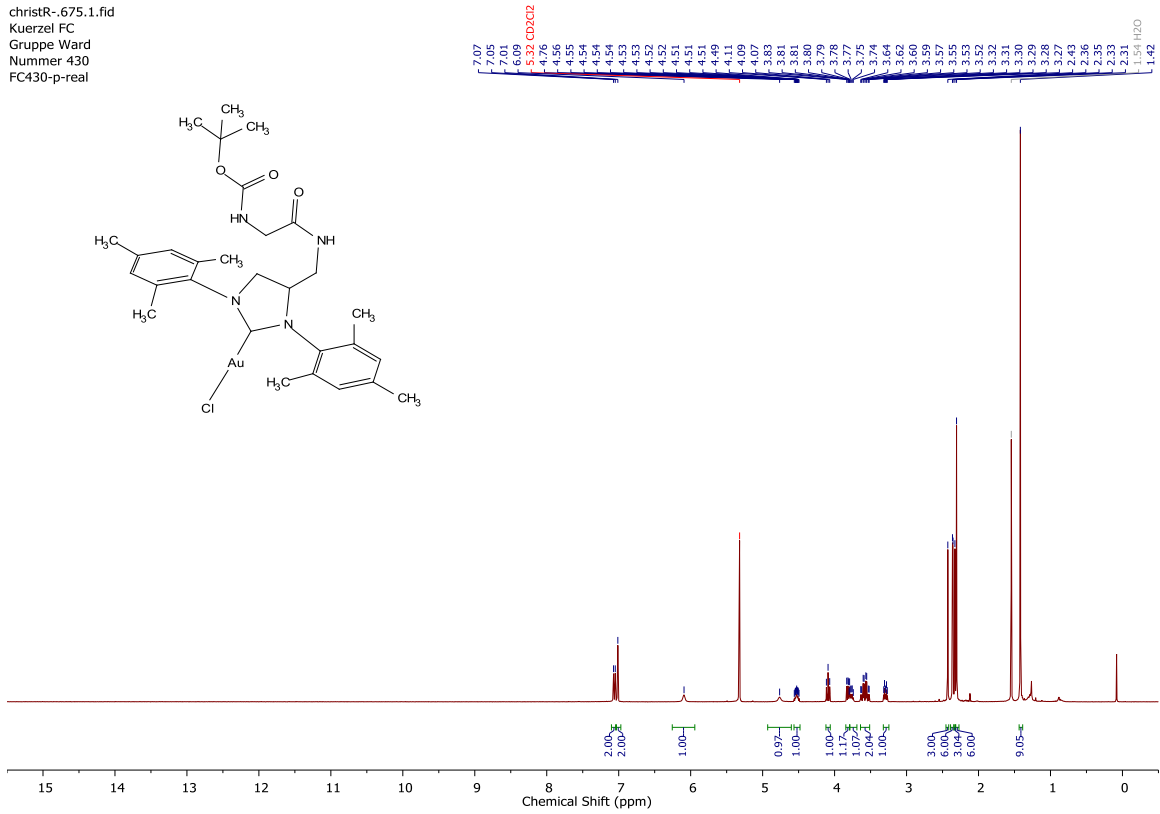


**Spectrum 78** <sup>1</sup>H NMR Spectrum of NHC 5 in DMSO-*d*<sub>6</sub>.



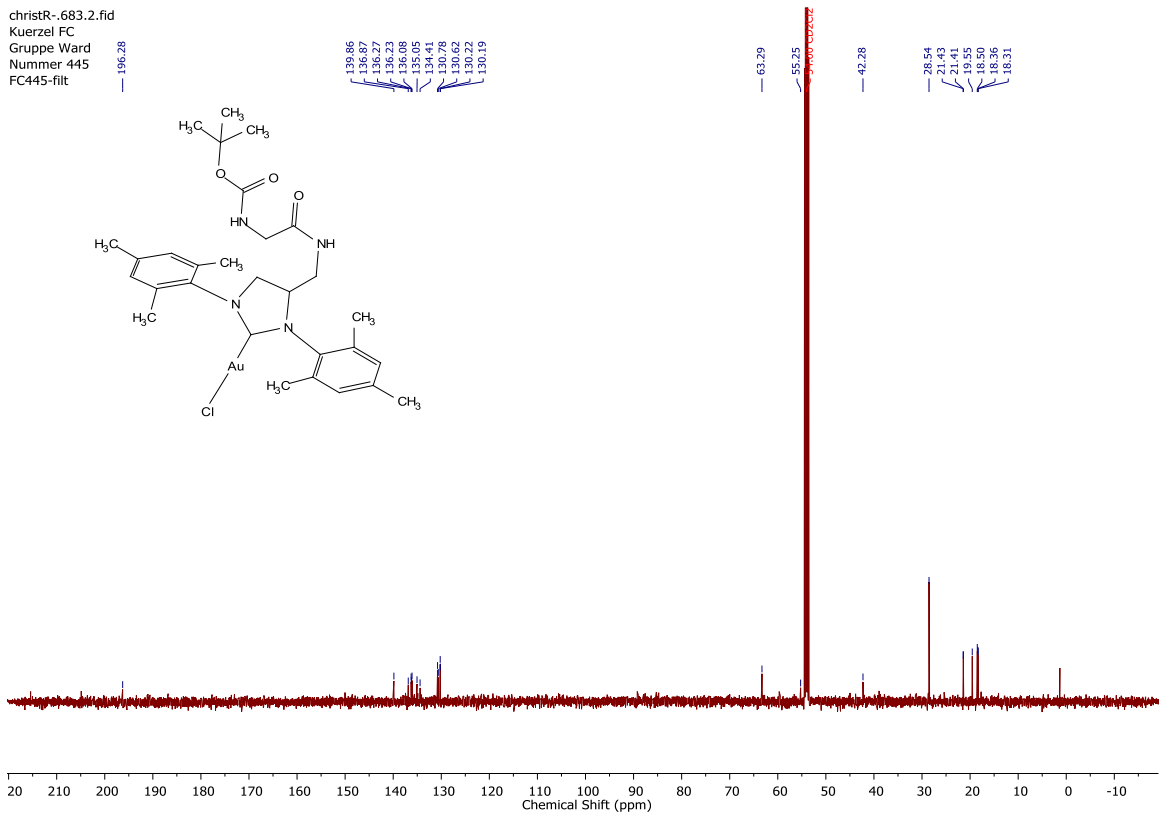
**Spectrum 79** <sup>13</sup>C NMR Spectrum of NHC 5 in DMSO-*d*<sub>6</sub>.

christR--675.1.fid  
 Kuerzel FC  
 Gruppe Ward  
 Nummer 430  
 FC430-p-real



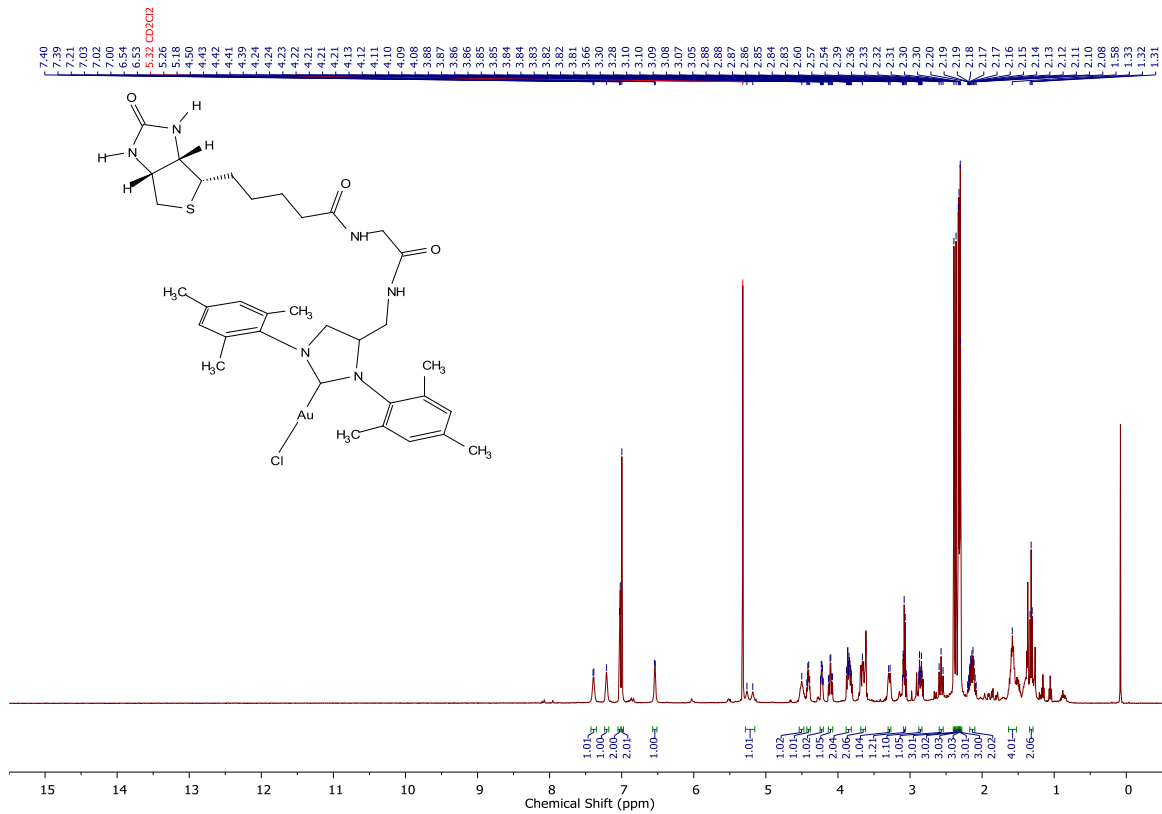
**Spectrum 80** <sup>1</sup>H NMR Spectrum of Gold complex **8** in Methylene chloride-*d*<sub>2</sub>.

christR--683.2.fid  
 Kuerzel FC  
 Gruppe Ward  
 Nummer 445  
 FC445-filt

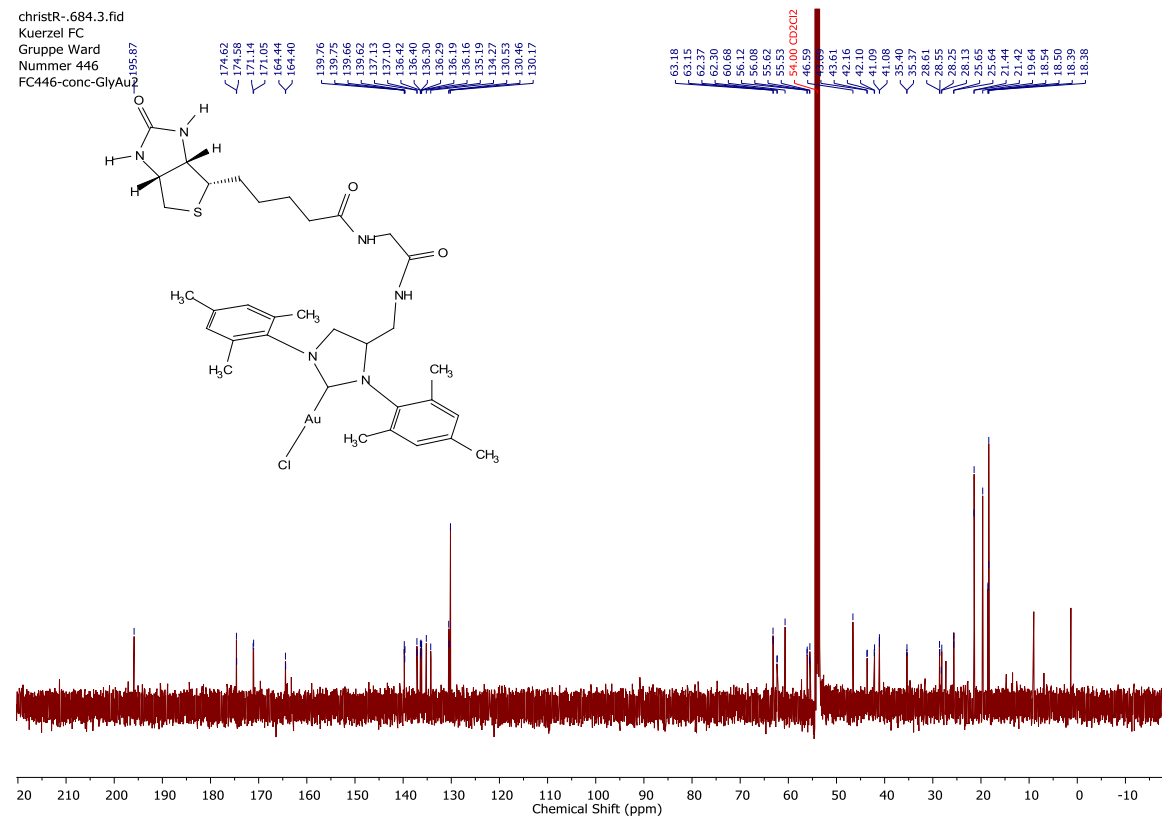


**Spectrum 81** <sup>13</sup>C NMR Spectrum of Gold complex **8** in Methylene chloride-*d*<sub>2</sub>.





**Spectrum 82** <sup>1</sup>H NMR Spectrum of biot-GlyAu 2 in Methylene chloride-d<sub>2</sub>.



**Spectrum 83** <sup>13</sup>C NMR Spectrum of biot-GlyAu 2 in Methylene chloride-d<sub>2</sub>.

## Diffusion Ordered Spectroscopy (DOSY) Data

### Summary:

**SI Table 8** Summary of Diffusion coefficients recorded via DOSY.

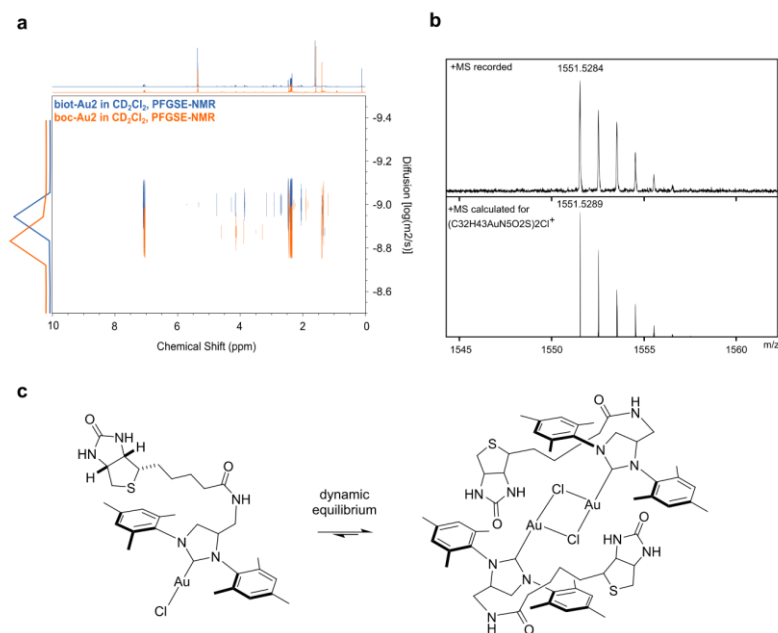
Gold Complex	Diff. Coef. ( $10^{-10} \text{ m}^2/\text{s}$ ) <sup>a</sup>	mass (g/mol)
<b>boc-Au 2</b>	10.08	667.22
<b>biot-Au 2</b>	7.857	793.25
<b>Me<sub>2</sub>biot-Au 2</b>	8.475	821.28

<sup>a</sup>Samples measured in CD<sub>2</sub>Cl<sub>2</sub> at a concentration of 5 mg/mL

Diffusion ordered spectroscopy (DOSY) of the biotinylated gold complex **biot-Au 2** revealed a significantly lower diffusion constant compared to the boc-protected gold complex **boc-Au 2** even taking into account the molecular weight difference. Rough calculations from the diffusion coefficients ( $7.9 \times 10^{-10} \text{ m}^2/\text{s}$  for **biot-Au 2** and  $10.1 \times 10^{-10} \text{ m}^2/\text{s}$  for **boc-Au 2**) suggest a predominantly dimeric nature for **biot-Au 2**. Further investigations under mild HR MS conditions allowed to record accurate mass spectra of dimeric **biot-Au 2** and other dimers of biotinylated gold complexes (see HR-MS spectra). While recording native MS spectra of **biot-Au 2** in Sav at high cone voltages a large peak at  $m/z=1551$  arose indicating the release of dimeric **biot-Au 2** under this harsh conditions (see SI Native MS spectrum 4). All these results lead us to the conclusions that biotinylated gold complexes have the tendency to dimerize and/or agglomerate. The increased diffusion constant of methylated **Me<sub>2</sub>biot-Au 2** compared to **biot-Au 2** may indicate, that the urea moiety of the biotin linker is involved in this agglomerating behavior.

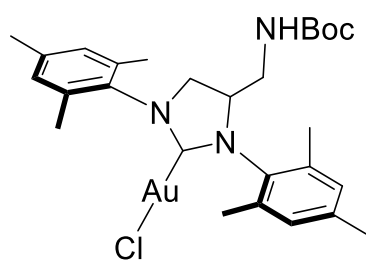
$$\frac{D1}{D2} = \frac{V1}{V2} \text{ and } \frac{V1}{V2} \approx \left(\frac{MW1}{MW2}\right)^3$$

$$\frac{MW_{\text{biotAu 2}^{\text{solv}}}}{MW_{\text{bocAu 2}}} \approx \left(\frac{V_{\text{biotAu 2}}}{V_{\text{bocAu 2}}}\right)^{-3} = \left(\frac{7.84}{10.05}\right)^{-3} = 2.11$$



**SI Figure 18 Aggregation of biotinylated gold complexes.** (a) Overlay of recorded DOSY spectra for boc protected gold complex **boc-Au 2** and biotinylated gold complexes **biot-Au 2** (b) HR MS spectrum (positive mode) of [(**biot-Au 2**)<sub>2</sub>-Cl]<sup>+</sup> (c) Plausible dynamic equilibrium of **biot-Au 2** in solution.

=====

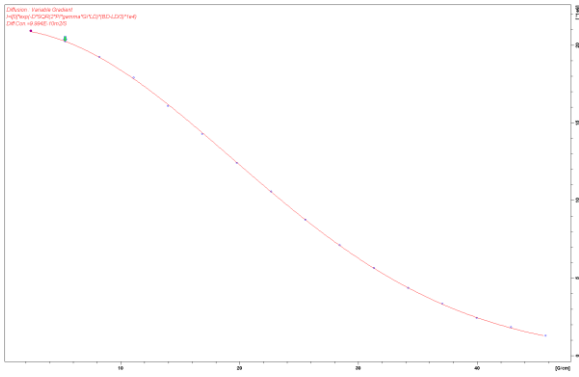


Molecular Weight:  
668.04  
**boc-Au 2**

Au Complex:		<b>boc-Au 2</b>
Proton	peak (ppm)	Diff Con (10 <sup>-10</sup> m <sup>2</sup> /s)
Aryl-H	7.05	9.994
NHC-H	4.13	10.11
Methyl-H	2.44	10.07
Mean Diff Con		10.058
STD Diff Con		0.048

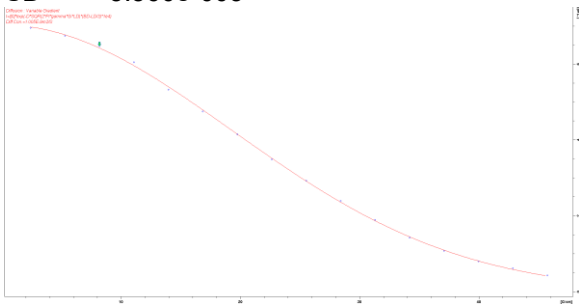
=====

SIMFIT RESULTS for Aryl Peak (s) at 7.054 ppm  
 INTENSITY fit : Diffusion : Variable Gradient :  
 $I = I[0] \cdot \exp(-D \cdot \text{SQR}(2 \cdot \text{PI} \cdot \text{gamma} \cdot \text{Gi} \cdot \text{LD}) \cdot (\text{BD} - \text{LD}/3)) \cdot 1e4$   
 16 points for Peak 1, Peak Point = 7.054 ppm  
 Converged after 35 iterations!  
 Results Comp. 1  
 I[0] = 1.005e+000  
 Diff Con. = 9.994e-010 m<sup>2</sup>/s  
 Gamma = 4.258e+003 Hz/G  
 Little Delta = 2.800m  
 Big Delta = 24.900m  
 RSS = 6.508e-005  
 SD = 2.017e-003



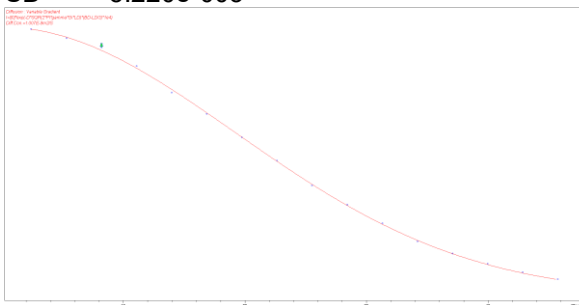
=====

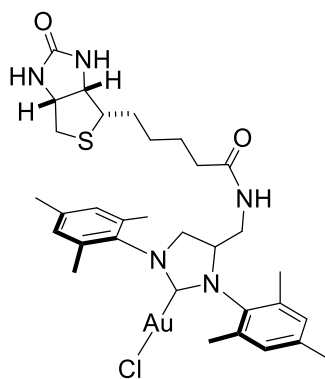
SIMFIT RESULTS for NHC-H (triplet) at 4.132 ppm  
 INTENSITY fit : Diffusion : Variable Gradient :  
 $I=I[0]*\exp(-D*\text{SQR}(2*\text{PI}*\text{gamma}*\text{Gi}*\text{LD})*(BD-\text{LD}/3)*1e4)$   
 16 points for Peak 1, Peak Point = 4.132 ppm  
 Converged after 24 iterations!  
 Results Comp. 1  
 I[0] = 1.011e+000  
 Diff Con. = 1.005e-009 m2/s  
 Gamma = 4.258e+003 Hz/G  
 Little Delta = 2.800m  
 Big Delta = 24.900m  
 RSS = 4.946e-004  
 SD = 5.560e-003



=====

SIMFIT RESULTS for methyl-H (s) at 2.444 ppm  
 INTENSITY fit : Diffusion : Variable Gradient :  
 $I=I[0]*\exp(-D*\text{SQR}(2*\text{PI}*\text{gamma}*\text{Gi}*\text{LD})*(BD-\text{LD}/3)*1e4)$   
 16 points for Peak 1, Peak Point = 2.444 ppm  
 Converged after 27 iterations!  
 Results Comp. 1  
 I[0] = 1.007e+000  
 Diff Con. = 1.007e-009 m2/s  
 Gamma = 4.258e+003 Hz/G  
 Little Delta = 2.800m  
 Big Delta = 24.900m  
 RSS = 4.359e-004  
 SD = 5.220e-003





Molecular Weight: 794.21

**biot-Au 2**

Au Complex:		<b>biot-Au 2</b>	
Proton	peak (ppm)	Diff ( $10^{-10}$ m <sup>2</sup> /s)	Con
Aryl-H	7.05	7.833	7.833
NHC-H	4.16	7.855	7.855
Methyl-H	2.46	7.824	7.824
Mean Diff Con		7.837	
STD Diff Con		0.013	

=====

SIMFIT RESULTS for Aryl-H (s) at 7.050 ppm  
 INTENSITY fit : Diffusion : Variable Gradient :  
 $I=I[0]*\exp(-D*\text{SQR}(2*\text{PI}*\text{gamma}*\text{Gi}*\text{LD})*(\text{BD}-\text{LD}/3)*1e4)$   
 16 points for Peak 1, Peak Point = 7.050 ppm  
 Converged after 32 iterations!

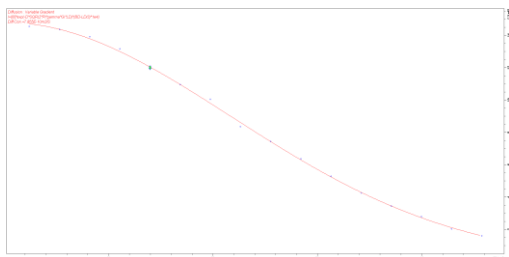
Results Comp. 1  
 I[0] = 1.010e+000  
 Diff Con. = 7.833e-010 m2/s  
 Gamma = 4.258e+003 Hz/G  
 Little Delta = 2.800m  
 Big Delta = 24.900m  
 RSS = 6.744e-005  
 SD = 2.053e-003



=====

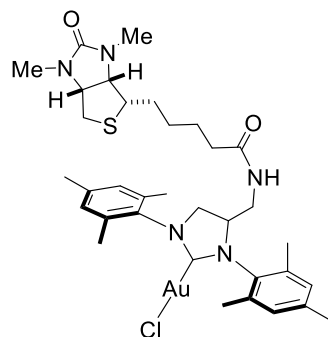
SIMFIT RESULTS for NHC-H (td) at 4.156 ppm  
 INTENSITY fit : Diffusion : Variable Gradient :  
 $I=I[0]*\exp(-D*\text{SQR}(2*\text{PI}*\text{gamma}*\text{Gi}*\text{LD})*(\text{BD}-\text{LD}/3)*1e4)$   
 16 points for Peak 1, Peak Point = 4.156 ppm  
 Converged after 31 iterations!

Results Comp. 1  
 I[0] = 1.017e+000  
 Diff Con. = 7.855e-010 m2/s  
 Gamma = 4.258e+003 Hz/G  
 Little Delta = 2.800m  
 Big Delta = 24.900m  
 RSS = 1.084e-003  
 SD = 8.229e-003



SIMFIT RESULTS for methyl-H (s) at 2.462 ppm  
 INTENSITY fit : Diffusion : Variable Gradient :  
 $I=I[0]*\exp(-D*SQR(2*PI*\gamma*Gi*LD)*(BD-LD/3)*1e4)$   
 16 points for Peak 1, Peak Point = 2.462 ppm  
 Converged after 32 iterations!

Results Comp. 1  
 I[0] = 9.993e-001  
 Diff Con. = 7.824e-010 m2/s  
 Gamma = 4.258e+003 Hz/G  
 Little Delta = 2.800m  
 Big Delta = 24.900m  
 RSS = 5.208e-004  
 SD = 5.706e-003



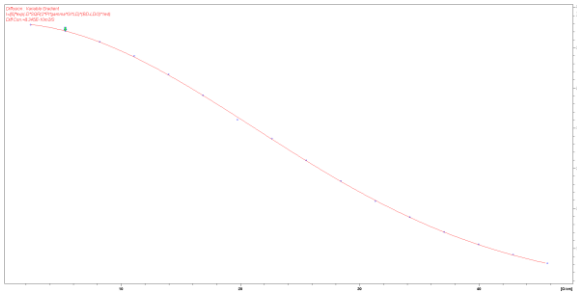
Molecular Weight:  
822.27

**Me<sub>2</sub>biot-Au 2**

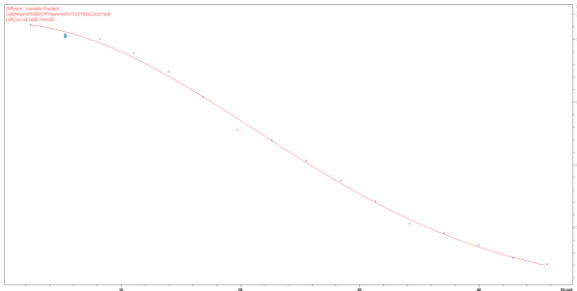
Au Complex:		<b>Me<sub>2</sub>biot-Au 2</b>	
Proton	peak (ppm)	Diff (10 <sup>-10</sup> m <sup>2</sup> /s)	Con
Aryl-H	7.05	8.345	8.345
NHC-H	4.14	8.392	8.392
Methyl-H	2.46	8.379	8.379
Mean Diff Con		8.372	
STD Diff Con		0.020	

SIMFIT RESULTS for Aryl-H (s) at 7.050 ppm  
 INTENSITY fit : Diffusion : Variable Gradient :  
 $I=I[0]*\exp(-D*SQR(2*PI*\gamma*Gi*LD)*(BD-LD/3)*1e4)$   
 16 points for Peak 1, Peak Point = 7.050 ppm  
 Converged after 31 iterations!

Results Comp. 1  
 I[0] = 1.008e+000  
 Diff Con. = 8.345e-010 m2/s  
 Gamma = 4.258e+003 Hz/G  
 Little Delta = 2.800m  
 Big Delta = 24.900m  
 RSS = 1.493e-004  
 SD = 3.055e-003

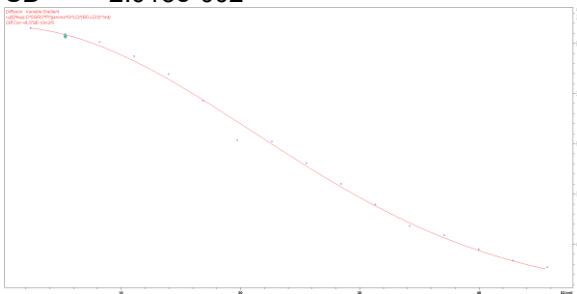


SIMFIT RESULTS for NHC-H (t) at 4.139 ppm  
 INTENSITY fit : Diffusion : Variable Gradient :  
 $I=I[0]*\exp(-D*\text{SQR}(2*\text{PI}*\text{gamma}*\text{Gi}*\text{LD})*(BD-\text{LD}/3)*1e4)$   
 16 points for Peak 1, Peak Point = 4.139 ppm  
 Converged after 32 iterations!  
 Results Comp. 1  
 I[0] = 1.007e+000  
 Diff Con. = 8.392e-010 m2/s  
 Gamma = 4.258e+003 Hz/G  
 Little Delta = 2.800m  
 Big Delta = 24.900m  
 RSS = 3.694e-003  
 SD = 1.520e-002



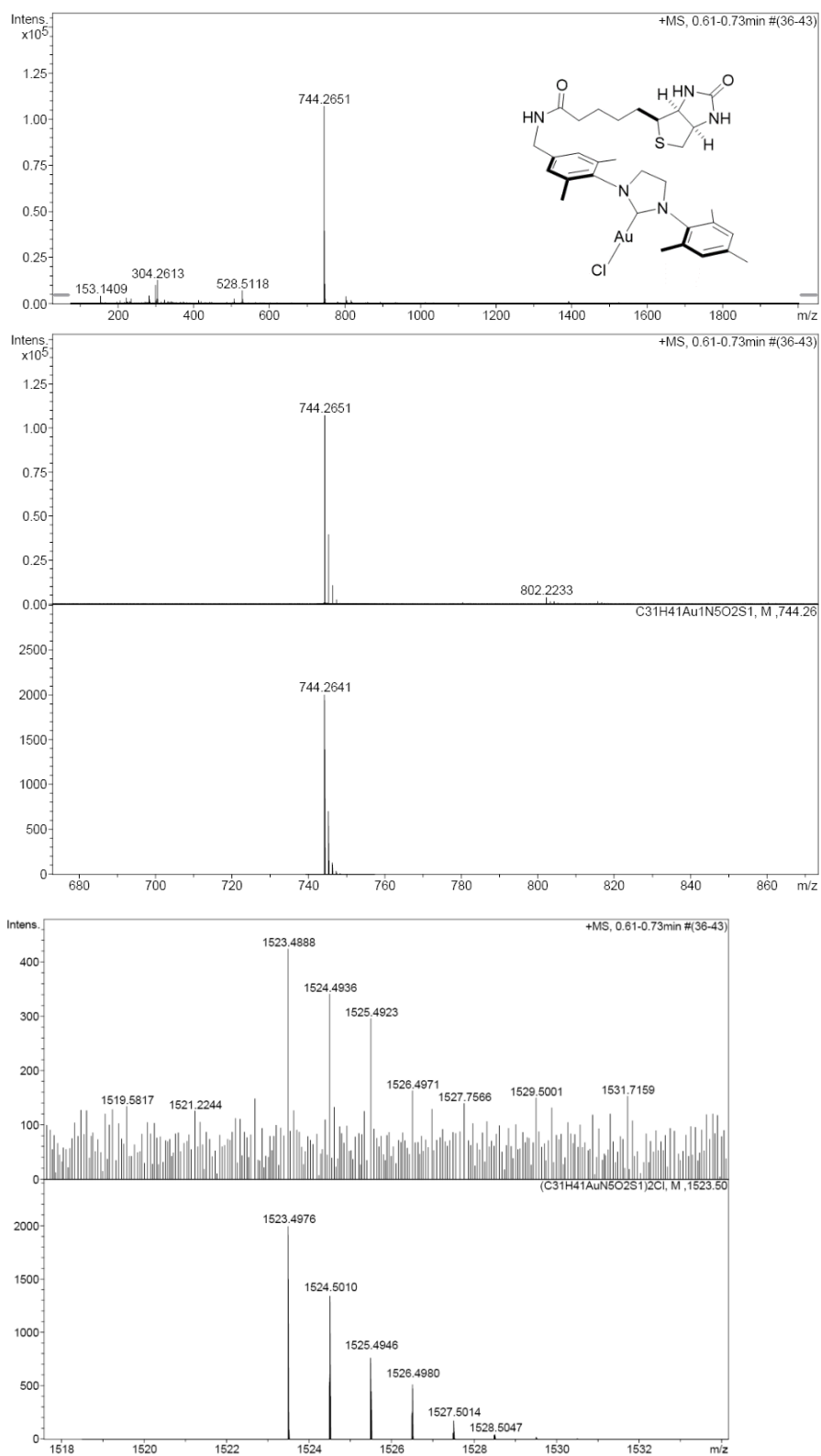
=====

SIMFIT RESULTS for Methyl-H (s) at 2.462 ppm  
 INTENSITY fit : Diffusion : Variable Gradient :  
 $I=I[0]*\exp(-D*\text{SQR}(2*\text{PI}*\text{gamma}*\text{Gi}*\text{LD})*(BD-\text{LD}/3)*1e4)$   
 16 points for Peak 1, Peak Point = 2.462 ppm  
 Converged after 28 iterations!  
 Results Comp. 1  
 I[0] = 1.007e+000  
 Diff Con. = 8.379e-010 m2/s  
 Gamma = 4.258e+003 Hz/G  
 Little Delta = 2.800m  
 Big Delta = 24.900m  
 RSS = 6.496e-003  
 SD = 2.015e-002



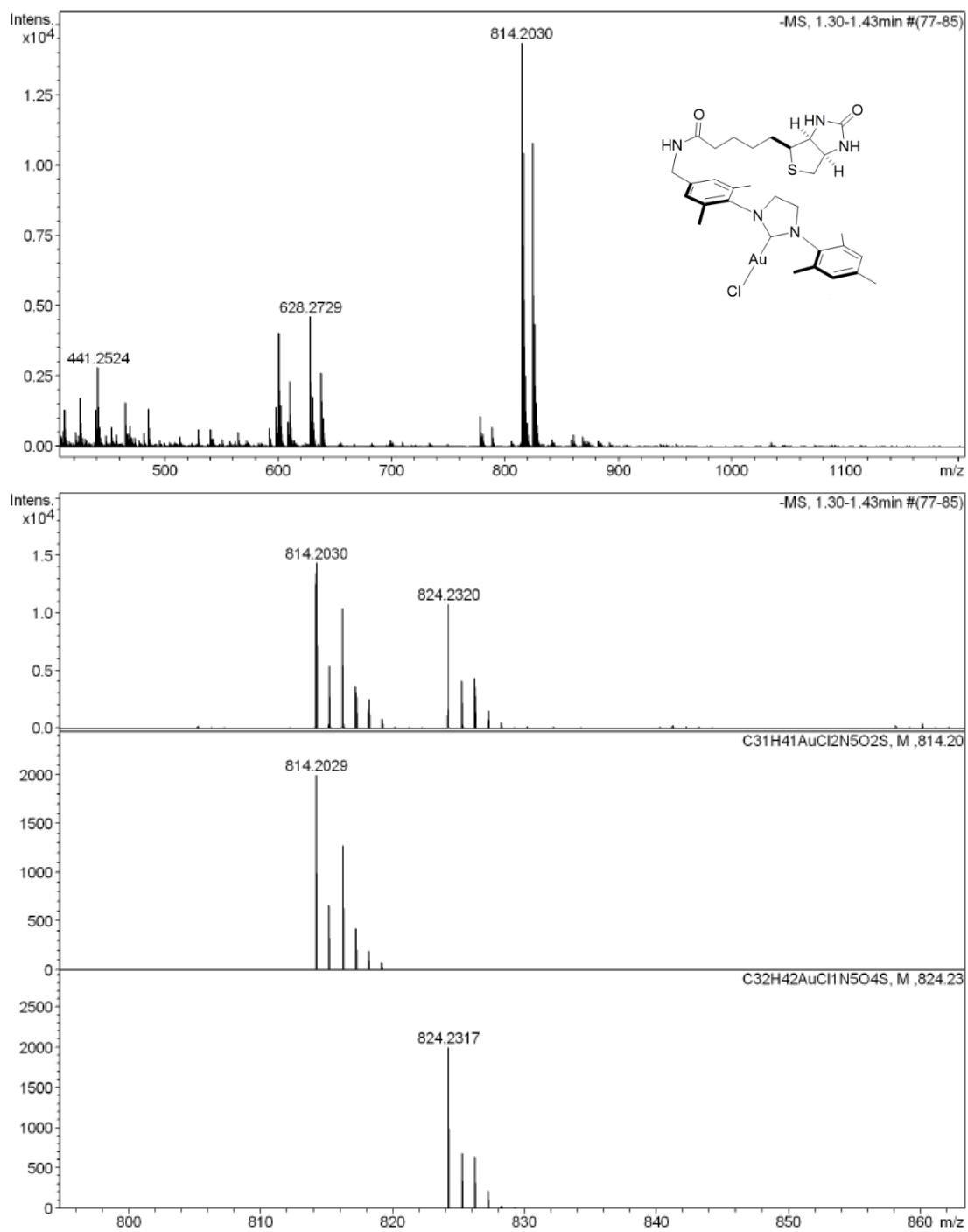
## Selected HR-MS spectra

### HR-MS spectra of biotinylated gold complexes recorded from MeOH

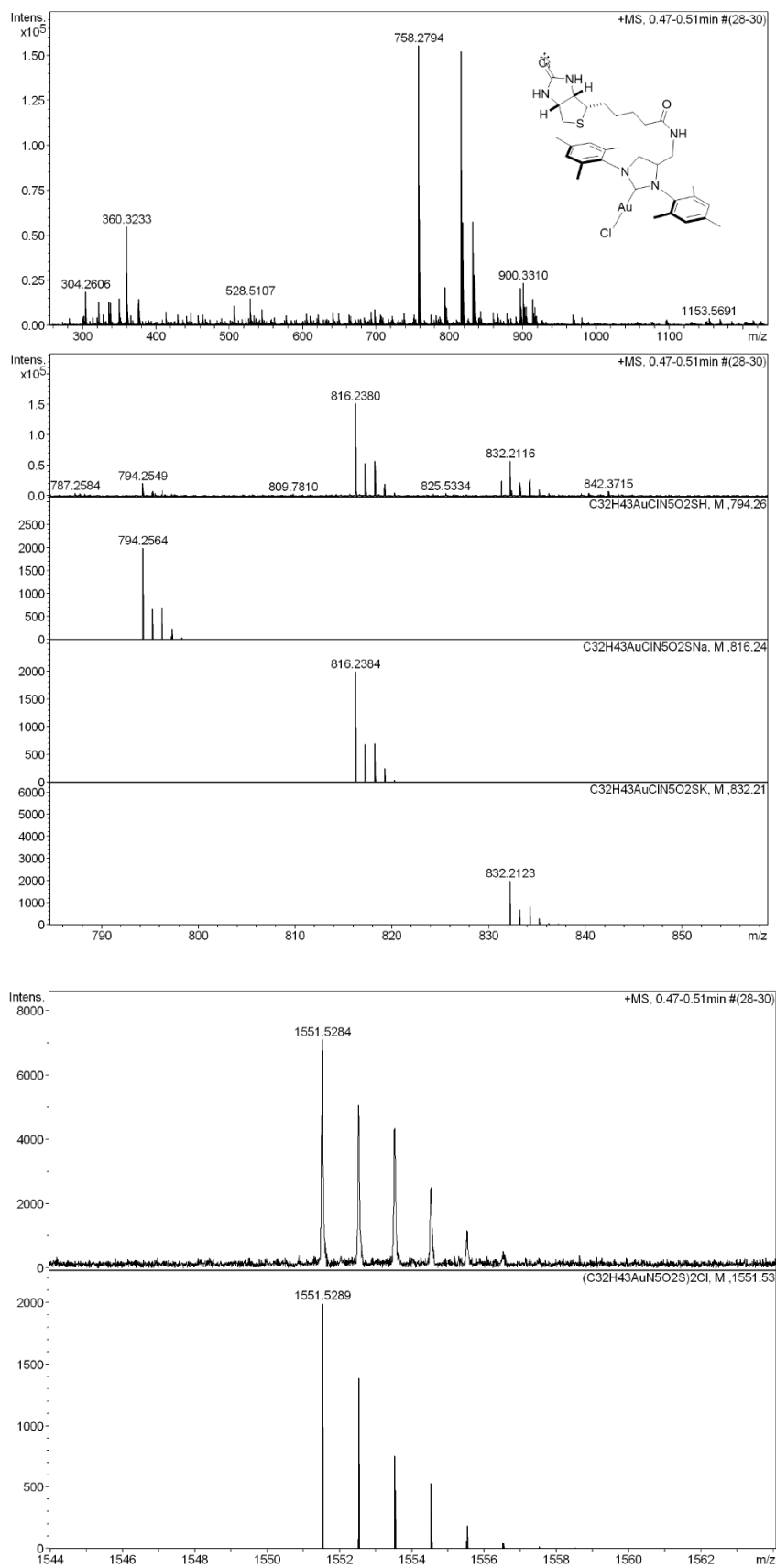


**Spectrum 84** HR-MS Spectrum of **biot-Au 1** in positive mode.

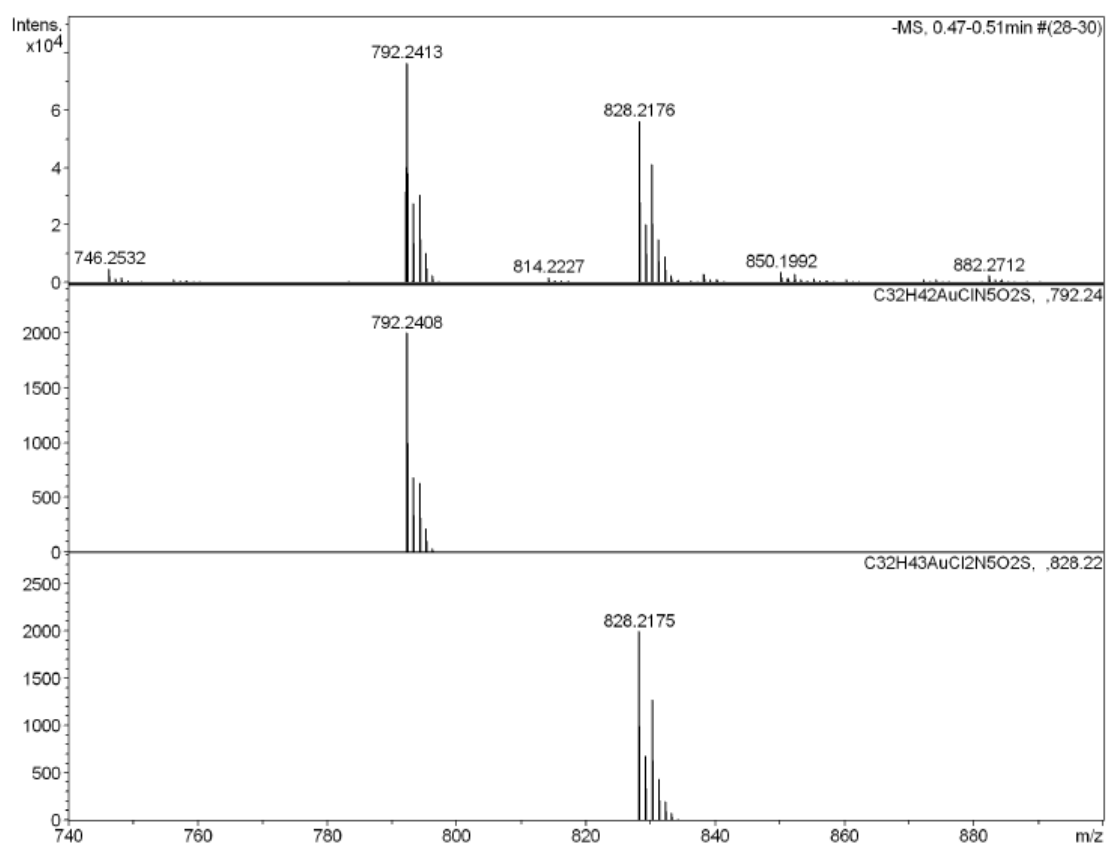
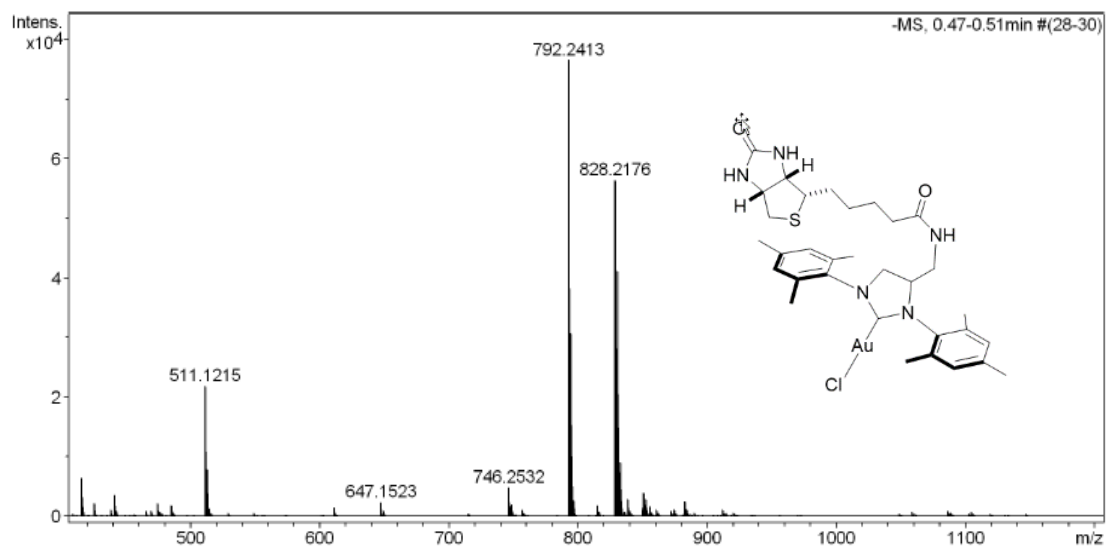




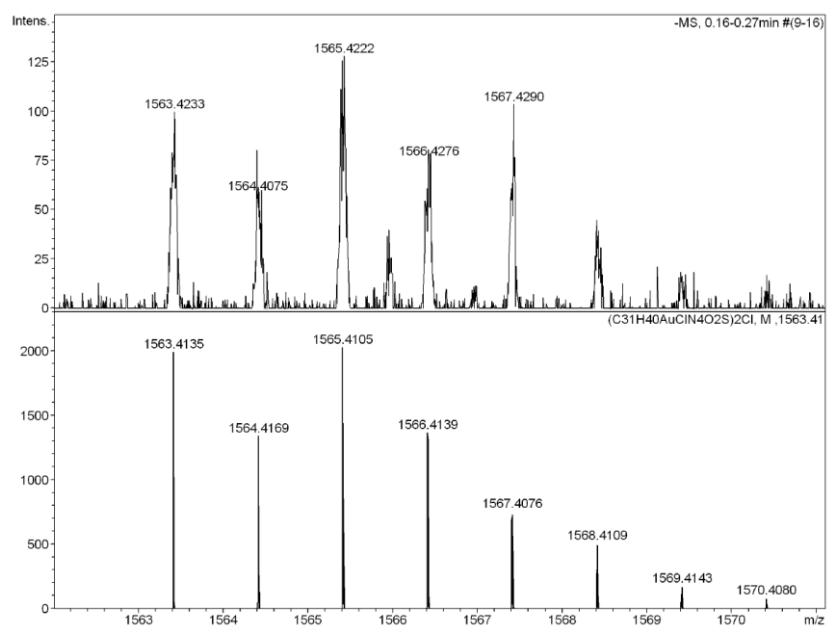
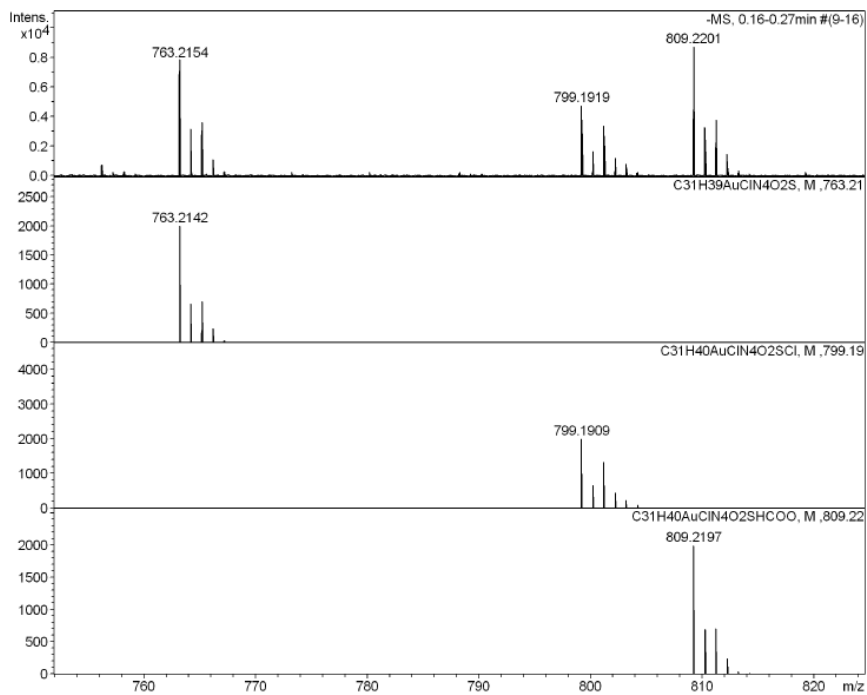
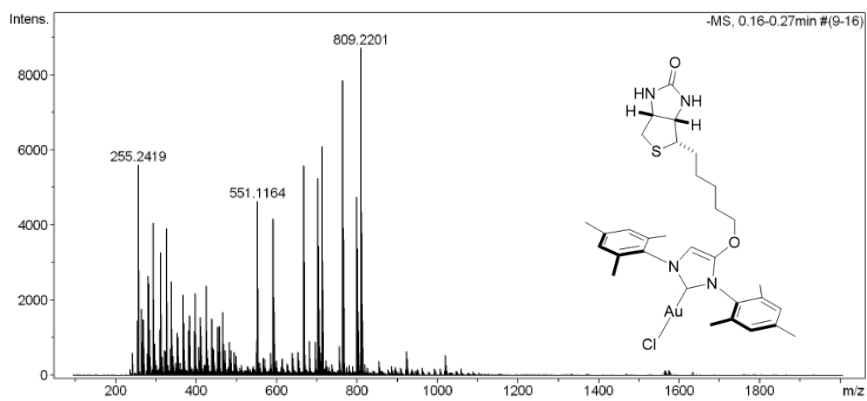
**Spectrum 85** HR-MS Spectrum of **biot-Au 1** in negative mode.



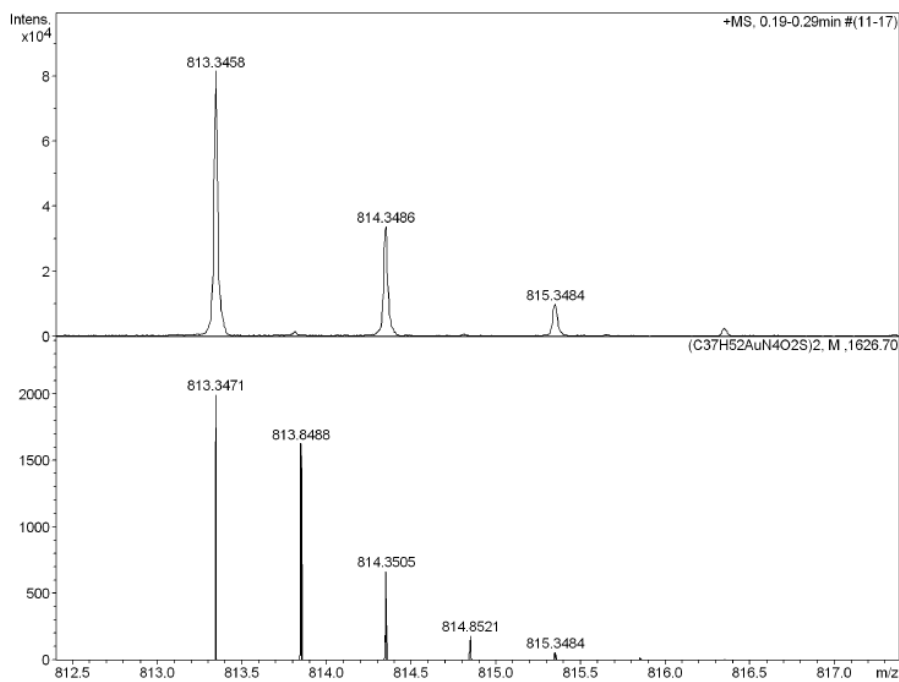
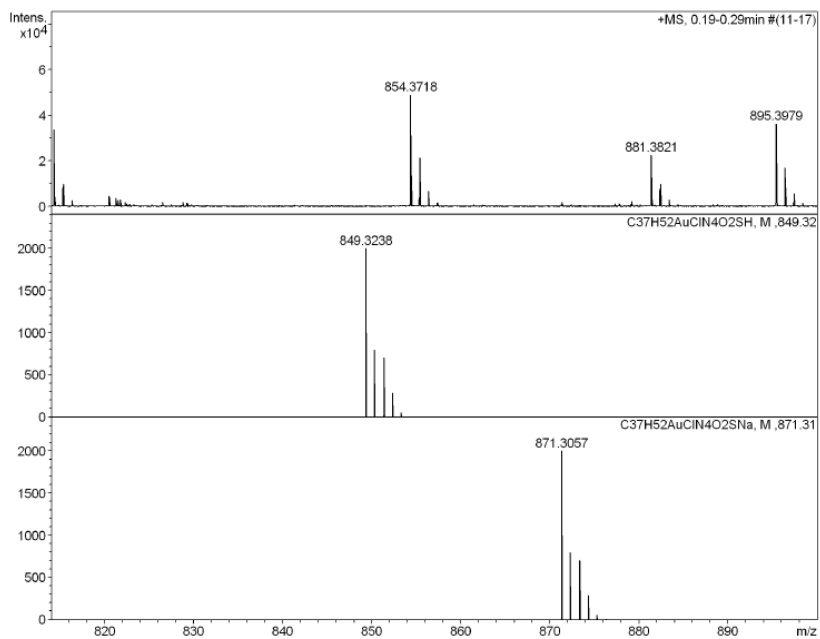
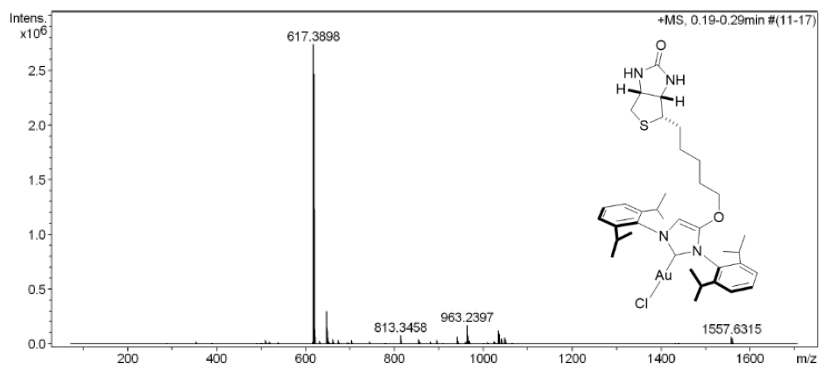
**Spectrum 86** HR-MS Spectrum of **biot-Au 2** in positive mode.



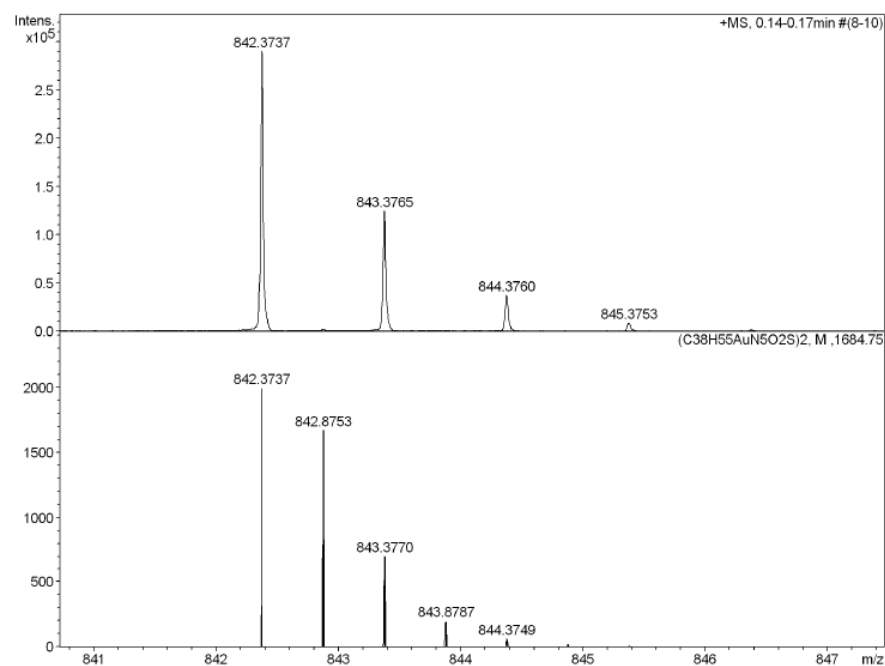
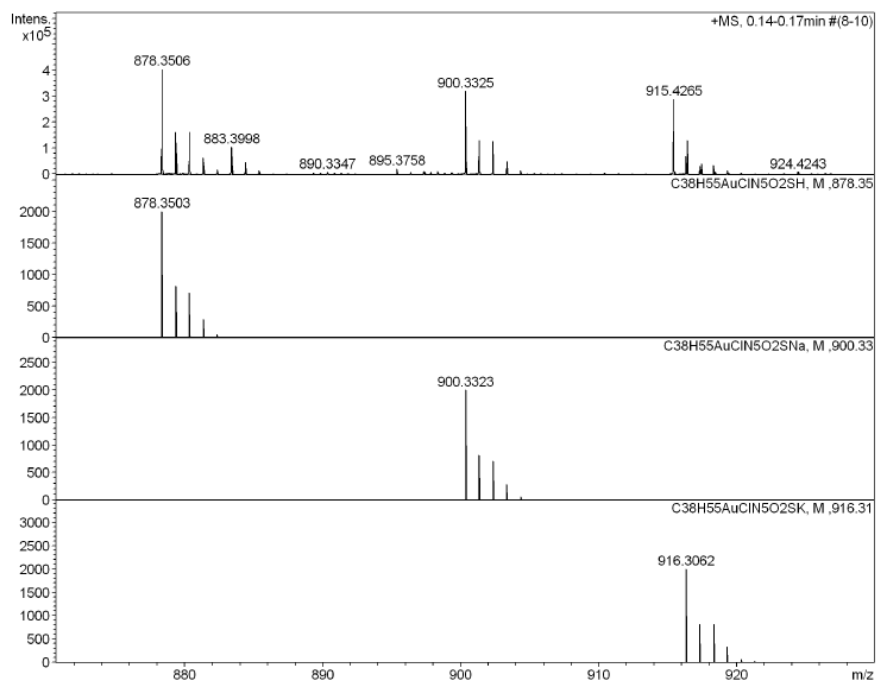
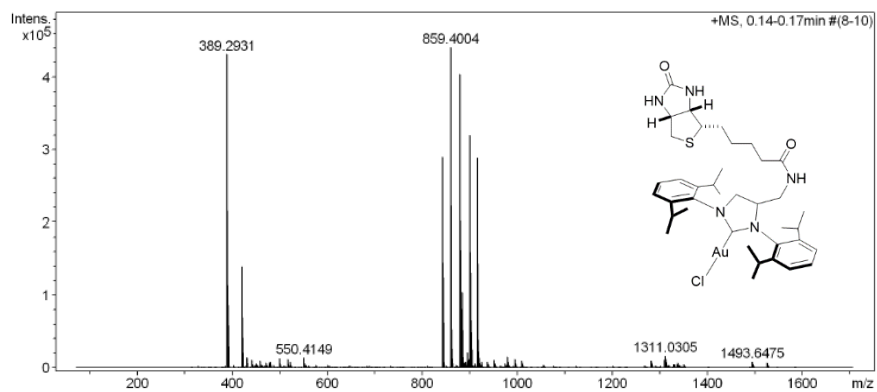
**Spectrum 87** HR-MS Spectrum of **biot-Au 2** in negative mode.



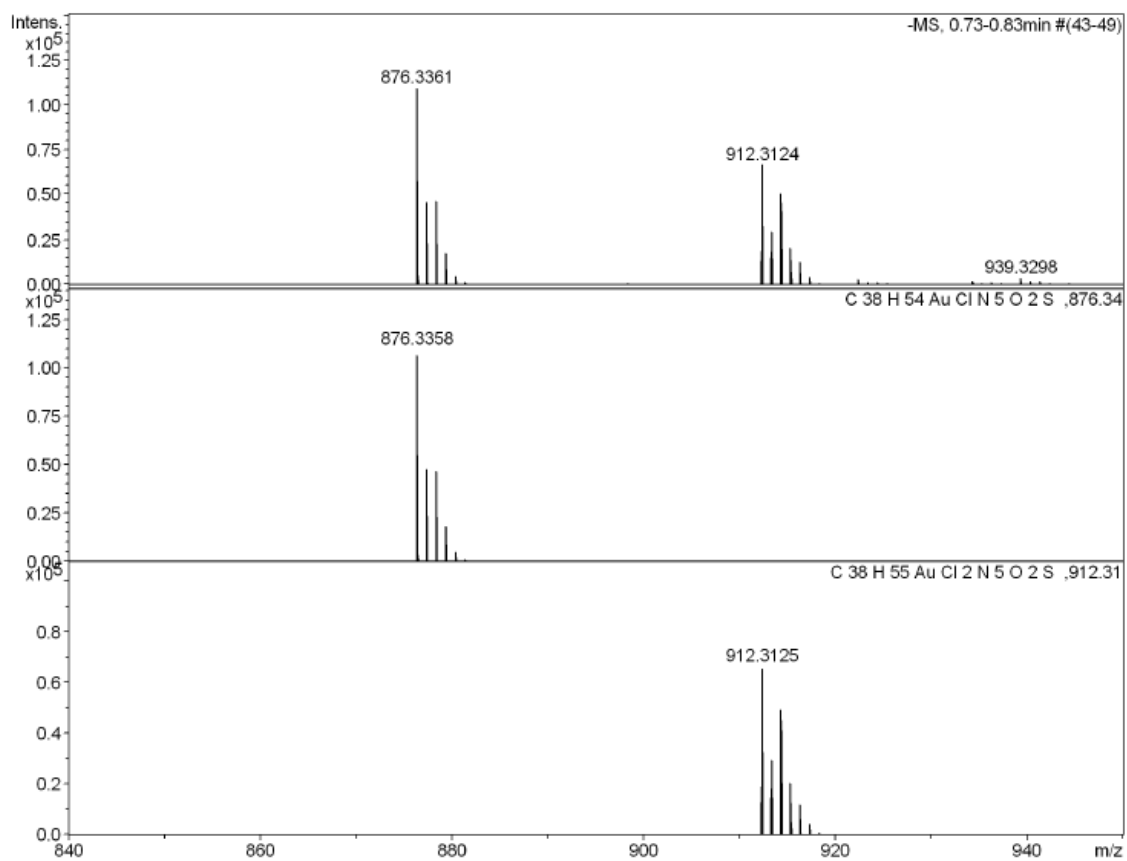
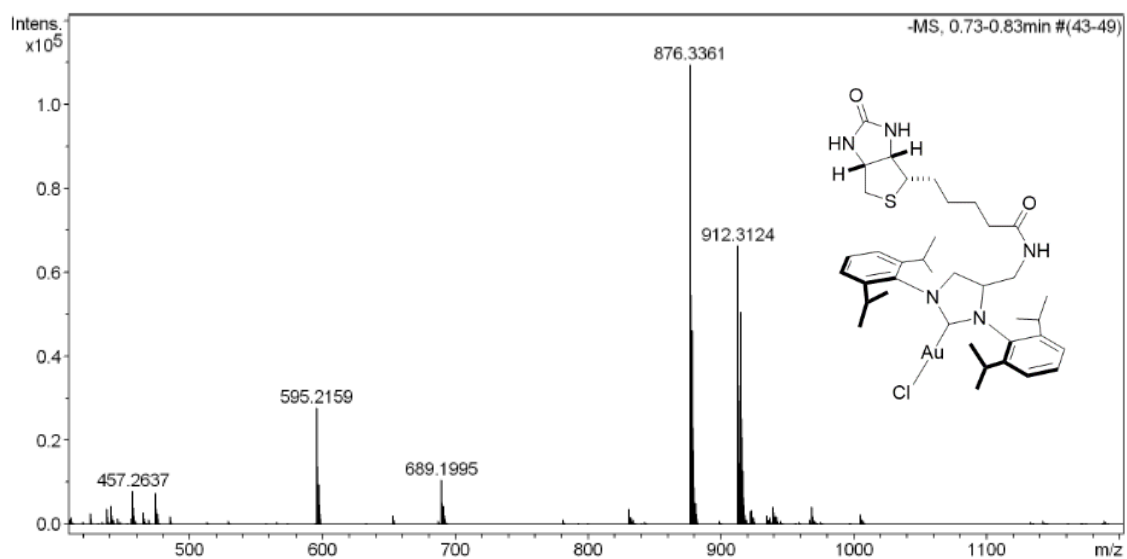
**Spectrum 88** HR-MS Spectrum of **biot-Au 3** in negative mode.



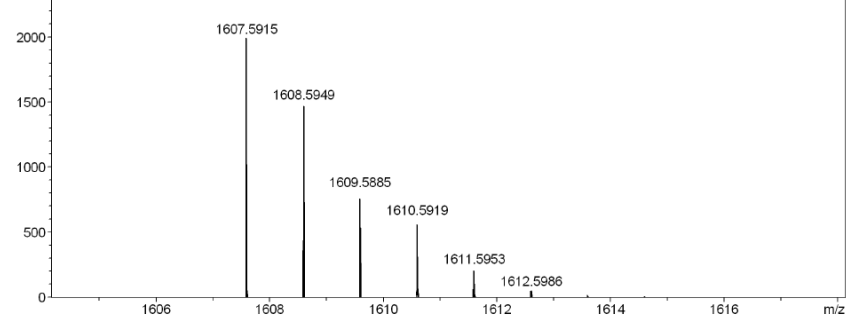
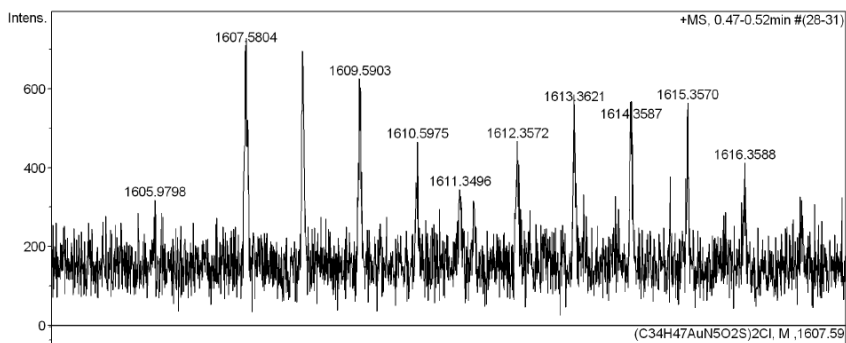
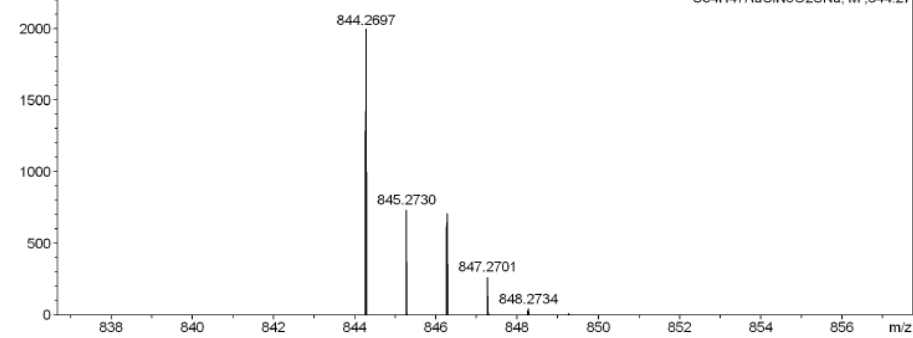
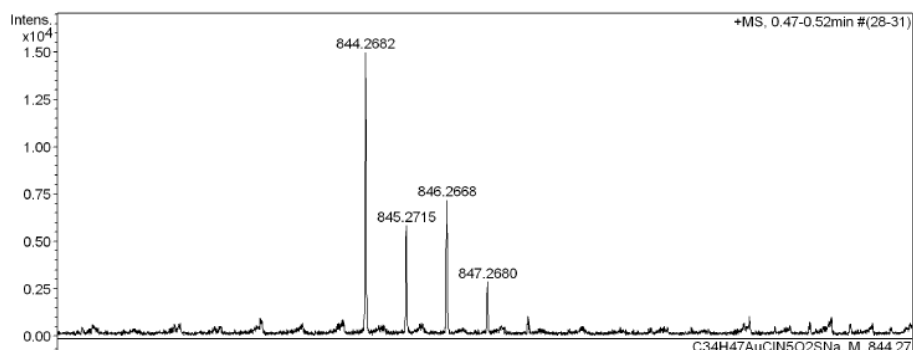
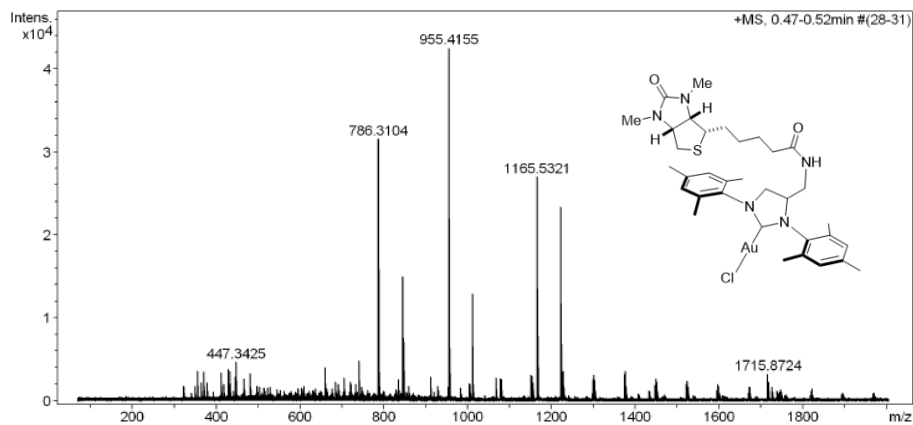
**Spectrum 89 HR-MS Spectrum of biot-Au 4.**



**Spectrum 90** HR-MS Spectrum of **biot-Au 5** in positive mode.

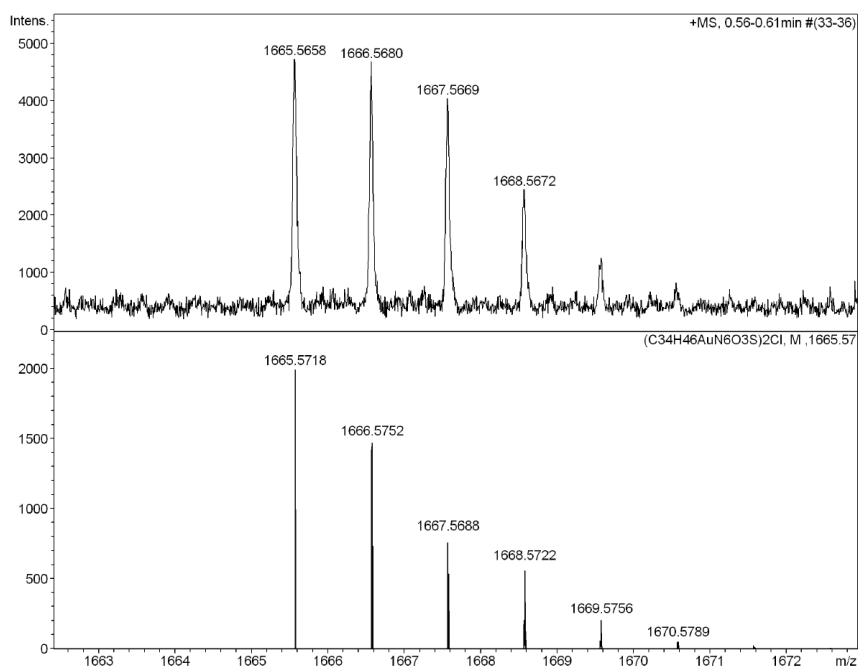
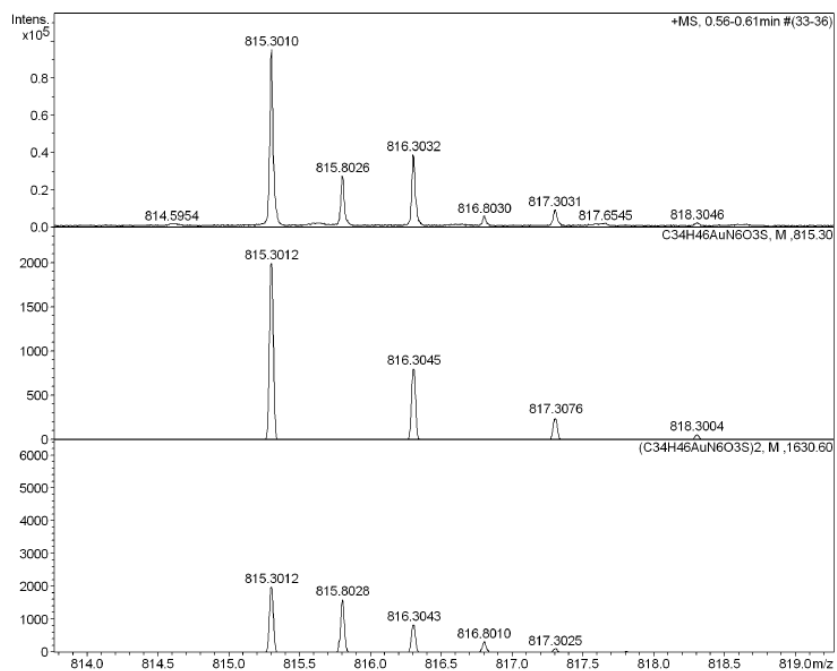
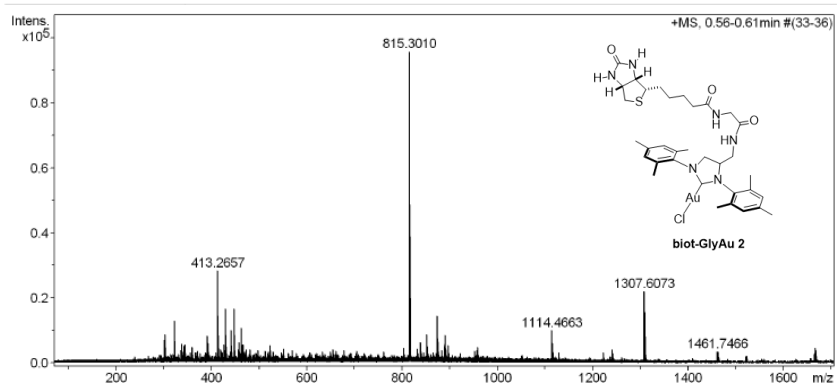


**Spectrum 91** HR-MS Spectrum of **biot-Au 5** in negative mode.



**Spectrum 92 HR-MS Spectrum of Me<sub>2</sub>biot-Au 2.**

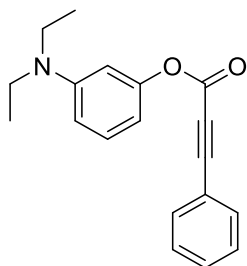




**Spectrum 93 HR-MS Spectrum of biot-GlyAu 2**

## 8.3 Chapter 2: Systematic Screening of Gold-based ArMs

### Substrate Synthesis

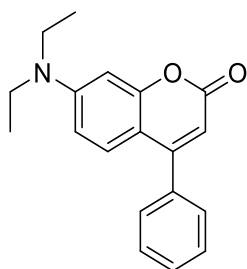


**3-(diethylamino)phenyl 3-phenylpropiolate (1):** Prepared according to a modified procedure of Do *et al*<sup>220</sup>. To a solution of 3-diethylaminophenol (826 mg, 5.00 mmol, 1.0 eq) in dry CH<sub>2</sub>Cl<sub>2</sub> (20 mL) was added a solution of 3-phenylpropionic acid (804 mg, 5.50 mmol, 1.1 eq) in dry CH<sub>2</sub>Cl<sub>2</sub> (10 mL). The solution was cooled to 0 °C before the dropwise addition of a solution of DMAP (305 mg, 2.50 mmol, 0.5 eq) and DCC (1.55 g, 7.50 mmol, 1.5 eq) in dry CH<sub>2</sub>Cl<sub>2</sub> (10 mL). The solution was stirred at room temperature for 16 h, then cooled to 0 °C and filtered to remove most of the formed dicyclohexylurea. The crude mixture was concentrated *in vacuo* and purified via automated flash column chromatography (KP-Sil 50g) to yield ester **1** as an orange oil (622 mg, 2.12 mmol, 42%).

<sup>1</sup>H NMR (500 MHz, DMSO-*d*<sub>6</sub>) δ 7.71 – 7.66 (m, 2H), 7.63 – 7.58 (m, 1H), 7.52 (t, J = 7.7 Hz, 2H), 7.19 (t, J = 8.2 Hz, 1H), 6.58 (dd, J = 8.4, 2.5 Hz, 1H), 6.50 (t, J = 2.3 Hz, 1H), 6.40 (dd, J = 7.8, 2.1 Hz, 1H), 3.32 (q, J = 7.2 Hz, 4H), 1.07 (t, J = 7.0 Hz, 6H).

<sup>13</sup>C NMR (126 MHz, DMSO-*d*<sub>6</sub>) δ 151.74, 151.17, 148.70, 132.95, 131.62, 129.96, 129.17, 118.15, 109.43, 107.36, 104.27, 87.95, 80.26, 43.73, 12.27.

HR-MS (ESI, pos): *m/z* calcd. for C<sub>19</sub>H<sub>19</sub>NO<sub>2</sub>H<sup>+</sup> 294.1489 found 294.1487 [M+H<sup>+</sup>]<sup>+</sup>; *m/z* calcd. for C<sub>19</sub>H<sub>19</sub>NO<sub>2</sub>Na<sup>+</sup> 316.1308 found 316.1306 [M+Na<sup>+</sup>]<sup>+</sup>.



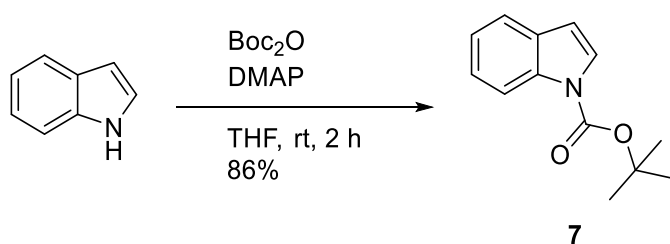
**7-(diethylamino)-4-phenyl-2H-chromen-2-one (2):** Prepared according to a modified procedure of Do *et al*<sup>220</sup>. In a reaction tube, ester **1** (96.8 mg, 0.33 mmol, 1.0 eq) was diluted with dry CH<sub>2</sub>Cl<sub>2</sub> (1.6 mL) and dry EtOH (0.4 mL) before adding hydrogen tetrachloroaurate(III)

hydrate (23.6 mg, 0.07 mmol, 0.2 eq). The reaction mixture was stirred at room temperature for 16 h in the dark. The solvents were removed *in vacuo* and the crude was purified via automated flash column chromatography (KP-Sil25g, ) to yield coumarin **2** as a yellow oil (43 mg, 0.15 mmol, 44%).

$^1\text{H}$  NMR (500 MHz,  $\text{DMSO-}d_6$ )  $\delta$  7.54 (dt,  $J = 5.0, 2.2$  Hz, 3H), 7.51 – 7.46 (m, 2H), 7.18 (d,  $J = 9.1$  Hz, 1H), 6.68 (dd,  $J = 9.1, 2.6$  Hz, 1H), 6.61 (d,  $J = 2.5$  Hz, 1H), 5.93 (s, 1H), 3.43 (q,  $J = 7.0$  Hz, 4H), 1.12 (t,  $J = 7.0$  Hz, 6H).

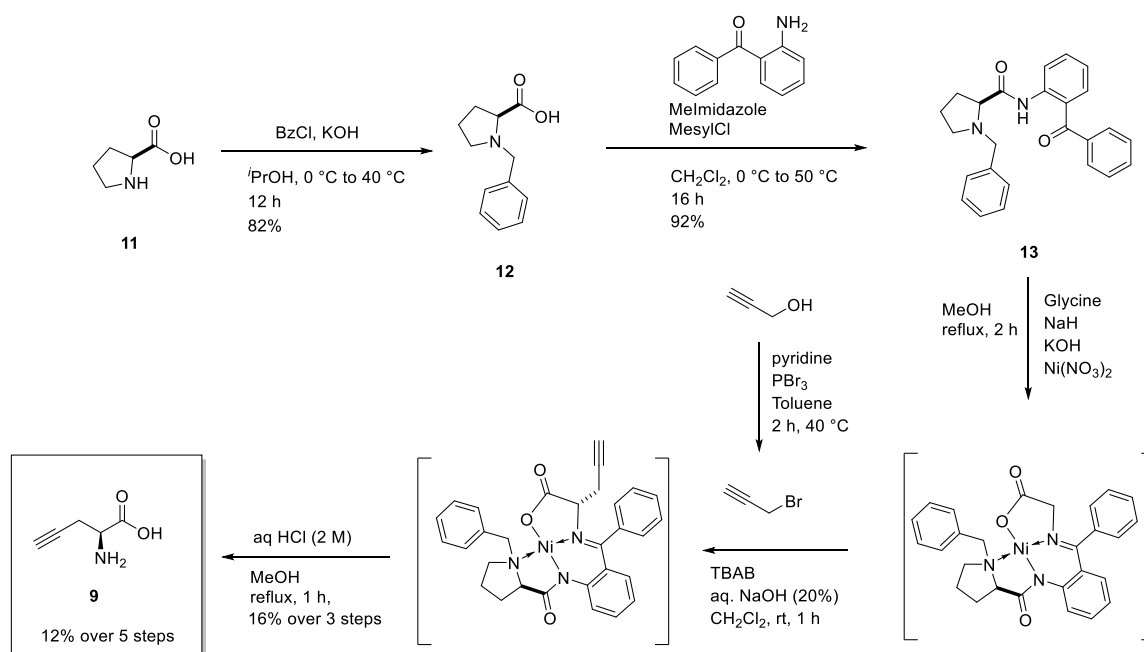
$^{13}\text{C}$  NMR (126 MHz,  $\text{DMSO-}d_6$ )  $\delta$  160.62, 156.37, 155.59, 150.50, 135.61, 129.42, 128.77, 128.30, 127.67, 108.91, 107.26, 106.77, 97.13, 44.02, 12.32.

HR-MS (ESI, pos):  $m/z$  calcd. for  $\text{C}_{19}\text{H}_{19}\text{NO}_2\text{H}^+$  294.1489 found 294.1491  $[\text{M}+\text{H}]^+$ ;  $m/z$  calcd. for  $\text{C}_{19}\text{H}_{19}\text{NO}_2\text{Na}^+$  316.1308 found 316.1310  $[\text{M}+\text{Na}]^+$ .



Protected indole **7**: Indole (351 mg, 3 mmol, 1 eq), di-tert-butyl dicarbonate ( $\text{Boc}_2\text{O}$ ) (0.77 mL, 3.6 mmol, 1.2 eq) and DMAP (73 mg, 0.6 mmol, 0.2 eq) were dissolved in dry THF (5 mL). The mixture was stirred (2 h, rt) before removing the solvent *in vacuo*. The product was purified by flash column chromatography (20% EtOAc/cyclohexane) to yield the product as a colourless oil (558 mg, 2.57 mmol, 86%).

$^1\text{H}$  NMR (500 MHz,  $\text{DMSO-}d_6$ )  $\delta$  8.06 (dd,  $J = 8.2, 1.1$  Hz, 1H), 7.67 (d,  $J = 3.7$  Hz, 1H), 7.65 – 7.58 (m, 1H), 7.35 – 7.29 (m, 1H), 7.27 – 7.21 (m, 1H), 6.71 (dd,  $J = 3.7, 0.8$  Hz, 1H), 1.63 (s, 9H).



The synthesis of substrate **9** was performed according to the procedure of Kent and co-workers.<sup>136</sup> The spectra were in agreement with literature data.

Amide **13**: <sup>1</sup>H NMR (500 MHz, CD<sub>3</sub>OD) δ 9.80 (s, 1H), 8.69 – 8.65 (m, 2H), 8.56 – 8.51 (m, 1H), 8.51 – 8.44 (m, 2H), 8.43 – 8.38 (m, 2H), 8.38 – 8.34 (m, 2H), 8.33 – 8.22 (m, 5H), 5.28 – 5.20 (m, 2H), 5.21 – 5.17 (m, 1H), 4.46 (ddd, *J* = 11.2, 7.5, 3.8 Hz, 1H), 4.28 – 4.23 (m, 1H), 3.29 (dddd, *J* = 13.3, 9.4, 8.3, 7.1 Hz, 1H), 3.12 – 2.96 (m, 1H), 2.84 – 2.70 (m, 1H), 2.53 (dtd, *J* = 13.6, 8.0, 5.5 Hz, 1H).

Substrate **9**: <sup>1</sup>H NMR (500 MHz, D<sub>2</sub>O) δ 3.92 (t, *J* = 5.5 Hz, 1H), 2.87 (d, *J* = 1.3 Hz, 2H), 2.53 (t, *J* = 2.7 Hz, 1H).

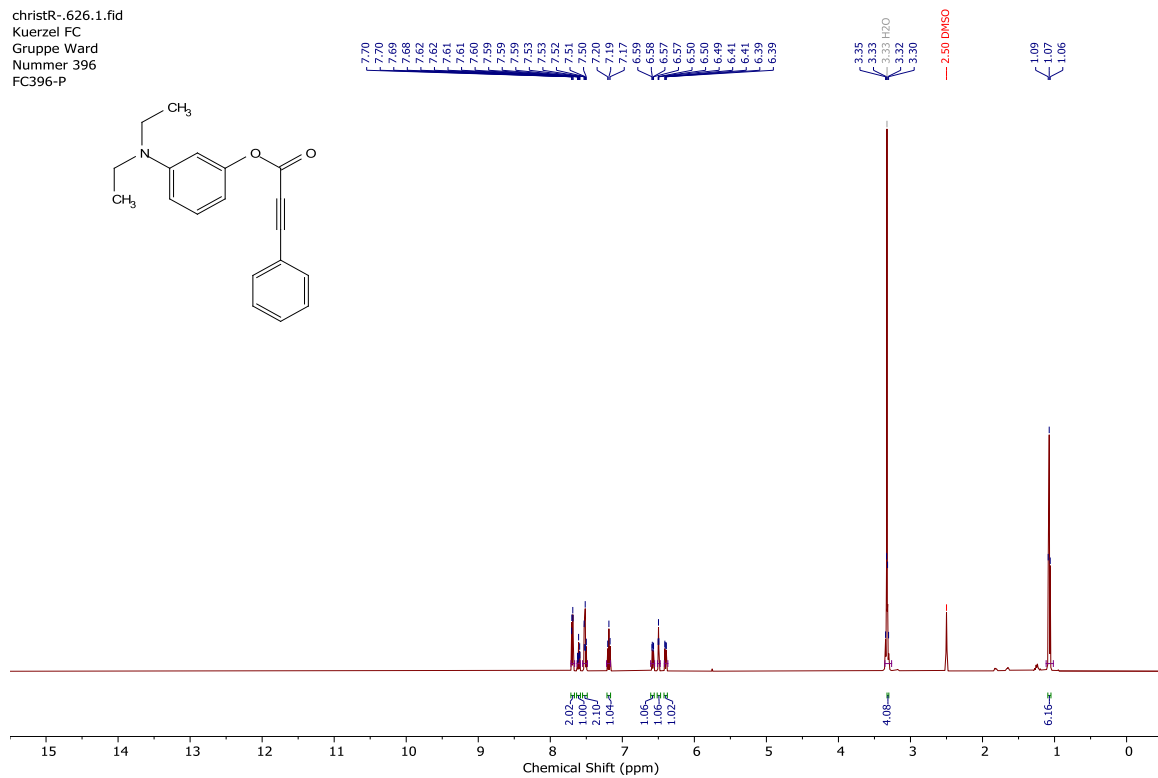
MS-Direct Injection (ESI, pos) *m/z*: 114.23 [100%, M+H]<sup>+</sup>.

### Catalysis Protocol

Pre-screening conditions: To a GC-MS vial (1.5 mL) was added MES-buffer (185 μL, 50 mM, pH 5.1), purified protein (4 μL of 1000 μM FBS in MQ-water) and cofactor (1 μL of 2 mM in DMSO). The tubes were incubated in a thermoshaker (20 min, 37 °C, 900 rpm). Afterwards, substrate (1 μL of 100 mM in DMSO) was added and the tubes were shaken in a thermoshaker for the corresponding reaction time. The reaction was quenched by the addition of methanol (200 μL) followed by centrifugation (14'000 rpm, 10 °C, 10 min). In UPLC vials, the reaction mixture (200 μL) was diluted in UPLC media (800 μL, 1:1 MeCN:MQ-Water) before UPLC-MS analysis.

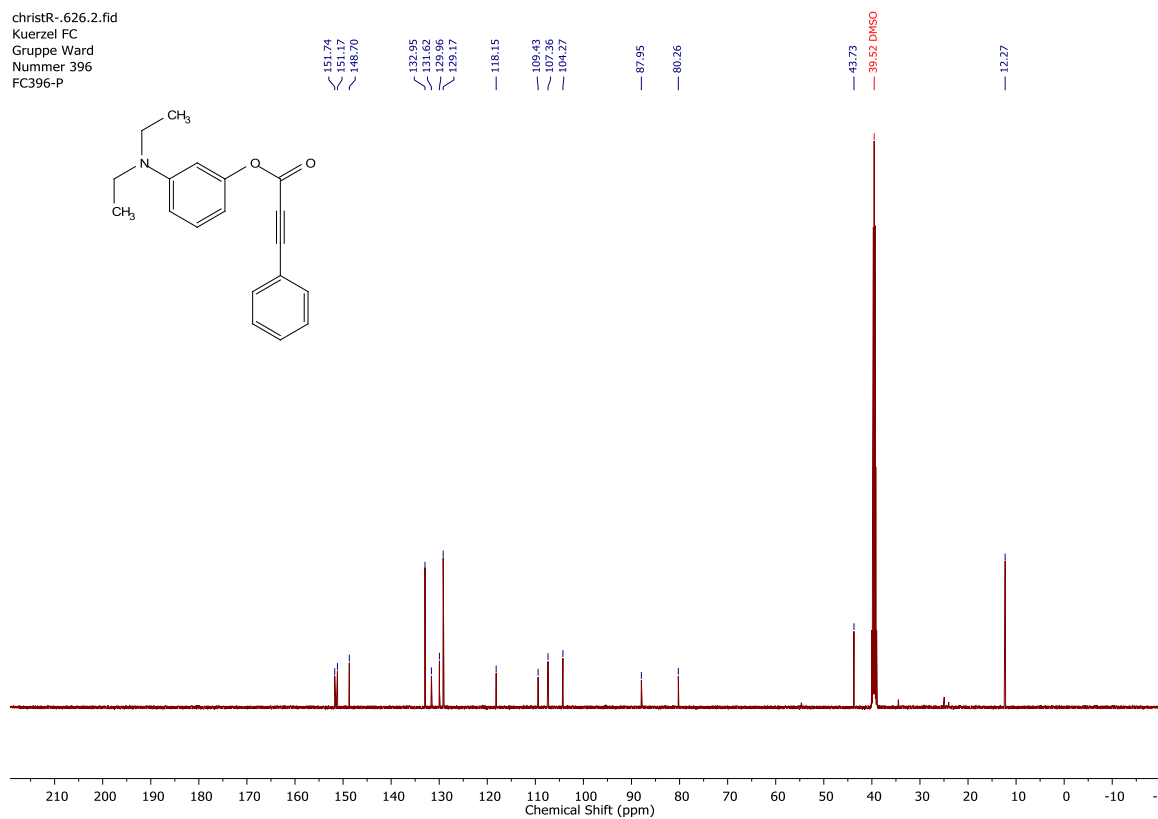
## NMR & Mass Spectra

christR-.626.1.fid  
Kuerzel FC  
Gruppe Ward  
Nummer 396  
FC396-P



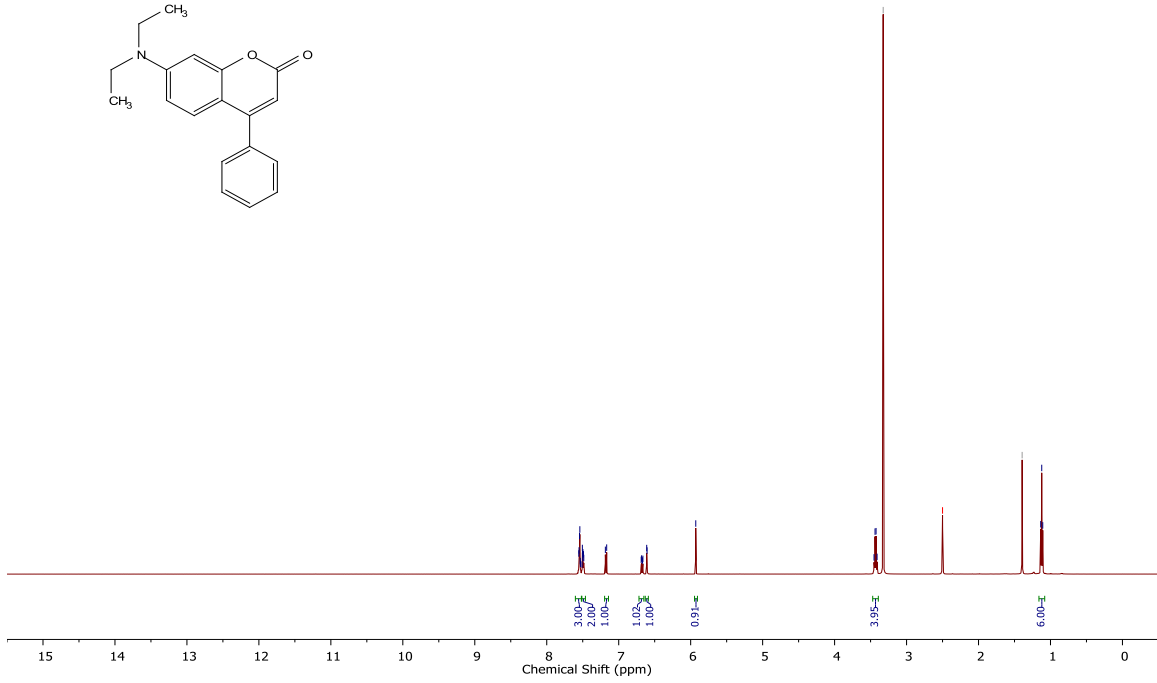
### Spectrum 94 <sup>1</sup>H-NMR spectrum of ester 1 in DMSO-*d*<sub>6</sub>.

christR-.626.2.fid  
Kuerzel FC  
Gruppe Ward  
Nummer 396  
FC396-P



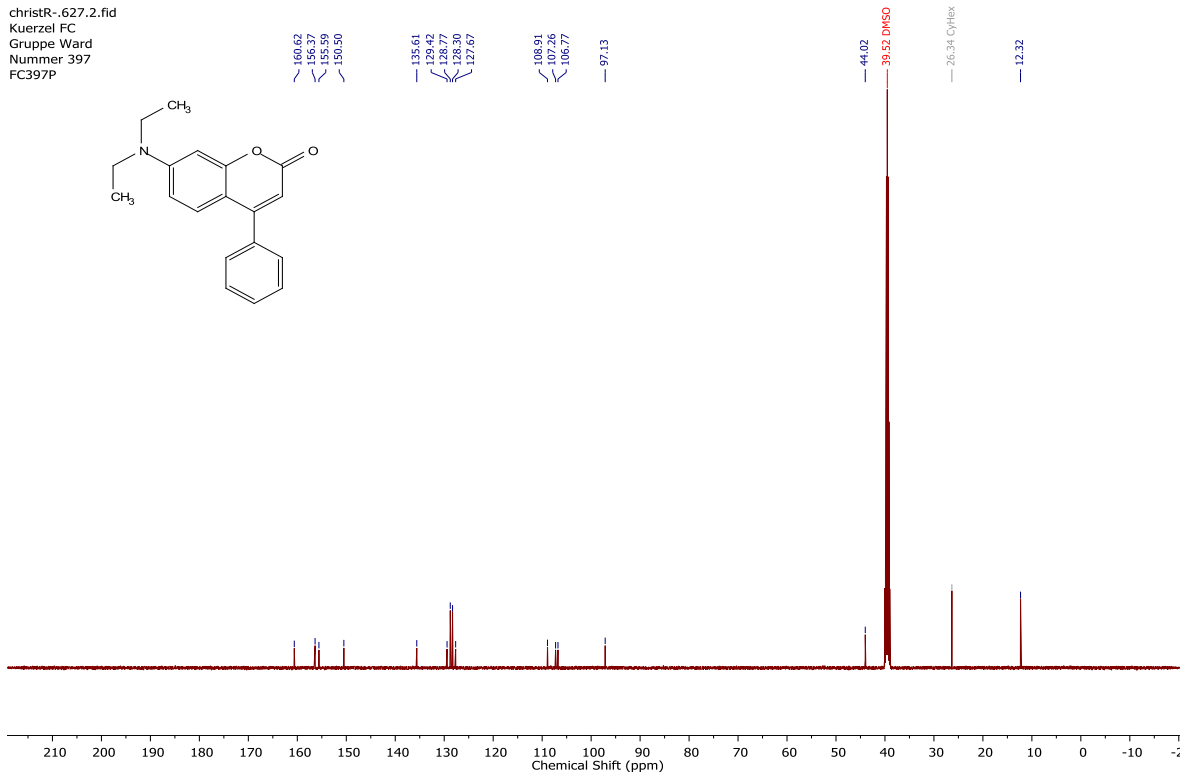
### Spectrum 95 <sup>13</sup>C-NMR spectrum of ester 2 in DMSO-*d*<sub>6</sub>.

christR--627.1.fid  
 Kuerzel FC  
 Gruppe Ward  
 Nummer 397  
 FC397P



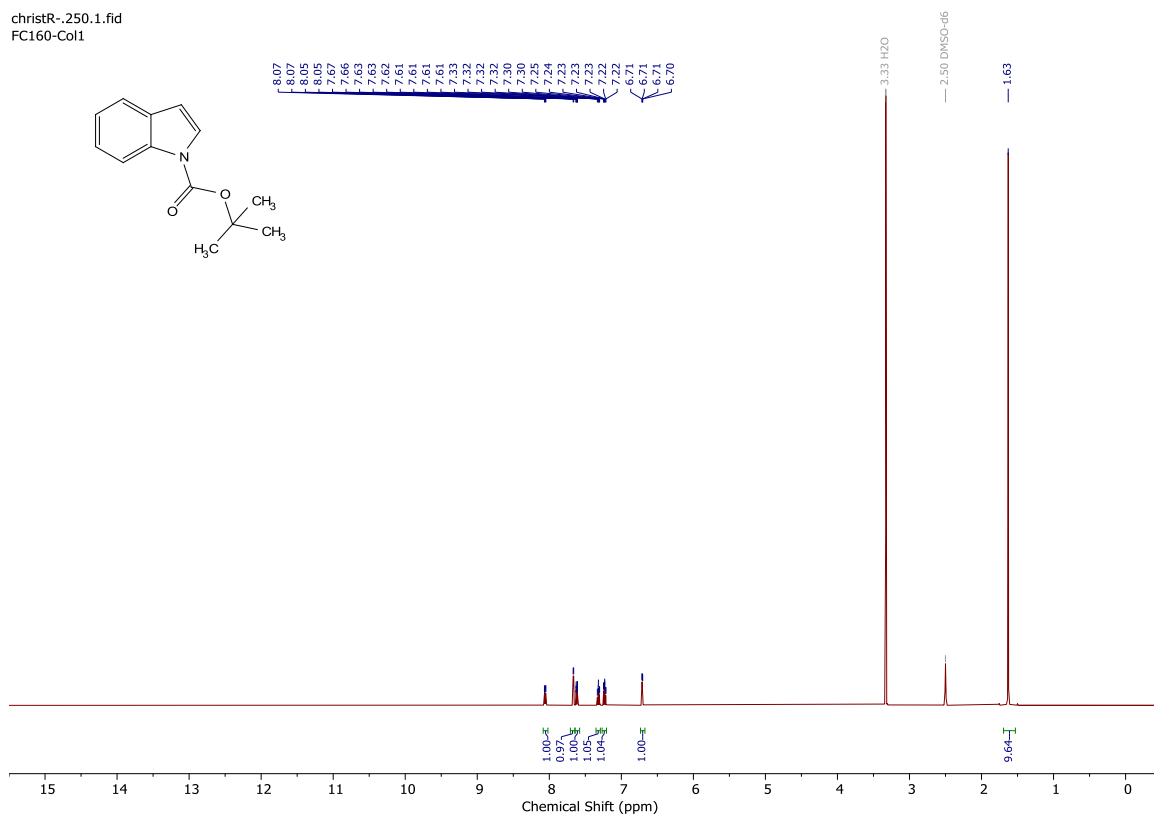
**Spectrum 96** <sup>1</sup>H-NMR spectrum of coumarin 2 in DMSO-d<sub>6</sub>.

christR--627.2.fid  
 Kuerzel FC  
 Gruppe Ward  
 Nummer 397  
 FC397P

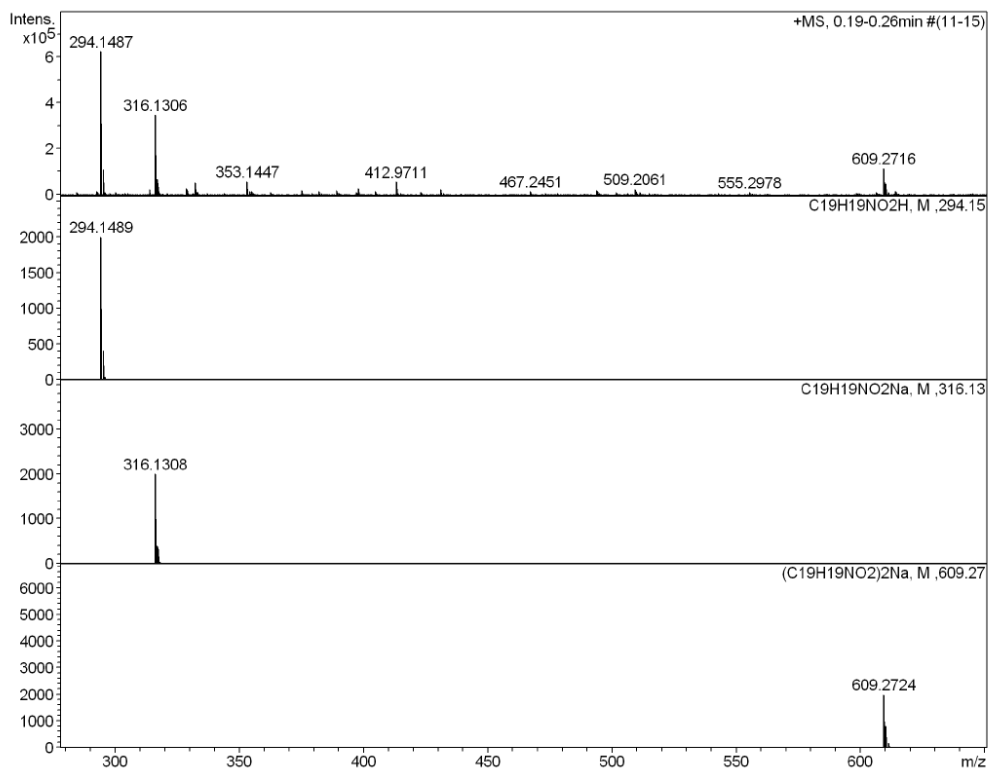


**Spectrum 97** <sup>13</sup>C-NMR spectrum of coumarin 2 in DMSO-d<sub>6</sub>.

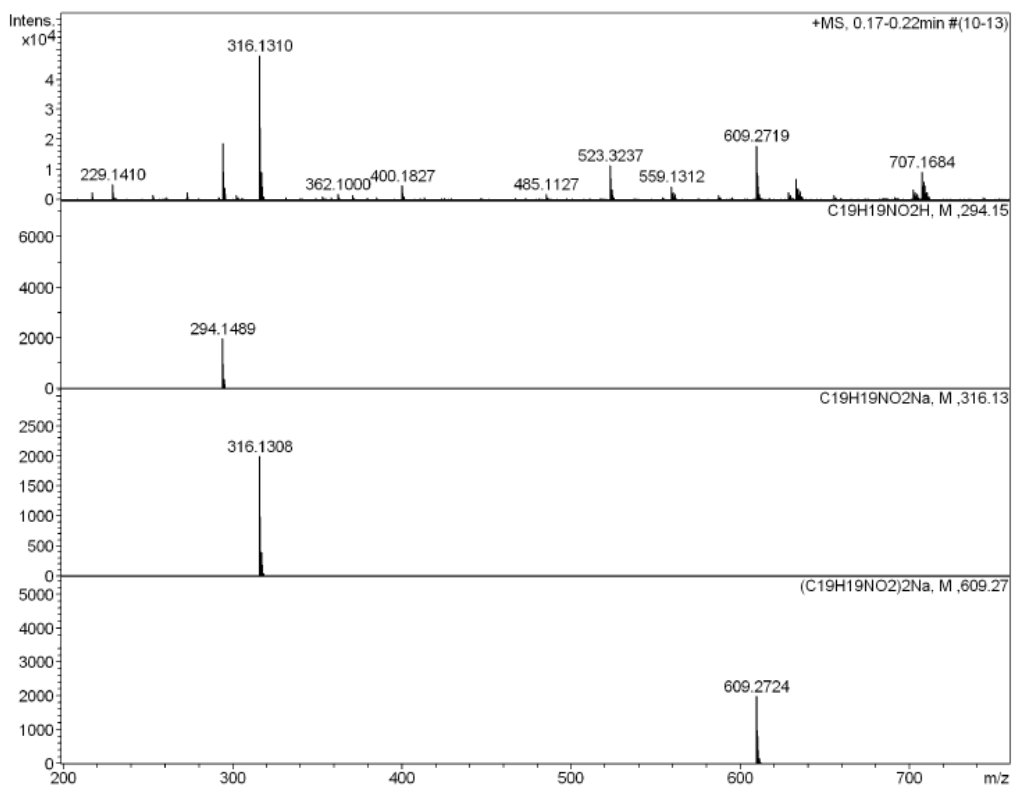
christR-.250.1.fid  
FC160-Col1



**Spectrum 98** <sup>1</sup>H-NMR spectrum of indole **7** in DMSO-*d*<sub>6</sub>.

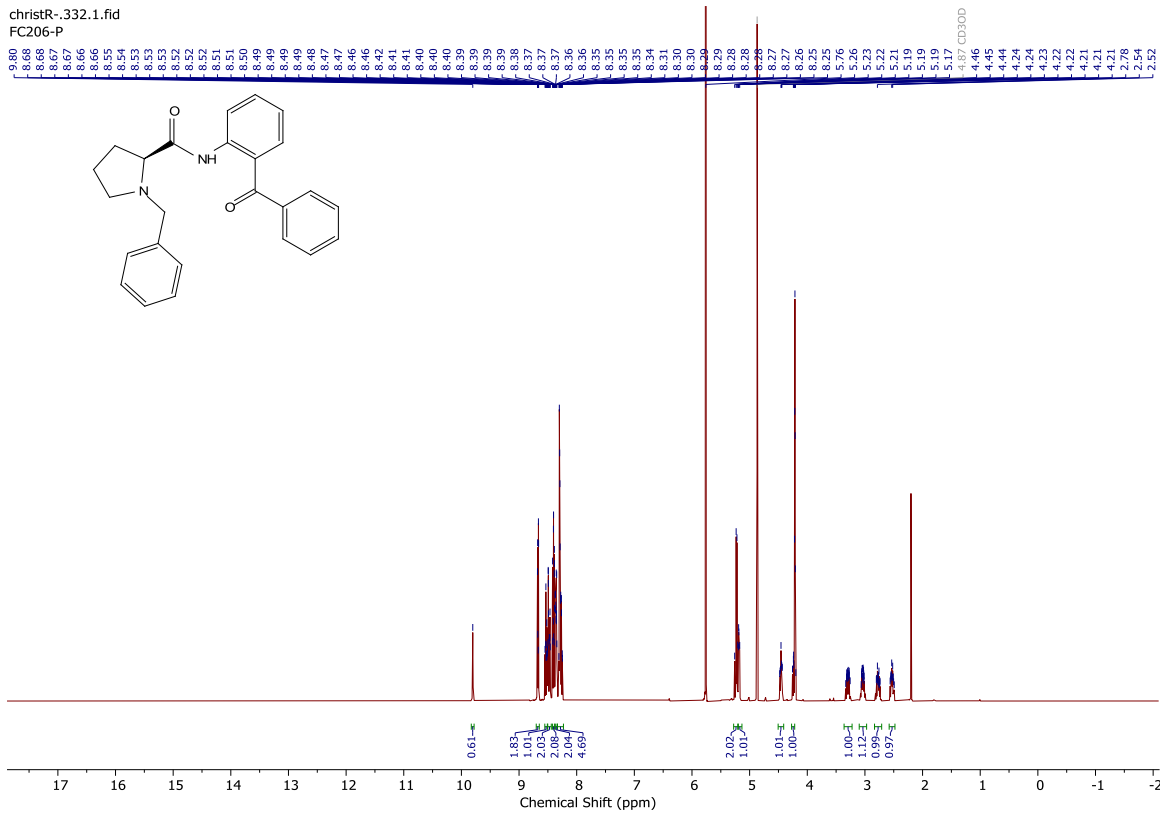


**Spectrum 99** HR-MS Spectrum of ester 1.

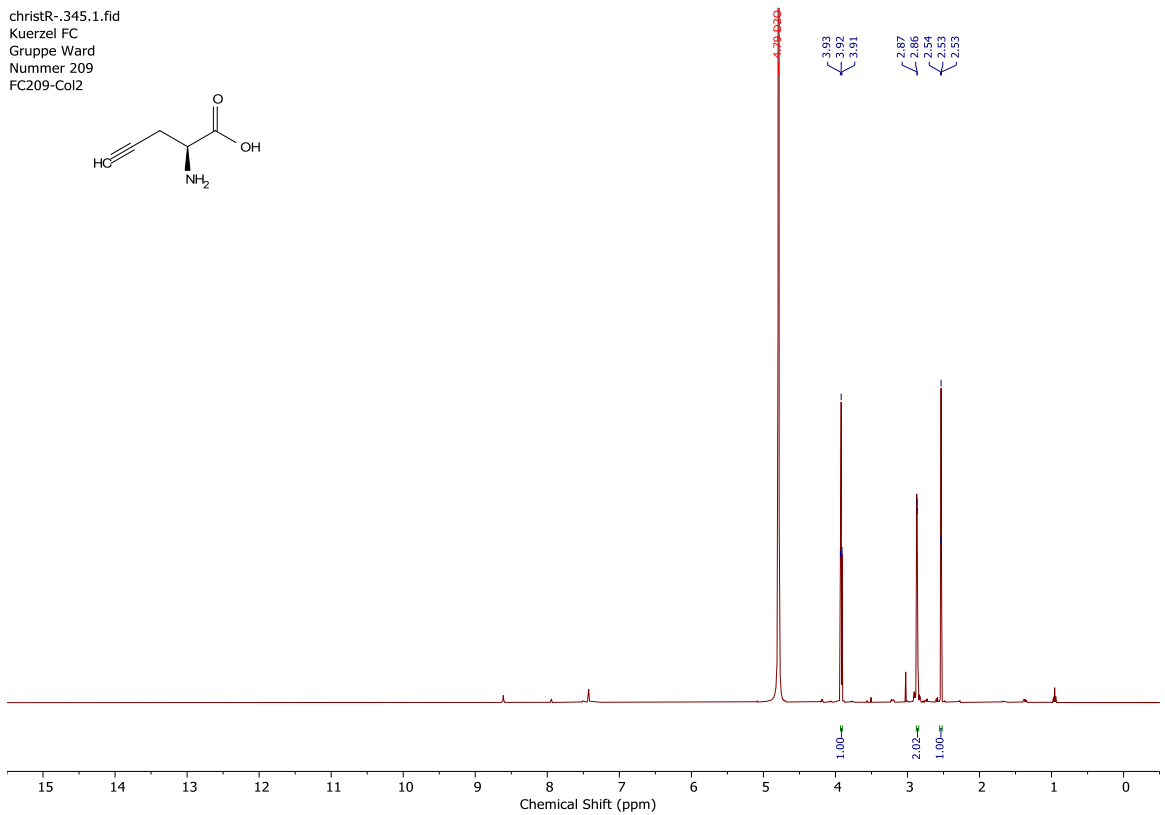


**Spectrum 100** HR-MS Spectrum of coumarin 2.





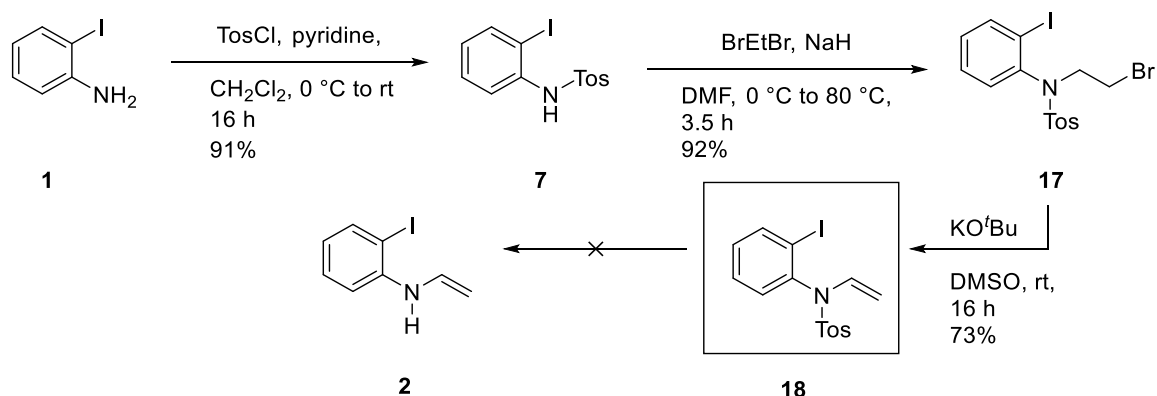
**Spectrum 101**  $^1\text{H-NMR}$  spectrum of amide **13** in MeOD.



**Spectrum 102**  $^1\text{H-NMR}$  spectrum of substrate **9** in  $\text{D}_2\text{O}$ .

## 8.4 Chapter 3: Palladium-based ArMs

### Substrate Synthesis



Tosyl amine **7**: Under inert atmosphere, a schlenk flask was charged with 2-Iodoaniline **1** (2.2 g, 10 mmol, 1 eq) and dry CH<sub>2</sub>Cl<sub>2</sub> (15 mL). The solution was cooled (0 °C) before adding TosCl (2.1 g, 10.9 mmol, 1.09 eq) and pyridine (24 mL, 30 mmol, 30 eq). After addition, the mixture was stirred (rt, colour change green, yellow then grey) and monitored by TLC. After consumption of the starting material, ethylenediamine (60 mg, 1.0 mmol, 0.1 eq) was added to quench the remaining TosCl. The mixture was stirred (rt, 2 h) before the addition of aq. HCl (10 mL, 0.1 M). The crude was extracted with CH<sub>2</sub>Cl<sub>2</sub> (3x20 mL), washed with brine (10 mL) and dried over MgSO<sub>4</sub>. The solvent was removed *in vacuo*. The crude was purified via flash column chromatography (20% EtOAc/cyclohexane) to yield the product as a slight yellow oil. Recrystallization (5% EtOAc/cyclohexane) gave the product as white crystals (3.4 g, 9.1 mmol, 91%). The mother liquor can be treated with drops of pentane to provoke further precipitation of the product. As an alternative, Kugelrohr distillation can be used (210 °C at 0.2 mbar). Spectra in agreement with literature data.<sup>221</sup>

<sup>1</sup>H NMR (500 MHz, DMSO-*d*<sub>6</sub>) δ 9.66 (s, 1H), 7.82 (dd, *J* = 7.9, 1.5 Hz, 1H), 7.63 – 7.55 (m, 2H), 7.37 (d, *J* = 8.0 Hz, 2H), 7.29 (td, *J* = 7.7, 1.5 Hz, 1H), 6.99 (dd, *J* = 8.0, 1.6 Hz, 1H), 6.96 (td, *J* = 7.6, 1.6 Hz, 1H), 2.38 (s, 3H).

Tosyl amine **17**: A dried Schlenk flask was charged with NaH (43 mg, 1.1 mmol, 60%, 2 eq) and dry DMF (3 mL) and cooled (0 °C). The amine **7** (200 mg, 0.53 mmol, 1 eq) in dry DMF (3 mL) was slowly added to the NaH-solution. The mixture was stirred (1 h, rt) before the addition dibromoethane (503 mg, 2.7 mmol, 5 eq). The mixture was heated (3.5 h, 80 °C). Reaction control via HPLC-MS revealed partial conversion. Thus, more NaH (43 mg, 1.1 mmol, 60%, 2 eq) and dibromoethane (503 mg, 2.7 mmol, 5 eq) were added and the mixture was heated again (3.5 h, 80 °C). After full conversion, the mixture was cooled (0 °C) and quenched by the slow addition of aq. NH<sub>4</sub>Cl (10 mL). The crude was extracted with EtOAc (3x50 mL), washed over brine (15 mL), dried over NaSO<sub>4</sub> and concentrated *in vacuo*.

Purification via flash column chromatography (10% EtOAc/cyclohexane) yielded the product as a colourless oil (237 mg, 0.49 mmol, 92%).

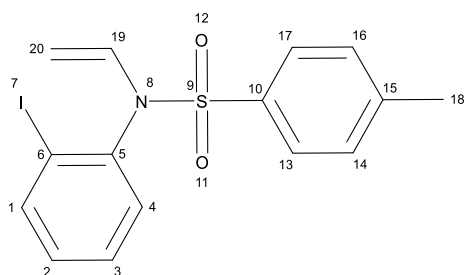
$^1\text{H}$  NMR (500 MHz,  $\text{DMSO-}d_6$ )  $\delta$  7.96 (dd,  $J = 7.9, 1.5$  Hz, 1H), 7.63 – 7.55 (m, 2H), 7.46 – 7.42 (m, 2H), 7.40 (td,  $J = 7.6, 1.5$  Hz, 1H), 7.15 (td,  $J = 7.6, 1.6$  Hz, 1H), 7.00 (dd,  $J = 7.9, 1.6$  Hz, 1H), 3.95 (ddd,  $J = 14.3, 8.3, 5.8$  Hz, 1H), 3.84 (ddd,  $J = 14.6, 8.1, 6.1$  Hz, 1H), 3.53 (ddd,  $J = 10.1, 8.1, 5.8$  Hz, 1H), 3.38 (ddd,  $J = 10.1, 8.3, 6.1$  Hz, 1H), 2.42 (s, 3H).

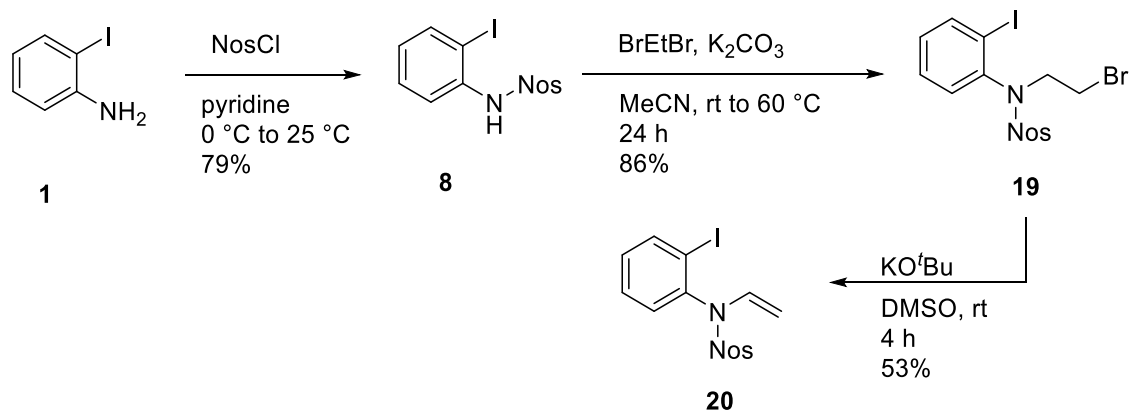
Tosy-vinyl amine **18**: To a solution of amine **17** (101 mg, 0.21 mmol, 1 eq) in dry DMSO (5 mL) was added tBuOK (31 mg, 0.28 mmol, 1.33 eq). The mixture was stirred (rt, colour change green to yellow then red). The reaction progress (every 30 min) was monitored via HPLC-MS. After full consumption of the substrate (2 h) the reaction was quenched with water (5 mL, 0 °C), extracted with EtOAc (3x5mL), washed with cold brine (3x1.5 mL) and dried over  $\text{NaSO}_4$ . The crude was concentrated *in vacuo* (<30 °C). Purification via flash column chromatography (10% EtOAc/cyclohexane) yielded the product as a white solid (61 mg, 0.15 mmol, 73%).

$^1\text{H}$  NMR (500 MHz,  $\text{DMSO-}d_6$ )  $\delta$  = 8.04 (dd,  $J=7.9, 1.5$ , 1H, C1H), 7.69 – 7.64 (m, 2H, C13H, C17H), 7.50 – 7.46 (m, 2H, C14H, C16H), 7.42 (td,  $J=7.6, 1.5$ , 1H, C2H), 7.21 (td,  $J=7.6, 1.6$ , 1H, C3H), 7.15 (dd,  $J=15.3, 8.8$ , 1H, C19H), 6.61 (dd,  $J=7.8, 1.5$ , 1H, C4H), 4.34 (dd,  $J=8.8, 1.0$ , 1H, C20H), 3.52 (dd,  $J=15.3, 1.0$ , 1H, C20H), 2.43 (s, 3H, C18H<sub>3</sub>).

$^{13}\text{C}$  NMR (126 MHz,  $\text{DMSO-}d_6$ )  $\delta$  = 144.42 (C10), 140.51 (C1), 138.14 (C6), 135.81 (C15), 133.46 (C19), 131.04 (C3), 130.13 (C14/C16), 129.64 (C4), 129.62 (C2), 127.24 (C13/C17), 102.90 (C5), 94.79 (C20), 21.10 (C18).

HR-MS (ESI, pos):  $m/z$  calcd. for  $\text{C}_{15}\text{H}_{14}\text{INO}_2\text{SH}^+$  399.9863 found 399.9862  $[\text{M}+\text{H}^+]^+$ ;  $m/z$  calcd. for  $\text{C}_{15}\text{H}_{14}\text{INO}_2\text{SNa}^+$  421.9682 found 421.9681  $[\text{M}+\text{Na}^+]^+$ ;





Nosyl amine **8**: To a cold solution (0 °C) of 2-iodoaniline **1** (241 mg, 1.1 mmol, 1.1 eq) in pyridine (15 mL) was added nosyl chloride (222 mg, 1 mmol, 1 eq). The mixture was stirred (3 h, 0-25 °C) before pyridine was removed *in vacuo*. The reaction mixture was poured into water and the crude was extracted with CH<sub>2</sub>Cl<sub>2</sub> (3x25 mL), dried over MgSO<sub>4</sub>, and concentrated *in vacuo*. Purification by column chromatography (15% EtOAc/cyclohexane) yielded nosyl-amine **8** as a pale yellow solid (321 mg, 0.79 mmol, 79%). Spectra in agreement with literature data.<sup>221</sup>

<sup>1</sup>H NMR (500 MHz, DMSO-*d*<sub>6</sub>) δ 10.27 (s, 1H), 8.46 – 8.35 (m, 2H), 7.96 – 7.90 (m, 2H), 7.87 – 7.81 (m, 1H), 7.38 – 7.28 (m, 1H), 7.07 – 6.98 (m, 2H).

Nosyl amine **19**: In a sealed tube, amine **8** (243 mg, 0.6 mmol, 1 eq) and K<sub>2</sub>CO<sub>3</sub> (249 mg, 1.8 mmol, 3 eq) were dried and diluted with dry acetonitrile (2 mL). The mixture was heated (1 h, 50 °C) before adding dibromoethane (451 mg, 2.4 mmol, 4 eq) under continued stirring (2 h, 50 °C). No full conversion was observed (HPLC-MS), thus more dibromoethane (1127 mg, 6 mmol, 10 eq) and K<sub>2</sub>CO<sub>3</sub> (415 mg, 3 mmol, 5 eq) were added and the mixture was heated again (24 h, 60 °C). The mixture was quenched with brine (20 mL), extracted with EtOAc (3x40 mL) and dried over NaSO<sub>4</sub>. Purification via flash column chromatography (15% EtOAc/cyclohexane) yielded amine **19** as a pale yellow solid (264 mg, 0.52 mmol, 86%).

<sup>1</sup>H NMR (500 MHz, DMSO-*d*<sub>6</sub>) δ 8.47 – 8.37 (m, 2H), 7.99 – 7.93 (m, 3H), 7.44 (td, *J* = 7.7, 1.5 Hz, 1H), 7.21 – 7.12 (m, 2H), 4.08 – 3.91 (m, 2H), 3.57 (ddd, *J* = 10.3, 7.5, 5.6 Hz, 1H), 3.39 (dt, *J* = 10.2, 7.2 Hz, 1H).

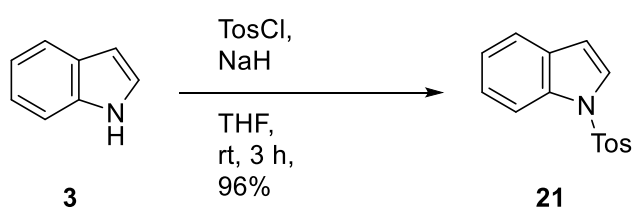
<sup>13</sup>C NMR (126 MHz, DMSO-*d*<sub>6</sub>) δ 150.15, 144.12, 140.47, 139.74, 131.70, 130.90, 129.37, 129.29, 124.80, 102.26, 52.62, 29.69.

Nosy-vinyl amine **20**: To a solution of amine **19** (102 mg, 0.2 mmol, 1 eq) in dry DMSO (5 mL) was added *t*BuOK (30 mg, 0.27 mmol, 1.33 eq). The mixture was stirred (rt, colour change green to yellow then red). The reaction progress (every 30 min) was monitored via HPLC-MS. After full consumption of the substrate (2 h) the reaction was quenched with water (5 mL, 0 °C),

extracted with EtOAc (3x5mL), washed with cold brine (3x1.5 mL) and dried over NaSO<sub>4</sub>. The crude was concentrated *in vacuo* (<30 °C). Purification via flash column chromatography (10% EtOAc/cyclohexane) yielded the product as a white solid (46 mg, 0.107 mmol, 54%).

<sup>1</sup>H NMR (500 MHz, DMSO-*d*<sub>6</sub>) δ 8.51 – 8.41 (m, 2H), 8.10 – 8.01 (m, 3H), 7.43 (td, *J* = 7.7, 1.5 Hz, 1H), 7.26 – 7.18 (m, 2H), 6.73 (dd, *J* = 7.8, 1.6 Hz, 1H), 4.44 (dd, *J* = 8.8, 1.2 Hz, 1H), 3.61 (dd, *J* = 15.3, 1.2 Hz, 1H).

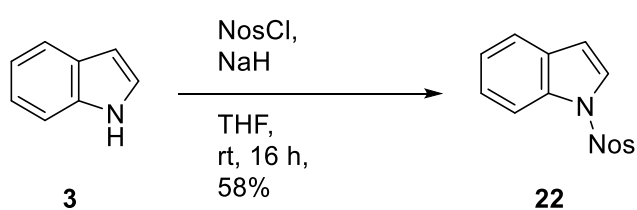
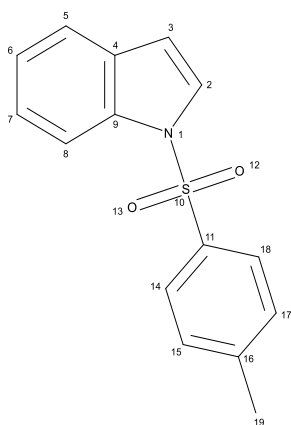
<sup>13</sup>C NMR (126 MHz, DMSO-*d*<sub>6</sub>) δ 150.37, 143.74, 140.70, 137.51, 132.94, 131.36, 130.19, 129.90, 128.88, 125.10, 102.48, 96.25.



Tosyl-indole **21** was prepared according to a modified procedure of Gagnon and co-workers.<sup>222</sup> Indole (250 mg, 2.1 mmol, 1 eq) was dissolved in dry THF (15 mL) and slowly added to a ice-cold mixture of sodium hydride (130 mg, 3.2 mmol, 60%) in dry THF (15 mL). The mixture was stirred until no gas formation was observed (ca. 90 min). To the mixture was slowly added tosyl chloride (447 mg, 2.34 mmol, 1.1 eq) in dry THF (5 mL). The mixture was stirred (16 h, rt) before quenching it with aq. NH<sub>4</sub>Cl (20 mL). The product was extracted with EtOAc (3x50 mL), washed with brine (20 mL) and dried over MgSO<sub>4</sub>. Purification via flash column chromatography (15% EtOAc/cyclohexane) yielded the product as a white solid (553 mg, 2.04 mmol, 96%).

<sup>1</sup>H NMR (500 MHz, DMSO-*d*<sub>6</sub>) δ = 7.92 (dd, *J*=8.4, 0.9, 1H, C8H), 7.85 (d, *J*=8.4, 2H, C15H/C17H), 7.78 (d, *J*=3.7, 1H, C2H), 7.62 – 7.57 (m, 1H, C5H), 7.38 (d, *J*=8.1, 2H, C14H/C18H), 7.33 (ddd, *J*=8.5, 7.2, 1.3, 1H, C7H), 7.24 (td, *J*=7.6, 1.0, 1H, C6H), 6.83 (dd, *J*=3.6, 0.8, 1H, C3H), 2.31 (s, 3H, C19H<sub>3</sub>).

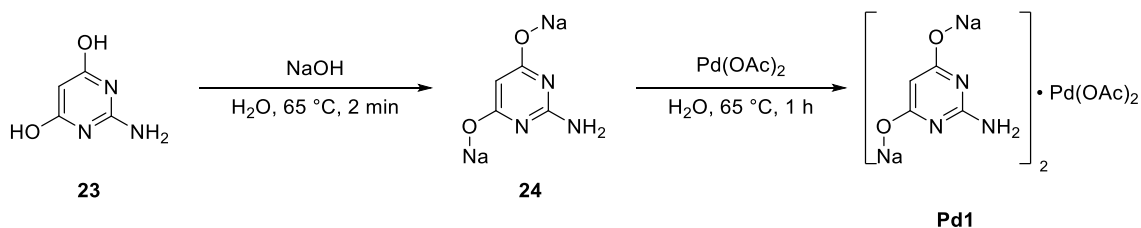
<sup>13</sup>C NMR (126 MHz, DMSO-*d*<sub>6</sub>) δ 145.45 (C16), 134.16 (C11), 134.08 (C9), 130.44 (C4), 130.21 (C14/C18), 126.91 (C2), 126.68 (C15/C17), 124.62 (C7), 123.41 (C6), 121.58 (C5), 113.05 (C8), 109.39 (C3), 21.00 (C19).



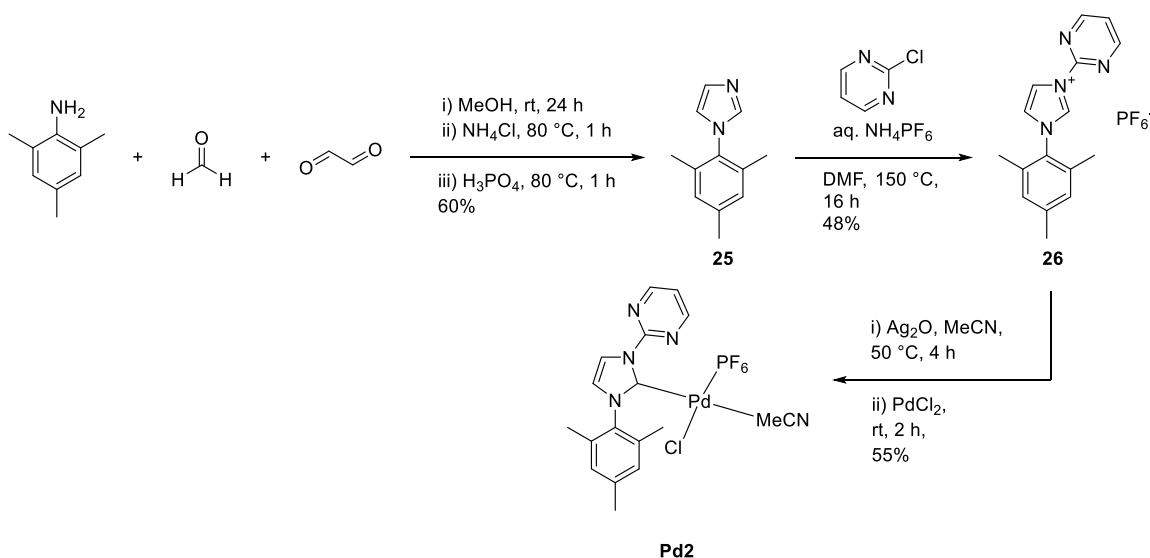
Nos-indole **22** was prepared according to a modified procedure of Carretero and co-workers.<sup>223</sup> Indole (900 mg, 7.68 mmol, 1 eq) was dissolved in dry THF (15 mL) and cooled (0 °C). To the mixture was added sodium hydride (258 mg, 10.8 mmol, 1.4 eq). The mixture was stirred until no gas formation was observed (ca. 90 min). To the mixture was slowly added nosyl chloride (2.38 g, 10.8 mmol, 1.4 eq) in dry THF (5 mL). The mixture was stirred (16 h, rt) before quenching it with aq. NH<sub>4</sub>Cl (20 mL). The product was extracted with EtOAc (3x50 mL), washed with brine (20 mL) and dried over MgSO<sub>4</sub>. Purification via flash column chromatography (15% EtOAc/cyclohexane) yielded the product as a white solid (1.34 g, 4.45 mmol, 58%).

<sup>1</sup>H NMR (500 MHz, DMSO-*d*<sub>6</sub>) δ 8.38 – 8.32 (m, 2H), 8.27 – 8.22 (m, 2H), 7.96 (dq, *J* = 8.4, 0.8 Hz, 1H), 7.86 (d, *J* = 3.7 Hz, 1H), 7.62 (dt, *J* = 7.7, 1.0 Hz, 1H), 7.38 (ddd, *J* = 8.5, 7.3, 1.3 Hz, 1H), 7.28 (ddd, *J* = 8.1, 7.3, 1.0 Hz, 1H), 6.92 (dd, *J* = 3.7, 0.8 Hz, 1H).

## Synthesis of Palladium Complexes



**Pd1** was prepared according to the procedure of Davis and co-workers and following their procedure without further isolation an characterization directly used for the catalysis after colour change of the aqueous mixture.<sup>161</sup>



**Pd2** was prepared according a modified procedure of Wang and co-workers.<sup>159</sup>

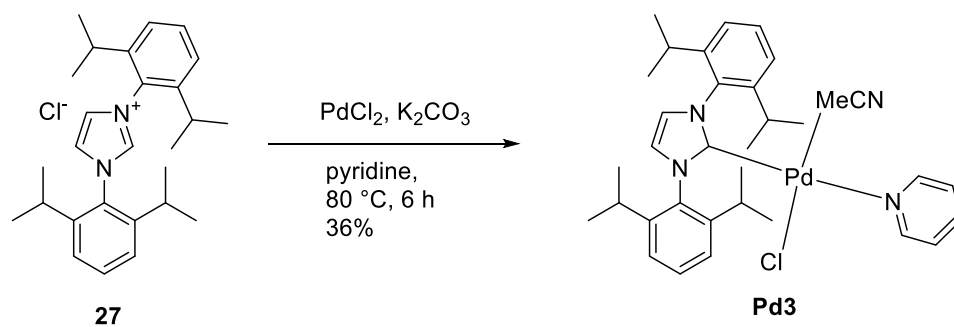
Ligand **26**: Imidazole **25** (93 mg, 0.5 mmol, 1 eq) and 2-chloro pyrimidine (63 mg, 0.55 mmol, 1.1 eq) were mixed in DMF and heated (reflux, 16 h). The cooled mixture was partitioned between EtOAc/brine (1:1, 50 mL). The aqueous phase was extracted with EtOAc (5x10 mL) and the organic solution was discarded. The aqueous phase was then transferred to an erlenmeyer. During vigorous stirring, a saturated solution of  $\text{NH}_4\text{PF}_6$  was added until no more precipitation took place. The mixture was stirred (1 h) before filtration. The filtercake was washed with cold water and extracted with  $\text{CH}_2\text{Cl}_2$  from the filter into a flask. The solvent was removed in vacuo to yield the product **26** as a white solid (63 mg, 0.24 mmol, 48%).

$^1\text{H NMR}$  (500 MHz,  $\text{DMSO-}d_6$ )  $\delta$  10.47 (d,  $J = 1.9$  Hz, 1H), 9.09 (d,  $J = 4.9$  Hz, 2H), 8.78 (d,  $J = 2.0$  Hz, 1H), 8.18 (d,  $J = 2.1$  Hz, 1H), 7.81 (t,  $J = 4.9$  Hz, 1H), 7.18 (s, 2H), 2.35 (s, 3H), 2.11 (s, 6H).

Complex **Pd2**: In a sealed tube, ligand **26** (53 mg, 0.2 mmol, 1 eq) and Ag<sub>2</sub>O (23 mg, 0.1 mmol, 0.5 eq) were dissolved in dry acetonitrile (3 mL) and heated (50 °C, 4 h). After the mixture was cooled to room temperature, [Pd(CH<sub>3</sub>CN)<sub>2</sub>]Cl<sub>2</sub> (53 mg, 0.2 mmol, 1 eq) was added to the solution, and the solution was stirred (rt, 2 h). Afterwards, the mixture was filtered through celite, and all volatiles removed *in vacuo*. The yellow residue was dissolved in dry acetonitrile and recrystallization by slow addition of diethyl ether to yield the product as a yellow solid (65.3 mg, 0.11 mmol, 55%).

<sup>1</sup>H NMR (500 MHz, CD<sub>2</sub>Cl<sub>2</sub>) δ 9.58 (s, 1H), 9.06 (dd, *J* = 5.0, 2.2 Hz, 1H), 8.28 (d, *J* = 5.6 Hz, 1H), 8.12 (s, 1H), 7.69 (d, *J* = 7.7 Hz, 1H), 7.66 – 7.61 (m, 1H), 7.19 (s, 1H), 7.17 – 7.10 (m, 2H), 6.64 (s, 1H), 2.37 (s, 3H), 2.19 (s, 3H), 2.16 (s, 1H), 2.09 (s, 1H), 2.05 (s, 3H), 1.91 (s, 3H).

<sup>19</sup>F NMR (471 MHz, CD<sub>2</sub>Cl<sub>2</sub>) δ -72.45, -73.96.



**Pd3** was prepared according to a modified procedure of Ananikov and co-workers.<sup>224</sup> The azolium salt (0.55 mmol), anhydrous K<sub>2</sub>CO<sub>3</sub> (345 mg, 2.5 mmol), and PdCl<sub>2</sub> (89 mg, 0.5 mmol) were charged in a glass tube. Dry pyridine was added (4 mL), the tube was capped with a screw cap, and the mixture was heated with vigorous stirring for 16 h at 80 °C. After it was cooled to 20 °C, the reaction mixture was diluted with CH<sub>2</sub>Cl<sub>2</sub> (5 mL) and passed through a short pad of silica gel with CH<sub>2</sub>Cl<sub>2</sub> as eluent until the product was completely recovered. The solvent was removed under vacuum (rotary evaporator) at room temperature. The residue that formed was treated with a small volume of hexane (~5 mL); the precipitate that formed was separated by filtration, washed with hexane (5 mL), and dried under vacuum at 20 °C. The crude was purified via flash column chromatography (15% EtOAc/cyclohexane) to give the complex **Pd3** as white solid (96 mg, 0.18 mmol, 36%).

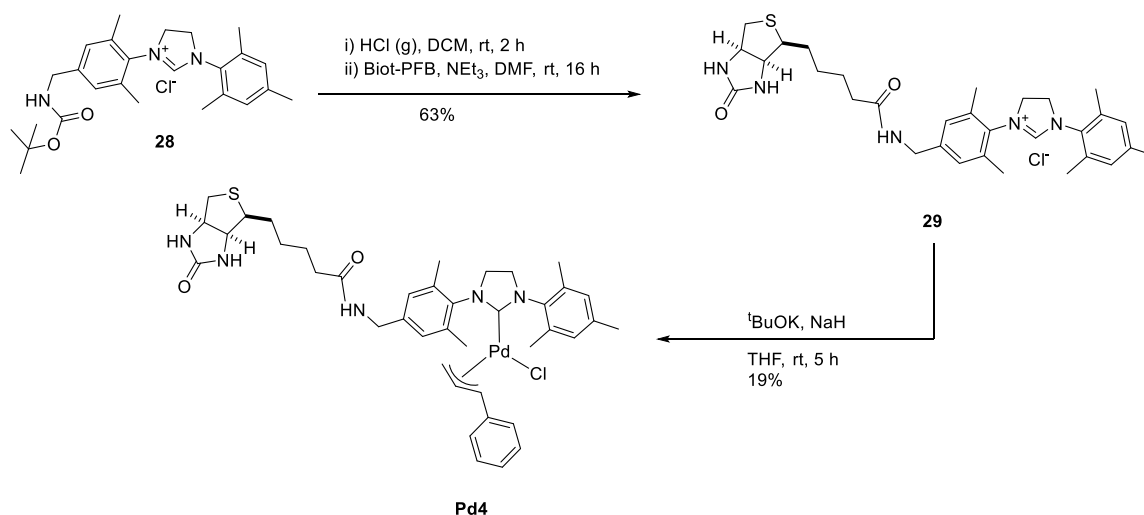
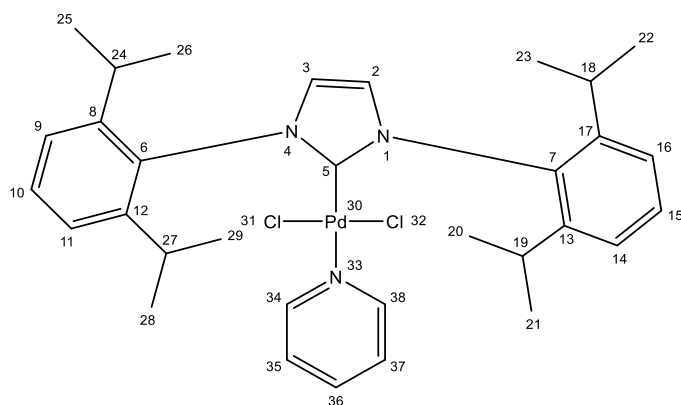
<sup>1</sup>H NMR (500 MHz, CD<sub>2</sub>Cl<sub>2</sub>) δ 8.55 (dt, *J* = 5.0, 1.6 Hz, 2H, C38H), 7.62 (tt, *J* = 7.7, 1.7 Hz, 1H, C36H), 7.51 (t, *J* = 7.8 Hz, 2H, C15H, C10H), 7.37 (d, *J* = 7.8 Hz, 4H, C16H, C14H, C9H, C11H), 7.16 (m, 4H, C37H, C35H, C2H, C3H), 3.16 (p, *J* = 6.7 Hz, 4H, C18H, C19H, C24H,



C27H), 1.45 (d,  $J = 6.6$  Hz, 12H, C22H<sub>3</sub>, C21H<sub>3</sub>, C28H<sub>3</sub>, C25H<sub>3</sub>), 1.11 (d,  $J = 6.9$  Hz, 12H, C23H<sub>3</sub>, C20H<sub>3</sub>, C26H<sub>3</sub>, C29H<sub>3</sub>).

<sup>13</sup>C NMR (126 MHz, CD<sub>2</sub>Cl<sub>2</sub>)  $\delta$  151.79 (C38, C34), 147.44 (C8, C12, C13, C17), 138.22 (C36), 135.88 (C6, C7), 130.55 (C10, C15), 125.79 ( $J = 198, 12.6$  Hz, C2, C3), 124.54 (C35, C37), 124.53 (C9, C11, C14, C16), 29.24 (C18, C19, C24, 27), 26.52 (C20, C23, C26, C29), 23.53 (C21, C22, C25, C28).

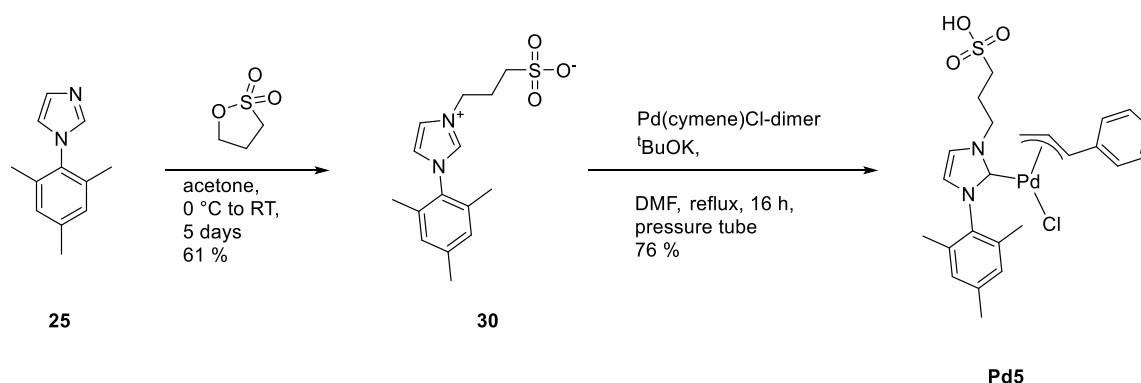
UPLC-MS (ESI, pos)  $m/z$ : 493.28, 534.26, 570.19, 613.23 [M-Pyr-Cl<sup>-</sup>+MeCN]<sup>+</sup>.



The complex **Pd4** was prepared according to the procedure of Ward and co-workers and purified via Pr<sup>ä</sup>pHPLC with additional recrystallization from CH<sub>2</sub>Cl<sub>2</sub>/hexane to yield the product as a white solid (11 mg, 0.014 mmol, 30%).<sup>149</sup> The spectra is difficult to assign but in agreement with literature data. As the catalyst did not prove efficient in catalysis, it was not characterized further.

<sup>1</sup>H NMR (500 MHz, CD<sub>2</sub>Cl<sub>2</sub>)  $\delta$  7.27 – 6.81 (m, 9H), 5.88 (s, 1H), 5.23 (td,  $J = 12.2, 6.8$  Hz, 1H), 4.88 (d,  $J = 7.1$  Hz, 1H), 4.72 (d,  $J = 11.9$  Hz, 1H), 4.52 – 4.40 (m, 2H), 4.33 – 4.13 (m, 1H),

4.06 (t,  $J = 11.1$  Hz, 1H), 3.81 (dd,  $J = 11.3, 6.8$  Hz, 1H), 3.57 (d,  $J = 35.5$  Hz, 1H), 3.28 (s, 1H), 3.13 (t,  $J = 11.9$  Hz, 1H), 2.91 (s, 1H), 2.66 (s, 1H), 2.57 – 2.21 (m, 16H), 2.07 (s, 1H), 1.46 – 1.18 (m, 2H).



Ligand **30**: The ligand was prepared by Dr. Isabel T. Alt according to the procedure of Shaughnessy and co-workers.<sup>163</sup> The spectra are in agreement with literature data.

<sup>1</sup>H NMR (500 MHz, DMSO-*d*<sub>6</sub>)  $\delta$  9.37 (t,  $J = 1.6$  Hz, 1H), 8.11 (t,  $J = 1.8$  Hz, 1H), 7.92 (t,  $J = 1.8$  Hz, 1H), 7.14 (d,  $J = 1.1$  Hz, 2H), 4.42 (t,  $J = 7.0$  Hz, 2H), 2.44 (t,  $J = 7.1$  Hz, 2H), 2.33 (s, 3H), 2.20 (p,  $J = 7.1$  Hz, 2H), 2.02 (s, 6H).

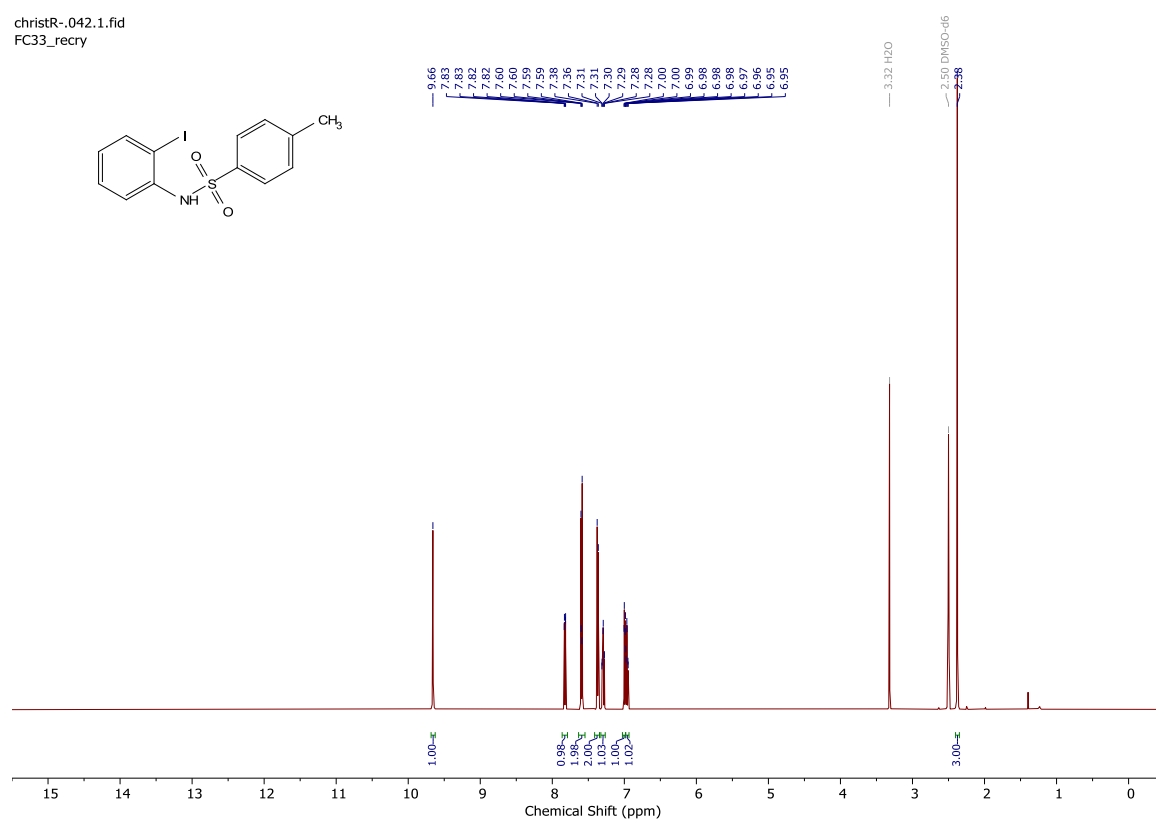
Complex **Pd5**: In a sealed tube, ligand **30** (50 mg, 0.15 mmol, 1 eq), Pd(cymene)Cl-dimer (39 mg, 0.073 mmol, 0.5 eq) and tBuOK (21 mg, 0.19 mmol, 1.3 eq) were dissolved in dry DMF (3 mL). The pressure tube was heated (130 °C, 16 h). After the reaction, the solvent was removed *in vacuo*. EtOAc was added to dissolve the crude. The mixture was filtered and hexane was added to precipitate the product **Pd5** as a white solid (63 mg, 0.11 mmol, 76%).

<sup>1</sup>H NMR (500 MHz, DMSO-*d*<sub>6</sub>)  $\delta$  7.62 (d,  $J = 1.9$  Hz, 1H), 7.38 – 7.29 (m, 3H), 7.26 – 7.15 (m, 3H), 7.03 (s, 2H), 5.60 (q,  $J = 10.4, 9.9$  Hz, 1H), 4.42 (d,  $J = 12.7$  Hz, 1H), 4.35 (t,  $J = 6.9$  Hz, 2H), 2.40 (dd,  $J = 8.9, 6.3$  Hz, 3H), 2.31 (s, 3H), 2.16 (t,  $J = 7.6$  Hz, 3H), 2.04 (s, 6H).

UPLC-MS (ESI, pos) *m/z*: 529.27, 530.27, 530.41, 531.34, 533.40, 535.33 [M-Cl]<sup>+</sup>.

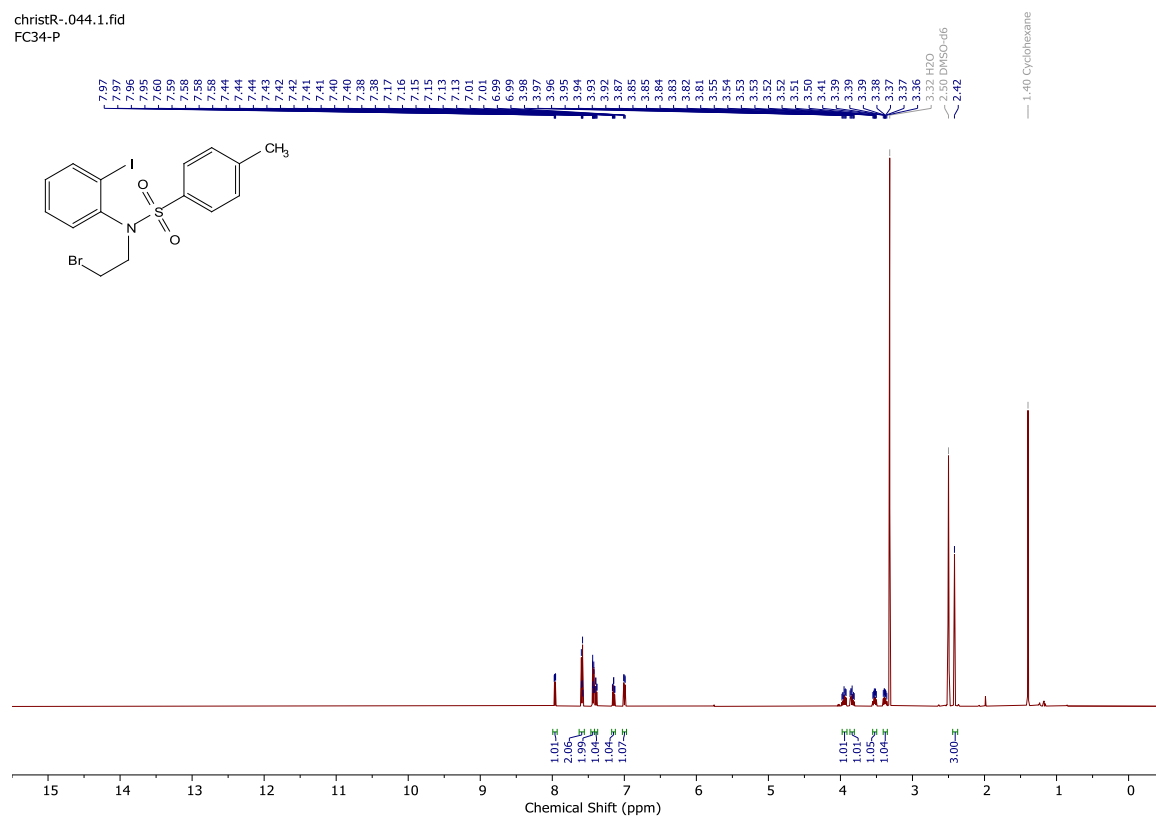
## NMR & Mass Spectra

christR-.042.1.fid  
FC33\_recry



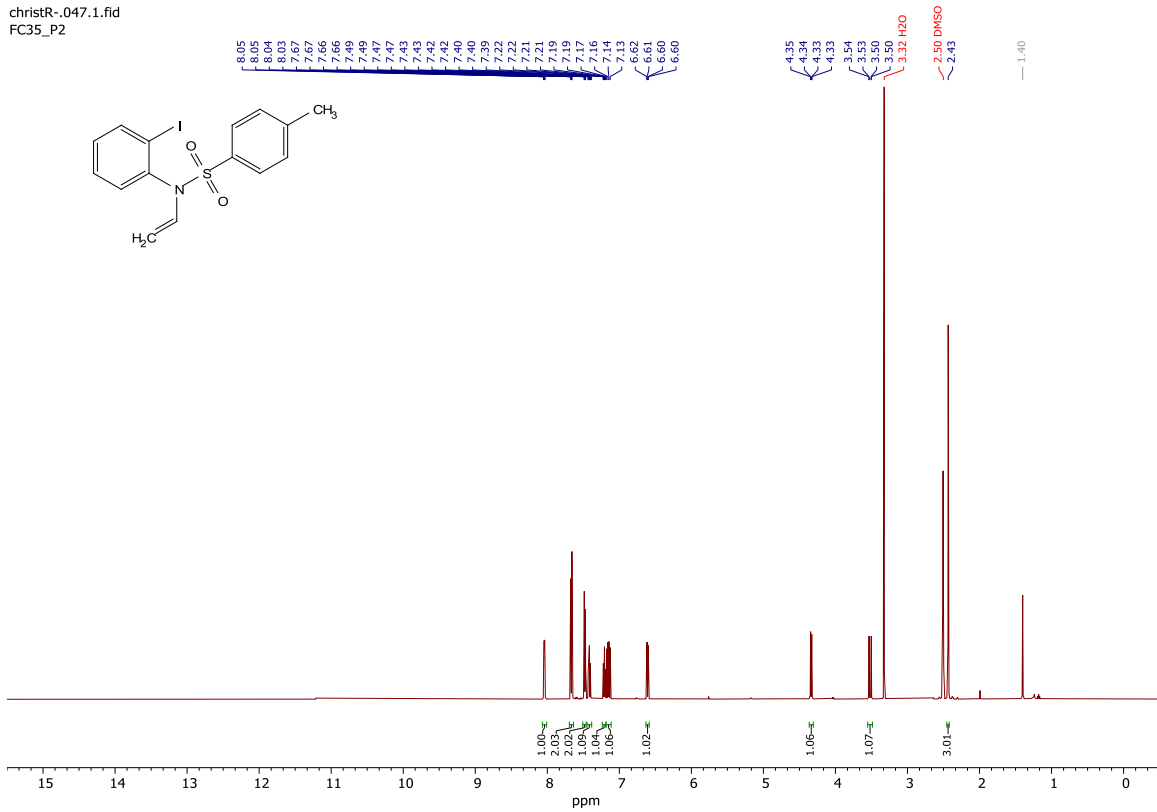
### Spectrum 103 <sup>1</sup>H NMR spectrum of tosy amine **7** in DMSO-*d*<sub>6</sub>.

christR-.044.1.fid  
FC34-P



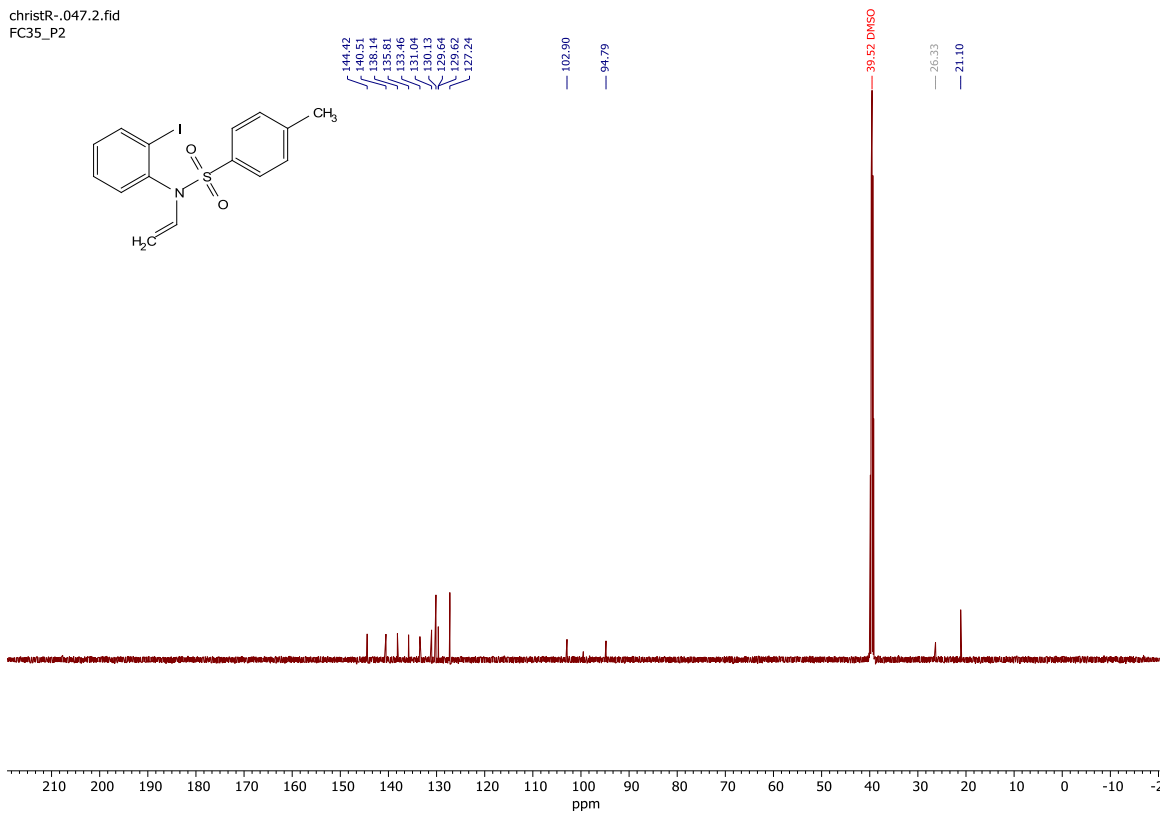
### Spectrum 104 <sup>1</sup>H NMR spectrum of tosy amine **17** in DMSO-*d*<sub>6</sub>.

christR-.047.1.fid  
FC35\_P2



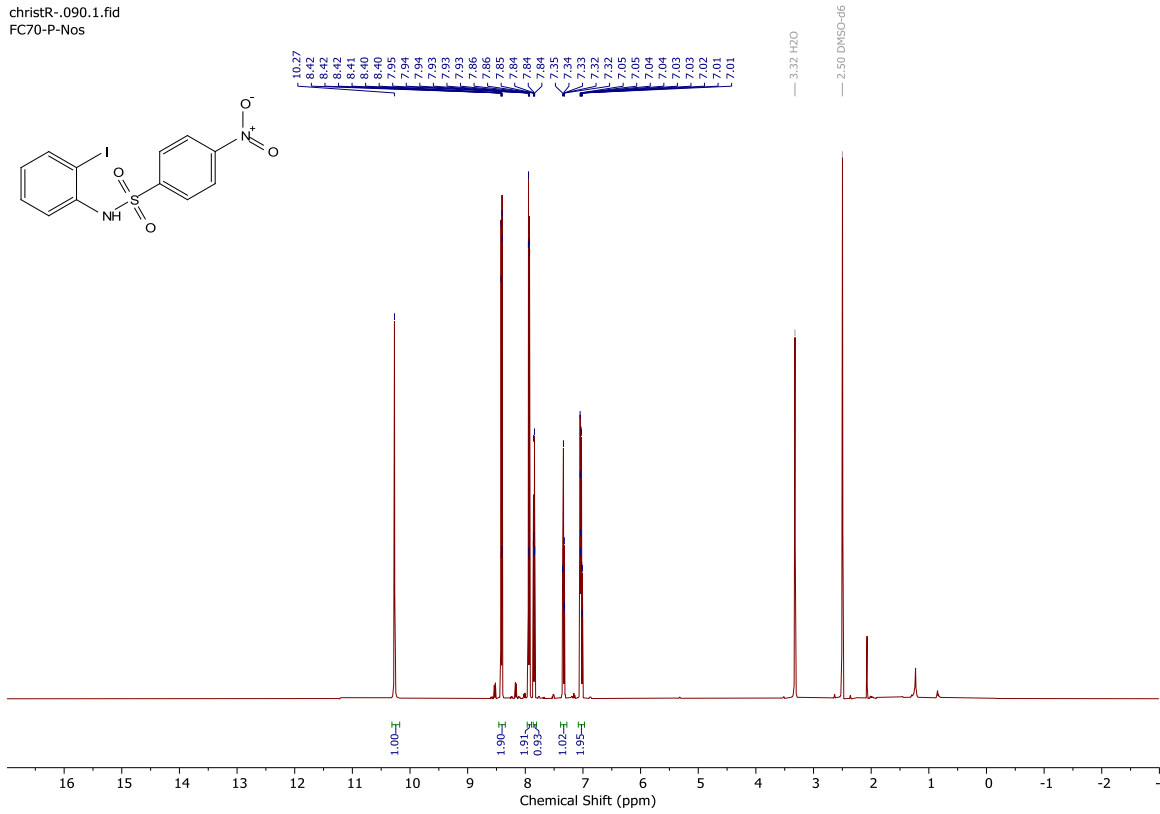
**Spectrum 105**  $^1\text{H}$  NMR spectrum of tosy-vinyl amine **18** in  $\text{DMSO-}d_6$ .

christR-.047.2.fid  
FC35\_P2



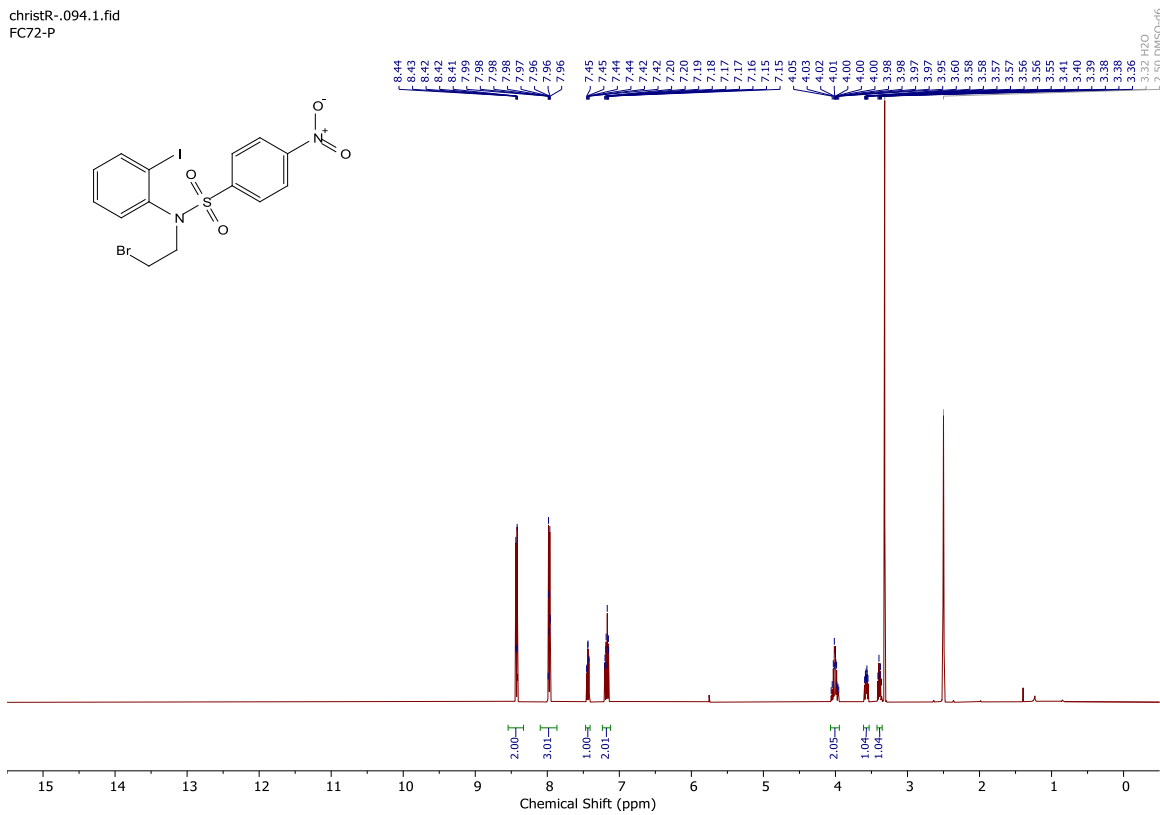
**Spectrum 106**  $^{13}\text{C}$  NMR spectrum of tosy-vinyl amine **18** in  $\text{DMSO-}d_6$ .

christR-.090.1.fid  
FC70-P-Nos



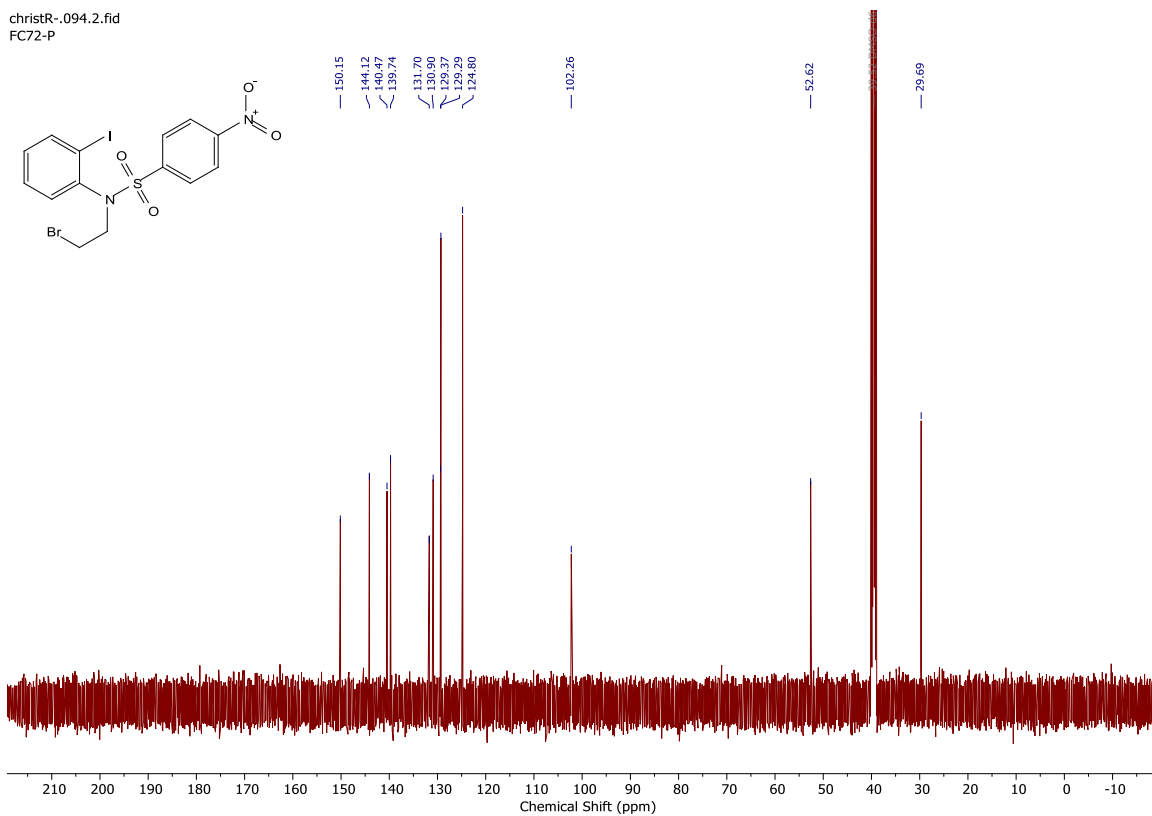
**Spectrum 107**  $^1\text{H}$  NMR spectrum of nosyl amine **8** in  $\text{DMSO-}d_6$ .

christR-.094.1.fid  
FC72-P



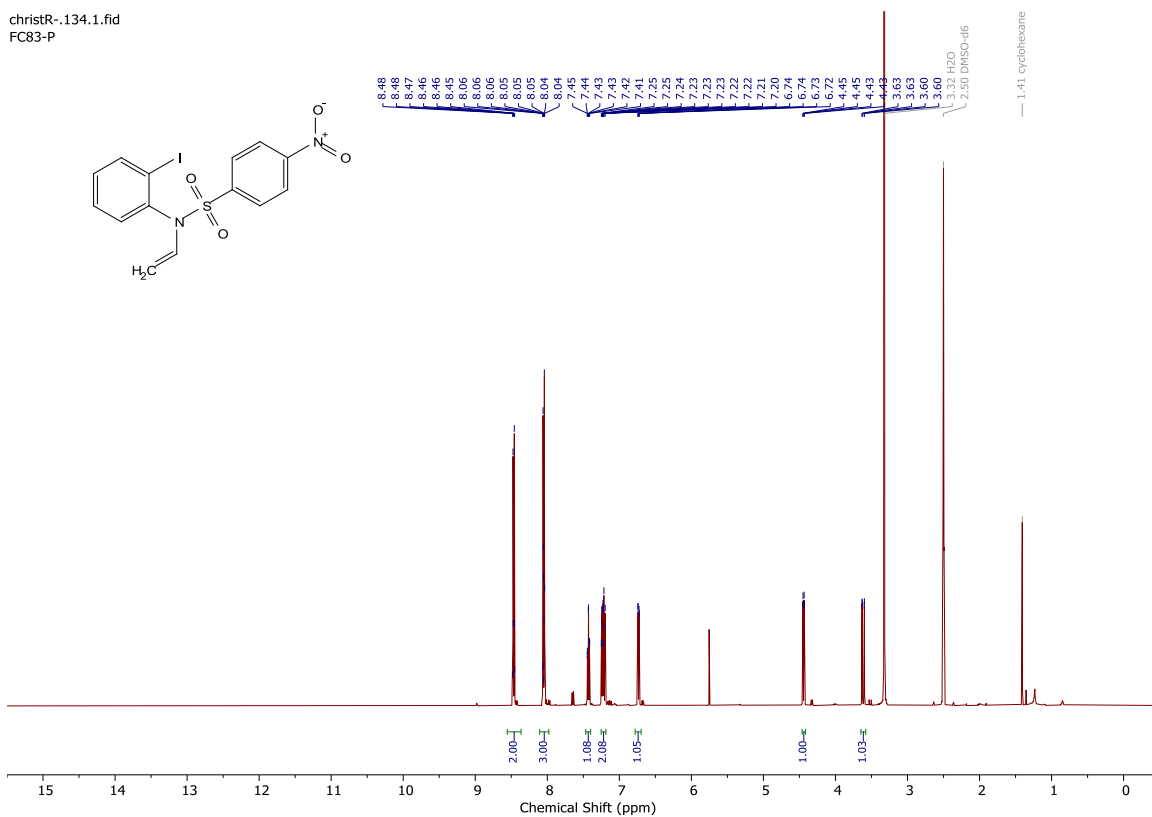
**Spectrum 108**  $^1\text{H}$  NMR spectrum of nosyl amine **19** in  $\text{DMSO-}d_6$ .

christR-.094.2.fid  
FC72-P



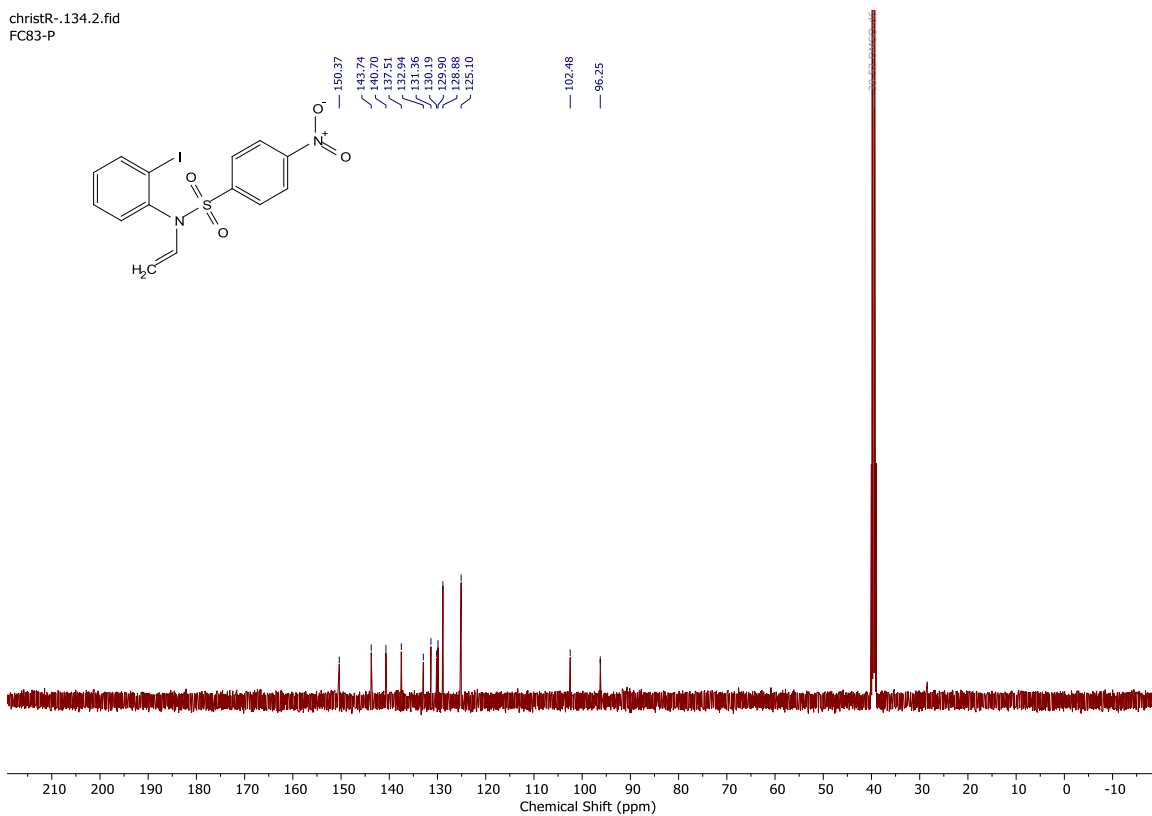
### Spectrum 109 <sup>13</sup>C NMR spectrum of nosyl amine 19 DMSO-*d*<sub>6</sub>.

christR-.134.1.fid  
FC83-P



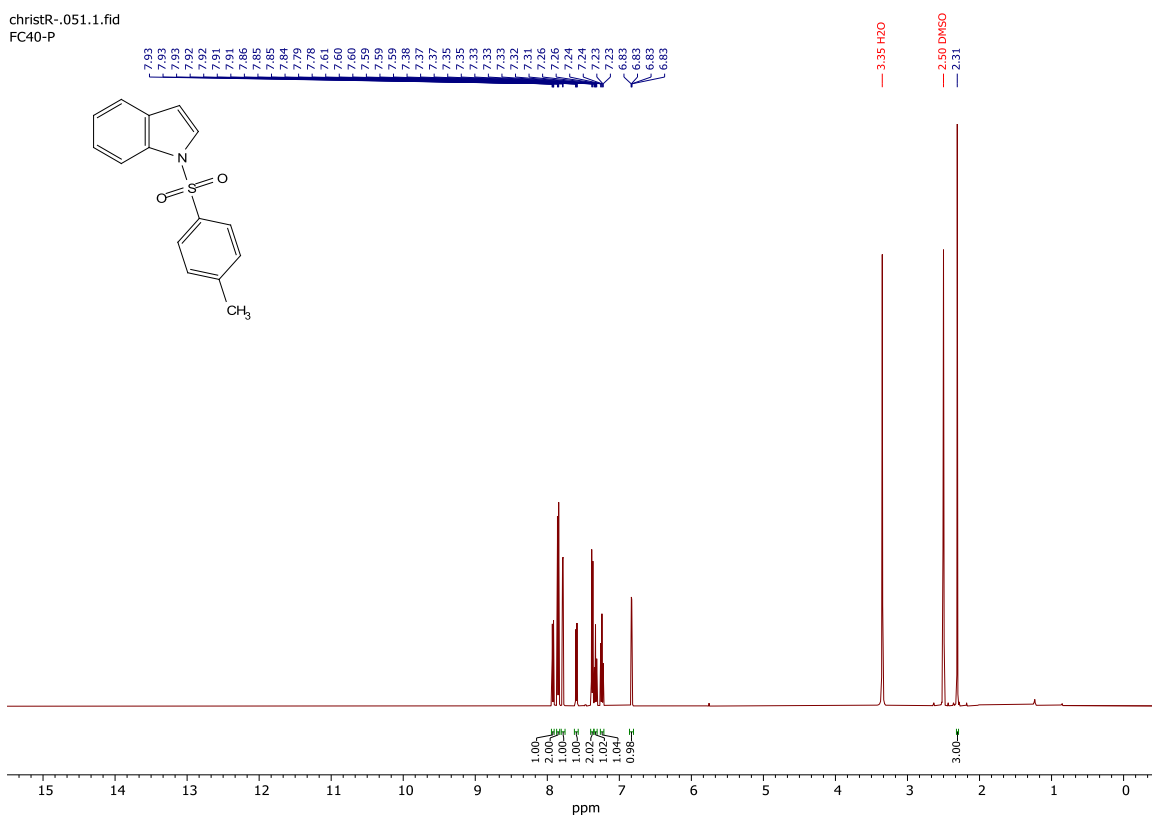
### Spectrum 110 <sup>1</sup>H NMR spectrum of nosyl vinyl amine 20 in DMSO-*d*<sub>6</sub>.

christR-.134.2.fid  
FC83-P



### Spectrum 111 <sup>13</sup>C NMR spectrum of nosyl vinyl amine 20 DMSO-d<sub>6</sub>.

christR-.051.1.fid  
FC40-P

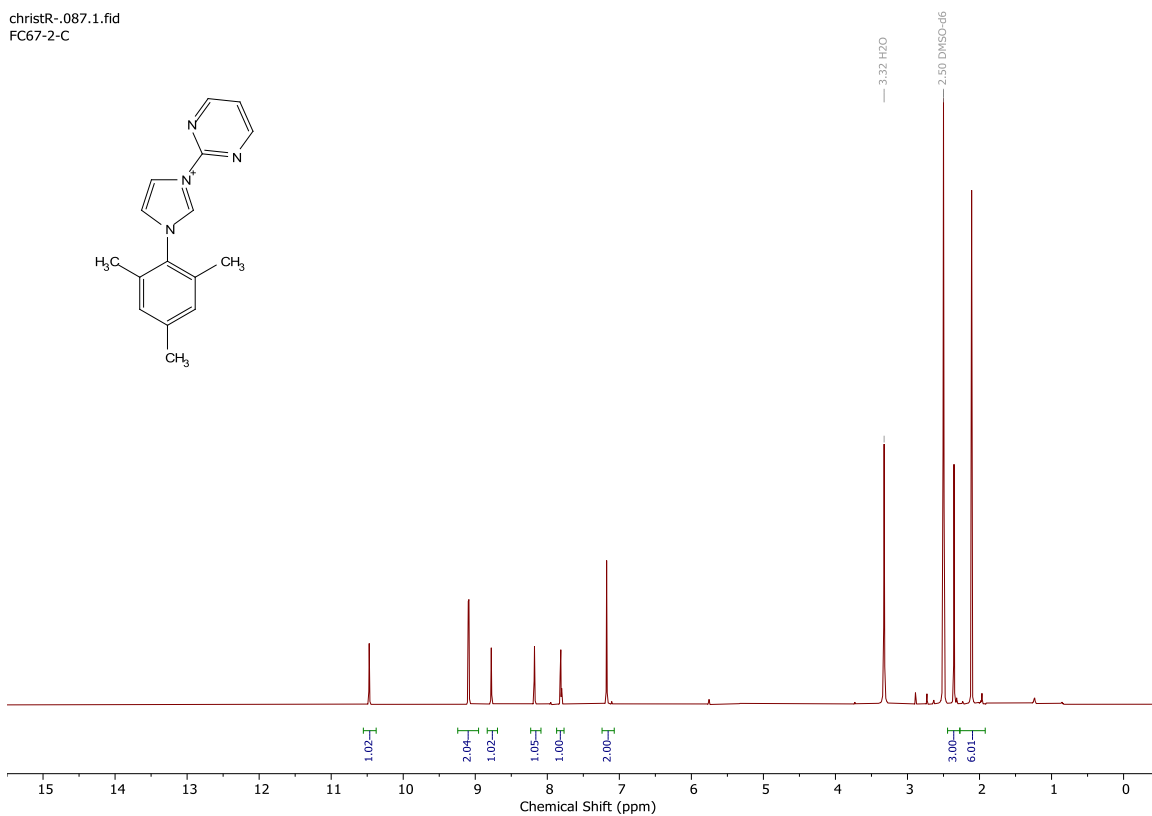


### Spectrum 112 <sup>1</sup>H NMR spectrum of tosyl-indole 21 in DMSO-d<sub>6</sub>.



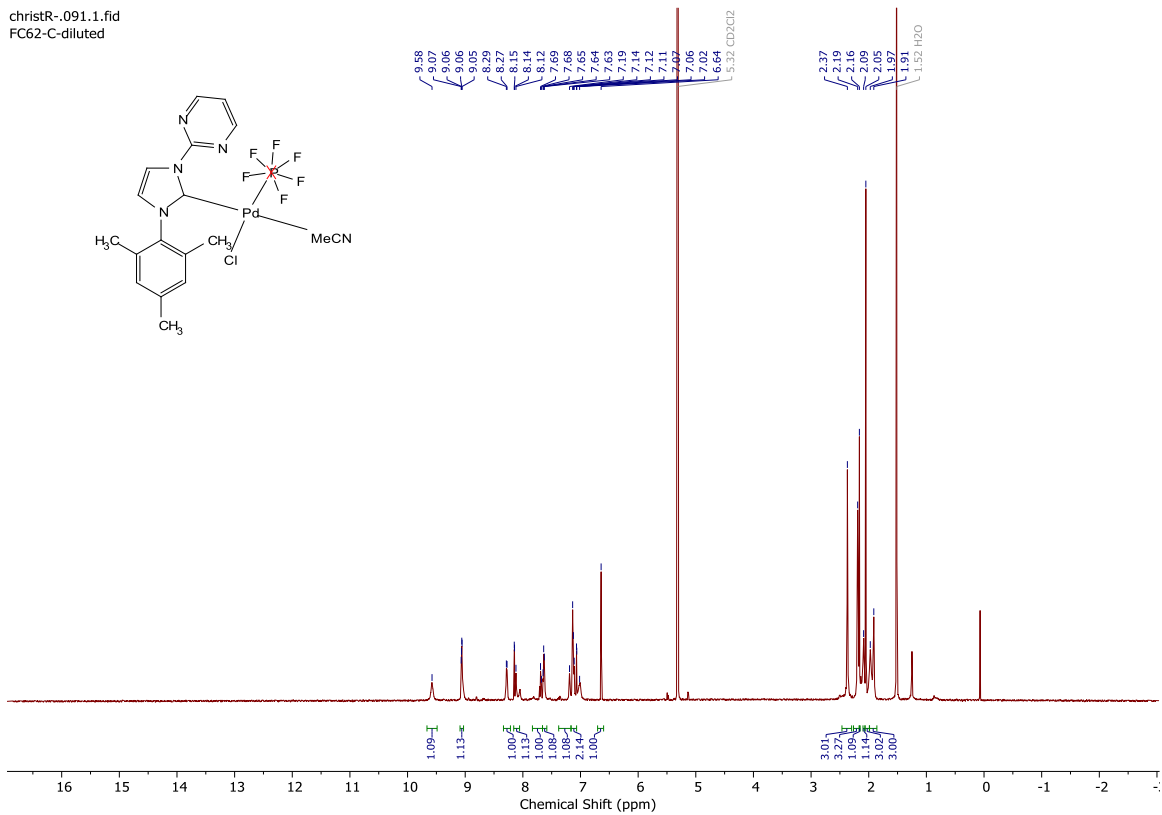


christR-.087.1.fid  
FC67-2-C



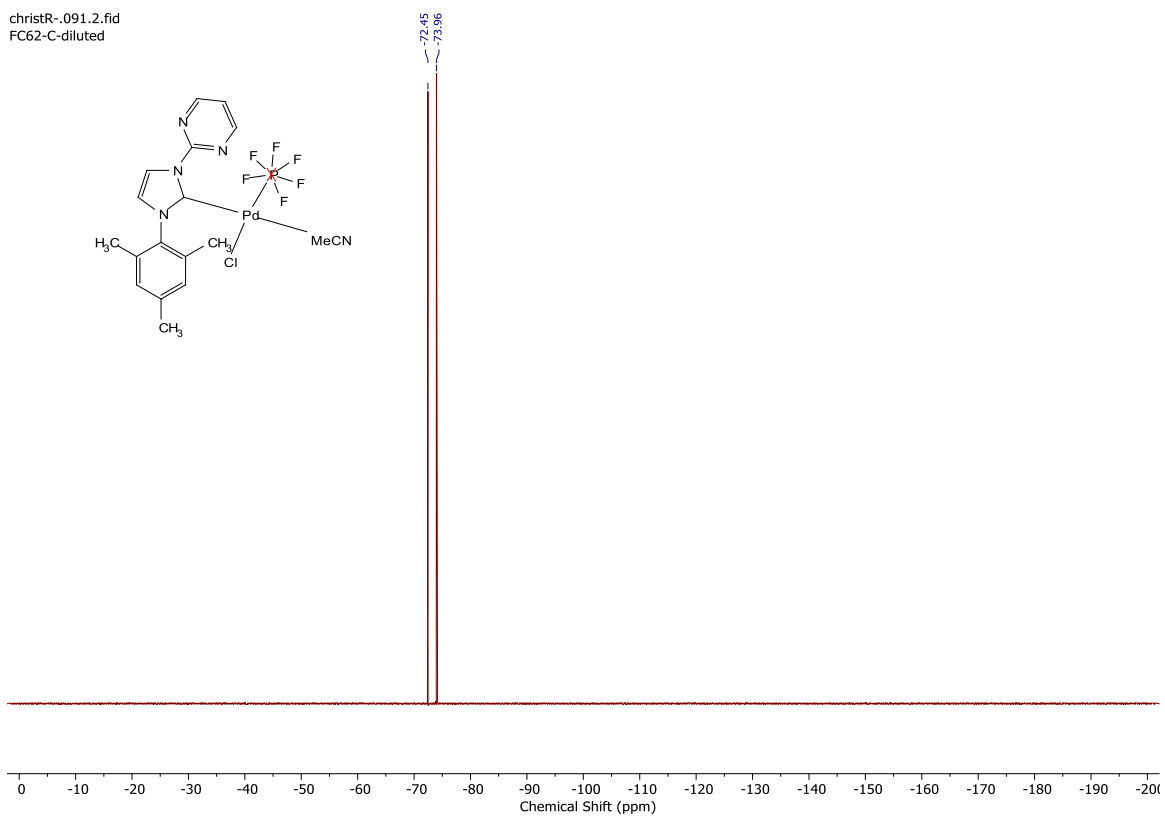
**Spectrum 115** <sup>1</sup>H NMR spectrum of ligand **26** in DMSO-*d*<sub>6</sub>.

christR-.091.1.fid  
FC62-C-diluted

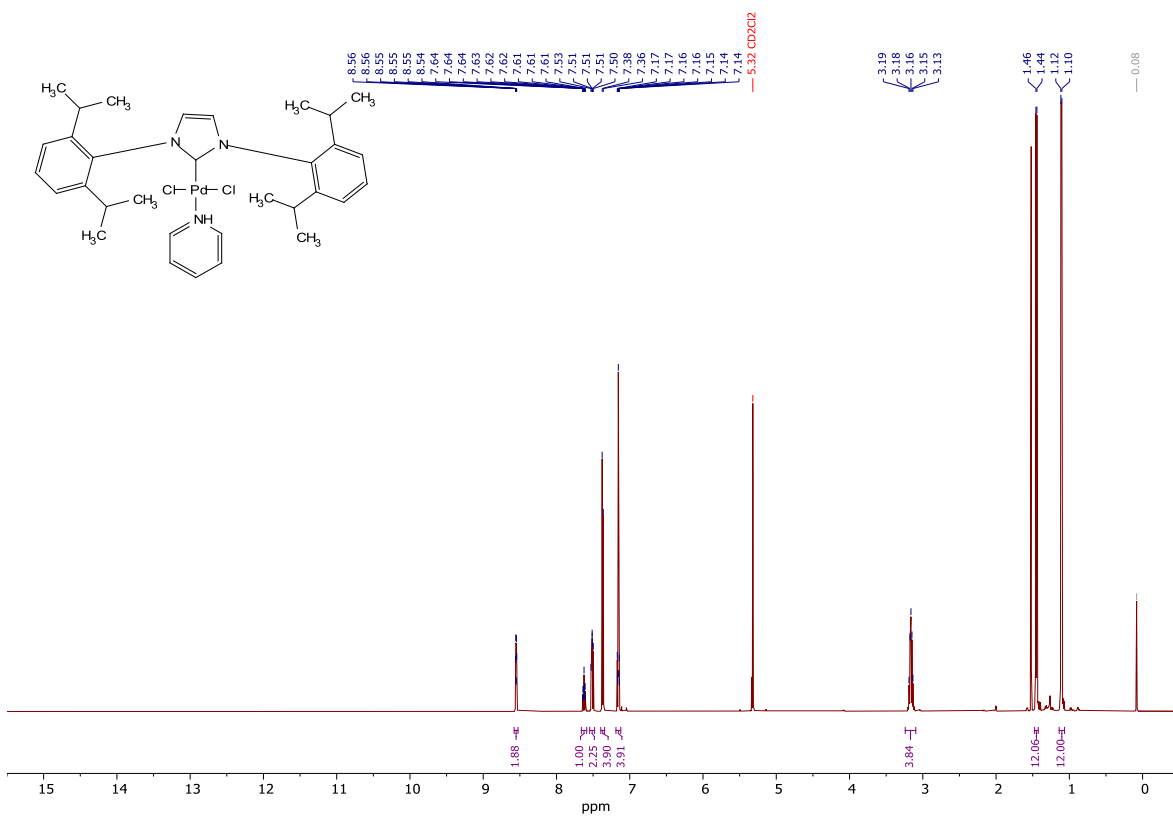


**Spectrum 116** <sup>1</sup>H NMR spectrum of complex **Pd2** in CD<sub>2</sub>Cl<sub>2</sub>.

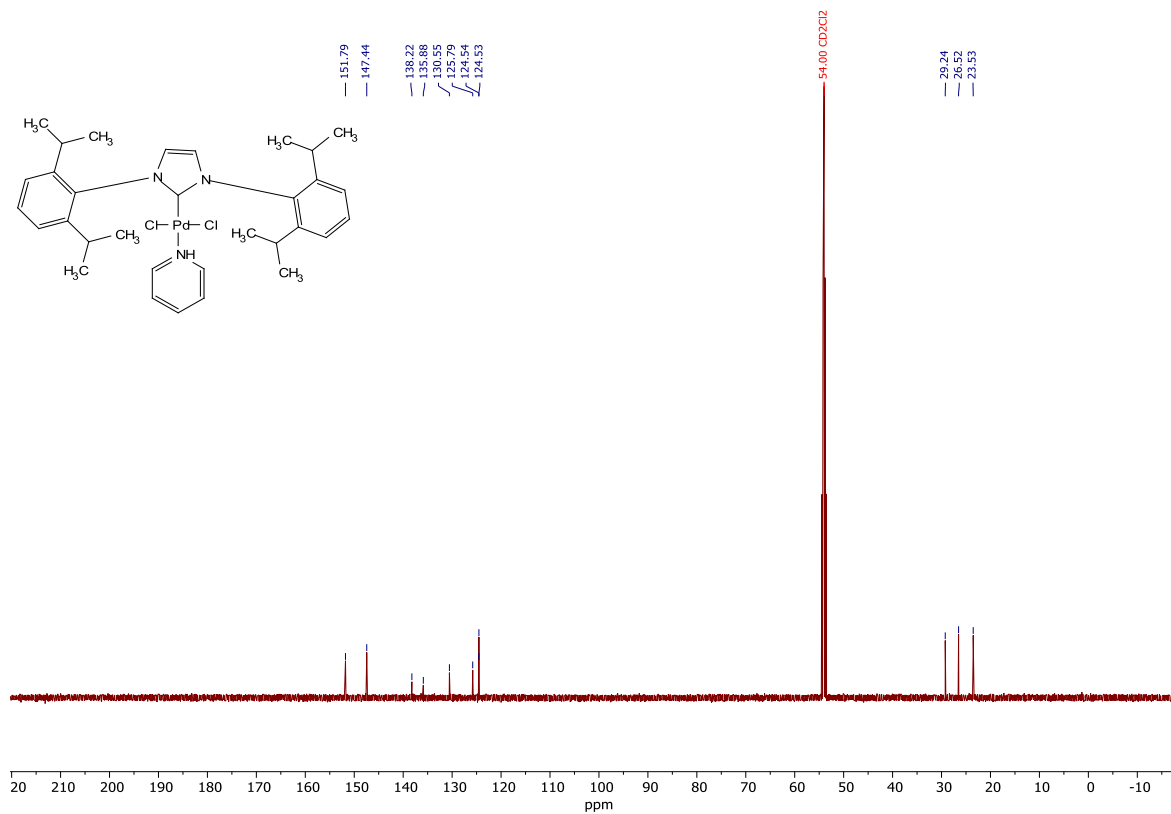
christR-.091.2.fid  
FC62-C-diluted



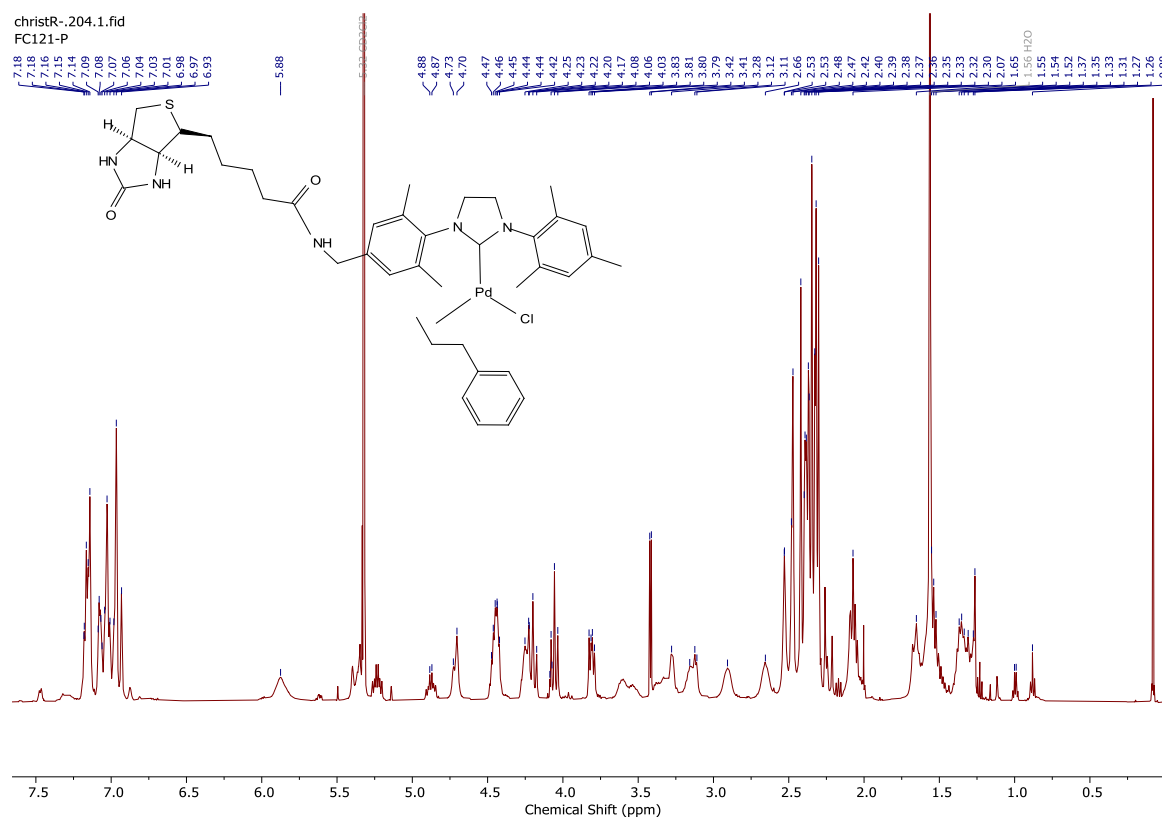
Spectrum 117 <sup>19</sup>F NMR spectrum of complex Pd2 in CD<sub>2</sub>Cl<sub>2</sub>.



Spectrum 118 <sup>1</sup>H NMR spectrum of complex Pd3 in DMSO-*d*<sub>6</sub>.

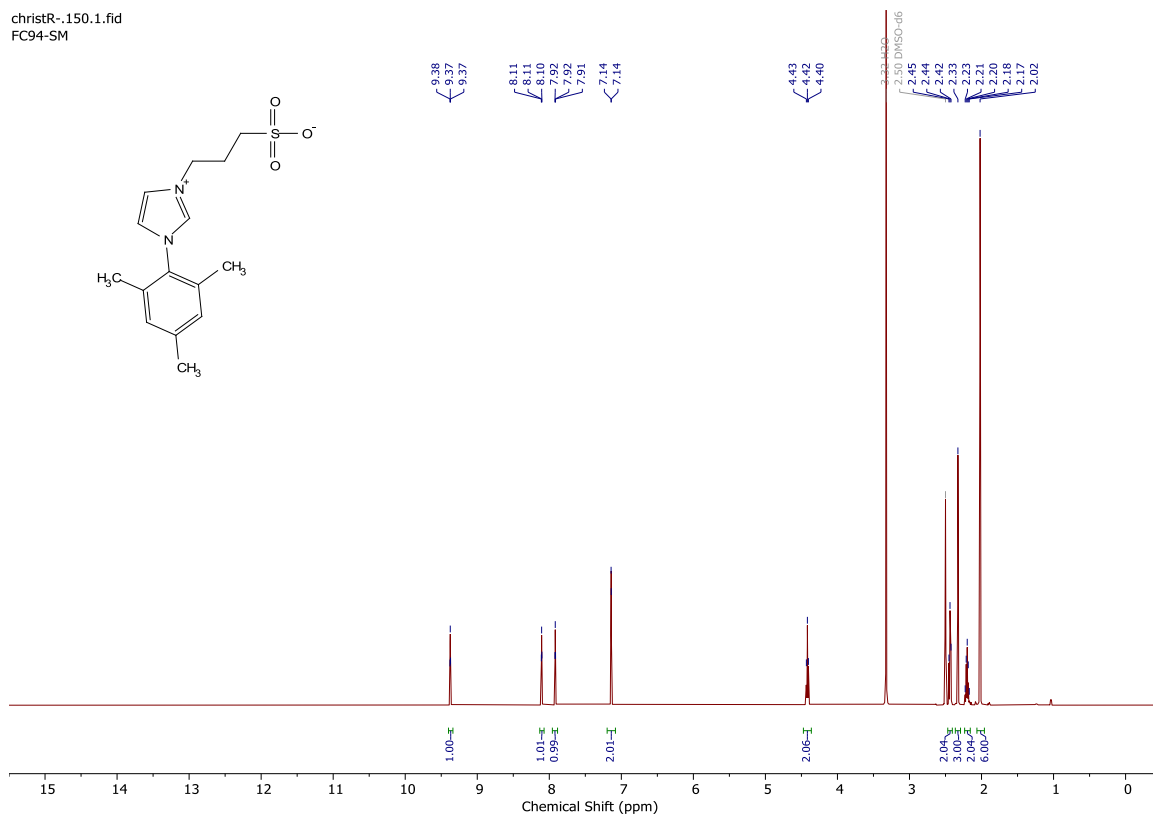


**Spectrum 119** <sup>13</sup>C NMR spectrum of complex Pd3 in DMSO-*d*<sub>6</sub>.



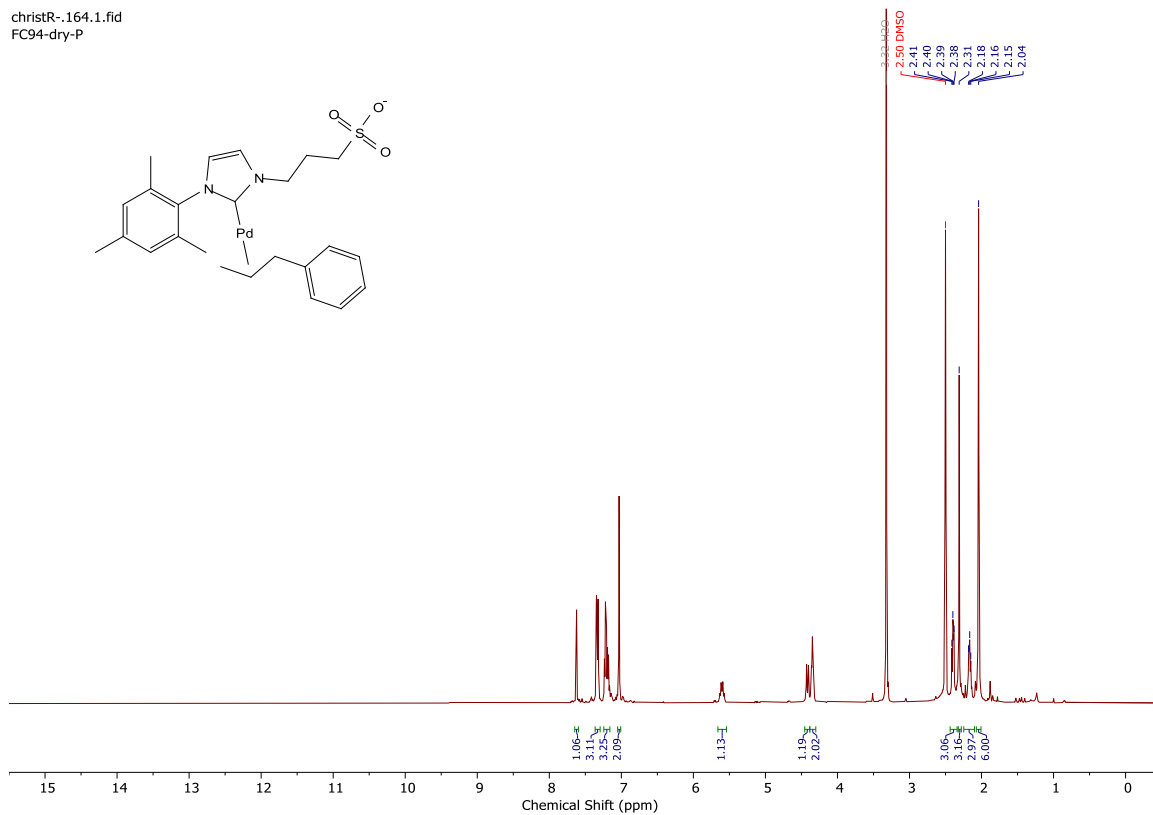
**Spectrum 120** <sup>1</sup>H NMR spectrum of complex Pd4 in CD<sub>2</sub>Cl<sub>2</sub>.

christR-.150.1.fid  
FC94-SM

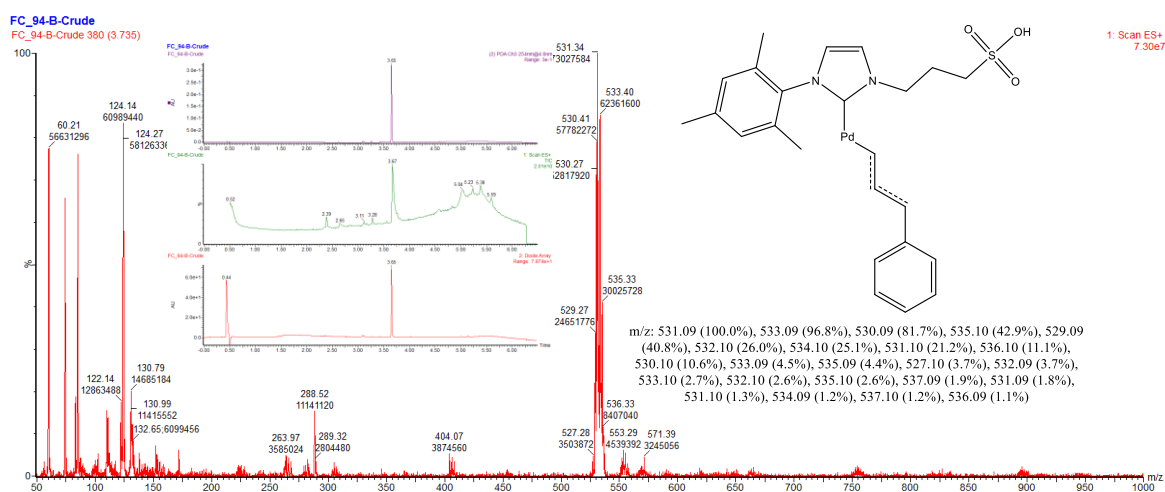


**Spectrum 121**  $^1\text{H}$  NMR spectrum of ligand **30** in  $\text{DMSO-}d_6$ .

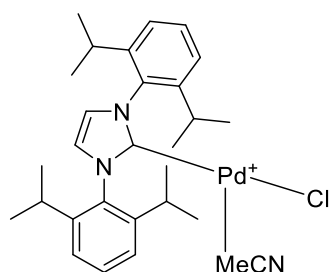
christR-.164.1.fid  
FC94-dry-P



**Spectrum 122**  $^1\text{H}$  NMR spectrum of complex **Pd5** in  $\text{DMSO-}d_6$ .

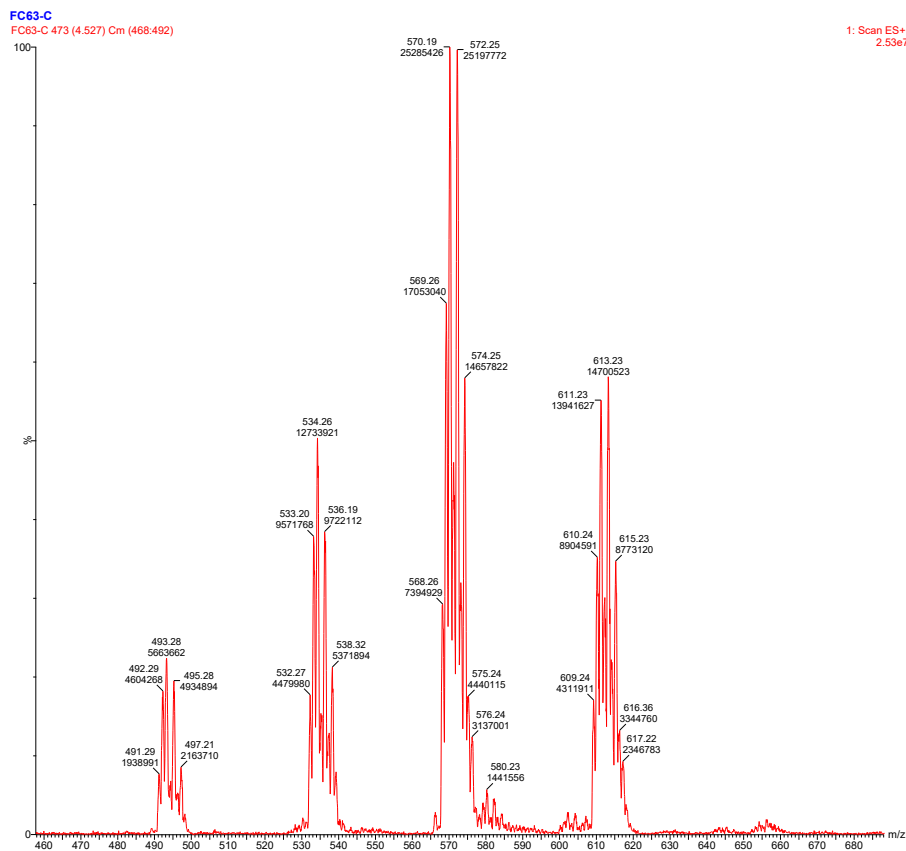


**Spectrum 123** UPLC-MS Spectrum of complex Pd5 from MeCN.



Chemical Formula:  $C_{29}H_{39}ClN_3Pd^+$

m/z: 570.19 (100.0%), 572.19 (86.0%), 569.19 (73.7%), 571.19 (48.3%), 574.19 (38.3%), 573.19 (32.9%), 568.19 (32.5%), 572.18 (25.0%), 574.18 (24.1%), 575.19 (18.7%), 576.19 (11.9%), 570.18 (10.1%), 577.19 (3.5%), 571.20 (3.3%), 566.19 (2.9%), 576.20 (1.7%), 573.18 (1.1%), 571.18 (1.0%).



**Spectrum 124** UPLC-MS spectrum of Pd3 from MeCN.

# Mass Spectrum SmartFormula Report

**Analysis Info**

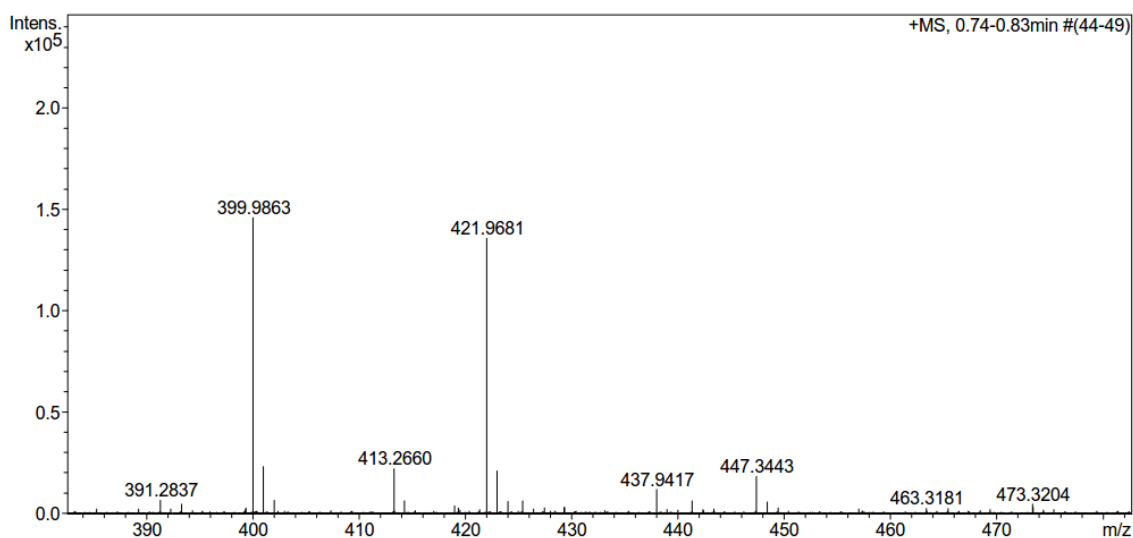
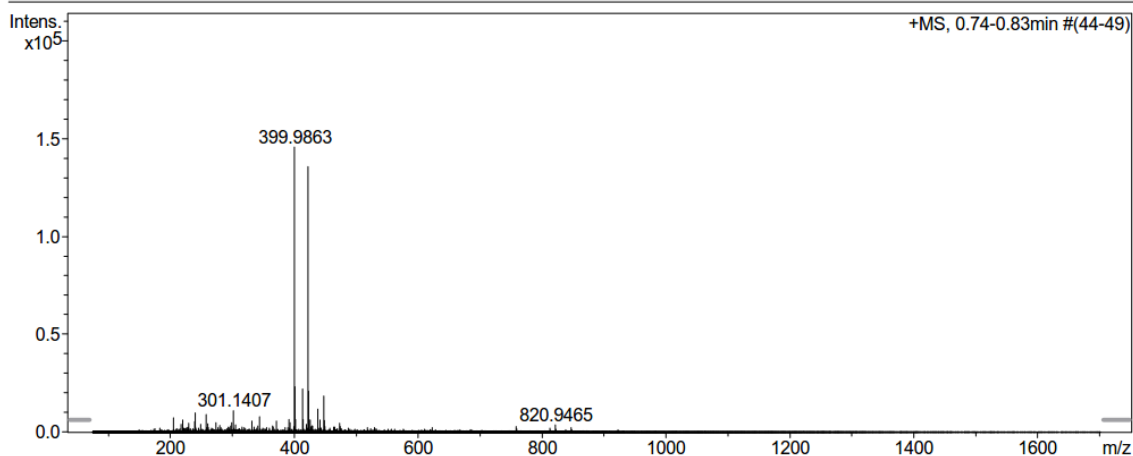
Analysis Name E:\acq data for data analysis\FC35-P 001.d  
 Method 22 Direct\_pos\_mid.m  
 Sample Name Fadri Christoffel  
 Comment FC-35-P, ca. 10 ug/ml MeCN

Acquisition Date 17.01.2018 10:12:00

Operator hn  
 Instrument / Ser# maXis 4G 21243

**Acquisition Parameter**

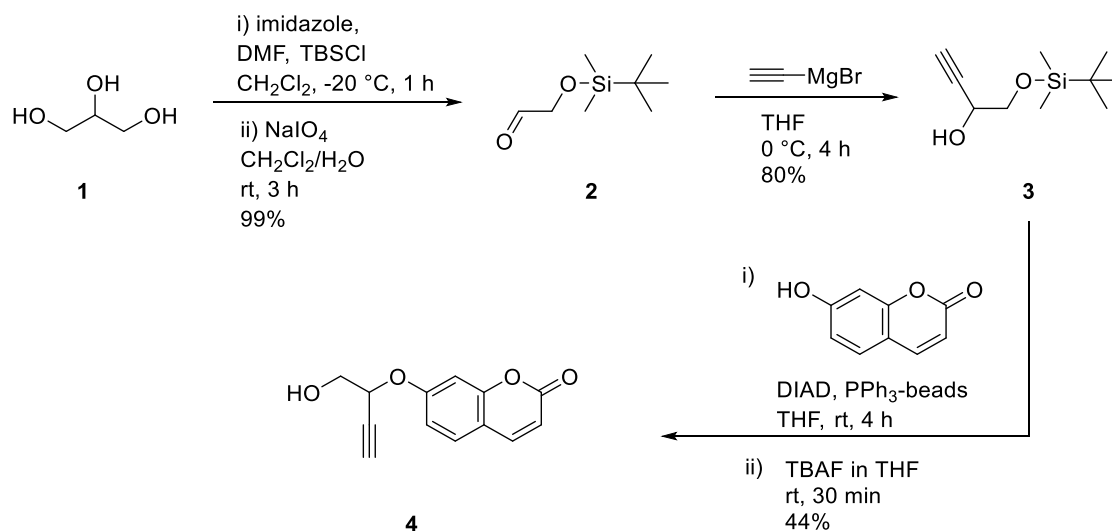
Source Type	ESI	Ion Polarity	Positive	Set Nebulizer	0.4 Bar
Focus	Not active	Set Capillary	3600 V	Set Dry Heater	180 °C
Scan Begin	75 m/z	Set End Plate Offset	-500 V	Set Dry Gas	4.0 l/min
Scan End	1700 m/z	Collision Energy	8.0 eV	Set Ion Energy ( MS only )	4.0 eV



Meas. m/z	#	Formula	Score	m/z	err [mDa]	err [ppm]	mSigma	rdb	e <sup>-</sup> Conf	z
399.9863	1	C <sub>15</sub> H <sub>15</sub> INO <sub>2</sub> S	100.00	399.9863	-0.0	-0.1	12.5	8.5	even	1+
421.9681	1	C <sub>15</sub> H <sub>14</sub> INaO <sub>2</sub> S	100.00	421.9682	0.1	0.2	13.9	8.5	even	
437.9417	1	C <sub>15</sub> H <sub>14</sub> IKNO <sub>2</sub> S	100.00	437.9422	0.4	0.9	5.7	8.5	even	

## 8.5 Chapter 4: Gold-triggered Drug-Release Systems

### Substrate Synthesis



TMS-protected aldehyde **2** was prepared from glycerol **1** according to the procedure of Paterson and co-workers.<sup>225</sup> The product was obtained quantitatively as a clear, colorless oil, the spectra were in agreement with literature data.

Butynol **3** was prepared via Grignard reaction with ethynylmagnesium bromide. The aldehyde **2** (2.00 g, 11.5 mmol, 1 eq) was added to a cold solution of dry THF (40 mL, 0 °C) followed by the dropwise addition of ethynylmagnesium bromide (27.6 mL, 13.8 mmol, 1.2 eq). The mixture was stirred (0 °C, ~4 h) until TLC stained with KMnO<sub>4</sub> revealed full conversion. The reaction mixture was quenched cold (0 °C) by the dropwise addition of aq. NH<sub>4</sub>Cl (40 mL). The crude was extracted with Et<sub>2</sub>O (3x50 mL), washed with brine (15 mL), dried with MgSO<sub>4</sub>, and gently reduced *in vacuo* (>100 mbar!). Purification by flash column chromatography (KP-Sil 50g, 10-20% Et<sub>2</sub>O/pentane) yielded butynol **3** as a colorless oil (1.83 g, 9.16 mmol, 80%).

<sup>1</sup>H NMR (500 MHz, DMSO-*d*<sub>6</sub>) δ 5.45 (d, *J* = 6.0 Hz, 1H), 4.17 (dd, *J* = 6.1, 2.2 Hz, 1H), 3.56 (dd, *J* = 6.2, 1.0 Hz, 2H), 0.87 (s, 9H), 0.05 (d, *J* = 1.1 Hz, 6H).

TMS-protected substrate **4** was prepared via Mitsunobu reaction. To a solution of butynol **3** (100 mg, 0.50 mmol, 1 eq), umbelliferone (81 mg, 0.50 mmol, 1 eq) and triphenylphosphine (beads, 0.75 mmol, 1.5 eq) was added dry THF (5 mL). DIAD (150 mg, 0.75 mmol, 1.5 eq) in dry THF (2 mL) was added dropwise. The mixture was stirred (90 min at rt). Afterwards, the mixture was diluted with EtOAc (20 mL), filtered, and extracted from aq. NH<sub>4</sub>Cl (20 mL) with EtOAc (3x40 mL). The crude was reduced *in vacuo* to yield the product as a yellow sticky oil, which can be directly transferred to the deprotection step (140 mg, 0.42 mmol, 83%).

$^1\text{H}$  NMR (500 MHz,  $\text{DMSO-}d_6$ )  $\delta$  8.00 (d,  $J = 9.5$  Hz, 1H), 7.66 (d,  $J = 8.7$  Hz, 1H), 7.07 (d,  $J = 2.4$  Hz, 1H), 7.00 (dd,  $J = 8.6, 2.4$  Hz, 1H), 6.32 (d,  $J = 9.5$  Hz, 1H), 5.22 (td,  $J = 5.5, 2.1$  Hz, 1H), 3.98 – 3.92 (m, 2H), 3.65 (d,  $J = 2.0$  Hz, 1H), 0.86 (s, 10H), 0.09 (d,  $J = 14.7$  Hz, 6H).

HR-MS (ESI, pos):  $m/z$  calcd. for  $\text{C}_{19}\text{H}_{24}\text{O}_4\text{SiH}^+$  345.1517 found 345.1518  $[\text{M}+\text{H}]^+$ ;  $m/z$  calcd. for  $\text{C}_{19}\text{H}_{24}\text{O}_4\text{SiNa}^+$  367.1336 found 367.1334  $[\text{M}+\text{Na}]^+$ ;

Substrate **5** was prepared via TBAF deprotection. TMS-substrate **4** (50 mg, 0.146 mmol, 1 eq) was diluted in dry THF (5 mL) and cooled (0 °C). A solution of TBAF in THF (0.146 mL, 0.146 mmol, 1 M in THF) was dropwise added. Reaction control via TLC (every 5 min) is required to avoid decomposition. After 15-20 min, the mixture was quenched by the addition of aq.  $\text{NaHCO}_3$  (10 mL). The crude was extracted with EtOAc (3x20 mL), washed with brine (10 mL), dried with  $\text{MgSO}_4$  and reduced in vacuo. Purification via flash column chromatography (KP-Sil 10g, 30-60% EtOAc/cyclohexane) yielded the product as a white solid (18 mg, 0.078 mmol, 54%).

$^1\text{H}$  NMR (500 MHz,  $\text{DMSO-}d_6$ )  $\delta$  8.00 (d,  $J = 9.5$  Hz, 1H), 7.66 (d,  $J = 8.6$  Hz, 1H), 7.07 (d,  $J = 2.4$  Hz, 1H), 7.01 (dd,  $J = 8.6, 2.5$  Hz, 1H), 6.32 (d,  $J = 9.5$  Hz, 1H), 5.37 (t,  $J = 6.1$  Hz, 1H), 5.11 (td,  $J = 5.5, 2.1$  Hz, 1H), 3.78 – 3.73 (m, 2H), 3.62 (d,  $J = 2.0$  Hz, 1H).

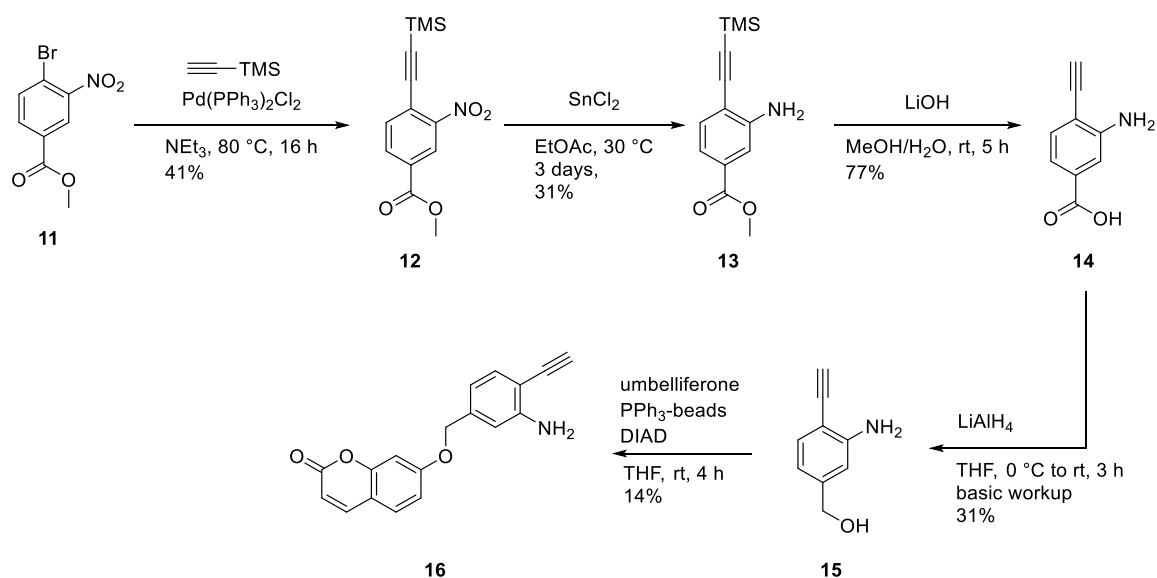
$^{13}\text{C}$  NMR (126 MHz,  $\text{DMSO-}d_6$ )  $\delta$  160.17, 155.05, 144.22, 129.47, 113.32, 112.95, 112.87, 102.42, 79.56, 78.69, 69.47, 63.61.

HR-MS (ESI, pos):  $m/z$  calcd. for  $\text{C}_{13}\text{H}_{10}\text{O}_4\text{H}^+$  231.0652 found 231.0649  $[\text{M}+\text{H}]^+$ .

Aryl acid **14** was prepared according to the procedure of Kirschning and co-workers.<sup>226</sup> The corresponding product was obtained as a pale yellow solid (497 mg, 3.08 mmol, 77%). The spectra are in agreement with literature data.

$^1\text{H}$  NMR (500 MHz,  $\text{DMSO-}d_6$ )  $\delta$  12.80 (s, 1H), 7.32 (d,  $J = 1.6$  Hz, 1H), 7.25 (d,  $J = 8.0$  Hz, 1H), 7.04 (dd,  $J = 8.0, 1.6$  Hz, 1H), 5.60 (s, 2H), 4.52 (s, 1H).





Benzyl alcohol **15** was prepared via reduction of aryl acid **14**. To a solution of dry THF (10 mL) was added aryl acid **14** (483 mg, 3 mmol, 1 eq). The mixture was cooled (0 °C) before slowly adding a solution of LiAlH<sub>4</sub> (4.5 mL, 4.5 mmol, 1 M in THF, 1.5 eq). Stirring was continued (3 h, 0 °C to rt) before slowly quenching the mixture with aq. NaHCO<sub>3</sub>. Upon dilution with EtOAc (50 mL) and aq. Rochelle Salt (20 mL), the crude was filtered and extracted with EtOAc (4x50 mL), washed with brine (15 mL) and dried with MgSO<sub>4</sub>. During the workup, the pH of the aqueous phase was checked, and if necessary adjusted (>7 pH). The crude was purified via flash column chromatography (KP-Sil 50 g, 30-60% EtOAc/cyclohexane) to yield the product as a pale yellow solid (137 mg, 0.93 mmol, 31%).

<sup>1</sup>H NMR (500 MHz, DMSO-*d*<sub>6</sub>) δ 7.10 (d, *J* = 7.8 Hz, 1H), 6.68 (d, *J* = 1.3 Hz, 1H), 6.48 – 6.41 (m, 1H), 5.30 (s, 2H), 5.09 (t, *J* = 5.8 Hz, 1H), 4.36 (dd, *J* = 5.8, 0.8 Hz, 2H), 4.25 (s, 1H).

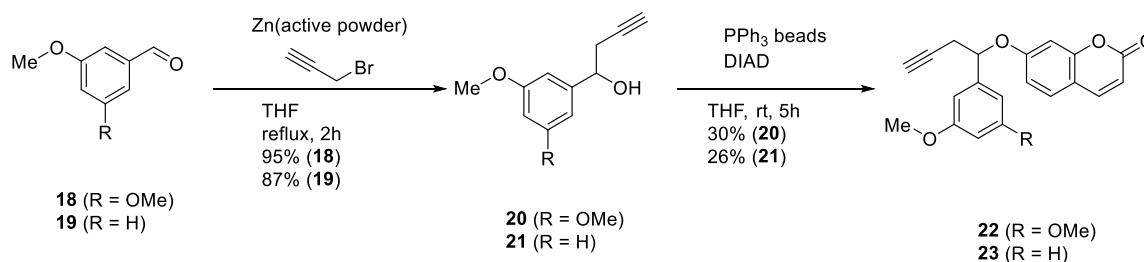
HR-MS (ESI, pos): *m/z* calcd. for C<sub>9</sub>H<sub>9</sub>OH<sup>+</sup> 148.0757 found 148.0754 [M+H]<sup>+</sup>.

Substrate **16** was prepared via a Mitsunobu reaction. To a solution of benzyl alcohol **15** (44 mg, 0.30 mmol, 1 eq), umbelliferone (39 mg, 0.24 mmol, 0.8 eq) and triphenylphosphine (beads, 0.36 mmol, 1.2 eq) was added dry THF (5 mL). DIAD (73 mg, 0.36 mmol, 1.2 eq) in dry THF (2 mL) was dropwise added. The mixture was stirred (4 h at rt). Afterwards, the mixture was diluted with EtOAc (20 mL), filtered, and extracted from aq. NH<sub>4</sub>Cl (20 mL) with EtOAc (3x40 mL). The crude was reduced in vacuo further purified via flash column chromatography (KP-Sil 25g, 20-80% EtOAc/cyclohexane) to yield the product as a white solid (12 mg, 0.04 mmol, 14%).

<sup>1</sup>H NMR (500 MHz, CD<sub>2</sub>Cl<sub>2</sub>) δ 7.65 (d, *J* = 9.5 Hz, 1H), 7.41 (d, *J* = 8.6 Hz, 1H), 7.32 (d, *J* = 7.8 Hz, 1H), 6.91 (dd, *J* = 8.6, 2.5 Hz, 1H), 6.86 (d, *J* = 2.5 Hz, 1H), 6.79 (d, *J* = 1.6 Hz, 1H), 6.72 (dd, *J* = 7.9, 1.6 Hz, 1H), 6.21 (d, *J* = 9.5 Hz, 1H), 5.05 (s, 2H), 4.37 (s, 2H), 3.45 (s, 1H).

$^{13}\text{C}$  NMR (126 MHz,  $\text{CD}_2\text{Cl}_2$ )  $\delta$  162.11, 161.15, 156.27, 149.45, 143.69, 138.79, 133.21, 129.31, 116.73, 113.64, 113.30, 113.12, 106.52, 102.24, 83.05, 80.47, 70.50.

HR-MS (ESI, pos):  $m/z$  calcd. for  $\text{C}_{18}\text{H}_{13}\text{NO}_3\text{H}^+$  292.0968 found 292.0966  $[\text{M}+\text{H}]^+$ ;  $m/z$  calcd. for  $\text{C}_{18}\text{H}_{13}\text{NO}_3\text{Na}^+$  314.0788 found 314.0788  $[\text{M}+\text{Na}]^+$ .



The synthesis of pro-naphthalene substrates **21** and **23** was performed by Philipp Meyer and is also described in his Master Thesis entitled "*Gold(I)-catalyzed bioorthogonal uncaging of fluorescent probes - towards in vivo imaging and prodrug activation.*", handed in to the Department of Chemistry at the University of Basel.

Alkynes **20** and **21** were prepared according to a modified procedure of Prisinzano and co-workers.<sup>227</sup> First, activated Zinc powder was prepared by suspending zinc powder in aq HCl (12 mL, 1 M). After stirring (30 min), the suspension was decanted, washed with water (3x6 mL), acetone (3x6 mL) and diethyl ether (2x3 mL) and dried *in vacuo*. The corresponding anisaldehyde **18** (831 mg, 5 mmol, 1 eq) or **19** (1.36 g, 10 mmol, 1 eq) was dissolved in THF/DMF (1:1, 100 mL). A solution of propargyl bromide (0.7 mL, 6.5 mmol or 1.4 mL, 13 mmol, 80% in toluene, 1.3 eq) and activated zinc powder (1.0 g, 15 mmol or 1.96 g, 30 mmol, 3 eq) was added. The reaction was heated (55 °C, 3 h) before quenching with sat. aq.  $\text{NH}_4\text{Cl}$  (50 mL). The mixture was filtered, extracted with diethyl ether (3x50 mL), washed with brine (3x75 mL), dried over  $\text{Na}_2\text{SO}_4$  and concentrated *in vacuo*. Purification by flash column chromatography (KP-Sil 50, 10% EtOAc/cyclohexane) yielded the corresponding alkynes **20** (982 mg, 4.8 mmol, 95%) and **21** (1.21 g, 6.9 mmol, 69%) as colorless oils. The spectra were in agreement with literature data.<sup>227</sup>

Alkyne **20**:  $^1\text{H}$  NMR (500 MHz,  $\text{DMSO}-d_6$ )  $\delta$  6.54 (d,  $J = 2.3$  Hz, 2H), 6.36 (t,  $J = 2.3$  Hz, 1H), 5.48 (d,  $J = 4.6$  Hz, 1H), 4.60 (td,  $J = 6.2, 4.5$  Hz, 1H), 2.73 (t,  $J = 2.6$  Hz, 1H), 2.50 – 2.43 (m, 2H).

Alkyne **21**:  $^1\text{H}$  NMR (500 MHz,  $\text{CDCl}_3$ ):  $\delta$  7.28 (1H, t,  $^3J = 8.2$  Hz), 6.97 (1H, s), 6.96 (1H, s), 6.85 (1H, s), 4.86 (1H, s), 3.82 (3H, s), 2.64 (2H, s), 2.35 (1H, d,  $^3J = 3.6$  Hz), 2.09 (1H, s).

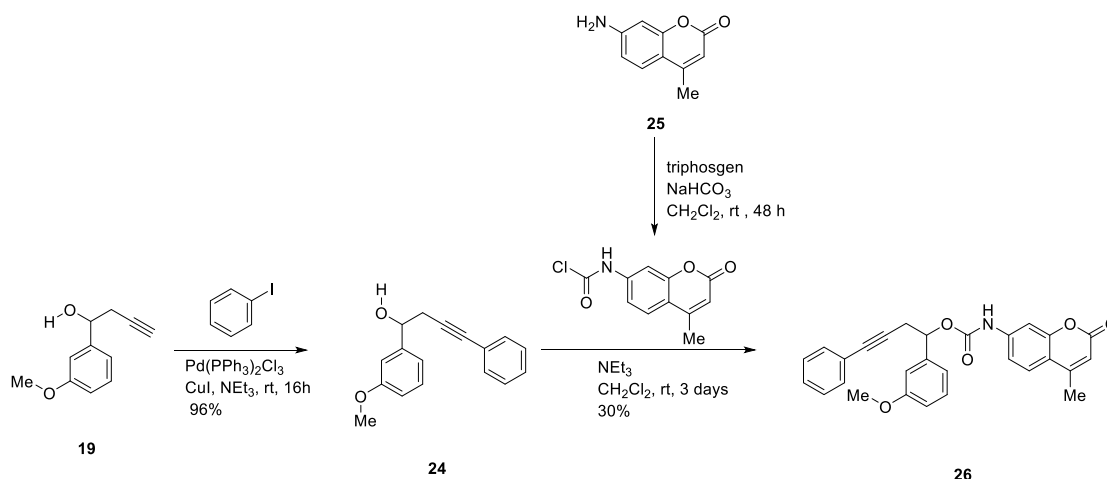
Substrates **22** and **23**: Alkynes **20** or **21** (227 mg, 1.1 mmol or 100 mg, 0.567 mmol, 1 eq), umbelliferone (162 mg, 1 mmol, or 91.9 mg, 0.567 mmol, 1 eq) and PPh<sub>3</sub> beads (1.7 g, 3.8 mmol or 826 mg, 1.9 mmol, 3.4 eq) were added to dry THF (10 mL or 5 mL). A solution of DIAD (0.32 mL, 1.9 mmol or 0.17 mL, 0.85 mmol, 1.5 eq) in dry THF (4 mL or 2 mL) was added and the mixture was stirred (16 h, rt). After filtration of the mixture, the crude was taken up in silica gel and purified by flash column chromatography (KP-Sil 25g, 10-20% EtOAc/cyclohexane) to yield substrates **22** (106 mg, 0.30 mmol, 30%) and **23** (55 mg, 4.5 mmol, 19%) as white oils.

Substrate **22**: <sup>1</sup>H NMR (500 MHz, DMSO-*d*<sub>6</sub>) δ 7.93 (d, *J* = 9.5 Hz, 1H), 7.57 (d, *J* = 8.7 Hz, 1H), 6.97 (dd, *J* = 8.6, 2.4 Hz, 1H), 6.94 (d, *J* = 2.4 Hz, 1H), 6.64 (d, *J* = 2.3 Hz, 2H), 6.41 (t, *J* = 2.3 Hz, 1H), 6.26 (d, *J* = 9.4 Hz, 1H), 5.58 (dd, *J* = 7.0, 5.4 Hz, 1H), 3.71 (s, 6H), 2.90 (t, *J* = 2.7 Hz, 1H), 2.88 – 2.82 (m, 1H), 2.78 (ddd, *J* = 16.9, 5.4, 2.7 Hz, 1H).

Substrate **23**: <sup>1</sup>H NMR (500 MHz, CD<sub>2</sub>Cl<sub>2</sub>): δ 7.59 (1H, d, <sup>3</sup>*J* = 9.5 Hz), 7.33 (1H, d, <sup>3</sup>*J* = 8.6 Hz), 7.27 (1H, pseudo-t, <sup>3</sup>*J* = 7.9 Hz), 6.98 (1H, d, <sup>3</sup>*J* = 7.6 Hz), 6.93 (1H, s), 6.86 (1H, dd, <sup>3</sup>*J* = 8.6 Hz, <sup>4</sup>*J* = 2.4 Hz), 6.83 (1H, d, <sup>3</sup>*J* = 8.2 Hz), 6.74 (d, <sup>3</sup>*J* = 2.4 Hz), 6.16 (1H, d, <sup>3</sup>*J* = 9.5 Hz), 5.32 (1H, s), 3.76 (3H, s), 2.90 (1H, ddd, <sup>2</sup>*J* = 16.4 Hz, <sup>3</sup>*J* = 6.13 Hz, <sup>4</sup>*J* = 2.6 Hz), 2.80 (1H, ddd, <sup>2</sup>*J* = 16.4 Hz, <sup>3</sup>*J* = 6.13 Hz, <sup>4</sup>*J* = 2.6 Hz), 2.08 (1H, s).

<sup>13</sup>C NMR (126 MHz, CD<sub>2</sub>Cl<sub>2</sub>): δ 160.70, 160.65, 159.99, 155.61, 143.18, 140.67, 129.83, 128.79, 118.40, 113.63, 113.59, 113.35, 112.98, 111.82, 103.07, 79.67, 78.72, 70.62, 55.19, 28.24.

HR-MS (ESI, pos): *m/z* calcd. for C<sub>20</sub>H<sub>16</sub>O<sub>4</sub>Na<sup>+</sup> 343.0941 found 343.0944 [M+Na<sup>+</sup>]<sup>+</sup>.



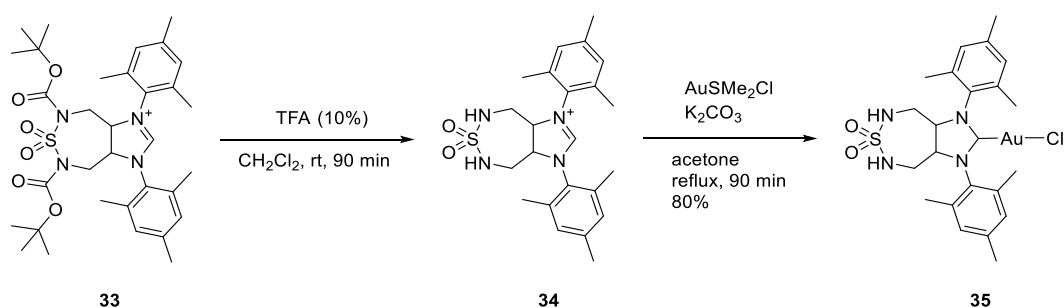
Carbamate **26** was prepared via chloroformate addition. To a solution of coumarin **25** (52.6 mg, 1.0 eq) in dry CH<sub>2</sub>Cl<sub>2</sub> (2 mL), triphosgene (44.5 mg, 0.15 mmol, 0.5 eq) and dry NaHCO<sub>3</sub> (75.6 mg, 0.9 mmol, 3.0 eq) were added. The mixture was stirred until reaction completion (monitored by TLC) and the volatiles were evaporated *in vacuo*. The crude material was

dissolved in dry  $\text{CH}_2\text{Cl}_2$  (2 mL) and added dropwise to a solution of benzyl alcohol **24** (75 mg, 1.0 eq) and triethylamine (0.08 mL, 2 eq) in dry  $\text{CH}_2\text{Cl}_2$  (3 mL). After reaction completion, the mixture was concentrated and purified by flash column chromatography (KP-Sil 25 g; 20-40% EtOAc/cyclohexane) to yield the product as a white solid (35 mg, 0.77 mmol, 26%).

$^1\text{H}$  NMR (500 MHz,  $\text{DMSO}-d_6$ )  $\delta$  10.41 (s, 1H), 7.69 (d,  $J = 8.7$  Hz, 1H), 7.54 (d,  $J = 2.1$  Hz, 1H), 7.44 (dd,  $J = 8.8, 2.1$  Hz, 1H), 7.34 (s, 1H), 7.32 (s, 5H), 7.12 – 7.06 (m, 2H), 6.92 (ddd,  $J = 8.3, 2.5, 1.1$  Hz, 1H), 6.23 (d,  $J = 1.3$  Hz, 1H), 5.93 (t,  $J = 6.3$  Hz, 1H), 3.77 (s, 3H), 3.09 (d,  $J = 6.3$  Hz, 2H), 2.38 (d,  $J = 1.3$  Hz, 3H).

MS-Direct Injection (ESI, pos)  $m/z$ : 454.1 [100%,  $\text{M}+\text{H}$ ] $^+$ ; 476.1 [21%,  $\text{M}+\text{Na}$ ] $^+$ ; (ESI, neg)  $m/z$ : 452.1 [100%,  $\text{M}-\text{H}$ ] $^-$ .

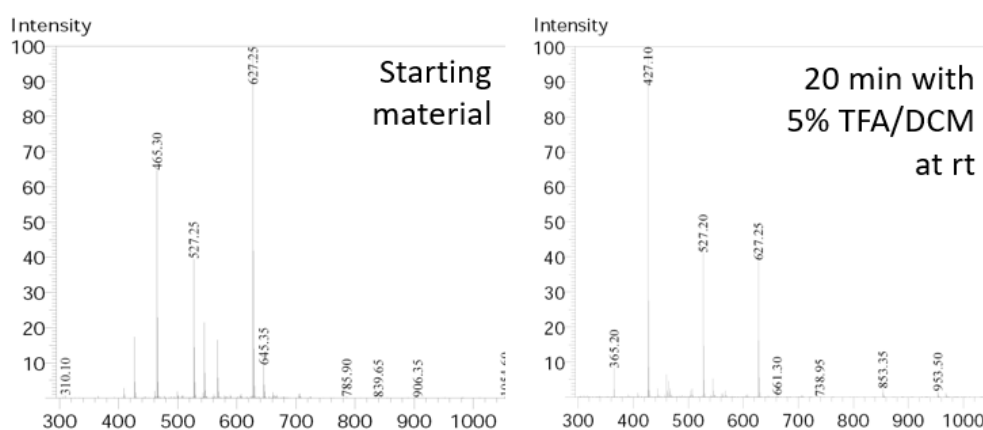
### Gold-Complex Synthesis

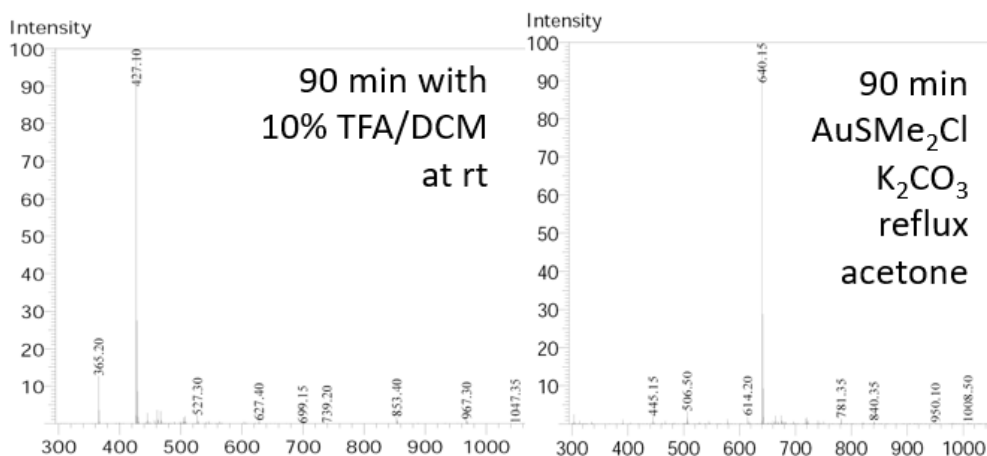


Sulfimide-NHC ligand **33** (20 mg, 0.03 mmol, 1 eq, prepared by Boris Lozhkin) was dissolved in dry  $\text{CH}_2\text{Cl}_2$  (1 mL). Trifluoroacetic acid (0.1 mL, 1.2 mmol, 40 eq) was added and the mixture was stirred (90 min at rt). The deprotection was monitored via ESI-MS direct injection (positive-mode). After deprotection, the solvent and the acid were removed under high vacuum to afford the desired ligand **34** as a yellow solid (13.8 mg, 0.03 mmol, 99%).

MS-Direct Injection of substrate **33** (ESI, pos)  $m/z$ : 627.25 [100%,  $\text{M}-\text{Cl}$ ] $^+$ .

MS-Direct Injection of product **34** (ESI, pos)  $m/z$ : 427.10 [100%,  $\text{M}-\text{Cl}$ ] $^+$ .





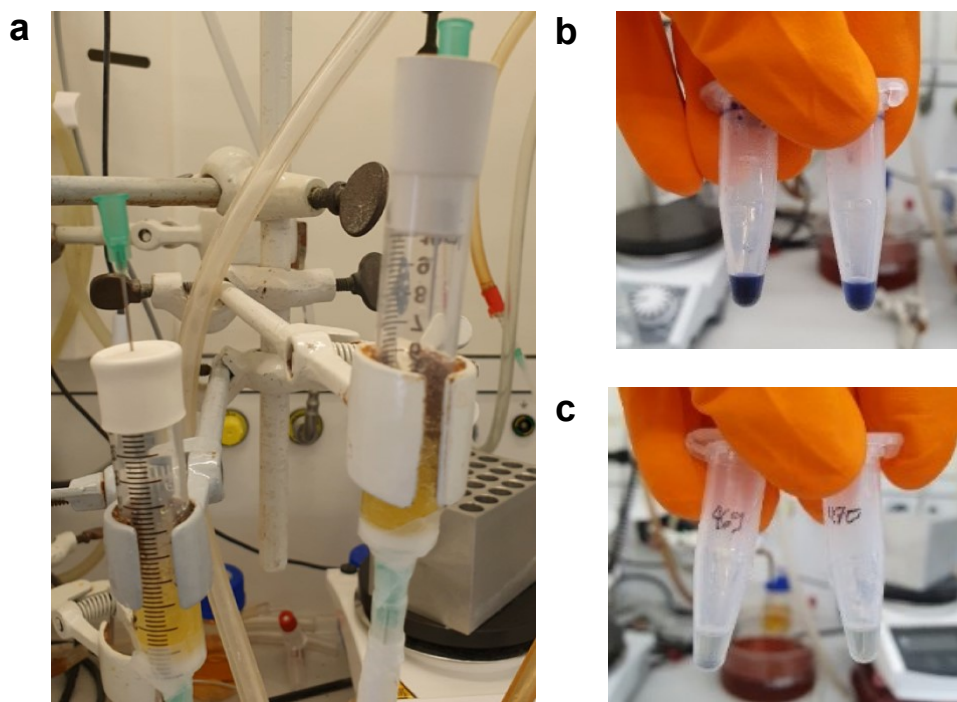
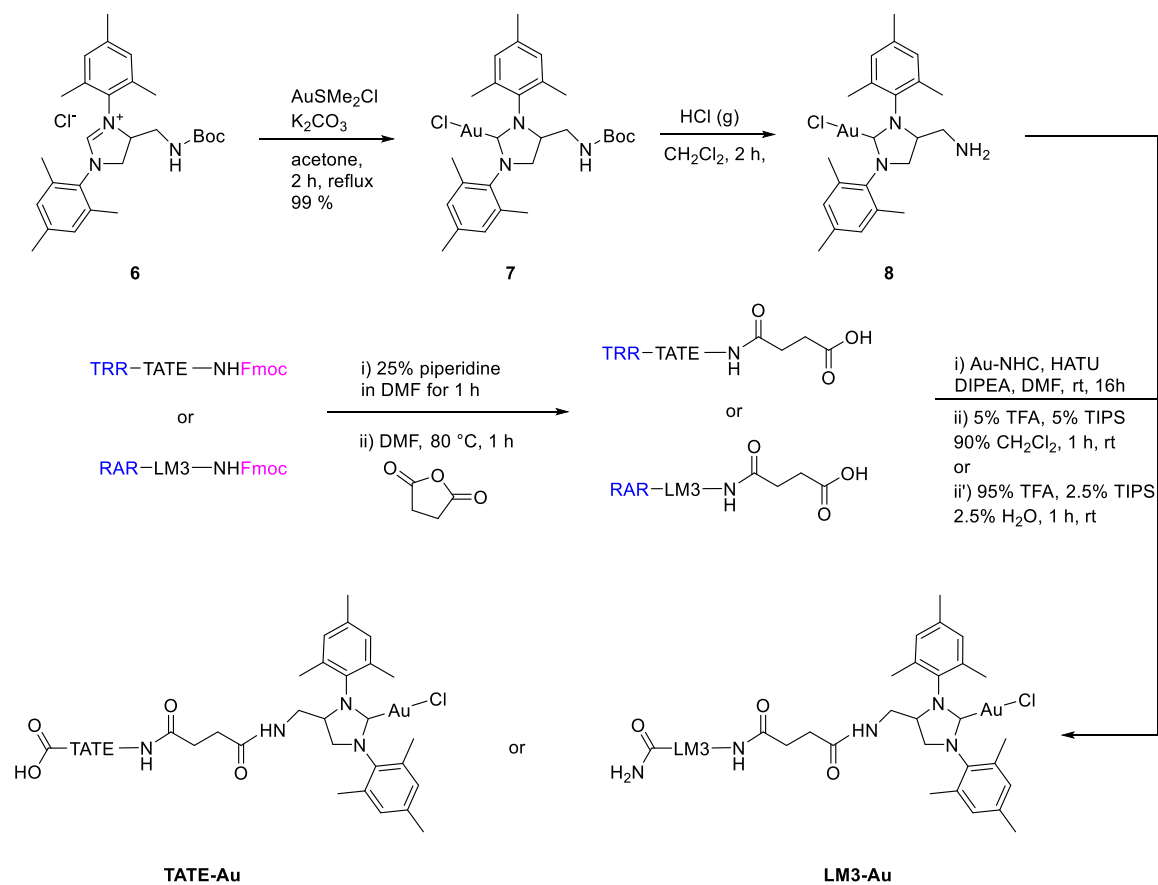
**SI Figure 19** Reaction control via ESI-MS direct injection.

To the crude ligand **34** (13.8 mg, 0.03 mmol, 1 eq) was added Au(Me<sub>2</sub>S)Cl (8.8 mg, 0.03 mmol, 1 eq), finely ground K<sub>2</sub>CO<sub>3</sub> (16.6 mg, 0.12 mmol, 4 eq) and acetone (3 mL). The pressure tube was sealed and heated (70 °C for 90 min). The solvent was removed *in vacuo* before adding dry CH<sub>2</sub>Cl<sub>2</sub> (5 mL). The mixture was filtered through Celite and the corresponding gold-complex was precipitated from little dry CH<sub>2</sub>Cl<sub>2</sub> by the addition of dry hexane to yield complex **35** as a white solid (3 mg, 0.005 mmol, 15%).

MS-Direct Injection (ESI, pos) m/z: 640.18 [100%, M-Cl+H<sub>2</sub>O]<sup>+</sup>.

HR-MS (ESI, pos): m/z calcd. for C<sub>23</sub>H<sub>30</sub>AuN<sub>4</sub>O<sub>2</sub>SCH<sub>3</sub>CN<sup>+</sup> 664.2015 found 664.2025 [M-Cl+MeCN]<sup>+</sup>; calcd. for C<sub>46</sub>H<sub>60</sub>Au<sub>2</sub>CIN<sub>8</sub>O<sub>4</sub>S<sub>2</sub><sup>+</sup> 1281.3193 found 1281.3207 [2M-Cl]<sup>+</sup>

## Gold Peptide Synthesis:



**SI Figure 20** a Peptide-coupling Setup and Kaiser test samples of b Fmoc-cleaved resin and c succinic acid coupled resin.

The cyclic peptides were prepared with the help of the M. Fani Group at the University Hospital of Basel according to reported procedures by Nico Igareta and Boris Lozhkin.<sup>209,210</sup> The gold complex **7** was prepared according to reported procedures, see also chapter 1 and 2.<sup>95</sup>

Setup: The **LM3** and **TATE** peptides were synthesized on rink amide and trityl resin, respectively. They were transferred into a peptide-synthesizer plastic vessel with filter inlet (10 mL) which was sealed with a septum. Nitrogen was purged from below through the vessel to guarantee a dry and oxygen-free environment while allowing for continuous mixing and easy access for the addition of further substrates via syringe. To remove the solvent through the bottom filter, the nitrogen line was swapped from bottom to top. Parafilm was used to seal the system for longer reaction times.

Fmoc-Cleaving Procedure: The Peptide-containing resin (ca 25 mg) was soaked in DMF (3 mL) under purging (30 min). The solvent was removed and the resin washed with DMF (2 mL). The Fmoc-group was removed by the addition of piperidine in DMF (25%, 3 mL). After purging (30 min), the solvent was removed, the resin was washed with DMF (2 mL) and the deprotection step was repeated one more time. Afterwards, the solvent was removed and the resin washed with DMF (3x2 mL). A spatula tip of resin was transferred to an Eppendorf vial to perform a Kaiser test.<sup>228</sup> In short, three solutions must be prepared for this test: (a) ninhydrin (500 mg) in ethanol (10 mL), (b) phenol (80 mg) in ethanol (10 mL) and (c) aq. KCN (2 mL, 0.001 M) in pyridine (100 mL). From each of these three solutions, ~20  $\mu$ L are transferred to the Eppendorf vial containing the sample. The vial is heated to reflux (>10 min) upon which the solution will turn blue if amines are present in the solution. The presence of a deep blue solution qualitatively confirms the successful deprotection of Fmoc from the peptide.

Coupling of Succinic anhydride: The resin was removed from the plastic vessel and transferred to a glass vial containing succinic anhydride (15 mg) and DMF (2 mL). The mixture was shaken in a thermoshaker (90 min, 80 °C). After the mixture cooled down (rt), it was transferred with the resin into the plastic vessel. The solvent was removed, and the resin was washed with **dry** DMF (3x2 mL). A second Kaiser test was performed in which the solution remains clear and thus confirms the absence of free amines.

Deprotection of gold complex **7**: The Boc-protected complex **7** (48 mg, 0.07 mmol) was dissolved in CH<sub>2</sub>Cl<sub>2</sub> (4 mL/mmol) and HCl gas was bubbled through the solution in the dark (1 h). The HCl gas was generated by the dropwise addition of concentrated sulfuric acid to ammonium chloride in a second flask and transferred via cannula into the reaction mixture (the controlled release of HCl gas from the system must be guaranteed to avoid overpressure). The solution was stirred in the dark (1 h, rt) while the deprotection step was monitored by thin-layer chromatography (MeOH/CH<sub>2</sub>Cl<sub>2</sub> 1:9) or Kaiser test. The solvent was evaporated (high vacuum) and the resulting solid was dissolved in dry DMF (2 mL).

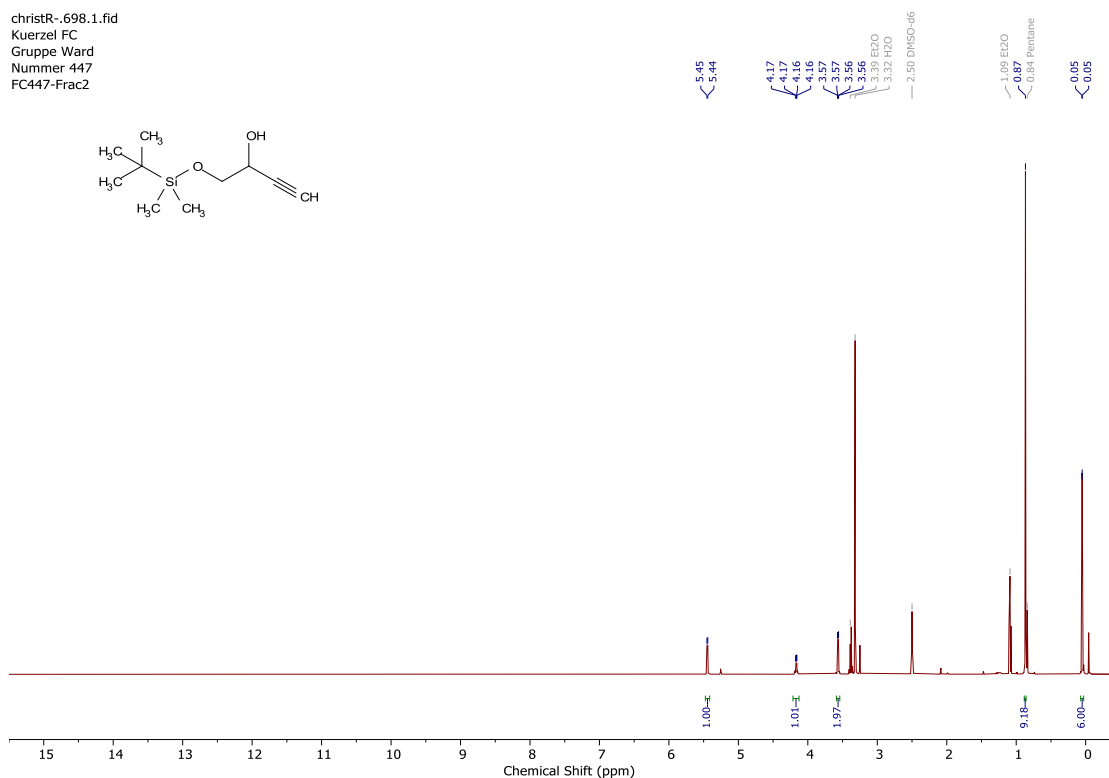
Coupling of gold complex **8** to the peptides: In case the resin was stored temporarily after the addition of succinic anhydride, the resin should be soaked with dry DMF (30 min), purged and then washed with dry DMF (2x2 mL) before further continuation. To the vessel was added HATU (27 mg, 0.07 mmol), DIPEA (24  $\mu$ L, 0.14 mmol) and dry DMF (1.5 mL). The mixture was purged (10 min) and the pH was checked (must be basic, else more DIPEA was added). Afterwards, the deprotected gold complex **8**, dissolved in dry DMF (2 mL) was added to the mixture. The seal was reinforced with Parafilm and the mixture was purged with N<sub>2</sub> overnight. The solvent was removed and the resin was washed with dry DMF (5x2 mL).

Cleaving from the resin:<sup>229</sup> Two cleaving procedures were tested: (1) harsh conditions with TFA:TIPS:H<sub>2</sub>O (95.0:2.5:2.5) and (2) mild conditions with CH<sub>2</sub>Cl<sub>2</sub>:TFA:TIPS (92.5:5.0:2.5). Therein, the corresponding cleaving mixtures (2 mL) were added to the resin in the plastic vessel. The mixtures were purged (90 min, rt). Under harsh conditions a color change from yellow to dark grey was observed. A pointed microwave vial was used to collect the filtrated mixture afterwards. The gold-functionalized peptides were precipitated by the addition of ice-cold diethyl ether and isolated via centrifugation of the precipitate. Further RP-HPLC may be necessary to further purify the desired compound.



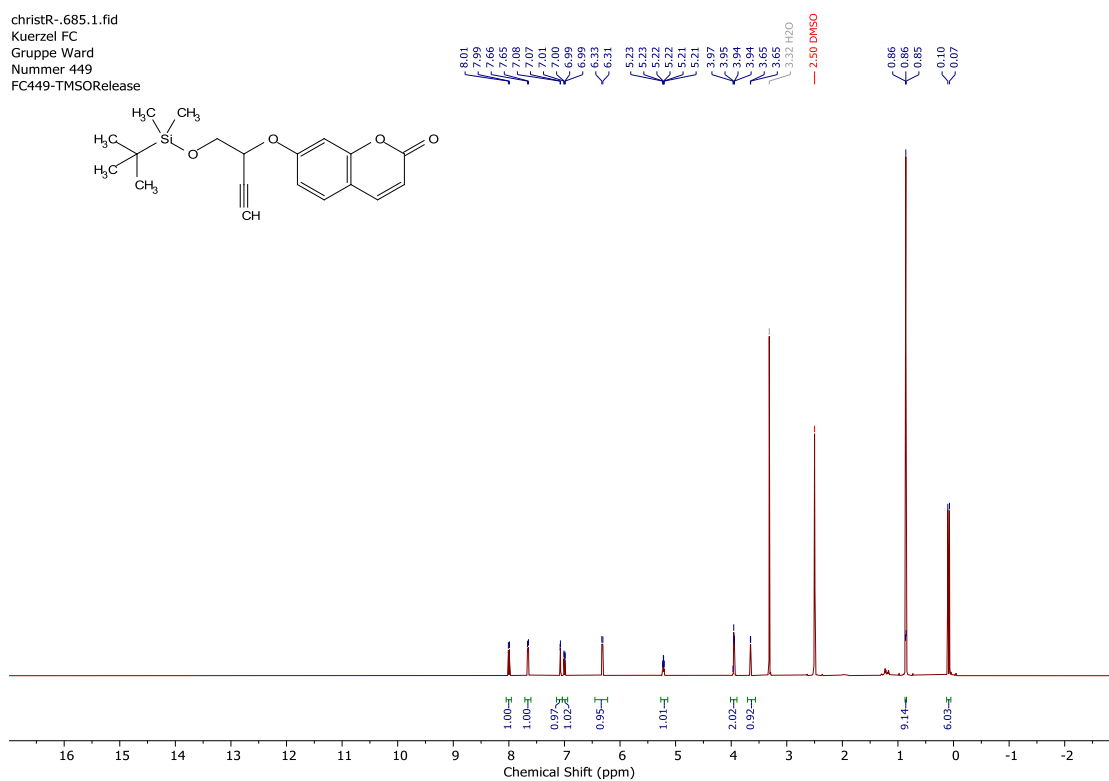
# NMR & Mass Spectra

christR--698.1.fid  
Kuerzel FC  
Gruppe Ward  
Nummer 447  
FC447-Frac2



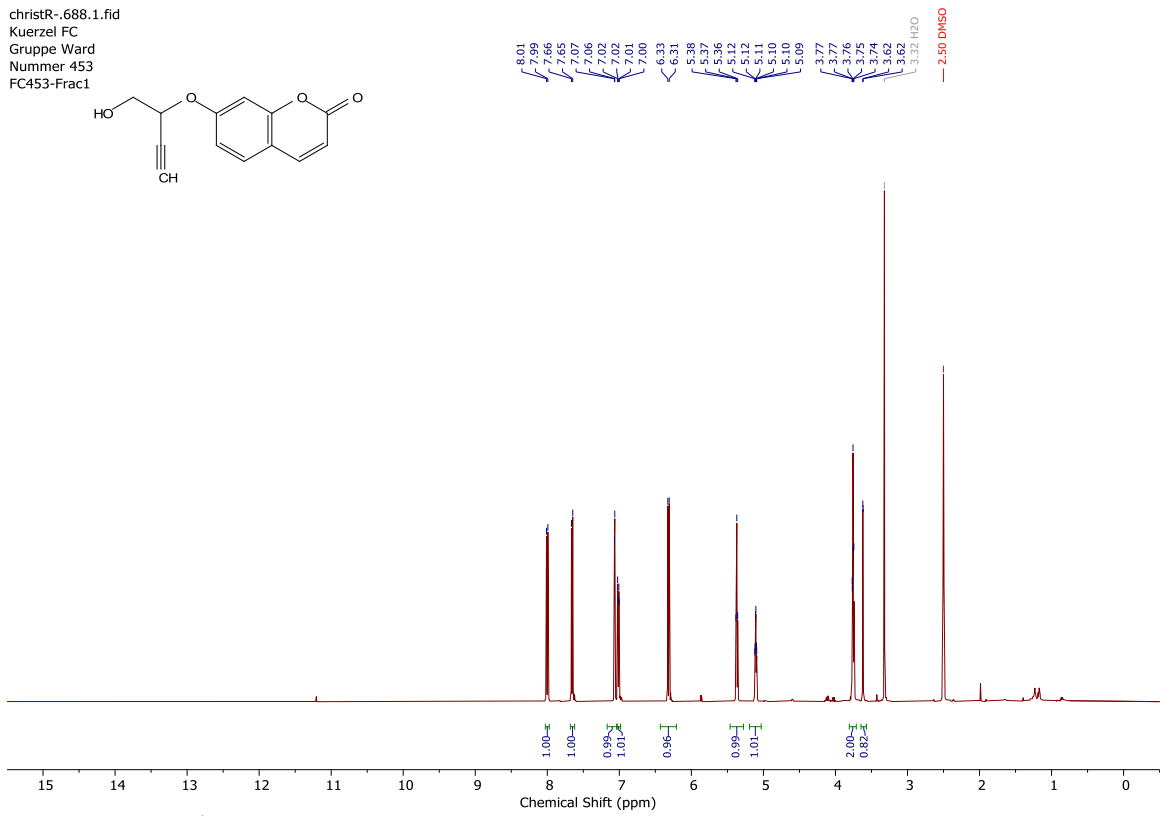
**Spectrum 126** <sup>1</sup>H NMR spectrum of butynol 3 in DMSO-d<sub>6</sub>.

christR--685.1.fid  
Kuerzel FC  
Gruppe Ward  
Nummer 449  
FC449-TMSORelease

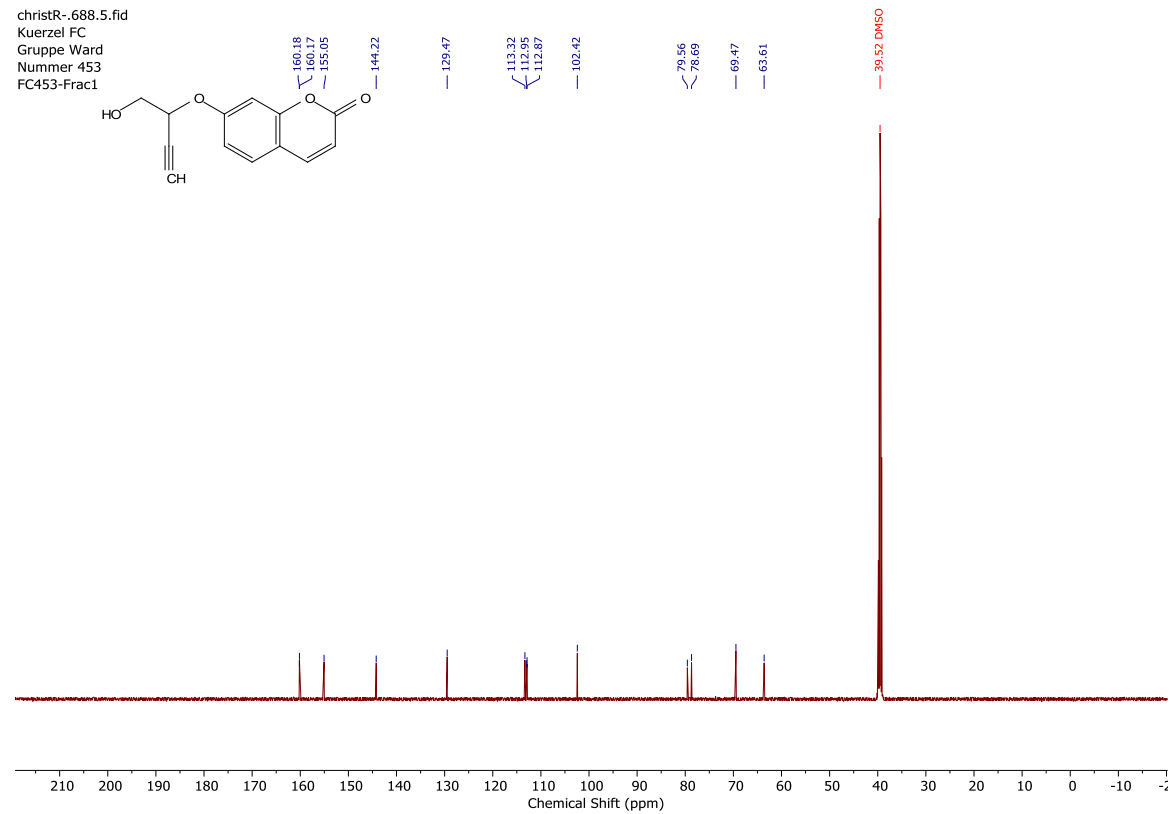


**Spectrum 127** <sup>1</sup>H NMR spectrum of TMS-protected substrate 4 in DMSO-d<sub>6</sub>.

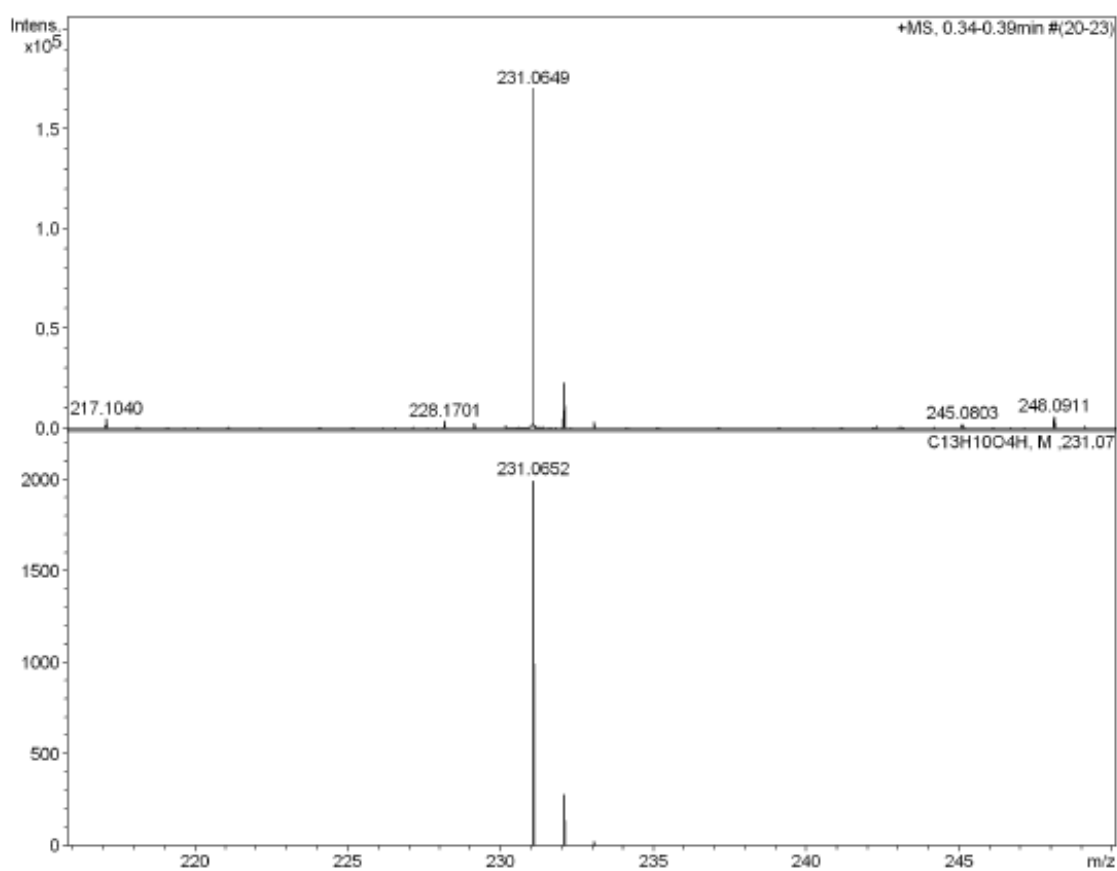
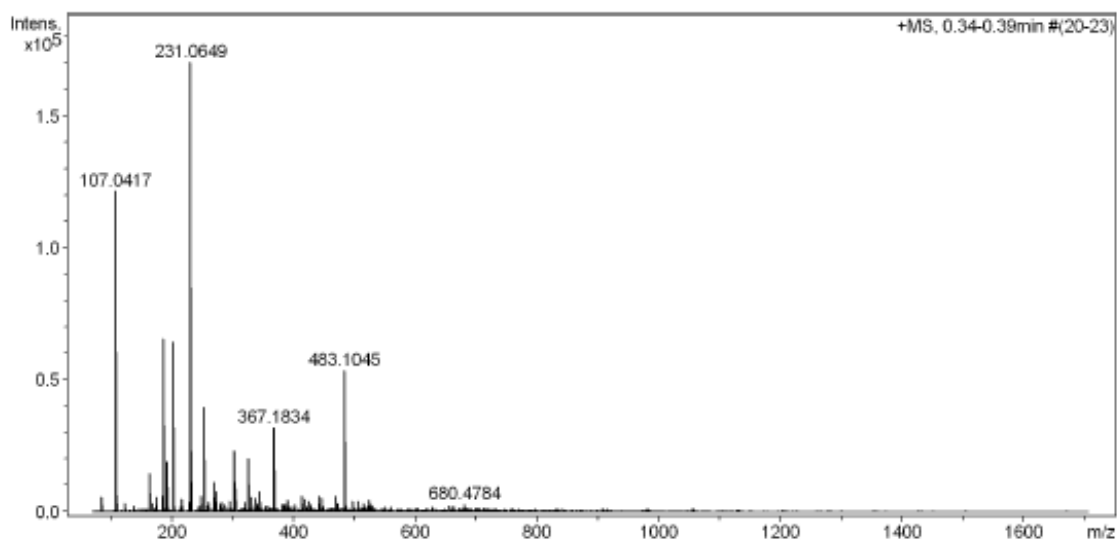
christR-.688.1.fid  
 Kuerzel FC  
 Gruppe Ward  
 Nummer 453  
 FC453-Frac1



**Spectrum 128**  $^1\text{H}$  NMR spectrum of substrate **5** in  $\text{DMSO-}d_6$ .

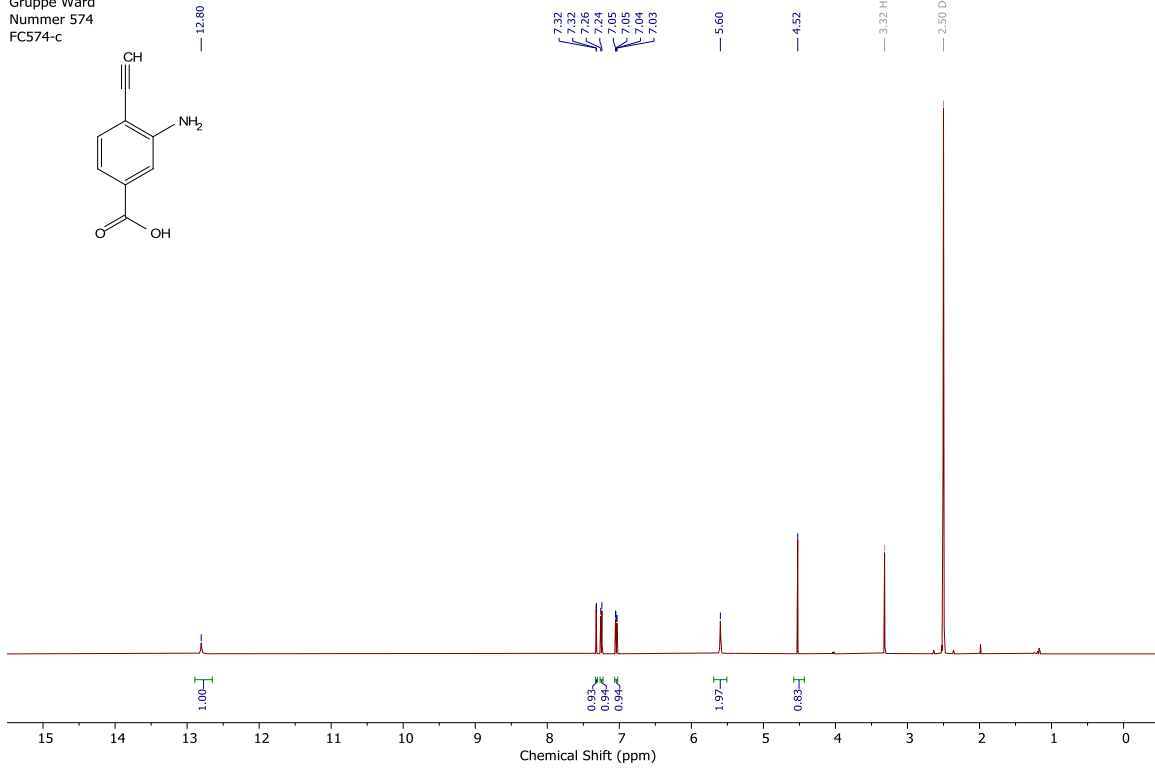


**Spectrum 129**  $^{13}\text{C}$  NMR spectrum of substrate **5** in  $\text{DMSO-}d_6$ .



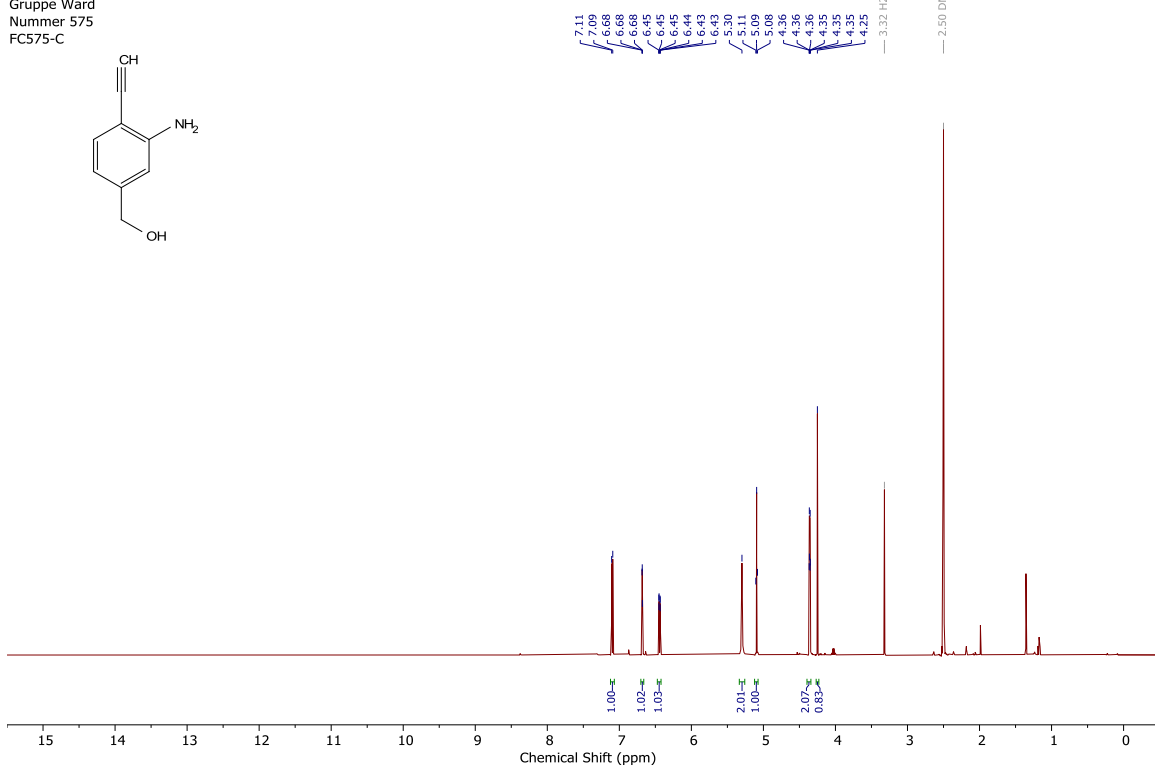
**Spectrum 130** HR-MS spectrum of substrate **5**.

christR-.829.1.fid  
Kuerzel FC  
Gruppe Ward  
Nummer 574  
FC574-c



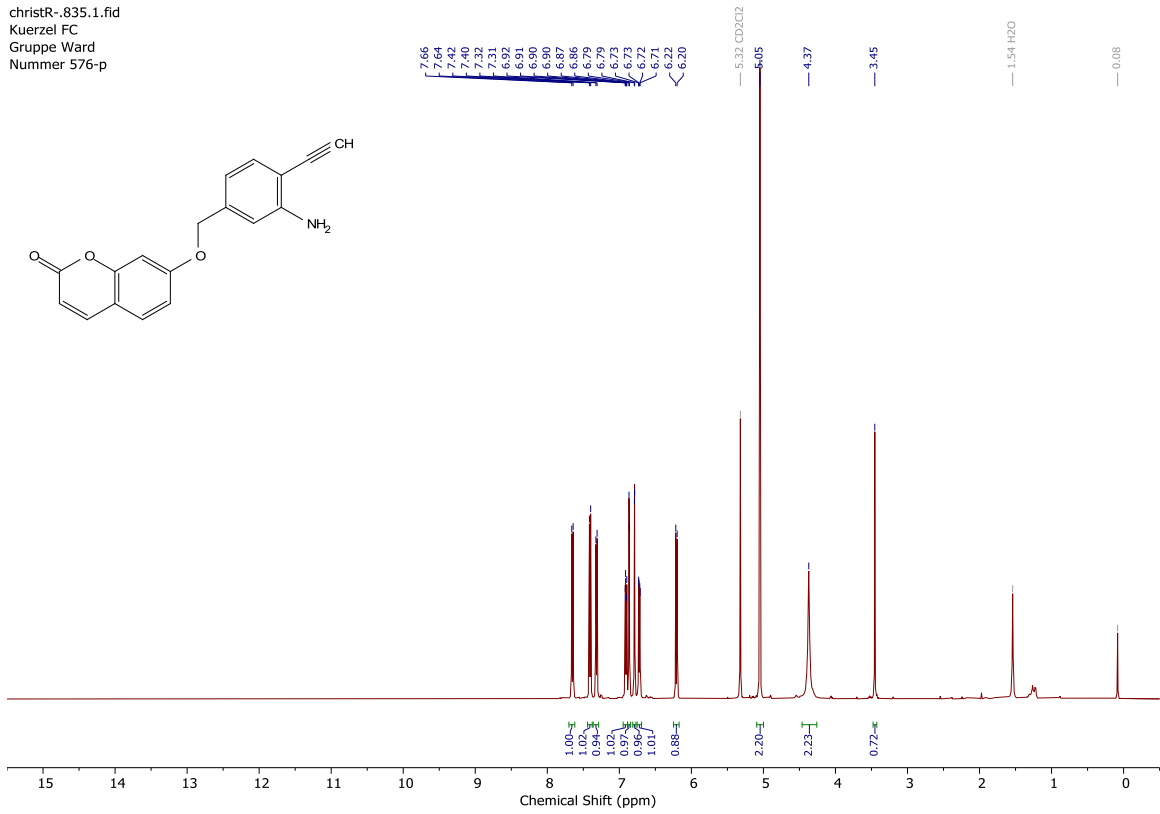
**Spectrum 131** <sup>1</sup>H NMR spectrum of arylacid **14** in DMSO-*d*<sub>6</sub>.

christR-.830.1.fid  
Kuerzel FC  
Gruppe Ward  
Nummer 575  
FC575-C



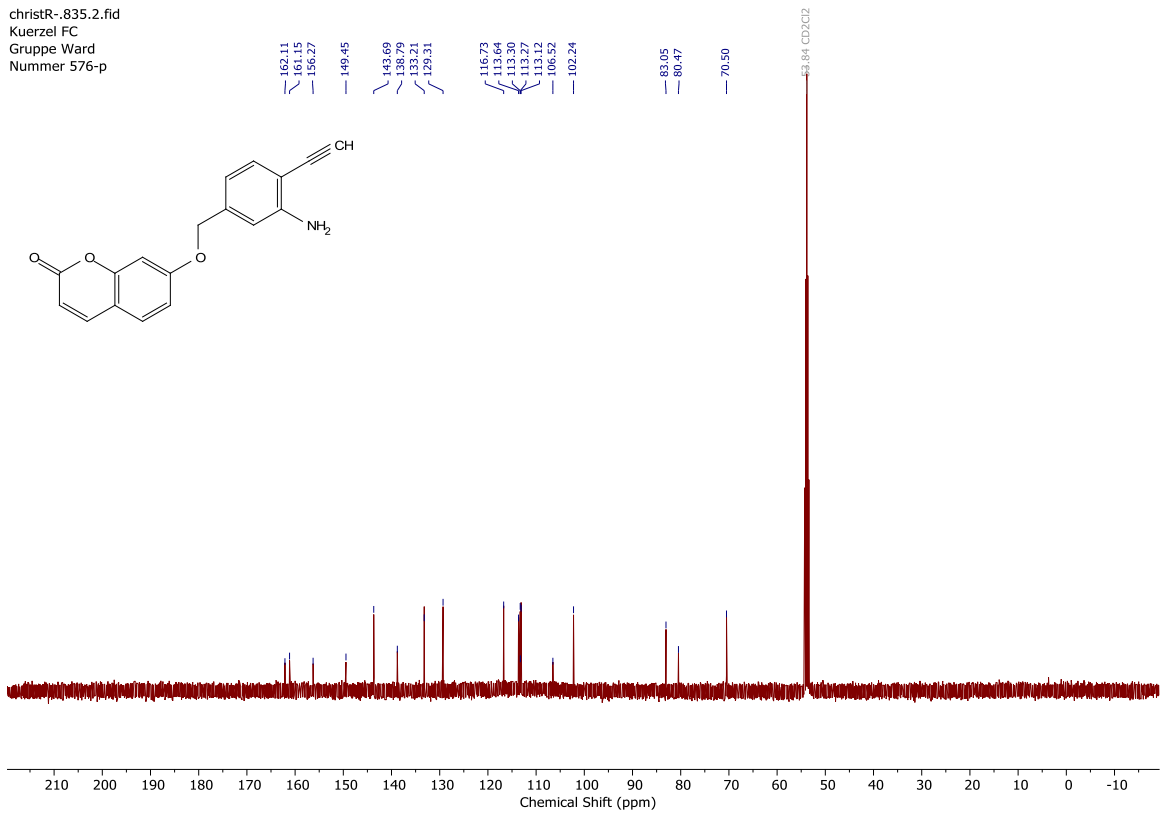
**Spectrum 132** <sup>1</sup>H NMR spectrum of benzylalcohol **15** in DMSO-*d*<sub>6</sub>.

christR-.835.1.fid  
Kuerzel FC  
Gruppe Ward  
Nummer 576-p



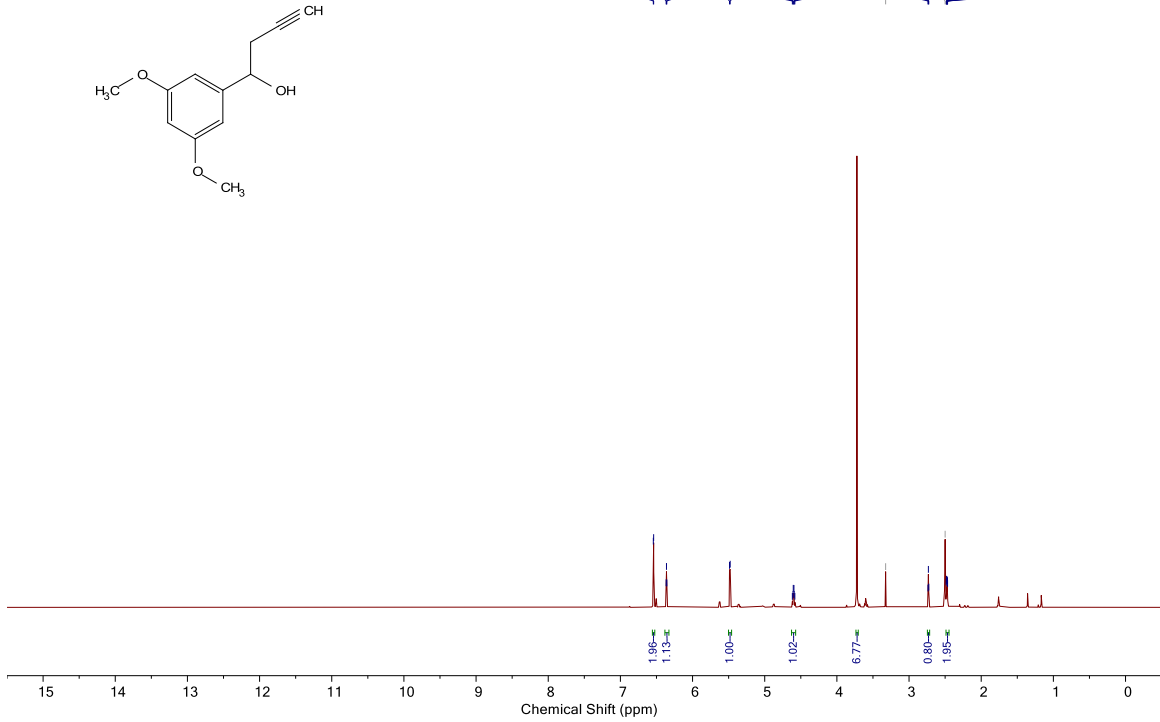
**Spectrum 133**  $^1\text{H}$  NMR spectrum of substrate **16** in  $\text{DMSO-}d_6$ .

christR-.835.2.fid  
Kuerzel FC  
Gruppe Ward  
Nummer 576-p

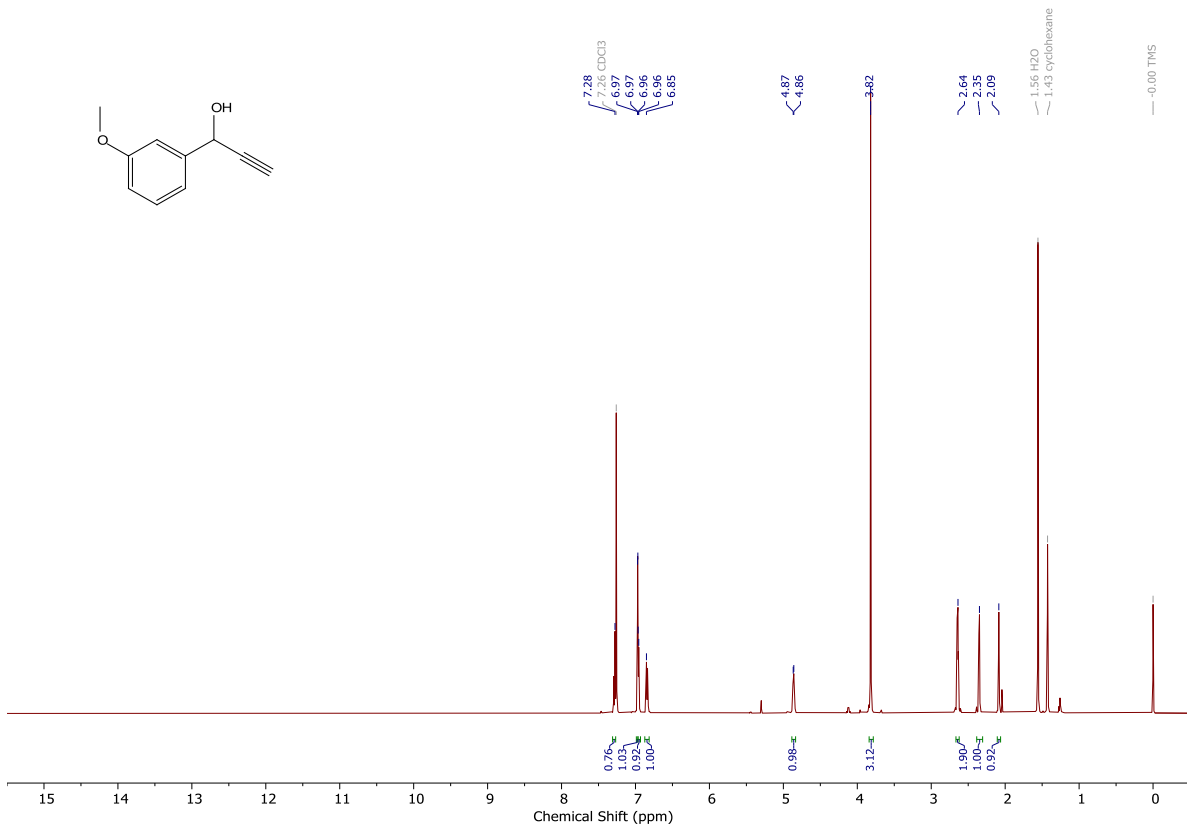


**Spectrum 134**  $^{13}\text{C}$  NMR spectrum of substrate **16** in  $\text{DMSO-}d_6$ .

christR-.771.1.fid  
Kuerzel FC  
Gruppe Ward  
Nummer 541  
FC541-c

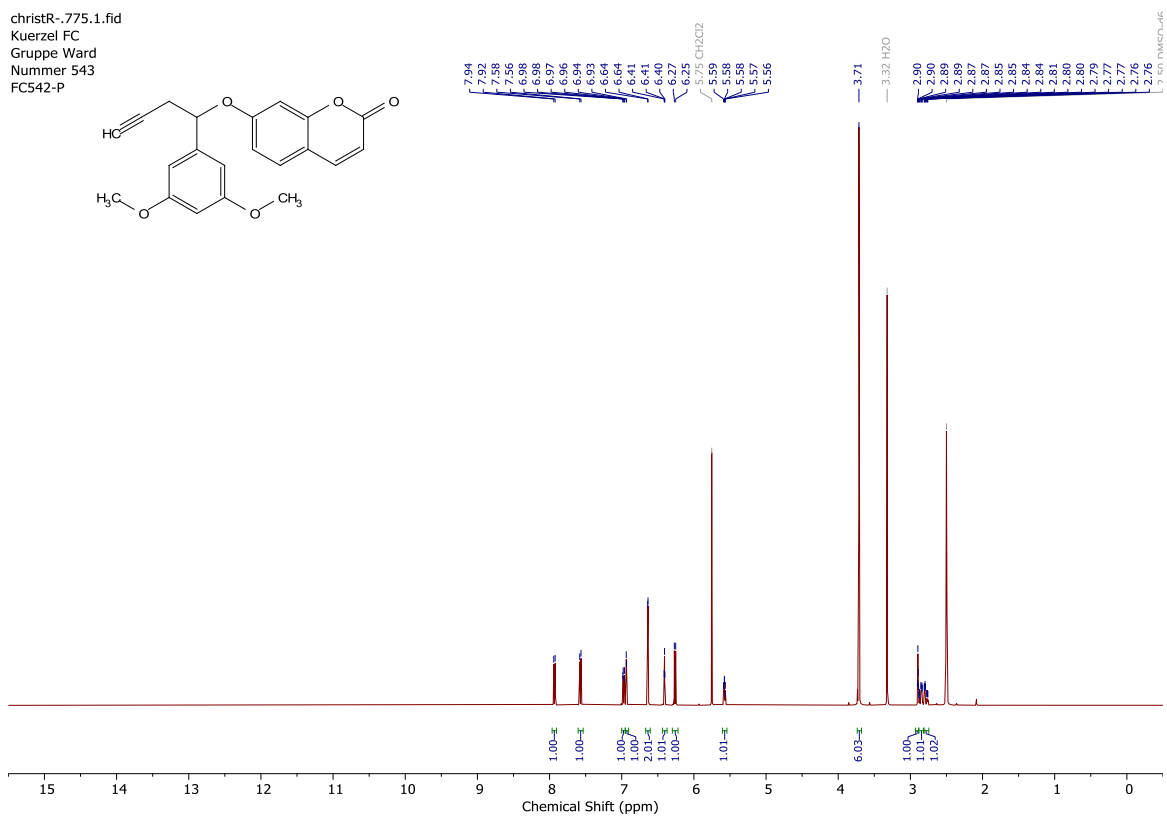


**Spectrum 135** <sup>1</sup>H NMR spectrum of substrate **20** in DMSO-d<sub>6</sub>.

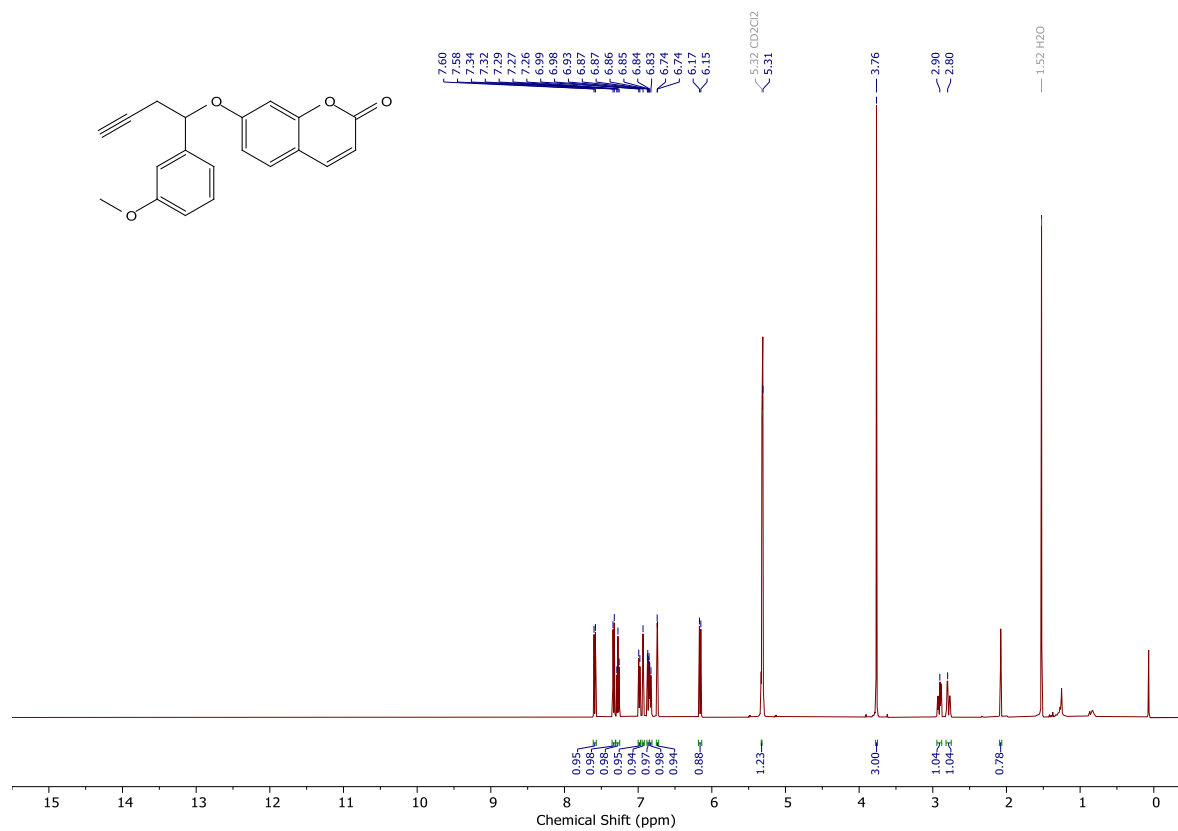


**Spectrum 136** <sup>1</sup>H NMR spectrum of substrate **21** in DMSO-d<sub>6</sub>.

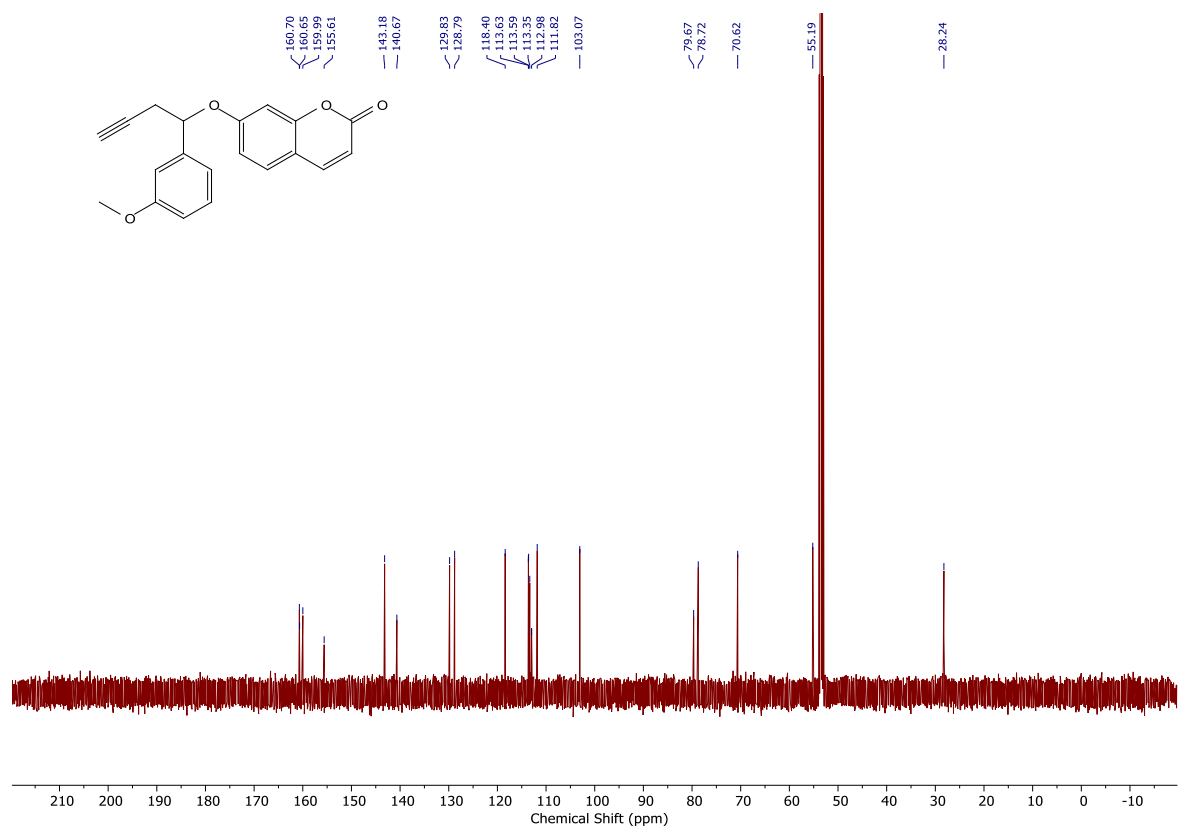
christR-.775.1.fid  
 Kuerzel FC  
 Gruppe Ward  
 Nummer 543  
 FC542-P



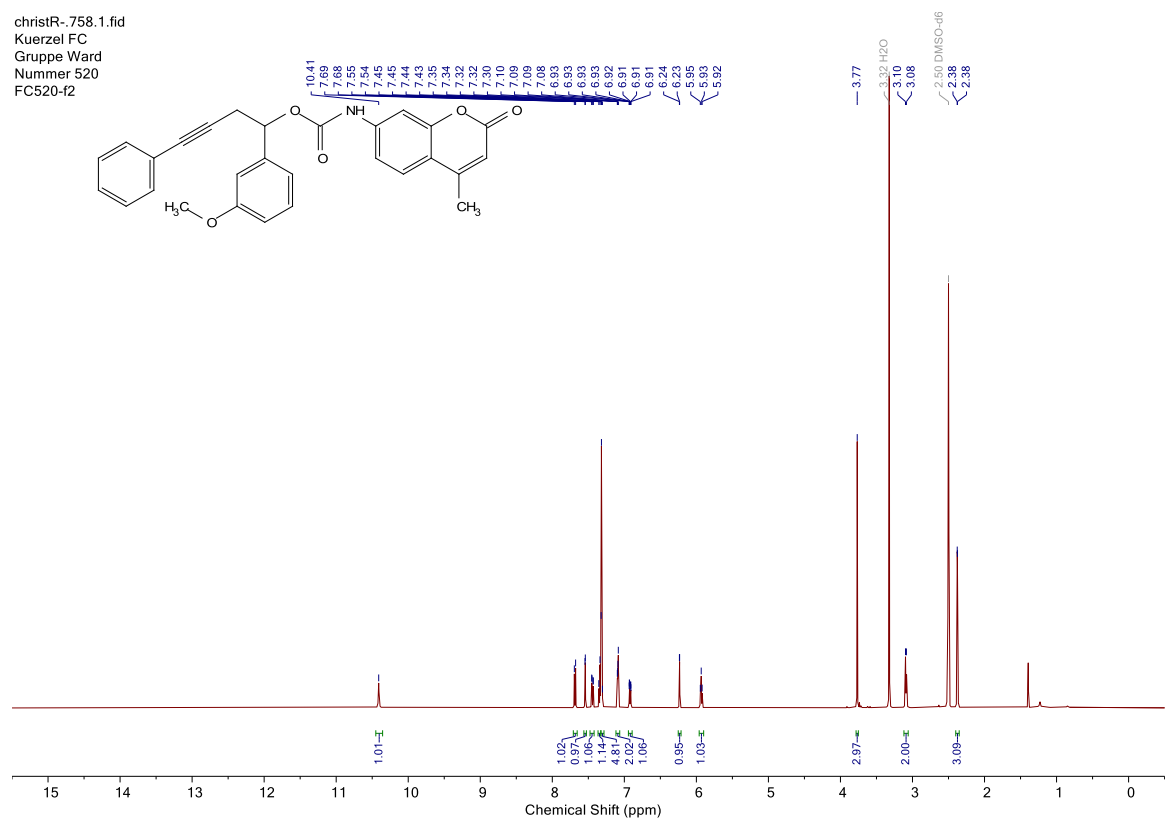
**Spectrum 137** <sup>1</sup>H NMR spectrum of substrate **22** in DMSO-*d*<sub>6</sub>.



**Spectrum 138** <sup>1</sup>H NMR spectrum of substrate **23** in DMSO-*d*<sub>6</sub>.



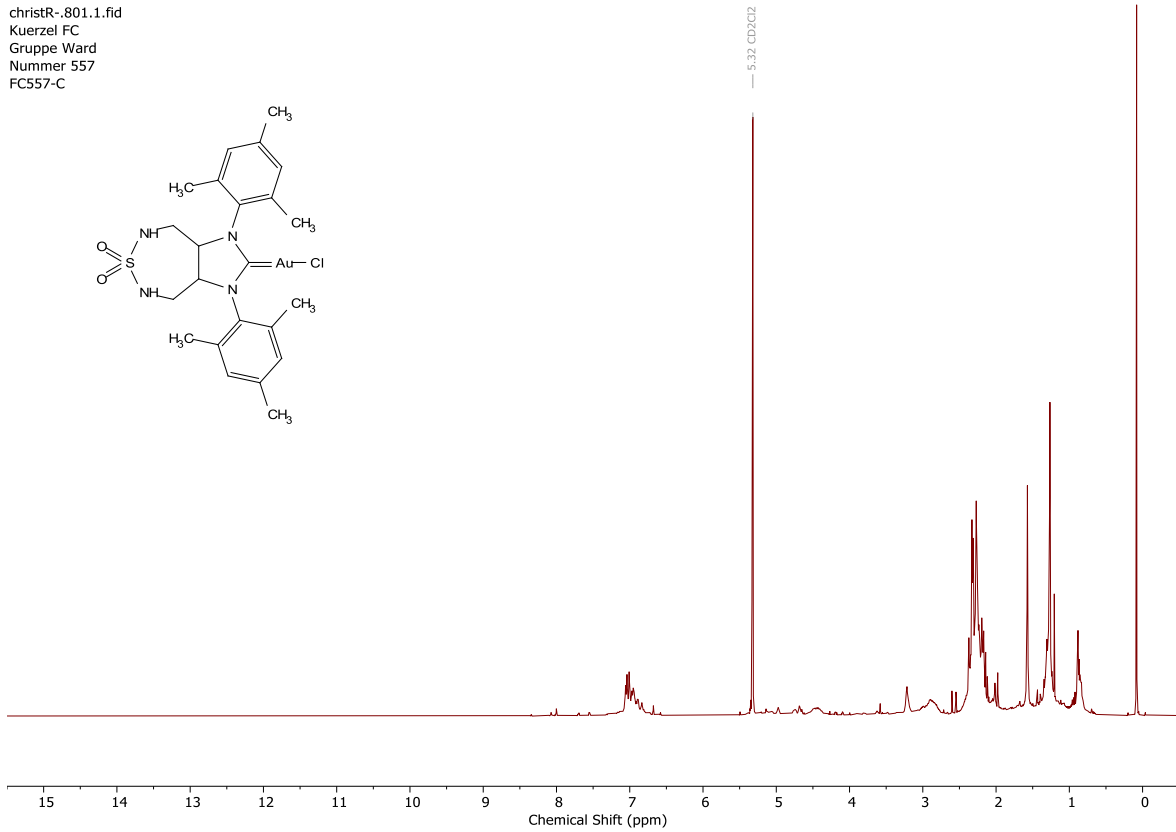
**Spectrum 139**  $^{13}\text{C}$  NMR spectrum of substrate **23** in  $\text{DMSO-}d_6$ .



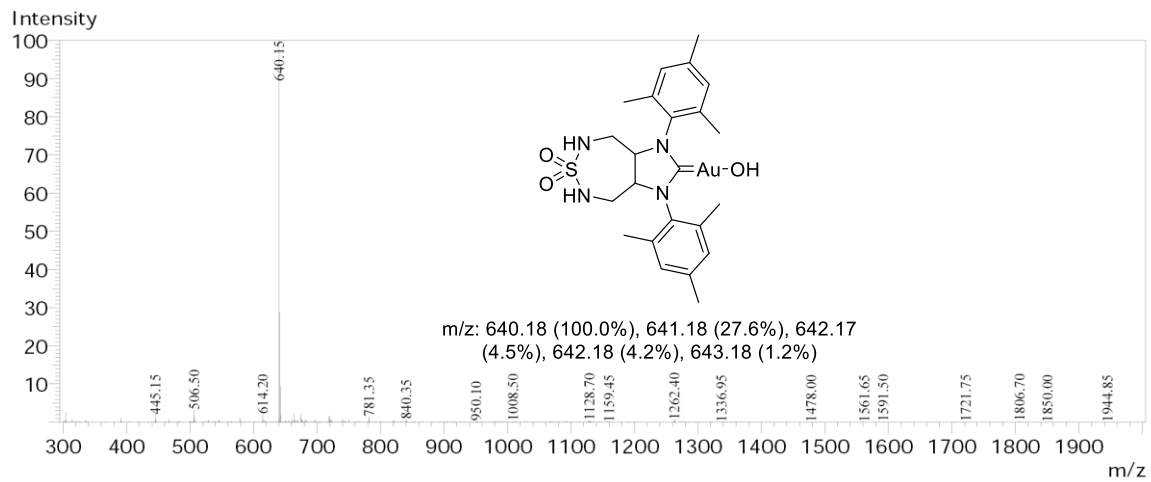
**Spectrum 140**  $^1\text{H}$  NMR spectrum of substrate **26** in  $\text{DMSO-}d_6$ .



christR-.801.1.fid  
Kuerzel FC  
Gruppe Ward  
Nummer 557  
FC557-C



**Spectrum 141**  $^1\text{H}$  NMR spectrum of gold-complex **35** in  $\text{CD}_2\text{Cl}_2$ .

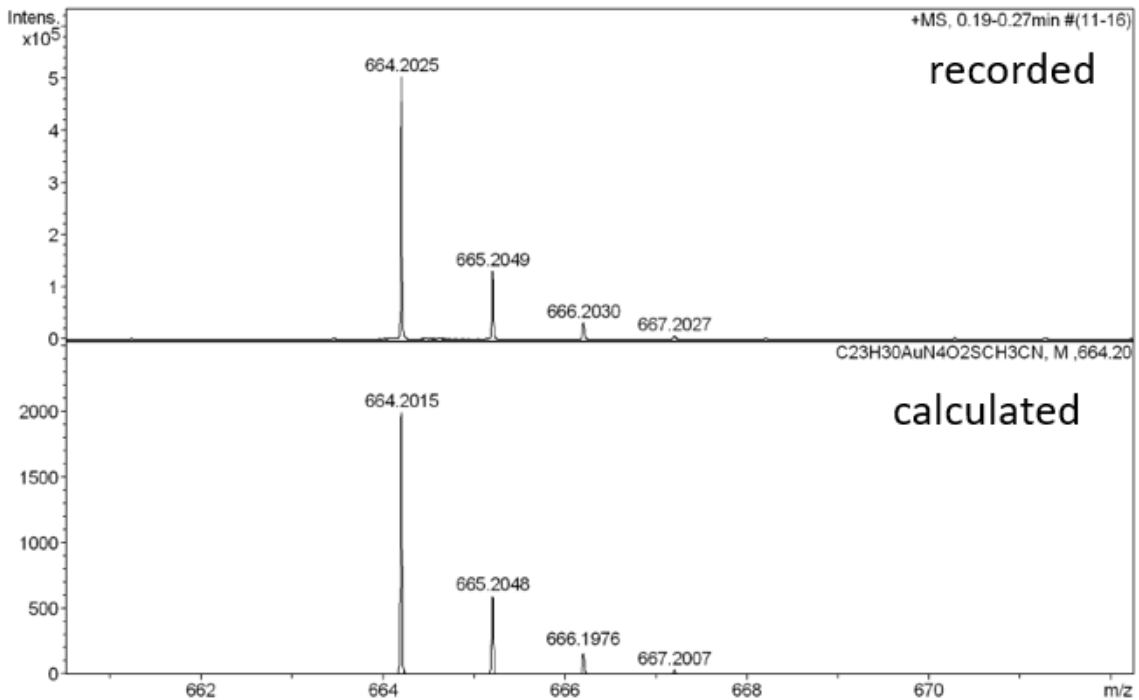
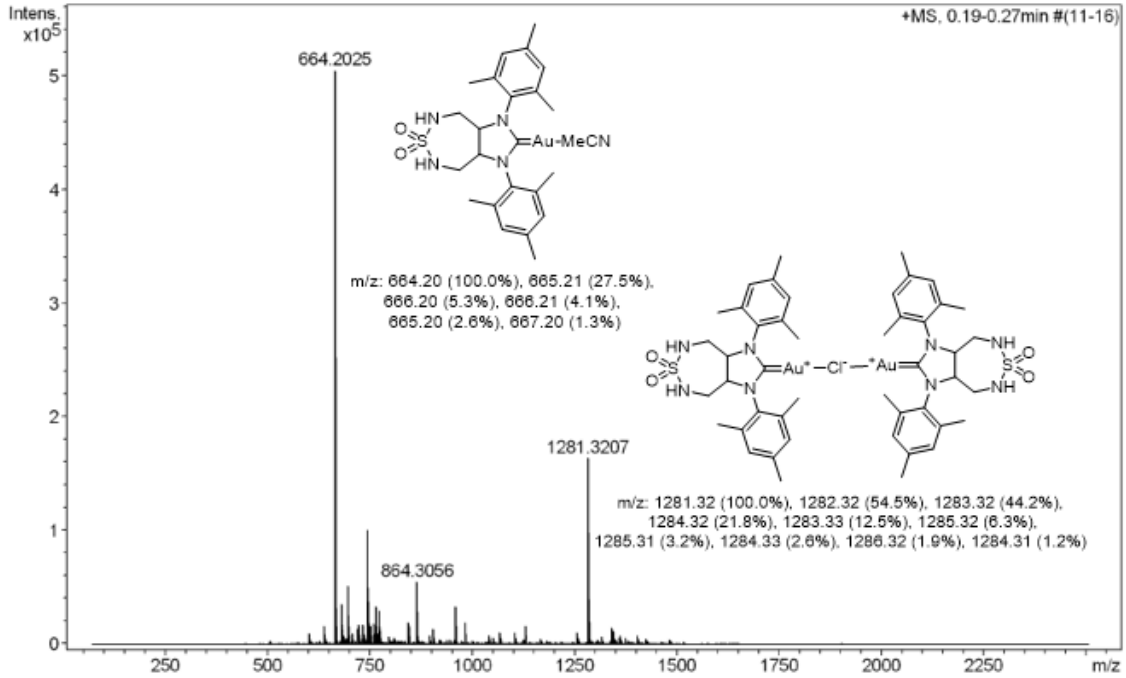


**Spectrum 142** ESI-MS (positive) direct-injection spectrum of gold complex **35**.

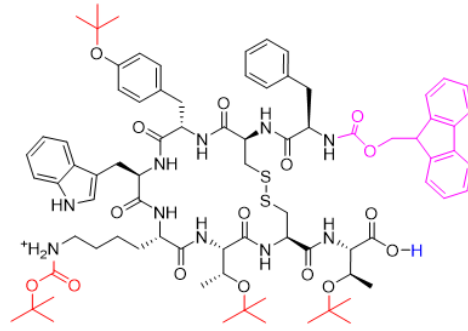
# High Resolution Mass Spectrometry Report

Sample Name **FC557**  
Comment

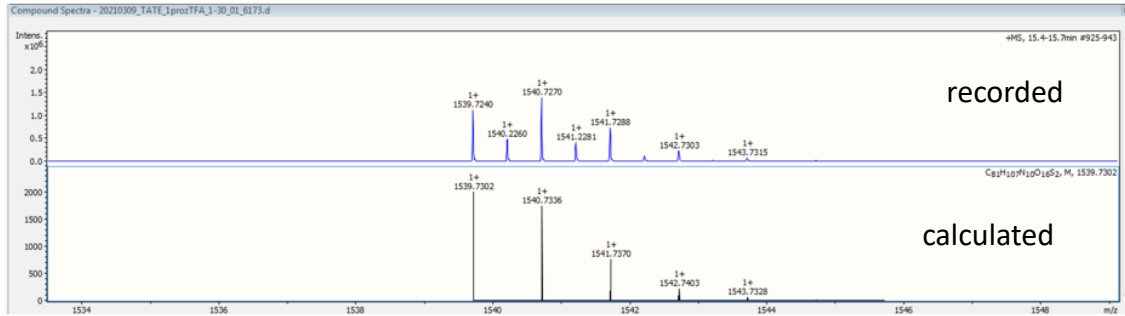
Instrument maXis 4G  
Method ms\_nocolumn\_high\_pos\_use\_acn.m



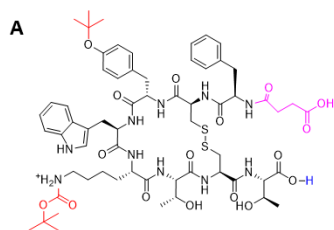
**Spectrum 143** HR-MS (positive) spectrum of gold-complex **35**.



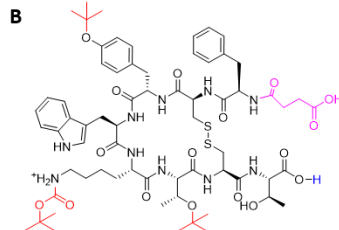
m/z: 1539.73 (100.0%), 1540.73 (92.9%), 1541.74 (42.8%), 1542.74 (15.1%), 1541.73 (13.8%), 1542.73 (9.8%), 1543.74 (4.5%), 1543.73 (4.2%), 1540.74 (1.8%), 1544.74 (1.3%)



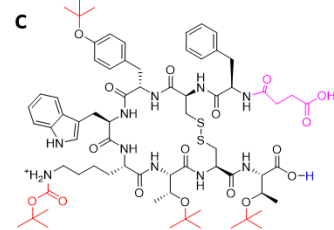
**Spectrum 144** HPLC into HR-MS (positive) spectrum of Fmoc-protected TATE.



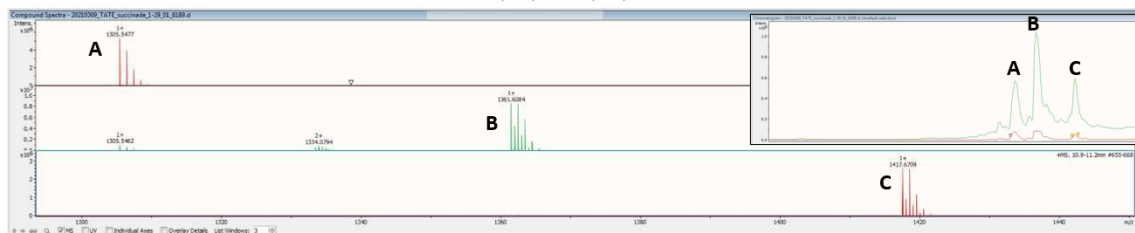
m/z: 1305.55 (100.0%), 1306.56 (68.7%), 1307.56 (27.8%), 1307.55 (11.7%), 1308.56 (8.7%), 1308.55 (6.7%), 1306.55 (5.3%), 1309.56 (3.3%)



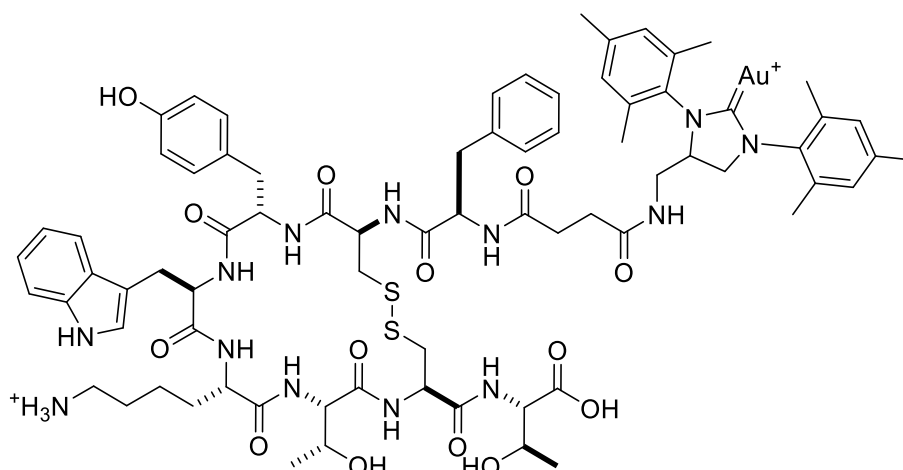
m/z: 1361.62 (100.0%), 1362.62 (74.7%), 1363.62 (32.9%), 1364.62 (10.7%), 1363.61 (9.2%), 1364.63 (6.3%), 1362.61 (3.7%), 1365.62 (3.1%), 1365.63 (2.1%)



m/z: 1417.68 (100.0%), 1418.68 (81.7%), 1419.69 (29.6%), 1420.69 (10.2%), 1419.67 (9.1%), 1420.68 (8.8%), 1419.68 (7.7%), 1421.68 (3.2%), 1421.69 (2.8%), 1418.69 (1.2%), 1422.68 (1.0%)

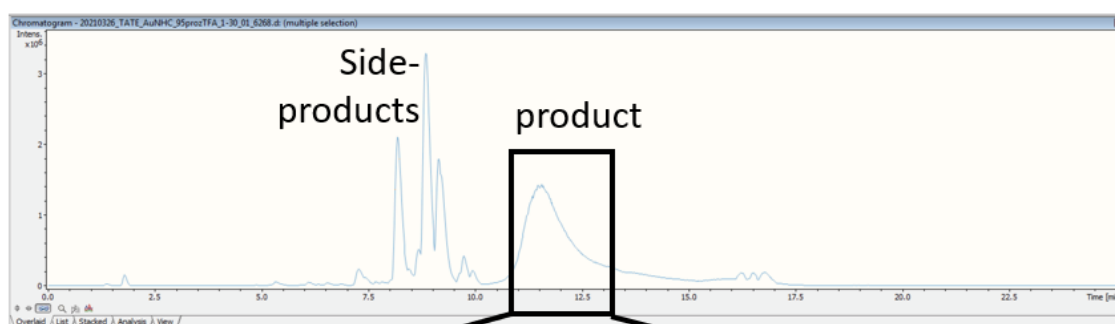


**Spectrum 145** HPLC into HR-MS (positive) spectrum of succinic acid coupled to TATE.

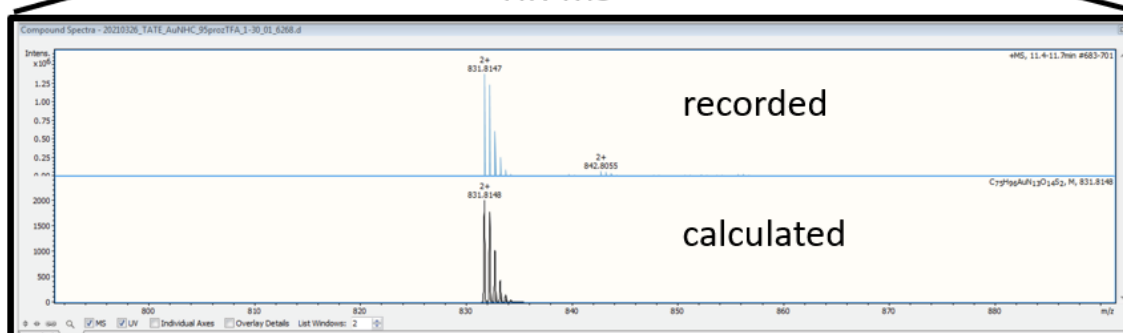


m/z: 831.81 (100.0%), 832.31 (88.1%), 832.82 (33.8%), 832.81 (17.3%), 833.32 (12.1%), 833.31 (9.4%), 833.81 (3.8%), 833.82 (3.5%), 834.32 (1.3%), 832.32 (1.1%)

### HPLC



### HR-MS



**Spectrum 146** HPLC into HR-MS (positive) spectrum of gold-functionalized **TATE**.

## 9. Bibliography:

---

1. Hartwig, J. F. & Ward, T. R. *Acc. Chem. Res.* **52**, 1145 (2019).
2. Kresge, N., Simoni, R. D. & Hill, R. L. *J. Biol. Chem.* **279**, e5–e6 (2004).
3. Acta, B. & Sciences, B. **670**, 207–213 (1981).
4. Laitinen, O. H. *et al. BMC Ecol. Evol.* **21**, 1–14 (2021).
5. Elo, H. A. & Korpela, J. *Comp. Biochem. Physiol. -- Part B Biochem.* **78**, 15–20 (1984).
6. Weber, P. C., Ohlendorf, D. H., Wendoloski, J. J. & Salemme, F. R. *Science* **243**, 85–88 (1989).
7. Green, N. M. *Adv. Protein Chem.* **29**, 85–133 (1975).
8. Wilson, M. E. & Whitesides, G. M. *J. Am. Chem. Soc.* **100**, 306–307 (1978).
9. Yamamura, K. & Kaiser, E. T. *J. Chem. Soc. Chem. Commun.* 830–831 (1976).
10. Schwizer, F. *et al. Chem. Rev.* **118**, 142–231 (2018).
11. Chodosh, L. A. *Curr. Protoc. Mol. Biol.* **36**, 1–9 (1996).
12. Chen, M. *et al. Anal. Methods* **10**, 1870–1874 (2018).
13. Zhang, C. *et al. Angew. Chemie - Int. Ed.* **51**, 3382–3385 (2012).
14. Ostojic, G. N. & Hersam, M. C. *Small* **8**, 1840–1845 (2012).
15. Syrkina, M. S. *et al. Protein Eng. Des. Sel.* **26**, 143–150 (2013).
16. McDevitt, T. C., Nelson, K. E. & Stayton, P. S. *Biotechnol. Prog.* **15**, 391–396 (1999).
17. Weir, C. *et al. Cancer Immunol. Res.* **2**, 469–479 (2014).
18. Jain, A., Barve, A., Zhao, Z., Jin, W. & Cheng, K. *Mol. Pharm.* **14**, 1517–1527 (2017).
19. Holmberg, A. *et al. Electrophoresis* **26**, 501–510 (2005).
20. Skander, M. *et al. J. Am. Chem. Soc.* **126**, 14411–14418 (2004).
21. Klein, G. *et al. Angew. Chemie - Int. Ed.* **44**, 7764–7767 (2005).
22. Pordea, A. *et al. J. Am. Chem. Soc.* **130**, 8085–8088 (2008).
23. Köhler, V. *et al. Angew. Chemie - Int. Ed.* **50**, 10863–10866 (2011).
24. Thomas, C. M., Letondor, C., Humbert, N. & Ward, T. R. *J. Organomet. Chem.* **690**, 4488–4491 (2005).
25. Creus, M. *et al. Angew. Chemie - Int. Ed.* **47**, 1400–1404 (2008).
26. Köhler, V. *et al. Nat. Chem.* **5**, 93–99 (2013).
27. Zhao, J. *et al. J. Am. Chem. Soc.* **140**, 13171–13175 (2018).
28. Chatterjee, A. *et al. Chem. Sci.* **7**, 673–677 (2016).
29. Hyster, T. K., Knörr, L., Ward, T. R. & Rovis, T. *Science* **338**, 500–503 (2012).
30. Jeschek, M. *et al. Nature* **537**, 661–665 (2016).
31. Hesticová, M. *et al. Angew. Chem. Int. Ed.* **57**, 1863–1868 (2018).
32. Heinisch, T. *et al. Chem. Sci.* **9**, 5383–5388 (2018).
33. Mallin, H., Hesticová, M., Reuter, R. & Ward, T. R. *Nat. Protoc.* **11**, 835–852 (2016).

34. Robinson, P. J. & Holbrook, K. A. *Nature* **376**, 238–240 (1995).
35. Bond, G. C., Sermon, P. A., Webb, G., Buchanan, D. A. & Wells, P. B. *J. Chem. Soc. Chem. Commun.* 444–445 (1973).
36. Thompson, D. *Gold Bull.* **31**, 111–118 (1998).
37. Knowles, W. S. *Adv. Synth. Catal.* **345**, 3–13 (2003).
38. Noyori, R. *Adv. Synth. Catal.* **345**, 15–32 (2003).
39. Grubbs, R. H. *Angew. Chemie - Int. Ed.* **45**, 3760–3765 (2006).
40. Negishi, E. I. *Angew. Chemie - Int. Ed.* **50**, 6738–6764 (2011).
41. Hashmi, A. S. K. 3180–3211 (2007).
42. Gorin, D. J. & Toste, F. D. *Nature* **446**, 395–403 (2007).
43. Hashmi, A. S. K. *Acc. Chem. Res.* **47**, 864–876 (2014).
44. McLean, E. B. & Lee, A. L. *Nat. Chem.* **11**, 760–761 (2019).
45. Dorel, R. & Echavarren, A. M. *Chem. Rev.* **115**, 9028–9072 (2015).
46. Jans, A. C. H., Caumes, X. & Reek, J. N. H. *ChemCatChem* **11**, 287–297 (2019).
47. Leyva-Pérez, A. & Corma, A. *Angew. Chem. Int. Ed.* **51**, 614–635 (2012).
48. Roşca, D. A., Wright, J. A. & Bochmann, M. (2015).
49. Pflästerer, D. & Hashmi, A. S. K. 1331–1367 (2016).
50. Cheong, P. H. Y., Morganelli, P., Luzung, M. R., Houk, K. N. & Toste, F. D. *J. Am. Chem. Soc.* **130**, 4517–4526 (2008).
51. Stephen, A., Hashmi, K., Braun, I., Rudolph, M. & Rominger, F. *Organometallics* **31**, 644–661 (2012).
52. Gimeno, A., Medio-Simón, M., De Arellano, C. R., Asensio, G. & Cuenca, A. B. *Org. Lett.* **12**, 1900–1903 (2010).
53. Ye, L., Wang, Y., Aue, D. H. & Zhang, L. *J. Am. Chem. Soc.* **134**, 31–34 (2012).
54. Zhao, X., Rudolph, M. & Hashmi, A. S. K. *Chem. Commun.* **55**, 12127–12135 (2019).
55. Wang, W. *et al. Chem. Soc. Rev.* (2021).
56. Maglio, O. *et al. Comptes Rendus Chim.* **10**, 703–720 (2007).
57. Nordlund, P., Sjöberg, B. M. & Eklund, H. *Nature* **345**, 593–598 (1990).
58. Chino, M. *et al. Eur. J. Inorg. Chem.* **2015**, 3371–3390 (2015).
59. Raines, D. J. *et al. Nat. Catal.* **1**, 680–688 (2018).
60. Changa, P. V. *et al. Proc. Natl. Acad. Sci. U. S. A.* **107**, 1821–1826 (2010).
61. Jewett, J. C. & Bertozzi, C. R. *Chem. Soc. Rev.* **39**, 1272–1279 (2010).
62. Devaraj, N. K. *ACS Cent. Sci.* **4**, 952–959 (2018).
63. Lauwaet, T. *et al. PLoS Negl. Trop. Dis.* **14**, 1–27 (2020).
64. Pickens, C. J., Johnson, S. N., Pressnall, M. M., Leon, M. A. & Berkland, C. J. *Bioconjug. Chem.* **29**, 686–701 (2018).
65. Boren, B. C. *et al. J. Am. Chem. Soc.* **130**, 8923–8930 (2008).

66. Vidal, C., Tomás-Gamasa, M., Destito, P., López, F. & Mascareñas, J. L. *Nat. Commun.* **9**, 1–9 (2018).
67. Tsubokura, K. *et al. Angew. Chemie - Int. Ed.* **56**, 3579–3584 (2017).
68. Pérez-López, A. M. *et al. Angew. Chemie - Int. Ed.* **56**, 12548–12552 (2017).
69. Jung Jou, M. *et al. Chem. Commun.* 7218–7220 (2009).
70. Wang, J. B., Wu, Q. Q., Min, Y. Z., Liu, Y. Z. & Song, Q. H. *Chem. Commun.* **48**, 744–746 (2012).
71. Huang, X. *et al. ACS Cent. Sci.* **4**, 760–767 (2018).
72. Yang, Y. K., Lee, S. & Tae, J. *Org. Lett.* **11**, 5610–5613 (2009).
73. Christoffel, F. *et al. Nat. Catal.* **4**, 643–653 (2021).
74. Chen, K. & Arnold, F. H. 203–213 (2020).
75. Reetz, M. T. *Acc. Chem. Res.* **52**, 336–344 (2019).
76. Studer, S. *et al. Science* **362**, 1285–1288 (2018).
77. Gu, Y., Natoli, S. N., Liu, Z., Clark, D. S. & Hartwig, J. F. *Angew. Chem. Int. Ed.* **58**, 13954–13960 (2019).
78. Roelfes, G. *Acc. Chem. Res.* 545–556 (2019).
79. Oohora, K., Miyazaki, Y. & Hayashi, T. *Angew. Chem. Int. Ed.* **58**, 13813–13817 (2019).
80. Song, W. J. & Tezcan, F. A. *Science* **346**, 1525–1528 (2014).
81. Watanabe, Y., Aiba, Y., Ariyasu, S. & Abe, S. *Bull. Chem. Soc. Jpn.* **93**, 379–392 (2020).
82. Nödling, A. R. *et al. Angew. Chemie Int. Ed.* **57**, 12478–12482 (2018).
83. Zhou, Z. & Roelfes, G. *Nat. Catal.* **3**, 289–294 (2020).
84. Alonso, S. *et al. Nat. Catal.* **3**, 319–328 (2020).
85. Martínez-Calvo, M. *et al. ACS Catal.* **8**, 6055–6061 (2018).
86. Heinisch, T. & Ward, T. R. *Acc. Chem. Res.* **49**, 1711–1721 (2016).
87. Monnard, F. W., Nogueira, E. S., Heinisch, T., Schirmer, T. & Ward, T. R. *Chem. Sci.* **4**, 3269–3274 (2013).
88. Oohora, K., Onoda, A. & Hayashi, T. *Acc. Chem. Res.* **52**, 945–954 (2019).
89. Mirts, E. N., Petrik, I. D., Hosseinzadeh, P., Nilges, M. J. & Lu, Y. *Science* 1098–1101 (2018).
90. Lewis, J. C. *Acc. Chem. Res.* 576–584 (2019).
91. Lombardi, A., Pirro, F., Maglio, O., Chino, M. & Degrado, W. F. *Acc. Chem. Res.* 1148–1159 (2019).
92. Schwaneberg, U. *Acc. Chem. Res.* 2611–2614 (2018).
93. Eda, S. *et al. Nat. Catal.* **2**, 780–792 (2019).
94. Liang, A. D., Serrano-plana, J., Peterson, R. L. & Ward, T. R. *Acc. Chem. Res.* 585–595 (2019).
95. Vornholt, T. *et al. Sci. Adv.* **7**, 1–12 (2021).

96. Gimeno, A. *et al.* *Chem. - A Eur. J.* **20**, 683–688 (2014).
97. Vreeken, V. *et al.* *Angew. Chem. Int. Ed.* **55**, 10042–10046 (2016).
98. Ye, D. *et al.* *Green Chem.* **11**, 1201–1208 (2009).
99. Le Trong, I. *et al.* *Acta Crystallogr. Sect. D Biol. Crystallogr.* **67**, 813–821 (2011).
100. Breker, V., Sak, H., Baracchi-Krause, G. & Krause, N. *Tetrahedron Lett.* **56**, 3390–3392 (2015).
101. Collado, A., Gómez-Suárez, A., Martín, A. R., Slawin, A. M. Z. & Nolan, S. P. *Chem. Commun.* **49**, 5541–5543 (2013).
102. Fre, P. De, Scott, N. M., Stevens, E. D. & Nolan, S. P. *Organometallics* 2411–2418 (2005).
103. Kajetanowicz, A., Chatterjee, A., Reuter, R. & Ward, T. R. *Catal. Letters* **144**, 373–379 (2014).
104. Jordan, J. P. & Grubbs, R. H. *Angew. Chem. Int. Ed.* **46**, 5152–5155 (2007).
105. Benhamou, L., César, V., Gornitzka, H., Lugan, N. & Lavigne, G. *Chem. Commun.* 4720–4722 (2009).
106. Collot, J., Humbert, N., Skander, M., Klein, G. & Ward, T. R. in 4868–4871 (Elsevier B.V., 2004).
107. Anhäuser, L., Teders, M., Rentmeister, A. & Glorius, F. *Nat. Protoc.* **14**, 2599–2626 (2019).
108. Pitzer, L., Schäfers, F. & Glorius, F. *Angew. Chem. Int. Ed.* **58**, 8572–8576 (2019).
109. Pellizzoni, M. M. *et al.* *ACS Catal.* **8**, 1476–1484 (2018).
110. Muñoz Robles, V., Vidossich, P., Lledós, A., Ward, T. R. & Maréchal, J. D. *ACS Catal.* **4**, 833–842 (2014).
111. Spagnolo, L. *et al.* *J. Biol. Chem.* **279**, 33447–33455 (2004).
112. Loving, G. & Imperiali, B. *Bioconjug. Chem.* **20**, 2133–2141 (2009).
113. Loving, G. & Imperiali, B. *J. Am. Chem. Soc.* **130**, 13630–13638 (2008).
114. Alonso-Cotchico, L., Rodríguez-Guerra, J., Lledós, A. & Maréchal, J. D. *Acc. Chem. Res.* **53**, 896–905 (2020).
115. Marenich, A. V., Cramer, C. J. & Truhlar, D. G. *J. Phys. Chem. B* **113**, 6378–6396 (2009).
116. Kiss, P. T. & Baranyai, A. *J. Chem. Phys.* **138**, 204507 (2013).
117. Webb, B. & Sali, A. *Curr. Protoc. Bioinforma.* **2016**, 5.6.1–5.6.37 (2016).
118. Case, D. A. *et al.* *Univ. California, San Fr. 2018* 1–923 (2018).
119. Rodríguez-Guerra Pedregal, J., Sciortino, G., Guasp, J., Municoy, M. & Maréchal, J.-D. *J. Comput. Chem.* **38**, 2118–2126 (2017).
120. Gareth Jones, Peter Willett, Robert C. Glen, Andrew R. Leach, R. T. *J. Mol. Biol.* **267**, 727–748 (1997).



121. Nanda, V. & Koder, R. L. *Nat. Chem.* **2**, 15–24 (2010).
122. Morris, J. H., Huang, C. C., Babbitt, P. C. & Ferrin, T. E. *Bioinformatics* **23**, 2345–2347 (2007).
123. Pettersen, E. F. *et al.* *J. Comput. Chem.* **25**, 1605–1612 (2004).
124. Wilson, Y. M., Dürrenberger, M., Nogueira, E. S. & Ward, T. R. *J. Am. Chem. Soc.* **136**, 8928–8932 (2014).
125. Rebelein, J. G., Cotelle, Y., Garabedian, B. & Ward, T. R. *ACS Catal.* **9**, 4173–4178 (2019).
126. Jeschek, M. *et al.* *Nature* **537**, 661–665 (2016).
127. Markel, U. *et al.* *Chem. Soc. Rev.* 233–262 (2020).
128. Tang, L. *et al.* *Biotechniques* **52**, 149–158 (2012).
129. Qu, G., Li, A., Acevedo-Rocha, C. G., Sun, Z. & Reetz, M. T. 13204–13231 (2020).
130. Takemiya, A. & Hartwig, J. F. 6042–6043 (2006).
131. Liu, Z. & Hartwig, J. F. *J. Am. Chem. Soc.* **130**, 1570–1571 (2008).
132. Miller, M. A. *et al.* *Nat. Commun.* **8**, 1–13 (2017).
133. Agostini, F. *et al.* *bioRxiv* (2019).
134. Akashi, H. & Gojobori, T. *Proc. Natl. Acad. Sci. U. S. A.* **99**, 3695–3700 (2002).
135. López-Soria, J. M. *et al.* *RSC Adv.* **5**, 6647–6651 (2015).
136. Lee, D. J., Mandai, K., Harris, P. W. R., Brimble, M. A. & Kent, S. B. H. *Org. Lett.* **11**, 5270–5273 (2009).
137. Christoffel, F. & Ward, T. R. *Catal. Letters* **148**, 489–511 (2018).
138. Heck, K. F. & Nolley, J. P. *J. Org. Chem.* **37**, 2320–2322 (1972).
139. Mizoroki, T., Mori, K. & Ozaki, A. 581–581 (1971).
140. Johansson Seechurn, C. C. C., Kitching, M. O., Colacot, T. J. & Snieckus, V. *Angew. Chemie - Int. Ed.* **51**, 5062–5085 (2012).
141. Alonso, F., Beletskaya, I. P. & Yus, M. *Tetrahedron* **61**, 11771–11835 (2005).
142. Heck, R. F. *Org. React.* **27**, 345–390 (1982).
143. Zafar, M. N., Mohsin, M. A., Danish, M., Nazar, M. F. & Murtaza, S. *Russ. J. Coord. Chem. Khimiya* **40**, 781–800 (2014).
144. Knowles, J. P. & Whiting, A. *Org. Biomol. Chem.* **5**, 31–44 (2007).
145. Beletskaya, I. P. & Cheprakov, A. V. *Chem. Rev.* **100**, 3009–3066 (2000).
146. Genet, J. P. & Savignac, M. *J. Organomet. Chem.* **576**, 305–317 (1999).
147. Lemaire-Audoire, S., Savignac, M., Dupuis, C. & Genêt, J. P. *Tetrahedron Lett.* **37**, 2003–2006 (1996).
148. Hervé, G. & Len, C. *RSC Adv.* **4**, 46926–46929 (2014).
149. Chatterjee, A. *et al.* *Chem. Sci.* **7**, 673–677 (2016).
150. Heinisch, T. & Ward, T. R. *Acc. Chem. Res.* **49**, 1711–1721 (2016).

151. Li, J. & Chen, P. R. *ChemBioChem* **13**, 1728–1731 (2012).
152. Bumagin, N. A., More, P. G. & Beletskaya, I. P. *J. Organomet. Chem.* **371**, 397–401 (1989).
153. Casalnuovo, A. L. & Calabrese, J. C. *J. Am. Chem. Soc.* **112**, 4324–4330 (1990).
154. Haque, R. A., Asekunowo, P. O., Budagumpi, S. & Shao, L. *Eur. J. Inorg. Chem.* **2015**, 3169–3181 (2015).
155. Hajipour, A. R. & Khorsandi, Z. *Appl. Organomet. Chem.* **30**, 256–261 (2016).
156. Hajipour, A. R., Abolfathi, P. & Mohammadsaleh, F. *RSC Adv.* **6**, 78080–78089 (2016).
157. Filice, M. *et al.* *Adv. Synth. Catal.* **357**, 2687–2696 (2015).
158. Liu, J. *et al.* *Synthesis (Stuttg.)* 2661–2666 (2003).
159. Chen, C., Zheng, Q., Ni, S. & Wang, H. *New J. Chem.* **42**, 4624–4630 (2018).
160. Astakhov, A. V. *et al.* *Organometallics* **36**, 1981–1992 (2017).
161. Chalker, J. M., Wood, C. S. C. & Davis, B. G. *J. Am. Chem. Soc.* **131**, 16346–16347 (2009).
162. Nagai, Y., Kochi, T. & Nozaki, K. *Organometallics* **28**, 6131–6134 (2009).
163. Moore, L. R. *et al.* *Organometallics* **25**, 5151–5158 (2006).
164. Chatterjee, A. & Ward, T. R. *Catal. Letters* **146**, 820–840 (2016).
165. Latocheski, E. *et al.* *Chem. Soc. Rev.* **49**, 7710–7729 (2020).
166. Thomson, A. J. & Grayt Addresses, H. B. *Curr. Opin. Chem. Biol.* **2**, 155–158 (1998).
167. Rebelein, J. G. & Ward, T. R. *Curr. Opin. Biotechnol.* **53**, 106–114 (2018).
168. Sasmal, P. K., Streu, C. N. & Meggers, E. *Chem. Commun.* **49**, 1581–1587 (2013).
169. Wang, J. *et al.* *J. Am. Chem. Soc.* **138**, 15118–15121 (2016).
170. Martínez-Calvo, M. & Mascareñas, J. L. *Coord. Chem. Rev.* **359**, 57–79 (2018).
171. Tomás-Gamasa, M., Martínez-Calvo, M., Couceiro, J. R. & Mascarenäs, J. L. *Nat. Commun.* **7**, (2016).
172. Tonga, G. Y. *et al.* *Nat. Chem.* **7**, 597–603 (2015).
173. Sancho-Albero, M. *et al.* *Nat. Catal.* **2**, 864–872 (2019).
174. Bray, T. L. *et al.* *Chem. Sci.* **9**, 7354–7361 (2018).
175. Adam, C. *et al.* *Chem. - A Eur. J.* **24**, 16783–16790 (2018).
176. Destito, P. *et al.* *Chem. Sci.* **10**, 2598–2603 (2019).
177. Torres-Sánchez, C., Pérez-López, A. M., Alqahtani, M. N., Unciti-Broceta, A. & Rubio-Ruiz, B. *New J. Chem.* **43**, 1449–1458 (2019).
178. Weiss, J. T. *et al.* *Nat. Commun.* **5**, (2014).
179. Clavadetscher, J., Indrigo, E., Chankeshwara, S. V., Lilienkampf, A. & Bradley, M. *Angew. Chemie - Int. Ed.* **56**, 6864–6868 (2017).
180. Liu, Y. *et al.* *J. Am. Chem. Soc.* **140**, 3423–3433 (2018).
181. Indrigo, E., Clavadetscher, J., Chankeshwara, S. V., Lilienkampf, A. & Bradley, M.

- Chem. Commun.* **52**, 14212–14214 (2016).
182. Stenton, B. J., Oliveira, B. L., Matos, M. J., Sinatra, L. & Bernardes, G. J. L. *Chem. Sci.* **9**, 4185–4189 (2018).
183. Wang, J. *et al.* *Angew. Chemie - Int. Ed.* **54**, 5364–5368 (2015).
184. Weiss, J. T. *et al.* *J. Med. Chem.* **57**, 5395–5404 (2014).
185. Li, J. *et al.* *Nat. Chem.* **6**, 352–361 (2014).
186. Yusop, R. M., Unciti-Broceta, A., Johansson, E. M. V. V., Sánchez-Martín, R. M. & Bradley, M. *Nat. Chem.* **3**, 239–243 (2011).
187. Unciti-Broceta, A., Johansson, E. M. V., Yusop, R. M., Sánchez-Martín, R. M. & Bradley, M. *Nat. Protoc.* **7**, 1207–1218 (2012).
188. Streu, C. & Meggers, E. *Angew. Chemie - Int. Ed.* **45**, 5645–5648 (2006).
189. Sasmal, P. K. *et al.* *ChemBioChem* **13**, 1116–1120 (2012).
190. Völker, T., Dempwolff, F., Graumann, P. L. & Meggers, E. *Angew. Chem. Int. Ed. Engl.* **53**, 10536–10540 (2014).
191. Völker, T. & Meggers, E. *ChemBioChem* **18**, 1083–1086 (2017).
192. Miller, M. A. *et al.* *ACS Nano* **12**, 12814–12826 (2018).
193. Das, R. *et al.* *ACS Nano* **13**, 229–235 (2019).
194. Gupta, A., Das, R., Yesilbag Tonga, G., Mizuhara, T. & Rotello, V. M. *ACS Nano* **12**, 89–94 (2018).
195. Sánchez, M. I., Penas, C., Vázquez, M. E. & Mascareñas, J. L. *Chem. Sci.* **5**, 1901–1907 (2014).
196. Sadhu, K. K., Eierhoff, T., Römer, W. & Winssinger, N. *J. Am. Chem. Soc.* **134**, 20013–20016 (2012).
197. Sabatino, V., Rebelein, J. G. & Ward, T. R. *J. Am. Chem. Soc.* **141**, 17048–17052 (2019).
198. Vong, K., Yamamoto, T., Chang, T. C. & Tanaka, K. *Chem. Sci.* **11**, 10928–10933 (2020).
199. Yada, Y., Miyake, Y. & Nishibayashi, Y. *Organometallics* **27**, 3614–3617 (2008).
200. Richard, J. A. *et al.* *Bioconjug. Chem.* **19**, 1707–1718 (2008).
201. de Souza, L. G., Rennã, M. N. & Figueroa-Villar, J. D. *Chem. Biol. Interact.* **254**, 11–23 (2016).
202. Barnard, D. L. *et al.* *Antivir. Chem. Chemother.* **13**, 39–59 (2002).
203. Saeed, A. *et al.* *Chem. Biodivers.* **14**, (2017).
204. Mishra, N., Maurya, A. K. & Mulpuru, V. *ACS Omega* **5**, 32234–32249 (2020).
205. Aponick, A., Li, C. Y., Malinge, J. & Marques, E. F. *Org. Lett.* **11**, 4624–4627 (2009).
206. Wild, D. *et al.* *J. Nucl. Med.* **52**, 1412–1417 (2011).
207. Laznicek, M. *et al.* *Cancer Biother. Radiopharm.* **17**, 527–533 (2002).

208. Hruby, V. J. *Nat. Rev. Drug Discov.* **1**, 847–858 (2002).
209. Wild, D. *et al. J. Nucl. Med.* **55**, 1248–1252 (2014).
210. Fani, M., Nicolas, G. P. & Wild, D. *J. Nucl. Med.* **58**, 61S-66S (2017).
211. Solvi, T. N., Reiersølmoen, A. C., Orthaber, A. & Fiksdahl, A. *European J. Org. Chem.* **2020**, 7062–7068 (2020).
212. Hashmi, A. S. K. *et al. Chem. - A Eur. J.* **16**, 8012–8019 (2010).
213. Hashmi, A. S. K., Weyrauch, J. P., Rudolph, M. & Kurpejović, E. *Angew. Chemie - Int. Ed.* **43**, 6545–6547 (2004).
214. Von Wachenfeldt, H. *et al. Dalt. Trans.* **44**, 5347–5353 (2015).
215. Schiller, T. L., Keddie, D. J., Blakey, I. & Fredericks, P. M. *Eur. Polym. J.* **87**, 508–518 (2017).
216. Zav, S. I. & Dorofeeva, O. V. *Russ. Chem. Bull.* **6**, 1634–1636 (1981).
217. Bergmann, M., Egert, M. & Plenio, H. *Chem. - A Eur. J.* **23**, 13328–13331 (2017).
218. Zhao, J., Kajetanowicz, A. & Ward, T. R. *Org. Biomol. Chem.* **13**, 5652–5655 (2015).
219. Keller, S. G. *et al. Org. Biomol. Chem.* **14**, 7197–7201 (2016).
220. Do, J. H., Kim, H. N., Yoon, J., Kim, J. S. & Kim, H. J. *Org. Lett.* **12**, 932–934 (2010).
221. Youn, S. W., Ko, T. Y. & Jang, Y. H. *Angew. Chemie - Int. Ed.* **56**, 6636–6640 (2017).
222. Hébert, M. *et al. J. Org. Chem.* **81**, 5401–5416 (2016).
223. García-Rubia, A., Urones, B., Arrayás, R. G. & Carretero, J. C. *Chem. - A Eur. J.* **16**, 9676–9685 (2010).
224. Astakhov, A. V. *et al. Organometallics* **36**, 1981–1992 (2017).
225. Paterson, I. *et al. J. Org. Chem.* **70**, 150–160 (2005).
226. Harmrolfs, K., Mancuso, L., Drung, B., Sasse, F. & Kirschning, A. *Beilstein J. Org. Chem.* **10**, 535–543 (2014).
227. Sherwood, A. M. *et al. J. Org. Chem.* **83**, 980–992 (2018).
228. Emil Thomas Kaiser, Robert L. Colescott, Charles D. Bossinger, P. I. C. *Anal. Biochem.* **34**, 595–598 (1970).
229. Alhassan, M., Al Musaimi, O., Collins, J. M., Albericio, F. & De La Torre, B. G. *Green Chem.* **22**, 2840–2845 (2020).

## 10. Self Citations & Reprint Permissions

---

During the course of my PhD at the University of Basel, three manuscripts were published. The preprints and the corresponding SI of these manuscripts are integrated in this thesis.

SPRINGER  
TERMS AND CONDITIONS  
Feb 18, 2021

NATURE

LICENSE

---

This Agreement between University of Basel -- Fadri Christoffel ("You") and Springer Nature ("Springer Nature") consists of your license details and the terms and conditions provided by Springer Nature and Copyright Clearance Center.

License Number	5011820540280
License date	Feb 18, 2021
Licensed Content Publisher	Springer Nature
Licensed Content Publication	Catalysis Letters
Licensed Content Title	Palladium-Catalyzed Heck Cross-Coupling Reactions in Water: A Comprehensive Review
Licensed Content Author	Fadri Christoffel et al
Licensed Content Date	Dec 30, 2017
Type of Use	Thesis/Dissertation
Requestor type	academic/university or research institute
Format	print and electronic
Portion	full article/chapter
Will you be translating?	no
Circulation/distribution	1 - 29
Author of this Springer Nature content	yes
Title	Directed Evolution of Gold-based Artificial Metalloenzymes and Design of Gold-triggered Drug-Release Systems
Institution name	University of Basel
Expected presentation date	Jul 2021
Requestor Location	University of Basel Mattenstrasse BPR1096 Basel, Switzerland Attn: University of Basel
Total	0.00 CHF
Requestor Location	Basel, Switzerland Basel 4058

**Springer Nature Customer Service Centre GmbH  
Terms and Conditions**

**AAAS MATERIAL:**

Tobias Vornholt, Fadri Christoffel et al., “Systematic engineering of artificial metalloenzymes for new-to-nature reactions” *Science Advances* 22 Jan 2021:

Vol. 7, no. 4, eabe4208 (DOI: 10.1126/sciadv.abe4208)

Dear Fadri:

Thank you very much for writing, I hope you are well. I apologize for the delay in my reply – we’ve had a high volume of email and it is taking me longer to respond.

After publication of a manuscript in *Science Advances*, per our License to Publish, the author may reprint the final published version of their manuscript (or figures, portions etc), in print & electronic formats, in a thesis or dissertation written by the author as part of a course of study at an educational institution. Credit must be given to the first appearance of the material in the appropriate issue of *Science Advances* and noted as being released under a CC BY-NC license.

Appropriate credit lines follow this format or something similar:

"Reprinted from (or modified from if applicable) [INSERT *Science Advances* REFERENCE CITATION].

© The Authors, some rights reserved; exclusive licensee AAAS. Distributed under a CC BY-NC 4.0 License, <http://creativecommons.org/licenses/by-nc/4.0/>"

Please note: Portions, images, or figures appearing in the original *Science Advances* article that are attributed to other publishers or individuals are not subject to the article's Creative Commons license. Permission from the credited party should be sought prior to reproduction of such material.

If you have any questions, please don't hesitate to contact me.

Kind regards,

Elizabeth Sandler (Ms.)

Rights & Permissions, *Science* family of journals

American Association for the Advancement of Science (AAAS)

1200 New York Avenue

Washington, DC 20005

E: [esandler@aaas.org](mailto:esandler@aaas.org)

Tel: +1-202-326-6765

Nature Catalysis Manuscript NATCATAL-20104618A:

**Christoffel, F.**, Igareta, N., Pellizzoni, M., Tiessler-Sala, L., Lozhkin, B., Spiess, D., Lledos, A., Maréchal, J., Peterson, R., Ward, T. R., Design and Evolution of Chimeric Streptavidin for Protein-Enabled Dual Gold Catalysis. *Nat. Catal.* **4**, 643-653 (2021).

Design and evolution of chimeric streptavidin for protein-enabled dual gold catalysis

**Author:**

Fadri Christoffel et al

**Publication:**

Nature Catalysis

**Publisher:**

Springer Nature

**Date:**

Aug 2, 2021

Copyright © 2021, The Author(s), under exclusive licence to Springer Nature Limited

Author Request

If you are the author of this content (or his/her designated agent) please read the following. If you are not the author of this content, please click the Back button and select no to the question "Are you the Author of this Springer Nature content?".

Ownership of copyright in original research articles remains with the Author, and provided that, when reproducing the contribution or extracts from it or from the Supplementary Information, the Author acknowledges first and reference publication in the Journal, the Author retains the following non-exclusive rights:

To reproduce the contribution in whole or in part in any printed volume (book or thesis) of which they are the author(s).

The author and any academic institution, where they work, at the time may reproduce the contribution for the purpose of course teaching.

To reuse figures or tables created by the Author and contained in the Contribution in oral presentations and other works created by them.

v1.0

## 11. Curriculum Vitae

---

### Fadri Christoffel

from Valsot GR, Switzerland

#### Personal Information:

Date of birth: 08.10.1992

Place of birth: Rorschach SG, Switzerland

Nationality: Swiss & Portuguese

#### Professional Experience:

##### 2021–now **QA Specialist BRR mRNA, Lonza**

Part of the IBEX QA Team responsible for releasing the Moderna Vaccine against SARS-CoV-2. Responsible for batch record reviews of mRNA batches, lipid nanoparticle batches, mRNA lipid nanoparticle batches (vaccine) and cleaning protocols including QC documentation and audit trails under cGMP. Release of Master Batch Records and labels for production. Training in cGMP and GDP for Operation.

##### 2016–2017 **Research Assistant MPI, Keiser Lab, Swiss TPH**

Helminth Drug Development in the group of Prof. Dr. Jennifer Keiser. Including *in vitro* assays with novel drug candidates, *in vivo* assays on mice and hamsters, maintenance of parasitic life cycles and data treatment of clinical trials.

#### Education:

##### 2017–2021 **Ph.D. in Chemistry, Ward Lab, University of Basel**

Title: *Directed evolution of gold-based artificial Metalloenzymes and design of gold-triggered drug-release systems.*

Supervisor: Prof. Dr. Thomas R. Ward,

Co-referee: Prof. Dr. Olivier Baudoin

Achievements: Established the first dual-gold catalysis *in vivo*. Developed and synthesized (>10 steps) Pd-, Ru and Au-based NHC complexes as protein cofactors. Optimized artificial Metalloenzymes via directed evolution. Synthesized cancer-targeting, gold-functionalized peptides and investigated their applicability as potential drug-therapeutics.

Supplementary: Board Member of the PhD Chemistry Community and Waters UPLC-MS responsible of the Group



- 2015–2016     **M.Sc. in Chemistry (5.9/6.0), Baudoin Lab, University of Basel**  
 Title: *Synthesis of sterically demanding azole-based phosphine ligands for direct Negishi cross coupling reactions.*  
 Supervisor: Prof. Dr. Olivier Baudoin,  
 Co-referee: Prof. Dr. Andreas Pfaltz  
 Achievements: Designed and synthesized eight new sterically crowded phosphine ligands from which two outperformed the best commercial ligands in terms of turnover and selectivity.
- 2012–2015     **Bilingual B.Sc. in Chemistry, University of Fribourg & HES-SO**  
 Major: “*Chemistry*” at the Department of Chemistry  
 Minor: “*Chimie industrielle*” at the HES-SO Fribourg  
 Supplementary Student representative in the security & safety commission, J&S-leader 2 in sports climbing
- 2011–2012     **Swiss Infantry, Inf S 11, Neuchlen & St. Luzisteig**  
 As part of the Inf Kdo-Spez Unit, I enjoyed an unforgettable team spirit, passed extreme physical and mental challenges, and acquired the persistence and dedication needed for the subsequent studies.
- 2007–2011     **Kantonsschule am Burggraben, St. Gallen**  
 Matura mit Schwerpunkt Biologie und Chemie

**Academic Supervision and Teaching:**

- 2020–2021     Master Thesis supervision of Philipp Meyer on "*Gold(I)-catalyzed bioorthogonal uncaging of fluorescent probes - towards in vivo imaging and prodrug activation.*"
- 2018–2020     Advanced Inorganic Chemistry Practicals for Chemists
- 2017–2018     General Chemistry Practicals for Pharmacists

## 12. Publication List

---

### Scientific Publications:

- Pub. 4      **Christoffel, F.**, Igareta, N., Pellizzoni, M., Tiessler-Sala, L., Lozhkin, B., Spiess, D., Lledos, A., Maréchal, J., Peterson, R., Ward, T., Design and Evolution of Chimeric Streptavidin for Protein-Enabled Dual Gold Catalysis. *Nat. Catal.* **4**, 643-653 (2021).
- Pub. 3      Vornholt, T., **Christoffel, F.**, Pellizzoni, M., Panke, S., Ward, T. & Jeschek, M. Systematic Engineering of Artificial Metalloenzymes for New-to-Nature Reactions. *Sci. Adv.* **7**, eabe4208 (2021).
- Pub. 2      **Christoffel, F.** & Ward, T. R. Palladium-Catalyzed Heck Cross-Coupling Reactions in Water: A Comprehensive Review. *Catal. Letters* **148**, 489–511 (2018).
- Pub. 1      Zhang, K.-F., **Christoffel, F.** & Baudoin, O. Barbier-Negishi Coupling of Secondary Alkyl Bromides with Aryl and Alkenyl Triflates and Nonaflates. *Angew. Chemie Int. Ed.* **57**, 1982–1986 (2018).

### Further Contributions:

- Pub. 3      Joss, D., Vallapurackal, J., Baiyoumy, A., Chimisso, V., **Christoffel, F.**, Herr, P., Meyer, C., Miarzlou, D., Murawska, G., Niggli, N., Reznikova, K., Urosev, I., Van Gerwen, P. Conference Report Christmas Symposium Basel, December 6, 2019. *CHIMIA* **74**, 63 (2020).
- Pub. 2      Joss, D., Rigo, S., **Christoffel, F.**, Herr, P., Murawska, G., Sauter, B., Stampfli, A., Urosev, I., Vallapurackal, J. Conference Report Christmas Symposium Basel, December 7, 2018. *CHIMIA* **73**, 98 (2019).
- Pub. 1      Kovac, J., Vargas, M. & Keiser, J. *In vitro* and *in vivo* activity of R- and S-praziquantel enantiomers and the main human metabolite trans-4-hydroxy-praziquantel against *Schistosoma haematobium*. *Parasites and Vectors* **10**, 365 (2017).